

# Selective C-X and C-H Borylation by N-Heterocyclic Carbene Nickel(0) Complex



Dissertation zur Erlangung des naturwissenschaftlichen Doktorgrades  
der Julius-Maximilians-Universität Würzburg

**Yaming Tian**

aus Hebei, V.R. China

Würzburg 2020



Eingereicht bei der Fakultät für Chemie und Pharmazie am

---

Gutachter der schriftlichen Arbeit

1. Gutachter: Prof. Dr. Dr. h. c. Todd B. Marder
2. Gutachter: Prof. Dr. rer. nat. habil. Udo Radius

Prüfer des öffentlichen Promotionskolloquiums

1. Prüfer: Prof. Dr. Dr. h. c. Todd B. Marder
2. Prüfer: Prof. Dr. rer. nat. habil. Udo Radius
3. Prüfer: Priv.-Doz. Dr. Florian Beuerle

Datum des öffentlichen Promotionskolloquiums

---

Doktorurkunde ausgehändigt am

---



谨此献给我的家人  
**Für meine Familie**



*“Our greatest glory consists not in never falling but in rising every time  
we fall.”*

— O. Goldsmith





Die Experimente zur vorliegenden Arbeit wurden in der Zeit von Oktober 2016 bis September 2020 am Institut für Anorganische Chemie der Julius-Maximilians-Universität Würzburg unter der Aufsicht von Prof. Dr. Dr. h. c. Todd B. Marder und Prof. Dr. rer. nat. habil. Udo Radius durchgeführt.



## Acknowledgements

First of all, I would like to thank **Prof. Dr. Dr. h. c. Todd B. Marder** for providing me the precious opportunity to do my PhD here. I still remember clearly the first time we met each other in Shanghai and you gave me infinite help in applying for the China Scholarship Council (CSC). I would like to thank you for your great help to let me have a good start in Würzburg. I am very grateful that you have been encouraging me to communicate with other people. I also appreciate your patient discussions, constant guidance in science and life during the past four years. Furthermore, I would like to thank you for providing me the opportunity to participate in the conference in Beijing which gave me a lot of fun. I would like to thank your wife **Anne** as well for her great support. It is a great honor and pleasure for me to be a member of “Marder” family.

I would like to thank **Prof. Dr. rer. nat. habil. Udo Radius** for the great opportunity to be part of the “Radius” family. I will never forget that at the beginning of my research, you greatly helped me in the NHC preparation training. I am very grateful for your patient discussions and explanations every time I had a question. I would like to thank you for your discussions, good ideas and the great time we had for the preparation of our papers. I also appreciate that you helped me revise my thesis and give a lot of useful comments. It is also a great honor for me to get your constant guidance during the past four years.

I would like to thank **Prof. Dr. Xiaoning Guo** for the great cooperation with me in science. In addition, I am also very grateful to you for your helpful suggestions and selfless help in life. I will never forget the great time of working in the lab, coffee breaks, lunches and beer time we had together. I also would like to thank your family who gave me great support and help during the past four years. I will never forget the great time I had with your family.

I would like to thank **Prof. Dr. Andreas Steffen** (Technische Universität Dortmund, Anorganische Chemie) for the helpful discussions, suggestions and great help on the DFT calculations for chapter two.

I would like to thank **Prof. Dr. Holger Braunschweig** for the helpful discussions and suggestions for my research work. I also appreciate that you helped correct the papers.

I would like to thank **Prof. Dr. Stephen A. Westcott** (Department of Chemistry and Biochemistry, Mount Allison University, Canada) for the helpful discussions and suggestions for Chapter four.

I would like to thank **Dr. Jörn Nitsch** for the great help with the photophysical measurements and the corrections of the paper.

I would like to thank **Dr. Ivo Krummenacher** for the CV and EPR measurements and analyses.

I would like to thank **Zhu Wu** for the kind help with the measurement of the crystal structures, photophysical measurements and proofreading of the paper.

I would like to thank **Dr. Alexandra Friedrich** for the kind help with the measurement of the crystal structures and proofreading of the paper.

I would like to thank **Zhiqiang Liu** for giving me helpful suggestions and countless help in my life. I will never forget the great time we had with **Tao Jin** and **Hongdong Yuan**.

I would like to thank **Dr. Julia Merz and Jan Maier** for the summary translation of the thesis and also great help for the preparation of the thesis.

I would like to thank **Dr. Florian Rauch** for teaching me to do the routine maintenance of the glovebox, the massive number of glovebox repair services and the great help for the preparation of the thesis.

I would like to thank **Florian Kerner** for the technique training and the kind help in the laboratory. I would like to thank **Sabine Lorenzen** for the safety training and general support in the laboratory. I would like to thank **Maximilian Kuntze-Fechner** for the

technique training and the contribution on chapter two. I would like to thank **Laura Kuehn** for the technique training.

I would like to thank **Jiang He** for the SPS solvent supply and general support in the laboratory. I would like to thank **Christoph Mahler** for countless HRMS measurements and general support in the laboratory. I want to thank **Dr. Stephan Wagner** for the GC-MS repair services. I would like to thank **Dr. Rüdiger Bertermann** and **Marie-Luise Schäfer** for their kind help with NMR spectroscopy. I would like to thank **Sabine Timmroth** and **Liselotte Michels** for the elemental analysis measurements. I would like to thank **Dr. Goutam Kumar Kole** for helping me check the crystals. I want to thank **Prof. Dr. Lei Ji** (Northwestern Polytechnical University) for the photophysical measurement in chapter two and also for the great help with my life.

I would like to thank the lunch group members, **Jiang He, Zhu Wu, Dr. Jiefeng Hu, Dr. Xiaolei Zhang**, I will never forget the great time we had in Mensa.

I want to thank **Yudha Prawira Budiman** for the suggestions on my research and great help for the preparation of the thesis.

I would like to thank **Prof. Dr. Xiaoling Luo, Prof. Dr. Qing Ye** (Southern University of Science and Technology), **Prof. Dr. Jian Zhao** (Nanjing University of Science and Technology), **Dr. Zhenguo Huang** (University of Technology Sydney), **Dr. Xiangqing Jia, Dr. Hua Wang, Dr. Lujia Mao, Dr. Wenbo Ming, Dr. Xiaocui Liu, Dr. Ying Ying Chia, Mingming Huang, Kun Peng** and **Xingxin Shao** for the helpful suggestions and discussions on my research and also for the kind help in science and life.

I would like to thank **Maria Eckhardt** for the great help with the preparation of the thesis and the assistance during my PhD study. I also want to thank **Cornelia Walter** for the assistance during my PhD study.

I would like to thank **Dr. Shishir Ghosh, Matthias Ferger, Johannes Krebs, Jan Maier**, and **Robert Ricker** for the great help in the laboratory. I want to thank **Hildegard**

**Holzinger** and **Sarina Berger** for the assistance in ordering chemicals and general lab supply.

I would like to thank the students, whom I supervised, for their assistance with synthesis:

**Andreas Helbig, Fridolin Saal** and **Maximilian Michel**.

I would like to thank **China Scholarship Council (CSC)** and the Chinese government for their kind and generous financial support of my studies in Germany. I also want to thank the staffs of the CSC and the Generalkonsulat der Volksrepublik China in München who helped me during my time in Germany.

I want to thank all of the people from AK Prof. Todd B. Marder, AK Prof. Udo Radius and the whole Inorganic Chemistry Institute for making my time here really enjoyable.

Last but not least, I would like to thank my family, the most important people in my life, thank you for always standing by me no matter what I do.

*Thank you!*

## List of Publications

The publications listed below are partly reproduced in this dissertation with permission from American Chemical Society. The table itemizes at which position in this work the paper have been reproduced.

Publication	Position
Y. M. Tian, X. N. Guo, M. Kuntze-Fechner, I. Krummenacher, H. Braunschweig, U. Radius, A. Steffen, T. B. Marder, <i>J. Am. Chem. Soc.</i> <b>2018</b> , <i>140</i> , 17612–17623.	Chapter 2
Y. M. Tian, X. N. Guo, I. Krummenacher, Z. Wu, J. Nitsch, H. Braunschweig, U. Radius, T. B. Marder, <i>submitted</i> .	Chapter 3
Y. M. Tian, X. N. Guo, Z. Wu, A. Friedrich, S. A. Westcott, H. Braunschweig, U. Radius, T. B. Marder, <i>J. Am. Chem. Soc.</i> <b>2020</b> , <i>142</i> , 13136-13144.	Chapter 4

### Further publications:

1. Z. F. Jiao, Y. M. Tian, B. Zhang, C. H. Hao, Y. Qiao, Y. X. Wang, Y. Qin, U. Radius, H. Braunschweig, T. B. Marder, X. N. Guo, X. Y. Guo, *J. Catal.* **2020**, *389*, 517-524.
2. Z. Liu, Y. P. Budiman, Y. M. Tian, A. Friedrich, M. Huang, S. A. Westcott, U. Radius, T. B. Marder, *Chem. Eur. J.* **2020**, DOI: 10.1002/chem.202002888.





## List of Abbreviations

APCI	Atmospheric-pressure chemical ionization
Ar	Argon
B <sub>2</sub> cat <sub>2</sub>	Bis(catecholato)diboron
B <sub>2</sub> neop <sub>2</sub>	Bis(neopentyl glycolato)diboron
BOC	<i>tert</i> -Butoxycarbonyl
B <sub>2</sub> pin <sub>2</sub>	Bis(pinacolato)diboron
cod	1,5-Cyclooctadiene
Cs <sub>2</sub> CO <sub>3</sub>	Cesium carbonate
CsF	Caesium fluoride
CV	Cyclic voltammetry
dba	Dibenzylideneacetone
DCM	Dichloromethane
DFT	Density functional theory
Eosin Y	2-(2,4,5,7-tetrabromo-6-oxido-3-oxo-3 <i>H</i> -xanthen-9-yl)benzoate
EPR	Electron paramagnetic resonance
equiv	Equivalents
Et <sub>2</sub> O	Ethoxyethane
EtOAc	Ethyl acetate
<i>fac</i> -[Ir(ppy) <sub>3</sub> ]	Tris[2-phenylpyridinato-C <sub>2</sub> ,N]iridium(III)
[Fe(acac) <sub>3</sub> ]	Iron(III) acetylacetonate
GC-MS	Gas chromatography-mass spectrometry
HBcat	Catecholborane
HBpin	4,4,5,5-Tetramethyl-1,3,2-dioxaborolane
HRMS	High-resolution mass spectrometry
IMes	1,3-Dimesitylimidazol-2-ylidene
IPr	1,3- <i>bis</i> (2,6-Diisopropylphenyl)imidazol-2-ylidene

KF	Potassium fluoride
KOAc	Potassium acetate
KOMe	Potassium methoxide
KO <sup>t</sup> Bu	Potassium <i>tert</i> -butoxide
Li <sub>2</sub> CO <sub>3</sub>	Lithium carbonate
MeCN	Acetonitrile
MTBE	Methyl <i>tert</i> -butyl ether
NaI	Sodium iodide
NaOAc	Sodium acetate
NaOMe	Sodium methoxide
NHC	<i>N</i> -Heterocyclic carbene
[NiCl <sub>2</sub> (PMe <sub>3</sub> ) <sub>2</sub> ]	Dichlorobis(trimethylphosphine)nickel(II)
NMR	Nuclear magnetic resonance
rt	Room temperature
[Ru(bpy) <sub>3</sub> ]Cl <sub>2</sub>	Tris(bipyridine)ruthenium(II) chloride
SED	Super electron donor
SET	Single electron transfer
TBAPF <sub>6</sub>	Tetrabutylammonium hexafluorophosphate
TD-DFT	Time-dependent density-functional theory
TEMPO	2,2,6,6-Tetramethylpiperidinyloxy
TET	Triplet energy transfer
THF	Tetrahydrofuran
tmly	1,3,4,5-tetramethylimidazol-2-ylidene
UV	Ultraviolet
UV-Vis	Ultraviolet-visible

## Table of Contents

1 Photoinduced C-X borylation for the synthesis of organoboron compounds.....	3
1.1 Abstract .....	3
1.2 Introduction .....	4
1.3 Photocatalytic C-X borylation .....	7
1.3.1 Transition-metal photocatalyst .....	7
1.3.2 Metal-free organocatalyst .....	15
1.3.3 Photochemical borylation.....	19
1.4 Conclusions and motivation .....	25
2 Selective photocatalytic C-F borylation of polyfluoroarenes by Rh/Ni dual catalysis....	29
2.1 Abstract .....	29
2.2 Introduction .....	30
2.3 Results and discussions.....	35
2.3.1 Photocatalytic borylation of 1,2,3,5-tetrafluorobenzene .....	35
2.3.2 Catalytic reactivity of different photocatalysts .....	38
2.3.3 Substrate scope .....	40
2.4 Mechanistic studies .....	42
2.4.1 Cyclic voltammetry .....	42
2.4.2 UV-vis absorption spectrum and stability upon irradiation of [Ni <sup>II</sup> ] .....	46
2.4.3 Control experiments for borylation of 1,2,3,5-tetrafluorobenzene.....	62
2.4.4 DFT calculations.....	98
2.4.5 Proposed mechanism.....	102
2.4.6 Possible role of CsF in the transmetalation step .....	103
2.5 Conclusions .....	104
2.6 Experimental procedures and characterization data.....	104
2.6.1 General information .....	104
2.6.2 Synthesis and stability of the Rh biphenyl complex.....	107
2.6.3 Synthesis and properties of [Ni <sup>II</sup> ].....	112

---

2.6.4	Experimental procedures .....	115
2.6.5	Compound characterization .....	116
3	Visible-light-induced Ni-catalyzed radical borylation of chloroarenes .....	125
3.1	Abstract.....	125
3.2	Introduction .....	126
3.3	Results and discussions .....	128
3.3.1	Photocatalytic borylation of 4-chloroanisole .....	128
3.3.2	Substrate scope .....	131
3.4	Mechanistic studies .....	137
3.4.1	Aryl radical trapping experiments .....	137
3.4.2	EPR investigations .....	139
3.4.3	Photophysical properties of different Ni catalysts .....	141
3.4.4	Photo-induced borylation of chlorobenzene with different Ni catalysts .....	142
3.4.5	Proposed mechanism .....	170
3.5	Conclusions.....	170
3.6	Experimental procedures and characterization data .....	171
3.6.1	General information .....	171
3.6.2	Experimental procedures .....	173
3.6.3	Synthesis of $[\text{Ni}^{\text{I}}(\text{IMes})_2\text{Cl}]$ .....	174
3.6.4	Synthesis of $[\text{Ni}^{\text{II}}(\text{IMes})_2\text{Cl}_2]$ .....	174
3.6.5	Compound characterization .....	175
3.6.6	Single-crystal X-ray diffraction analyses.....	193
4	Ni-catalyzed traceless, directed C3-selective C-H borylation of indoles .....	197
4.1	Abstract.....	197
4.2	Introduction .....	198
4.3	Results and discussions .....	200
4.3.1	Borylation of indole .....	200
4.3.2	Substrate scope .....	203
4.4	Mechanistic studies .....	204
4.4.1	Monitoring the borylation of indole at different times .....	204

---

4.4.2	Investigation of the installation of the directing group.....	206
4.4.3	Investigation of the catalytic selective C3-H borylation step.....	210
4.4.4	Investigation of the removal of the directing group.....	211
4.4.5	Proposed mechanism.....	212
4.4.6	Synthetic applications of C3-borylated indoles.....	213
4.5	Conclusions .....	213
4.6	Experimental procedures and characterization data.....	214
4.6.1	General information .....	214
4.6.2	Experimental procedures.....	216
4.6.3	Synthesis of [Ni(IMes) <sub>2</sub> (H)(indole)] and [Ni(IMes) <sub>2</sub> (H)(6F-indole)] .....	217
4.6.4	Synthesis of 1,3-(Bpin) <sub>2</sub> -indole .....	219
4.6.5	Synthesis of methyl-4-(1H-indol-3-yl)-benzoate .....	220
4.6.6	Compound characterization.....	221
4.6.7	Single-crystal X-ray diffraction analyses of C3-borylated indoles .....	228
	Summary .....	229
	Zusammenfassung .....	235
	Notes and References .....	241
	Appendix.....	261
	Affidavit.....	275
	Eidesstaatliche Erklärung.....	275



# **Chapter One**

## **Photoinduced C-X borylation for the synthesis of organoboron compounds**





# 1 Photoinduced C-X borylation for the synthesis of organoboron compounds

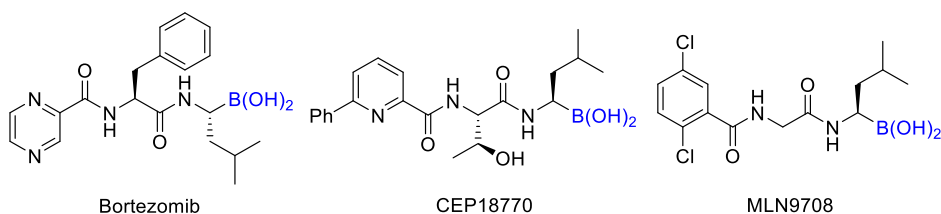
## 1.1 Abstract

Organoboron compounds are important building blocks in organic synthesis, materials science, and drug discovery. The development of practical and convenient ways to synthesize boronate esters attracted significant interest. Photoinduced borylations originated with stoichiometric reactions of arenes and alkanes with well-defined metal-boryl complexes. Now photoredox-initiated borylations, catalyzed either by transition-metal or organic photocatalysts, and photochemical borylations with high efficiency have become a burgeoning area of research. In this chapter, we summarize research in the field of photocatalytic C-X borylation, especially emphasizing recent developments and trends, based on transition-metal catalysis, metal-free organocatalysis and direct photochemical activation. We focus on reaction mechanisms involving single electron transfer (SET), triplet energy transfer (TET), and other radical processes.

## 1.2 Introduction

Organoboron compounds are key building blocks in organic synthesis, materials science, and drug discovery.<sup>1-4</sup> The boronate group in organoboronate esters can not only be converted to virtually all functional groups, but the boronate esters themselves can be employed in various cross-coupling reactions to synthesize a wide range of valuable organic compounds, and can also be used to catalyze enantioselective Diels-Alder reactions and chemo- or regioselective activation of pyruvic acids, diols, and carbohydrates.<sup>5-7</sup> Recently, organoboron compounds have emerged as useful synthons for conjugated materials,<sup>8-12</sup> covalent organic frameworks<sup>13-15</sup> and hydrogels.<sup>16-18</sup> Their low toxicity and easy-handling make them widely applicable in the total synthesis of bioactive natural products. In addition, organoboronic acids can be utilized directly as therapeutic agents and biological probes.<sup>19-21</sup> For example, bortezomib and its derivatives (Scheme 1-1) as carboxylic bioisosteres can replace motifs with similar chemical and physical properties and act as proteasome inhibitors.<sup>19</sup>

### Scheme 1-1. Structures of important $\alpha$ -aminoboronic acid-based pharmaceuticals

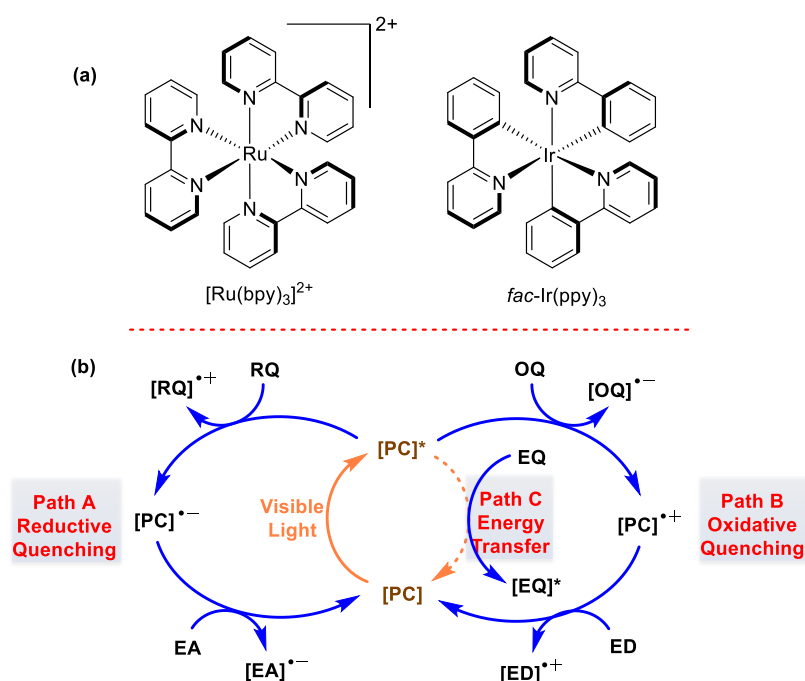


The development of practical and convenient ways to synthesize boronate esters has gained broad interest over the past few decades. The classical method for the preparation of boronic acids is based on the use of highly reactive organolithium or Grignard reagents in combination with suitable boron precursors, followed by transesterification or hydrolysis.<sup>22,23</sup> Recently, a series of new borylation protocols, including transition-metal-catalyzed hydroborations and diborations of alkenes and alkynes,<sup>2,24-36</sup> C-H<sup>4,37-45</sup> and C-X<sup>46-49</sup> borylations, which display a high degree of functional group tolerance, and transition-metal-free borylations,<sup>3,50</sup> etc., have been developed to achieve the borylation of different classes of organic compounds.

Photoinduced borylation is emerging as an important approach for the synthesis of organoboron compounds.<sup>38,45,51-53</sup> Photoinduced organic synthesis focuses on electronically excited molecules and light-induced chemical processes. Because the reactivity of excited molecules is fundamentally different from that in their ground state, photo-mediated chemistry has the possibility to generate highly reactive intermediates, and then to achieve reactions that are difficult or even impossible via conventional ground-state pathways. Photocatalytic borylation originated with the photoinduced stoichiometric borylations of arenes and alkanes with well-defined metal-boryl complexes. Now, photoredox-initiated borylations catalyzed either by transition-metal complexes or organic photoredox catalysts are gradually becoming a popular light-driven synthetic strategy.

Ruthenium bipyridyl<sup>54</sup> and iridium 2-phenylpyridine<sup>55</sup> complexes (Scheme 1-2a) are typical metal photocatalysts (PC).<sup>54-63</sup> Generally, an electron of a [PC] is excited from a metal-centered orbital to a ligand-centered  $\pi^*$  orbital (MLCT) via photon absorption giving [PC]\*. The singlet MLCT state undergoes rapid intersystem crossing (ISC) to give a triplet MLCT state, the long-lived photoexcited species that engages in single electron transfer (SET). It is both a strong electron donor and acceptor, and is easily reduced to [PC]<sup>-</sup> or oxidized to [PC]<sup>++</sup> through SET processes, triggering key organic reactions (Scheme 1-2b, Paths A & B); it can also directly transfer energy to a substrate or other metal complex, thus initiating subsequent reactions (Scheme 1-2b, Path C). Because both oxidants and reductants are generated in the same system, under extremely mild conditions, typically using household light bulb photoredox processes, they can promote reactions requiring both the donation and receipt of electrons at disparate points in the reaction sequence. Therefore, many side reactions can be avoided. Beside photoredox catalysis, direct photochemical activation of organic molecules has also become a widely used tool for the synthesis of organoboron compounds. For example, photoinduced homolytic or heterolytic cleavage of Ar-X bonds is an efficient method to generate reactive intermediates, which enables the construction of many important carbon-carbon and carbon-heteroatom bonds.<sup>45,51,52</sup>

**Scheme 1-2. (a) Prototypical ruthenium bipyridyl photocatalyst (left) and iridium 2-phenylpyridine photocatalyst (right); (b) Electron transfer and energy transfer processes of a photocatalyst ([PC]) under visible light irradiation (RQ = reductive quencher, OQ = oxidative quencher, EQ = energy quencher, EA = electron acceptor, ED = electron donor)**



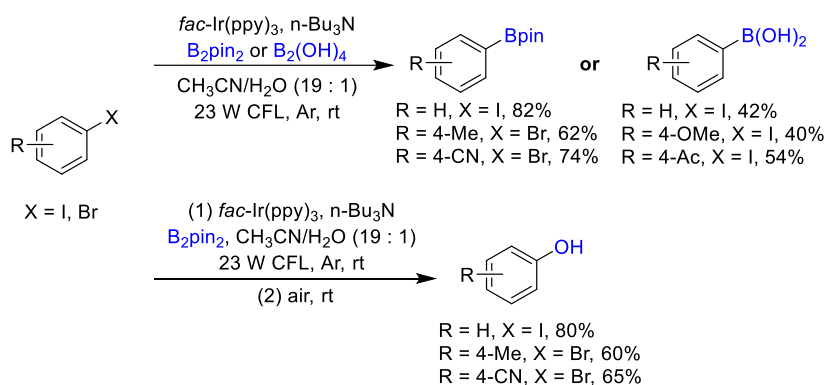
Herein, we systematically and comprehensively summarize research in the field of photocatalytic C-X borylation from 1995 to 2020, especially emphasizing recent developments and trends. Different approaches to improve reactivity and selectivity are analyzed, and their commonalities and differences are addressed. This chapter guides the reader through three types of photocatalysis, i.e., transition-metal catalysis, metal-free organocatalysis, and photochemical activation, focusing on the reaction mechanisms involving single electron transfer (SET), triplet energy transfer (TET), or other radical processes.

### 1.3 Photocatalytic C-X borylation

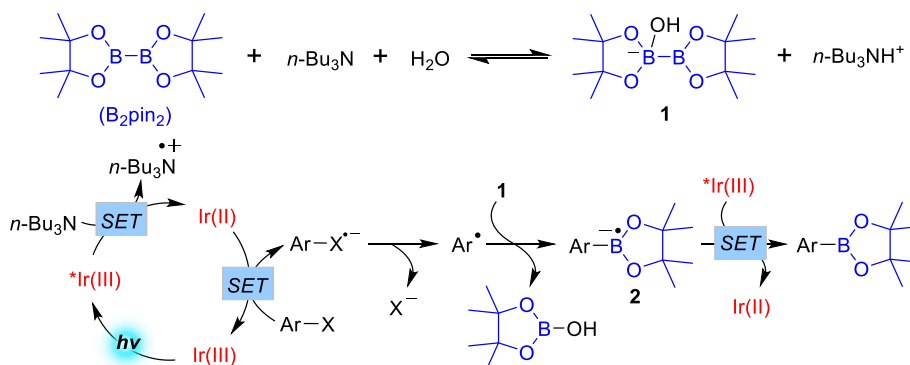
Since Miyaura et al. achieved the borylation of aryl halides with bis(pinacolato)diboron ( $B_2pin_2$ ) using a palladium catalyst in 1995,<sup>64</sup> catalytic C-X borylation has become one of the fundamental methods to construct C-B bonds due to the high functional group tolerance of the method employed and the excellent availability of aryl and alkyl halides.<sup>46-49</sup> Photo-excited photocatalysts have a much more negative reduction potential and high triplet (singlet) energies, which can efficiently reduce aryl/alkyl halides, cleaving the C-X bonds, and even activating and borylating less reactive C-Cl and C-F bonds.

#### 1.3.1 Transition-metal photocatalyst

**Scheme 1-3. Visible light photoredox-induced borylation of aryl halides and one-pot, two-step synthesis of phenols from aryl halides**



**Scheme 1-4. Mechanism of visible light photoredox-induced borylation of aryl halides with  $B_2pin_2$**

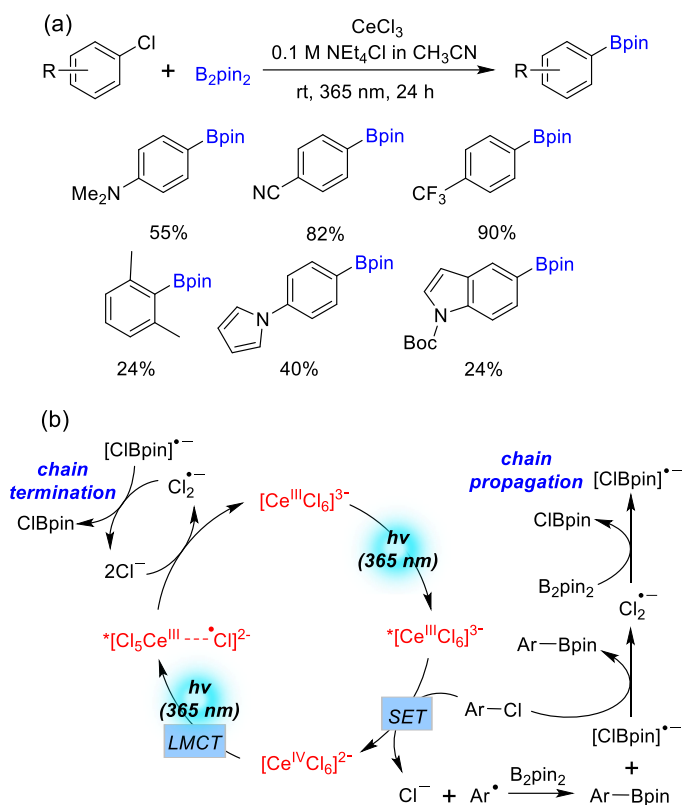


In 2016, Fu et al. reported a visible light photoredox-induced borylation of aryl halides with  $B_2pin_2$  using  $fac\text{-Ir(ppy)}_3$  as the photocatalyst with irradiation by a 23 W compact

fluorescent light (CFL), (Scheme 1-3).<sup>65</sup> Tributylamine ( ${}^n\text{Bu}_3\text{N}$ ) as a sacrificial electron donor and aqueous acetonitrile as solvent proved to be optimal. The reaction did not proceed in the absence of  ${}^n\text{Bu}_3\text{N}$  or light. With triethylamine ( $\text{Et}_3\text{N}$ ) and diisopropylethylamine (DIPEA) as additives instead of the  ${}^n\text{Bu}_3\text{N}$ , the product yield is lower. The substrate scope for the borylation of aryl iodides and bromides with  $\text{B}_2\text{pin}_2$  was studied, and good functional group tolerance for ethers, ketone, aldehyde, nitriles, esters, and  $\text{CF}_3$  was observed. Aryl iodides not only show higher reactivity than bromides, but those bearing either electron-withdrawing and electron-donating groups performed equally well. However, as is typical for thermal metal-catalyzed borylation,<sup>46-49</sup> electron-rich aryl bromides gave lower yields of the corresponding borylated products than electron-deficient aryl bromides. This protocol was applied to the synthesis of phenylboronic acid, using  $\text{B}_2(\text{OH})_4$  as the boron source, but this was only successful with aryl iodides (Scheme 1-3). In addition, a one-pot, two-step borylation of aryl halides and oxidation of the resulting arylboronic esters for the direct synthesis of phenols was also developed. After borylation of the aryl halides, exposing the reaction system to air for 16 h gave the corresponding phenols moderate to good yields (Scheme 1-3).

Based on an electron spin resonance (ESR) investigation, a possible mechanism involving a radical process was proposed (Scheme 1-4). Treatment of  $\text{B}_2\text{pin}_2$  with  ${}^n\text{Bu}_3\text{N}$  in aqueous solution forms a hydroxide-diboron adduct **1**. Upon irradiation, a SET from  ${}^n\text{Bu}_3\text{N}$  to the excited  ${}^*\text{Ir}(\text{III})$  generates a  $[{}^n\text{Bu}_3\text{N}]^{+\bullet}$  radical cation and  $\text{Ir}(\text{II})$ , which further reacts with aryl halide to form an  $[\text{ArX}]^{\bullet-}$  anion radical regenerating  $\text{Ir}(\text{III})$ . Then, the  $\text{Ar}^{\bullet}$  produced from  $[\text{ArX}]^{\bullet-}$  reacts with the anionic hydroxide-diboron adduct **1** to generate an aryl Bpin radical anion **2**, which further undergoes a SET process with  ${}^*\text{Ir}(\text{III})$  to form the borylated product. However, there may be a problem with this mechanism, as the oxidation potential of the tertiary amine is 0.99 V in  $\text{CH}_3\text{CN}$ ,<sup>66</sup> which is not sufficient for electron transfer to  ${}^*\text{Ir}(\text{III})$  [ $E_{1/2}({}^*\text{Ir}(\text{III})/\text{Ir}(\text{II})) = 0.31 \text{ V}$ ].<sup>54,55</sup> However, in the following step, the  $\text{Ir}(\text{II})$  radical anion intermediate is a strong reductant [ $E_{1/2}(\text{Ir}(\text{III})/\text{Ir}(\text{II})) = -2.19 \text{ V}$ ],<sup>54,55</sup> and may donate an electron to aryl iodides and bromides.

## Scheme 1-5. Hexachlorocerate anion-photocatalyzed borylation of aryl chlorides

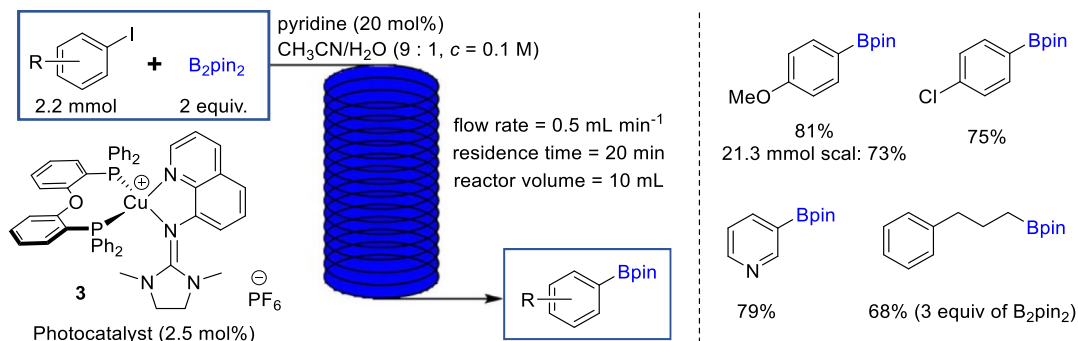


Lanthanide photosensitizers have been recognized as potential substitutes for Ru or Ir photocatalysts as they can generate various active intermediates, including aryl and alkyl radicals, via SET or hydrogen atom transfer (HAT) processes under mild conditions. Schelter, et al. developed a series of Ce(III)-photocatalysts, e.g.,  $\text{Ce}[\text{N}(\text{SiMe}_3)_2]_3$  and  $[(\text{Me}_3\text{Si})_2\text{NC}(\text{CyN})_2]\text{Ce}[\text{N}(\text{SiMe}_3)_2]_2$ , which exhibited two absorption maxima at ca. 420 nm (corresponding to a  $4f \rightarrow 5d_z^2$  electronic transition, 2.89-2.99 eV) and ca. 360 nm (corresponding to a  $4f \rightarrow 5d_{xy}, 5d_{xz}, 5d_{yz}$  electronic transition, 3.38-3.52 eV) to access organic transformations.<sup>67-70</sup> Upon photoexcitation of the Ce(III) cation under ca. 420 nm irradiation, its long-lived  $^2\text{D}$  excited state, a highly reactive metalloradical and strong reductant, can readily reduce organic substrates by SET. Recently, they reported a photocatalyzed borylation of aryl chlorides using the hexachlorocerate ( $[\text{Ce}^{\text{III}}\text{Cl}_6]^{3-}$ ) anion,<sup>71</sup> which was generated *in situ* by reaction of  $\text{CeCl}_3$  with  $\text{NEt}_4\text{Cl}$  in acetonitrile, at room temperature. Aryl and heteroaryl halides with electron-donating, electron-neutral, and electron-withdrawing groups at the *para*, *meta*, or *ortho* positions, including methyl, cyano, ester, and trifluoromethyl groups, gave the corresponding borylated products under the

optimized conditions (Scheme 1-5a).

A radical-trapping experiment, and the high quantum yield ( $\Phi = 6.1$ ) of the reaction, showed that the reaction probably goes through a radical chain pathway (Scheme 1-5b). The reaction is initiated by SET from the *in situ* generated  $[\text{Ce}^{\text{III}}\text{Cl}_6]^{3-}$  to an aryl chloride producing a  $\text{Cl}^-$  anion and an aryl radical, which further reacts with  $\text{B}_2\text{pin}_2$  to form the borylated product and the  $[\text{ClBpin}]^-$  radical anion. Chain propagation is achieved by the reaction of  $[\text{ClBpin}]^-$  with additional aryl chloride giving the borylated product and another radical anion  $\text{Cl}_2^-$ , which is trapped by  $\text{B}_2\text{pin}_2$  to regenerate  $[\text{ClBpin}]^-$ .<sup>72,73</sup> The  $[\text{Ce}^{\text{IV}}\text{Cl}_6]^{2-}$  formed is reduced via photoinduced ligand-to-metal charge transfer (LMCT), followed by reaction of a chlorine anion with  $\text{Cl}^-$  from the excess  $\text{NEt}_4\text{Cl}$  to generate  $\text{Cl}_2^-$ , which then reacts with  $[\text{ClBpin}]^-$  to terminate the radical chain process.<sup>74-76</sup>

### Scheme 1-6. Copper-photocatalyzed borylation of aryl and alkyl iodides under continuous-flow conditions

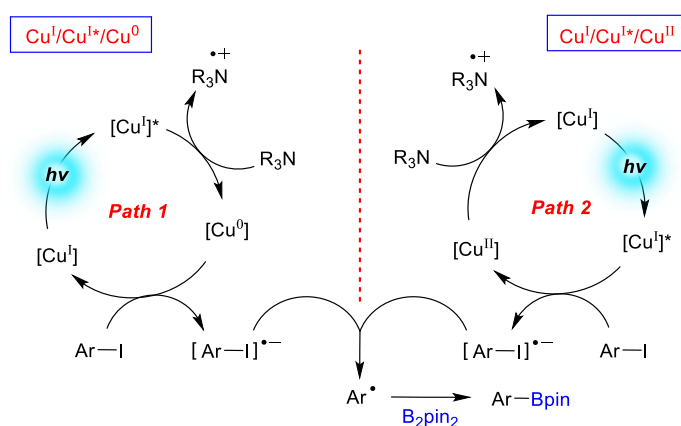


Poisson et al. reported a heteroleptic Cu complex  $[\text{Cu}(\text{DPEPhos})(\text{DMEGqu})]\text{PF}_6$  (**3**)-photocatalyzed borylation of organic iodides at room temperature with irradiation by blue LEDs.<sup>77</sup> The mixture of  $\text{CH}_3\text{CN}/\text{H}_2\text{O}$  as the solvent and 20 mol% of pyridine as an additive gave the boronic ester product. The protocol provided a wide range of aryl, heteroaryl, vinyl and alkyl boronates in moderate to high yields using  $\text{B}_2\text{pin}_2$  as the boron source and  $N,N$ -diisopropylethylamine (DIPEA) as the base. Five aryl and heteroaryl bromides were also successfully borylated using this method. The reactions were conducted under continuous-flow conditions with a 20 min residence time and 0.5 mL



min<sup>-1</sup> flow rate (Scheme 1-6). Using 21.3 mmol of 4-iodoanisole as substrate yielded 73% of isolated product. Two pathways including a Cu<sup>I</sup>/Cu<sup>I\*</sup>/Cu<sup>0</sup> cycle based on a reductive quenching with DIPEA and a Cu<sup>I</sup>/Cu<sup>I\*</sup>/Cu<sup>II</sup> cycle based on an oxidative quenching with the aryl iodides are presumed involving in the reaction, and the former is the predominant process (Scheme 1-7).

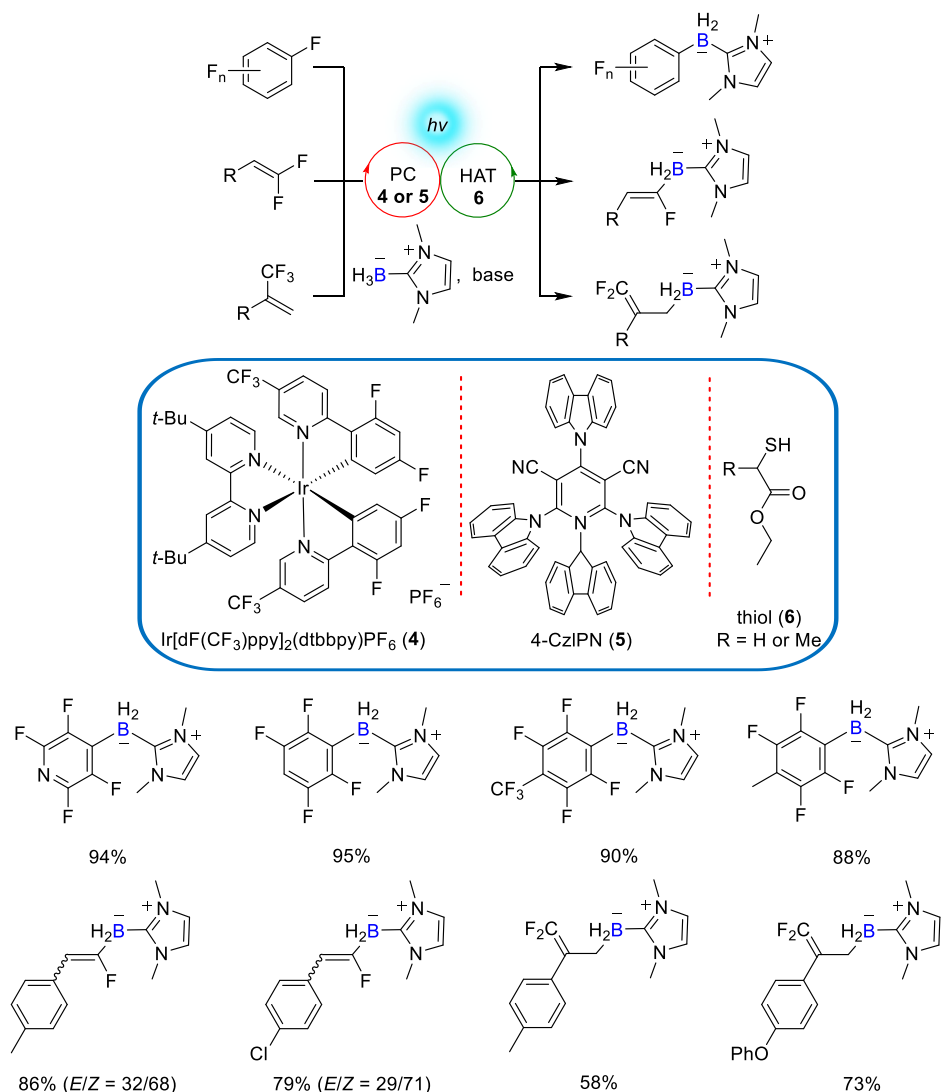
**Scheme 1-7. Proposed mechanism of the copper-photocatalyzed borylation of aryl iodides**



Recently, Wu et al. developed a general defluoroborylation protocol that employed Ir[dF(CF<sub>3</sub>)ppy]<sub>2</sub>(dtbbpy)PF<sub>6</sub> (**4**) and 4-CzIPN (**5**) as photoredox catalysts and thiol (**6**) as a HAT agent to achieve the activation and borylation of C-F bonds of a wide range of polyfluoroarenes, *gem*-difluoroalkenes, and trifluoromethylalkenes (Scheme 1-8).<sup>78</sup> Upon excitation of the Ir<sup>III</sup> photocatalyst, it is reduced by the thiol via a SET process to produce an Ir<sup>II</sup> complex and a thiyl radical, which further reacts with NHC-boranes to form an NHC-boryl radical and regenerate the thiol through a HAT process (Scheme 1-9a). Then, the fluoroarene or *gem*-difluoroalkene is reduced by the Ir<sup>II</sup> complex to regenerate the Ir<sup>III</sup> catalyst and a fluoroaryl radical anion, which combines with the NHC-boryl radical, followed by the extrusion of fluoride to give the final product (Scheme 1-9a). When a proton is located at the *para*-position of an electron-withdrawing group in the polyfluoroarene, the dearomatized hydroboration product is formed by protonation after the radicals combine (Scheme 1-9b). With the defluoroborylation of trifluoromethylalkenes, the generated NHC-boryl radical first undergoes a radical addition to the alkene, which is

followed by fluoride elimination to give the *gem*-difluoroallylborane product (Scheme 1-9c). However, it should be pointed out that the redox potential of the Ir<sup>II</sup> complex [ $E_{1/2}(\text{Ir}^{\text{III}}/\text{Ir}^{\text{II}} = -1.37 \text{ V})$ ] is not sufficient to reduce the fluoroarene ( $E_{1/2}^{\text{red}} = -2.38 \text{ V}$ ) and, therefore, there is a problem with the SET mechanism proposed in the work.

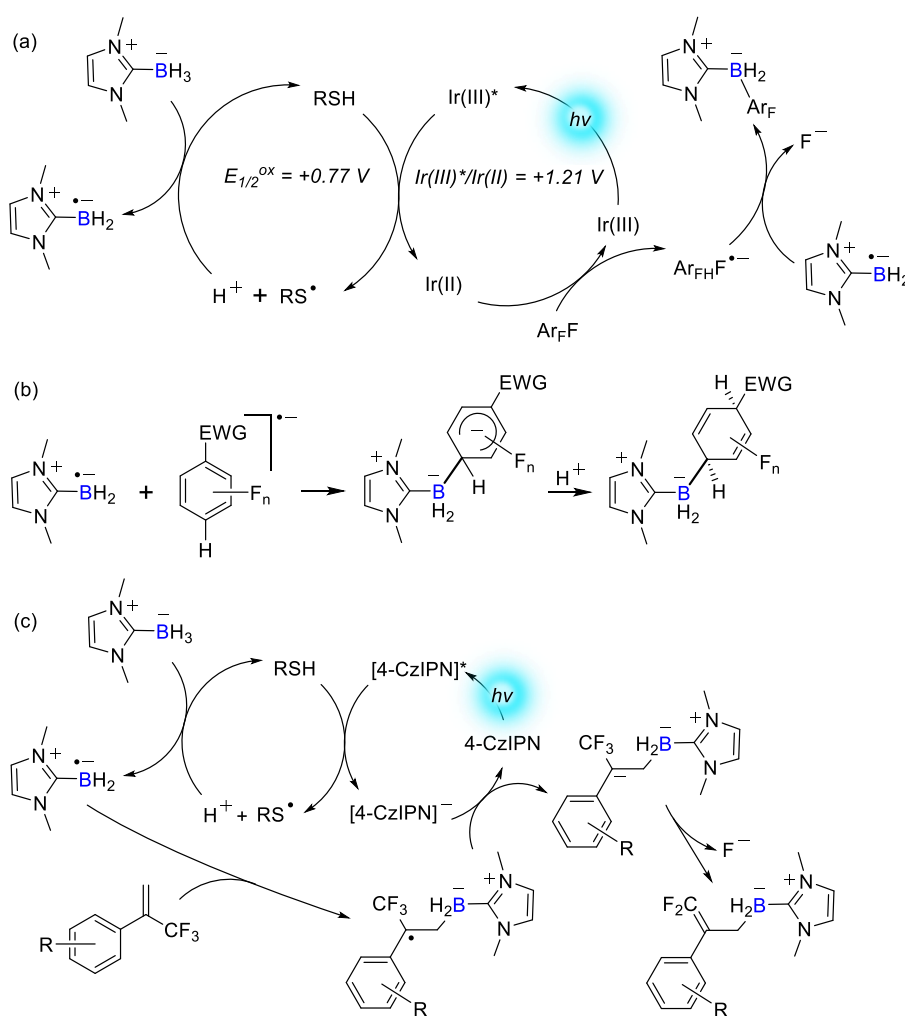
### Scheme 1-8. Photocatalytic defluoroborylation of aryl and alkenyl fluorides



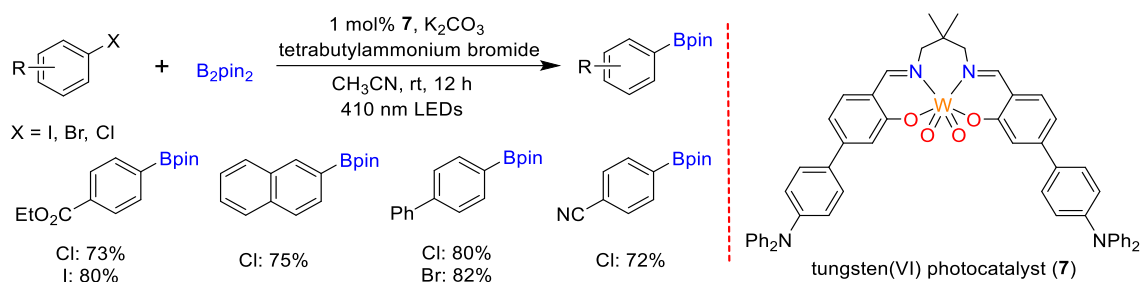
Che et al. developed an air-stable and visible light-responsive tungsten(VI) photocatalyst (7) that can be prepared on a gram scale. The tungsten(VI) complex exhibited good activity for the borylation of aryl halides, including aryl chlorides, with high product yields and broad functional group tolerance (Scheme 1-10).<sup>79</sup> Liang et al. employed Pd(PPh<sub>3</sub>)<sub>4</sub> complex as a visible light photocatalyst to achieve the borylation of aryl and alkyl bromides

via a SET process (Scheme 1-11).<sup>80</sup> The excited Pd(0) catalyst undergoes SET with aryl/alkyl halides to give a Pd(I) complex and an aryl/alkyl radical, which adds to B<sub>2</sub>Pin<sub>2</sub> to form an sp<sup>2</sup>-sp<sup>3</sup> diboron adduct **8**. Upon reaction with K<sub>3</sub>PO<sub>4</sub>, complex **8** is converted into the sp<sup>3</sup>-sp<sup>3</sup> diboron adduct **9**, which yields the final borylated product and intermediate **10** via an energy favorable homolysis process. Finally, the Pd(I) complex formed is reduced by **10** via another SET to regenerate the Pd(0) catalyst. The protocol was also successfully extended to the silylation of aryl bromides.

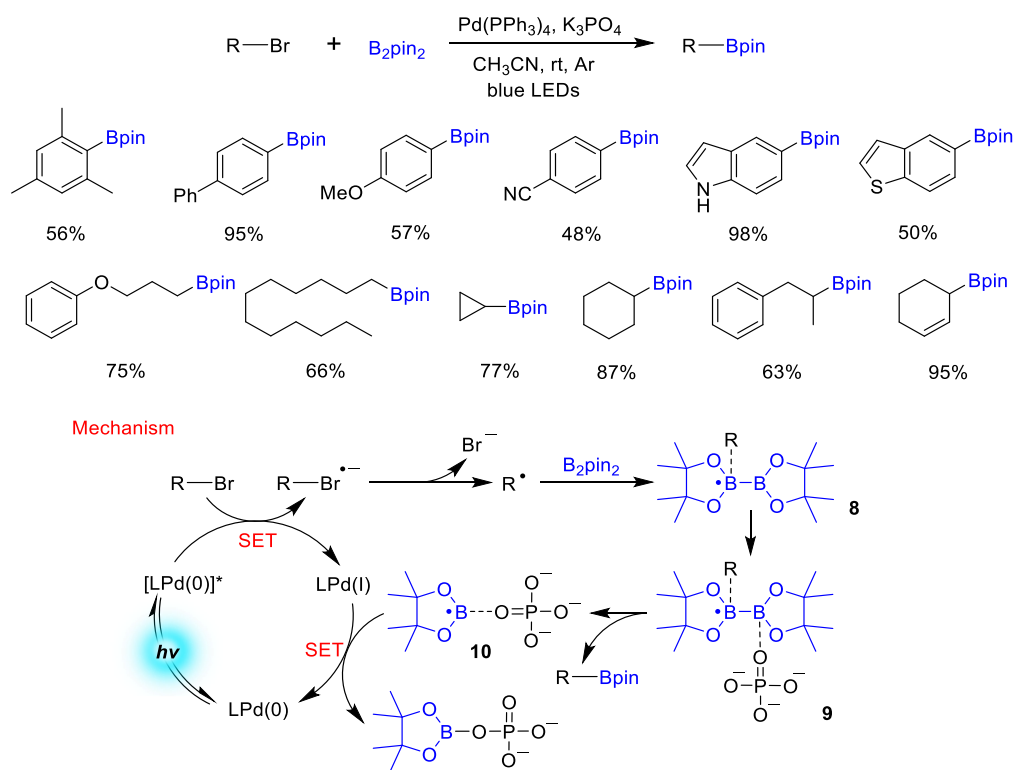
**Scheme 1-9. Proposed mechanism of the photocatalytic defluoroborylation process in Scheme 1-8**



### Scheme 1-10. Photoinduced borylation of aryl halides with a tungsten(VI) photocatalyst



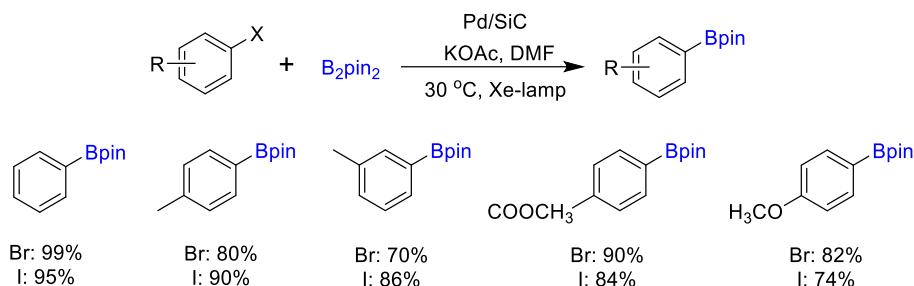
### Scheme 1-11. Pd(PPh<sub>3</sub>)<sub>4</sub>-photocatalyzed borylation of aryl and alkyl bromides and its reaction mechanism



Heterogeneous processes have also attracted attention due to their ease of recycling. Guo et al. developed a hierarchical silicon carbide (SiC) nanowire-supported Pd nanoparticle system for the photocatalytic borylation of aryl halides at 30 °C (Scheme 1-12).<sup>81</sup> Under irradiation by a Xe lamp, the photogenerated electrons transfer from SiC to Pd through the Schottky contact between them, leading to a negatively charged Pd, which can facilitate the cleavage of C-X bonds. The Pd/SiC photocatalyst is applicable to catalyzing the conversion of various aryl bromides and iodides to the corresponding

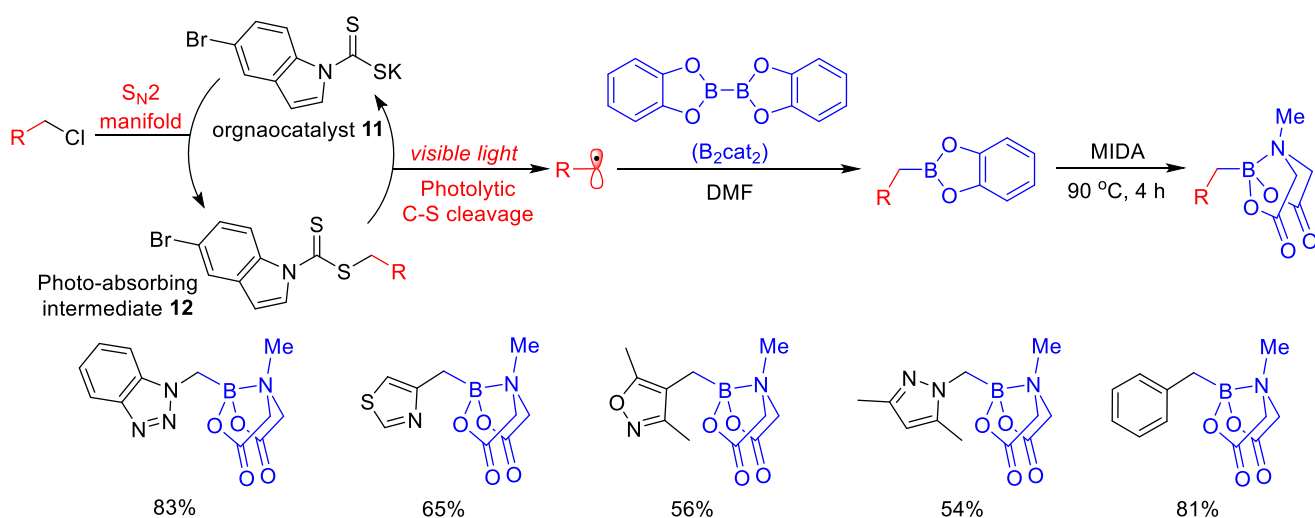
borylated products with excellent yields under visible light irradiation.

### Scheme 1-12. Heterogeneous Pd/SiC photocatalyzed borylation of aryl halides



### 1.3.2 Metal-free organocatalyst

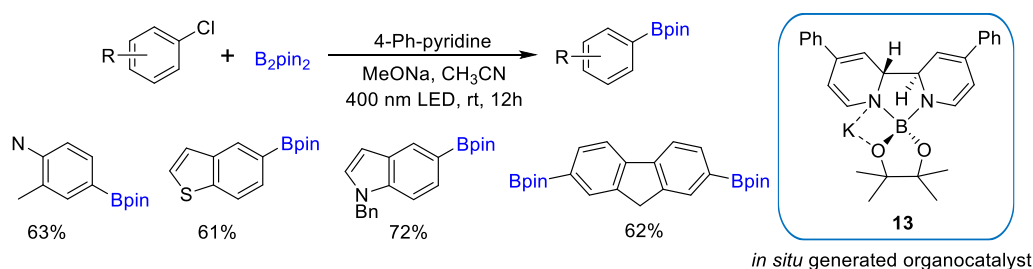
#### Scheme 1-13. Photoinduced borylation of alkyl halides via an $\text{S}_{\text{N}}2$ pathway



As an alternative to transition-metal photocatalysis, organic photoredox catalysis can afford high reactivity, allowing access to selective transformations of a large variety of substrates that are unreactive in most synthetic contexts.<sup>59</sup> Most photoinduced organocatalysis involve a radical pathway. Melchiorre, et al. reported an  $\text{S}_{\text{N}}2$ -based photochemical protocol for the borylation of alkyl halides using a nucleophilic dithiocarbamate anion as the organocatalyst and bis(catecholato)diboron ( $\text{B}_2\text{cat}_2$ ) as the boron source.<sup>82</sup> As the method does not depend on the redox properties of the substrates and catalysts, it is very suitable for substrates that are difficult to reduce, such as benzylic

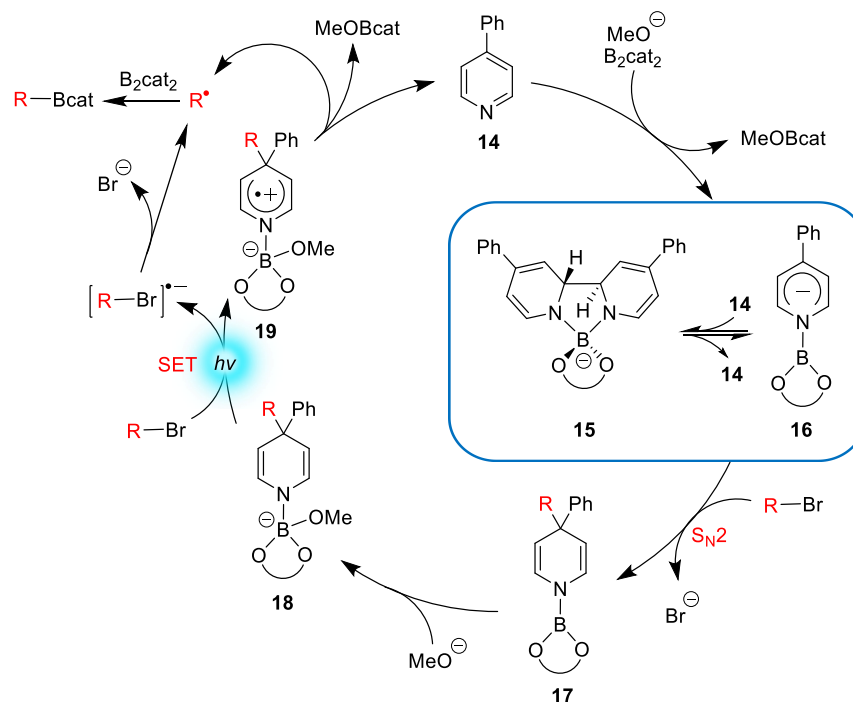
and allylic chlorides, bromides, and mesylates, and substrates that are not compatible with strong redox-active reagents or metal-based protocols. The chloride-leaving group in alkyl chlorides is substituted by the nucleophilic dithiocarbamate anion organocatalyst (**11**) to generate a photon-absorbing intermediate (**12**) via an S<sub>N</sub>2 pathway (Scheme 1-13).<sup>82,83</sup> Upon excitation by visible light, photolytic cleavage of the weak C-S bond of intermediate **12** produces a C(sp<sup>3</sup>)-centered radical, which is captured by B<sub>2</sub>cat<sub>2</sub> in DMF solvent to form the alkylboronic ester. Then, the borylated product is further treated with methyliminodiacetic acid (MIDA) at 90 °C for 4 h to generate the more-stable MIDA boronate (Scheme 1-13).

**Scheme 1-14. Photoinduced radical borylation of aryl chlorides with an organocatalyst generated *in situ* from B<sub>2</sub>pin<sub>2</sub>/methoxide/4-Ph-pyridine**



Jiao et al. developed a B<sub>2</sub>pin<sub>2</sub>/methoxide/4-Ph-pyridine reaction system for the radical borylation of aryl iodides and bromides, and observed an intermediate, **13**,<sup>72,84</sup> which exhibits a broad absorption in the range of 300–500 nm and fluorescent emission ( $\lambda_{\text{max}} = 547 \text{ nm}$ ) with lifetime of 6.1 ns. The reduction potential of excited complex **13** is calculated to be  $-3.87 \text{ V}$ , showing it to be a strong reducing agent. Therefore, Jiao's group employed the same system to generate intermediate **13** *in situ* as an organic photocatalyst to achieve the borylation of aryl chlorides (Scheme 1-14).<sup>85</sup> After complex **13** is excited to the S<sub>1</sub> state, it undergoes SET with chloroarenes to produce chloroarene radical anions, which further form aryl radicals via the dissociation of Cl<sup>-</sup>. Then, the reaction of aryl radicals with B<sub>2</sub>pin<sub>2</sub> gives the corresponding arylboronic esters. The protocol is applicable to a broad range of chloroarenes.

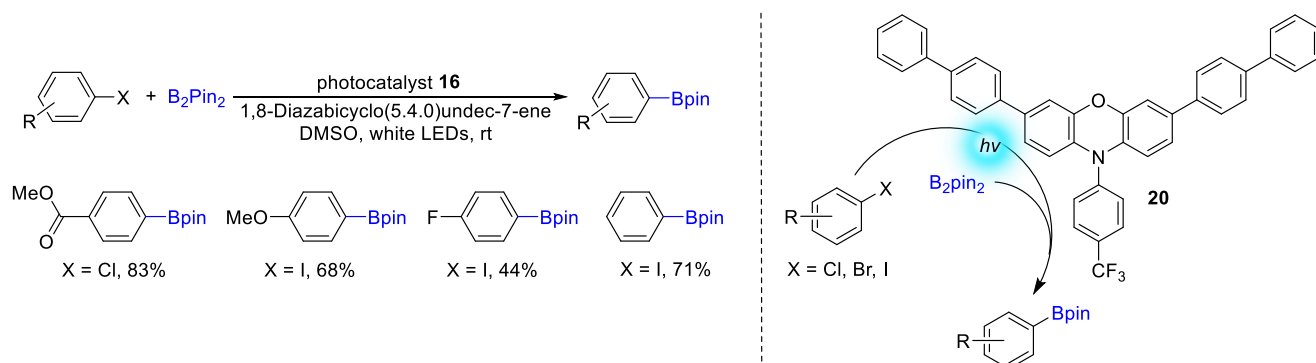
## Scheme 1-15. Photoinduced radical borylation of alkyl bromides with 4-Ph-pyridine



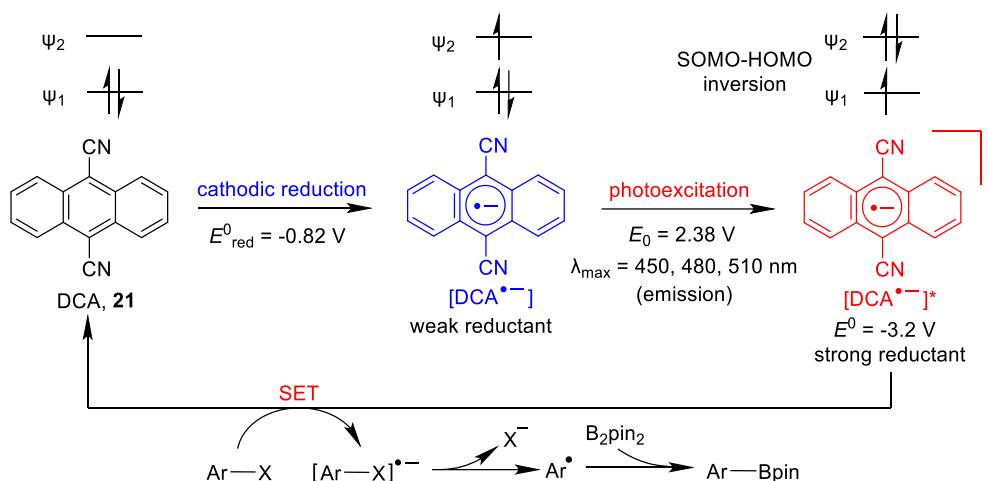
Jiao's group also employed a B<sub>2</sub>cat<sub>2</sub>/methoxide/4-Ph-pyridine system to achieve the radical borylation of alkyl bromides (Scheme 1-15).<sup>86</sup> Similarly, a mixture of nucleophilic intermediates **15** and **16** is formed first, which react with alkyl bromides to generate 4-alkyl-1,4-dihydropyridine (**17**). Upon reaction of **17** with methoxide, the electron-rich complex **18** undergoes photoinduced SET to the alkyl bromide to produce an alkyl radical and radical intermediate **19**. The facile homolytic cleavage of a C-C bond in complex **19** generates another alkyl radical with re-aromatization of the pyridine moiety, regenerating the 4-Ph-pyridine (**14**) catalyst. The alkyl radicals formed react with B<sub>2</sub>cat<sub>2</sub> to produce the alkylboronate product. A series of primary, secondary and tertiary alkyl bromides with different functional groups were successfully borylated using this method.

The use of 3,7-di-([1,1'-biphenyl]-4-yl)-10-(4-(trifluoromethyl)phenyl)-10*H*-phenoxazine (**20**) as a photosensitizer was developed by Son, Cho, et al. (Scheme 1-16). Its excited state has a highly negative photoexcited reduction potential (-2.56 V), allowing it to reduce aryl halides. Using **20** as a photocatalyst, borylation proceeded smoothly with various aryl chlorides, bromides and iodides bearing electron-withdrawing and electron-donating substituents.<sup>87</sup>

## Scheme 1-16. Organic photosensitizer 16-catalyzed borylation of aryl halides



## Scheme 1-17. Reductive electrophotocatalysis for the borylation of aryl halides



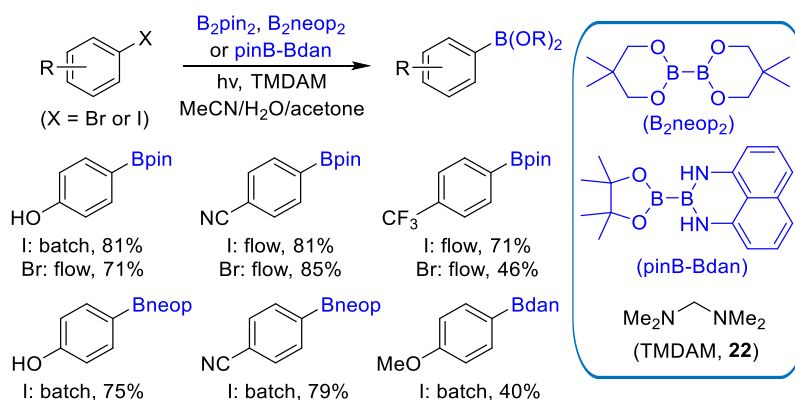
Lambert, Lin, et al. reported a new electrophotocatalytic protocol merging the power of electrical with photochemical energy to achieve extremely high reduction potentials (Scheme 1-17).<sup>88</sup> When dicyanoanthracene (DCA, **21**) is used as an organocatalyst, a radical anion  $\text{DCA}^{\bullet-}$  is produced after cathodic reduction of DCA ( $E_{1/2} = -0.82$  V). The  $\text{DCA}^{\bullet-}$  exhibits a broad absorption with maxima at 375, 395 and 420 nm and displays an intense fluorescence emission with maxima at 450, 480, and 510 nm (excitation energy,  $E_0 = 2.38$  eV) with a lifetime of 13.5 ns. Therefore, the reduction potential of excited  $\text{DCA}^{\bullet-}$  is calculated to be  $-3.2$  V. TD-DFT calculations show that upon photoexcitation, an inversion of the SOMO-HOMO results in a very unstable electronic structure with the lower energy orbital  $\psi_1$  becoming the SOMO and the higher energy orbital  $\psi_2$  becoming filled. Via SET, aryl halides are reduced to aryl halide anion radicals, and the excited  $\text{DCA}^{\bullet-}$  reforms to the DCA. Upon dissociation of halide anion, the aryl radicals formed react with  $\text{B}_2\text{pin}_2$  to give



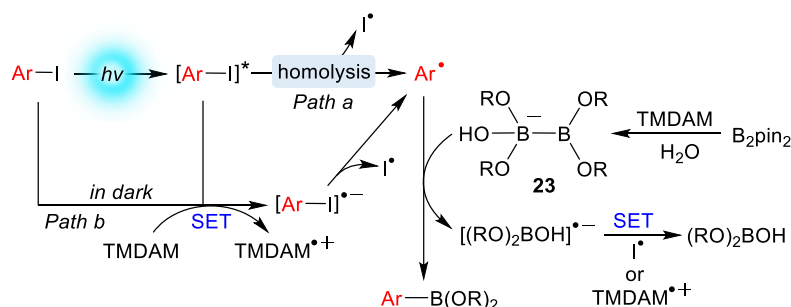
the arylboronic esters. Various aryl bromides and chlorides with very high reduction potentials ( $E_{\text{red}} \approx -1.9$  to  $-2.9$  V) are smoothly activated and borylated through this electrophotocatalytic protocol.

### 1.3.3 Photochemical borylation

#### Scheme 1-18. Substrate scope of the batch/continuous-flow photolytic borylation of aryl halides



#### Scheme 1-19. Mechanism for the photolytic borylation of aryl halides

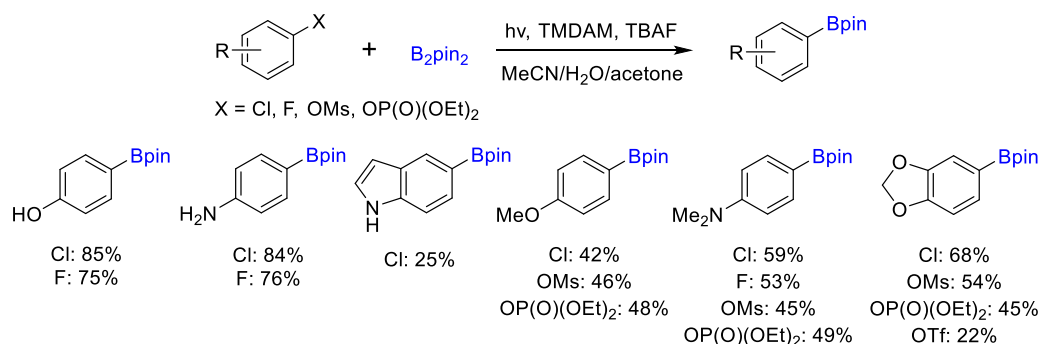


The photochemical activation of molecules can provide possible pathways which are difficult to achieve from their ground states.<sup>89-91</sup> The homolytic and heterolytic processes being accessed from singlet and triplet excited states afford many synthetic possibilities. In 2016, Li et al. showed that aryl halides can be photochemically borylated with high efficiency and chemo-selectivity in the absence of metals under batch and continuous-flow conditions (Schemes 1-18 and 1-19).<sup>74</sup> Aryl iodides and bromides bearing a variety of functional groups were efficiently converted to the corresponding arylboronic esters in good to excellent yields using *N,N,N',N'*-tetramethyldiaminomethane (TMDAM, **22**) as the

photocatalyst (Scheme 1-18). Bis-boronic acid  $[B_2(OH)_4]$  also can be employed as the boron source. After borylation, aqueous  $KHF_2$  was added to form the more stable potassium aryltrifluoroborate salts.

Mechanistically, the photoinduced homolytic cleavage of the C(aryl)-I bond is considered as initiating the borylation (Scheme 1-19). The reaction of **22** with  $B_2pin_2$  in the presence of water generates a  $sp^2$ - $sp^3$  diboron adduct (**23**),<sup>92,93</sup> which further reacts with the above formed aryl radical to produce the final borylation product and a boron-containing radical anion. Without irradiation, a low yield of the target product was achieved with **22**, suggesting the important role of **22** in the dark reaction. This is consistent with the comments on an uncatalyzed background borylation of aryl iodides with  $B_2pin_2$  and  $KO^tBu$  in the absence of Cu catalyst by Lin, Marder et al. in their Cu catalyzed aryl halides borylation work.<sup>94</sup> The ground-state and excited-state aryl iodides undergo a SET pathway with **22** to give a TMDAM<sup>++</sup> radical cation and an  $[Ar-I]^-$  radical anion, which further produces another  $Ar^*$  radical. Finally, the boron-containing radical anion is quenched by SET with an iodine radical or TMDAM<sup>++</sup> radical cation.

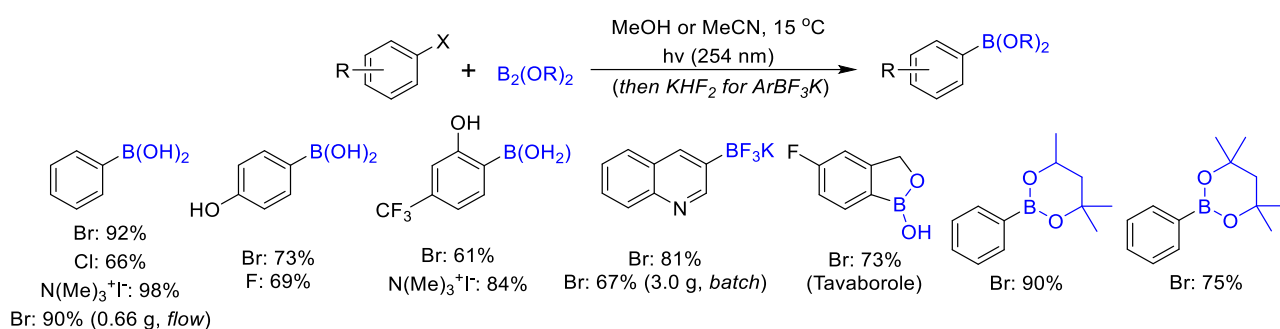
### Scheme 1-20. Photoinduced borylation of electron-rich aryl chlorides, fluorides, mesylates and phosphates



Then, Li et al. expanded the substrate scope of the photochemical borylation protocol to electron-rich aryl chlorides, fluorides, mesylates and phosphates (Scheme 1-20).<sup>95</sup> Aryl chlorides with strong electron-donating substituents in the *ortho*- or *para*-position were smoothly converted to the corresponding boronates in moderate to good yields. However, electron-neutral and electron-deficient aryl chlorides were inert using this protocol.

Mechanistic studies showed that a triplet aryl cation ( $^3\text{Ar}^+$ ), whose energy is  $1.4 \text{ kcal mol}^{-1}$  lower than that of the singlet species, is formed by the photoinduced heterolytic cleavage of a C(aryl)-X bond in the beginning of the reaction. Then, a three-component interaction among the  $^3\text{Ar}^+$ ,  $\text{Cl}^-$  and  $\text{B}_2\text{pin}_2$  occurs until a minimum energy crossing point (MECP) between the triplet and singlet potential energy surfaces is achieved and, subsequently, the reaction crosses to the singlet surface to form the final product.

**Scheme 1-21. Metal- and additive-free photoinduced borylation of aryl halides and arylammonium salts**

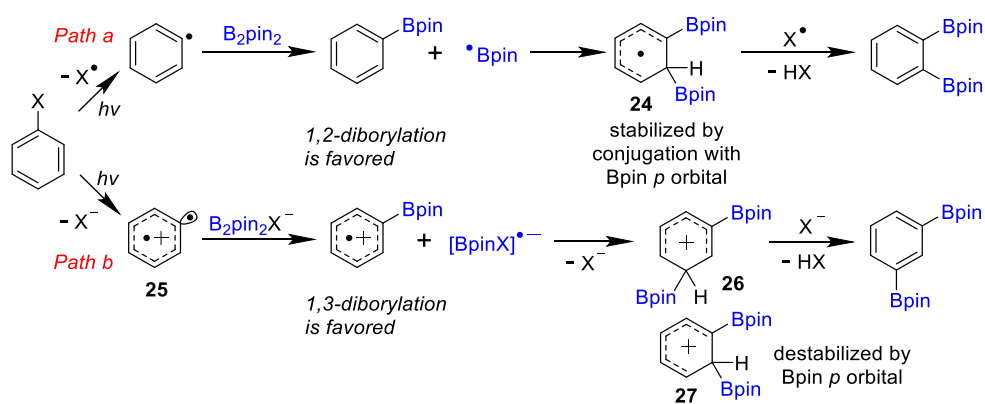


Larionov and coworkers also reported a metal- and additive-free photoinduced borylation of aryl halides and quaternary arylammonium salts in the same year.<sup>73</sup> The reactions are operationally simple, allowing borylation of a variety of aryl iodides, bromides, chlorides and fluorides, as well as arylammonium salts with different diboron esters in good to excellent yields in methanol with UV irradiation ( $\lambda = 254 \text{ nm}$ ) under batch and continuous-flow conditions (Scheme 1-21). No product was detected in the dark reaction and the photoinduced reaction showed a good quantum yield ( $\Phi = 0.34$ ). The group subsequently reported a detailed experimental procedure to describe the borylation protocol in detail.<sup>96</sup>

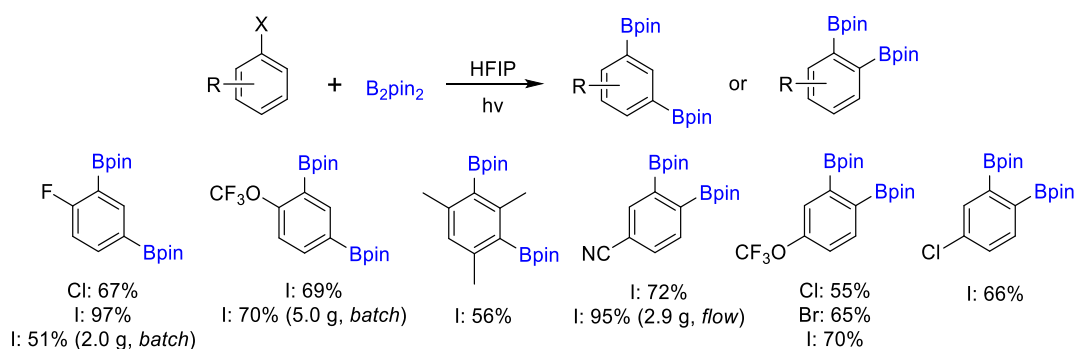
Aromatic polyboronic acids are highly valuable organoboron materials. Notably, Marder et al. developed a Zn-catalyzed 1,2-selective dual C-H/C-X borylation of aryl iodides and bromides in 2015.<sup>97</sup> Then, Larionov et al. reported an additive- and metal-free photoinduced regioselective 1,2- and 1,3-C-H/C-X diborylation of aryl halides under batch and continuous flow conditions.<sup>75</sup> The most typical feature of this strategy is that the

regioselectivity of the dual borylation depends on the solvent and the substituents on the parent haloarenes. A solvent cage-assisted radical pathway was proposed to explain the mechanism. Low and medium polarity solvents, such as isopropanol, favor the 1,2-diborylation (Scheme 1-22, path a). Photoinduced homolysis of aryl bromides and iodides tends to occur in isopropanol to produce  $\text{Ar}^\bullet$  and  $\text{X}^\bullet$  radicals. The reaction of  $\text{B}_2\text{pin}_2$  with  $\text{Ar}^\bullet$  gives the monoborylation product  $\text{Ar-Bpin}$  and a  $\text{Bpin}^\bullet$  radical and, subsequently, the two under the confinement of the solvent cage, form radical intermediate **24**, which can be stabilized by conjugation by the empty  $p_z$  orbital of Bpin. Then, the combination of radical **24** with  $\text{X}^\bullet$  generate the final product. In contrast, highly polar solvents, such as hexafluoroisopropanol (HFIP), favor 1,3-diborylation (Scheme 1-22, path b). In this case, the photoinduced heterolysis of the aryl halide forms a triplet aryl cation **25**, which further reacts with the  $\text{sp}^2\text{-sp}^3$  diboron adduct  $[\text{B}_2\text{pin}_2\text{X}]^-$  to form an  $[\text{Ar-Bpin}]^{+\bullet}$  radical cation and a  $[\text{BpinX}]^{\bullet-}$  radical anion. The confinement of the two in the HFIP cage favors a 1,3-addition intermediate **26**, which give the 1,3-diborylation product after reacting with  $\text{X}^-$ ; while 1,2- and 1,4-addition would produce cationic intermediates **27** that are destabilized by the  $\pi$ -acceptor boryl group. However, if there is a strong electron-withdrawing or electron-donating group at the *para*- or *meta*-positions of the aryl halide, the weak  $\pi$ -acceptor boryl group-induced 1,3-diborylation will revert to 1,2-diborylation.

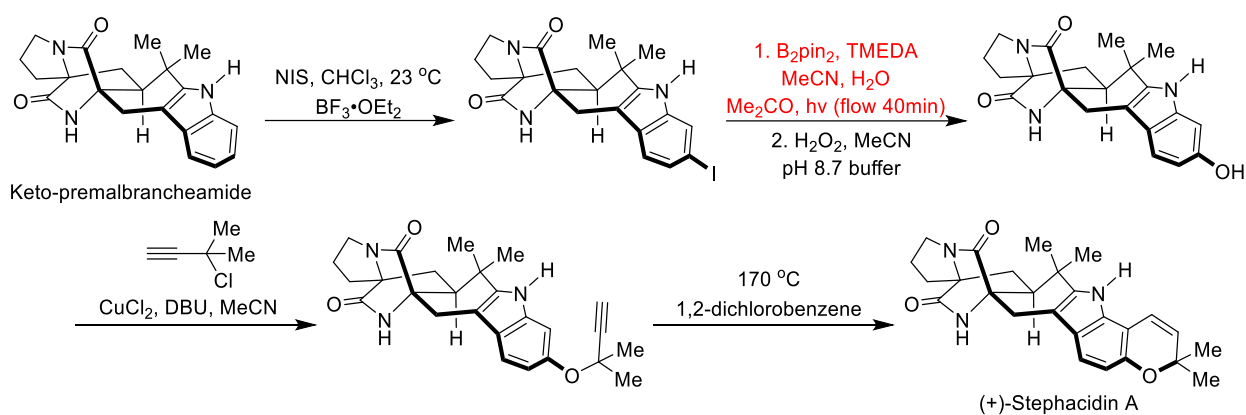
### Scheme 1-22. Plausible reaction pathways for the photoinduced dual C-H/C-X borylation



## Scheme 1-23. Photoinduced dual C-H/C-X borylation of aryl halides in HFIP

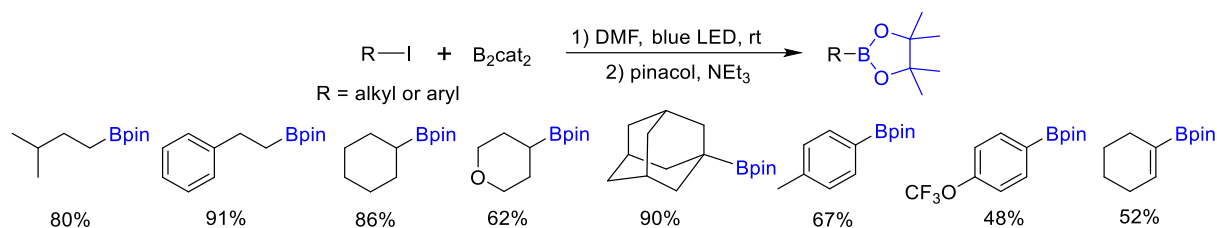


## Scheme 1-24. Synthesis of (+)-stephacidin A congeners from keto-premalbrancheamide

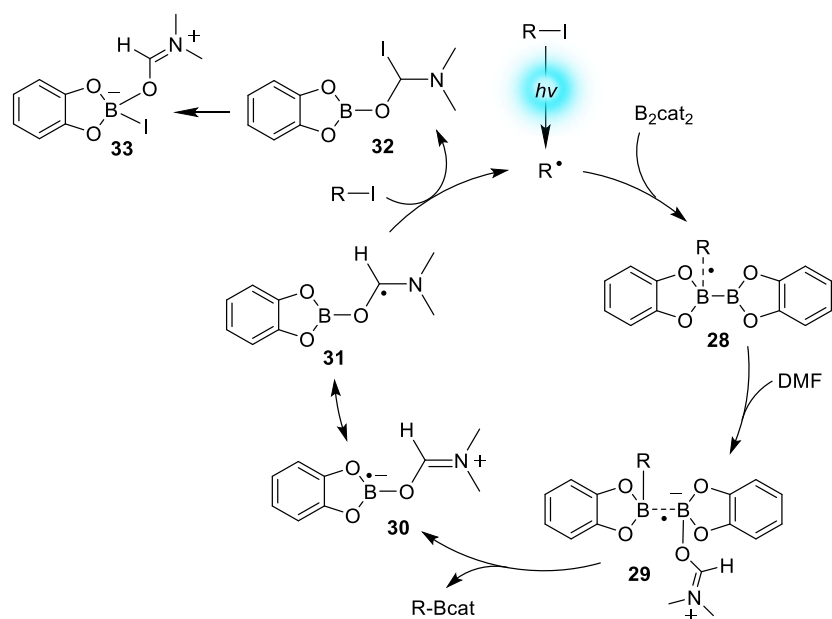


Both 2- and 4-alkyl-substituted aryl halides were converted to 1,3- diborylated products as single isomers in excellent yields (Scheme 1-23). F-, Cl- and CF<sub>3</sub>O-groups were tolerated and showed good directing ability. Sterically hindered iodomesitylene was successfully diborylated in modest yield. Haloarenes with 3-F-, 3-Cl-, 3-CF<sub>3</sub>O-, and 4-CN-groups gave the corresponding 1,2-diborylated products in good yields in HFIP. In 2018, Sarpong et al. employed the photoinduced borylation method proposed by Li et al. and Larionov et al. to achieve the total synthesis of monomeric and dimeric stephacidin A congeners from keto-premalbrancheamide (Scheme 1-24).<sup>98</sup>

### Scheme 1-25. Photoinduced metal-free radical borylation of alkyl and aryl iodides



### Scheme 1-26. Mechanism for photoinduced borylation of alkyl and aryl iodides



The methods developed by Li et al. and Larionov et al. are efficient; however, the necessary high-intensity UV irradiation poses potential limitations on their applicability. Studer and coworkers also reported a metal-free radical borylation of alkyl and aryl iodides with  $\text{B}_2\text{cat}_2$  under irradiation using blue LEDs at ambient temperature (Scheme 1-25).<sup>99</sup> Primary alkyl iodides bearing different functional groups, such as alkynyl, nitrile, ester, ketone, and aldehyde, etc. were smoothly converted to the corresponding products in good yields. Secondary alkyl iodides containing cyclohexyl, tetrahydropyranyl, Boc-protected piperidine (Boc = *tert*-butoxycarbonyl), aryl and phenyl alkyl ether groups, and 1-iodoadamantane can also be borylated. Aryl iodides were compatible substrates for this method, but the yields were lower compared with those from alkyl iodides.

The alkyl/aryl radical formed by photoinduced homolysis of alkyl/aryl iodide undergoes

addition to  $B_2cat_2$  to generate radical **28** (Scheme 1-26), which is trapped by DMF to form intermediate **29**, which further homolyzes to give the borylated product and the DMF-complexed boryl radicals **30/31**. Then, I-atom transfer from the alkyl/aryl iodide via **32** propagates the radical chain giving **33** and another alkyl/aryl radical.

## 1.4 Conclusions and motivation

Organoboron compounds have become increasingly important and key synthons in the fields of synthetic chemistry, materials science, and pharmacy et al. Photoinduced borylation, as a new and efficient method of constructing C-B bond, has developed rapidly from the stoichiometric reaction of metal boryl complexes with substrate to the catalytic reaction using transition-metal or organic photocatalyst in the past two decades. The protocol usually operates under mild and environment friendly conditions and shows a high tolerance to functional groups. Aryl/alkyl halides are suitable substrates with high reactivity and selectivity. Most reactions proceed via radical pathways initiated by photochemical activation or SET from an excited photocatalyst.





## **Chapter Two**

# **Selective photocatalytic C-F borylation of polyfluoroarenes by Rh/Ni dual catalysis**



## 2 Selective photocatalytic C-F borylation of polyfluoroarenes by Rh/Ni dual catalysis

### 2.1 Abstract

A highly selective and general photocatalytic C-F borylation protocol that employs a rhodium biphenyl complex as a triplet sensitizer and the nickel catalyst  $[\text{Ni}(\text{IMes})_2]$  (IMes = 1,3-dimesitylimidazolin-2-ylidene) for the C-F bond activation and defluoroborylation process was developed. This tandem catalyst system operates with visible (400 nm) light and achieves borylation of a wide range of fluoroarenes with  $\text{B}_2\text{pin}_2$  at room temperature in excellent yields and with high selectivity. Direct irradiation of the intermediary C-F bond oxidative addition product *trans*- $[\text{NiF}(\text{Ar}^{\text{F}})(\text{IMes})_2]$  leads to fast decomposition when  $\text{B}_2\text{pin}_2$  is present. This destructive pathway can be bypassed by indirect excitation of the triplet states of the nickel(II) complex via the photoexcited rhodium biphenyl complex. Mechanistic studies suggest that the exceptionally long-lived triplet excited state of the Rh biphenyl complex used as the photosensitizer allows for efficient triplet energy transfer to *trans*- $[\text{NiF}(\text{Ar}^{\text{F}})(\text{IMes})_2]$ , which leads to dissociation of one of the NHC ligands. This contrasts with the majority of current photocatalytic transformations, which employ transition metals as excited state single electron transfer agents. We have previously reported that C(arene)-F bond activation with  $[\text{Ni}(\text{IMes})_2]$  is facile at room temperature, but that the transmetalation step with  $\text{B}_2\text{pin}_2$  is associated with a high energy barrier. Thus, this triplet energy transfer ultimately leads to a greatly enhanced rate constant for the transmetalation step and thus for the whole borylation process. While addition of a fluoride source such as CsF enhances the yield, it is not absolutely required. We attribute this yield-enhancing effect to (i) formation of an anionic adduct of  $\text{B}_2\text{pin}_2$ , i.e.  $\text{FB}_2\text{pin}_2^-$ , as an efficient, much more nucleophilic {Bpin} transfer reagent for the borylation/transmetalation process, and/or (ii) trapping of the Lewis acidic side product FBpin by formation of  $[\text{F}_2\text{Bpin}]^-$  to avoid the formation of a significant amount of NHC-FBpin and consequently of decomposition of  $\{\text{Ni}(\text{NHC})_2\}$  species in the reaction mixture.

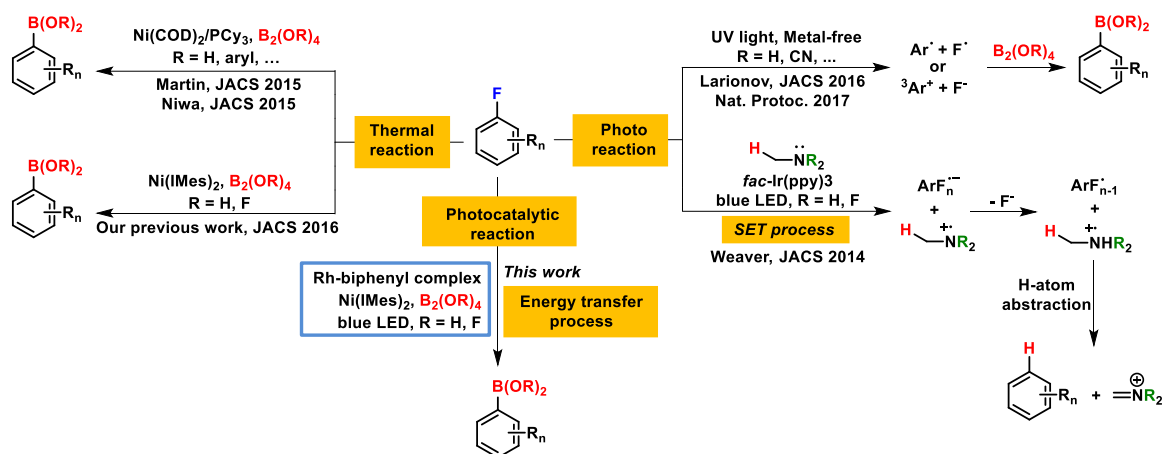
## 2.2 Introduction

The development of methods to introduce fluorinated aromatic building blocks selectively into organic molecules is of great importance, as fluorinated organic compounds have exceptional properties that are being exploited in many applications including materials, pharmaceuticals, and agrochemicals.<sup>100-112</sup> A promising strategy to achieve this goal would be to transform commercially available fluoroaromatics into fluoroarylboronic acid esters by transition-metal-catalyzed selective C-F borylation, which could then be further used in Suzuki-Miyaura and other cross-coupling reactions and numerous functional group transformations.<sup>4,38,94,97,113-116</sup> The challenge of this method is the selective cleavage of a very stable C-F bond,<sup>117,118</sup> while simultaneously forming an easily transformable C-B bond.

Early work of the groups of Smith, Zhang, Braun, Perutz and Marder have demonstrated that borylation of C-F bonds can be achieved by using different Rh complexes as catalysts.<sup>119-123</sup> Subsequently, *in situ*-generated Ni phosphine complexes were employed by the Martin, Niwa and Hosoya groups to avoid noble metal catalysts for C-F borylation of monofluoroarenes (Scheme 2-1).<sup>124,125</sup> However, the catalytic activity of Ni complexes has only been reported for monofluoroarenes, which removes the only C-F bond present, and is very sensitive to changes of the reaction conditions. We recently reported an efficient thermal catalytic procedure for the selective C-F borylation of polyfluoroaromatic compounds using the *N*-heterocyclic carbene (NHC) nickel(0) complex [Ni(IMes)<sub>2</sub>] (IMes = 1,3-dimesitylimidazolin-2-ylidene) as a catalyst and bis(pinacolato)diboron (B<sub>2</sub>pin<sub>2</sub>) as the boron source (Scheme 2-1).<sup>126</sup> One particularly interesting finding of our study was that activation of the very strong C-F bond by the Ni(0) complex to give the oxidative addition product *trans*-[NiF(Ar<sup>F</sup>)(IMes)<sub>2</sub>] (Ar<sup>F</sup> = fluoroarene) is very fast at room temperature,<sup>127-133</sup> but the transmetalation step with B<sub>2</sub>pin<sub>2</sub> is rate determining, requiring elevated temperatures for efficient catalysis. Often, C-F oxidative addition is the rate determining step in catalytic cross-coupling reactions of polyfluoroarenes, while transmetalation is generally facile.<sup>130,134,135</sup> Although conversion of several polyfluorinated arenes into their corresponding boronate esters was successful, the efficiency for difluoroarenes is still

unsatisfactory even at 100 °C.

### Scheme 2-1. Examples of C-F bond activation of fluoroarenes in thermal- and photo-reactions



An alternative to thermally induced C-F bond activation and subsequent borylation of fluoroarenes by transition metals, that may enhance the efficiency of this process, could be visible light photocatalysis, which has recently emerged as a powerful tool in organic synthesis.<sup>136,137</sup> However, for photolytically-induced borylation reactions in general, only very recently has significant progress been achieved. For example, Li et al.<sup>74,95</sup> and Larionov et al.<sup>73,75,96</sup> showed that aryl halides, mesitylates, and ammonium salts can be photochemically borylated (Scheme 2-1), affording the corresponding aromatic boronic acids and esters in moderate to good yields. It is worth mentioning that our group has developed a Zn-catalyzed 1,2-selective dual C-H/C-X borylation of aryl halides in 2016,<sup>97</sup> and subsequently an additive- and metal-free photoinduced 1,2- or 1,3-selective dual C-H/C-X borylation of haloarenes was described by Larionov et al.<sup>75,96</sup> The necessary high intensity UV irradiation, which poses potential limitations to the applicability of this method, leads directly to homolytic cleavage of the C(arene)-X bond, creating an aryl radical which can then further react with, e.g., B<sub>2</sub>pin<sub>2</sub>. Heterolytic cleavage also appears to play a role in the above mentioned dual C-H/C-X borylation reaction.<sup>75,96</sup> Aryl radical formation by homolytic C-X cleavage can also be achieved by single electron transfer (SET) from a potent donor to the arene, as has been shown for the UV light-initiated borylation of aryl

triflates with  $B_2pin_2$  in the presence of NaI.<sup>76</sup> Employing photoredox catalysts, such as Eosin Y or *fac*-[Ir(ppy)<sub>3</sub>], also allows the generation of aryl boronates from aryl diazonium salts or aryl halides in the same manner, but with visible light.<sup>65,138,139</sup> Very recently, Glorius et al. achieved a denitrogenative borylation of benzotriazoles to *o*-borylated *N*-arylbenzamides using blue light LEDs and [Ir(ppy)<sub>2</sub>(NHC-F<sub>2</sub>)] (NHC-F<sub>2</sub> = 1-(2,4-difluorophenyl)-3-methyl-2,3-dihydro-1*H*-imidazolylidene) as a photoredox catalyst, which was chosen by a mechanism-based luminescence screening method.<sup>140</sup> Li et al. prepared primary and secondary alkyl boronates by visible-light-promoted decarboxylative borylation of aliphatic esters in non-anhydrous solvents using [Ir(ppy)<sub>2</sub>(dtbpy)]PF<sub>6</sub> as an SET catalyst.<sup>141</sup>

Surprisingly, decarboxylative borylation of aryl and alkyl *N*-hydroxyphthalimide esters with visible light is also possible in a metal-free fashion. For the former, Glorius et al. suggest that the SET process leading to CO<sub>2</sub> release and aryl radical formation occurs from a pyridine- $B_2pin_2$  adduct to the photoexcited ester in its triplet state.<sup>142</sup> In the case of the alkyl esters, Aggarwal and co-workers claim that the radical process is initiated by irradiation of an adduct which is formed by simultaneous binding of the solvent *N,N*-dimethylacetamide and the ester via its phthalimide moiety to the diboron reagent  $B_2cat_2$ .<sup>143</sup>

Apart from these photo-initiated borylations based on the formation of aryl or alkyl radicals, transition metal-mediated C-H borylation of arenes has also been achieved by photolytic ligand dissociation as the crucial step, producing an unsaturated and highly reactive metal complex fragment. For example, the bimetallic catalyst [(IPr)Cu-Fe( $\eta^5$ -C<sub>5</sub>H<sub>5</sub>)(CO)<sub>2</sub>] has been found to undergo oxidative addition of HBCat to give [(IPr)CuH] and [Fe(BCat)( $\eta^5$ -C<sub>5</sub>H<sub>5</sub>)(CO)<sub>2</sub>].<sup>144</sup> The latter then releases CO upon UV irradiation and reacts with arenes to form the respective aryl boronates and [FeH( $\eta^5$ -C<sub>5</sub>H<sub>5</sub>)(CO)<sub>2</sub>], presumably by a  $\sigma$ -bond metathesis mechanism.<sup>144-150</sup> Beller et al. reported the catalytic dehydrogenative C-H borylation of (hetero)arenes with high TON by dissociation of CO from *trans*-[RhCl(CO)(PMe<sub>3</sub>)<sub>2</sub>] when irradiated with 320-400 nm light, which allows for facile

C(arene)-H or H-Bpin activation and subsequent coupling with the other.<sup>151</sup> Dihydrogen release from  $[\text{Fe}(\text{H})_2(\text{dmpe})_2]$  under UV irradiation gives an iron(0) bis(diphosphine) complex which can insert into the pinB-H bond, forming  $[\text{FeH}(\text{Bpin})(\text{dmpe})_2]$  and then generate aryl boronic esters by reaction with arenes.<sup>152</sup>

In order to overcome the problems of requiring harsh UV irradiation for direct C-X bond cleavage and breaking the very strong C-F bond under mild conditions, a cooperative catalysis approach combining the benefits of photocatalysis and transition metal catalysis appears attractive. For some organic transformations, this general concept has been demonstrated to be very efficient. Examples include the trifluoromethylation of aryl boronic acids and C-H arylation by Sanford et al. and Glorius et al., respectively.<sup>153-156</sup> In such cases, the organic radical, initially formed by an SET process from a  $[\text{Ru}(\text{bpy})_3]^{2+}$  photoredox catalyst to the substrate, can be trapped by a second transition metal catalyst and is then available for further complex transformations, which would not be possible with one SET step. The groups of Doyle and MacMillan, and Molander showed that merging  $[\text{Ir}(\text{ppy})_2(\text{bpy})]^+$ -based photoredox catalysts with nickel(0) diimine catalysts allows for cross-coupling of potassium benzyl- and secondary ( $\alpha$ -alkoxy)alkyltrifluoroborates with an array of aryl bromides, and cross-coupling of  $\alpha$ -carboxyl  $\text{sp}^3$ -carbons with aryl halides, respectively, at ambient temperature under visible light irradiation.<sup>57,58</sup> A photo-assisted Suzuki-Miyaura coupling reaction mediated by a bimetallic catalyst containing a Ru(II)-polypyridyl moiety undergoing, according to the authors, intramolecular SET to a Pd(0) complex fragment as the reactive center to enhance oxidative addition of arylbromides upon irradiation was reported by Mori and Yamashita et al.<sup>157</sup> Weaver et al. also showed that an SET from photoexcited *fac*- $[\text{Ir}(\text{ppy})_3]$  to polyfluoroarenes leads to fluoride extrusion and formation of a fluoroaryl radical, which can further be selectively functionalized (Scheme 2-1).<sup>158-161</sup> These few examples showcase the potential of this cooperative catalysis approach.

The current photocatalysts for borylation reactions are mostly confined to Eosin Y, or Ru and Ir complexes, which exhibit strong, broad absorptions in the visible region, and which

can form triplet excited states with lifetimes of hundreds of nanoseconds up to a few microseconds in solution upon irradiation and with vastly different redox potentials than their respective ground states.<sup>54,55</sup> However, exploring other metal complexes with even longer-lived triplet excited states is expected to provide access to more efficient photocatalysts because long excited state lifetimes increase the probability of electron or energy transfer to the substrate.<sup>162-164</sup> In the course of our studies of the formation of novel fluorescent rhodacyclopentadienes via couplings of 1,3-diyne,<sup>165-169</sup> our group also synthesized an interesting rhodium biphenyl complex (**[Rh]**),<sup>170</sup> which shows a broad absorption between 390-440 nm ( $\epsilon_{400\text{nm}} = 4400 \text{ M}^{-1} \text{ cm}^{-1}$ ) and displays intense phosphorescence in the visible region ( $\lambda_{\text{em}} = 540 \text{ nm}$ ,  $\phi = 0.14$ ) with lifetimes of over 100  $\mu\text{s}$  in toluene or 2-MeTHF solution at room temperature (Figure 2-1). The lifetimes are almost a hundred times longer than those of the traditional metal complex photocatalysts *fac*-[Ir(ppy)<sub>3</sub>] (1.9  $\mu\text{s}$ ) and [Ru(bpy)<sub>3</sub>]<sup>2+</sup> (1.1  $\mu\text{s}$ ), and even five times longer than that of Eosin Y (24  $\mu\text{s}$ ).<sup>54,55,171</sup> Moreover, the redox potentials of **[Rh]** in the triplet excited state ( $E_{1/2}^{\text{IV}^*/\text{III}} = -1.73 \text{ V}$ ,  $E_{1/2}^{\text{III}/\text{III}^*} = 0.04 \text{ V}$ ) are close to those of *fac*-[Ir(ppy)<sub>3</sub>] ( $E_{1/2}^{\text{IV}^*/\text{III}} = -1.73 \text{ V}$ ,  $E_{1/2}^{\text{III}/\text{III}^*} = 0.31 \text{ V}$ ) (Figure 2-2). All of these properties suggested that our Rh biphenyl complex might indeed be a very promising candidate as a photoredox or energy transfer catalyst for borylation reactions (Scheme 2-1).

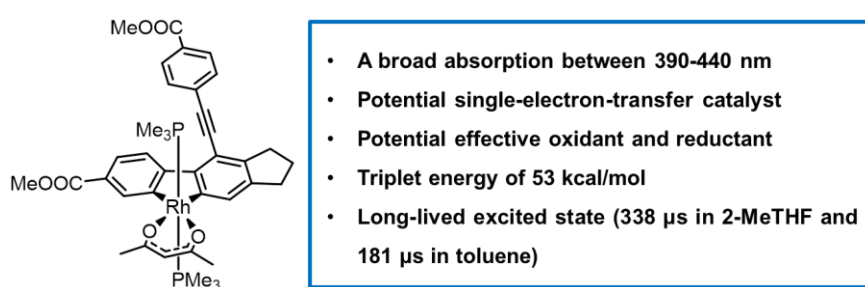


**Figure 2-1.** Key properties of a potential Rh biphenyl complex **[Rh]** photocatalyst. The compound is easily prepared in one step from reaction of [Rh( $\kappa^2$ -O,O-acac)(PMe<sub>3</sub>)<sub>2</sub>] (acac = acetylacetonato) and readily accessible MeO<sub>2</sub>C-C<sub>6</sub>H<sub>4</sub>-C $\equiv$ C-C $\equiv$ C-(CH<sub>2</sub>)<sub>3</sub>-C $\equiv$ C-C $\equiv$ C-C<sub>6</sub>H<sub>4</sub>-CO<sub>2</sub>Me.<sup>170</sup>

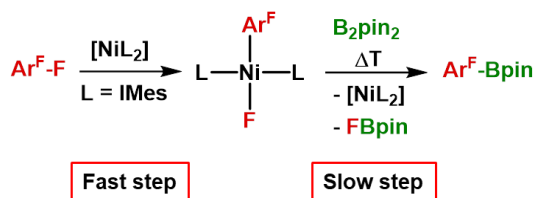


## 2.3 Results and discussions

### 2.3.1 Photocatalytic borylation of 1,2,3,5-tetrafluorobenzene

Given our long-standing interest in borylation chemistry,<sup>2,4,94,97,123,126,172-177</sup> we were interested in studying the influence of photoexcited and, in its triplet excited state  $T_1$ , exceptionally long-lived **[Rh]** on the  $[\text{Ni}(\text{IMes})_2]$ -catalyzed borylation of fluorobenzenes, which we previously reported to proceed via very fast oxidative addition of a C-F bond and rate-determining thermally driven transmetalation (Scheme 2-2).<sup>126</sup> Because aromatic C-F bond activation is very fast at  $[\text{Ni}(\text{IMes})_2]$ , the oxidative addition product *trans*- $[\text{NiF}(\text{Ar}^{\text{F}})(\text{IMes})_2]$  is the resting state of the catalytic cycle, and  $[\text{Ni}(\text{IMes})_2]$  is thus only ever present in very small amounts in the solution (vide infra). Consequently, the already facile oxidative addition step is not an issue for an efficient catalytic process, but we envisaged that photoredox or energy transfer catalysis may enhance the rate of the transmetalation step.

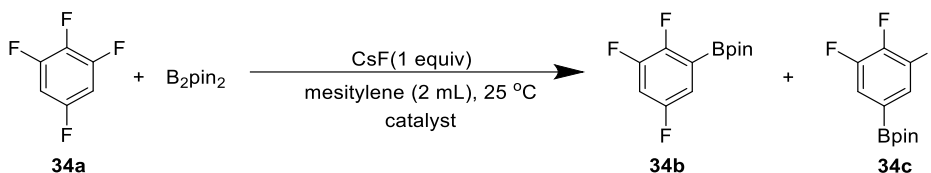
**Scheme 2-2. Thermal borylation of fluoroarenes with  $\text{B}_2\text{pin}_2$  mediated by  $[\text{Ni}(\text{IMes})_2]$  via the oxidative addition product *trans*- $[\text{NiF}(\text{Ar}^{\text{F}})(\text{IMes})_2]$** <sup>126</sup>



In order to evaluate the photocatalytic effect, we investigated the efficiency of the thermal borylation reaction of **34a** with  $\text{B}_2\text{pin}_2$  in the presence of CsF using 10 mol%  $[\text{Ni}(\text{IMes})_2]$  as the catalyst at 25 °C, which gave 6, 12 and 20% yields of **34b** after 1, 6 and 12 hours, respectively (Table 2-1, entry 1). Irradiation of the reaction mixture with a 400 nm LED for 30 minutes gave approximately stoichiometric conversion of the nickel complex, or ca. 1 turn-over, to the fluoroaryl boronate product **34b**, but with complete decomposition of the Ni species (Table 2-1, entry 2), which is in line with our observations of the decomposition of  $[\text{Ni}^{\text{II}}]$  under irradiation in the presence of  $\text{B}_2\text{pin}_2$  (Figure 2-19). The reaction carried out in the dark for 6 hours in the presence of 5 mol% **[Rh]** yielded ca. 15% of **34b** (Table 2-1,

entry 3), indicating that the rhodium biphenyl complex had no effect on the thermal borylation reaction.

**Table 2-1. Photocatalytic borylation of 34a**



Entry	[Rh] (5 mol%)	[Ni(IMes) <sub>2</sub> ] (10 mol%)	400 nm LED	t (h)	Yield (%) <sup>a</sup>	
					34b	34c
1	✗	✓	✗	1/6/12	6/12/20	trace
2 <sup>b</sup>	✗	✓	✓	0.5/6	13/13	trace
3	✓	✓	✗	6	15	trace
4	✓	✓	✓	6	95	trace
5	✗	✗	✓	6	0	0
6	✓	✗	✓	6	2	0

However, highly efficient and selective borylation of **34a** with  $B_2pin_2$  in the presence of CsF, using 5 mol% [Rh]/10 mol% [Ni(IMes)<sub>2</sub>] as a dual photocatalytic system, was observed under 400 nm light irradiation at 25 °C, giving **34b** in excellent yield (95%) after 6 hours with only traces of 5-Bpin-1,2,3-C<sub>6</sub>F<sub>3</sub>H<sub>2</sub> (**34c**) formed (Table 2-1, entry 4). It is important to note that the reaction did not occur under light irradiation without the Rh and Ni complexes, and that employing only 5 mol% [Rh] without the nickel complex gave **34b** in only 2% yield (Table 2-1, entries 5 and 6).

We screened a range of solvents of varying polarity, with mesitylene proving to be optimal (Table 2-2). The product yield decreased with shorter reaction times. Although photocatalytic borylation of **34a** can also occur without a fluoride additive in 60% yield in 6 hours, we found that CsF has a beneficial effect on the product yield (Table 2-2). We also note that the yield is significantly influenced by both [Rh] and [Ni(IMes)<sub>2</sub>] concentrations, with 5 mol% of the former and 10 mol% of the latter providing an excellent yield (Table 2-3).

The crude product from the synthesis of the Rh-biphenyl complex **[Rh]** contains a small amount of its fluorescent (ns lifetime) 2,5-bis-(arylethynyl)rhodacyclopenta-2,4-diene isomer; the NMR yield of **[Rh]** is 96%.<sup>170</sup> As column chromatographic purification leads to a significant loss of **[Rh]**, we tested a 96 : 4 mixture of the two isomeric Rh-complexes in the photocatalytic borylation of **34a**. The 82% yield of **34b** obtained is comparable with that using pure **[Rh]** as photocatalyst, so the costly purification of the **[Rh]** complex can be avoided.

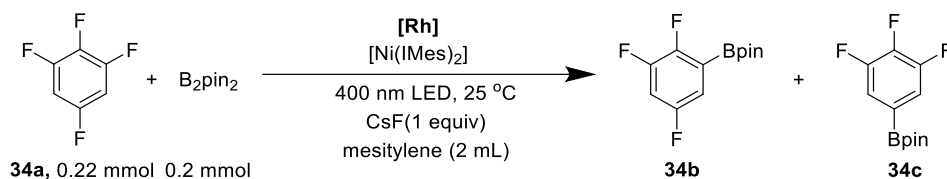
**Table 2-2. Screening of solvents and time for the photocatalytic borylation of 34a with or without added CsF**

$\text{34a, 0.22 mmol} + \text{B}_2\text{pin}_2 \text{ 0.2 mmol} \xrightarrow[\text{400 nm LED, 25 }^\circ\text{C}]{\text{[Rh] (5 mol\%), [Ni(IMes)}_2\text{] (10 mol\%), CsF (1 equiv)}} \text{34b} + \text{34c}$

Entry	Solvent (2 mL)	t (h)	Yield (%) <sup>a</sup>	
			<b>34b</b>	<b>34c</b>
1	mesitylene	6	95 (60)	trace (6)
2	hexane	6	75 (35)	10 (4)
3	THF	6	45 (10)	6 (trace)
4	MTBE	6	40 (11)	5 (trace)
5	1,4-dioxane	6	35 (8)	8 (trace)
6	MeCN	6	2 (0)	0 (0)
7	mesitylene	3	68 (-)	trace (-)
8	mesitylene	5	85 (-)	trace (-)
9	mesitylene	10	- (70)	- (6)
10	mesitylene	12	- (75)	- (4)

<sup>a</sup>Yields without added CsF are given in parentheses.

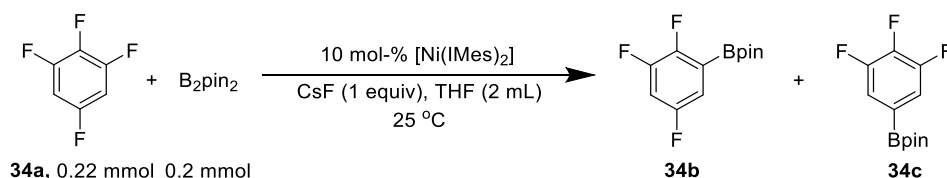
**Table 2-3. The dependence of photocatalytic borylation of 34a on different amounts of Rh biphenyl complex [Rh] or [Ni(IMes)<sub>2</sub>]**



Entry	[Rh] (mol%)	[Ni(IMes) <sub>2</sub> ] (mol%)	t (h)	Yield (%)	
				34b	34c
1	1	10	6	45	trace
2	2	10	6	67	trace
3	3	10	6	82	trace
4	4	10	6	90	trace
5	5	10	6	95	trace
6	5	8	6	72	trace
7	5	6	6	55	trace
8	5	4	6	34	trace
9	5	2	6	13	trace

### 2.3.2 Catalytic reactivity of different photocatalysts

**Table 2-4. Influence of various photocatalysts on the [Ni(IMes)<sub>2</sub>]-catalyzed borylation of 34a**



Entry	Photocatalyst (5 mol%)	$\lambda_{\text{ex}}$ (nm)	$\epsilon$ (M <sup>-1</sup> cm <sup>-1</sup> ) @ $\lambda_{\text{ex}}$	t (h)	Yield (%) <sup>a,b</sup>	
					34b	34c
1	[Rh]	400	4,400	6	45	6
2	<i>fac</i> -[Ir(ppy) <sub>3</sub> ] <sup>c</sup>	400	9,000	6	21 (10)	4 (2)
3	Eosin Y	516	12,000	6	13 (5)	3 (1)
4	[Ru(bpy) <sub>3</sub> ]Cl <sub>2</sub>	457	14,000	6	9 (3)	trace
5	-	400	-	6	6	trace

<sup>a</sup>The yields were determined by GC-MS analysis vs. a calibrated internal standard and are averages of two runs. <sup>b</sup>Yields scaled to the  $\epsilon$  of [Rh] are given in parentheses. <sup>c</sup>We may have underestimated the activity of *fac*-[Ir(ppy)<sub>3</sub>] as there may have been a small amount of undissolved Ir(ppy)<sub>3</sub> in the dark solution.

In order to compare the photosensitizing performance of our Rh biphenyl complex with that of other commonly employed photocatalysts, we studied the efficiency of the photocatalytic borylation of **34a** using  $[\text{Ni}(\text{IMes})_2]$  in combination with *fac*- $[\text{Ir}(\text{ppy})_3]$ , Eosin Y, and  $[\text{Ru}(\text{bpy})_3]\text{Cl}_2$  (Table 2-4). Due to their limited solubility in mesitylene, the experiments were conducted in THF as the solvent. Although **[Rh]** exhibits the smallest extinction coefficient  $\epsilon$  of all tested sensitizers at the respective excitation wavelength, it nonetheless shows the best catalytic activity with a yield of 45% for the formation of **34b** after 6 h (entry 1), while *fac*- $[\text{Ir}(\text{ppy})_3]$ , Eosin Y, and  $[\text{Ru}(\text{bpy})_3]\text{Cl}_2$  gave only 21%, 13% and 9% yields, respectively (entries 2-4). We note that the yield obtained with  $[\text{Ru}(\text{bpy})_3]\text{Cl}_2$  as sensitizer is close to that of the background reaction mediated by  $[\text{Ni}(\text{IMes})_2]$  alone (entry 5). The difference in activity is even more pronounced when the yields are scaled to the extinction coefficient of **[Rh]**, showing that it is superior by a factor of 4-15. We attribute the much higher efficiency of our rhodium biphenyl complex as sensitizer to its exceptionally long-lived triplet excited state, for which lifetimes of 338  $\mu\text{s}$  and 181  $\mu\text{s}$  were observed in 2-MeTHF and toluene, respectively. In contrast, the triplet excited states of *fac*- $[\text{Ir}(\text{ppy})_3]$  (1.9  $\mu\text{s}$ ),<sup>55</sup> Eosin Y (24  $\mu\text{s}$ ),<sup>171</sup> and  $[\text{Ru}(\text{bpy})_3]\text{Cl}_2$  (1.1  $\mu\text{s}$ )<sup>54</sup> are much shorter lived, decreasing the probability of triplet energy transfer as other relaxation pathways, such as collisions with other chemical species in the complex reaction mixture, become more competitive than for **[Rh]**. However, an alternative explanation or additional effect may be that the conjugated extended ligand system of our rhodium complex provides a better orbital overlap integral than the other photosensitizers with the sensitized Ni species. Weaver et al. found indications that the product distribution of photocatalytic C-F bond alkenylation of perfluoropyridine using a series of  $\text{Ir}(\text{ppy})_3$ -type photocatalysts correlates better with their size than their triplet state energy.<sup>178</sup> This suggests that energy transfer rather than electron transfer is occurring and, in that particular case, orbital overlap may be an important factor for the photocatalytic activity. For our study, it is important to note that the shape and size of **[Rh]** is significantly different than those of the other sensitizers tested, and thus, the triplet state electron density distribution is different. A simple comparative size analysis of the sensitizers tested is therefore not sufficient to understand the differences in their photocatalytic activities. The better performance of **[Rh]** may very

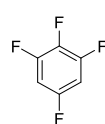
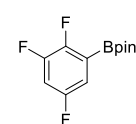
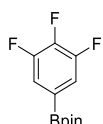
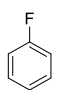
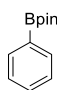
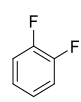
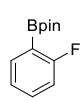
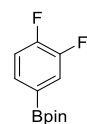
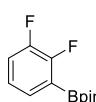
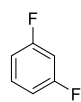
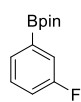
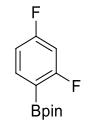
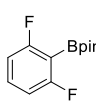
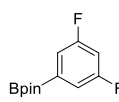
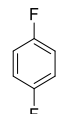
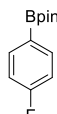
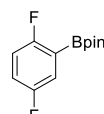
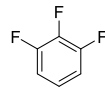
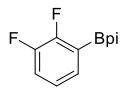
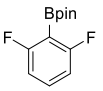
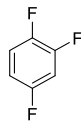
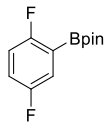
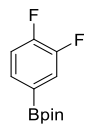
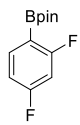
well be due to a combination of its longer excited state lifetime in the reaction mixture and better orbital overlap integral with the Ni complex.

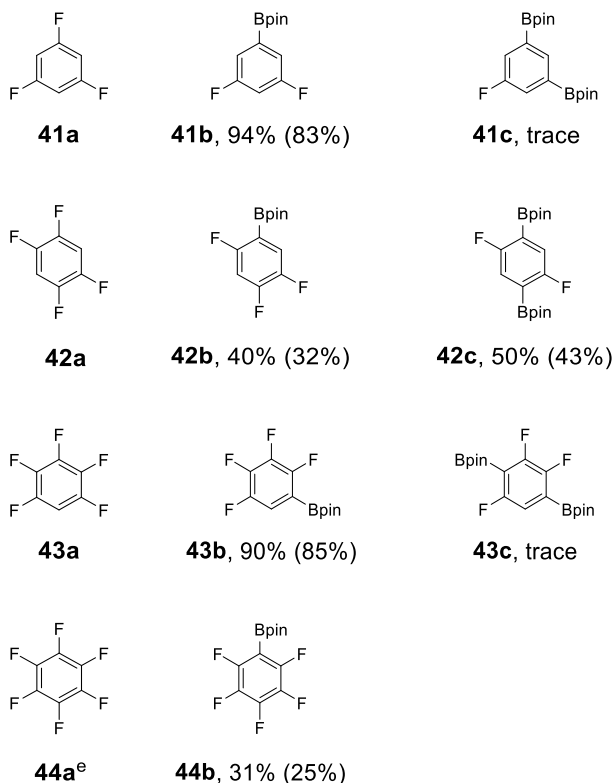
### 2.3.3 Substrate scope

We further examined the scope of fluoroarenes for our photocatalytic borylation under the optimized conditions, and the results are summarized in Table 2-5. The borylations of most fluoroarenes were achieved in good to excellent yields. As we have shown previously,<sup>126</sup> borylation of mono- and difluoroarenes with B<sub>2</sub>pin<sub>2</sub> is particularly challenging, and the yields obtained from the thermal borylation reaction catalyzed by [Ni(IMes)<sub>2</sub>] were unsatisfactory even at 100 °C (20% for fluorobenzene, and ca. 50% for 1,2- and 1,3-difluorobenzene). In contrast, the conversion of C<sub>6</sub>H<sub>5</sub>F (**35a**) to give C<sub>6</sub>H<sub>5</sub>Bpin (**35b**) is greatly improved under visible light irradiation at room temperature, giving a 49% yield. Employing 1,2-difluorobenzene (**36a**), 1,3-difluorobenzene (**37a**) and 1,4-difluorobenzene (**38a**), the borylation products **36b-38b** were obtained in 62%, 67% and 42% yields, respectively. However, we also observed a degree of competing C-H borylation for the difluorobenzenes,<sup>179,180</sup> transforming **36a-38a** to **39b** (17%), **41b** (10%), and **40b** (29%), respectively, apart from traces of other products given in Table 2-4. We do see a little more C-H borylation in the photocatalytic reactions using **36a-38a** as substrates compared to the analogous thermal reactions.<sup>126</sup> Further studies are underway to understand better the Ni-catalyzed C-H borylation process and its regioselectivity in the photocatalytic reaction. The borylation of 1,2,3-trifluorobenzene (**39a**) is highly selective for the 1-position (**39b**, 84%) and for 1,2,4-trifluorobenzene (**40a**) at the 2-position (**40b**, 88%), with C-F borylation at other positions being detected only in trace amounts. Symmetrically substituted 1,3,5-trifluorobenzene (**41a**) is selectively monoborylated to give **41b** in excellent yield (94%), whereas diborylation is observed only in trace amounts. For 1,2,4,5-tetrafluorobenzene (**42a**), both monoborylated **42b** and diborylated **42c** were obtained as the main products in 40% and 50% yields, respectively, based on the amount of added B<sub>2</sub>pin<sub>2</sub>. However, the relative formation of **42b** and **42c** can be controlled by the ratio of fluoroarene **42a** and B<sub>2</sub>pin<sub>2</sub> used. For example, diborylation is achieved in 83% yield when **42a** and B<sub>2</sub>pin<sub>2</sub> are employed in a 1:2 ratio, while a 4:1 ratio of **42a** and B<sub>2</sub>pin<sub>2</sub>

gives monoborylated product in 77% yield with only small amounts of **42c**. Selective borylation of pentafluorobenzene (**43a**) at the 1-position was also accomplished, giving **43b** in excellent yield (90%). Monoborylation of hexafluorobenzene (**44a**) is also possible, leading to C<sub>6</sub>F<sub>5</sub>Bpin (**44b**) in 31% yield after 12 hours.

**Table 2-5. Substrate scope for the photocatalyzed C-F borylation reaction<sup>a</sup>**

			
<b>34a</b>	<b>34b</b> , 95% <sup>b</sup> (86%) <sup>c</sup>	<b>34c</b> , trace	
			
<b>35a<sup>d</sup></b>	<b>35b</b> , 49% (41%)		
			
<b>36a</b>	<b>36b</b> , 62% (58%)	<b>36c</b> , trace	<b>39b</b> , 17% (14%)
			
<b>37a</b>	<b>37b</b> , 67% (59%)	<b>37c</b> , trace	<b>37d</b> , trace
			
			<b>41b</b> , 10% (5%)
			
<b>38a<sup>d</sup></b>	<b>38b</b> , 42% (31%)	<b>40b</b> , 29% (20%)	
			
<b>39a</b>	<b>39b</b> , 84% (65%)	<b>37d</b> , trace	
			
<b>40a</b>	<b>40b</b> , 88% (82%)	<b>36c</b> , trace	<b>37c</b> , trace



<sup>a</sup>Reaction conditions: B<sub>2</sub>pin<sub>2</sub> (0.20 mmol), fluoroarene (0.22 mmol), CsF (0.20 mmol), **[Rh]** (5 mol%), [Ni(IMes)<sub>2</sub>] (10 mol%), mesitylene (2 mL), at room temperature under irradiation with a 400 nm-LED for 6 h unless otherwise stated. <sup>b</sup>The yields are based on B<sub>2</sub>pin<sub>2</sub> and were determined by GC-MS analysis vs. a calibrated internal standard and are averages of two runs.

<sup>c</sup>Isolated yields are given in parentheses. <sup>d</sup>The reaction time was 12 h. <sup>e</sup>The reaction time was 15 h.

## 2.4 Mechanistic studies

### 2.4.1 Cyclic voltammetry

Photoredox catalysis takes advantage of the ground- and excited-state redox properties of the photocatalyst and is based on photoinitiated SET between the catalyst and the substrates. Cyclic voltammetry (CV) is the most common way to measure the groundstate redox potentials of a compound. We first investigated the redox potentials of the participating known metal complexes to elucidate the potential for SET processes between **[Rh]** and any of the Ni species and chose 1,2,3,5-tetrafluorobenzene (**34a**) as model substrate for the oxidative addition. The cyclic voltammogram of the **[Rh]** in CH<sub>3</sub>CN is shown in Figure 2-2 and those of the nickel complexes [Ni(IMes)<sub>2</sub>] and *trans*-[NiF(2,3,5-C<sub>6</sub>F<sub>3</sub>H<sub>2</sub>)(IMes)<sub>2</sub>] (**[Ni<sup>II</sup>]**), and of the reactants 1,2,3,5-tetrafluorobenzene



(**34a**) and  $B_2pin_2$ , are displayed in Figure 2-3. The oxidation of the metal center ( $Rh^{IV}/Rh^{III}$ ) occurs at about 0.57 V, while the reduction of the metal center ( $Rh^{III}/Rh^{II}$ ) occurs at about -2.26 V. Assuming that the all the excited state energy is available as free energy (i.e., the entropic contribution is neglected),<sup>181</sup> the excited state redox potentials can be calculated using eq. (1) and (2).<sup>60,182,183</sup> Herein, the  $E_0$  is emission energy.

$$E(Rh^{*III}/Rh^{II}) = E(Rh^{III}/Rh^{II}) + E_0 = -2.26 \text{ V} + 2.3 \text{ V} = 0.04 \text{ V} \quad (1)$$

$$E(Rh^{IV}/Rh^{*III}) = E(Rh^{IV}/Rh^{III}) - E_0 = 0.57 \text{ V} - 2.3 \text{ V} = -1.73 \text{ V} \quad (2)$$

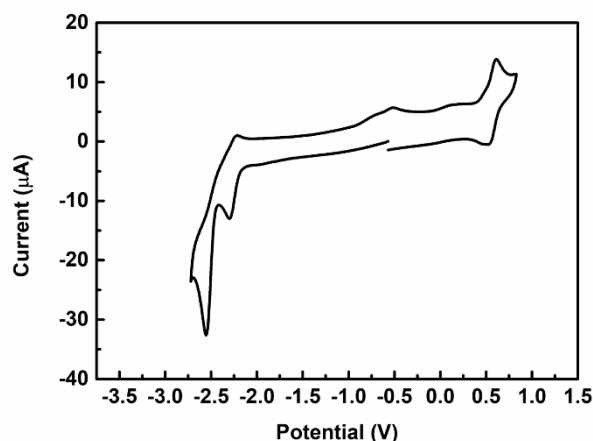


**Figure 2-2.** Cyclic voltammogram of **[Rh]** in  $CH_3CN$ , using 0.1 M tetrabutylammonium hexafluorophosphate ( $TBAPF_6$ ) as supporting electrolyte. Potentials are referenced to the ferrocene/ferrocenium couple.

The reversible one-electron-oxidation of  $[Ni(IMes)_2]$  in THF solution occurs at about -1.9 V, which is higher than that of  $Rh^{III/II}$  (-2.26 V) and lower than that of  $Rh^{IV/III}$  (-1.73 V). The cyclic voltammogram of **[Ni<sup>II</sup>]** in  $CH_3CN$  shows the oxidation of the metal center ( $Ni^{III}/Ni^{II}$ ) at ca. 0.4 V, which is higher than that of  $Rh^{*III/II}$  (0.04 V) and lower than that of  $Rh^{IV/III}$  (0.57 V). Therefore, the **[Rh]** can not undergoes a electron transfer to  $[Ni(IMes)_2]$  or **[Ni<sup>II</sup>]** (Scheme 2-3). The triplet excited state reduction potential at 0.04 V of  $^3[Rh]$  would be sufficient to oxidize  $[Ni(IMes)_2]$ , which shows reversible oxidation at -1.90 V. However, this process is not relevant for transmetalation and therefore not relevant for a photocatalytic process, and would likely inhibit the initial C-F activation step. It is important to note that  $^3[Rh]$  cannot reduce **[Ni<sup>II</sup>]**, a process which could influence the transmetalation step. For **34a** and  $B_2pin_2$ , no reduction or oxidation peaks were observed within the electrochemical

window of the solvent, suggesting that  $B_2pin_2$  and **34a** cannot be reduced or oxidized by the  $^3IL$  state of  $[Rh]$  either. This excludes photoinitiated SET processes relevant for transmetalation in general.

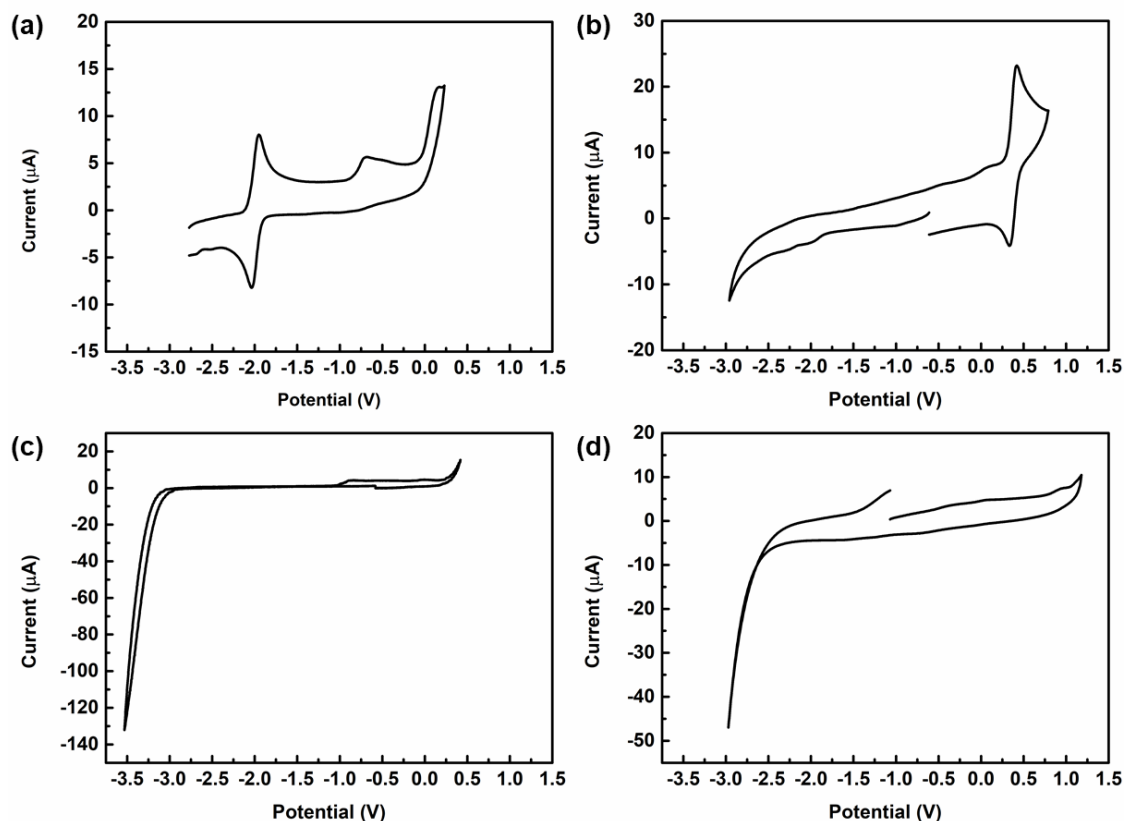


**Figure 2-3.** Cyclic voltammograms of  $[Ni(IMes)_2]$  (a) in THF,  $[Ni^{II}]$  (b) in  $CH_3CN$ , 1,2,3,5-tetrafluorobenzene **34a** (c) in THF, and  $B_2pin_2$  (d) in  $CH_3CN$ , using 0.1 M  $TBAPF_6$  as supporting electrolyte. Potentials are referenced to the ferrocene/ferrocenium couple.

To confirm that  $B_2pin_2$  does not react with the electrolyte  $TBAPF_6$  (e.g., by fluoride ion abstraction), we compared the NMR spectra of pure  $B_2pin_2$  with that of a mixture of  $B_2pin_2$  and  $TBAPF_6$  which had been allowed to stand for 10 min. From Figures 2-4 - 2-6, we see that there is no change in the  $^{11}B$  NMR spectrum of  $B_2pin_2$  upon addition of  $TBAPF_6$ , and that the  $^{19}F$  NMR spectrum of the mixture is the same as that of pure  $TBAPF_6$ , indicating that  $B_2pin_2$  does not react with  $TBAPF_6$ .

**Scheme 2-3. Redox potentials of the nickel and rhodium species potentially involved in the photocatalytic borylation reaction of fluoroaromatics ( $\text{Ni}^0 = [\text{Ni}^0(\text{IMes})_2]$ ;  $\text{Ni}^{\text{I}} = [\text{Ni}^{\text{I}}(\text{IMes})_2]^+$ ;  $\text{Ni}^{\text{II}} = [\text{Ni}^{\text{II}}]$ ;  $\text{Ni}^{\text{III}} = \text{trans}-[\text{Ni}^{\text{III}}\text{F}(2,3,5\text{-C}_6\text{F}_3\text{H}_2)(\text{IMes})_2]^+$ ;  $\text{Rh}^{\text{I}} = [\text{Rh}]$ ;  $\text{Rh}^{\text{II}} = [\text{Rh}]$ ;  $^*\text{Rh}^{\text{III}} = ^3[\text{Rh}]$ ;  $\text{Rh}^{\text{IV}} = [\text{Rh}]^+$ )**

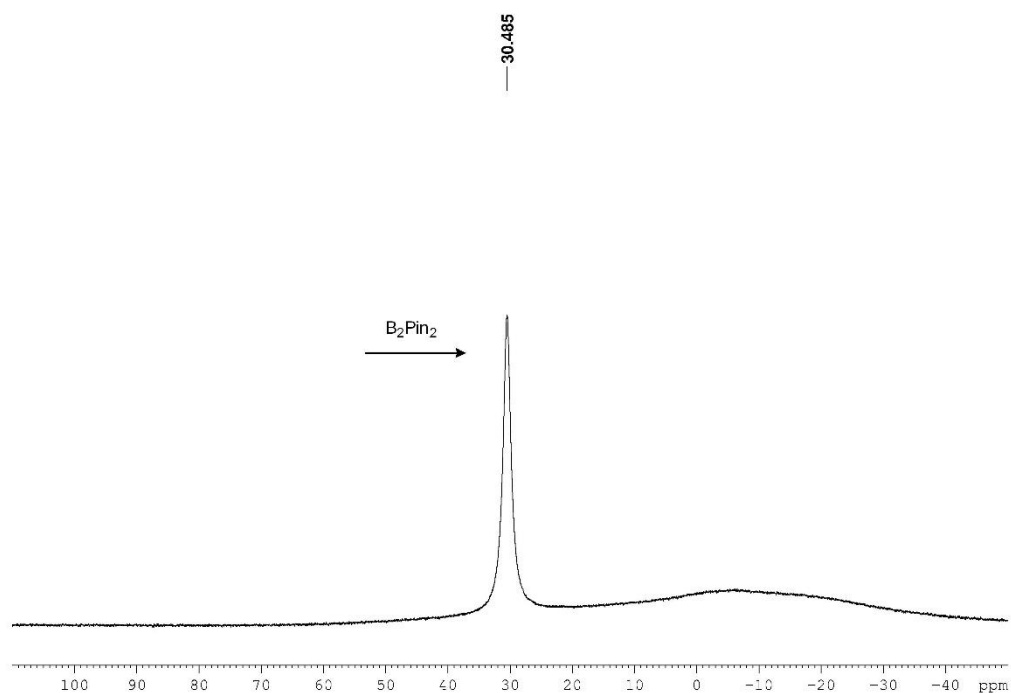
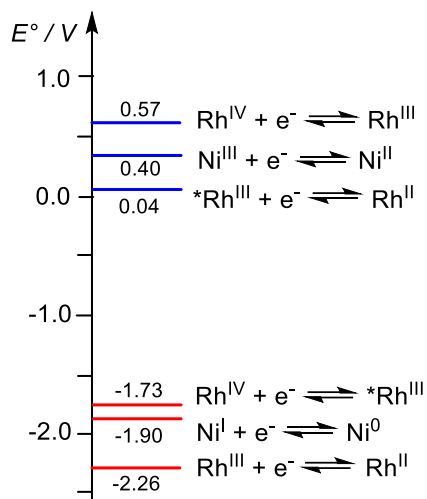


**Figure 2-4.**  $^{11}\text{B}$  NMR spectrum of  $\text{B}_2\text{pin}_2$  (128 MHz,  $\text{CD}_3\text{CN}$ ).

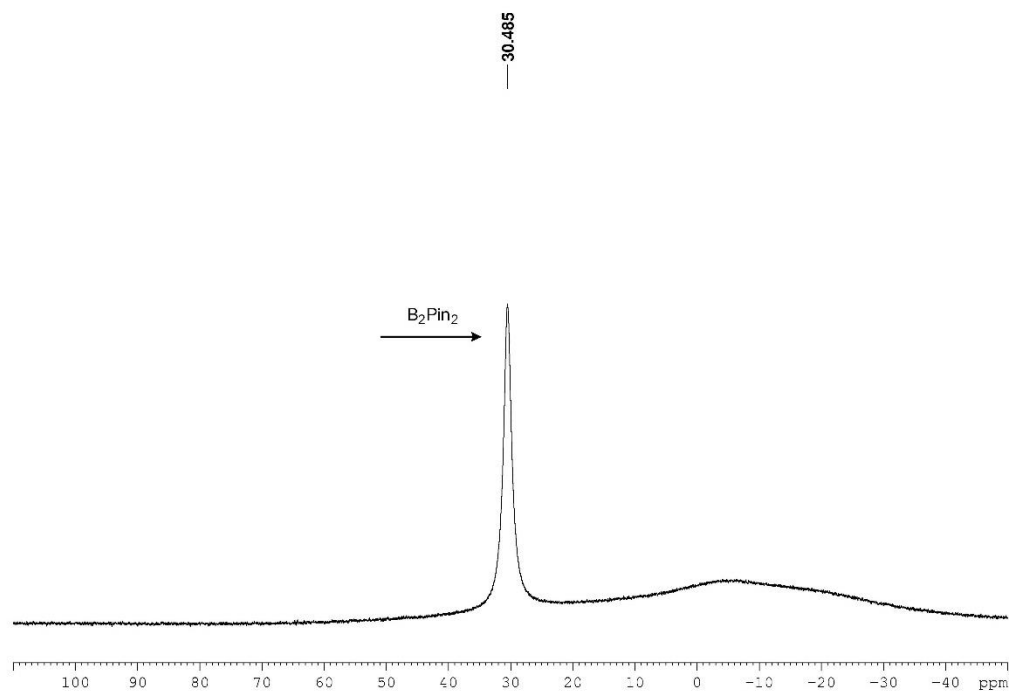


**Figure 2-5.**  $^{11}\text{B}$  NMR spectrum of  $\text{B}_2\text{pin}_2$  with  $\text{TBAPF}_6$  (128 MHz,  $\text{CD}_3\text{CN}$ ).

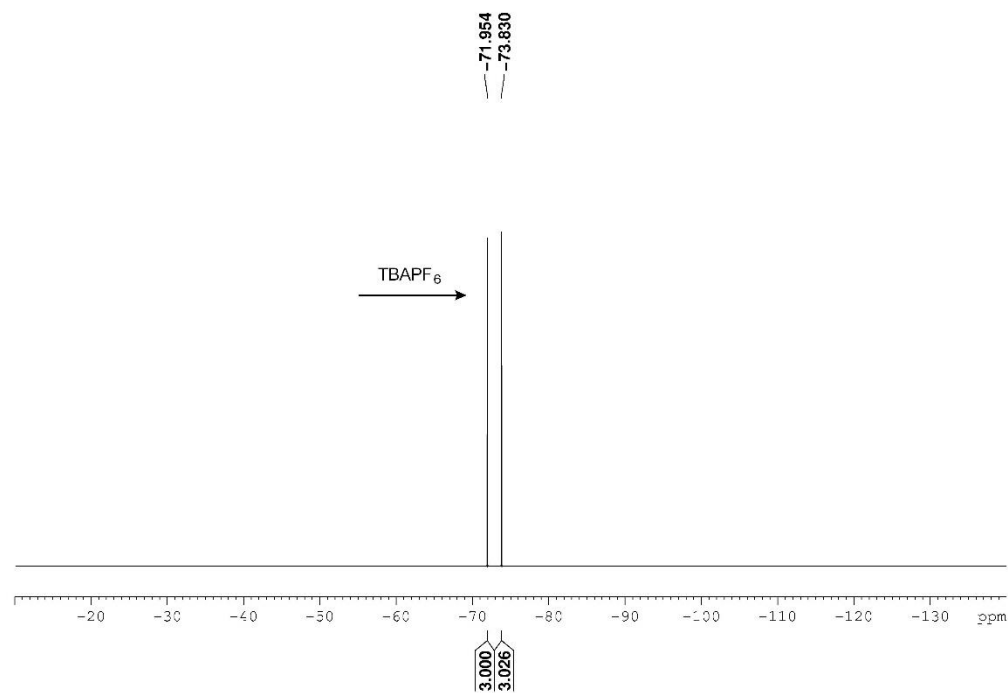


**Figure 2-6.**  $^{19}\text{F}$  NMR spectrum of  $\text{B}_2\text{pin}_2$  with  $\text{TBAPF}_6$  (376 MHz,  $\text{CD}_3\text{CN}$ ).

#### 2.4.2 UV-vis absorption spectrum and stability upon irradiation of $[\text{Ni}^{\text{II}}]$

With photoinduced SET processes being excluded, we were curious to see if formation of a photoexcited state of the resting state complex  $[\text{Ni}^{\text{II}}]$  could enhance the borylation efficiency. The photophysics investigation showed that The  $\text{Ni}^{\text{II}}$  intermediate absorbs very weakly ( $\epsilon \approx 500 \text{ M}^{-1} \text{ cm}^{-1}$ ) at 400 nm (Figure 2-7). To test the stability of the  $[\text{Ni}^{\text{II}}]$  upon

irradiation, a Young's tap NMR tube containing 15 mg of  $[\text{Ni}^{\text{II}}]$  in 0.7 mL  $\text{C}_6\text{D}_6$  was placed between two 400 nm-LEDs for 1 h. The NMR spectra show no signs of decomposition (Figure 2-8 - 2-10).

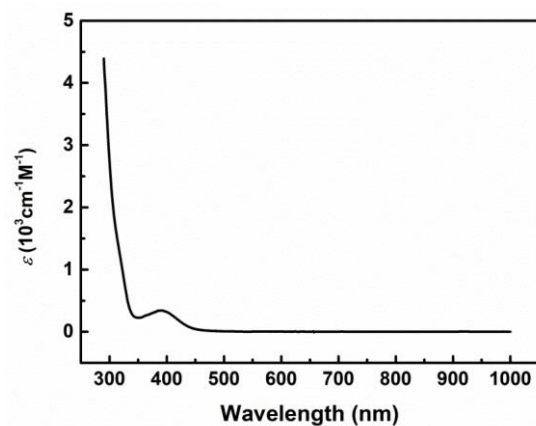


Figure 2-7. UV-visible absorption of  $\text{trans-}[\text{NiF}(2,3,5\text{-C}_6\text{F}_3\text{H}_2)(\text{IMes})_2]$  in THF.

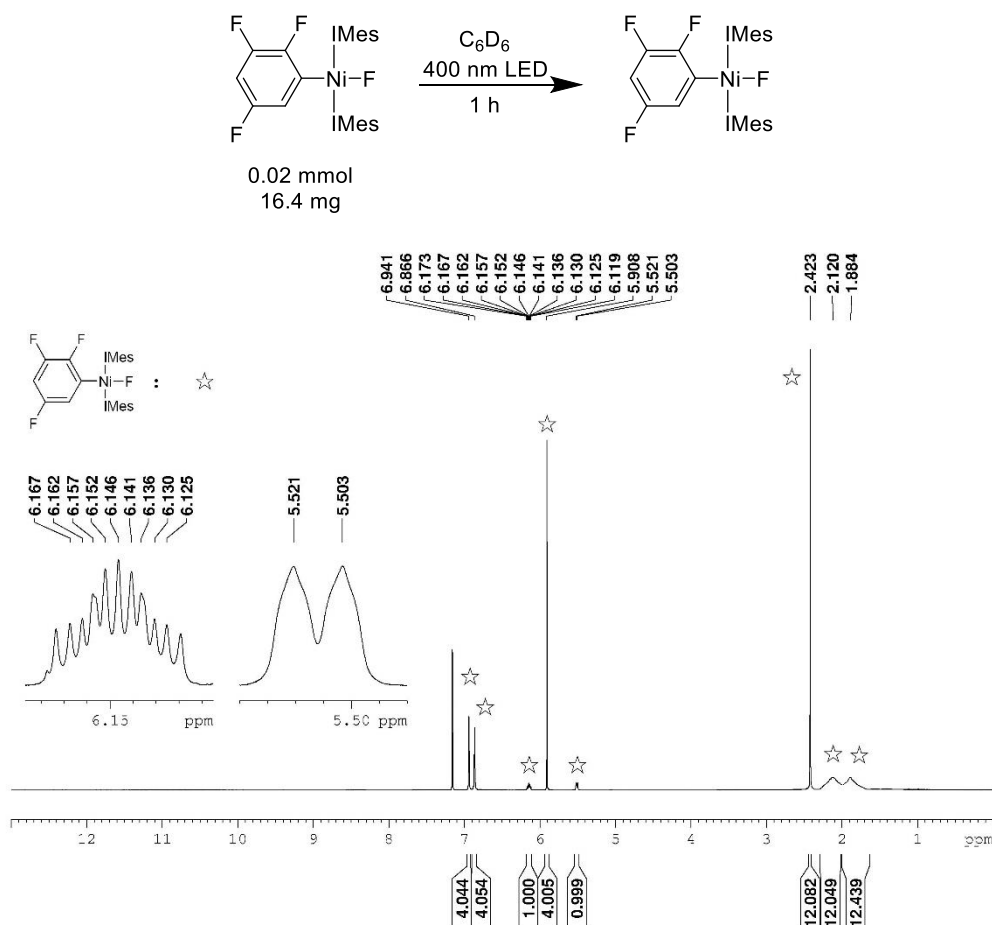
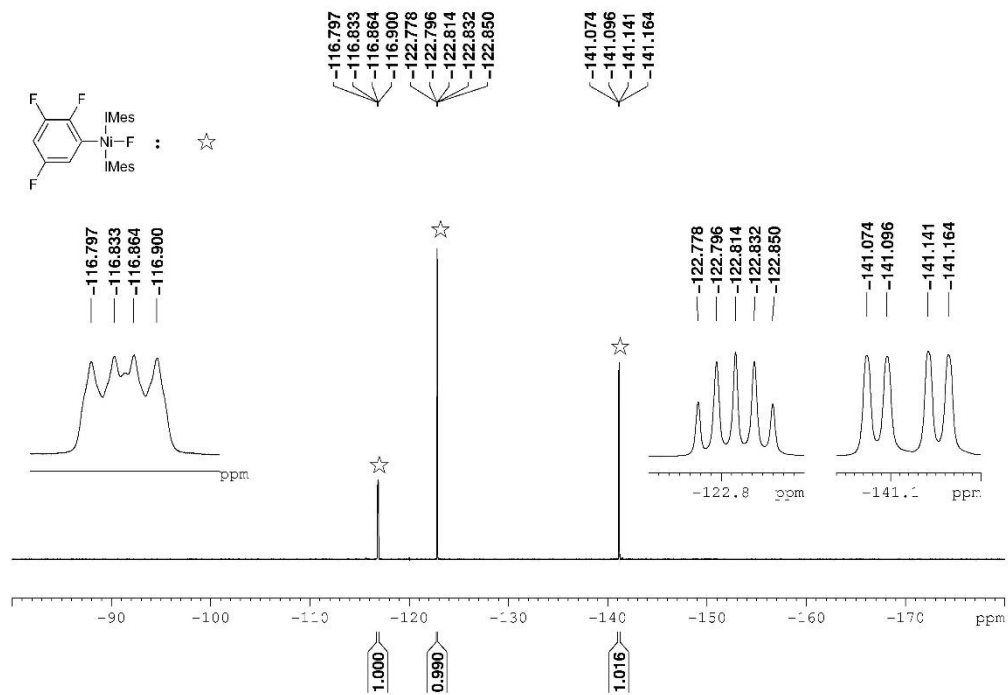
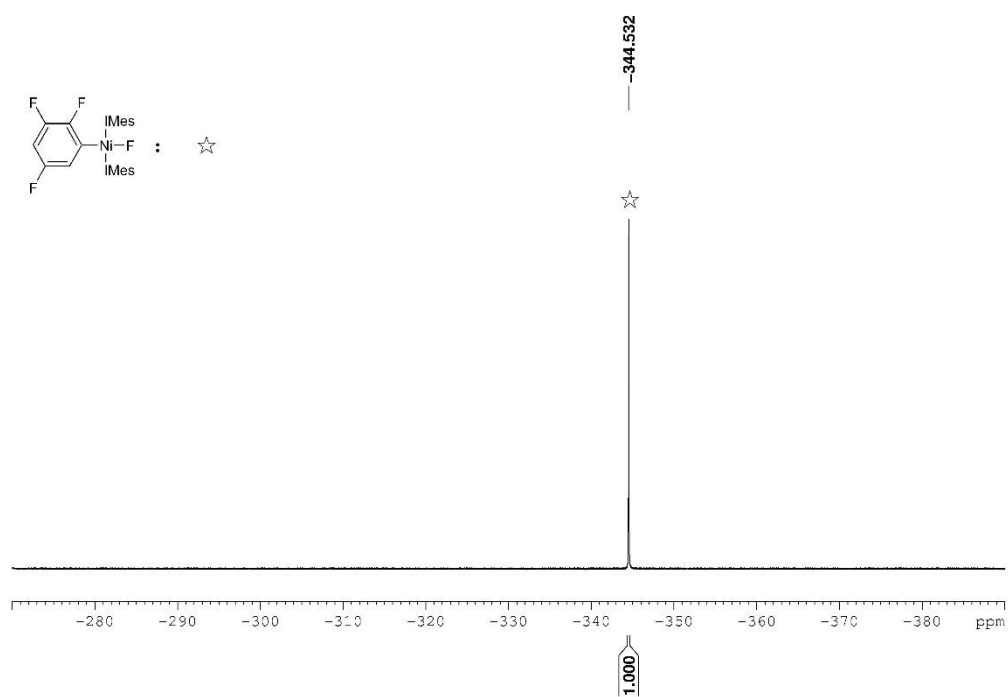


Figure 2-8.  $^1\text{H}$  NMR spectrum after 1 h irradiation (500 MHz,  $\text{C}_6\text{D}_6$ ).



**Figure 2-9.**  $^{19}\text{F}$  NMR spectrum of aromatic region after 1 h irradiation (471 MHz,  $\text{C}_6\text{D}_6$ ).



**Figure 2-10.**  $^{19}\text{F}$  NMR spectrum of Ni-F resonance after 1 h irradiation (471 MHz,  $\text{C}_6\text{D}_6$ ).

We further studied the reactivity of  $[\text{Ni}^{\text{II}}]$  with stoichiometric amounts of  $\text{B}_2\text{pin}_2$ . A mixture of  $[\text{Ni}^{\text{II}}]$  (0.02 mmol, 16.4 mg) and  $\text{B}_2\text{pin}_2$  (0.02 mmol, 5.1 mg, 1eq.) was dissolved in 0.7 mL  $\text{C}_6\text{D}_6$  in a Young's tap NMR tube. For those components of which less than 6 mg were required, we firstly prepared a stock solution of known concentration and then added the respective volume as needed. The  $^1\text{H}$ -,  $^{11}\text{B}$ -, and  $^{19}\text{F}$ -NMR spectra of the mixture kept in the dark were immediately recorded. No reaction was observed, but upon irradiation with 400 nm LEDs for 10 minutes, the reaction mixture turned black due to significant decomposition of the  $\text{Ni}^{\text{II}}$  complex and the formation of nickel particles in conjunction with the formation of small quantities of the borylation product 1-Bpin-2,3,5- $\text{C}_6\text{F}_3\text{H}_2$  (**34b**) and FBpin (Figures 2-11 - 2-18)

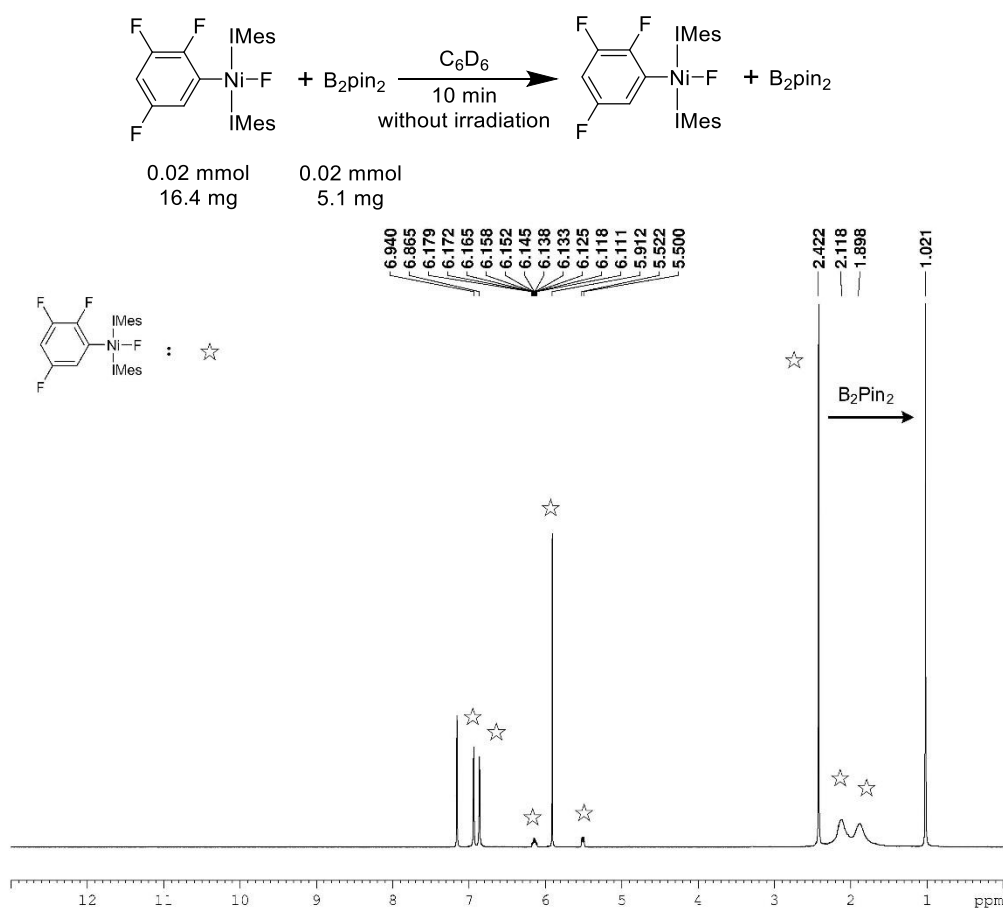


**Figure 2-11.**  $^1\text{H}$  NMR spectrum after 10 min in the dark (400 MHz,  $\text{C}_6\text{D}_6$ ).

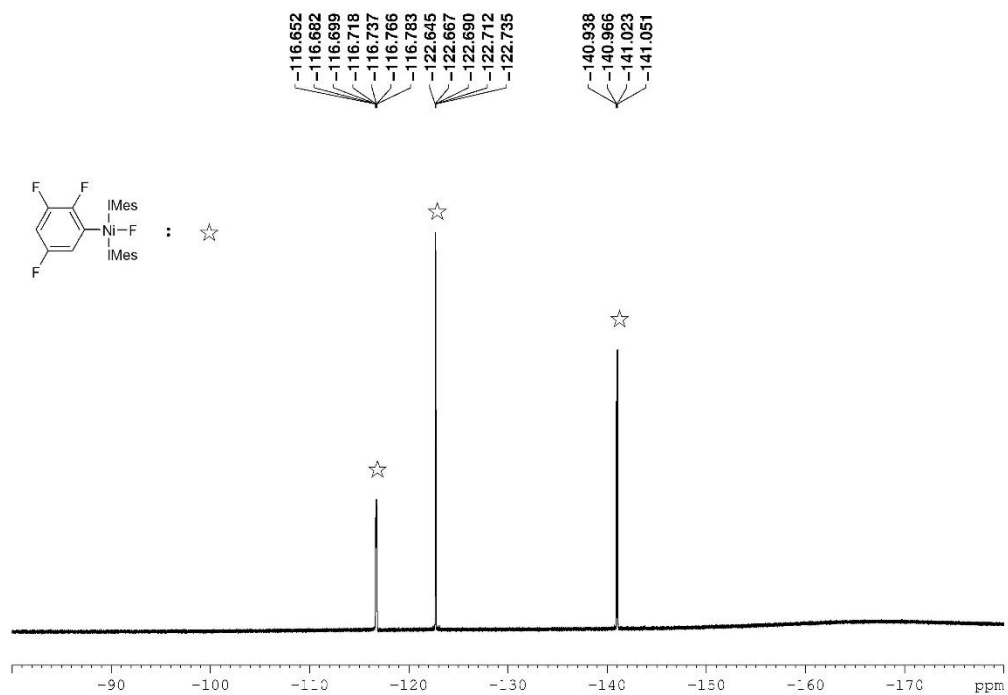


**Figure 2-12.**  $^{19}\text{F}$  NMR spectrum of aromatic region after 10 min in the dark (376 MHz,  $\text{C}_6\text{D}_6$ ).

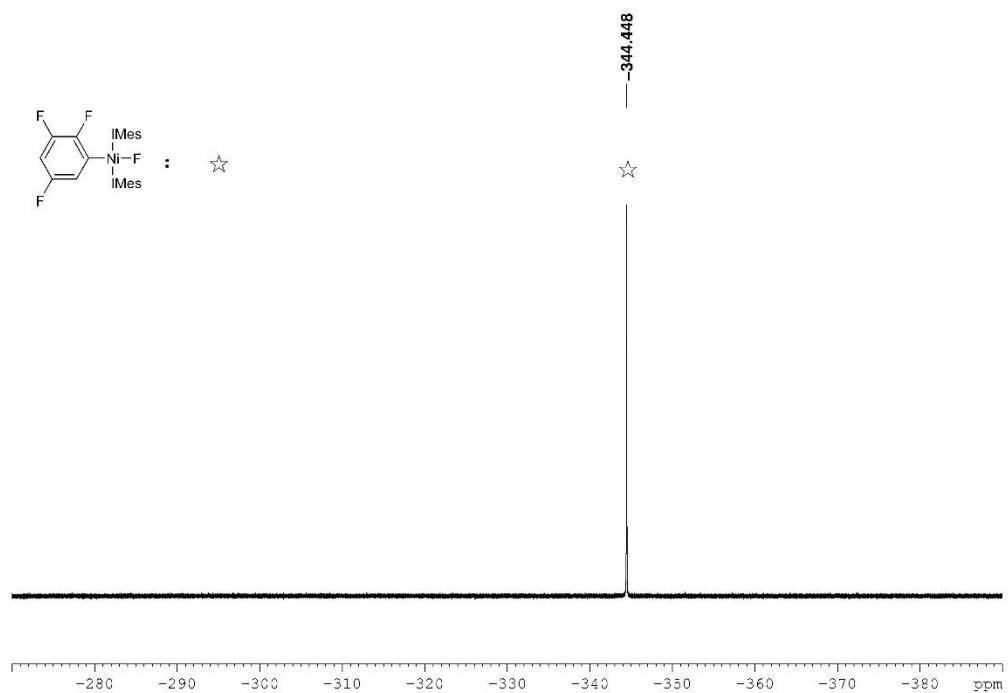


**Figure 2-13.**  $^{19}\text{F}$  NMR spectrum of Ni-F resonance after 10 min in the dark (376 MHz,  $\text{C}_6\text{D}_6$ ).



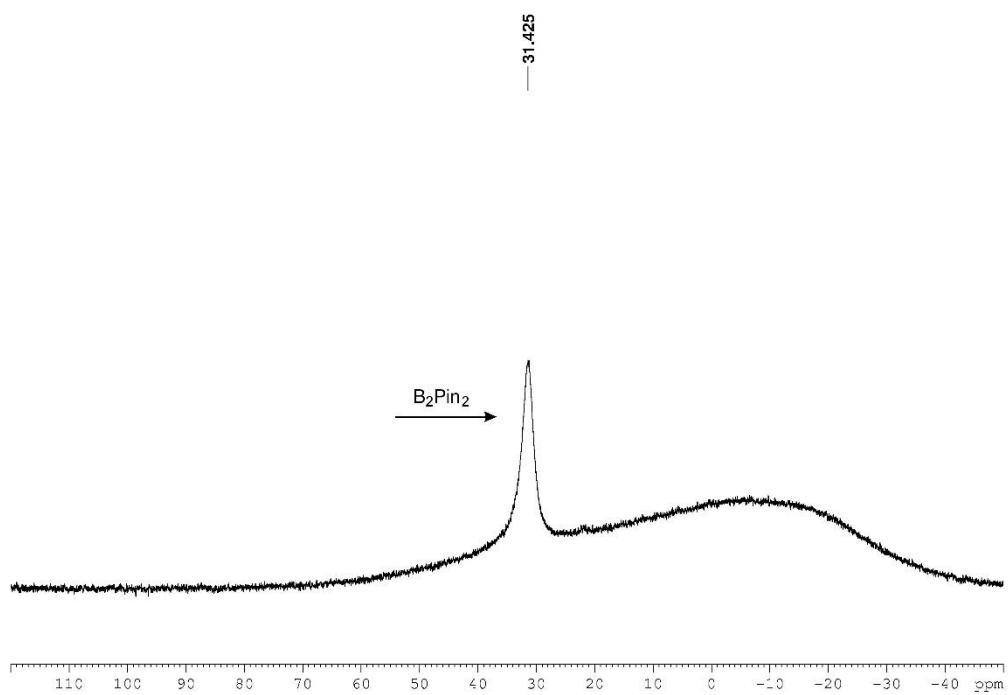


**Figure 2-14.**  $^{11}\text{B}$  NMR spectrum after 10 min in the dark (128 MHz,  $\text{C}_6\text{D}_6$ ).

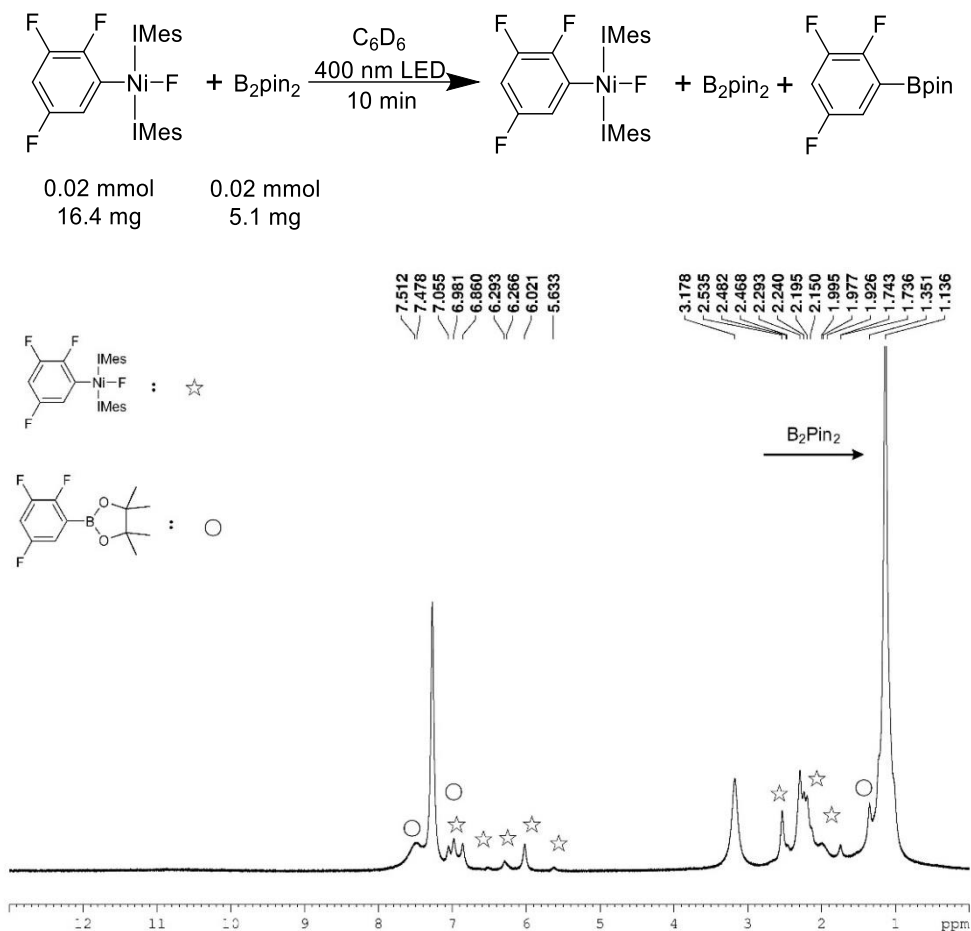


**Figure 2-15.**  $^1H$  NMR spectrum after 10 min irradiation (400 MHz,  $C_6D_6$ ).

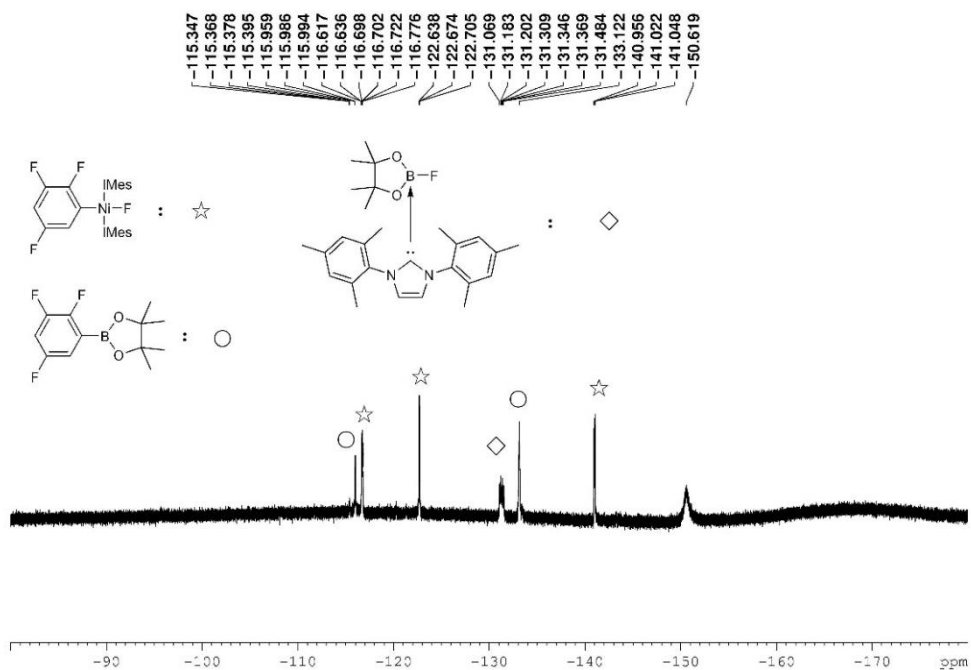


**Figure 2-16.**  $^{19}F$  NMR spectrum of aromatic region after 10 min irradiation (376 MHz,  $C_6D_6$ ).

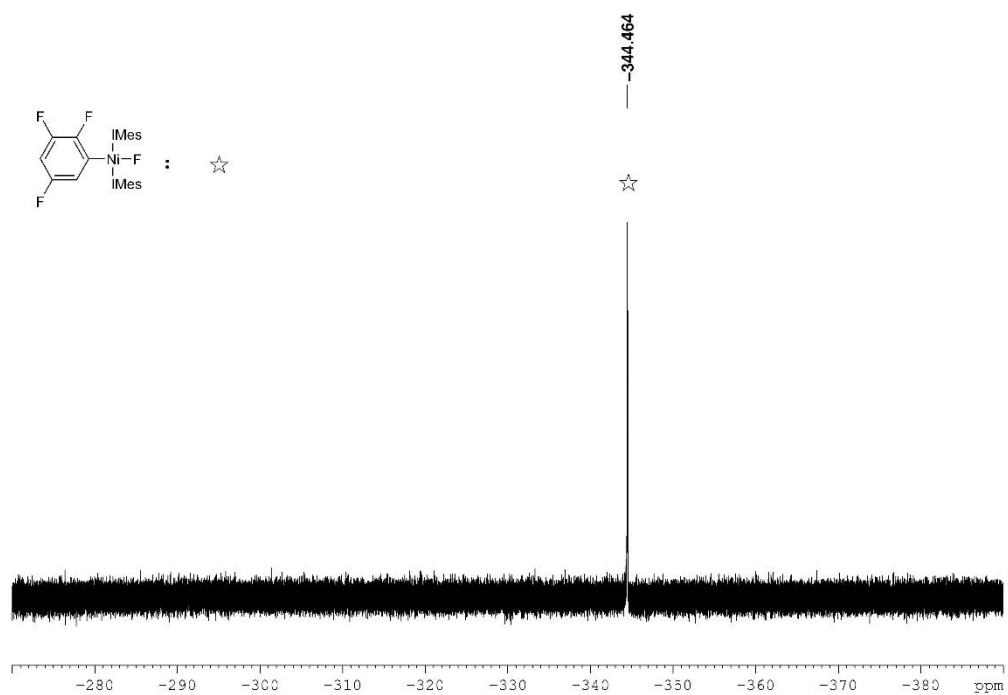


**Figure 2-17.**  $^{19}\text{F}$  NMR spectrum of Ni-F resonance after 10 min irradiation (376 MHz,  $\text{C}_6\text{D}_6$ ).

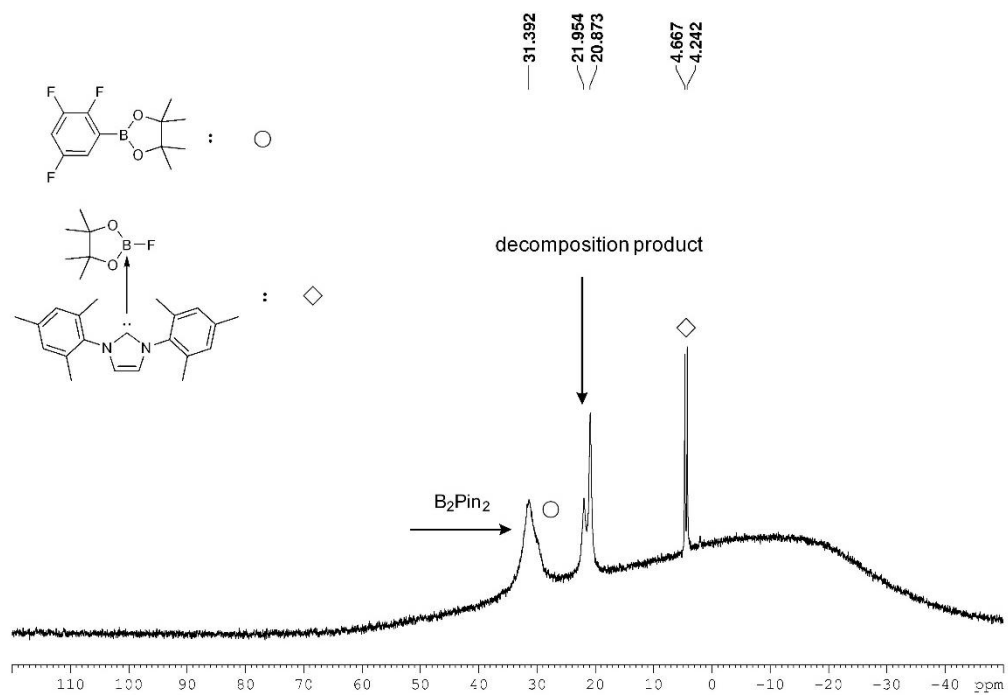


**Figure 2-18.**  $^{11}\text{B}$  NMR spectrum after 10 min irradiation (128 MHz,  $\text{C}_6\text{D}_6$ ).

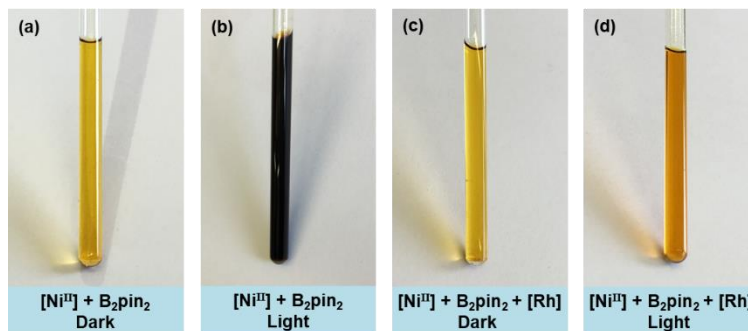


**Figure 2-19.** Photographs of the reaction of  $[\text{Ni}^{\text{II}}]$  with  $\text{B}_2\text{pin}_2$  after 10 minutes in the dark (a), upon irradiation with a 400 nm LED (b), in the presence of  $[\text{Rh}]$  in the dark (c) and upon irradiation (d).

If 0.02 mmol of CsF (3.0 mg, 1eq.) was added into the above reaction system, the same experimental phenomenon was observed (Figures 2-20 - 2-27).

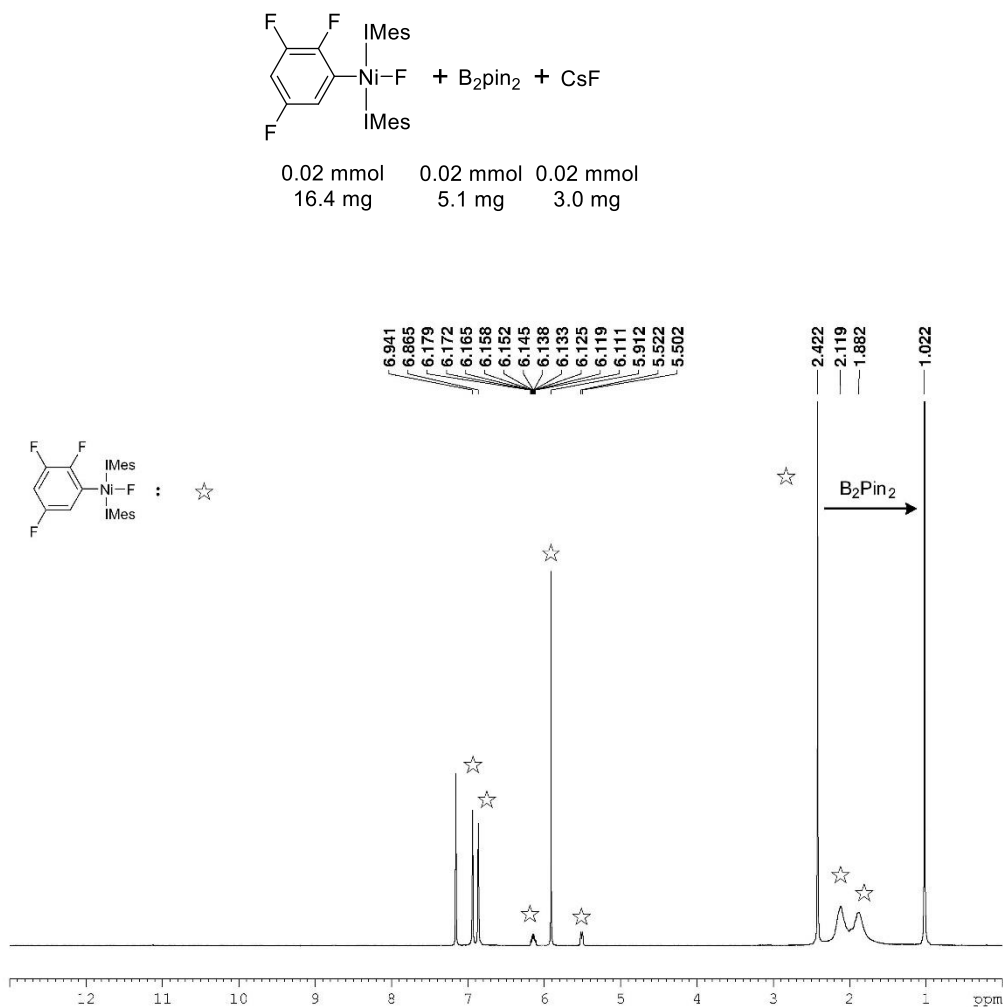


**Figure 2-20.**  $^1\text{H}$  NMR spectrum in the dark (400 MHz,  $\text{C}_6\text{D}_6$ ).

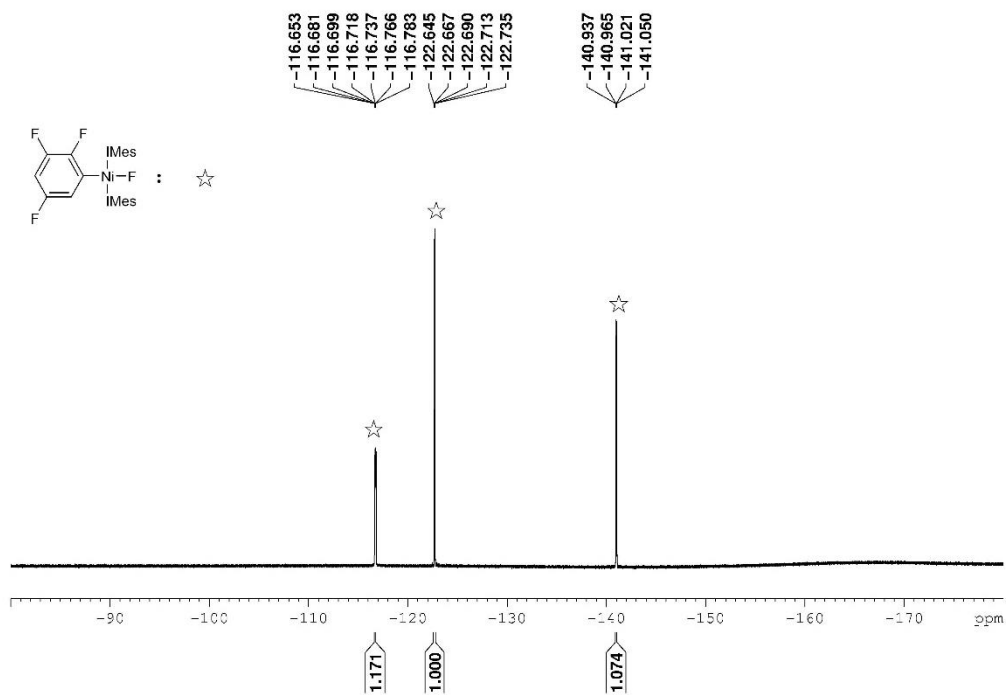


**Figure 2-21.**  $^{19}\text{F}$  NMR spectrum of aromatic region in the dark (376 MHz,  $\text{C}_6\text{D}_6$ ).

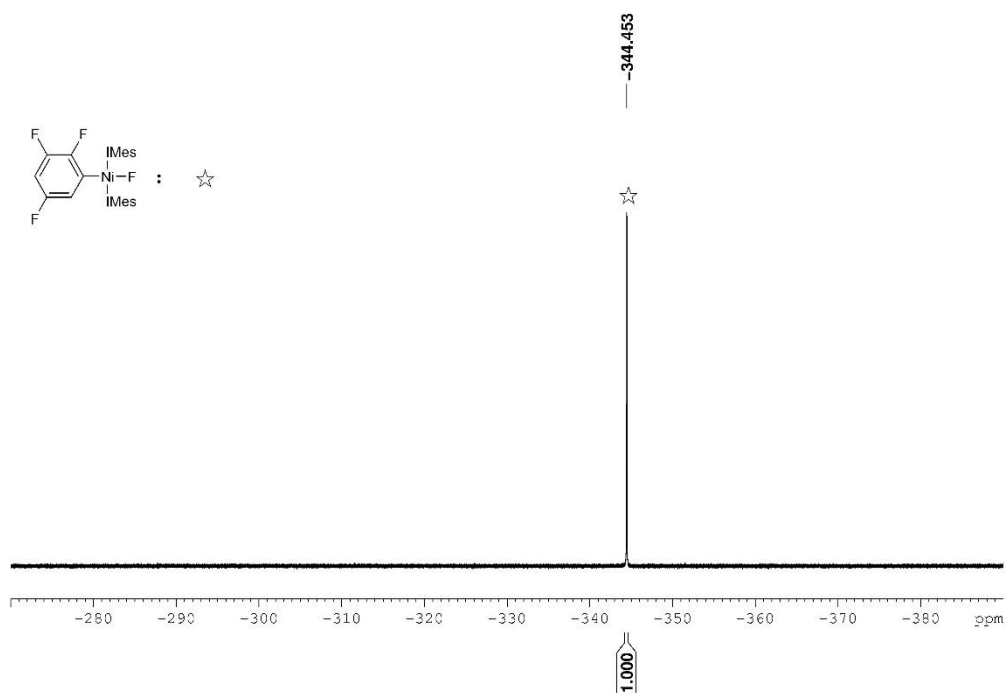


**Figure 2-22.**  $^{19}\text{F}$  NMR spectrum of Ni-F resonance in the dark (376 MHz,  $\text{C}_6\text{D}_6$ ).

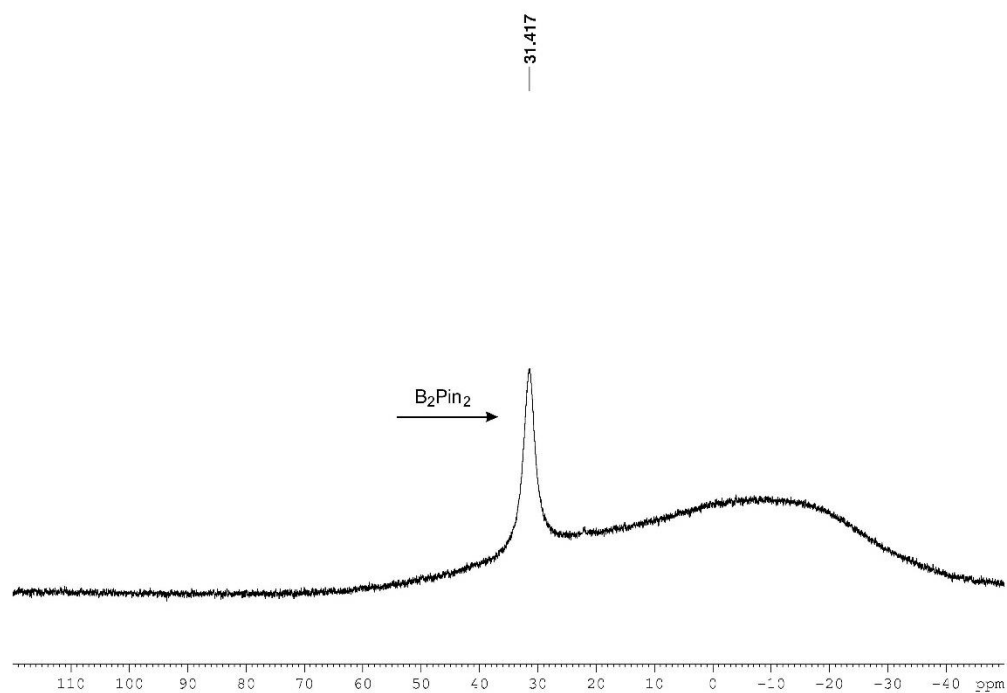


Figure 2-23.  $^{11}\text{B}$  NMR spectrum in the dark (128 MHz,  $\text{C}_6\text{D}_6$ ).

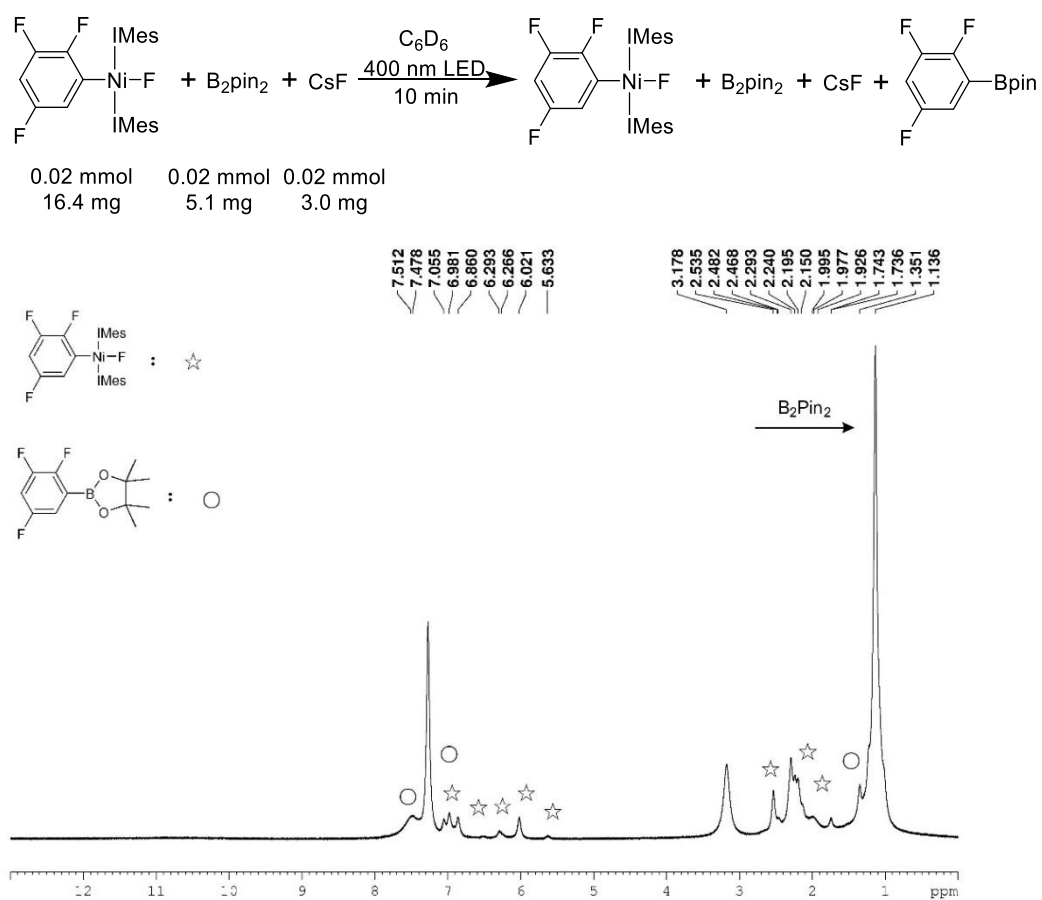
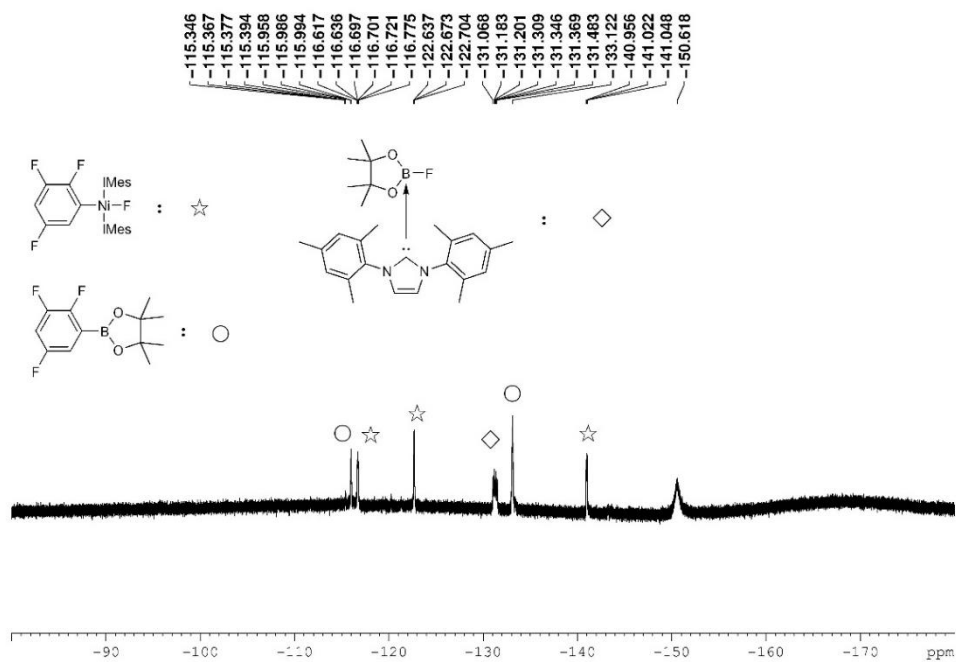
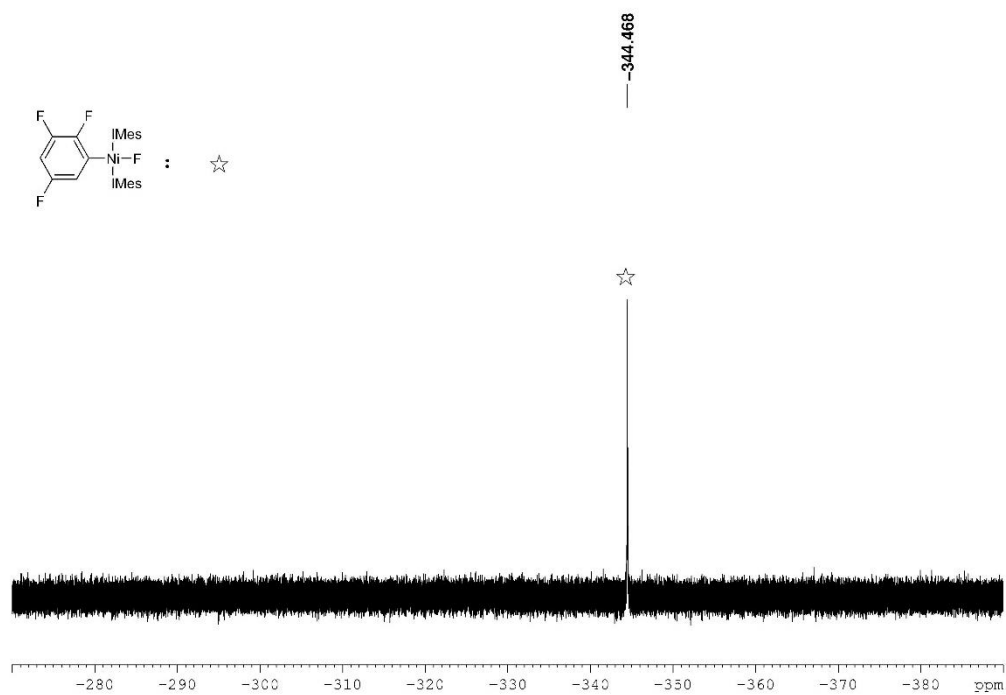


Figure 2-24.  $^1\text{H}$  NMR spectrum after 10 min irradiation (400 MHz,  $\text{C}_6\text{D}_6$ ).



**Figure 2-25.**  $^{19}\text{F}$  NMR spectrum of aromatic region after 10 min irradiation (376 MHz,  $\text{C}_6\text{D}_6$ ).



**Figure 2-26.**  $^{19}\text{F}$  NMR spectrum of Ni-F resonance after 10 min irradiation (376 MHz,  $\text{C}_6\text{D}_6$ ).

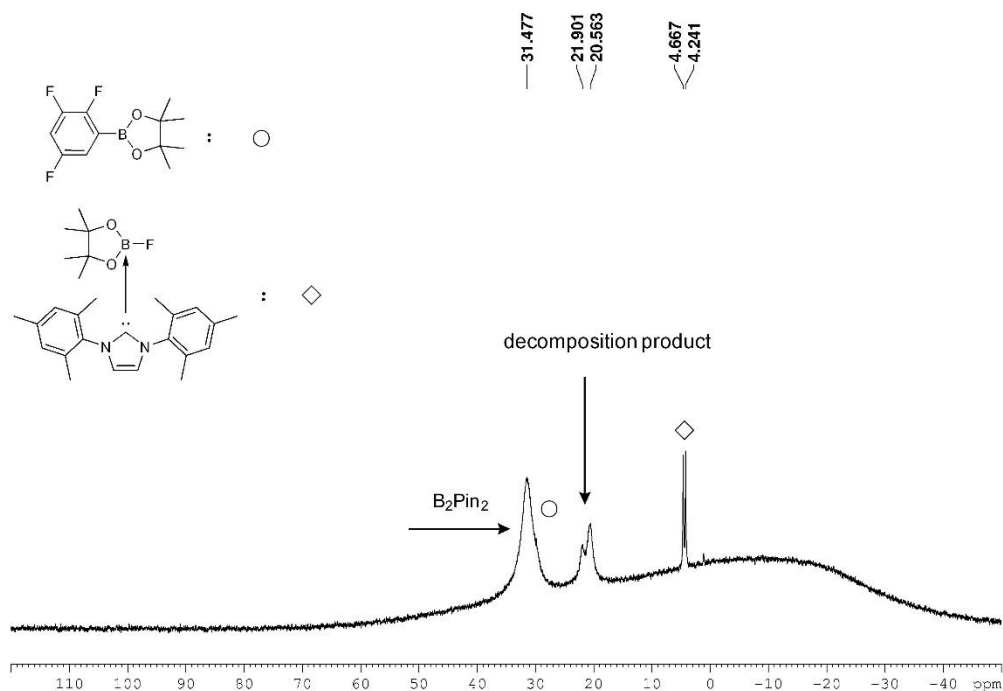


**Figure 2-27.**  $^{11}\text{B}$  NMR spectrum after 10 min irradiation (128 MHz,  $\text{C}_6\text{D}_6$ ).

In order to test whether the fluoroarene can trap any  $\text{Ni}^0$  species that should be formed after photoinitiated borylation of the fluoroarene ligand by direct irradiation of *trans*- $[\text{NiF}(\text{2,3,5-}\text{C}_6\text{F}_3\text{H}_2)(\text{IMes})_2]$  in the presence of stoichiometric amounts of  $\text{B}_2\text{pin}_2$ , a 10-fold excess of 1,2,3,5- $\text{C}_6\text{F}_4\text{H}_2$  has been added and the reactions mixture has been irradiated for 10 minutes with 400 nm LEDs. We note that the presence of a 10-fold excess of fluoroarene to trap any  $\{\text{Ni}^0\text{L}_n\}$  species which might be formed upon formal reductive elimination, did improve the stability to some extent, but was still insufficient to prevent fast decomposition of the nickel complex.



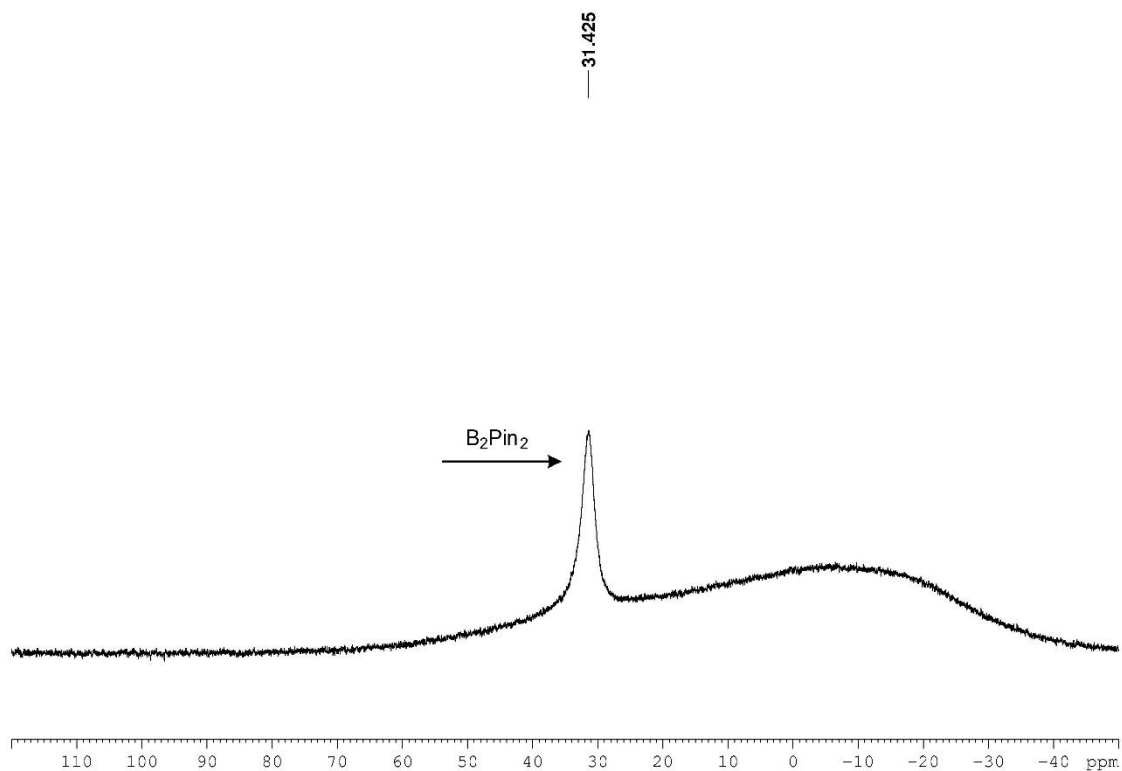


Figure 2-28.  $^{11}\text{B}$  NMR spectrum after 10 min in the dark (128 MHz,  $\text{C}_6\text{D}_6$ ).

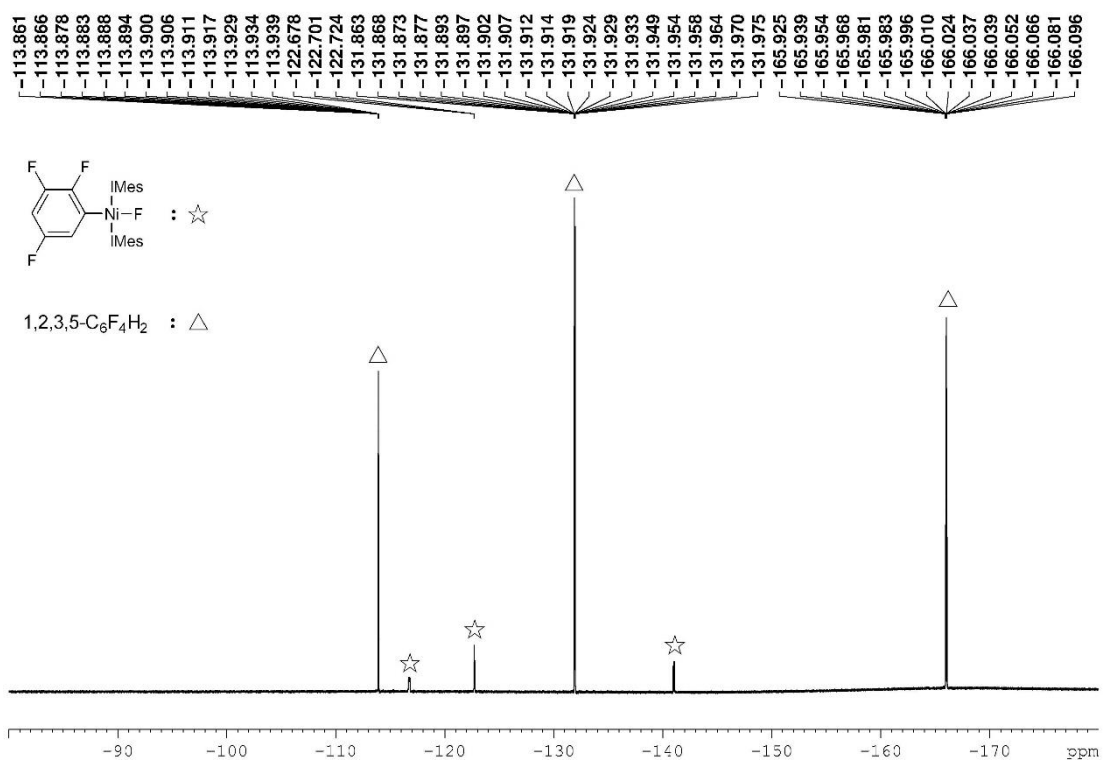
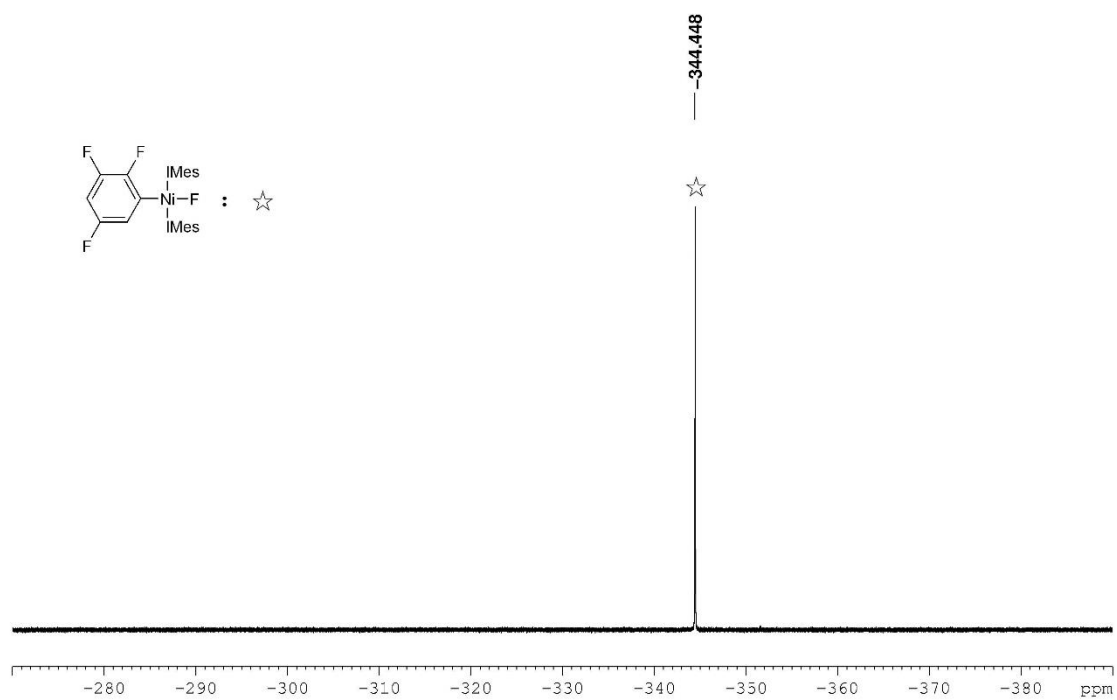
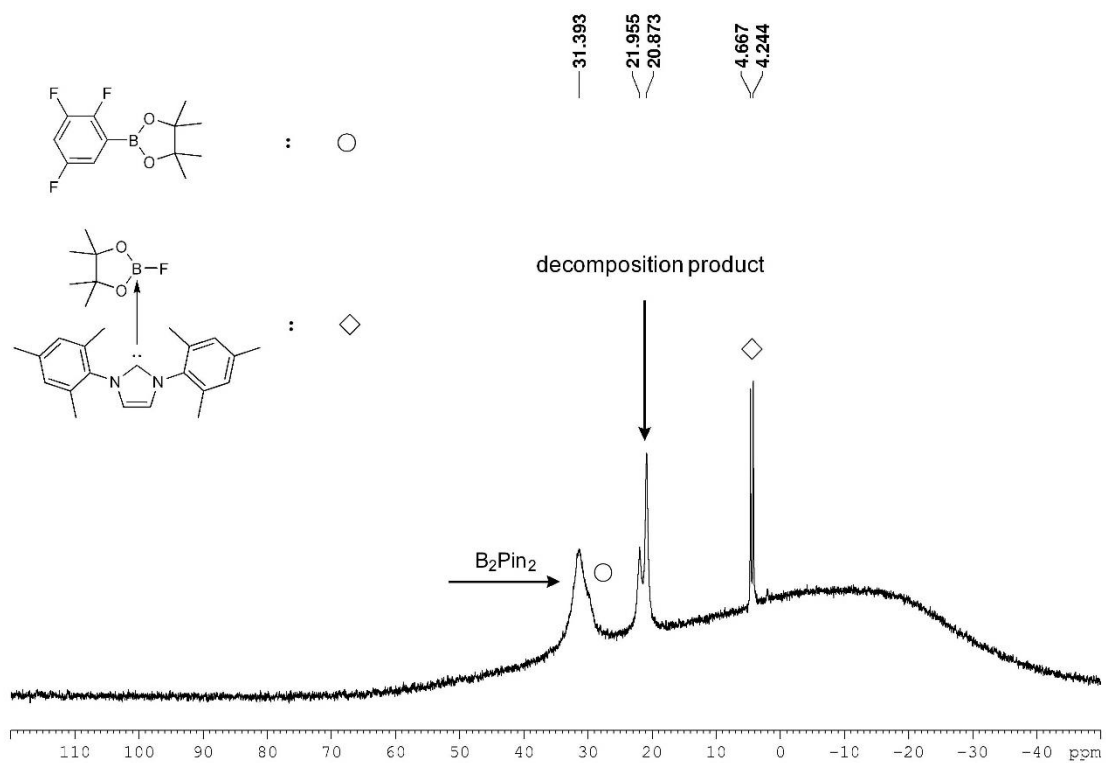


Figure 2-29.  $^{19}\text{F}$  NMR spectrum of aromatic region after 10 min in the dark (376 MHz,  $\text{C}_6\text{D}_6$ ).



**Figure 2-30.**  $^{19}\text{F}$  NMR spectrum of Ni-F resonance after 10 min in the dark (376 MHz,  $\text{C}_6\text{D}_6$ ).



**Figure 2-31.**  $^{11}\text{B}$  NMR spectrum after 10 min irradiation (128 MHz,  $\text{C}_6\text{D}_6$ ).

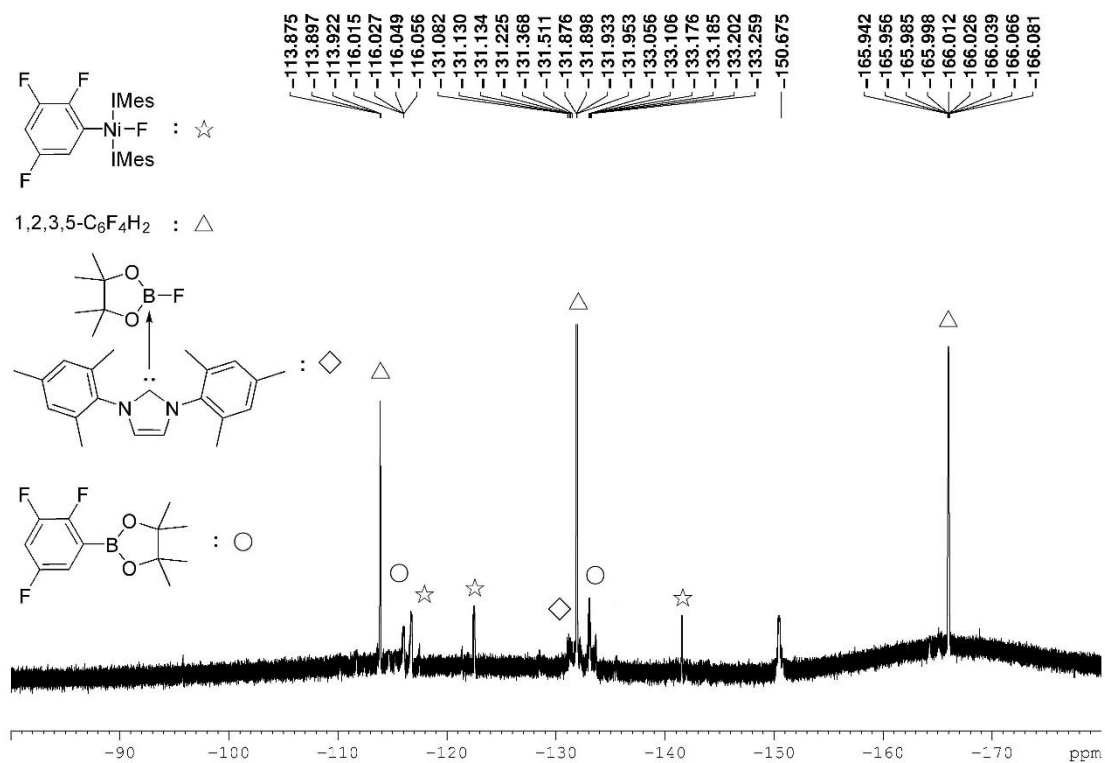


**Figure 2-32.**  $^{19}\text{F}$  NMR spectrum of aromatic region after 10 min irradiation (376 MHz,  $\text{C}_6\text{D}_6$ ).

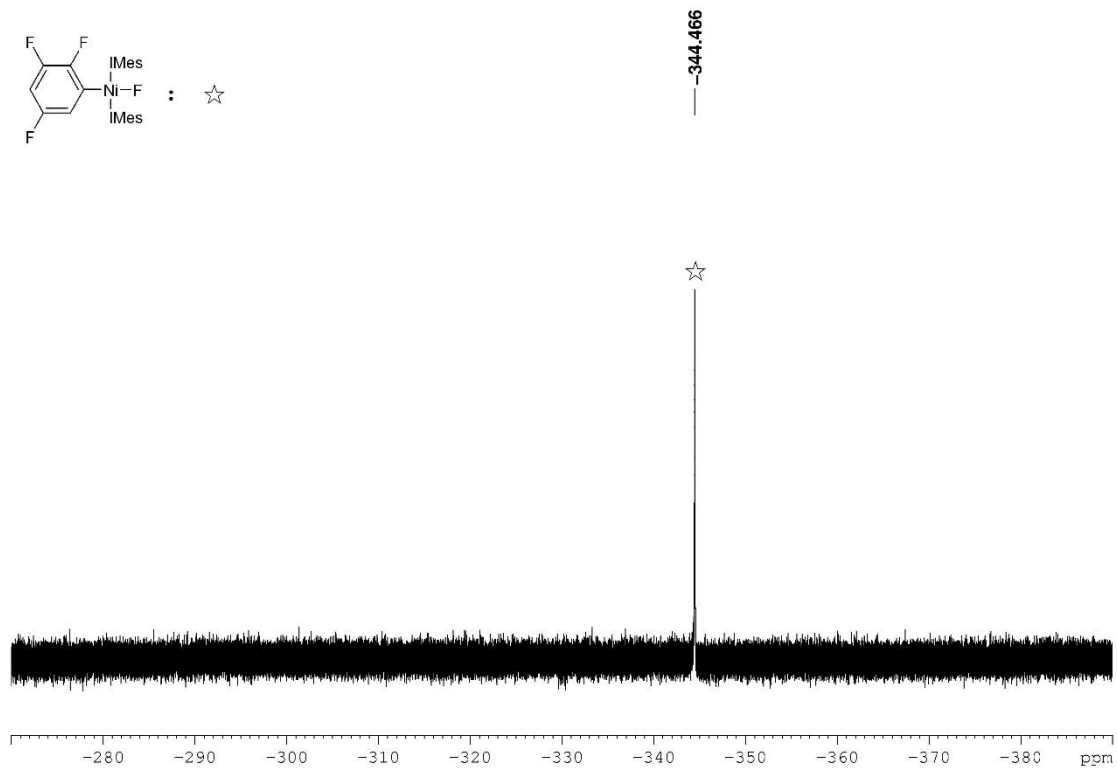
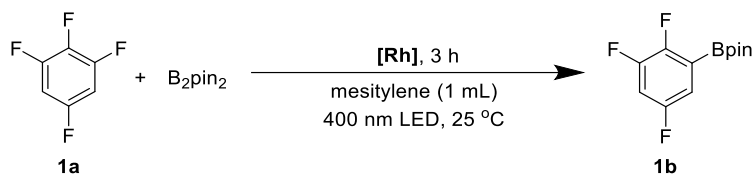


**Figure 2-33.**  $^{19}\text{F}$  NMR spectrum of Ni-F resonance after 10 min irradiation (376 MHz,  $\text{C}_6\text{D}_6$ ).

### 2.4.3 Control experiments for borylation of 1,2,3,5-tetrafluorobenzene

The photocatalytic borylation of **34a** with B<sub>2</sub>pin<sub>2</sub> using [Rh]/[Ni(IMes)<sub>2</sub>] in the presence of CsF was conducted for only 3 h, giving a 68% yield of **34b** (Table 2-6, entry 1) and, as observed for all other following *in situ* studies, FBpin. In another experiment, we first ensured that all [Ni(IMes)<sub>2</sub>] of the above mentioned reaction mixture reacted with **34a** in the dark to form [Ni<sup>II</sup>], which is quantitative within the few minutes it takes to record an NMR spectrum, and confirmed its stability towards the other reagents by leaving the solution in the dark for 3 h at room temperature. Then the system was irradiated for 3 h (Table 2-6, entry 2), giving a yield of **34b** that is identical, within experimental error, to that from the reaction with immediate irradiation (Table 2-6, entry 1). This suggests that the C-F bond oxidative addition product is a crucial intermediate for the photocatalytic borylation reaction, which is consistent with our previous report on the thermal process.<sup>126</sup>

**Table 2-6. Control experiments of photocatalytic borylation of 34a**



Entry	Ni <sup>0</sup> (mmol) <sup>a</sup>	[Ni <sup>II</sup> ] (mmol) <sup>b</sup>	[Rh] (mmol)	<b>34a</b> (mmol)	B <sub>2</sub> pin <sub>2</sub> (mmol)	CsF (mmol)	Yield ( <b>34b</b> , %) <sup>b</sup>
1	0.02	/	0.01	0.22	0.2	0.2	68
2 <sup>c</sup>	0.02	/	0.01	0.22	0.2	0.2	65
3	/	0.02	0.01	0.2	0.2	0.2	61
4	/	0.02	0.01	/	0.2	0.2	10
5	0.01	0.01	0.01	0.21	0.2	0.2	66
6	0.02	/	0.01	0.22	0.2	/	45
7 <sup>c</sup>	0.02	/	0.01	0.22	0.2	/	42
8	/	0.02	0.01	/	0.2	/	10
9	/	0.02	0.01	0.2	0.2	/	40
10	0.01	0.01	0.01	0.21	0.2	/	44

<sup>a</sup>Ni<sup>0</sup> = [Ni(IMes)<sub>2</sub>]. <sup>b</sup>The yields are based on B<sub>2</sub>pin<sub>2</sub> and were determined by GC-MS analysis vs. a calibrated internal standard and are averages of two runs. <sup>c</sup>The reaction was first stirred for 3 h in the dark and was then irradiated with a 400 nm-LED.

Further evidence is provided by using independently prepared **[Ni<sup>II</sup>]** as the catalyst instead of **[Ni(IMes)<sub>2</sub>]** under otherwise the same conditions, which gave a 61% conversion to **34b** (Table 2-6, entry 3). We note that when **[Ni<sup>II</sup>]** is employed (10 mol% with regard to **B<sub>2</sub>pin<sub>2</sub>**) together with **B<sub>2</sub>pin<sub>2</sub>**, **[Rh]** and CsF in the absence of substrate **34a**, the formation of borylation product **1b** in 10% yield is observed, indicating full stoichiometric conversion of the nickel(II) complex (Table 2-6, entry 4). The latter experiment provides important deeper insight because direct irradiation with 400 nm LEDs of stoichiometric amounts of the **[Ni<sup>II</sup>]** complex and **B<sub>2</sub>pin<sub>2</sub>** without **[Rh]** being present leads to decomposition (vide supra). This suggests that one of the directly accessible singlet excited states **S<sub>1</sub>** or **S<sub>2</sub>** of **[Ni<sup>II</sup>]** reacts with **B<sub>2</sub>pin<sub>2</sub>** with decomposition of the nickel(II) complex, whereas indirect excitation of the nickel(II) complex by triplet energy transfer (TET) from **<sup>3</sup>[Rh]** bypasses this decomposition pathway (Figure 2-19)!

When **[Ni(IMes)<sub>2</sub>]** and **[Ni<sup>II</sup>]** were employed simultaneously as catalyst precursors, we obtained the same conversion as with either of them alone (Table 2-6, entry 5). These results confirm that the photosensitized reaction of **[Ni<sup>II</sup>]** with **B<sub>2</sub>Pin<sub>2</sub>** regenerates a **Ni<sup>0</sup>** carbene species, either **[Ni(IMes)<sub>2</sub>]** or **[Ni(IMes)]**, which participates in the next catalytic cycle.

We tested the stability of **[Ni<sup>II</sup>]** in the presence of **[Rh]** in the dark and under irradiation with 400 nm LEDs. For this, **[Ni<sup>II</sup>]** (0.02 mmol, 16.4 mg) and the rhodium biphenyl complex (0.01 mmol, 7.6 mg) were dissolved in 0.7 mL **C<sub>6</sub>D<sub>6</sub>** in a Young's tap NMR tube, and the <sup>1</sup>H-, <sup>19</sup>F-, and <sup>31</sup>P-NMR spectra were immediately recorded in the dark. No decomposition was observed. Then the NMR tube was placed between two LEDs for 1 h and investigated by NMR spectroscopy. Again, no reaction between the two metal complexes could be observed.

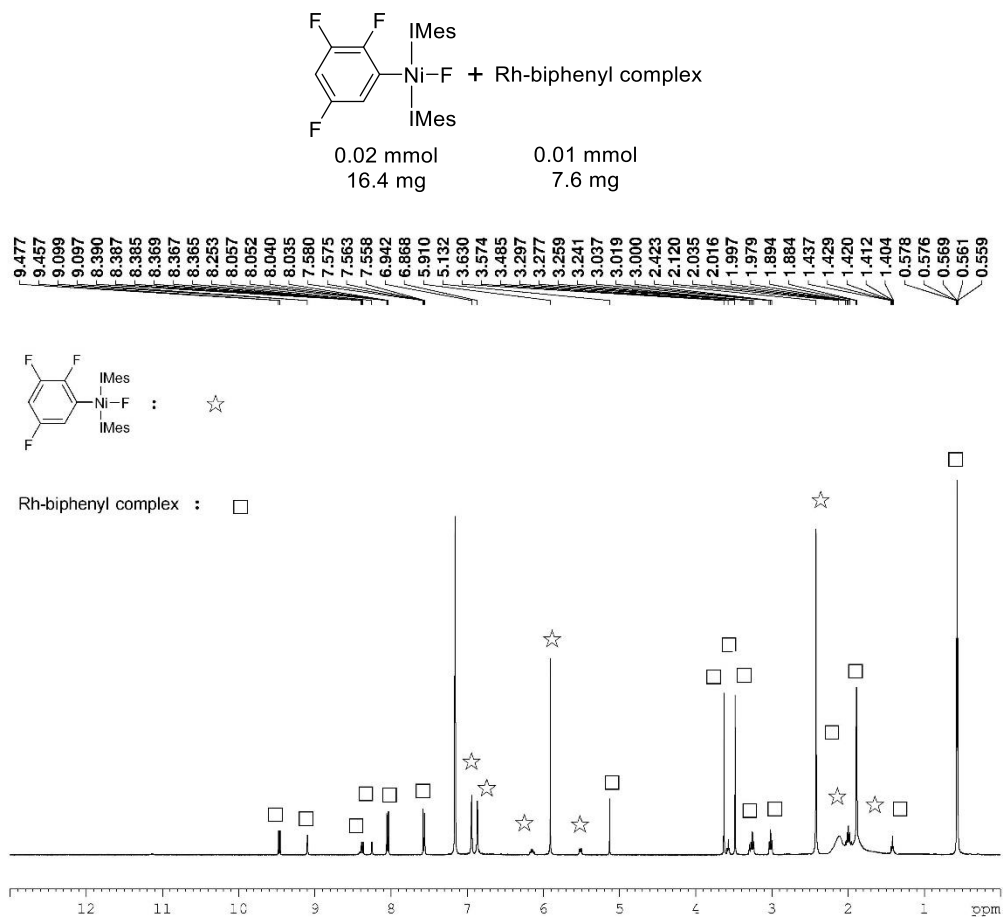


Figure 2-34.  $^1\text{H}$  NMR spectrum in the dark (400 MHz,  $\text{C}_6\text{D}_6$ ).

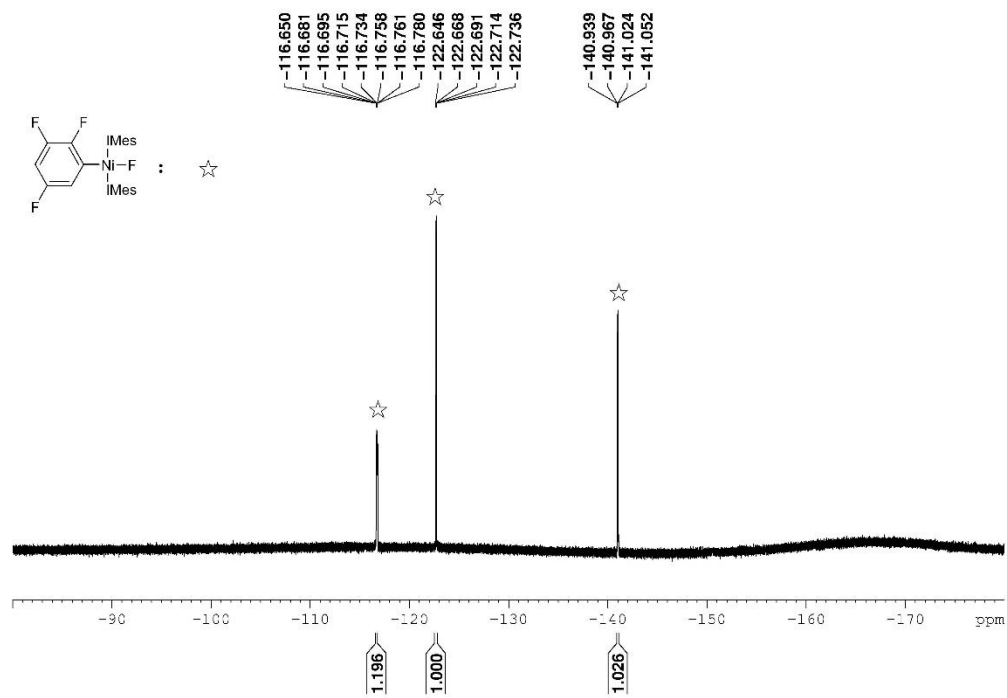
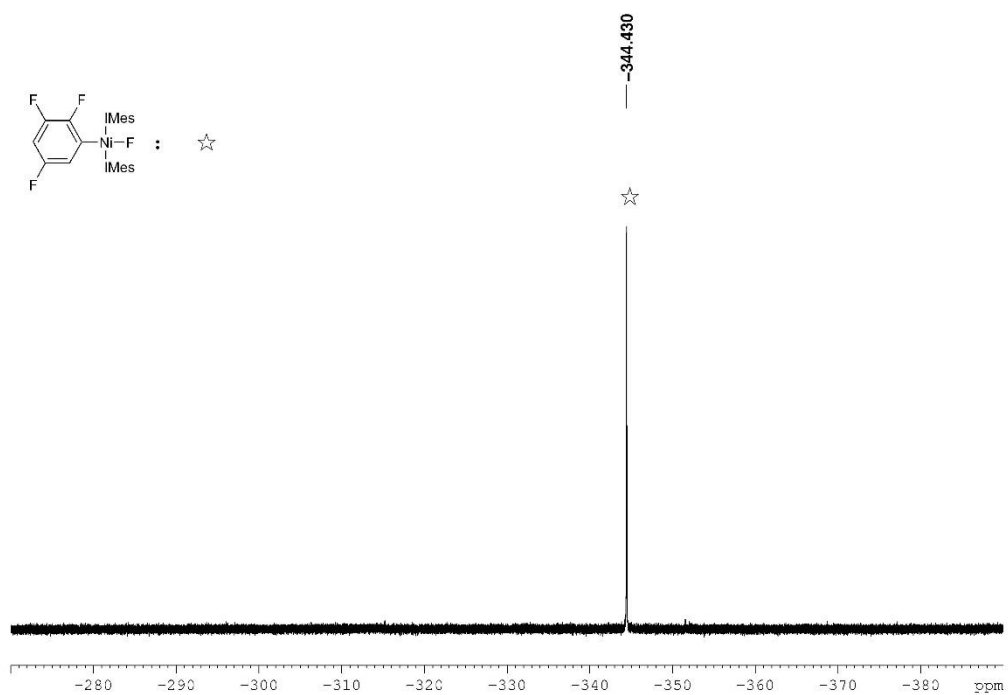
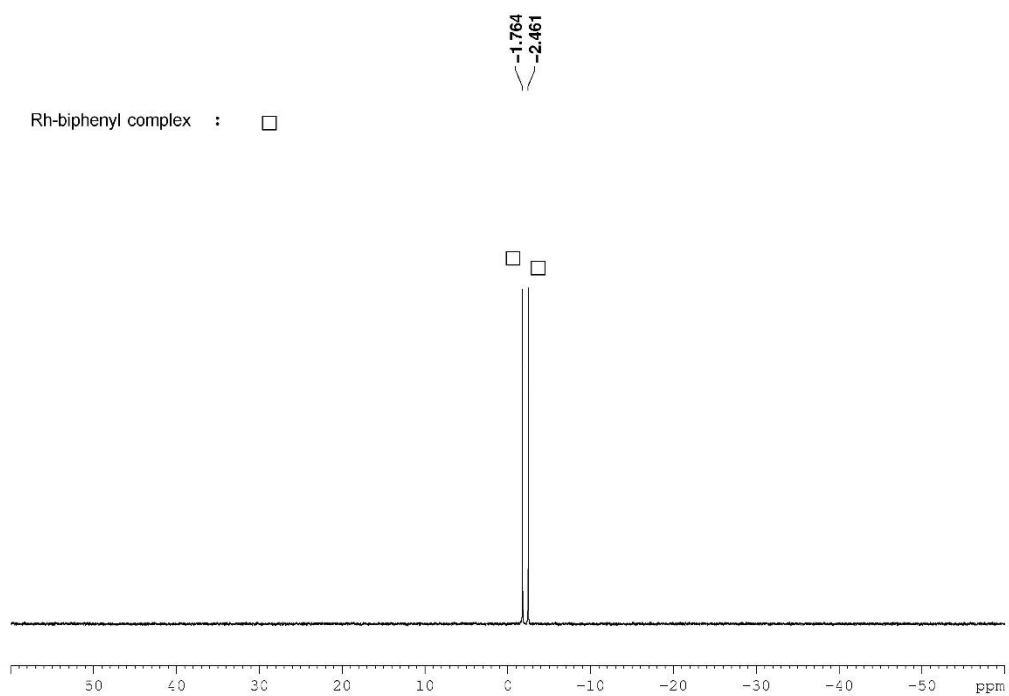


Figure 2-35.  $^{19}\text{F}$  NMR spectrum of aromatic region in the dark (376 MHz,  $\text{C}_6\text{D}_6$ ).



**Figure 2-36.**  $^{19}\text{F}$  NMR spectrum of Ni-F resonance in the dark (376 MHz,  $\text{C}_6\text{D}_6$ ).



**Figure 2-37.**  $^{31}\text{P}$  NMR spectrum in the dark (162 MHz,  $\text{C}_6\text{D}_6$ ).

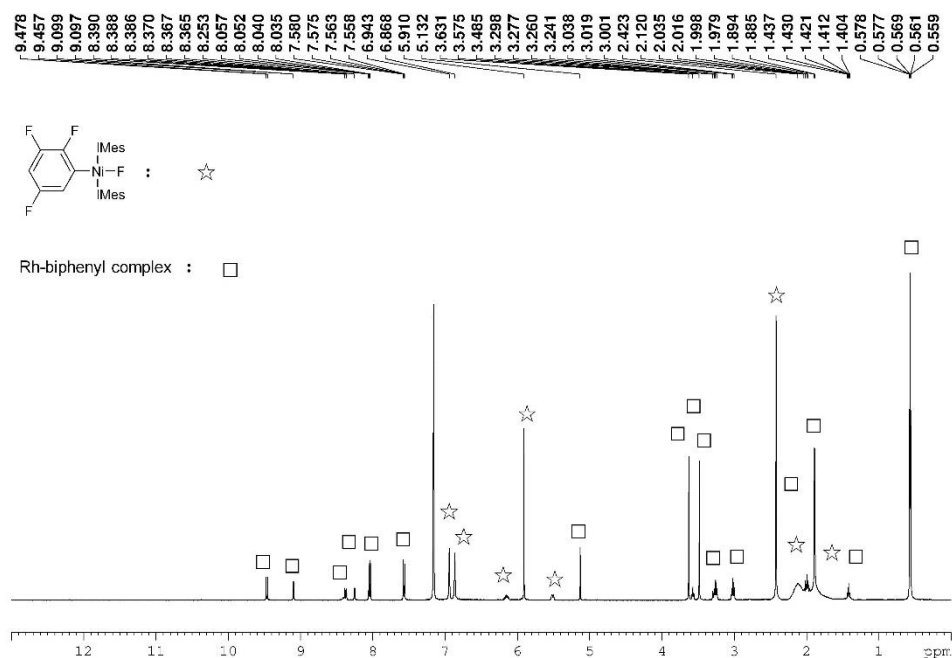
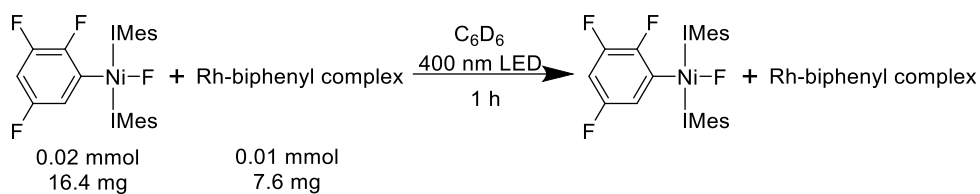


**Figure 2-38.**  $^1\text{H}$  NMR spectrum after 1 h irradiation (400 MHz,  $\text{C}_6\text{D}_6$ ).

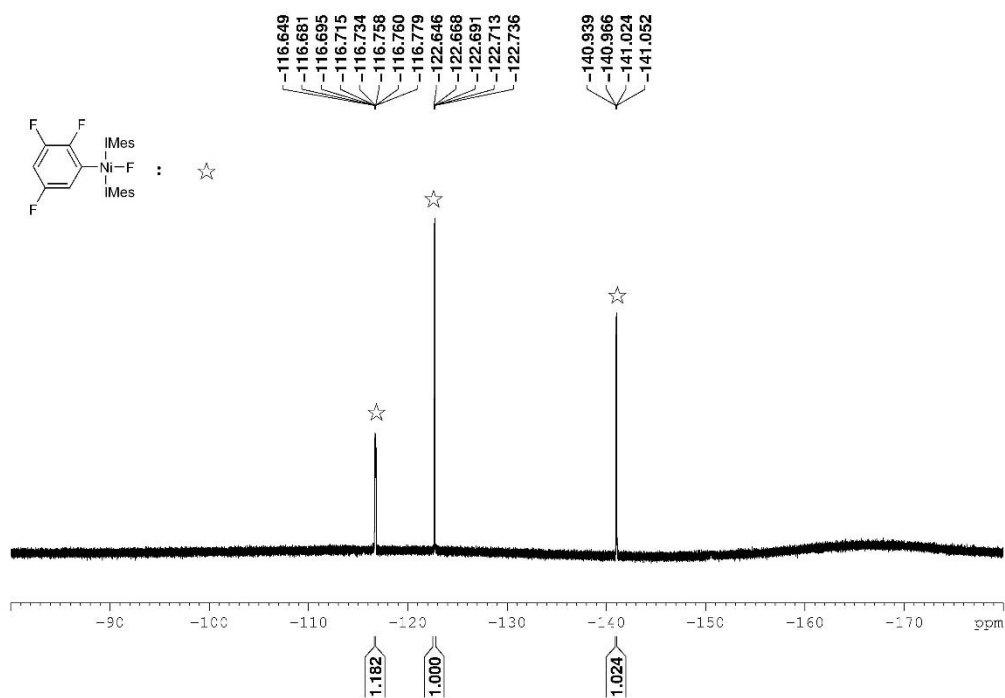


**Figure 2-39.**  $^{19}\text{F}$  NMR spectrum of aromatic region after 1 h irradiation (376 MHz,  $\text{C}_6\text{D}_6$ ).



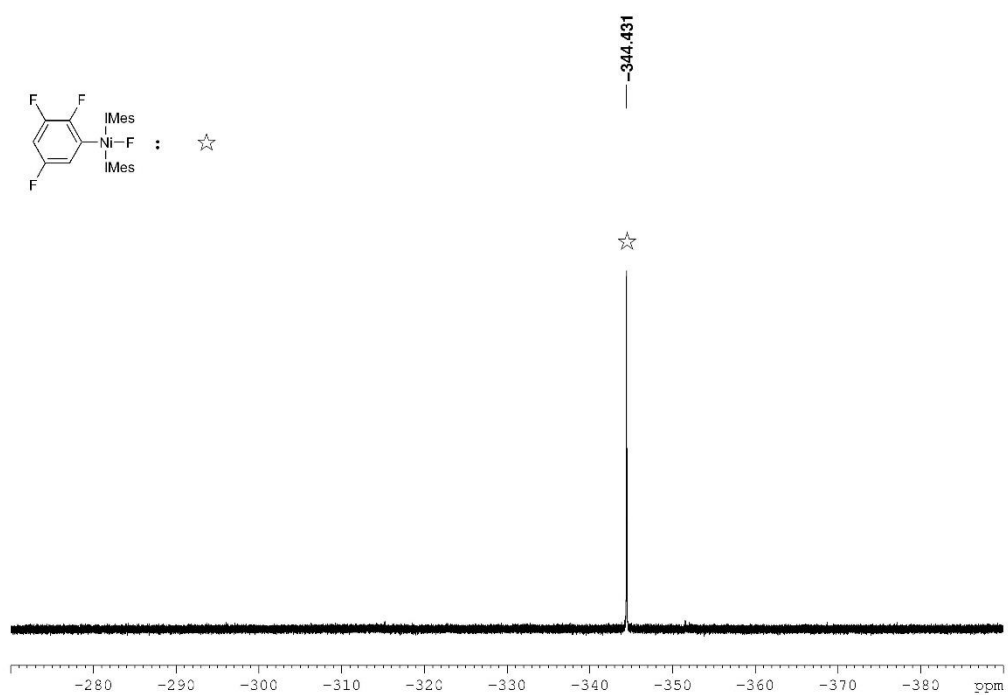


**Figure 2-40.** <sup>19</sup>F NMR spectrum of Ni-F resonance after 1 h irradiation (376 MHz, C<sub>6</sub>D<sub>6</sub>).

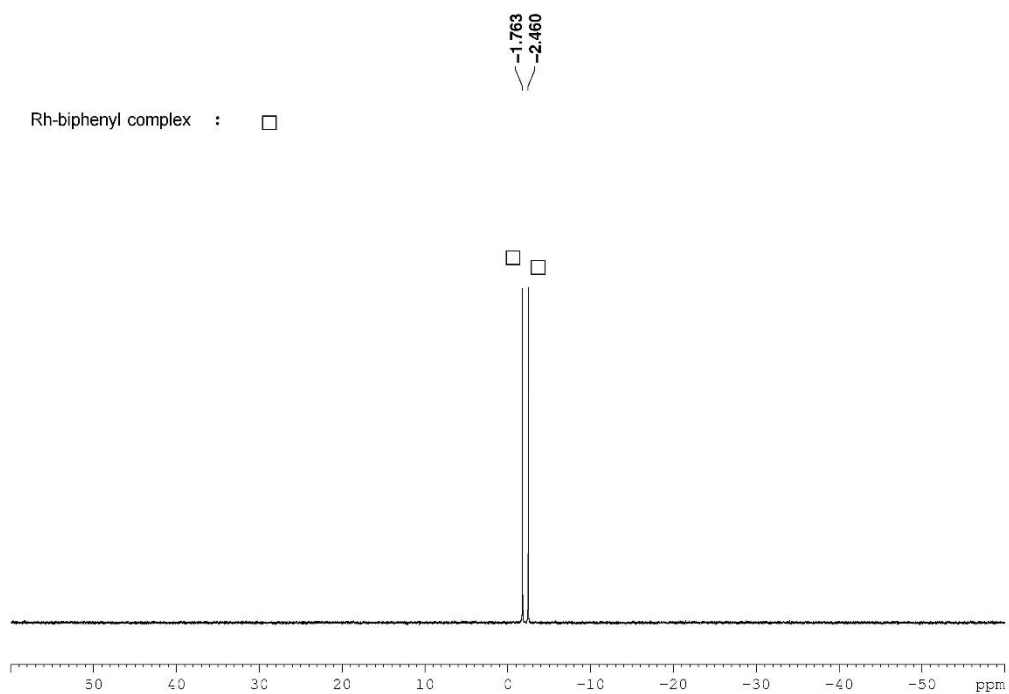


**Figure 2-41.** <sup>31</sup>P NMR spectrum after 1 h irradiation (162 MHz, C<sub>6</sub>D<sub>6</sub>).

We then added 0.22 mmol (33.4 mg) of 1,2,3,5-tetrafluorobenzene (**34a**) into the reaction mixture of  $[\text{Ni}^{\text{II}}]$  (0.02 mmol, 16.4 mg) and the rhodium biphenyl complex (0.01 mmol, 7.6 mg) in 0.7 mL  $\text{C}_6\text{D}_6$  in a Young's tap NMR tube and recorded the  $^1\text{H}$ -,  $^{19}\text{F}$ -, and  $^{31}\text{P}$ -NMR spectra in the dark as well as after 1 h of irradiation with 400 nm LEDs. No reaction was observed in each case.

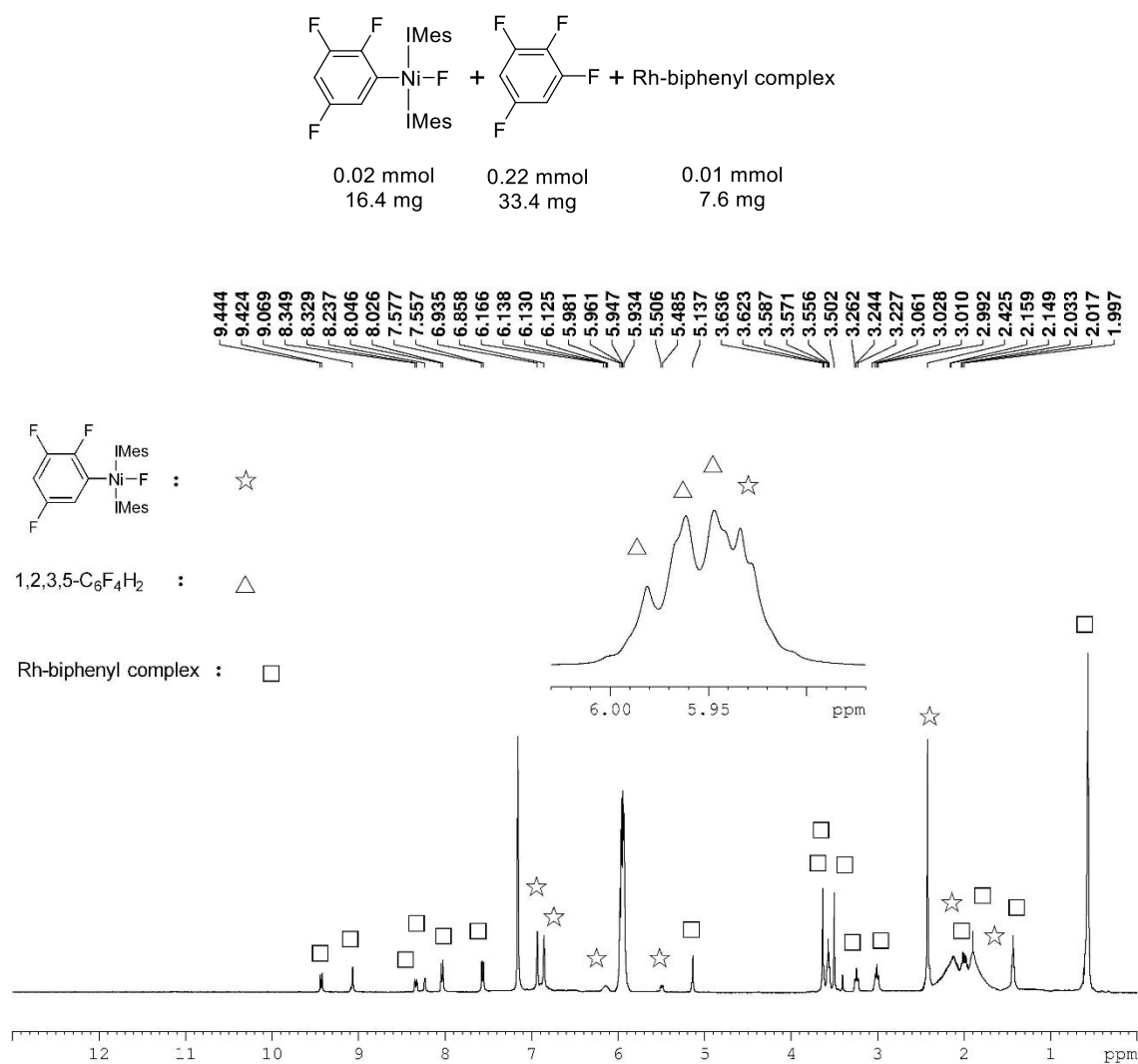


**Figure 2-42.**  $^1\text{H}$  NMR spectrum in the dark (400 MHz,  $\text{C}_6\text{D}_6$ ).

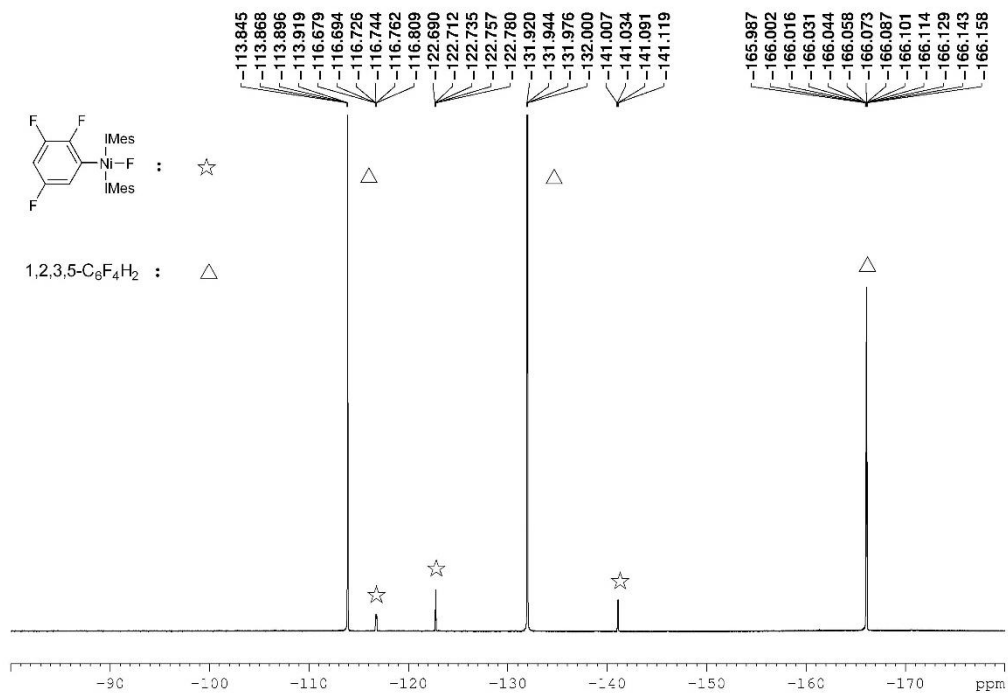


**Figure 2-43.**  $^{19}\text{F}$  NMR spectrum of aromatic region in the dark (376 MHz,  $\text{C}_6\text{D}_6$ ).

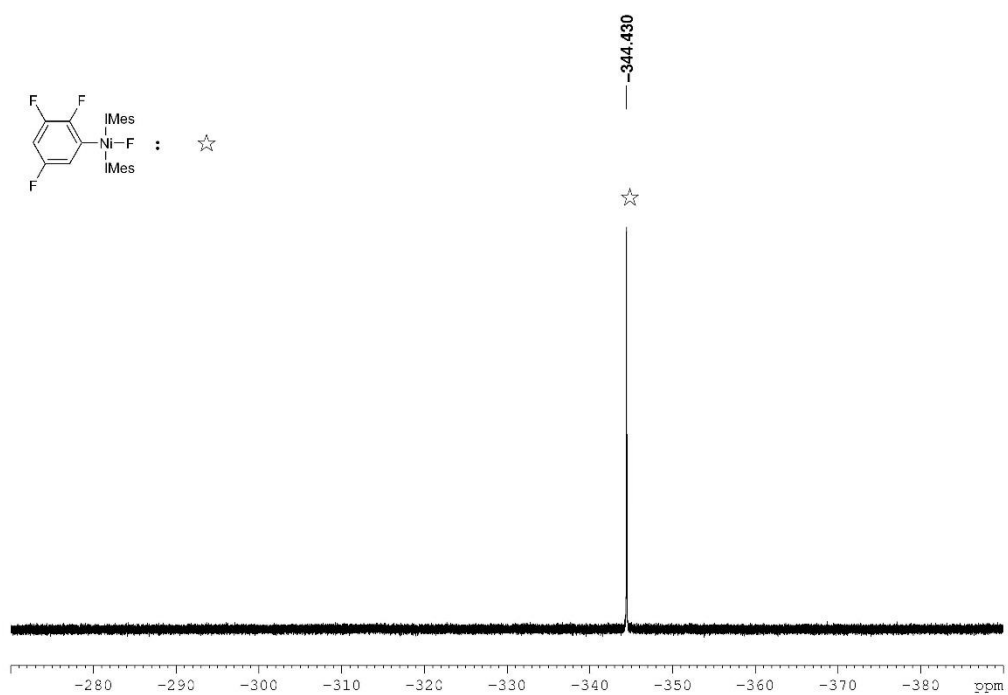


**Figure 2-44.**  $^{19}\text{F}$  NMR spectrum of Ni-F resonance in the dark (376 MHz,  $\text{C}_6\text{D}_6$ ).

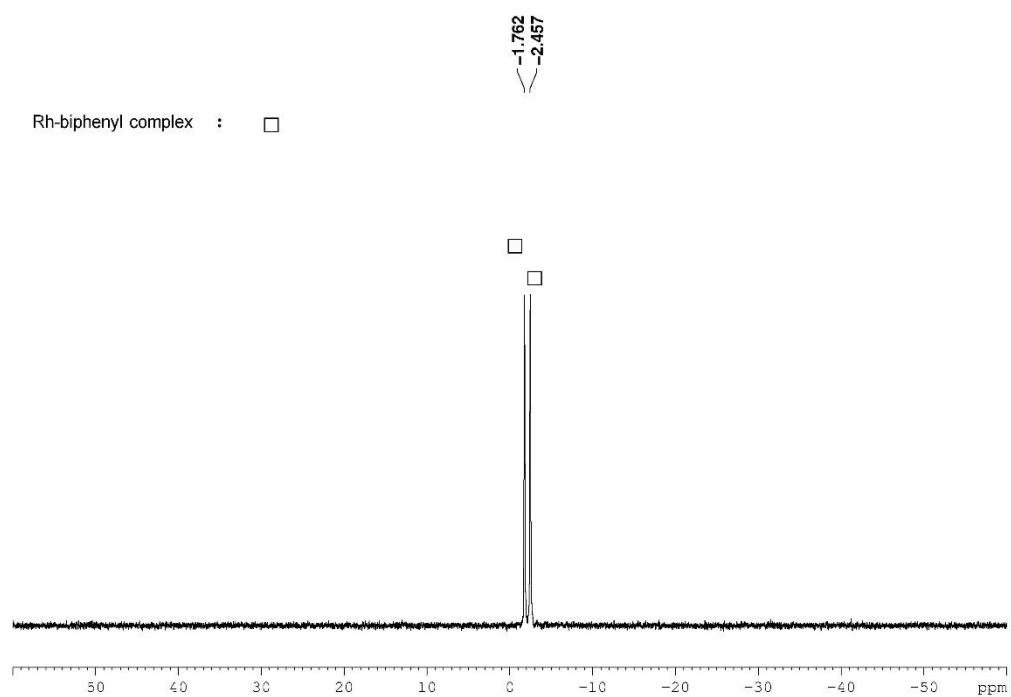


**Figure 2-45.**  $^{31}\text{P}$  NMR spectrum in the dark (162 MHz,  $\text{C}_6\text{D}_6$ ).

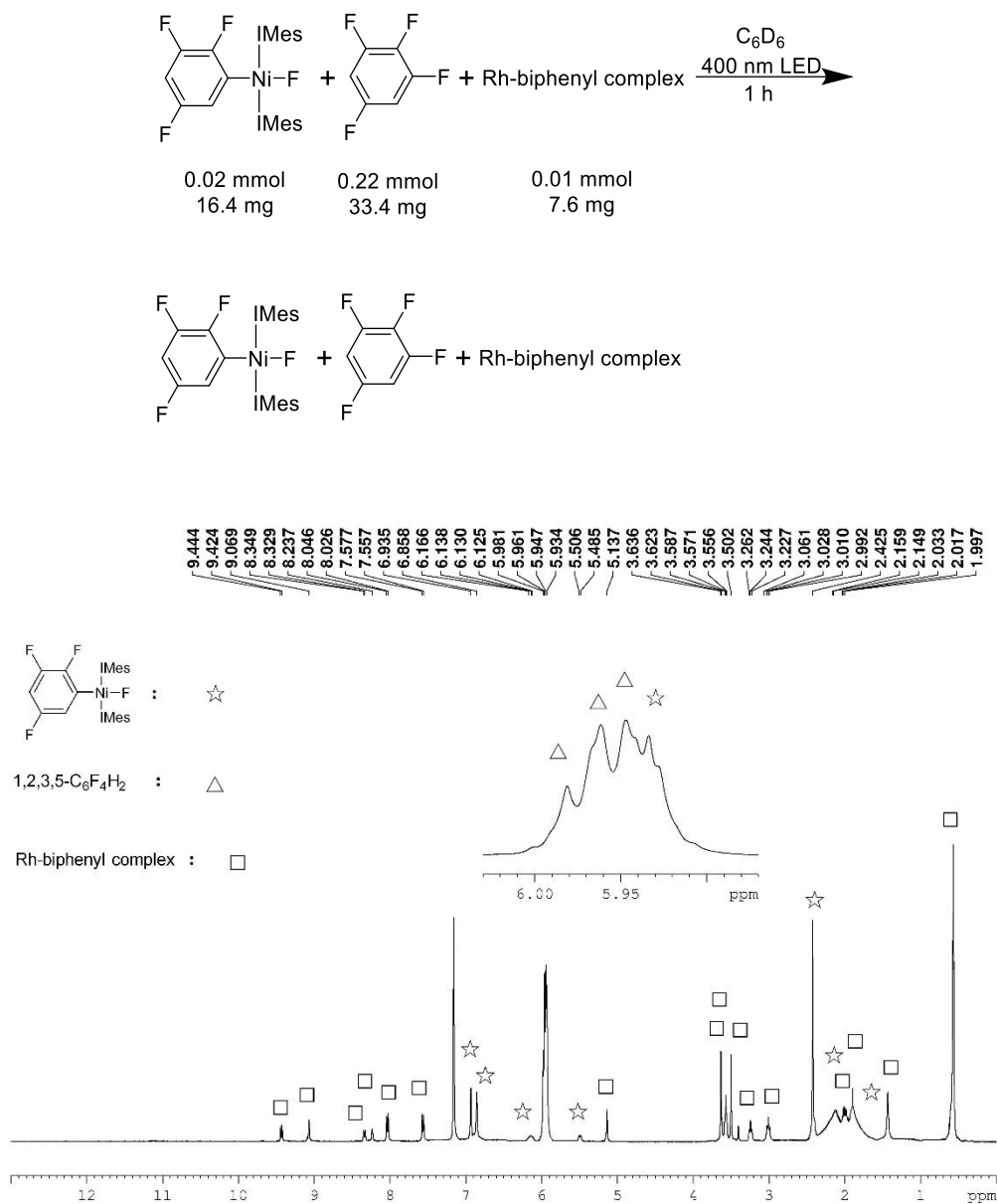


**Figure 2-46.** <sup>1</sup>H NMR spectrum after 1 h irradiation (400 MHz, C<sub>6</sub>D<sub>6</sub>).

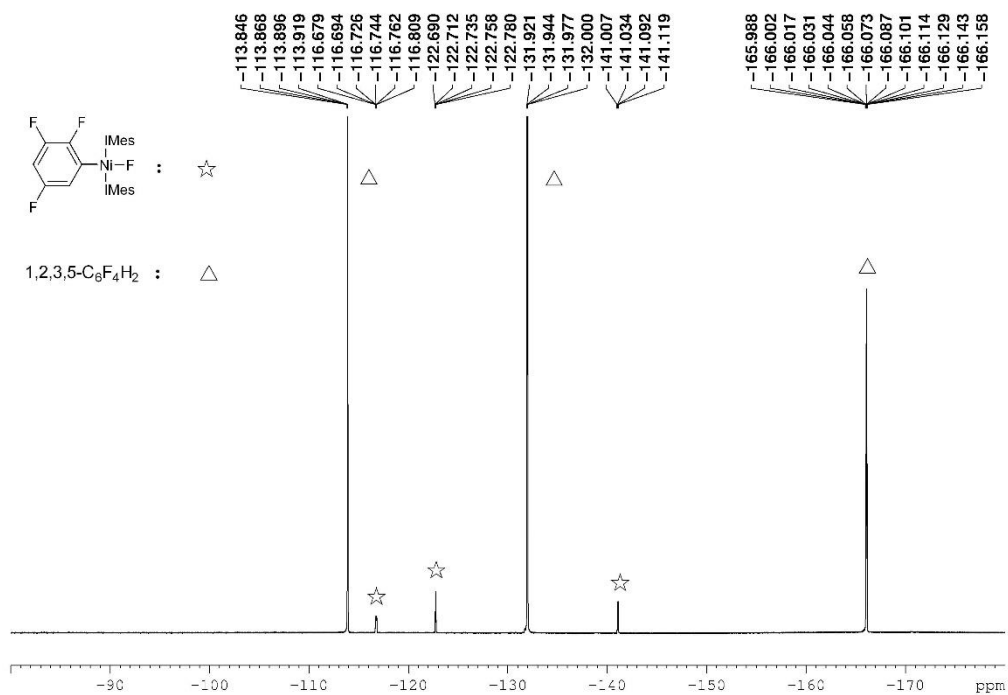


Figure 2-47.  $^{19}\text{F}$  NMR spectrum of aromatic region after 1 h irradiation (376 MHz,  $\text{C}_6\text{D}_6$ ).

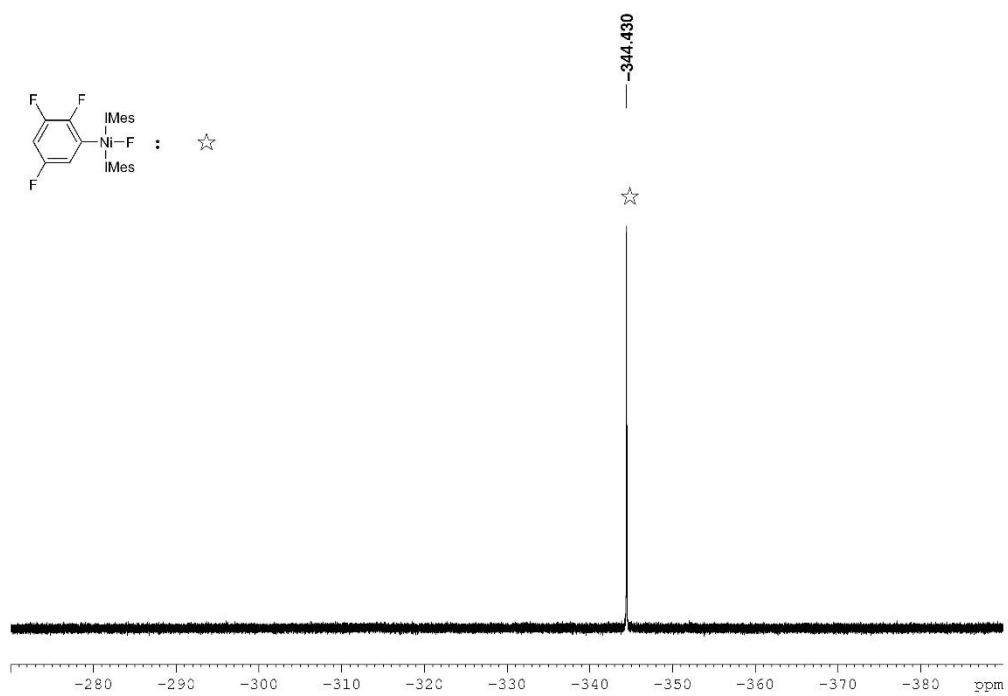
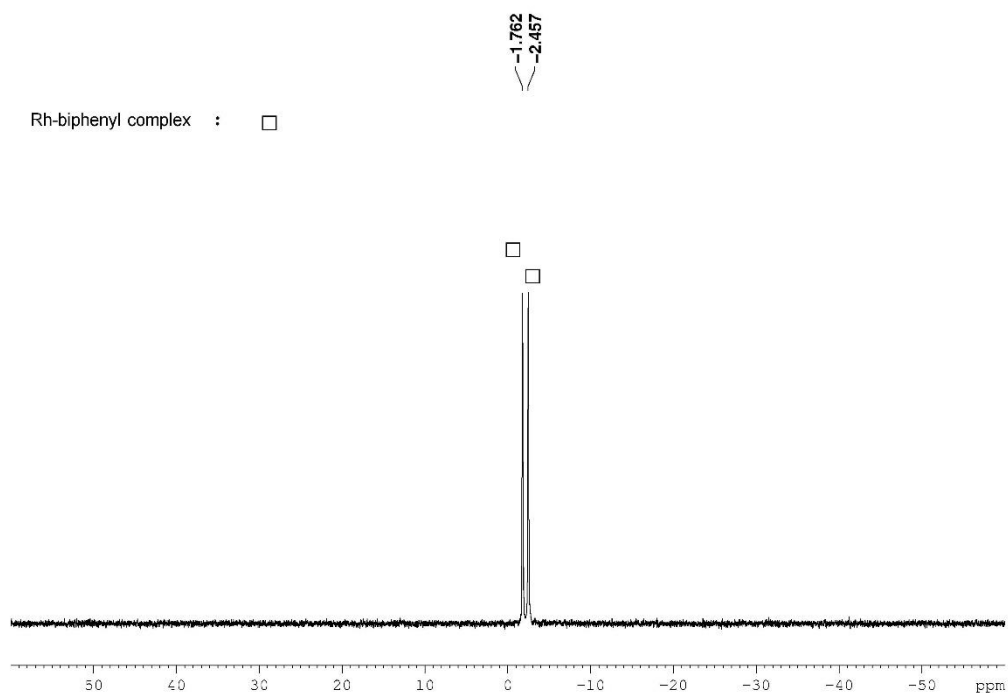
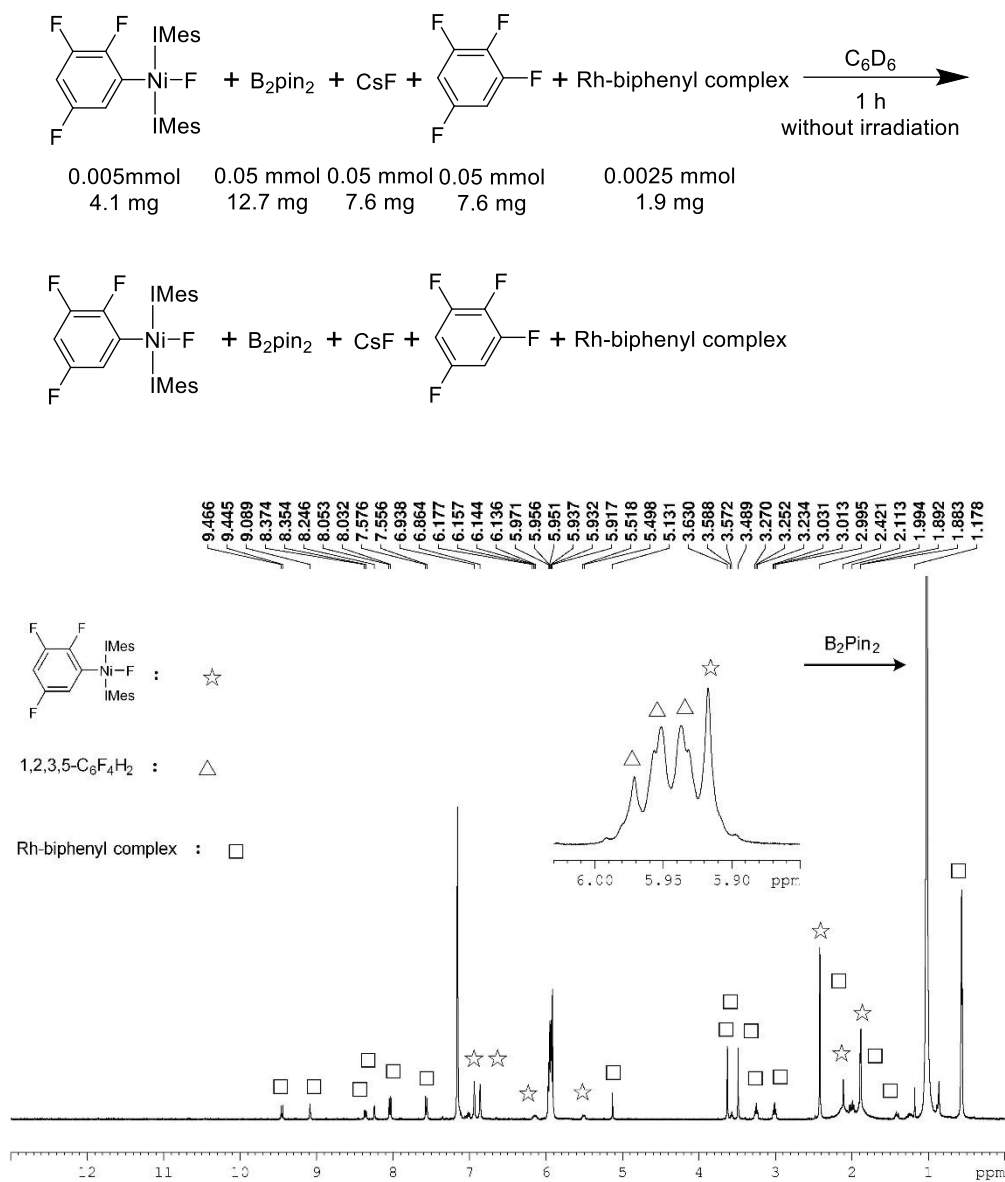


Figure 2-48.  $^{19}\text{F}$  NMR spectrum of Ni-F resonance after 1 h irradiation (376 MHz,  $\text{C}_6\text{D}_6$ ).



**Figure 2-49.**  $^{31}\text{P}$  NMR spectrum after 1 h irradiation (162 MHz,  $\text{C}_6\text{D}_6$ ).

In order to test whether  $[\text{Ni}^{\text{II}}]$  is an intermediate in the photocatalytic borylation of polyfluoroarenes, a mixture of  $\text{B}_2\text{pin}_2$  (0.05 mmol, 12.7 mg), 1,2,3,5-tetrafluorobenzene (0.05 mmol, 7.6 mg, 1 eq.),  $\text{CsF}$  (0.05 mmol, 7.6 mg, 1 eq.),  $[\text{Ni}^{\text{II}}]$  (0.005 mmol, 4.1 mg, 10 mol%) and  $[\text{Rh}]$  (0.0025 mmol, 1.9 mg, 5 mol%) was suspended in 0.7 mL  $\text{C}_6\text{D}_6$  in a Young's tap NMR tube. Then the mixture was studied by NMR spectroscopy after 1 h in the dark, which revealed no reactivity, and upon irradiation at 400 nm with LEDs for 1 h, showing significant borylation product.



**Figure 2-50.** <sup>1</sup>H NMR spectrum after 1 h in the dark (400 MHz, C<sub>6</sub>D<sub>6</sub>).



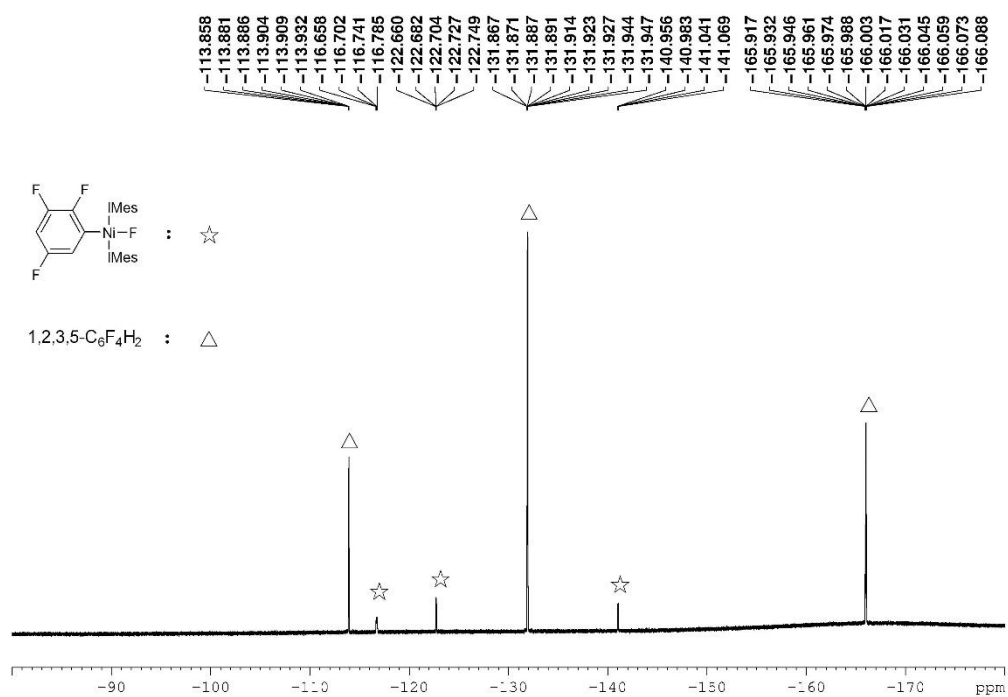


Figure 2-51.  $^{19}\text{F}$  NMR spectrum of aromatic region after 1 h in the dark (376 MHz,  $\text{C}_6\text{D}_6$ ).

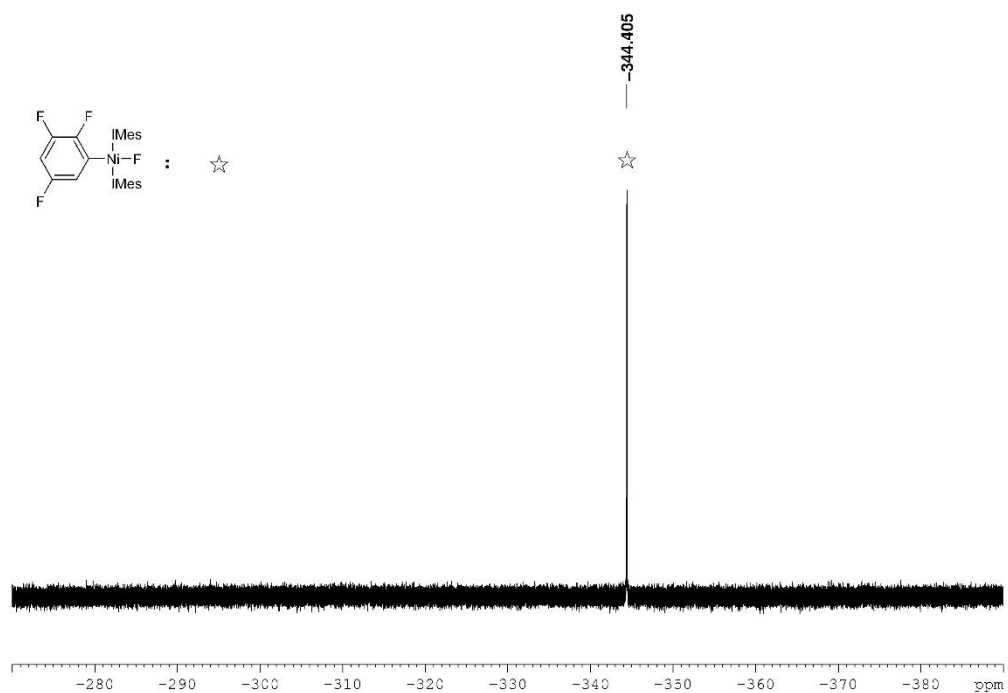
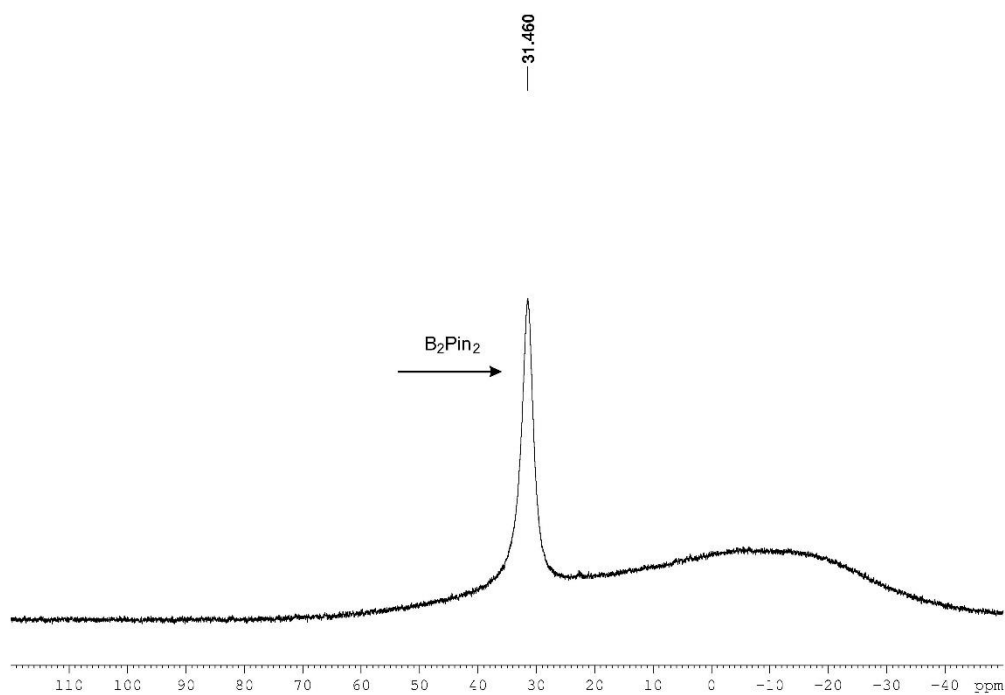
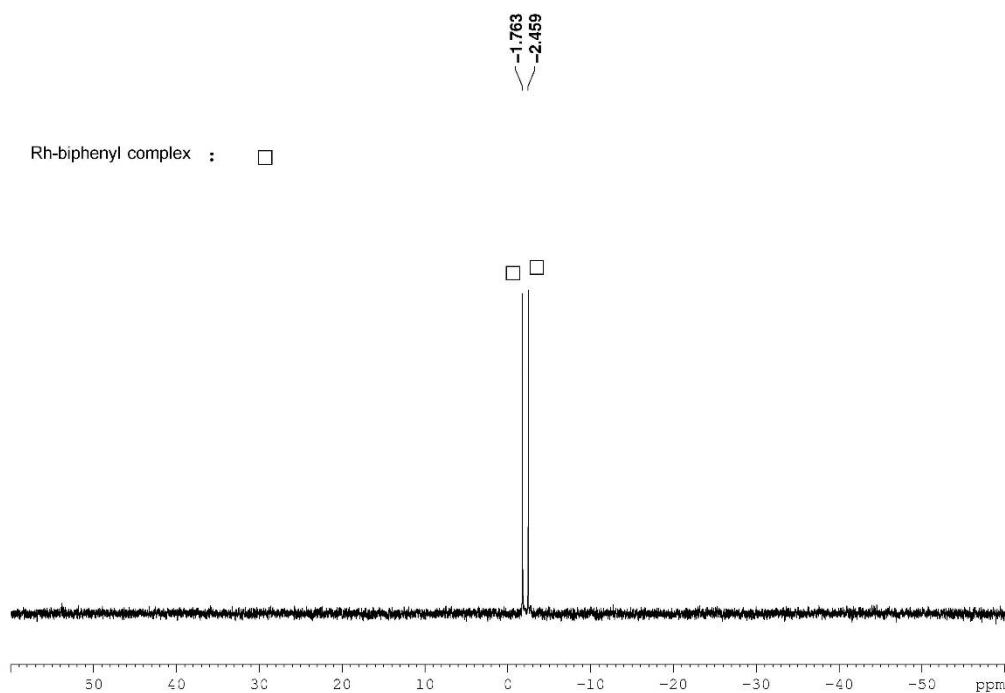


Figure 2-52.  $^{19}\text{F}$  NMR spectrum of Ni-F resonance after 1 h in the dark (376 MHz,  $\text{C}_6\text{D}_6$ ).



**Figure 2-53.**  $^{11}\text{B}$  NMR spectrum after 1 h in the dark (128 MHz,  $\text{C}_6\text{D}_6$ ).



**Figure 2-54.**  $^{31}\text{P}$  NMR spectrum after 1 h in the dark (162 MHz,  $\text{C}_6\text{D}_6$ ).

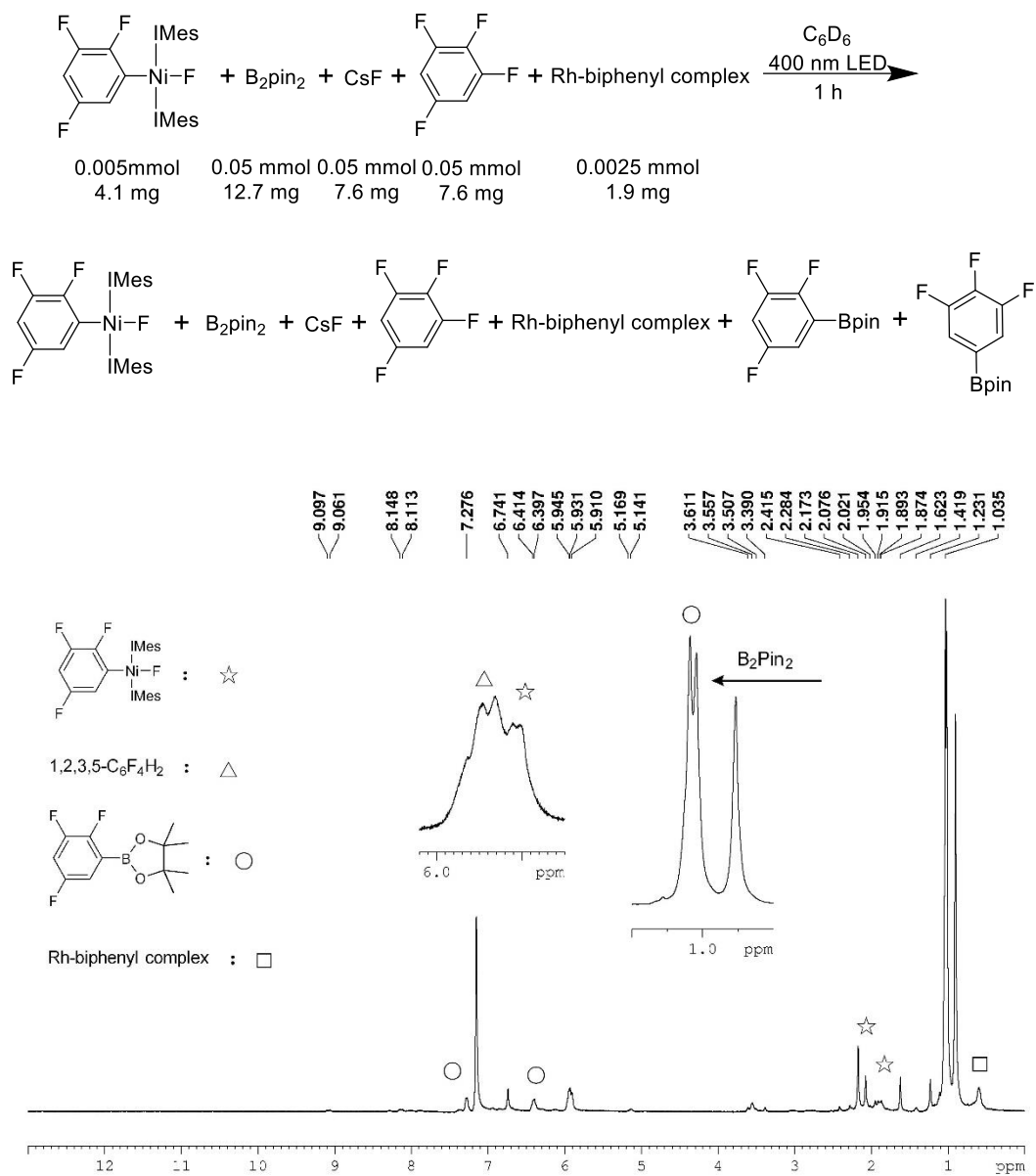


**Figure 2-55.** <sup>1</sup>H NMR spectrum after 1 h irradiation (400 MHz, C<sub>6</sub>D<sub>6</sub>).

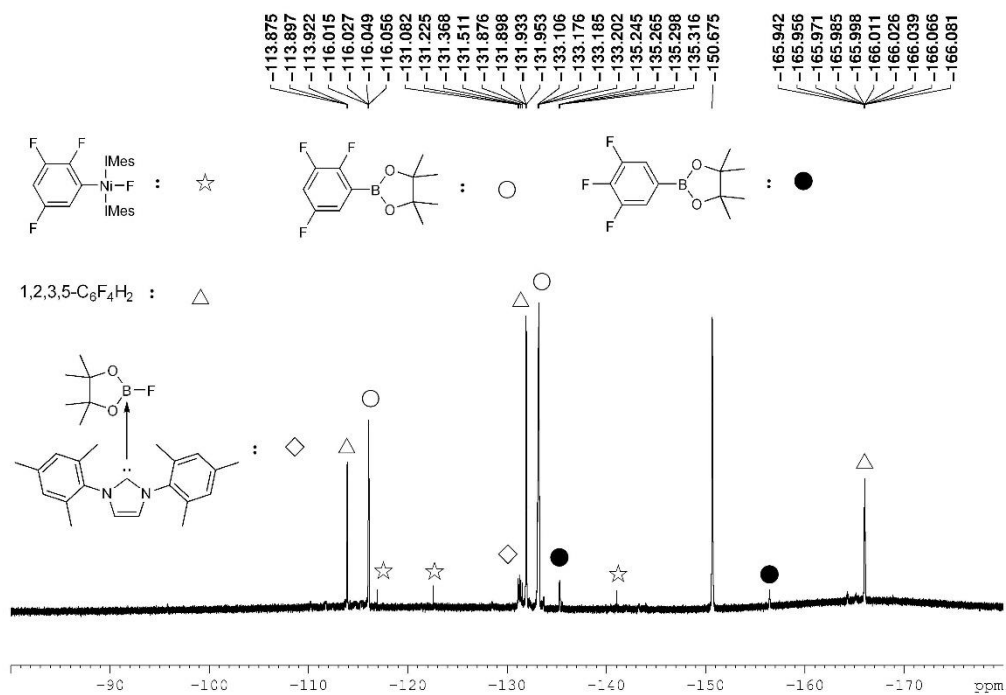


**Figure 2-56.**  $^{19}\text{F}$  NMR spectrum of aromatic region after 1 h irradiation (376 MHz,  $\text{C}_6\text{D}_6$ ).

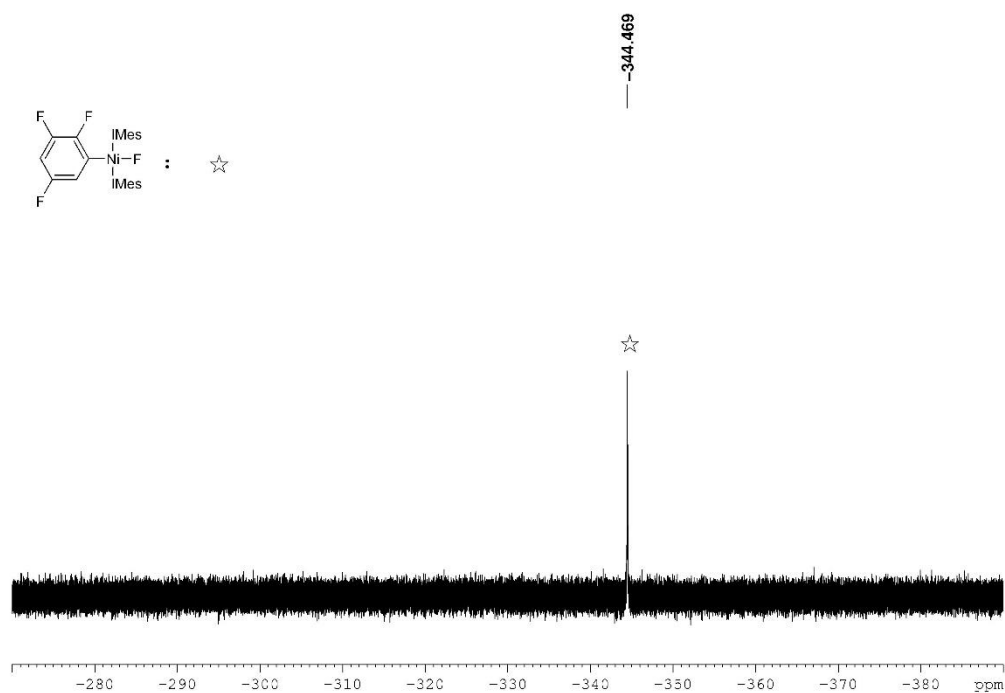


**Figure 2-57.**  $^{19}\text{F}$  NMR spectrum of Ni-F resonance after 1 h irradiation (376 MHz,  $\text{C}_6\text{D}_6$ ).

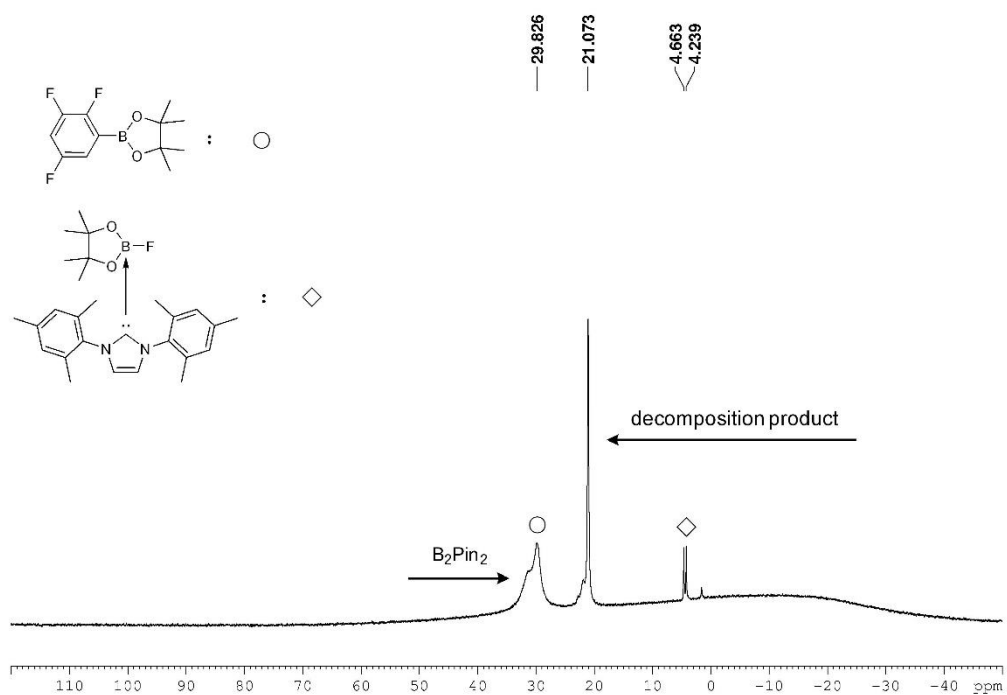


Figure 2-58.  $^{11}\text{B}$  NMR spectrum after 1 h irradiation (128 MHz,  $\text{C}_6\text{D}_6$ ).

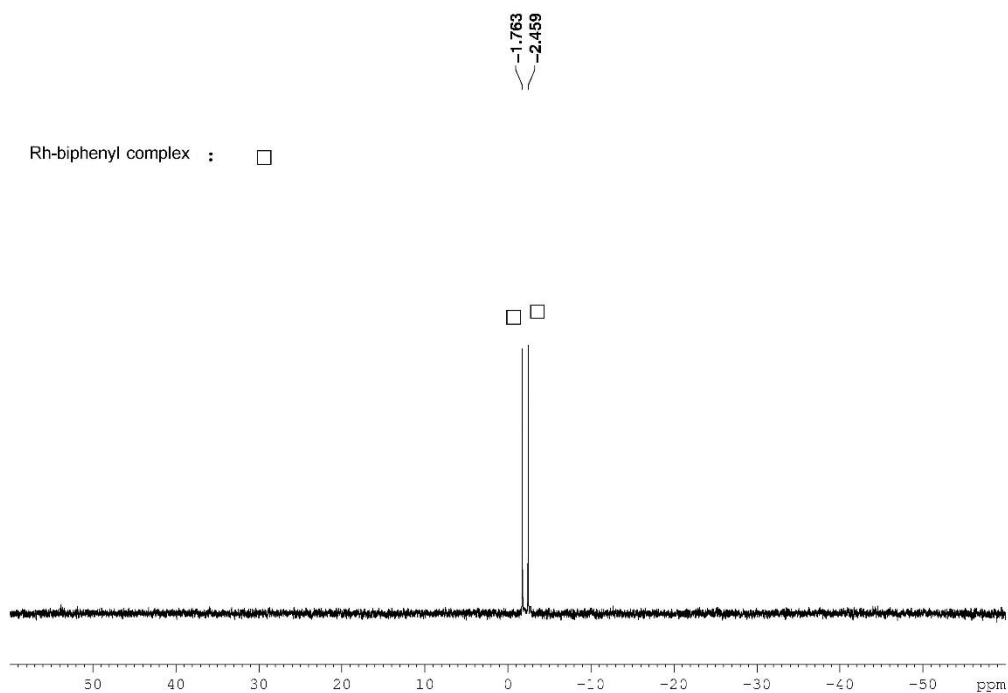
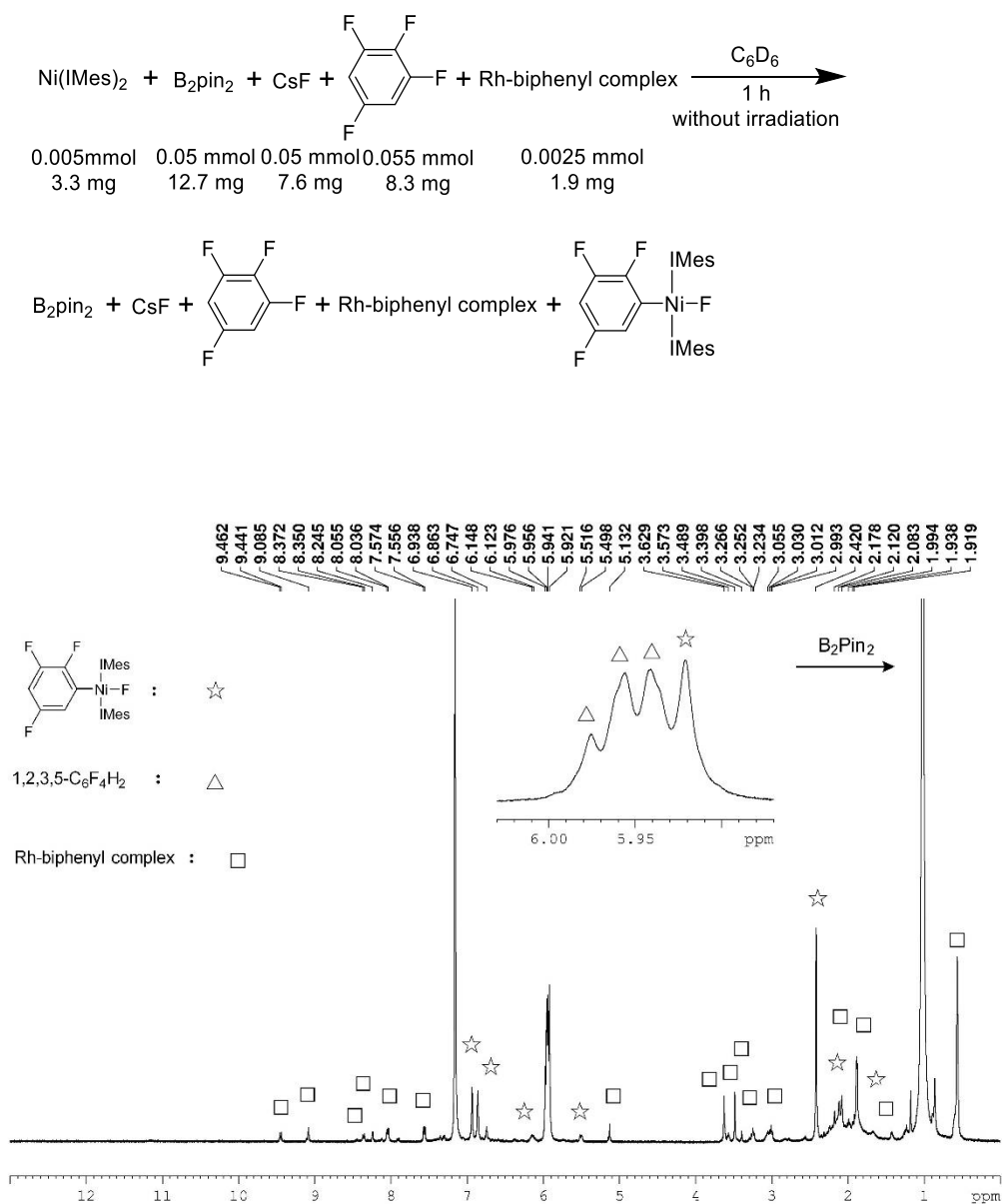
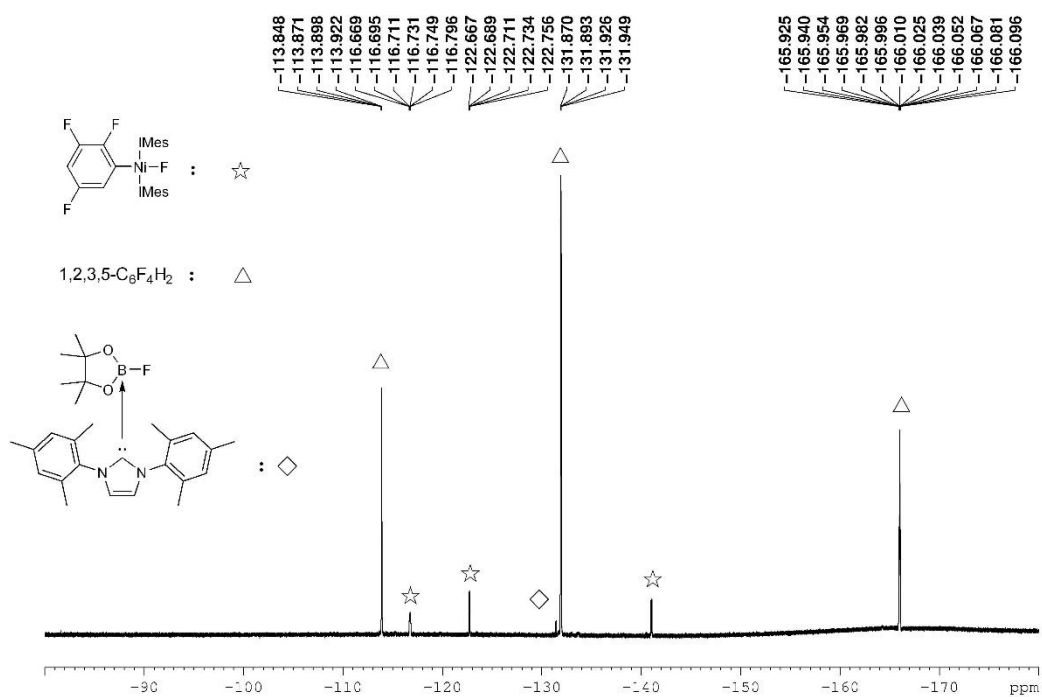


Figure 2-59.  $^{31}\text{P}$  NMR spectrum after 1 h irradiation (162 MHz,  $\text{C}_6\text{D}_6$ ).

To test the catalytic reactivity of  $[\text{Ni}(\text{IMes})_2]$ , a mixture of  $\text{B}_2\text{pin}_2$  (0.05 mmol, 12.7 mg), 1,2,3,5-tetrafluorobenzene (0.005 mmol, 8.3 mg, 1.1 eq.),  $\text{CsF}$  (0.05 mmol, 7.6 mg, 1 eq.),  $[\text{Ni}(\text{IMes})_2]$  (0.005 mmol, 3.3 mg, 10 mol%) and Rh biphenyl complex (0.0025 mmol, 1.9 mg, 5 mol%) was suspended in 0.7 mL  $\text{C}_6\text{D}_6$  in a Young's tap NMR tube. Then the mixture was studied by NMR spectroscopy after 1 h in the dark, which revealed only the formation of  $[\text{Ni}^{\text{II}}]$ ; however, upon irradiation at 400 nm with LEDs for 1 h, it showed significant borylation product and the presence of  $[\text{Ni}^{\text{III}}]$ .



**Figure 2-60.**  $^1\text{H}$  NMR spectrum after 1 h in the dark (400 MHz,  $\text{C}_6\text{D}_6$ ).



**Figure 2-61.**  $^{19}\text{F}$  NMR spectrum of aromatic region after 1 h in the dark (376 MHz,  $\text{C}_6\text{D}_6$ ).

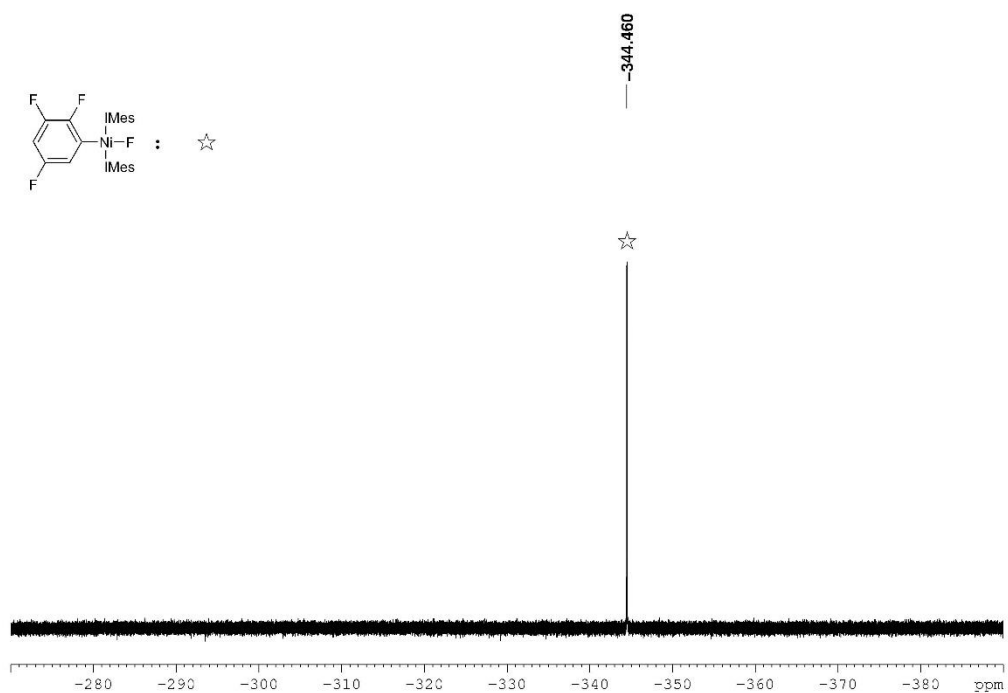


**Figure 2-62.**  $^{19}\text{F}$  NMR spectrum of Ni-F resonance after 1 h in the dark (376 MHz,  $\text{C}_6\text{D}_6$ ).

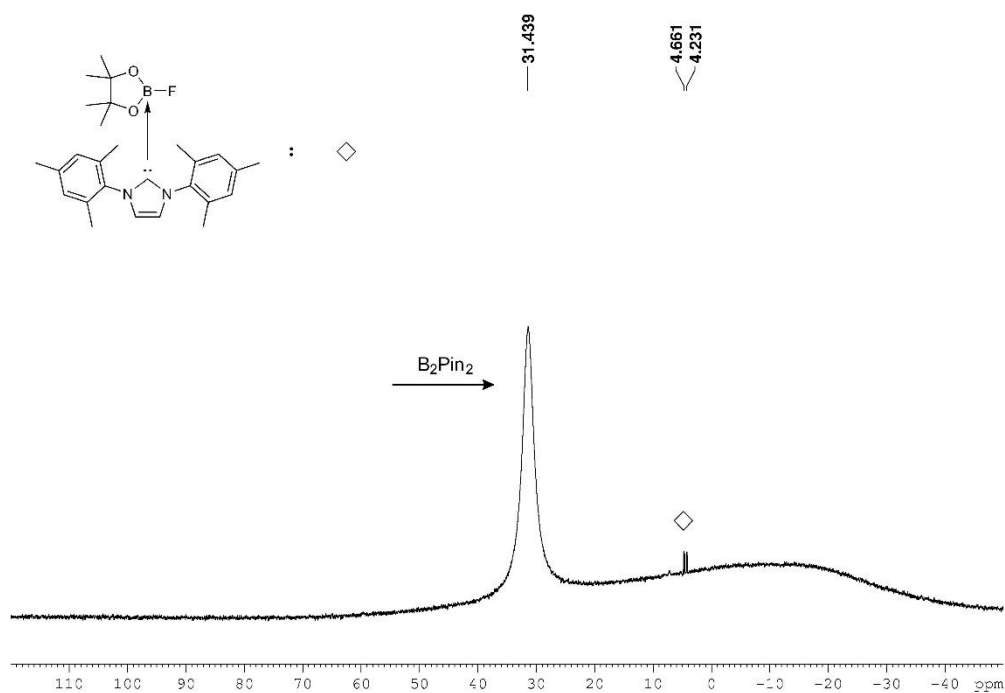


**Figure 2-63.** <sup>11</sup>B NMR spectrum after 1 h in the dark (128 MHz, C<sub>6</sub>D<sub>6</sub>).

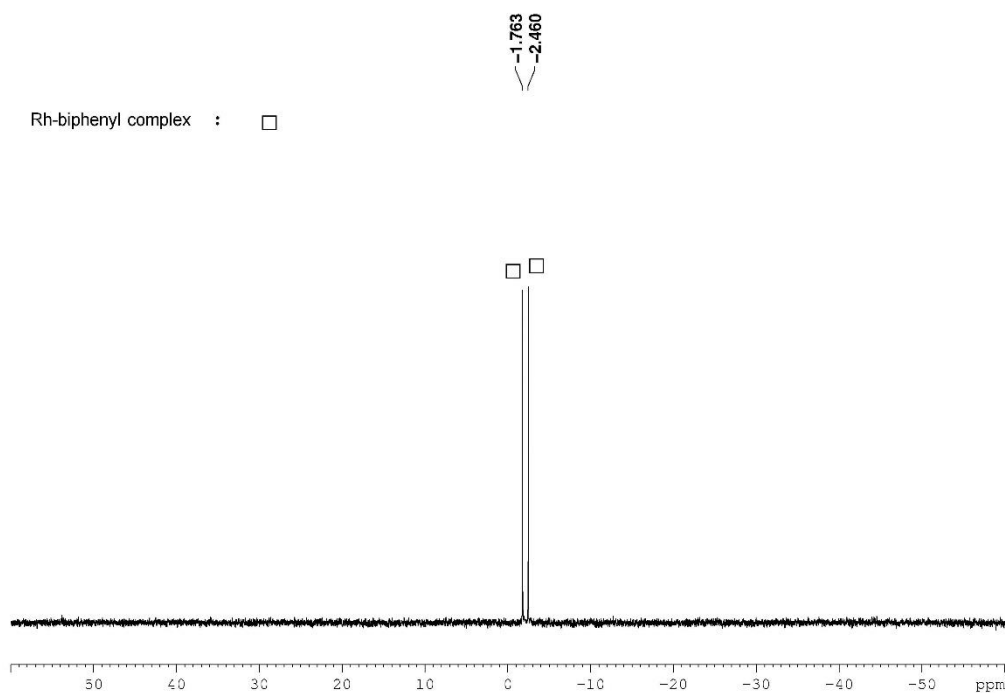


**Figure 2-64.** <sup>31</sup>P NMR spectrum after 1 h in the dark (162 MHz, C<sub>6</sub>D<sub>6</sub>).



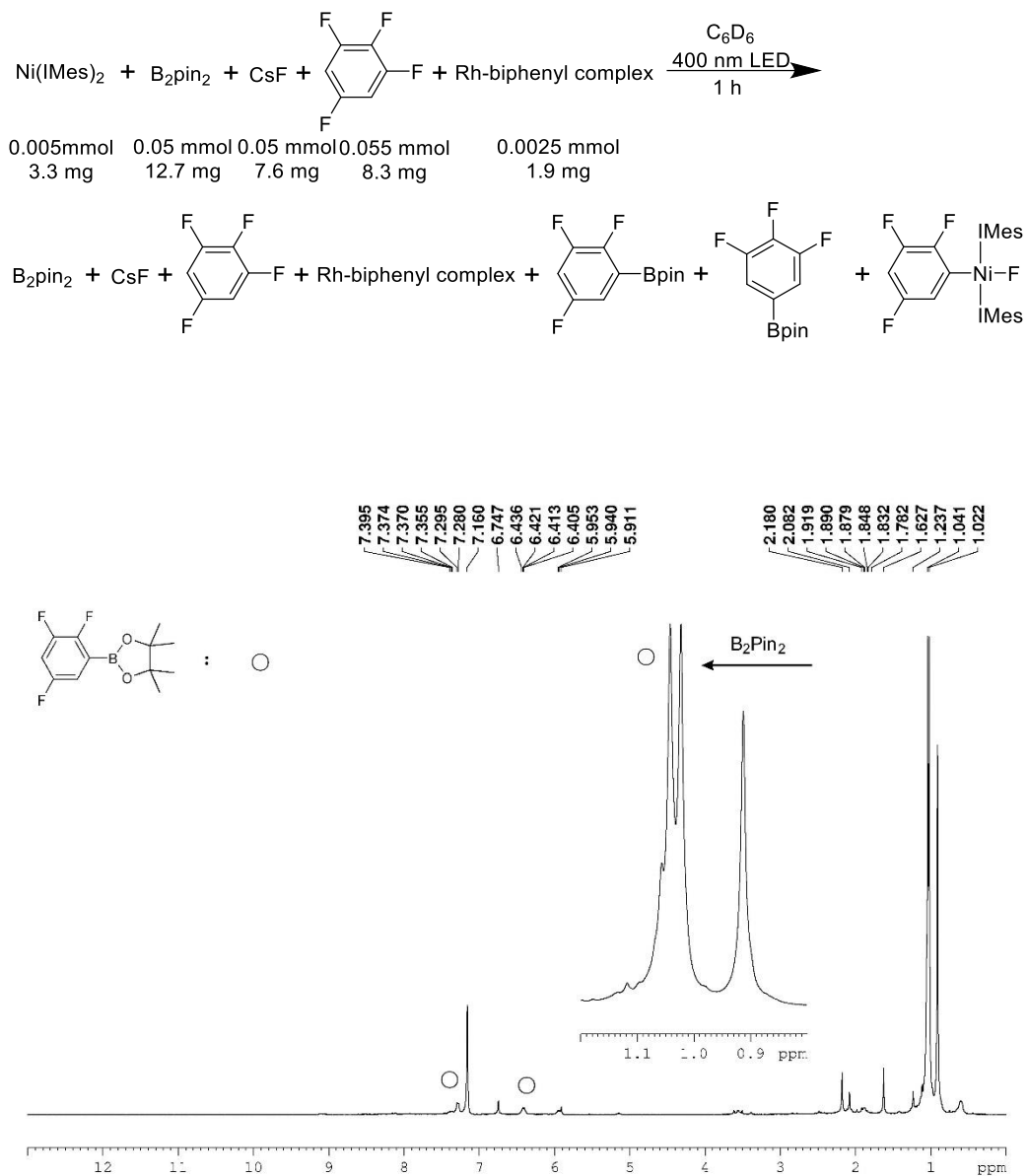
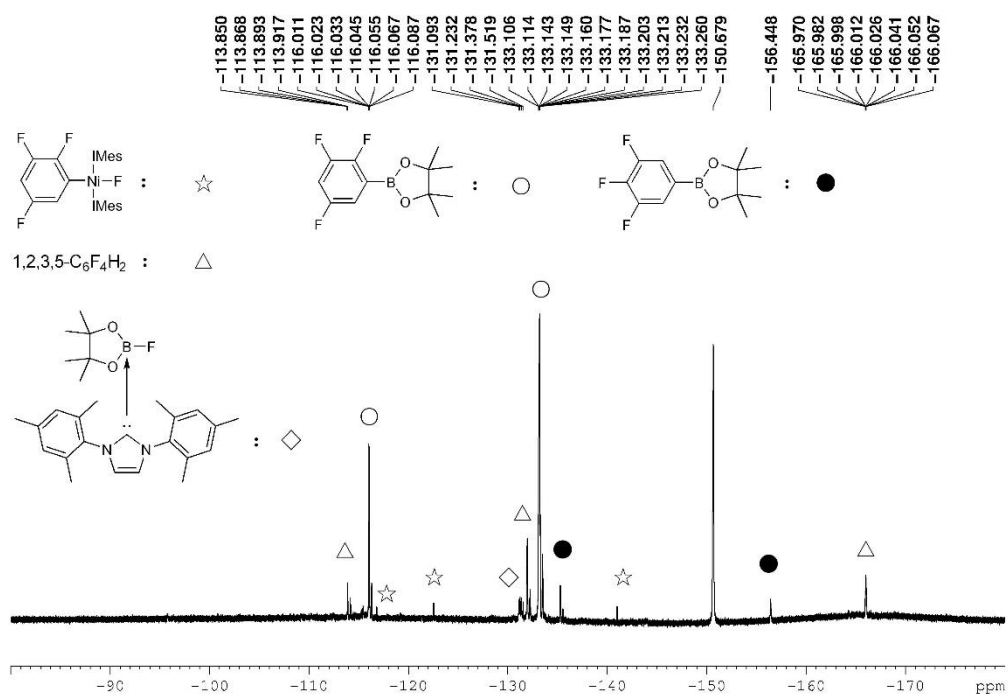
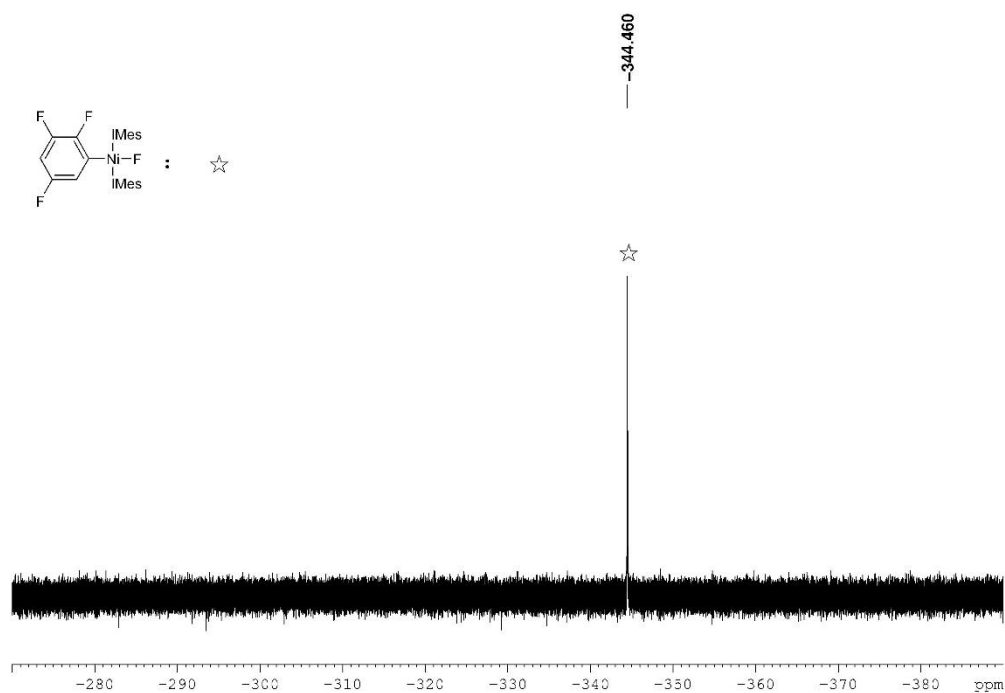


Figure 2-65.  $^1\text{H}$  NMR spectrum after 1 h irradiation (400 MHz,  $\text{C}_6\text{D}_6$ ).



**Figure 2-66.**  $^{19}\text{F}$  NMR spectrum of aromatic region after 1 h irradiation (376 MHz,  $\text{C}_6\text{D}_6$ ).



**Figure 2-67.**  $^{19}\text{F}$  NMR spectrum of Ni-F resonance after 1 h irradiation (376 MHz,  $\text{C}_6\text{D}_6$ ).

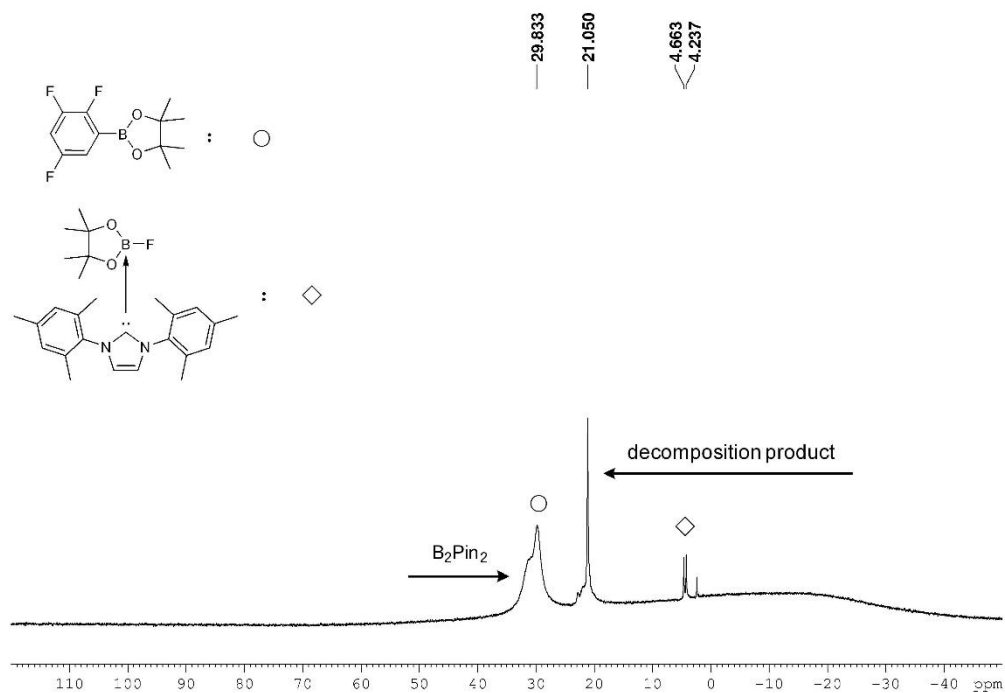


Figure 2-68.  $^{11}\text{B}$  NMR spectrum after 1 h irradiation (128 MHz,  $\text{C}_6\text{D}_6$ ).

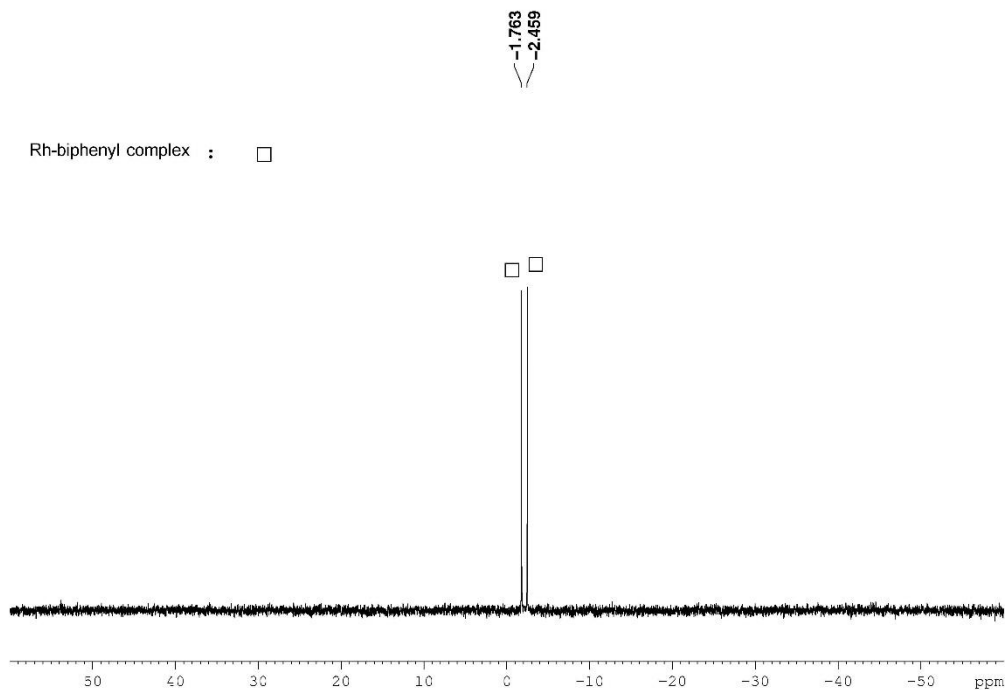
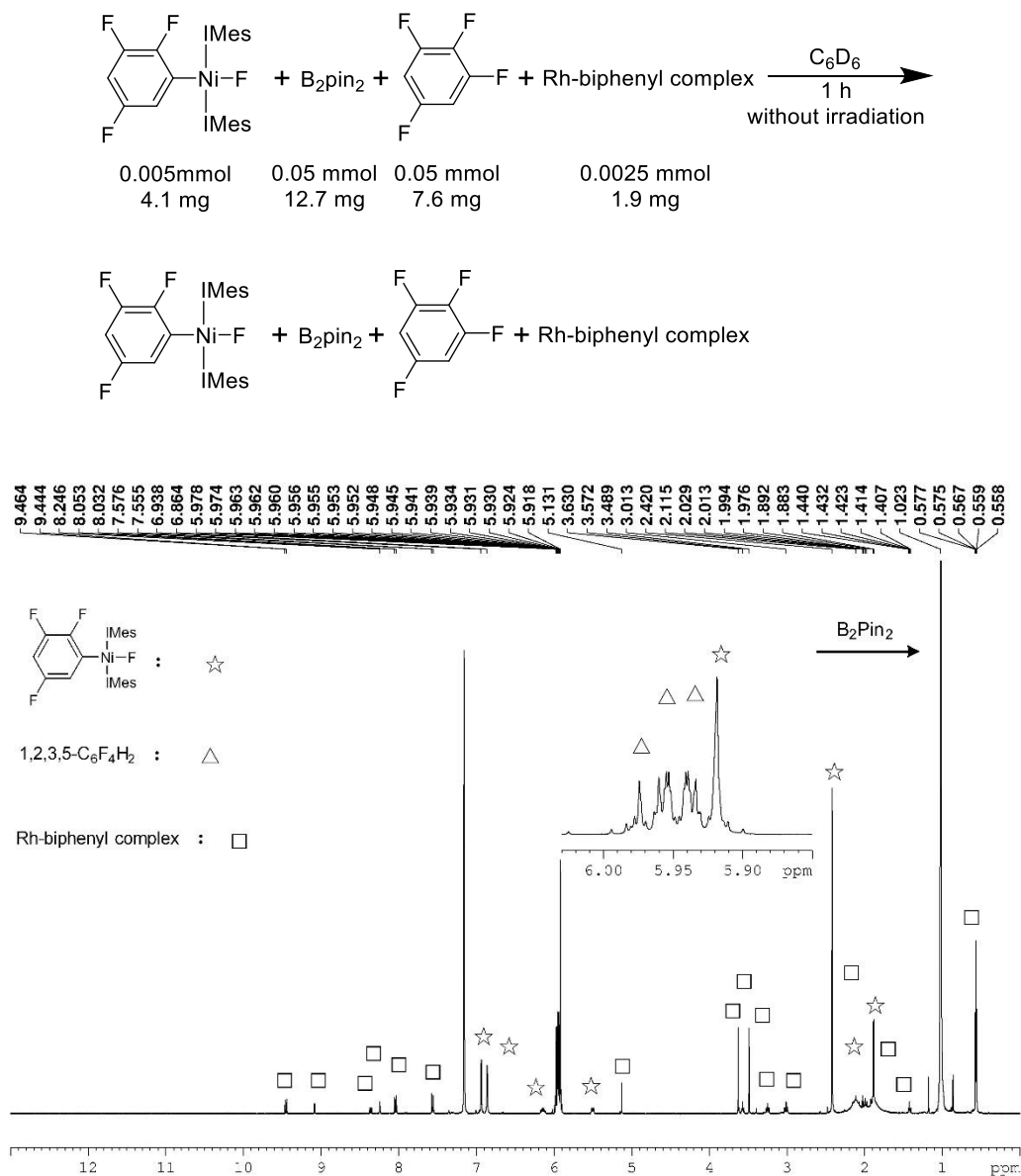


Figure 2-69.  $^{31}\text{P}$  NMR spectrum after 1 h irradiation (162 MHz,  $\text{C}_6\text{D}_6$ ).

The above catalytic test reactions can also be carried out in the absence of CsF, albeit with lower efficiency of the photoinitiated borylation of 1,2,3,5-tetrafluorobenzene, leading to the same general conclusions. The respective experiments and the NMR spectra are listed below.



**Figure 2-70.**  $^1\text{H}$  NMR spectrum after 1 h in the dark (400 MHz,  $\text{C}_6\text{D}_6$ ).

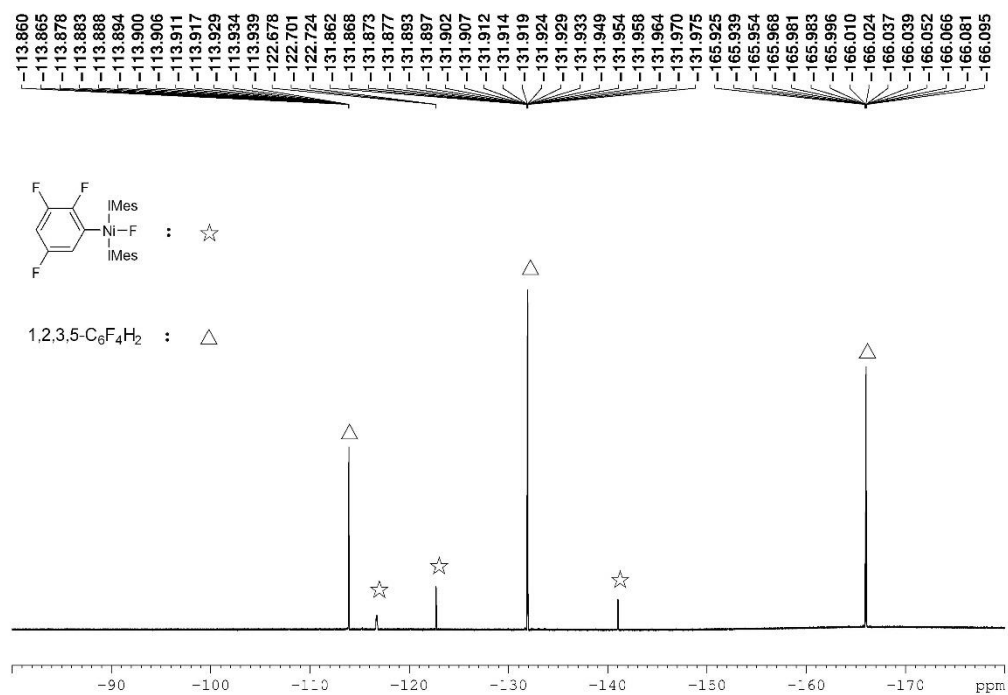


Figure 2-71. <sup>19</sup>F NMR spectrum of aromatic region after 1 h in the dark (376 MHz, C<sub>6</sub>D<sub>6</sub>).

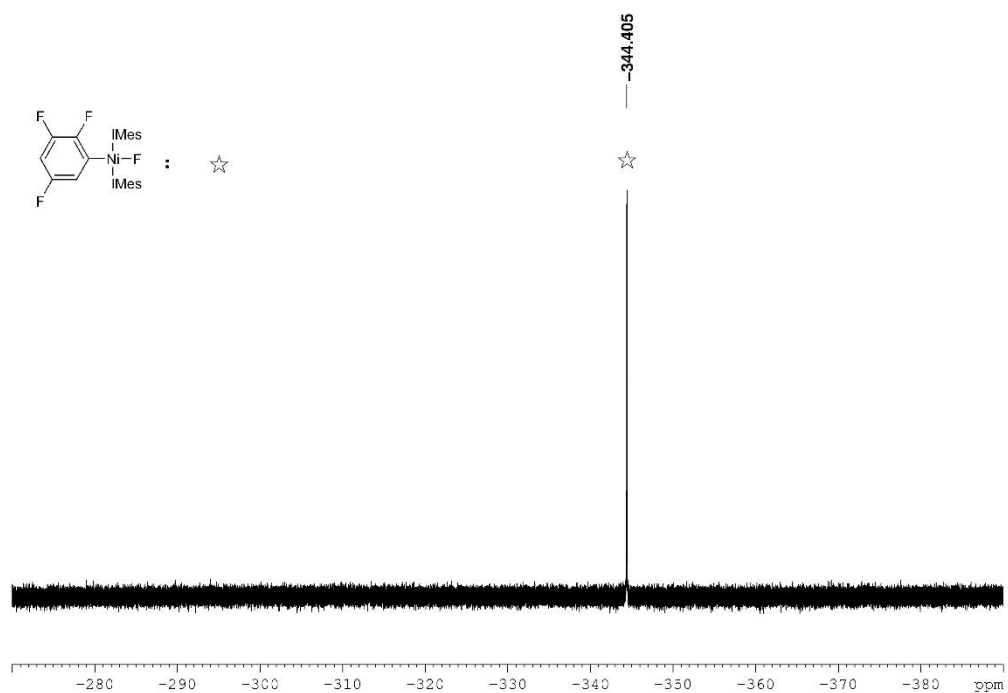
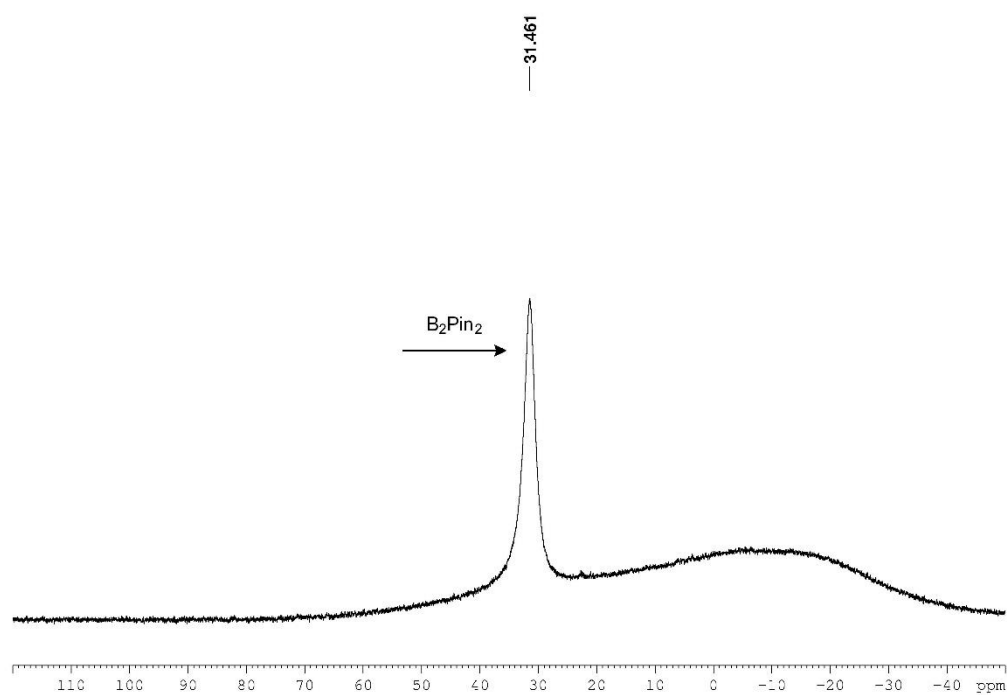
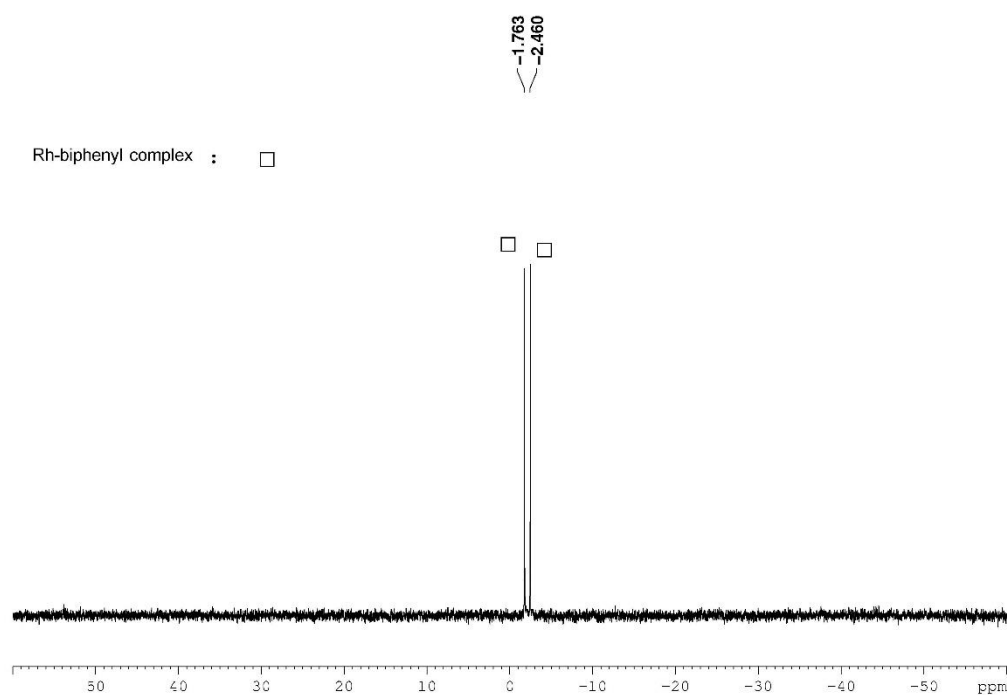


Figure 2-72. <sup>19</sup>F NMR spectrum of Ni-F resonance after 1 h in the dark (376 MHz, C<sub>6</sub>D<sub>6</sub>).



**Figure 2-73.**  $^{11}\text{B}$  NMR spectrum after 1 h in the dark (128 MHz,  $\text{C}_6\text{D}_6$ ).



**Figure 2-74.**  $^{31}\text{P}$  NMR spectrum after 1 h in the dark (162 MHz,  $\text{C}_6\text{D}_6$ ).

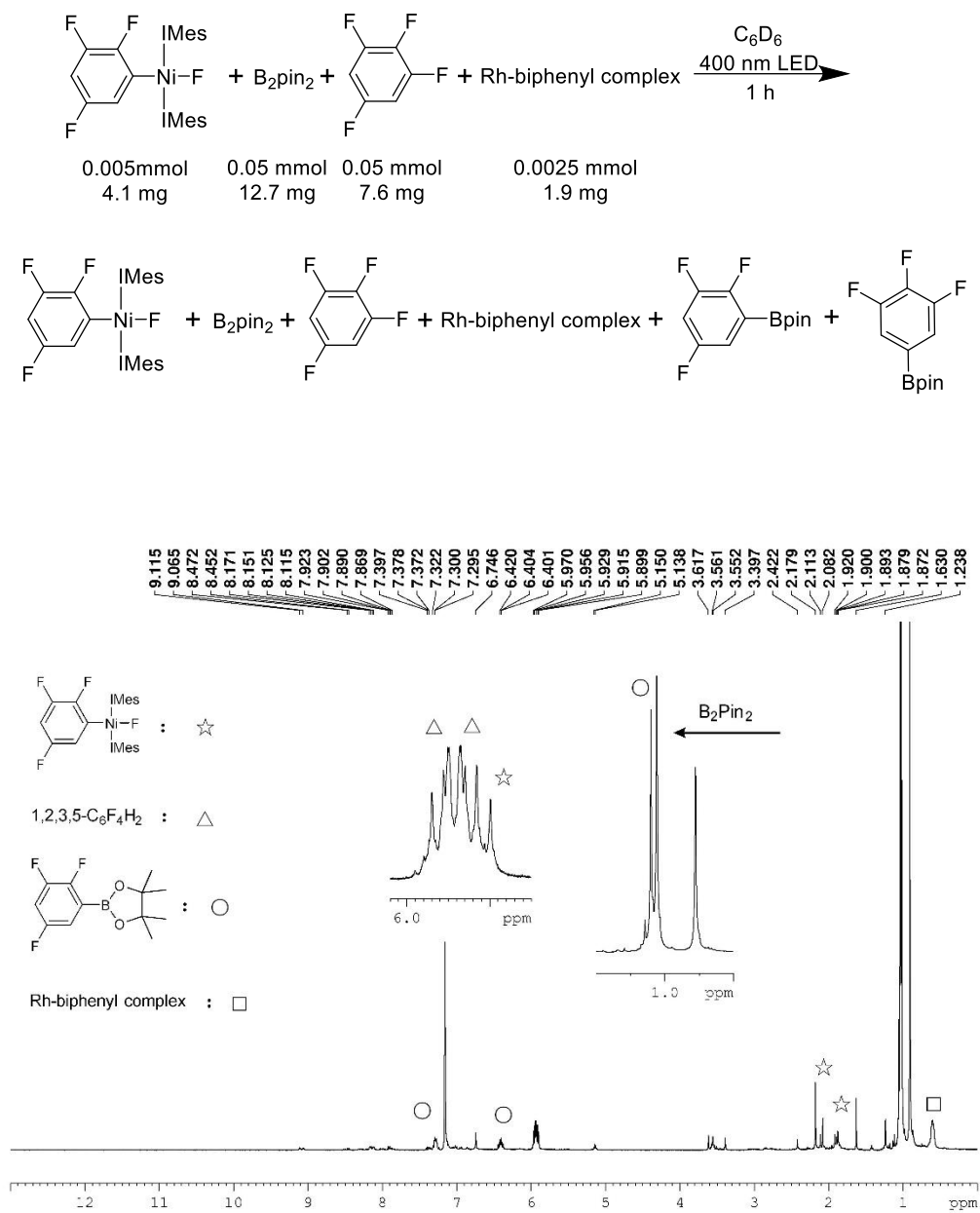


**Figure 2-75.** <sup>1</sup>H NMR spectrum after 1 h irradiation (400 MHz, C<sub>6</sub>D<sub>6</sub>).

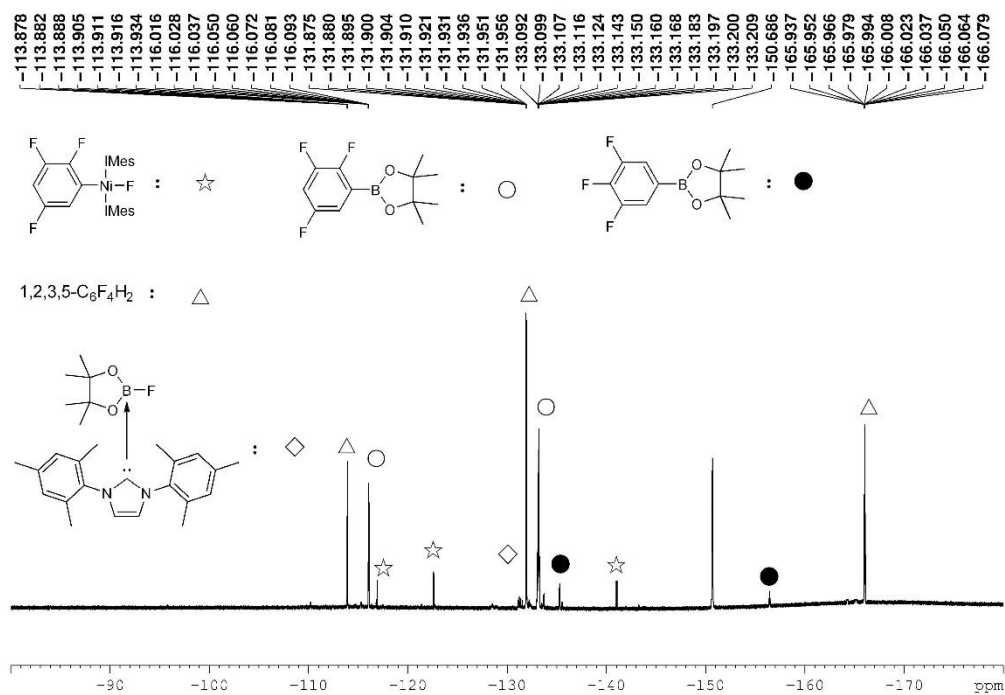


**Figure 2-76.** <sup>19</sup>F NMR spectrum of aromatic region after 1 h irradiation (376 MHz, C<sub>6</sub>D<sub>6</sub>).

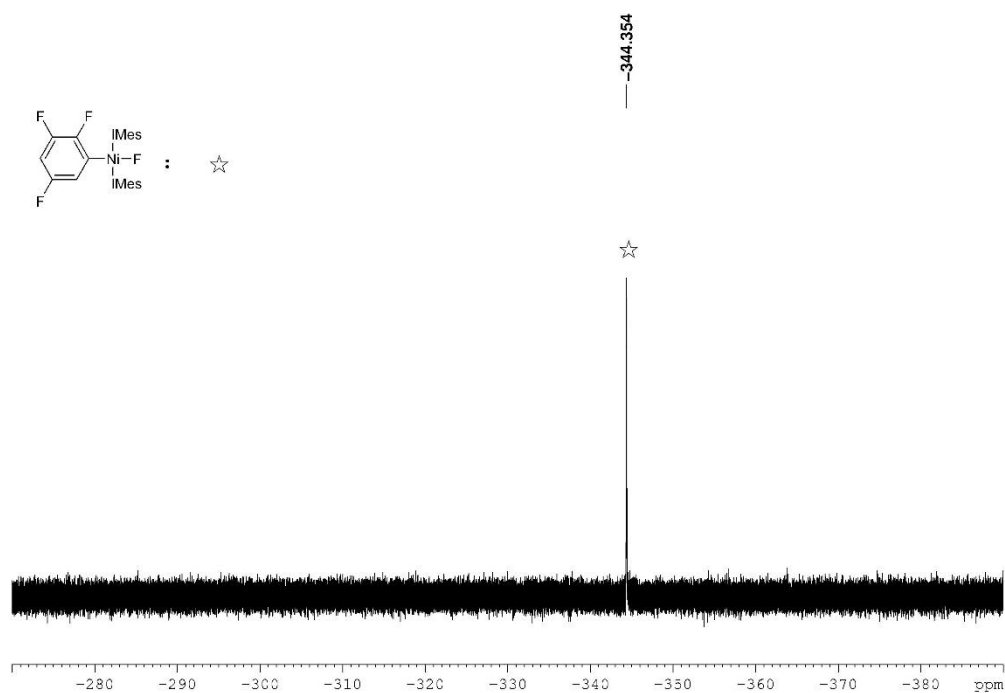


**Figure 2-77.** <sup>19</sup>F NMR spectrum of Ni-F resonance after 1 h irradiation (376 MHz, C<sub>6</sub>D<sub>6</sub>).



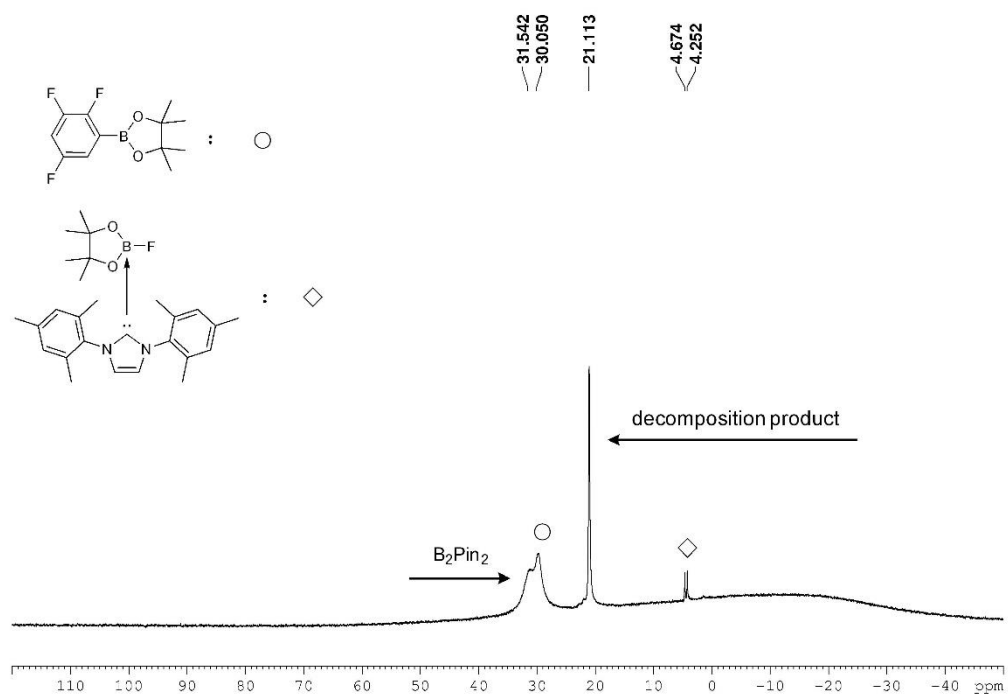


Figure 2-78.  $^{11}\text{B}$  NMR spectrum after 1 h irradiation (128 MHz,  $\text{C}_6\text{D}_6$ ).

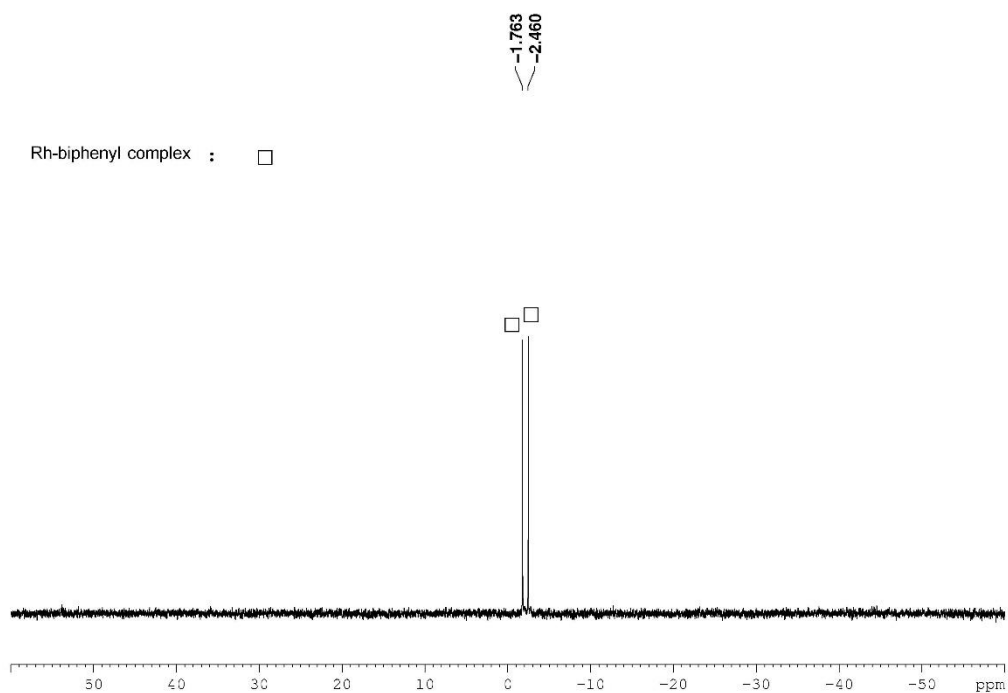
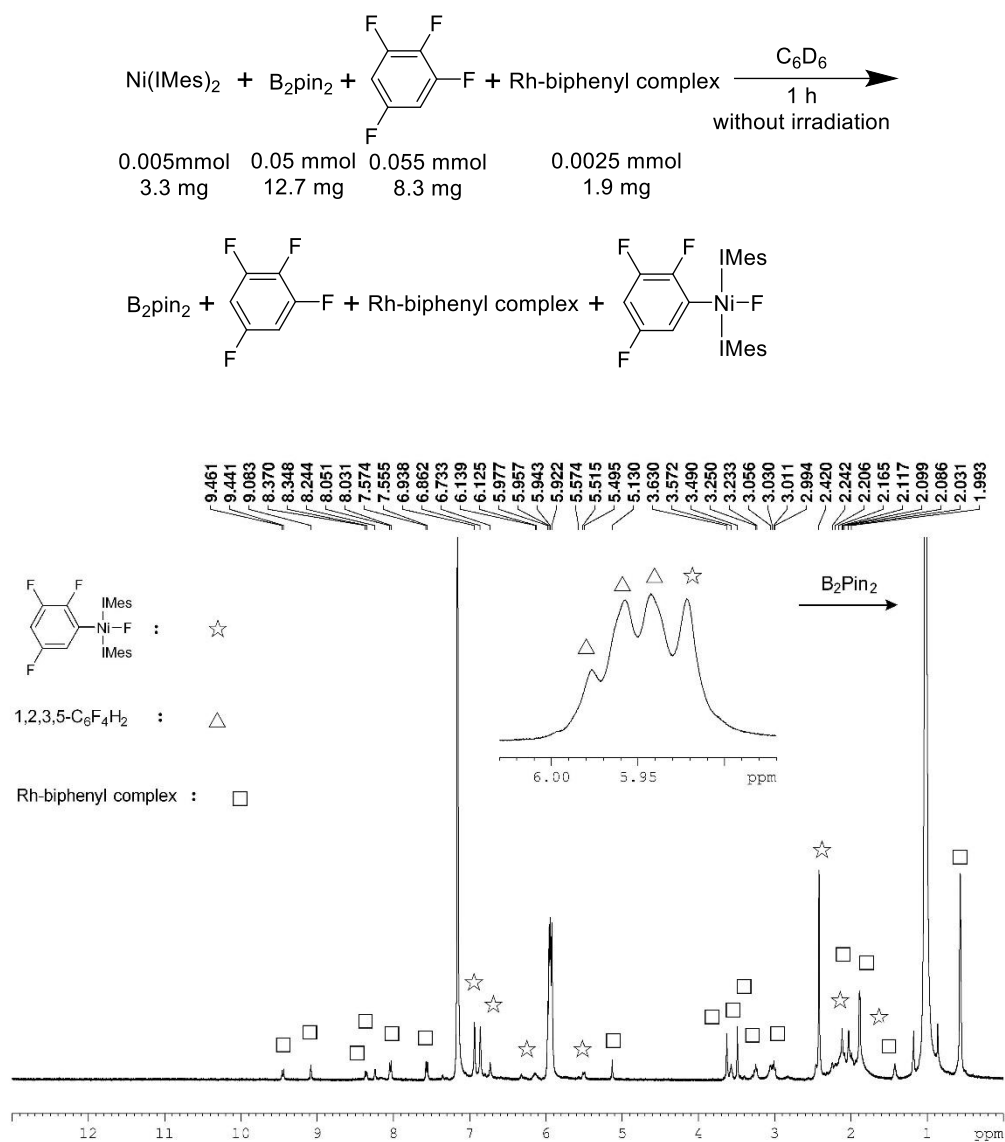


Figure 2-79.  $^{31}\text{P}$  NMR spectrum after 1 h irradiation (162 MHz,  $\text{C}_6\text{D}_6$ ).



**Figure 2-80.**  $^1\text{H}$  NMR spectrum after 1 h in the dark (400 MHz,  $\text{C}_6\text{D}_6$ ).

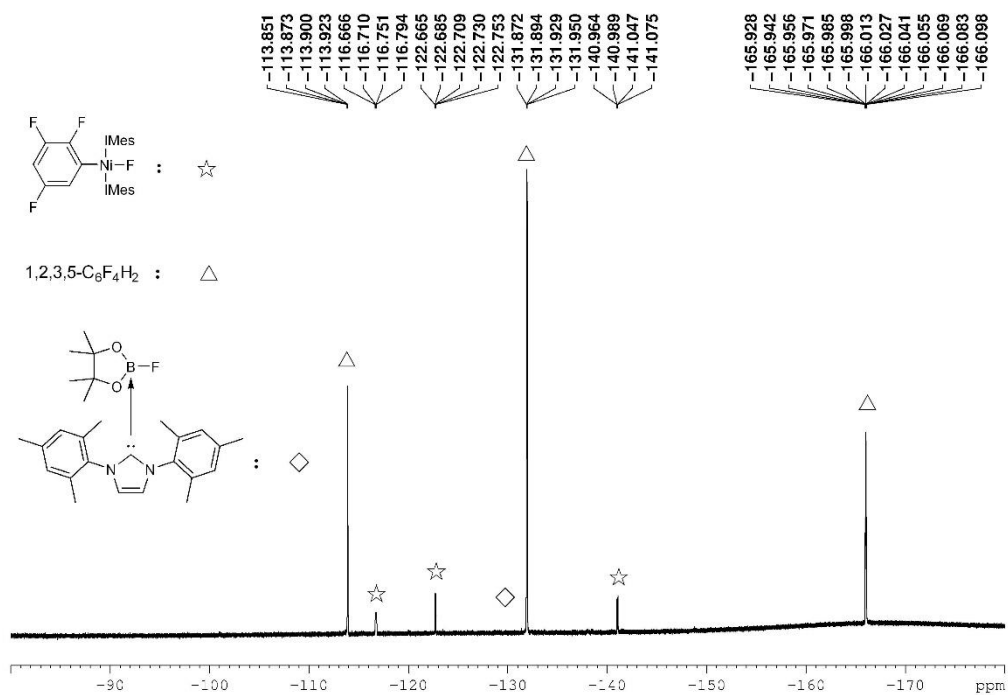


Figure 2-81. <sup>19</sup>F NMR spectrum of aromatic region after 1 h in the dark (376 MHz, C<sub>6</sub>D<sub>6</sub>).

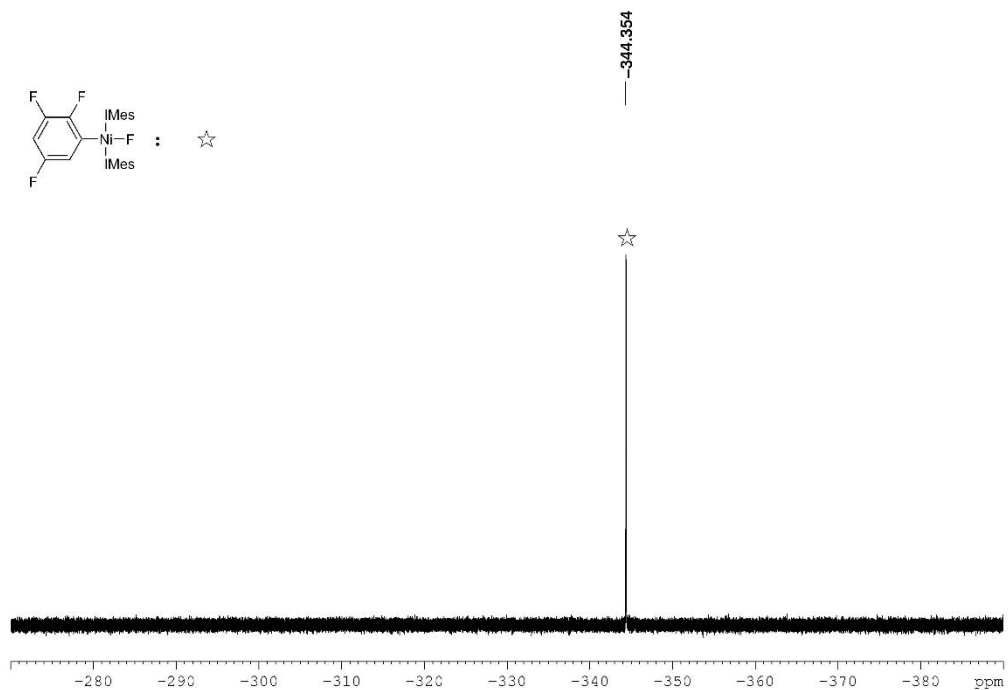
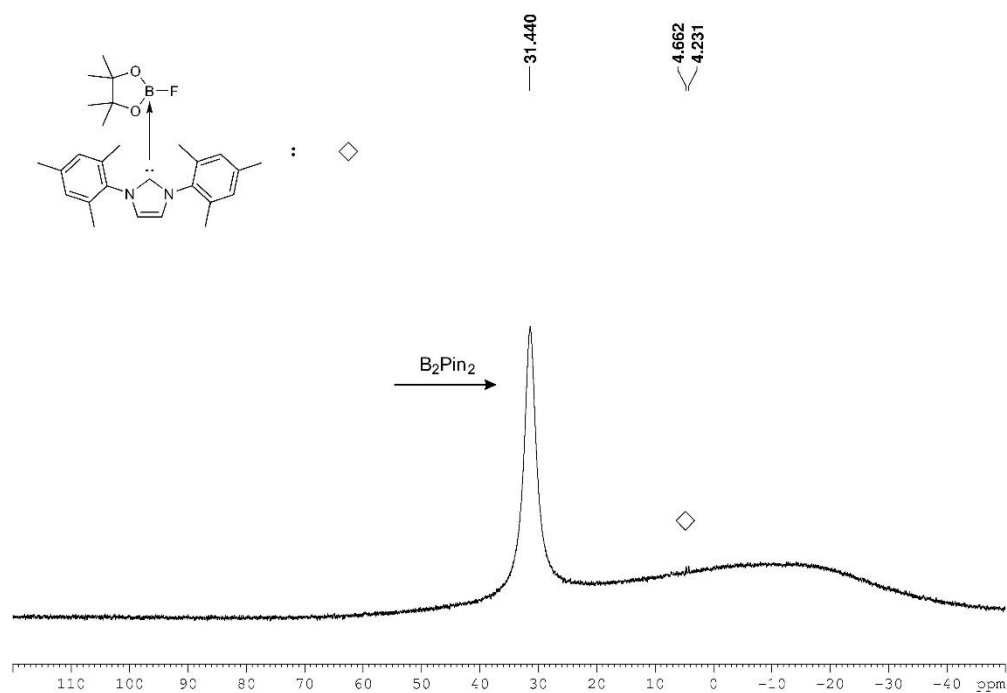
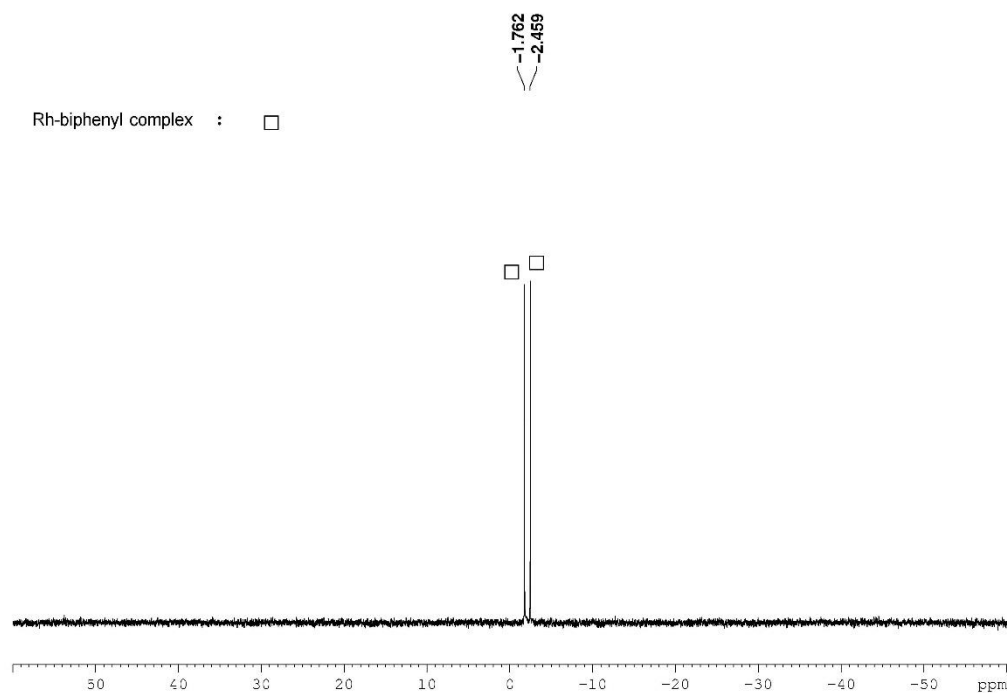


Figure 2-82. <sup>19</sup>F NMR spectrum of Ni-F resonance after 1 h in the dark (376 MHz, C<sub>6</sub>D<sub>6</sub>).



**Figure 2-83.** <sup>11</sup>B NMR spectrum after 1 h in the dark (128 MHz, C<sub>6</sub>D<sub>6</sub>).



**Figure 2-84.** <sup>31</sup>P NMR spectrum after 1 h in the dark (162 MHz, C<sub>6</sub>D<sub>6</sub>).

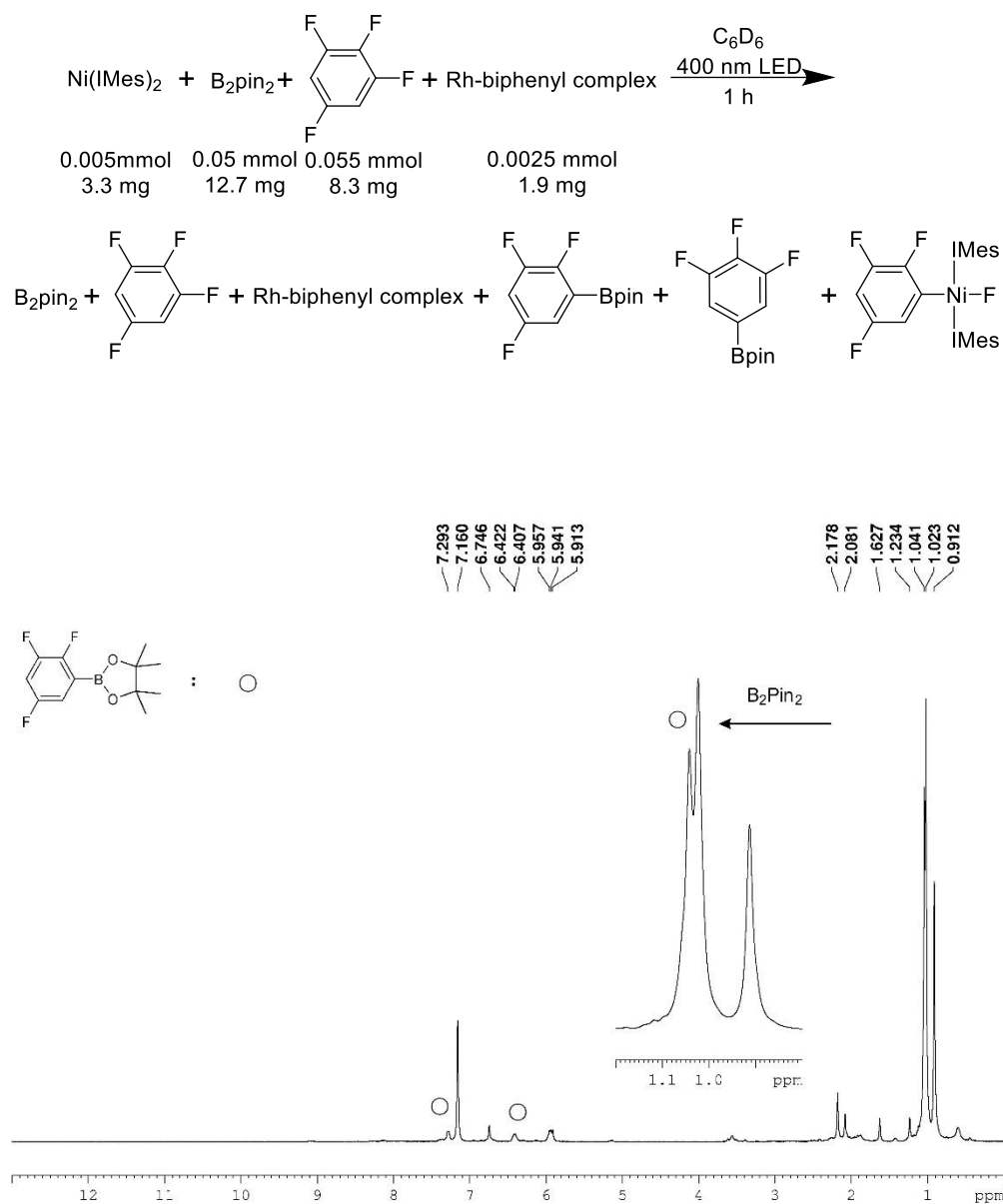


**Figure 2-85.**  $^1\text{H}$  NMR spectrum after 1 h irradiation (400 MHz,  $\text{C}_6\text{D}_6$ ).

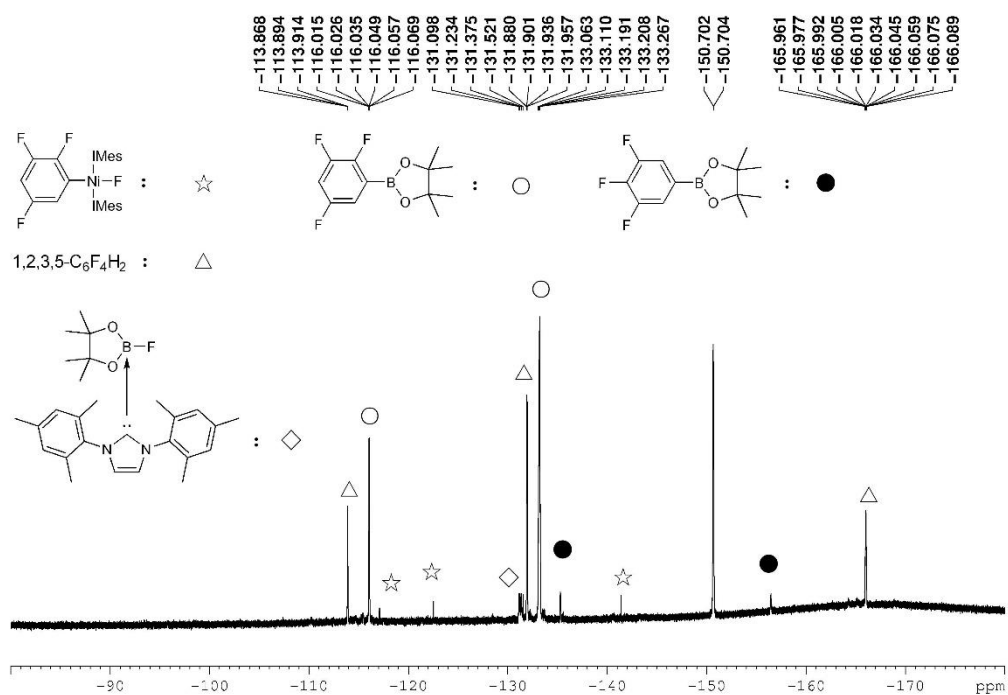


**Figure 2-86.**  $^{19}\text{F}$  NMR spectrum of aromatic region after 1 h irradiation (376 MHz,  $\text{C}_6\text{D}_6$ ).

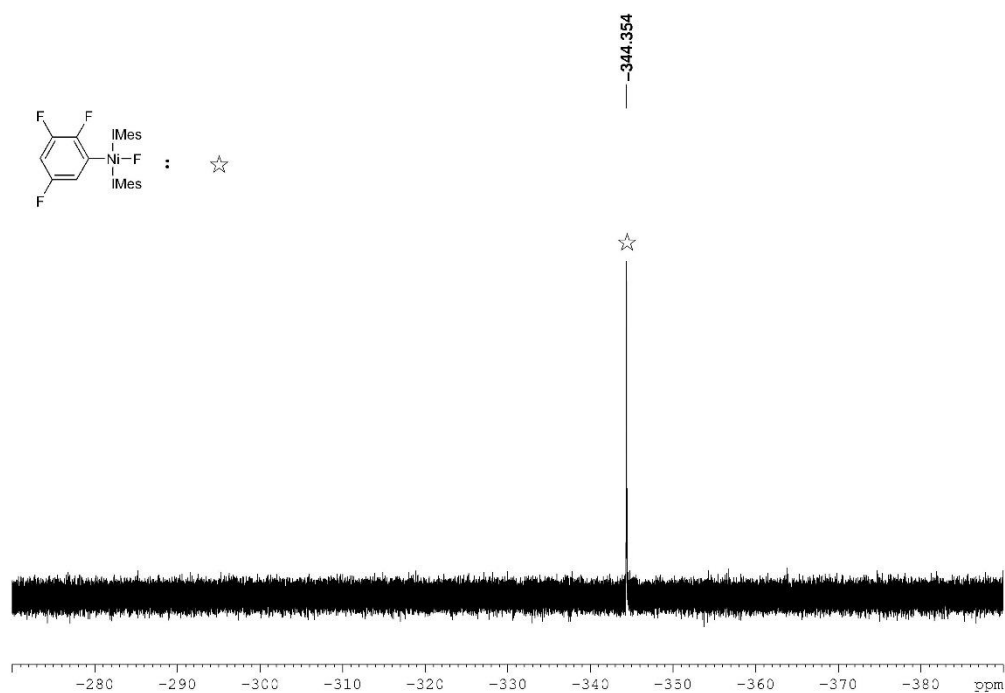


**Figure 2-87.**  $^{19}\text{F}$  NMR spectrum of Ni-F resonance after 1 h irradiation (376 MHz,  $\text{C}_6\text{D}_6$ ).

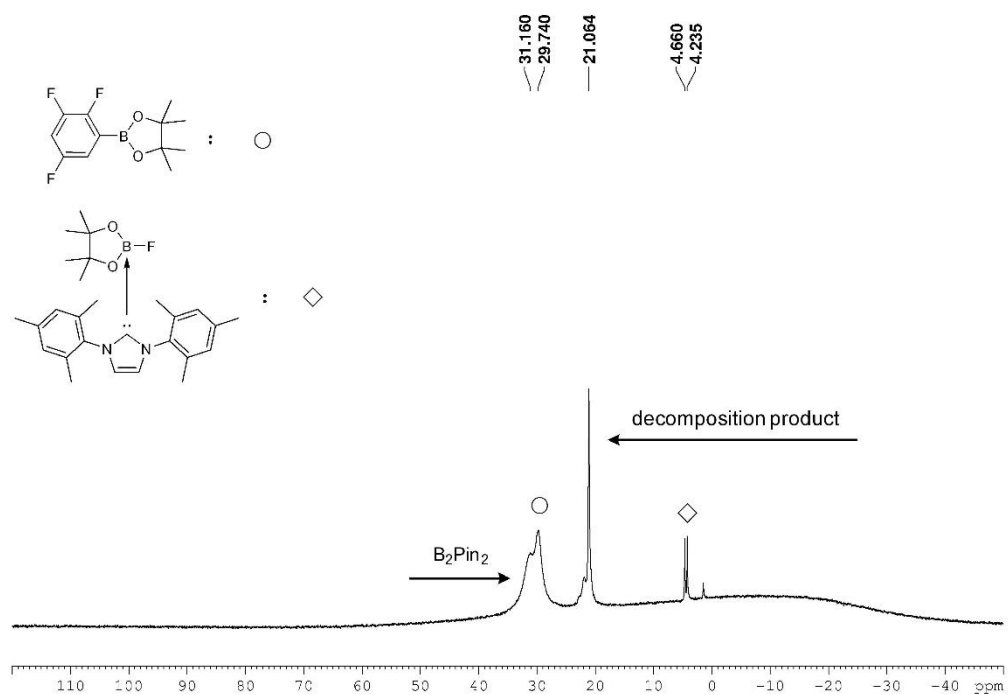


Figure 2-88.  $^{11}\text{B}$  NMR spectrum after 1 h irradiation (128 MHz,  $\text{C}_6\text{D}_6$ ).

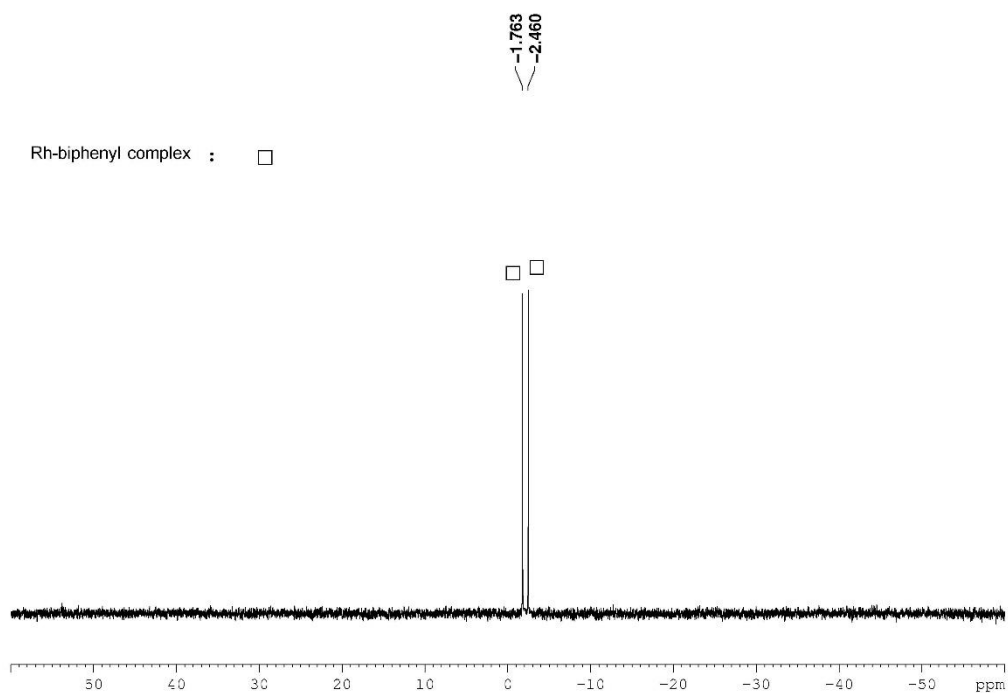


Figure 2-89.  $^{31}\text{P}$  NMR spectrum after 1 h irradiation (162 MHz,  $\text{C}_6\text{D}_6$ ).

#### 2.4.4 DFT calculations

Calculations regarding the properties of the ground state  $S_0$  and of the first triplet excited state  $T_1$  of *trans*-[NiF(2,3,5-C<sub>6</sub>F<sub>3</sub>H<sub>2</sub>)(IMes)<sub>2</sub>] were carried out in the gas-phase with the ORCA 4.0.1 program suite.<sup>184,185</sup> Geometry optimizations were performed starting from the molecular structures obtained from experimental single crystal X-ray diffraction studies, employing the PBE0<sup>186-192</sup> functional together with Grimme's empirical dispersion correction (D3BJ)<sup>193,194</sup> to account for van der Waals interactions. The def2-TZVP<sup>195,196</sup> basis set was used for nickel in combination with the auxiliary basis set def2-TZVP/J<sup>197</sup> in order to accelerate the computations within the framework of the resolution of identity (RI) approximation, whereas for all other atoms the def2-SVP(/J)<sup>196,197</sup> basis sets were used. Frequency analyses ensured that the optimized structures correspond to energy minima. TD-DFT calculations were carried out for the first 20 singlet and triplet excited states employing the same functional and basis sets. Representations of molecular orbitals and transition density differences were produced with orca\_plot as provided by ORCA 4.0.1 and with gOpenMol 3.00.<sup>198,199</sup> TD-DFT geometry optimizations of the excited states  $T_1$ ,  $T_2$  and  $T_3$  were performed with Gaussian16<sup>200</sup> using the same functional and basis sets as chosen for the  $S_0$  and  $T_1$  state.

Our TD-DFT studies of **[Ni<sup>II</sup>]** (Table 2-7, Figure 2-86), which is the resting state of the catalytic cycle, show that the experimentally observed weak absorption band at  $\lambda_{\text{abs}} = 400$  nm ( $\epsilon = 500 \text{ M}^{-1} \text{ cm}^{-1}$ ) is due to metal-centered MC(d-d) transitions. More importantly, the triplet excited states  $T_1$ - $T_4$  were found between ca. 14,000-21,000  $\text{cm}^{-1}$  (727-477 nm). Thus, they are energetically close to or below the  $T_1$  state of **[Rh]** (18,000  $\text{cm}^{-1}$ ; 540 nm) and thus available for energy transfer. It has previously been shown that ISC in square-planar nickel(II) complexes can be very slow (timescale of ns).<sup>201,202</sup> It is thus feasible that ISC  $S_1 \rightarrow T_n$  in **[Ni<sup>II</sup>]** is also slow and not competitive with a decomposition reaction of its photoexcited  $S_1$  state with B<sub>2</sub>pin<sub>2</sub>. However, **[Ni<sup>II</sup>]** exhibits a number of energetically low-lying triplet excited states in the visible region which could be sensitized by the exceptionally long-lived triplet state of **[Rh]** (Table 2-7). Indeed, irradiation of a reaction mixture containing the nickel(II) complex, B<sub>2</sub>pin<sub>2</sub> and **[Rh]** with a 400 nm LED



gave borylation product 1-Bpin-2,3,5-C<sub>6</sub>F<sub>3</sub>H<sub>2</sub> (**34b**) with little sign of decomposition (Figures 2-19).

To show that the Rh-triplet is quenched by the [Ni<sup>II</sup>] and thus that energy transfer occurs from [Rh] to [Ni<sup>II</sup>], we prepared six toluene solutions with a [Rh] concentration of 3.9 μM and [Ni<sup>II</sup>] concentrations of 0, 2.7, 10.8, 18.9, 27, and 35.1 μM, respectively. Phosphorescence spectra of these solutions are shown in Figure 2-91a. The photoluminescence intensity decreased gradually with increasing concentration of [Ni<sup>II</sup>]. The photoluminescence quenching data were analyzed using the Stern-Volmer eq. (1):<sup>221</sup>

$$I_0/I = 1 + K_{SV}[Q] \quad (1)$$

where  $I_0$  and  $I$  are the steady-state phosphorescence intensities of [Rh] in the absence and in the presence of a quencher [Ni<sup>II</sup>], respectively.  $[Q]$  is the molar concentration of the quencher [Ni<sup>II</sup>].  $K_{SV}$  is the Stern-Volmer constant. The resulting plot is given in Figure 2-91b, which shows an excellent linear relationship ( $R = 0.99962$ ).  $K_{SV}$ , which is a measure of the efficiency of the quencher, is  $3.15 \times 10^4 \text{ M}^{-1}$ . Such a large  $K_{SV}$  value indicates that [Ni<sup>II</sup>] is very efficient in quenching the phosphorescence of [Rh], confirming the high efficient TET from [Rh] to [Ni<sup>II</sup>].

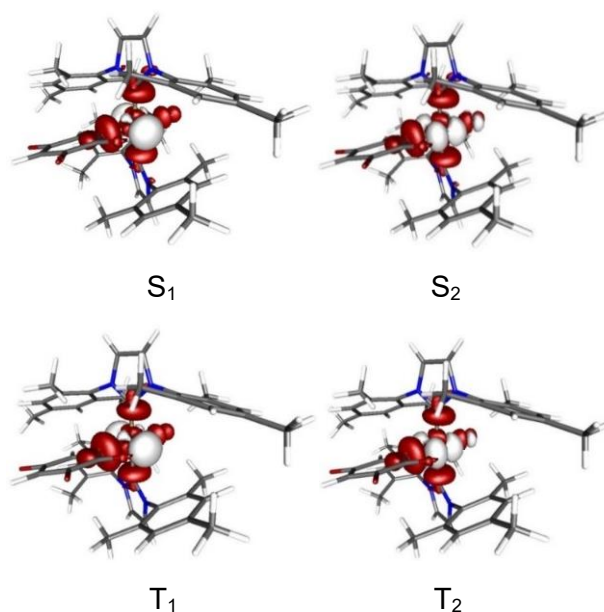


**Figure 2-90.** Electron density differences (white: depletion, red: population) in [Ni<sup>II</sup>] for the excitations from the ground state  $S_0$  to  $S_1$ ,  $S_2$ ,  $T_1$ , and  $T_2$ .

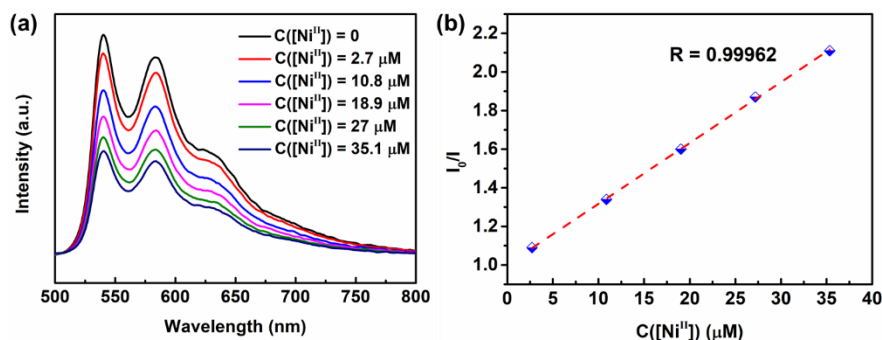


**Figure 2-91.** (a) Emission spectra of **[Rh]** in toluene at a concentration of 3.9 μM with quencher concentration of **[Ni<sup>II</sup>]** varying from 0.00 to 35.1 μM; (b) Stern-Volmer plot of  $I_0/I$  vs.  $[Q]$ .

Due to the mainly MC(d-d) nature of the  $T_1$  to  $T_4$  states of **[Ni<sup>II</sup>]**, all of which populate the M–L  $\sigma$ -antibonding  $d_{x^2-y^2}$  orbital, their TD-DFT-optimized geometries exhibit a significant elongation of the Ni–C(NHC) bonds by ca. 0.141–0.186 Å (Figure 2-93), implying that NHC ligand dissociation can be facilitated by triplet sensitization. A space-filling model of **[Ni<sup>II</sup>]** clearly demonstrates that the square-planar **[Ni<sup>II</sup>]** complex is sterically too crowded for  $B_2pin_2$  to interact with the metal or the fluoride ligand (Figure 2-92). However, the photoinitiated formation of 3-coordinate  $[NiF(2,3,5-C_6F_3H_2)(IMes)]$  would allow for facile transmetalation with  $B_2pin_2$  or  $FB_2pin_2^-$ , which is apparently the rate-determining step, as **[Ni<sup>II</sup>]** is the only nickel species observed in the catalytic cycle in solution during catalysis. The proposed NHC ligand dissociation would also be in line with our observation of a four-coordinate boron species in all of our photoinitiated borylation experiments, exhibiting a doublet at 4.4 ppm in the  $^{11}B$  NMR spectrum ( $J_{BF} = 68$  Hz) and a quartet at -131 ppm in the  $^{19}F$  NMR spectrum ( $J_{FB} = 66$  Hz), which we tentatively assign to  $IMes-FBpin$ .

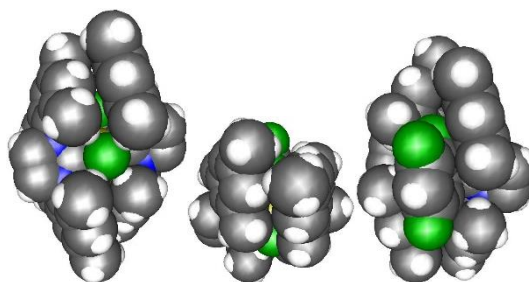


**Figure 2-92.** Space-filling representations of **[Ni<sup>II</sup>]** viewed along the F–Ni–Ar axis (left), from the top (middle), and along the Ar–Ni–F axis (right). H white, C grey, N blue, F green.

**Table 2-7. Calculated transitions of [Ni<sup>II</sup>] obtained by TD-DFT (D3-PBE0/def2-SVP/def2-TZVP), and experimental values for the S<sub>0</sub>→S<sub>1</sub>/T<sub>1</sub> transitions of [Rh]<sup>a</sup>**

Cpd.	State	Energy / cm <sup>-1</sup>	λ <sub>abs</sub> / nm (f)	Exp. λ <sub>abs</sub> / nm (ε / M <sup>-1</sup> cm <sup>-1</sup> )	Nature
[Rh] <sup>a</sup>	S <sub>1</sub>	25,000		400 (4400)	IL/ILCT
	T <sub>1</sub>	18,519 <sup>b</sup>			IL/ILCT
[Ni <sup>II</sup> ]	S <sub>1</sub>	24,416	410 (0.00099)	400 (500)	d(z <sup>2</sup> )→d(x <sup>2</sup> -y <sup>2</sup> )
	S <sub>2</sub>	24,816	403 (0.00004)		d(xz)→d(x <sup>2</sup> -y <sup>2</sup> )
	T <sub>1</sub>	13,760	727		d(z <sup>2</sup> )→d(x <sup>2</sup> -y <sup>2</sup> )
	T <sub>2</sub>	15,172	659		d(xz)→d(x <sup>2</sup> -y <sup>2</sup> )
	T <sub>3</sub>	18,114	552		d(yz)→d(x <sup>2</sup> -y <sup>2</sup> )
	T <sub>4</sub>	20,946	477		d(xy)→d(x <sup>2</sup> -y <sup>2</sup> )

<sup>a</sup>Experimental data for [Rh] taken from ref. 29. <sup>b</sup>Phosphorescence energy with wavelength maximum of 540 nm.

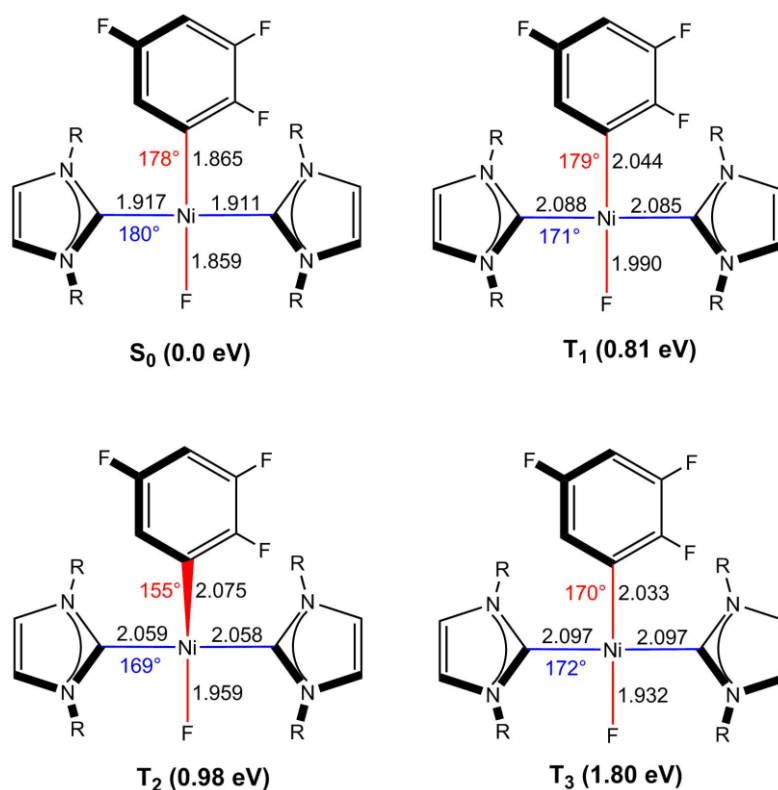
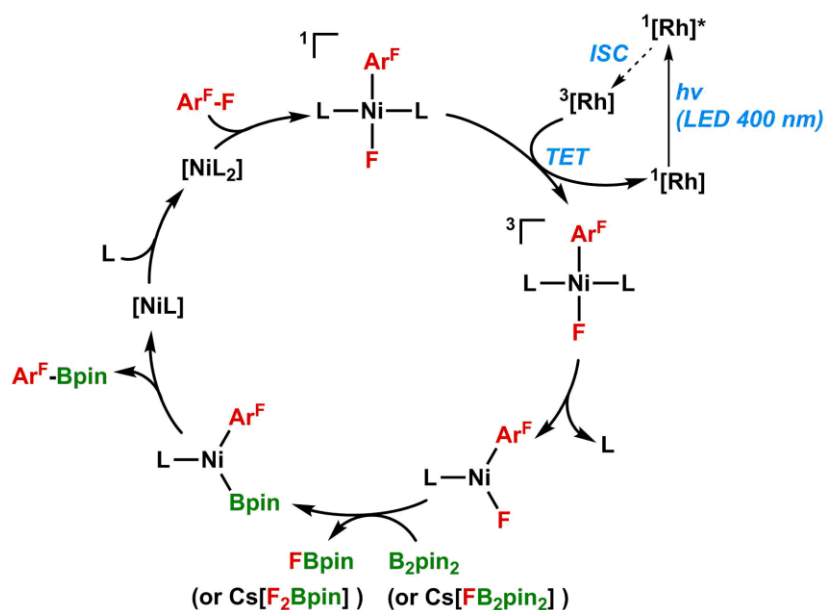


**Figure 2-93.** Structural parameters of the geometry optimized ground state S<sub>0</sub>, and the triplet excited states T<sub>1</sub>, T<sub>2</sub> and T<sub>3</sub>. Energies given relative to the optimized ground state S<sub>0</sub>.

### 2.4.5 Proposed mechanism

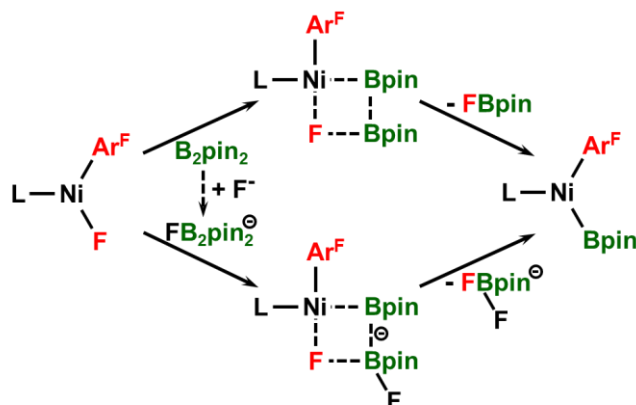
In light of these findings, we thus propose the following mechanism for the photocatalytic borylation of fluoroarenes via C-F bond activation (Scheme 2-4).  $[\text{Ni}(\text{IMes})_2]$  undergoes very fast oxidative addition of the  $\text{C}(\text{Ar}^{\text{F}})\text{-F}$  bond to give *trans*- $[\text{NiF}(\text{Ar}^{\text{F}})(\text{IMes})_2]$ , which is the resting state of the catalytic cycle.<sup>126</sup> The rhodium biphenyl complex **[Rh]** is excited to the  $\text{S}_1$  state by the 400 nm LED and, following ISC, energy transfer from its triplet excited state  $\text{T}_1$  to *trans*- $[\text{NiF}(\text{Ar}^{\text{F}})(\text{IMes})_2]$  occurs. The triplet sensitization of the **[Ni<sup>II</sup>]** complex, which bypasses its  $\text{S}_1$  state and thus its decomposition reaction with  $\text{B}_2\text{pin}_2$  that forms nickel black (vide supra), leads to NHC ligand dissociation. The resulting trigonal  $[\text{NiF}(\text{Ar}^{\text{F}})(\text{IMes})]$  is sterically much less encumbered and then reacts with  $\text{B}_2\text{pin}_2$ . Upon transmetalation, for which the rate constant may be enhanced by the formation of  $\text{FB}_2\text{pin}_2^-$  from  $\text{B}_2\text{pin}_2$  and  $\text{CsF}$ , reductive elimination of  $\text{Ar}^{\text{F}}\text{-Bpin}$  is fast,<sup>126,204</sup> and the resulting  $\text{Ni}(0)$  species is then stabilized by re-coordination of  $\text{IMes}$ , giving  $[\text{Ni}(\text{IMes})_2]$ . Alternatively, TET from  $^3[\text{Rh}]$  to *trans*- $[\text{NiF}(\text{Ar}^{\text{F}})(\text{IMes})_2]$  could lead to  $\text{F}^-$  dissociation, which would also serve as a means by which to facilitate transmetalation producing nucleophilic  $[\text{FB}_2\text{pin}_2]^-$  and electrophilic  $[\text{Ni}(\text{Ar}^{\text{F}})(\text{IMes})_2]^+$ .

**Scheme 2-4. Proposed mechanism for the photocatalytic borylation of fluoroarenes by **[Rh]**/**[Ni(IMes)<sub>2</sub>]** using triplet energy transfer (TET). L = IMes;  $\text{Ar}^{\text{F}}$  = fluoroarene; ISC = intersystem-crossing**



## 2.4.6 Possible role of CsF in the transmetalation step

Scheme 2-5. Possible transmetalation route with or without CsF



Photocatalytic borylations without CsF gave lower yields of product **34b** of ca. 45% (Table 2-6, entries 6, 7, 9 and 10), except for the experiment equivalent to entry 3, which gave the expected 10% yield. Thus, the addition of CsF has a yield-enhancing effect, although the reaction proceeds in modest yields without CsF. There are two reasonable explanations of the effect of added CsF, based on our previous studies of anionic adducts of  $B_2pin_2$ , and their reactivity with electrophiles.<sup>92,93</sup> Thus, formation of  $[FB_2pin_2]^-$  would create a much more nucleophilic  $\{Bpin\}^-$  fragment, which would be expected to enhance the rate constant for transmetalation (Scheme 2-5).<sup>92,93,126</sup> Alternatively, or in addition, partial trapping of the observed Lewis acidic  $FBpin$  by formation of  $Cs[F_2Bpin]$ ,<sup>126</sup> would reduce the formation of an NHC- $FBpin$  adduct (vide infra) and thus enhance the stability of  $\{Ni(NHC)_2\}$  species in the reaction mixture.

Although the critical aspect of our photocatalytic borylation of fluoroaromatics at room temperature is clearly triplet energy transfer from **[Rh]** to  $trans-[NiF(Ar^F)(IMes)_2]$ , we cannot exclude the possibility that SET processes are involved *after* the sensitization process. For example, the redox potentials of the assumed 3-coordinate  $[NiF(Ar^F)(IMes)]$  are unknown because this species is experimentally not accessible for CV studies. However, our proposed mechanism in Scheme 2-4, which does not involve SET, is in line with our experimental observations.

## 2.5 Conclusions

In contrast to the majority of current photocatalytic transformations, which employ transition metals as excited state SET agents, we have developed a bimetallic photocatalytic system, that consists of a rhodium biphenyl complex as a triplet sensitizer and  $[\text{Ni}(\text{IMes})_2]$  as a catalyst, operating with 400 nm light for the borylation of a wide range of fluoroarenes with  $\text{B}_2\text{pin}_2$  via selective C-F bond activation. In contrast to the majority of cross-coupling reactions for which C-X/H bond oxidative addition is rate determining, we have previously reported that C(arene)-F bond activation with this particular nickel bis(NHC) complex is facile at room temperature, but that the transmetalation step with  $\text{B}_2\text{pin}_2$  is associated with a high energy barrier.<sup>126</sup> The exceptionally long-lived triplet excited state of the Rh biphenyl complex<sup>170</sup> and perhaps a very efficient orbital overlap integral allow for efficient triplet energy transfer to the intermediary C-F bond oxidative addition product *trans*- $[\text{NiF}(\text{Ar}^{\text{F}})(\text{IMes})_2]$ , which leads to ligand dissociation and subsequently to a greatly enhanced rate constant for the transmetalation step at room temperature. The photocatalytic borylation of the fluoroarenes occurs with high selectivity in good to excellent yields. For the particularly challenging monoborylation of mono- and difluorobenzenes, the yields are significantly higher than found for our previously reported thermal catalytic borylation with  $[\text{Ni}(\text{IMes})_2]$ .<sup>126</sup> Direct irradiation of *trans*- $[\text{NiF}(\text{Ar}^{\text{F}})(\text{IMes})_2]$  populates the  $\text{S}_1$  state, which leads to very fast decomposition when  $\text{B}_2\text{pin}_2$  is present. This destructive pathway can be bypassed by indirect excitation of the triplet states of the nickel(II) complex via photoexcited  $^3[\text{Rh}]$ . The efficient photo-induced borylation of fluoroarenes with visible light reported herein is only possible due to this beneficial excited state discrimination of the nickel catalyst.

## 2.6 Experimental procedures and characterization data

### 2.6.1 General information

Unless otherwise noted, all manipulations were performed using standard Schlenk or glovebox (Innovative Technology Inc.) techniques under argon. All reagents were purchased from Alfa-Aesar, Aldrich, ABCR or VWR, and were checked for purity by

GC-MS and/or  $^1\text{H}$  NMR spectroscopy and used as received. Bis(pinacolato)diboron ( $\text{B}_2\text{pin}_2$ ) was kindly provided by AllylChem Co. Ltd. (Dalian, China). HPLC grade solvents were argon saturated, dried using an Innovative Technology Inc. Pure-Solv Solvent Purification System, and further deoxygenated using the freeze-pump-thaw method.  $\text{C}_6\text{D}_6$  and  $\text{CDCl}_3$  were purchased from Cambridge Isotope Laboratories, and dried over 4 Å molecular sieves, deoxygenated using the freeze-pump-thaw method and vacuum transferred into a sealed vessel. The rhodium biphenyl complex ( $[\text{Rh}]$ )<sup>170</sup>, IMes (1,3-bis-(2,4,6-trimethylphenyl)-imidazol-2-ylidene),<sup>205</sup> and  $[\text{Ni}(\text{IMes})_2]$ <sup>206</sup> were prepared according to the literature.

UV-visible absorption spectra were obtained on an Agilent 1100 Series Diode Array spectrophotometer using standard 1 cm path length quartz cells. Emission spectra were recorded on an Edinburgh Instruments FLSP920 spectrometer, equipped with a 450W Xenon arc lamp, double monochromators for the excitation and emission pathways, and a red-sensitive photomultiplier tube (R928-P PMT) as the detector. Cyclic voltammetry measurements were performed in 0.2 M TBA-PF<sub>6</sub> in CH<sub>3</sub>CN or THF under an argon atmosphere. CH<sub>3</sub>CN or THF was distilled over sodium wire prior to use and stored under argon over molecular sieves (3 Å) overnight. The synthesis of TBA-PF<sub>6</sub> is described elsewhere.<sup>207</sup> Voltammograms were recorded using a Gamry Reference 600 Potentiostat and a three electrode cell (1 mm Pt-disc working electrode, Pt counter and pseudoreference electrode). All voltammograms were referenced to the Fc/Fc<sup>+</sup> redox couple. Substance concentration was  $\sim 1.5 \times 10^{-3}$  M.

Automated flash chromatography was performed using a Biotage<sup>®</sup> Isolera Four system on silica gel (Biotage SNAP cartridge KP-Sil 10 g and KP-Sil 25 g). Commercially available, precoated TLC plates (Polygram<sup>®</sup> Sil G/UV254) were purchased from Machery-Nagel. The removal of solvent was performed on a rotary evaporator *in vacuo* at a maximum temperature of 30 °C. GC-MS analyses were performed using an Agilent 7890A gas chromatograph (column: HP-5MS 5 % phenylmethylsiloxane, 10 m, Ø 0.25 mm, film 0.25 µm; injector: 250 °C; oven: 40 °C (2 min), 40 °C to 280 °C (20 °C·min<sup>-1</sup>); carrier gas: He

(1.2 mL·min<sup>-1</sup>) equipped with an Agilent 5975C inert MSD with triple-axis detector operating in EI mode and an Agilent 7693A series auto sampler/injector. HRMS were measured on a Thermo Scientific Exactive Plus equipped with an Orbitrap. ESI measurements were conducted using a HESI source with an aux-gas temperature of 50 °C. Measurements were conducted using an APCI source with a corona needle; aux-gas temperature was 400 °C.

All NMR spectra were recorded at ambient temperature using Bruker Avance III HD 300 NMR (<sup>1</sup>H, 300 MHz; <sup>13</sup>C{<sup>1</sup>H}, 75 MHz; <sup>11</sup>B, 96 MHz), or Bruker Avance 400 NMR (<sup>1</sup>H, 400 MHz; <sup>13</sup>C{<sup>1</sup>H}, 100 MHz; <sup>11</sup>B, 128 MHz), or Bruker Avance 500 NMR (<sup>1</sup>H, 500 MHz; <sup>13</sup>C{<sup>1</sup>H}, 126 MHz; <sup>11</sup>B, 160 MHz; <sup>19</sup>F, 471 MHz) spectrometers. <sup>1</sup>H NMR chemical shifts are reported relative to TMS and were referenced via residual proton resonances of the corresponding deuterated solvent (CDCl<sub>3</sub>: 7.26 ppm, C<sub>6</sub>D<sub>6</sub>: 7.16 ppm) whereas <sup>13</sup>C{<sup>1</sup>H} NMR spectra are reported relative to TMS *via* the carbon signals of the deuterated solvent (CDCl<sub>3</sub>: 77.16 ppm, C<sub>6</sub>D<sub>6</sub>: 128.06 ppm). <sup>11</sup>B NMR chemical shifts are quoted relative to BF<sub>3</sub>·Et<sub>2</sub>O as external standard. <sup>19</sup>F NMR chemical shifts are quoted relative to CFCl<sub>3</sub> as external standard. All <sup>13</sup>C NMR spectra were broad-band <sup>1</sup>H decoupled.

Output spectrum of the used 400 nm light emitting diodes is below.

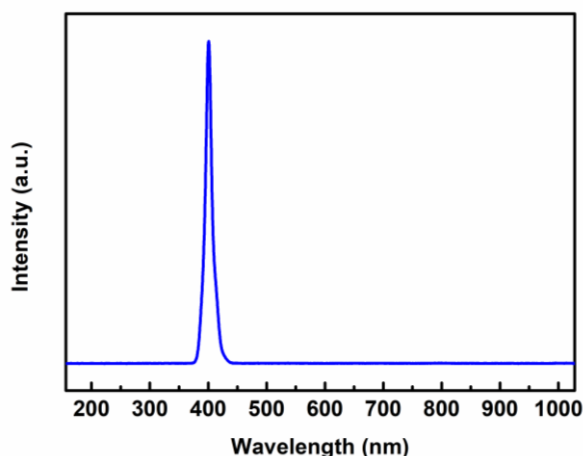


**Figure 2-94.** Output spectrum of the used 400 nm light emitting diodes (centered at 400 nm, output range: 375-440 nm).



## 2.6.2 Synthesis and stability of the Rh biphenyl complex

The compound is easily prepared in one step by reaction of  $[\text{Rh}(\kappa^2\text{-O,O-acac})(\text{PMe}_3)_2]$  (acac = acetylacetonato) with readily accessible  $\text{MeO}_2\text{C-C}_6\text{H}_4\text{-C}\equiv\text{C-C}\equiv\text{C-(CH}_2\text{)}_3\text{-C}\equiv\text{C-C}\equiv\text{C-C}_6\text{H}_4\text{-CO}_2\text{Me}$  as we previously reported in detail.<sup>170</sup> The structure of **[Rh]** is shown in Figure 2-95.

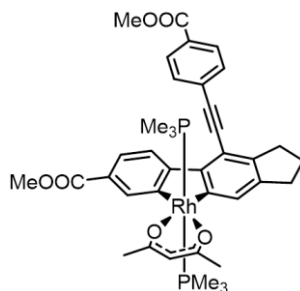


**Figure 2-95.** The structure of the Rh-biphenyl **[Rh]** photocatalyst.

**$^1\text{H NMR}$**  (500 MHz,  $\text{C}_6\text{D}_6$ ):  $\delta$  9.46 (d,  $J = 8$  Hz, 1H,  $\text{CH}_{\text{arom}}$ ), 9.09 (d,  $J = 1$  Hz, 1H,  $\text{CH}_{\text{arom}}$ ), 8.37 (dt,  $J = 1$  Hz,  $J = 8$  Hz, 1H,  $\text{CH}_{\text{arom}}$ ), 8.25 (s, 1H,  $\text{CH}_{\text{arom}}$ ), 8.05 (d,  $J = 9$  Hz, 2H,  $\text{CH}_{\text{arom}}$ ), 7.57 (d,  $J = 9$  Hz, 2H,  $\text{CH}_{\text{arom}}$ ), 5.13 (s, 1H, CH), 3.63 (s, 3H,  $\text{CH}_3$ ), 3.49 (s, 3H,  $\text{CH}_3$ ), 3.26 (t,  $J = 7$  Hz, 2H,  $\text{CH}_2$ ), 3.02 (t,  $J = 7$  Hz, 2H,  $\text{CH}_2$ ), 2.00 (m, 2H,  $\text{CH}_2$ ), 1.89 (s, 3H,  $\text{CH}_3$ ), 1.88 (s, 3H,  $\text{CH}_3$ ), 0.57 ppm (vt,  $J_{\text{P-H}} = 4$  Hz, 18H,  $\text{PMe}_3$ ).

**$^{13}\text{C}\{^1\text{H}\}$  NMR** (126 MHz,  $\text{C}_6\text{D}_6$ ):  $\delta$  188.0, 187.3, 167.8, 165.9, 164.9 (dt,  $^1J_{\text{Rh-C}} = 11$  Hz,  $^2J_{\text{P-C}} = 32$  Hz), 158.2, 148.5, 142.9, 140.2, 133.0, 131.1, 129.7, 129.4, 129.3, 129.1, 126.2, 124.2, 122.7, 113.0, 98.9, 96.6, 93.4, 67.5, 51.3, 51.0, 33.5, 33.0, 28.4, 28.3, 25.5, 24.6, 10.2 ppm (vt,  $J_{\text{C-P}} = 14$  Hz). Due to the low intensity, the  $^1J_{\text{Rh-C}}$  and  $^2J_{\text{P-C}}$  coupling of the second quat. carbon atom could not be determined.

**$^{31}\text{P}\{^1\text{H}\}$  NMR** (202 MHz,  $\text{C}_6\text{D}_6$ ):  $\delta$  -2.2 ppm (d,  $J_{\text{Rh-P}} = 113$  Hz, 2P).

Spectroscopic data for **[Rh]** match with those previously reported.<sup>170</sup>

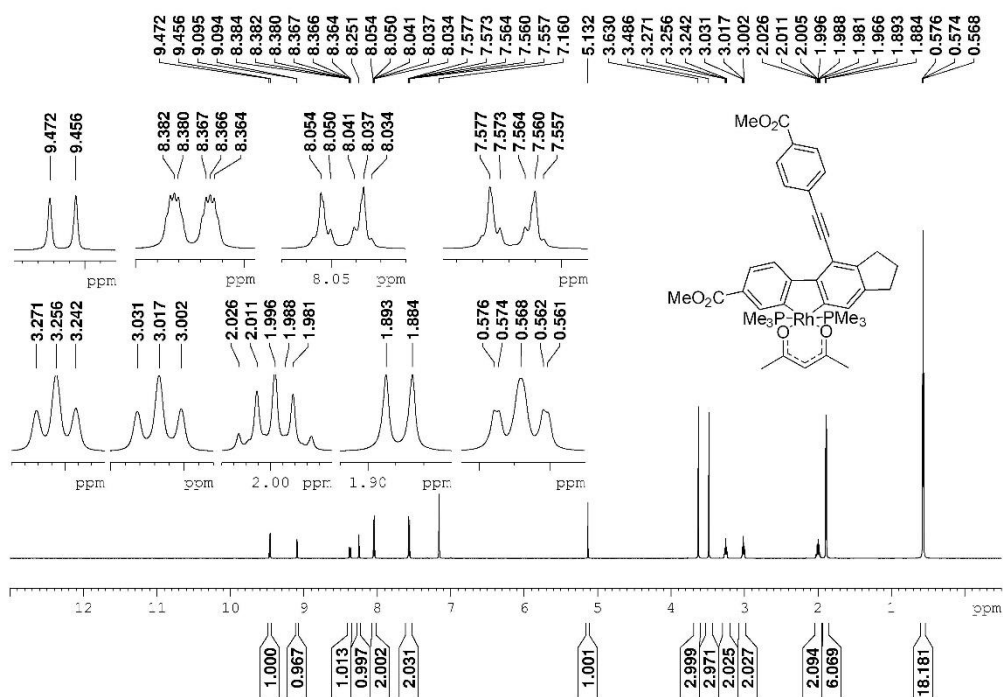


Figure 2-96. <sup>1</sup>H NMR spectrum (500 MHz, C<sub>6</sub>D<sub>6</sub>) of Rh-biphenyl complex.

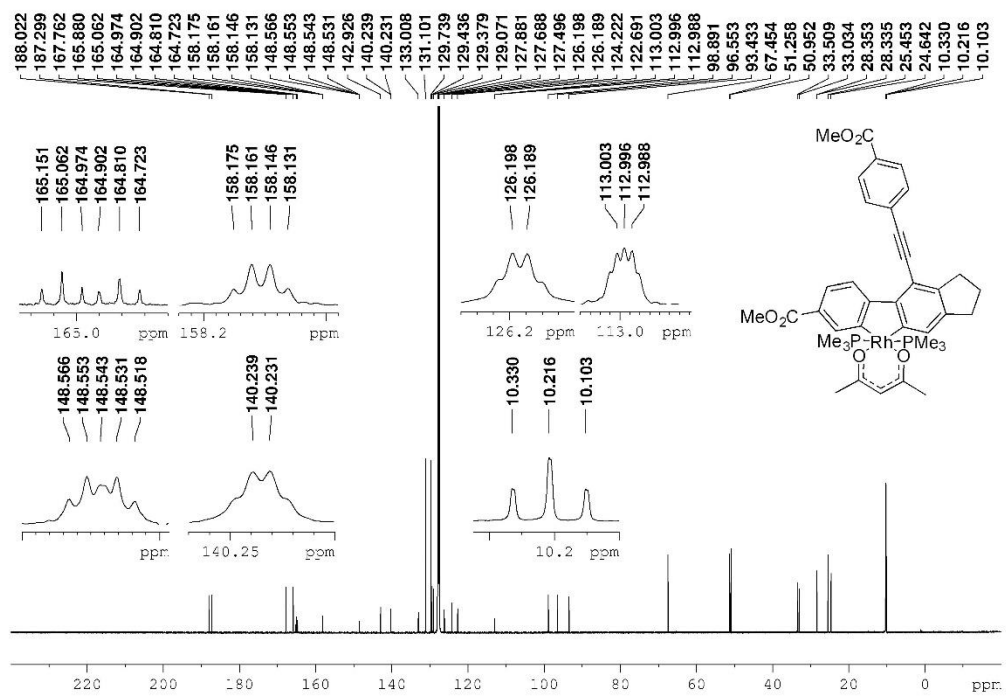
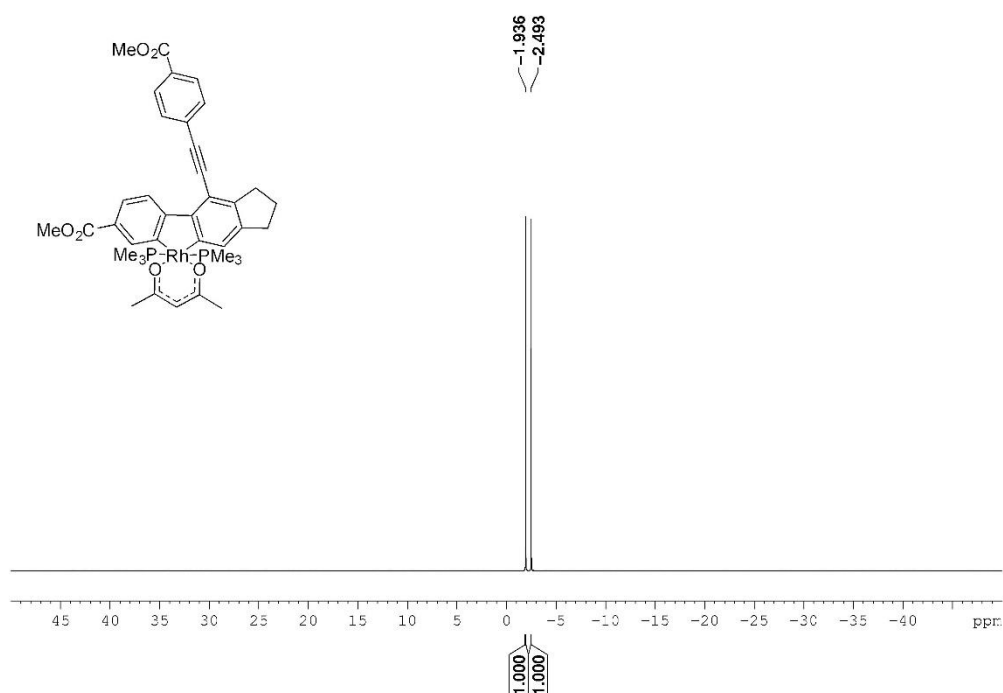
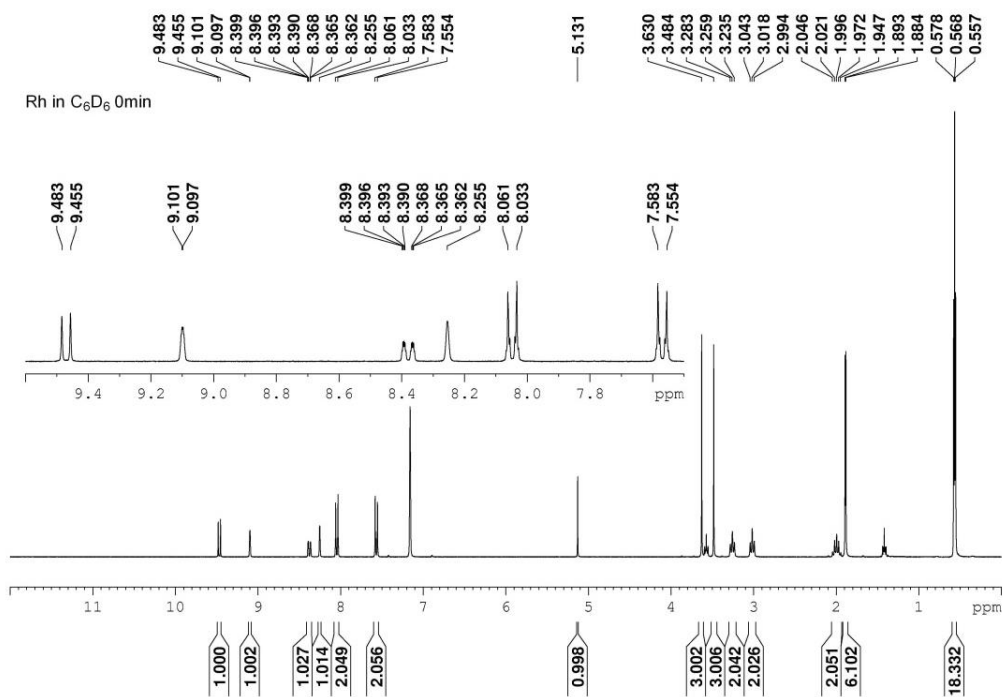


Figure 2-97. <sup>13</sup>C{<sup>1</sup>H} NMR spectrum (126 MHz, C<sub>6</sub>D<sub>6</sub>) of Rh-biphenyl complex.



**Figure 2-98.**  $^{31}\text{P}\{^1\text{H}\}$  NMR spectrum (202 MHz,  $\text{C}_6\text{D}_6$ ) of Rh-biphenyl complex.

The **[Rh]** can be chromatographed in air. As a solid, it is stable in air for at least 2 days. To test the stability of **[Rh]** in solution in air, 0.02 mmol of **[Rh]** (15.2 mg) was dissolved in 0.7 mL of  $\text{C}_6\text{D}_6$  in a Young's tap NMR tube in a glovebox. The  $^1\text{H}$ - and  $^{31}\text{P}$ -NMR spectra were recorded immediately (Figures 2-99 and 2-100). Then the tube was opened and kept in air for 48 h, and then the NMR spectra were recorded again. Small but noticeable changes were observed in the spectra, suggesting that **[Rh]** is unstable in  $\text{C}_6\text{D}_6$  in air. Thus, the solid can be weighed in air, but exposure to air while in solution should be avoided.



**Figure 2-99.** <sup>1</sup>H NMR spectrum of **[Rh]** in C<sub>6</sub>D<sub>6</sub> under Ar (300 MHz, C<sub>6</sub>D<sub>6</sub>).

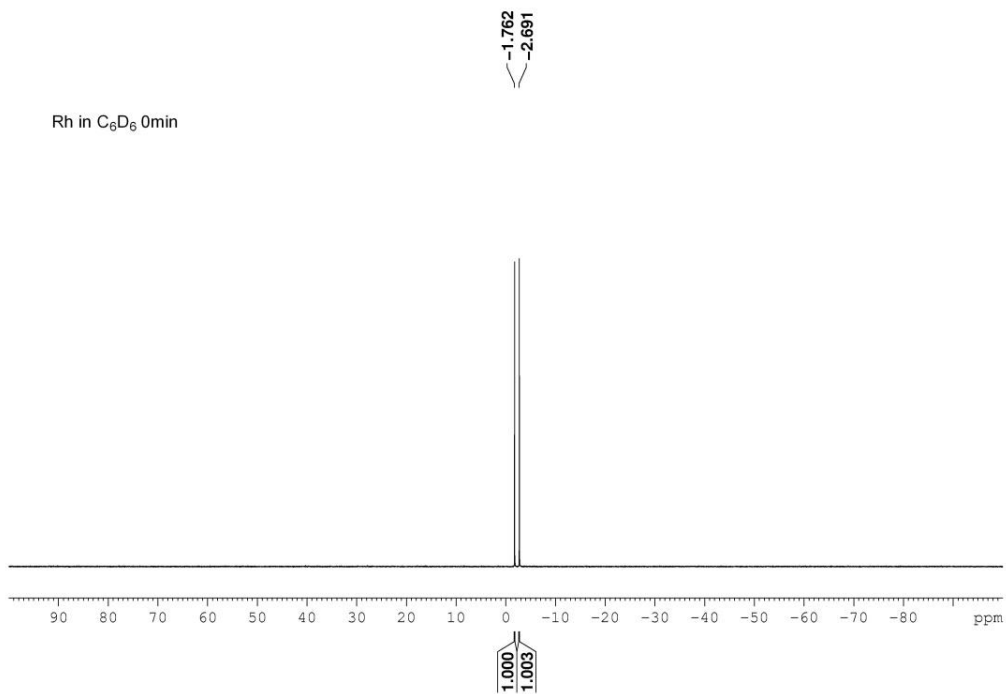


**Figure 2-100.** <sup>31</sup>P NMR spectrum of **[Rh]** in C<sub>6</sub>D<sub>6</sub> under Ar (122 MHz, C<sub>6</sub>D<sub>6</sub>).

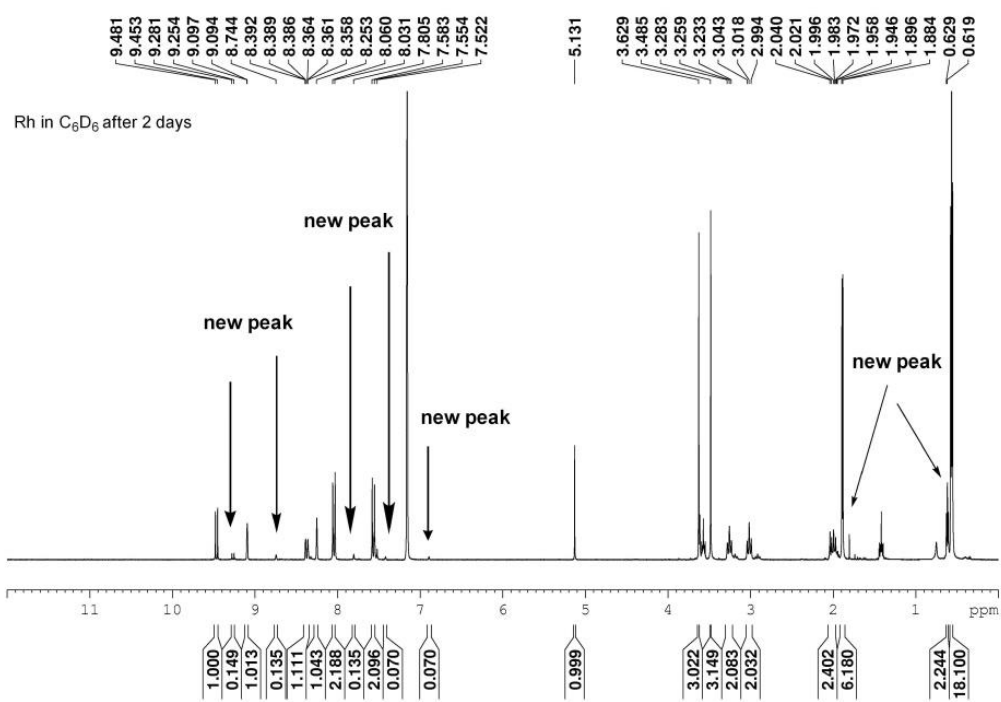


Figure 2-101. <sup>1</sup>H NMR spectrum of [Rh] in C<sub>6</sub>D<sub>6</sub> in air for 48 h (300 MHz, C<sub>6</sub>D<sub>6</sub>).

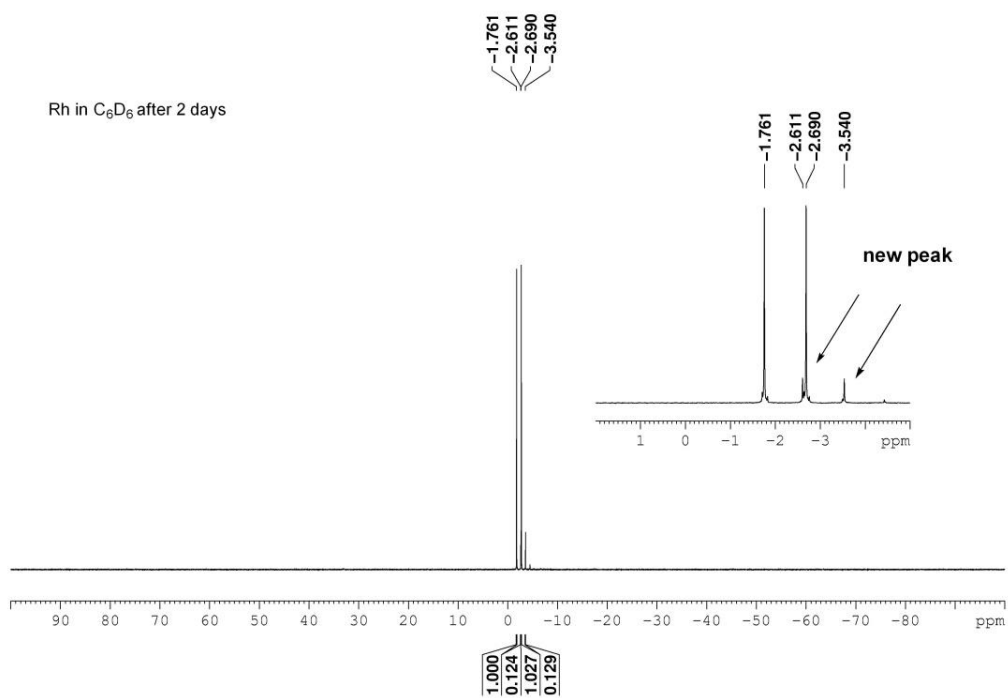
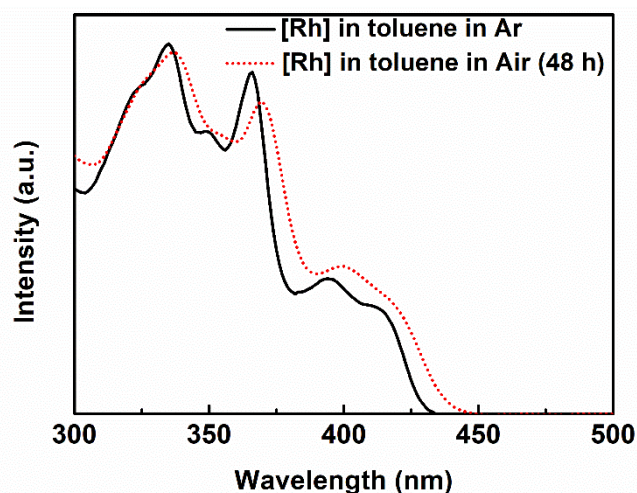


Figure 2-102. <sup>31</sup>P NMR spectrum of [Rh] in C<sub>6</sub>D<sub>6</sub> in air for 48 h (122 MHz, C<sub>6</sub>D<sub>6</sub>).

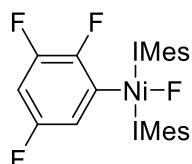
We also prepared two toluene solutions of **[Rh]**. One was kept under Ar, while another one was kept in air for 48 h. Then, their UV-Vis absorption spectra were recorded (Figure 2-103). Again, small but clear changes were observed which suggest that the **[Rh]** is unstable in toluene with some decomposition taking place over 2 days. Therefore, we conducted all experiments in our study under Ar using Schlenk techniques or a glovebox.



**Figure 2-103.** UV-Vis absorption spectra of **[Rh]** in toluene in Ar and in air (48 h).

### 2.6.3 Synthesis and properties of **[Ni<sup>II</sup>]**

Our previous work showed that  $[\text{Ni}(\text{IMes})_2]$  readily inserts into C-F bonds of polyfluorinated aromatics to give the oxidative addition product  $[\text{Ni}^{\text{II}}]$ , which is the first step of their borylation.<sup>26</sup> To investigate the mechanism of photocatalytic borylation of polyfluoroarenes, we prepared  $[\text{Ni}^{\text{II}}]$ . **34a** (39  $\mu\text{L}$ , 0.36 mmol) was added to a solution of  $[\text{Ni}(\text{IMes})_2]$  (239 mg, 0.35 mmol) in toluene (20 mL) and the reaction was stirred overnight. All volatiles were removed *in vacuo* and the remaining solid was suspended in 5 mL hexane. The product was collected by filtration and dried *in vacuo* to give a yellow product.



**Isolated yield:** 73% (208.6 mg, yellow solid).

**<sup>1</sup>H NMR** (500 MHz,  $\text{C}_6\text{D}_6$ ):  $\delta$  6.94 (s, 4H), 6.87 (s, 4H), 6.18-6.12 (m, 1H), 5.91 (s, 4H), 5.52-5.50 (m, 1H), 2.42 (s, 12H), 2.12 (br s, 12H), 1.88 (br s, 12H).

$^{13}\text{C}\{^1\text{H}\}$  NMR (126 MHz,  $\text{C}_6\text{D}_6$ ):  $\delta$  180.0 (d,  $^2J_{\text{C-F}} = 8$  Hz), 153.7 (dd,  $J_{\text{F-C}} = 7$  Hz,  $^1J_{\text{F-C}} = 244$  Hz), 150.3 (ddd,  $J_{\text{F-C}} = 3$  Hz,  $J_{\text{F-C}} = 8$  Hz,  $^1J_{\text{F-C}} = 227$  Hz), 146.7 (ddd,  $J_{\text{F-C}} = 12$  Hz,  $J_{\text{F-C}} = 22$  Hz,  $^1J_{\text{F-C}} = 252$  Hz), 140.8 (br dd,  $J_{\text{F-C}} = 28$  Hz,  $J_{\text{F-C}} = 46$  Hz), 137.4, 136.7 (br), 128.7, 128.6, 121.8, 120.6 (ddd,  $J_{\text{F-C}} = 4$  Hz,  $J_{\text{F-C}} = 18$  Hz,  $J_{\text{F-C}} = 18$  Hz), 95.8 (dd,  $J_{\text{F-C}} = 21$  Hz,  $J_{\text{F-C}} = 28$  Hz), 21.1, 17.9 (br), 17.8 (br).

$^{19}\text{F}$  NMR (471 MHz,  $\text{C}_6\text{D}_6$ ):  $\delta$  -116.8 - -116.9 (m, 1F), -122.8 (dt,  $^3J_{\text{F-H}} = 8$  Hz,  $^4J_{\text{F-F}} = 17$  Hz, 1F), -141.1 (dd,  $^3J_{\text{F-H}} = 10$  Hz,  $^3J_{\text{F-F}} = 32$  Hz, 1F), -344.5 (s, NiF, 1F) ppm.

HRMS:  $m/z$  for  $[\text{C}_{48}\text{H}_{51}\text{F}_4\text{N}_4\text{Ni}]^+ [\text{M}+\text{H}^+]$  calcd: 817.3398, found: 817.3390.

Spectroscopic data for *trans*- $[\text{NiF}(\text{2,3,5-C}_6\text{F}_3\text{H}_2)(\text{IMes})_2]$  match with those previously reported.<sup>26</sup>

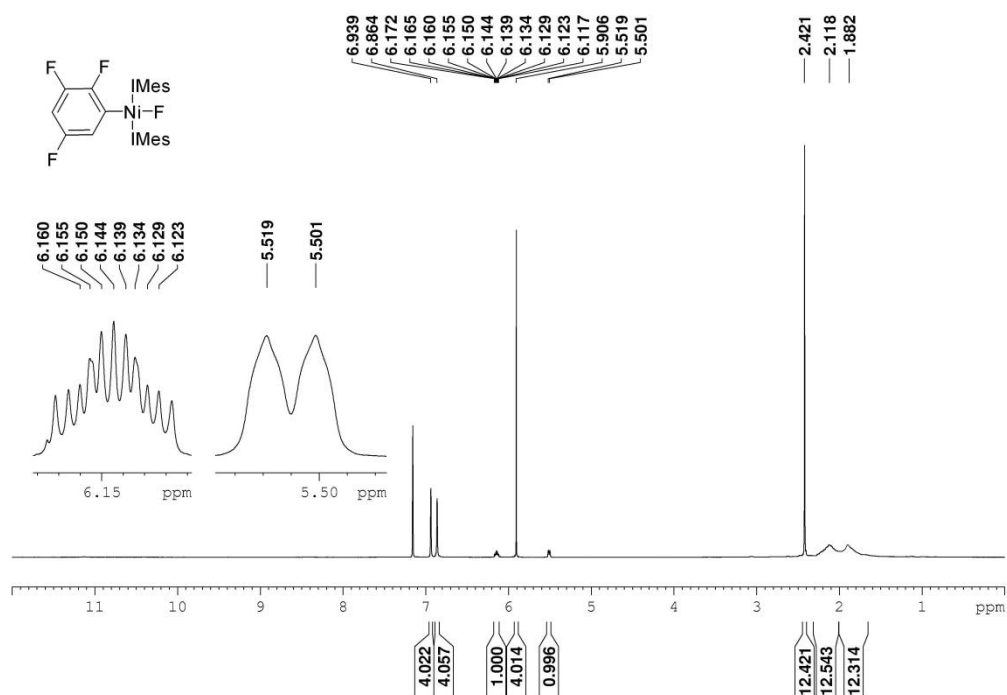


Figure 2-104.  $^1\text{H}$  NMR spectrum (500 MHz,  $\text{C}_6\text{D}_6$ ).

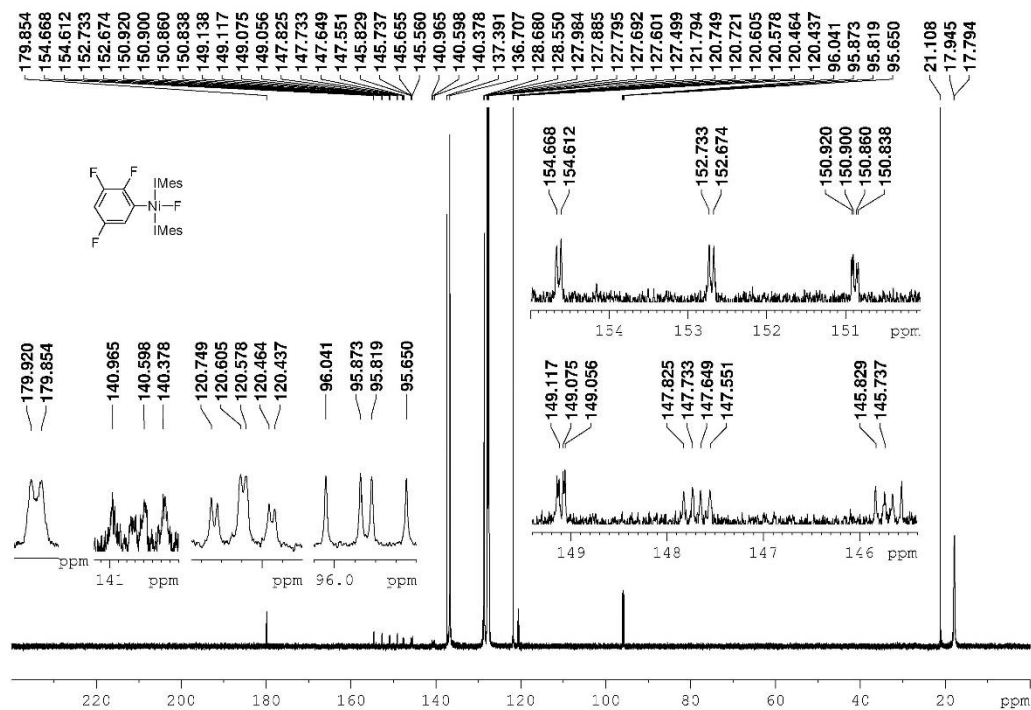


Figure 2-105.  $^{13}\text{C}\{^1\text{H}\}$  NMR spectrum (126 MHz,  $\text{C}_6\text{D}_6$ ).

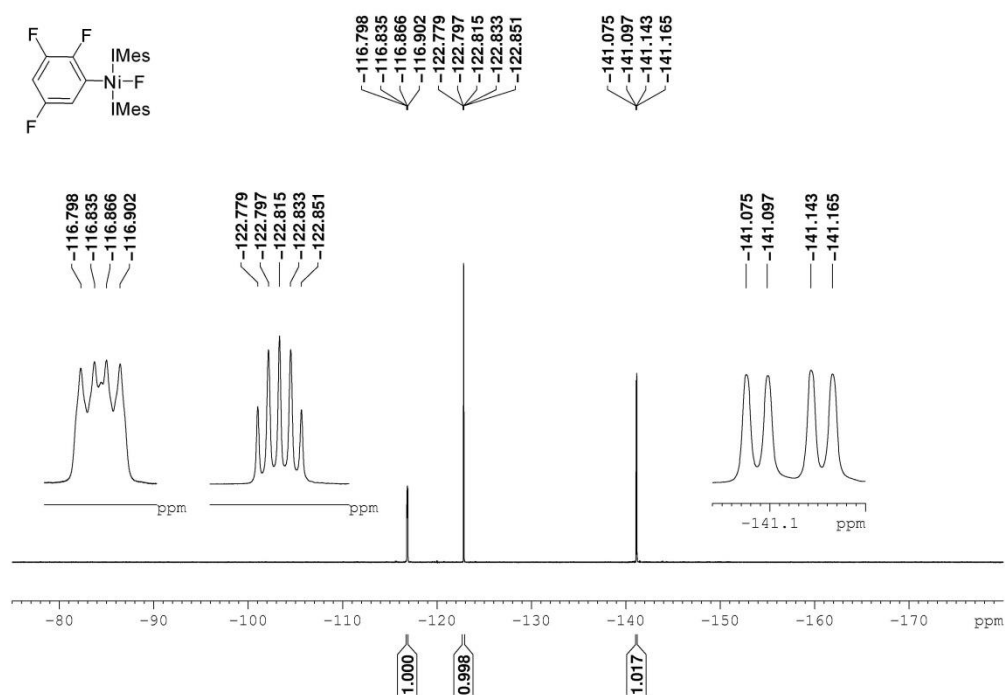
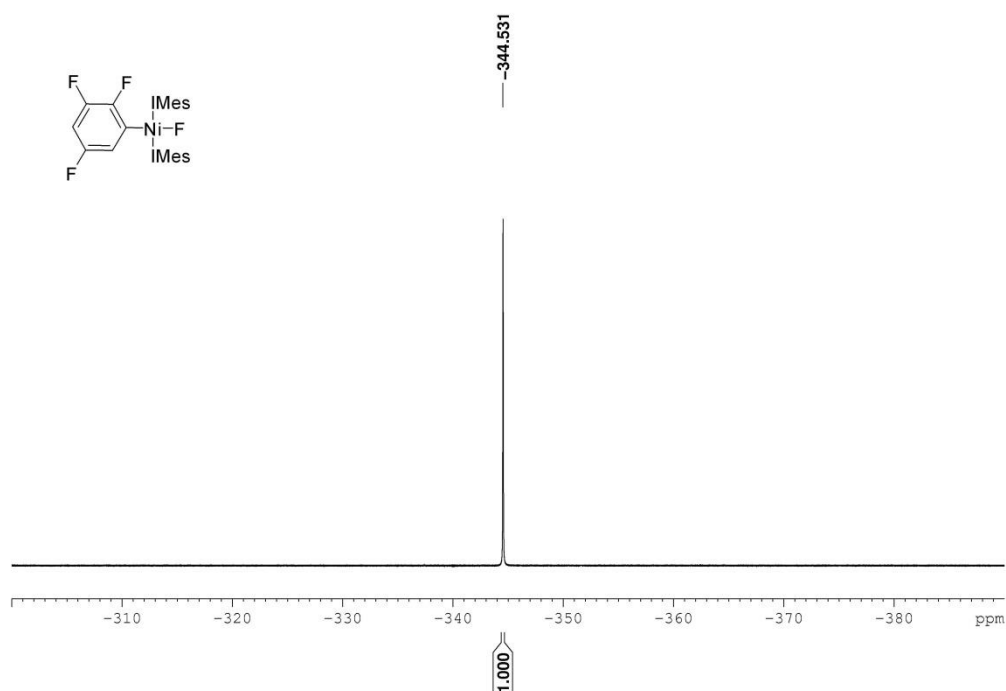


Figure 2-106.  $^{19}\text{F}$  NMR spectrum of aromatic region (471 MHz,  $\text{C}_6\text{D}_6$ ).





**Figure 2-107.**  $^{19}\text{F}$  NMR spectrum of Ni-F resonance (471 MHz,  $\text{C}_6\text{D}_6$ ).

## 2.6.4 Experimental procedures

### Method A

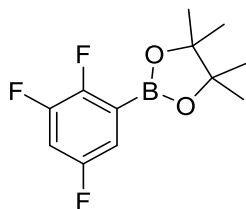
Unless specified otherwise, a mixture of  $[\text{Ni}(\text{IMes})_2]$  (0.02 mmol, 13 mg), **[Rh]** (0.01 mmol, 7.6 mg),  $\text{B}_2\text{pin}_2$  (0.2 mmol, 51 mg) and CsF (0.2 mmol, 31mg) was suspended in the respective solvent (2 mL) in an oven-dried 10 mL vial equipped with a magnetic stirring bar. The fluoroarene (0.22 mmol) was added to the suspension, and then the vial was sealed. The vial was placed between two 400 nm LEDs (1W, the output spectrum is displayed in Figure 2-94) in 1 cm distance from either of them. A fan was used to avoid heating of the reaction system due to the illumination. The reaction mixture was stirred at 25 °C for 6 h, then diluted with dichloromethane (DCM, 2 mL) and filtered through a plug of celite ( $\varnothing$  3 mm  $\times$  8 mm). After addition of *n*-dodecane (34 mg, 0.2 mmol) as an internal standard for calibration, the product yield was determined by GC-MS based on  $\text{B}_2\text{pin}_2$  if not mentioned otherwise.

## Method B

A mixture of [Ni(IMes)<sub>2</sub>] (0.10 mmol, 65 mg), **[Rh]** (0.05 mmol, 38 mg), B<sub>2</sub>pin<sub>2</sub> (1.00 mmol, 254 mg) and CsF (1.00 mmol, 152 mg) was suspended in mesitylene (5 mL) in a Schlenk tube equipped with a magnetic stirring bar. The fluoroarene (1.10 mmol) was added and the Schlenk tube was placed between two 400 nm LEDs (1 W, the output spectrum is displayed in Figure 2-94) in 1 cm distance from either of them. A fan was used to avoid heating of the reaction system due to the illumination. The reaction mixture was stirred at 25 °C for 6 h, was then filtered and the remaining solid was washed with diethyl ether (5 mL Et<sub>2</sub>O). The filtrate was concentrated *in vacuo* and purified by silica-gel column chromatography with hexane, and afterwards with a hexane and ethyl acetate mixture (hexane/EtOAc = 100/1), as eluent. The solvent of the product containing fraction of the eluent was evaporated *in vacuo*. Yields are based on B<sub>2</sub>pin<sub>2</sub>.

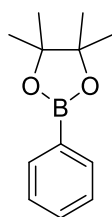
## 2.6.5 Compound characterization

### 4,4,5,5-tetramethyl-2-(2,3,5-trifluorophenyl)-1,3,2-dioxaborolane (**34b**)



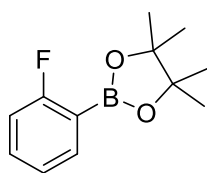
**Isolated yield:** 86 % (222.0 mg, pale yellow liquid).

**<sup>1</sup>H NMR** (500 MHz, CDCl<sub>3</sub>): δ 7.19-7.16 (m, 1H), 7.02-7.00 (m, 1H), 1.36 (s, 12H). **<sup>13</sup>C{<sup>1</sup>H} NMR** (126 MHz, CDCl<sub>3</sub>): δ 157.4 (ddd, *J*<sub>F-C</sub> = 3 Hz, *J*<sub>F-C</sub> = 9 Hz, <sup>1</sup>*J*<sub>F-C</sub> = 246 Hz), 151.0 (ddd, *J*<sub>F-C</sub> = 3 Hz, *J*<sub>F-C</sub> = 11 Hz, <sup>1</sup>*J*<sub>F-C</sub> = 248 Hz), 150.2 (ddd, *J*<sub>F-C</sub> = 10 Hz, *J*<sub>F-C</sub> = 13 Hz, <sup>1</sup>*J*<sub>F-C</sub> = 248 Hz), 116.6 (ddd, *J*<sub>F-C</sub> = 4 Hz, *J*<sub>F-C</sub> = 7 Hz, <sup>2</sup>*J*<sub>F-C</sub> = 22 Hz), 108.3 (ddd, *J*<sub>F-C</sub> = 1 Hz, *J*<sub>F-C</sub> = 21 Hz, *J*<sub>F-C</sub> = 28 Hz), CB not detected, 84.6, 24.8. **<sup>11</sup>B NMR** (160 MHz, CDCl<sub>3</sub>): δ 29.7. **<sup>19</sup>F NMR** (471 MHz, CDCl<sub>3</sub>): δ -116.2- -116.3 (m, 1F), -133.5- -133.6 (m, 1F), -133.9- -134.0 (m, 1F). **HRMS:** *m/z* for [C<sub>12</sub>H<sub>15</sub>BF<sub>3</sub>O<sub>2</sub>]<sup>+</sup> [M+H<sup>+</sup>] calcd: 259.1112, found: 259.1108. Spectroscopic data for **1b** match with those previously reported in the literature.<sup>26</sup>

**4,4,5,5-tetramethyl-2-phenyl-1,3,2-dioxaborolane (35b)**

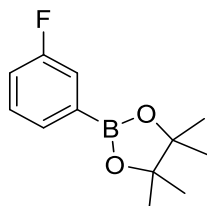
**Isolated yield:** 41% (83.7 mg, pale yellow liquid).

**<sup>1</sup>H NMR** (500 MHz, CDCl<sub>3</sub>): δ 7.85-7.83 (m, 2H), 7.50-7.46 (m, 1H), 7.41-7.37 (m, 2H), 1.37 (s, 12H). **<sup>13</sup>C{<sup>1</sup>H} NMR** (126 MHz, CDCl<sub>3</sub>): δ 134.8, 131.3, 127.7, CB not detected, 83.8, 24.9. **<sup>11</sup>B NMR** (160 MHz, CDCl<sub>3</sub>): δ 31.1. **HRMS:** *m/z* for [C<sub>12</sub>H<sub>18</sub>BO<sub>2</sub>]<sup>+</sup> [M+H<sup>+</sup>] calcd: 205.1394, found: 205.1392. Spectroscopic data for **2b** match with those previously reported in the literature.<sup>26,97</sup>

**2-(2-fluorophenyl)-4,4,5,5-tetramethyl-1,3,2-dioxaborolane (36b)**

**Isolated yield:** 58 % (128.8 mg, pale yellow liquid).

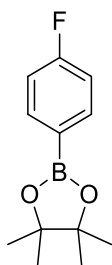
**<sup>1</sup>H NMR** (500 MHz, CDCl<sub>3</sub>): δ 7.76-7.73 (m, 1H), 7.46-7.41 (m, 1H), 7.15-7.12 (m, 1H), 7.05-7.01 (m, 1H), 1.37 (s, 12H). **<sup>13</sup>C{<sup>1</sup>H} NMR** (126 MHz, CDCl<sub>3</sub>): δ 167.2 (d, <sup>1</sup>J<sub>F-C</sub> = 251 Hz), 136.8 (d, <sup>3</sup>J<sub>F-C</sub> = 8 Hz), 133.2 (d, <sup>3</sup>J<sub>F-C</sub> = 9 Hz), 123.6 (d, <sup>4</sup>J<sub>F-C</sub> = 3 Hz), 115.8 (br, CB), 115.2 (d, <sup>2</sup>J<sub>F-C</sub> = 24 Hz), 83.9, 24.8. **<sup>11</sup>B NMR** (160 MHz, CDCl<sub>3</sub>): δ 30.3. **<sup>19</sup>F NMR** (471 MHz, CDCl<sub>3</sub>): δ -102.5- -102.6 (m, 1F). **HRMS:** *m/z* for [C<sub>12</sub>H<sub>17</sub>BFO<sub>2</sub>]<sup>+</sup> [M+H<sup>+</sup>] calcd: 223.1300, found: 223.1297. Spectroscopic data for **3b** match with those previously reported in the literature.<sup>26,208</sup>

**2-(3-fluorophenyl)-4,4,5,5-tetramethyl-1,3,2-dioxaborolane (37b)**

**Isolated yield:** 59% (131.1mg, pale yellow liquid).

**<sup>1</sup>H NMR** (500 MHz, CDCl<sub>3</sub>): δ 7.60-7.58 (m, 1H), 7.51-7.49 (m, 1H), 7.35-7.32 (m, 1H), 7.16-7.14 (m, 1H), 1.35 (s, 12H). **<sup>13</sup>C{<sup>1</sup>H} NMR** (126 MHz, CDCl<sub>3</sub>): δ 162.5 (d, <sup>1</sup>J<sub>F-C</sub> = 247 Hz), 131.2 (br, CB), 130.3 (d, <sup>4</sup>J<sub>F-C</sub> = 3 Hz), 129.5 (d, <sup>3</sup>J<sub>F-C</sub> = 7 Hz), 121.0 (d, <sup>2</sup>J<sub>F-C</sub> = 19 Hz), 118.2 (d, <sup>2</sup>J<sub>F-C</sub> = 21 Hz), 84.1, 24.9. **<sup>11</sup>B NMR** (160 MHz, CDCl<sub>3</sub>): δ 30.6. **<sup>19</sup>F NMR** (471 MHz, CDCl<sub>3</sub>): δ -114.1- -114.2 (m, 1F). **HRMS:** *m/z* for [C<sub>12</sub>H<sub>17</sub>BFO<sub>2</sub>]<sup>+</sup> [M+H<sup>+</sup>] calcd: 223.1300, found: 223.1297. Spectroscopic data for **4b** match with those previously reported in the literature.<sup>26,208</sup>

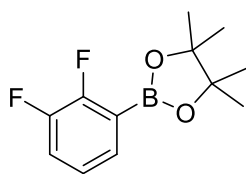
### 2-(4-Fluorophenyl)-4,4,5,5-tetramethyl-1,3,2-dioxaborolane (**38b**)



**Isolated yield:** 31% (68.9 mg, white solid).

**<sup>1</sup>H NMR** (500 MHz, CDCl<sub>3</sub>): δ 7.84-7.80 (m, 2H), 7.08-7.03 (m, 2H), 1.34 (s, 12H). **<sup>13</sup>C{<sup>1</sup>H} NMR** (126 MHz, CDCl<sub>3</sub>): δ 165.1(d, *J*<sub>F-C</sub> = 311 Hz), 137.0 (d, *J*<sub>F-C</sub> = 10 Hz), 124.8 (br, CB), 114.8 (d, *J*<sub>F-C</sub> = 25 Hz), 83.9, 24.8. **<sup>11</sup>B NMR** (160 MHz, CDCl<sub>3</sub>): δ 30.6. **<sup>19</sup>F NMR** (471 MHz, CDCl<sub>3</sub>): δ -108.4- -108.5 (m, 1F). **HRMS:** *m/z* for [C<sub>12</sub>H<sub>17</sub>BFO<sub>2</sub>]<sup>+</sup> [M+H<sup>+</sup>] calcd: 223.1300, found: 223.1297. Spectroscopic data for **5b** match with those previously reported in the literature.<sup>208,209</sup>

### 2-(2,3-difluorophenyl)-4,4,5,5-tetramethyl-1,3,2-dioxaborolane (**39b**)



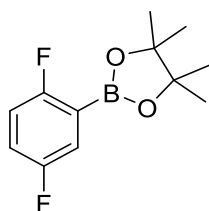
**Isolated yield:** 65% (156.1 mg, pale yellow liquid).

**<sup>1</sup>H NMR** (500 MHz, CDCl<sub>3</sub>): δ 7.47-7.45 (m, 1H), 7.25-7.21 (m, 1H), 7.09-7.05 (m, 1H), 1.37 (s, 12H). **<sup>13</sup>C{<sup>1</sup>H} NMR** (126 MHz, CDCl<sub>3</sub>): δ 154.5 (dd, <sup>1</sup>J<sub>F-C</sub> = 251 Hz, <sup>2</sup>J<sub>F-C</sub> = 12 Hz),

150.4 (dd,  $^1J_{F-C} = 247$  Hz,  $^2J_{F-C} = 14$  Hz), 131.1 (dd,  $J_{F-C} = 4$  Hz,  $J_{F-C} = 7$  Hz), 124.1 (dd,  $J_{F-C} = 4$  Hz,  $J_{F-C} = 6$  Hz), 120.2 (dd,  $^2J_{F-C} = 17$  Hz,  $J_{F-C} = 1$  Hz), 118.6 (br, CB), 84.2, 24.8.  **$^{11}B$  NMR** (160 MHz,  $CDCl_3$ ):  $\delta$  30.0.  **$^{19}F$  NMR** (471 MHz,  $CDCl_3$ ):  $\delta$  -129.0- -129.1 (m, 1F), -139.0- -139.1 (m, 1F).

**HRMS:**  $m/z$  for  $[C_{12}H_{16}BF_2O_2]^+ [M+H^+]$  calcd: 241.1206, found: 241.1197. Spectroscopic data for **6b** match with those previously reported in the literature.<sup>26,210</sup>

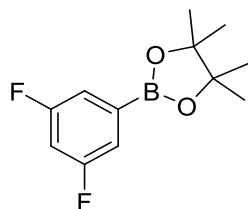
### 2-(2,5-difluorophenyl)-4,4,5,5-tetramethyl-1,3,2-dioxaborolane (40b)



**Isolated yield:** 82% (196.9 mg, pale yellow liquid).

**$^1H$  NMR** (500 MHz,  $CDCl_3$ ):  $\delta$  7.40-7.37 (m, 1H), 7.11-7.07 (m, 1H), 7.00-6.97 (m, 1H), 1.36 (s, 12H).  **$^{13}C\{^1H\}$  NMR** (126 MHz,  $CDCl_3$ ):  $\delta$  163.0 (dd,  $^1J_{C-F} = 247$  Hz,  $^4J_{C-F} = 2$  Hz), 158.4 (dd,  $^1J_{C-F} = 243$  Hz,  $^4J_{C-F} = 3$  Hz), 122.2 (dd,  $^2J_{C-F} = 23$  Hz,  $^3J_{C-F} = 9$  Hz), 119.7 (dd,  $^2J_{C-F} = 24$  Hz,  $^3J_{C-F} = 10$  Hz), 116.6 (dd,  $^2J_{C-F} = 27$  Hz,  $^3J_{C-F} = 8$  Hz), CB not detected, 84.2, 24.8.  **$^{11}B$  NMR** (160 MHz,  $CDCl_3$ ):  $\delta$  29.9.  **$^{19}F$  NMR** (471 MHz,  $CDCl_3$ ):  $\delta$  -109.4- -109.5 (m, 1F), -120.5- -120.6 (m, 1F). **HRMS:**  $m/z$  for  $[C_{12}H_{16}BF_2O_2]^+ [M+H^+]$  calcd: 241.1206, found: 241.1201. Spectroscopic data for **7b** match with those previously reported in the literature.<sup>26,210</sup>

### 2-(3,5-difluorophenyl)-4,4,5,5-tetramethyl-1,3,2-dioxaborolane (41b)

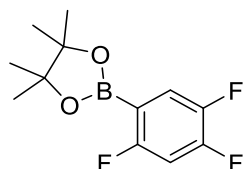


**Isolated yield:** 83% (199.3 mg, colorless solid).

**$^1H$  NMR** (500 MHz,  $CDCl_3$ ):  $\delta$  7.30-7.28 (m, 2H), 6.87 (tt,  $^3J_{F-H} = 9$  Hz,  $^4J_{H-H} = 2$  Hz, 1H), 1.34 (s, 12H).  **$^{13}C\{^1H\}$  NMR** (126 MHz,  $CDCl_3$ ):  $\delta$  162.8 (dd,  $^1J_{F-C} = 246$  Hz,  $^3J_{F-C} = 11$  Hz),

116.8 (m), 106.5 (t,  $^2J_{F-C} = 25$  Hz), CB not detected, 84.4, 24.8.  **$^{11}\text{B}$  NMR** (160 MHz,  $\text{CDCl}_3$ ):  $\delta$  30.1.  **$^{19}\text{F}$  NMR** (471 MHz,  $\text{CDCl}_3$ ):  $\delta$  -110.7- -110.8 (m, 2F). **HRMS**:  $m/z$  for  $[\text{C}_{12}\text{H}_{16}\text{BF}_2\text{O}_2]^+ [\text{M}+\text{H}^+]$  calcd: 241.1206, found: 241.1201. Spectroscopic data for **8b** match with those previously reported in the literature.<sup>26,208</sup>

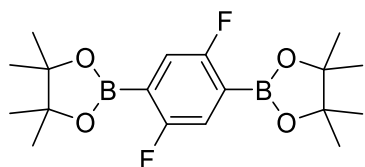
#### 4,4,5,5-tetramethyl-2-(2,4,5-trifluorophenyl)-1,3,2-dioxaborolane (**42b**)



**Isolated yield**: 32% (82.6 mg, pale yellow liquid).

**$^1\text{H}$  NMR** (500 MHz,  $\text{CDCl}_3$ ):  $\delta$  7.51 (td,  $^4J_{F-H} = 5$  Hz,  $^3J_{F-H} = 10$  Hz, 1H), 6.88 (ddd,  $^4J_{F-H} = 6$  Hz,  $^4J_{F-H} = 8$  Hz,  $^3J_{F-H} = 10$  Hz, 1H), 1.35 (s, 12H).  **$^{13}\text{C}\{^1\text{H}\}$  NMR** (126 MHz,  $\text{CDCl}_3$ ):  $\delta$  162.6 (ddd,  $^4J_{F-C} = 2$  Hz,  $^3J_{F-C} = 10$  Hz,  $^1J_{F-C} = 251$  Hz), 152.5 (ddd,  $J_{F-C} = 13$  Hz,  $J_{F-C} = 15$  Hz,  $^1J_{F-C} = 255$  Hz), 146.8 (ddd,  $^4J_{F-C} = 4$  Hz,  $^2J_{F-C} = 12$  Hz,  $^1J_{F-C} = 245$  Hz), 123.8 (ddd,  $J_{F-C} = 2$  Hz,  $J_{F-C} = 10$  Hz,  $J_{F-C} = 18$  Hz), 112.5 (br, CB), 105.5 (dd,  $J_{F-C} = 20$  Hz,  $J_{F-C} = 31$  Hz), 84.3, 24.8.  **$^{11}\text{B}$  NMR** (160 MHz,  $\text{CDCl}_3$ ):  $\delta$  29.7.  **$^{19}\text{F}$  NMR** (471 MHz,  $\text{CDCl}_3$ ):  $\delta$  -104.1- -104.2 (m, 1F), -128.4- -128.5 (m, 1F), -144.1- -144.2 (m, 1F). **HRMS**:  $m/z$  for  $[\text{C}_{12}\text{H}_{15}\text{BF}_3\text{O}_2]^+ [\text{M}+\text{H}^+]$  calcd: 259.1112, found: 259.1107. Spectroscopic data for **9b** match with those previously reported in the literature.<sup>26</sup>

#### 2,2'-(2,5-difluoro-1,4-phenylene)bis(4,4,5,5-tetramethyl-1,3,2-dioxaborolane) (**42c**)

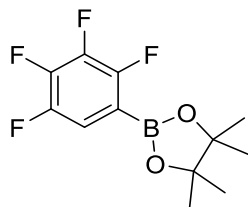


**Isolated yield**: 43% (157.5 mg, white solid).

**$^1\text{H}$  NMR** (500 MHz,  $\text{CDCl}_3$ ):  $\delta$  7.35 (AA'XX' – system,  $|^3J_{F-H} + ^4J_{F-H}| = 13$  Hz, 2H), 1.35 (s, 24H).  **$^{13}\text{C}\{^1\text{H}\}$  NMR** (126 MHz,  $\text{CDCl}_3$ ):  $\delta$  162.5 (dd,  $^1J_{F-C} = 250$  Hz,  $^4J_{F-C} = 4$  Hz), 122.4 (AXX' – system,  $|^2J_{F-C} + ^3J_{F-C}| = 34$  Hz), 121.0 (br, CB), 84.3, 24.8.  **$^{11}\text{B}$  NMR** (160 MHz,  $\text{CDCl}_3$ ):  $\delta$  29.8.  **$^{19}\text{F}$  NMR** (471 MHz,  $\text{CDCl}_3$ ):  $\delta$  -111.0 (AA'XX' – system,  $|^3J_{F-H} + ^4J_{F-H}| = 13$  Hz, 2F). **HRMS**:  $m/z$  for  $[\text{C}_{18}\text{H}_{27}\text{B}_2\text{F}_2\text{O}_4]^+ [\text{M}+\text{H}^+]$  calcd: 367.2058, found: 367.2054.

Spectroscopic data for **9c** match with those previously reported in the literature.<sup>26,211</sup>

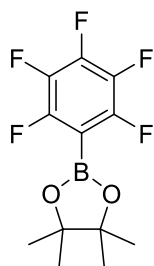
#### 4,4,5,5-tetramethyl-2-(2,3,4,5-tetrafluorophenyl)-1,3,2-dioxaborolane (**43b**)



**Isolated yield:** 85% (234.7 mg, pale yellow liquid).

**<sup>1</sup>H NMR** (500 MHz, CDCl<sub>3</sub>): δ 7.33-7.28 (m, 1H), 1.35 (s, 12H). **<sup>13</sup>C{<sup>1</sup>H} NMR** (126 MHz, CDCl<sub>3</sub>): δ 151.5 (dddd,  $J_{F-C} = 2$  Hz,  $J_{F-C} = 3$  Hz,  $J_{F-C} = 9$  Hz,  $^1J_{F-C} = 250$  Hz), 147.0 (ddd,  $J_{F-C} = 3$  Hz,  $J_{F-C} = 10$  Hz,  $^1J_{F-C} = 247$  Hz), 142.6 (dddd,  $J_{F-C} = 4$  Hz,  $J_{F-C} = 12$  Hz,  $J_{F-C} = 17$  Hz,  $^1J_{F-C} = 255$  Hz), 140.5 (dddd,  $J_{F-C} = 3$  Hz,  $J_{F-C} = 12$  Hz,  $J_{F-C} = 19$  Hz,  $^1J_{F-C} = 253$  Hz), 116.5 (ddd,  $J_{F-C} = 4$  Hz,  $J_{F-C} = 8$  Hz,  $^2J_{F-C} = 18$  Hz), 112.2 (br, CB), 84.6, 24.7. **<sup>11</sup>B NMR** (160 MHz, CDCl<sub>3</sub>): δ 29.5. **<sup>19</sup>F NMR** (471 MHz, CDCl<sub>3</sub>): δ -128.9- -129.0 (m, 1F), -139.7- -139.8 (m, 1F), -150.9- -151.0 (m, 1F), -156.0- -156.1 (m, 1F). **HRMS:**  $m/z$  for [C<sub>12</sub>H<sub>14</sub>BF<sub>4</sub>O<sub>2</sub>]<sup>+</sup> [M+H<sup>+</sup>] calcd: 277.1017, found: 277.1009. Spectroscopic data for **10b** match with those previously reported in the literature.<sup>26</sup>

#### 4,4,5,5-tetramethyl-2-(2,3,4,5,6-pentafluorophenyl)-1,3,2-dioxaborolane (**44b**)



**Isolated yield:** 25% (73.5mg, white solid).

**<sup>1</sup>H NMR** (500 MHz, CDCl<sub>3</sub>): δ 1.37 (s, 12H). **<sup>13</sup>C{<sup>1</sup>H} NMR** (126 MHz, CDCl<sub>3</sub>): δ 150.3 (m), 148.3 (m), 144.0 (m), 141.9 (m), 138.3 (m), 136.3 (m), 84.9, 24.7. **<sup>11</sup>B NMR** (160 MHz, CDCl<sub>3</sub>): δ 29.1. **<sup>19</sup>F NMR** (471 MHz, CDCl<sub>3</sub>): δ -129.5- -129.6 (m, 2F), -149.7- -149.8 (m, 1F), -161.9- -162.0 (m, 2F). **HRMS:**  $m/z$  for [C<sub>12</sub>H<sub>13</sub>BF<sub>5</sub>O<sub>2</sub>]<sup>+</sup> [M+H<sup>+</sup>] calcd: 295.0923, found: 295.0918. Spectroscopic data for **11b** match with those previously reported in the literature.<sup>212</sup>





## **Chapter Three**

# **Visible-light-induced Ni-catalyzed radical borylation of chloroarenes**



## 3 Visible-light-induced Ni-catalyzed radical borylation of chloroarenes

### 3.1 Abstract

A highly selective and general photo-induced C-Cl borylation protocol that employs  $[\text{Ni}(\text{IMes})_2]$  (IMes = 1,3-dimesitylimidazoline-2-ylidene) for the radical borylation of chloroarenes is reported. This photo-induced system operates with visible light (400 nm) and achieves borylation of a wide range of chloroarenes with  $\text{B}_2\text{pin}_2$  at room temperature in excellent yields and with high selectivity, thereby demonstrating its broad utility and functional group tolerance. Mechanistic investigations suggest that the borylation reactions proceed via a radical process. EPR studies demonstrate that  $[\text{Ni}(\text{IMes})_2]$  undergoes very fast chlorine atom abstraction from aryl chlorides to give  $[\text{Ni}^{\text{I}}(\text{IMes})_2\text{Cl}]$  and aryl radicals. Control experiments indicate that light promotes the reaction of  $[\text{Ni}^{\text{I}}(\text{IMes})_2\text{Cl}]$  with aryl chlorides generating additional aryl radicals and  $[\text{Ni}^{\text{II}}(\text{IMes})_2\text{Cl}_2]$ . The aryl radicals react with an anionic  $\text{sp}^2\text{-sp}^3$  diborane  $[\text{B}_2\text{pin}_2(\text{OMe})]^-$  formed from  $\text{B}_2\text{pin}_2$  and KOMe to yield the corresponding borylation product and the  $[\text{Bpin}(\text{OMe})]^-$  radical anion, which reduces  $[\text{Ni}^{\text{II}}(\text{IMes})_2\text{Cl}_2]$  under irradiation to regenerate  $[\text{Ni}^{\text{I}}(\text{IMes})_2\text{Cl}]$  and  $[\text{Ni}(\text{IMes})_2]$  for the next catalytic cycle.

## 3.2 Introduction

Arylboronic esters have been recognized as key building blocks in organic synthesis, materials science, and drug discovery.<sup>1-4,38-40,44,45,53</sup> Recently, highly selective transition metal-catalyzed borylations of aryl halides, based on Pd,<sup>46,47,64,80,213-234</sup> Ni,<sup>124,235-244</sup> Fe,<sup>245-250</sup> Cu,<sup>77,94,125,251-256</sup> Co,<sup>257-262</sup> Zn,<sup>97,116,263</sup> have been developed as an efficient method to synthesize arylboronic esters. Aryl iodides and bromides are frequently employed as precursors to aryl boronate esters. However, although widely available and inexpensive, chloroarene borylation is more challenging due to the relatively high C-Cl bond energy. Ishiyama et al. first achieved the borylation of C-Cl bonds by using a Pd(0)-tricyclohexylphosphine complex as a catalyst in 2001.<sup>215</sup> The groups of Yamakawa<sup>242</sup> and Nakamura<sup>249</sup> showed that employing  $[\text{NiCl}_2(\text{PMe}_3)_2]$  and  $[\text{Fe}(\text{acac})_3]$  as catalyst efficiently borylate chloroarenes in the presence of cesium 2,2,2-trifluoroethoxide and KO<sup>t</sup>Bu at 100 and 130 °C, respectively. Our groups recently reported an efficient catalytic procedure for the C-Cl borylation of chloroarenes using NHC-Ni (NHC = N-heterocyclic carbene) complexes as catalysts and bis(pinacolato)diboron ( $\text{B}_2\text{pin}_2$ ) as the boron source at 100 °C.<sup>244</sup> In 2016, we showed that the selective C-F borylation of polyfluoroaromatic compounds can be catalyzed by  $[\text{Ni}(\text{IMes})_2]$  in the presence of  $[\text{NMe}_4]\text{F}$  or CsF at 80 °C.<sup>126</sup> Geetharani et al. also reported an efficient catalytic system based on a Co(II)-NHC precursor for the borylation of chloroarenes at 50 °C, affording the aryl boronates in good to excellent yields.<sup>262</sup> Recently, our groups developed an efficient Cu-catalyzed borylation of aryl chlorides at 90 °C.<sup>256</sup> Jiao et al. recently developed a pyridine-catalyzed transition-metal-free radical borylation of aryl halides at 85 °C, but only two chloroarenes were described in this report.<sup>92,93,264-272</sup>

Photocatalysis, as an alternative to the thermally induced borylation of aryl halides by transition metals, has recently emerged as a powerful tool for the synthesis of aryl boronate esters due to the great enhancement of the catalytic efficiency.<sup>54,55,136,137</sup> For example, Li et al.<sup>74,95</sup> and Larionov et al.<sup>73,75,96</sup> showed that aryl halides, mesitylates, and ammonium salts can be photochemically borylated. Aryl radicals, produced by photoinduced homolytic or heterolytic cleavage of the C(arene)-X bond, react with a boron

source to form the target aryl boronates. However, the necessary high-intensity UV irradiation poses potential limitations to the applicability of this method. Visible light photoredox catalysts can also be employed to generate aryl boronates from aryl halides. Fu et al. developed a visible-light photoredox borylation of aryl halides with  $B_2pin_2$  using of *fac*-Ir(ppy)<sub>3</sub> as the photocatalyst.<sup>65</sup> The method displays high tolerance for various functional groups; however, it is limited to aryl iodides and bromides. The photocatalytic conversion of widely available aryl pseudohalides, carboxylic acids, aryldiazonium salts, and aromatic amines into versatile boronic esters has been reported by Li, Glorius, Aggarwal, Yan and Ranu et al.<sup>138-143</sup> Very recently, Jiao et al. reported a visible-light-induced organocatalytic method for the borylation of unactivated chloroarenes, and even fluorides, by photoactivation of the super electron donor (SED) complex generated *in situ* in a diboron/methoxide/pyridine reaction system.<sup>85,273-276</sup> Our group recently reported a photocatalytic C-F borylation protocol that employs a Rh biphenyl complex (**[Rh]**) as a triplet sensitizer and the nickel catalyst [Ni(IMes)<sub>2</sub>] for the borylation of C-F bonds on arylfluorides.<sup>277</sup> Further mechanistic studies showed that the exceptionally long-lived triplet excited state of the Rh biphenyl complex allows for efficient triplet energy transfer to the oxidative addition product *trans*-[Ni<sup>II</sup>F(Ar<sup>F</sup>)(IMes)<sub>2</sub>] to greatly enhance the rate constant for the transmetalation step with  $B_2pin_2$  at room temperature.<sup>170,277</sup>

Cavell et al. found that small NHC ligands with less steric hindrance, such as 1,3,4,5-tetramethylimidazol-2-ylidene (tmiy), permit oxidative addition to form Ni<sup>II</sup> complexes,<sup>278</sup> while Matsubara et al. found that larger NHC ligands, such as 1,3-bis-(2,6-diisopropylphenyl)imidazolin-2-ylidene (IPr), favour halide abstraction to form Ni<sup>I</sup> complexes plus aryl radicals.<sup>279</sup> Louie et al. and Nelson et al. further confirmed that the products of the reactions of [Ni(NHC)<sub>2</sub>] with aryl halides are mainly dominated by the steric impact of the NHC ligand, based on experimental and computational investigations, respectively.<sup>280,281</sup> With this information, and the fact that aryl radicals are well-known as one of the intermediates in some catalytic borylation processes, we hoped to achieve the activation of chloroarenes to form the corresponding arylboronic esters utilizing [Ni(IMes)<sub>2</sub>] as the catalyst.

### 3.3 Results and discussions

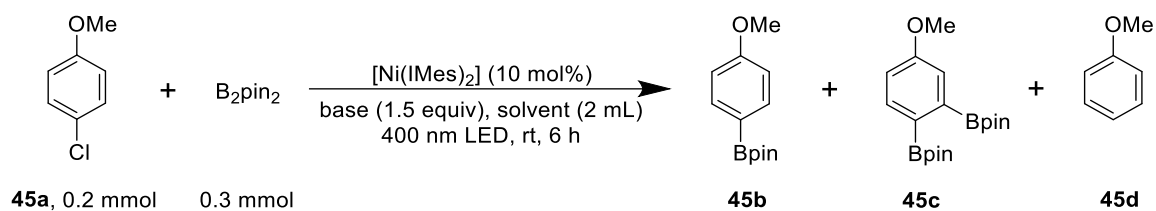
#### 3.3.1 Photocatalytic borylation of 4-chloroanisole

We first investigated the efficiency of the borylation reaction of 4-chloroanisole (**45a**) with  $B_2pin_2$  in the presence of KOMe using 10 mol %  $[Ni(IMes)_2]$  as the catalyst at 25 °C, which gave a 12% yield of 1-Bpin-4-methoxybenzene (**45b**) after 2 h (Table 3-1, entry 1). When the reaction time was extended to 6 h, the yield of **45b** was almost the same, suggesting that the protocol is inefficient.

**Table 3-1. Photo-induced borylation of 45a**

Entry	[Ni(IMes) <sub>2</sub> ] (10 mol%)	[Rh] (5 mol%)	400 nm LED	Time	Yield (%) <sup>a</sup>		
					<b>45b</b>	<b>45c</b>	<b>45d</b>
1	✓	✗	✗	6 h (2 h)	14 (12)	3 (2)	3 (trace)
2	✓	✗	✓	6 h (2 h)	86 (35)	11 (8)	2 (2)
3	✓	✓	✗	2 h	13	4	2
4	✓	✓	✓	2 h	72	13	15
5	✗	✓	✓	2 h	0	0	0
6	✗	✗	✓	2 h	0	0	0

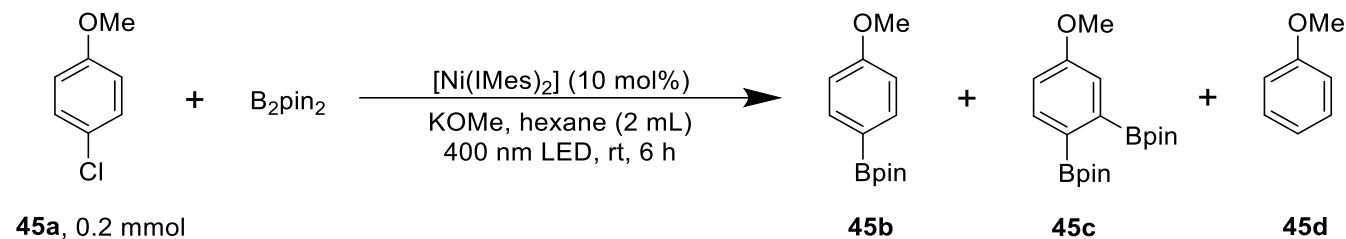
<sup>a</sup>The yields were determined by GC-MS analysis vs. a calibrated internal standard and are averages of two runs.

**Table 3-2. Optimization of the reaction conditions for the photo-induced borylation of 4-chloroanisole**

Entry	Base (1.5 equiv)	Solvent (2 mL)	Yield (%) <sup>a</sup>		
			<b>45b</b>	<b>45c</b>	<b>45d</b>
1	KOMe	hexane	86	11	2
2	KOMe	methylcyclohexane	79	9	7
3	KOMe	toluene	71	5	15
4	KOMe	THF	67	4	23
5	KOMe	THF-d <sub>8</sub>	61	3	20 <sup>b</sup>
6	KOMe	MTBE	45	13	5
7	KOMe	Et <sub>2</sub> O	16	trace	12
8	NaOMe	hexane	21	5	5
9	KO <sup>t</sup> Bu	hexane	72	13	9
10	Li <sub>2</sub> CO <sub>3</sub>	hexane	13	7	3
11	Cs <sub>2</sub> CO <sub>3</sub>	hexane	18	8	4
12	KOAc	hexane	54	4	3
13	NaOAc	hexane	53	4	3
14	KF	hexane	9	6	4
15	CsF	hexane	12	8	5
16	-	hexane	4	3	trace

<sup>a</sup>The yields were determined by GC-MS analysis vs. a calibrated internal standard and are averages of two runs. <sup>b</sup>The ratio of anisole-4-d<sub>1</sub> to anisole was ca. 1:1.

**Table 3-3. The dependences of activity of photocatalytic borylation of 4-chloroanisole on different amount of B<sub>2</sub>pin<sub>2</sub> or KOMe**



Entry	Amount of B <sub>2</sub> Pin <sub>2</sub> (mmol)	Amount of KOMe (mmol)	Yield (%) <sup>a</sup>		
			<b>45b</b>	<b>45c</b>	<b>45d</b>
1	0.2 (1 equiv)	0.3 (1.5 equiv)	59	8	2
2	0.3 (1.5 equiv)	0.3 (1.5 equiv)	86	11	2
3	0.4 (2 equiv)	0.3 (1.5 equiv)	87	10	3
4	0.5 (2.5 equiv)	0.3 (1.5 equiv)	83	10	2
5	0.3 (1.5 equiv)	0.02 (0.1 equiv)	24	14	2
6	0.3 (1.5 equiv)	0.06 (0.3 equiv)	30	12	2
7	0.3 (1.5 equiv)	0.1 (0.5 equiv)	41	12	1
8	0.3 (1.5 equiv)	0.2 (1 equiv)	75	12	2
9	0.3 (1.5 equiv)	0.4 (2 equiv)	78	10	3
10	0.3 (1.5 equiv)	0.5 (2.5 equiv)	72	8	4

<sup>a</sup>The yields were determined by GC-MS analysis vs a calibrated internal standard and are averages of two runs.

In the light of our previous work,<sup>277</sup> the 5 mol% **[Rh]**/10 mol% [Ni(IMes)<sub>2</sub>] catalyst system was then examined as a dual photocatalytic system. First, a reaction carried out in the dark for 2 h yielded ca. 13% of **45b** (Table 3-1, entry 3), indicating that the **[Rh]** complex has no effect on the thermal borylation reaction. The yield of **45b** reached 72% after only 2 h of irradiation of the reaction mixture with a 400 nm LED (Table 3-1, entry 4), suggesting that the dual photocatalytic system works efficiently for the borylation of aryl chlorides. However, the photocatalytic process yielded more dechlorohydrogenated byproduct anisole (**45d**, 15%) compared with that obtained when the reaction was performed in the



dark. Interestingly, highly efficient and selective borylation of **45a** under visible light (400 nm) irradiation at 25 °C was observed using only [Ni(IMes)<sub>2</sub>] as the photocatalyst without [Rh] complex, giving **45b** in 86% yield after 6 h (Table 3-1, entry 2). It is worth mentioning that our group developed a Zn-catalyzed 1,2-selective dual C-H/C-X borylation of aryl iodides and bromides in 2015.<sup>97</sup> In this work, we also observed both C-Cl and C-H borylation of chloroarenes, and the yield of 1,2-(Bpin)<sub>2</sub>-4-methoxybenzene (**45c**) in the photo-induced reaction is slightly higher compared to that from the reaction without irradiation (Table 3-1, entries 1-4). It is important to note that the reaction did not occur under light irradiation in the absence of [Ni(IMes)<sub>2</sub>] (Table 3-1, entries 5 and 6).

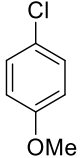
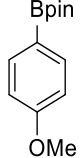
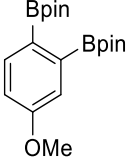
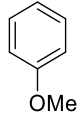
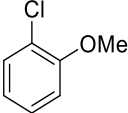
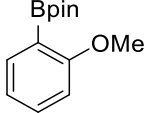
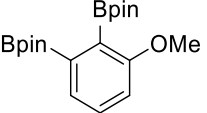
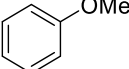
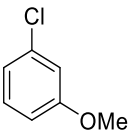
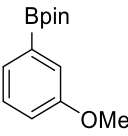
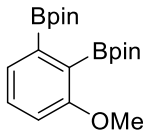
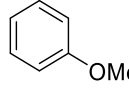
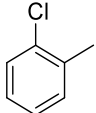
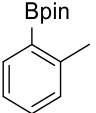
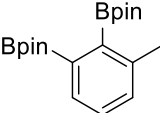
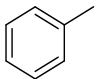
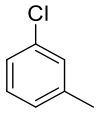
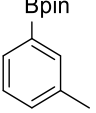
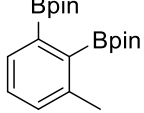
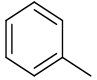
We screened a range of solvents and bases, with hexane and KOMe proving to be optimal (Table 3-2). Importantly, THF gave more of the hydrodehalogenation product ArH (Table 3-2, entry 4) than other solvents and there was significant deuterium incorporation when THF-d<sub>8</sub> was used (Table 3-2, entry 5), suggesting a radical process. The yield is significantly influenced by the amount of both B<sub>2</sub>pin<sub>2</sub> and KOMe amounts, with 1.5 equiv of each providing an excellent yield (Table 3-3).

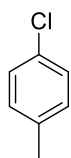
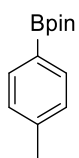
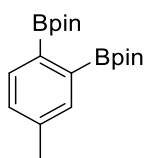
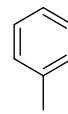
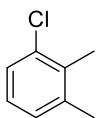
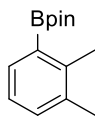
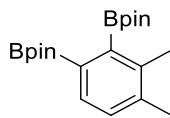
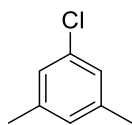
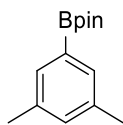
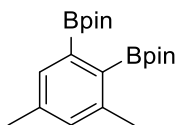
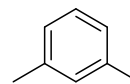
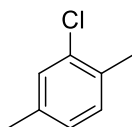
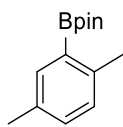
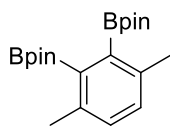
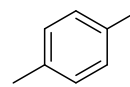
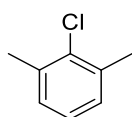
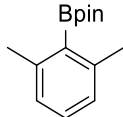
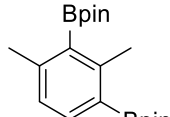
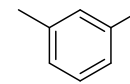
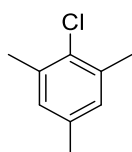
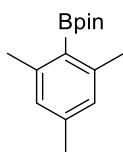
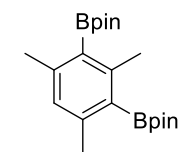
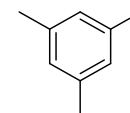
### 3.3.2 Substrate scope

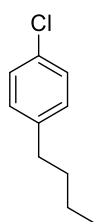
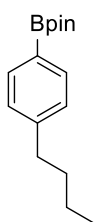
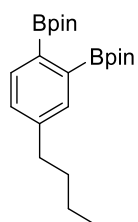
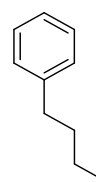
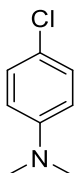
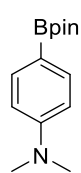
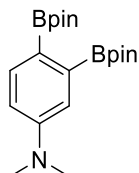
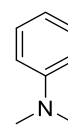
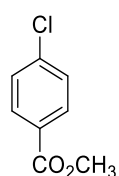
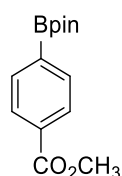
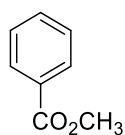
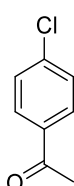
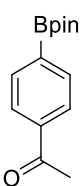
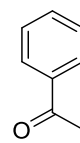
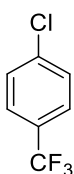
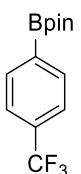
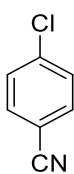
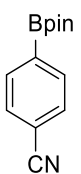
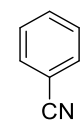
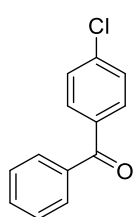
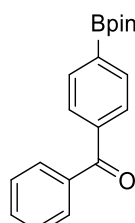
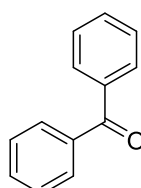
We further examined the scope of chloroarene substrates for the photo-induced borylation under the optimized conditions, and the results are summarized in Table 3-4. Chloroarenes with either electron-donating (**45a-57a**) or electron-withdrawing (**58a-62a**) groups including esters, ketones, and nitriles reacted smoothly to afford the corresponding arylboronic esters in good to excellent yields, highlighting the excellent functional group tolerance of this method. *Ortho*-substitution with MeO (**46a**) or Me (**48a, 51a, 53a**) groups did not significantly lower the yield of product while substitution with two *ortho*-methyl groups (**54a, 55a**) somewhat reduced the yield. Importantly, both strong π-donor (NMe<sub>2</sub>, **57a**) and π-acceptor (CO<sub>2</sub>CH<sub>3</sub>, **58a**; COCH<sub>3</sub>, **59a**) substituents as well as the inductively withdrawing CF<sub>3</sub> group (CF<sub>3</sub>, **60a**) at the *para*-position, resulted in excellent yields of product. 4-Chlorobiphenyl (**64a**), naphthyl chlorides (**65a, 66a**), and several chloroheteroarenes (**67a-71a**), are also compatible substrates which produced the

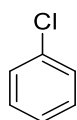
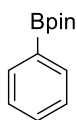
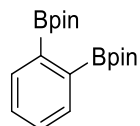
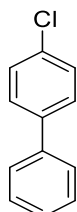
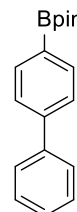
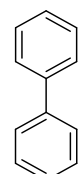
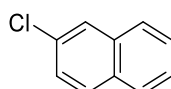
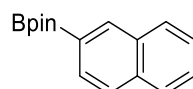
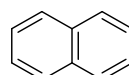
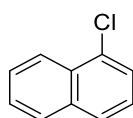
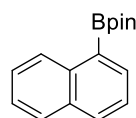
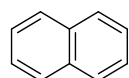
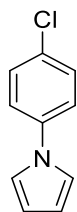
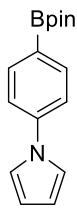
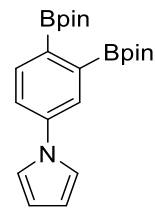
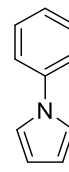
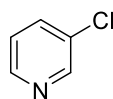
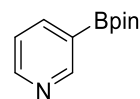
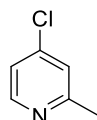
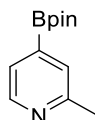
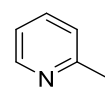
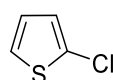
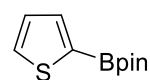
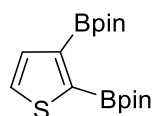
borylation product in good yields. Notably, the protocol worked well with 5-chloroindole bearing an NH group (**72a**), enabling convenient borylation of such substrates without the need for a protecting group. High yields of diborylation products were also achieved with dichlorobenzenes as substrates (**73a** and **74a**). Not only does the reaction show wide scope with respect to  $B_2pin_2$ , but bis(neopentyl glycolato)diboron ( $B_2neop_2$ )<sup>282</sup> can be substituted for  $B_2pin_2$  as the diboron reagent to give the corresponding aryl neopentylglycolato boronate ester products (**75b-78b**) in similar yields to those observed with  $B_2pin_2$ .

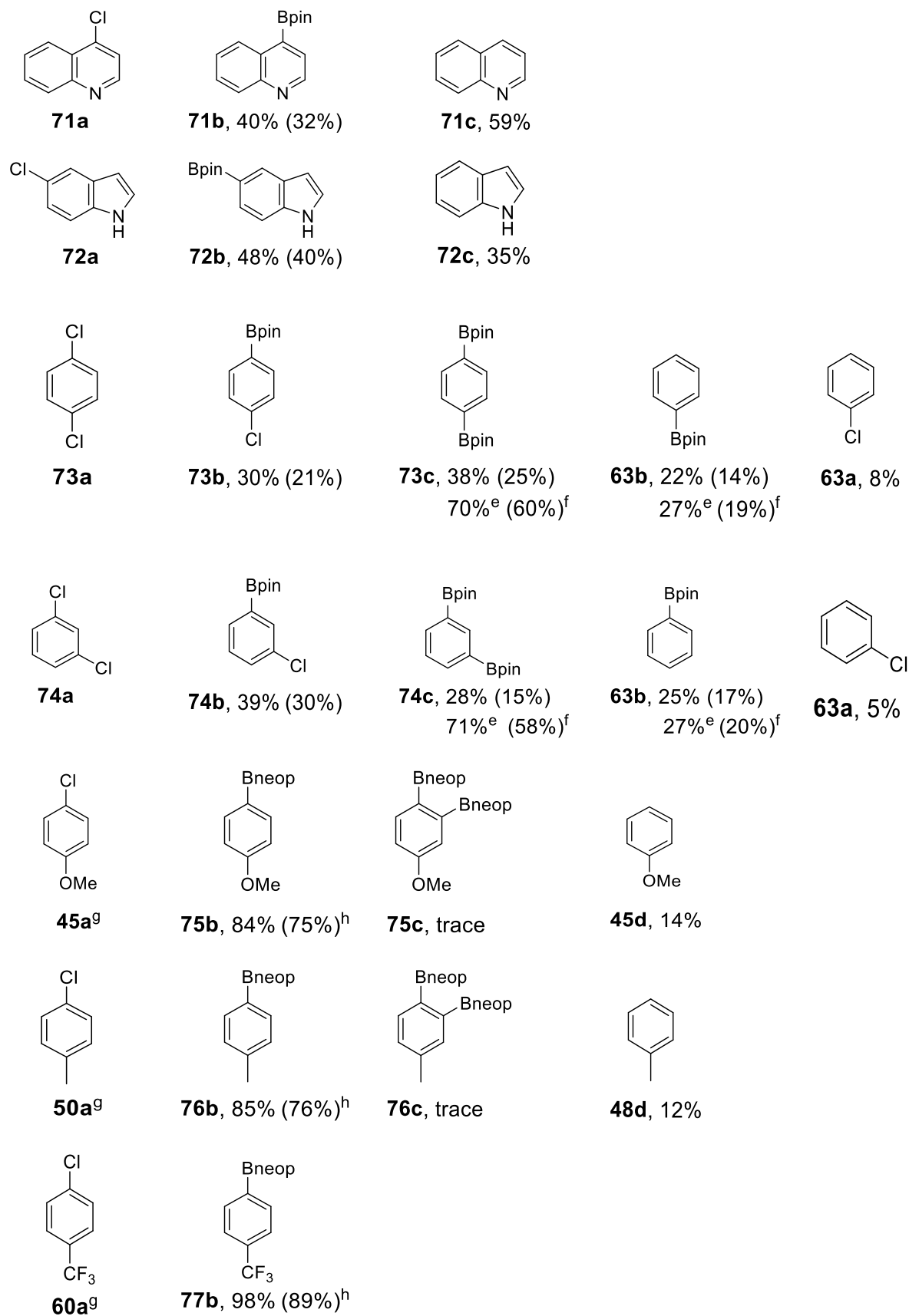
**Table 3-4. Scope of the photo-induced borylation of chloroarenes<sup>a</sup>**

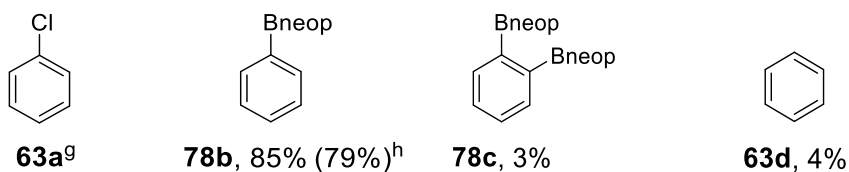
			
<b>45a</b>	<b>45b</b> , 86% <sup>b</sup> (79%) <sup>c</sup>	<b>45c</b> , 11% (5%)	<b>45d</b> , 2%
			
<b>46a</b>	<b>46b</b> , 69% (60%)	<b>46c</b> , 3%	<b>45d</b> , 28%
			
<b>47a</b>	<b>47b</b> , 70% (63%)	<b>46c</b> , 9% (2%)	<b>45d</b> , 20%
			
<b>48a</b>	<b>48b</b> , 70% (62%)	<b>48c</b> , 5%	<b>48d</b> , 25%
			
<b>49a</b>	<b>49b</b> , 73% (64%)	<b>48c</b> , 9% (3%)	<b>48d</b> , 17%

**50a****50b**, 75% (67%)**50c**, 14% (5%)**48d**, 11%**51a****51b**, 65% (55%)**51c**, 7%**51d**, 18%**52a****52b**, 70% (61%)**52c**, 11% (3%)**52d**, 19%**53a****53b**, 74% (66%)**53c**, 6%**53d**, 20%**54a<sup>d</sup>****54b**, 46% (38%)**54c**, 7%**54d**, 47%**55a<sup>d</sup>****55b**, 45% (35%)**55c**, 18% (9%)**55d**, 32%

**56a****56b**, 71% (63%)**56c**, 2%**56d**, 27%**57a****57b**, 89% (80%)**57c**, trace**57d**, 5%**58a****58b**, 90% (82%)**58c**, 10%**59a****59b**, 84% (75%)**59c**, 16%**60a****60b**, 99% (90%)**61a****61b**, 25% (15%)**61c**, 8%**62a****62b**, 51% (42%)**62c**, 47%

**63a****63b**, 68% (60%)**63c**, 9% (4%)**63d**, 20%**64a****64b**, 85% (76%)**64c**, 13%**65a****65b**, 71% (62%)**65c**, 22%**66a****66b**, 80% (71%)**65c**, 18%**67a****67b**, 74% (67%)**67c**, 3%**67d**, 23%**68a****68b**, 90% (50%)**68c**, 9%**69a****69b**, 64% (55%)**69c**, 10%**70a****70b**, 62% (53%)**70c**, 7%**70d**, 12%



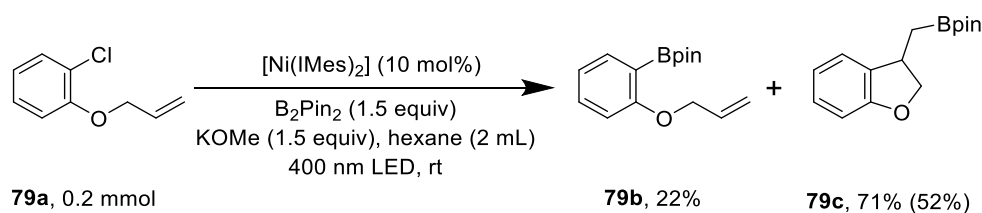


<sup>a</sup>Reaction conditions: B<sub>2</sub>pin<sub>2</sub> (0.3 mmol), chloroarene (0.2 mmol), KOMe (0.3 mmol), [Ni(IMes)<sub>2</sub>] (10 mol%), hexane (2 mL), at room temperature under irradiation with a 400 nm LED for 6 h unless otherwise stated. <sup>b</sup>The yields are based on aryl chlorides and were determined by GC-MS analysis vs. a calibrated internal standard and are averages of two runs. <sup>c</sup>Isolated yields based on 1 mmol of aryl chloride are given in parentheses. <sup>d</sup>The reaction time was 24 h. <sup>e</sup>B<sub>2</sub>pin<sub>2</sub> (0.6 mmol) and KOMe (0.6 mmol) were used. <sup>f</sup>B<sub>2</sub>pin<sub>2</sub> (3 mmol) and KOMe (3 mmol) were used. <sup>g</sup>B<sub>2</sub>neop<sub>2</sub> (0.3 mmol) was used. <sup>h</sup>B<sub>2</sub>neop<sub>2</sub> (1.5 mmol) was used.

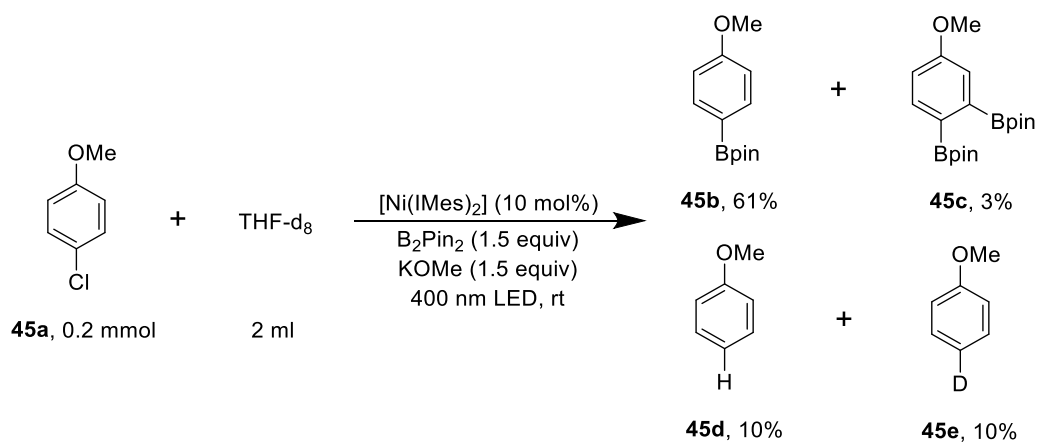
### 3.4 Mechanistic studies

#### 3.4.1 Aryl radical trapping experiments

##### Scheme 3-1. Aryl radical trapping



##### Scheme 3-2. Hydrogen atom transfer from THF-d<sub>8</sub>



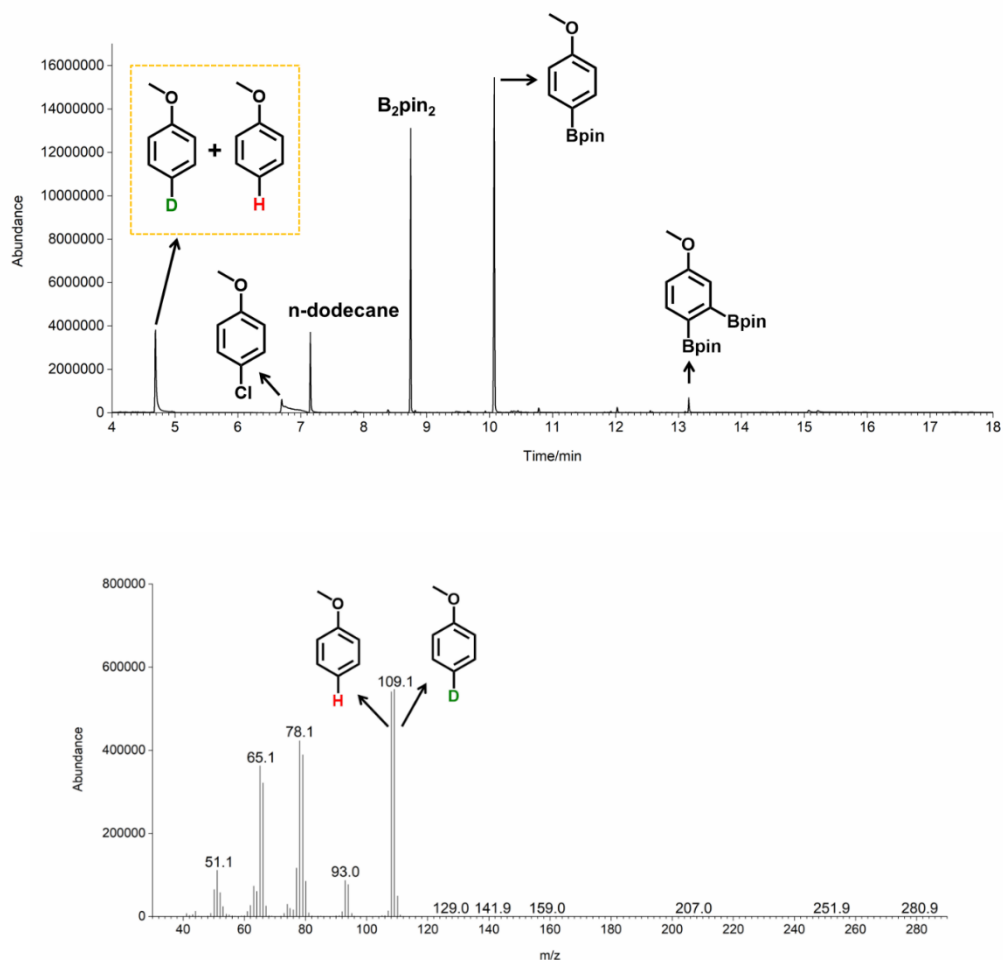


**Figure 3-1.** GC chromatogram of the reaction mixture of 4-chloroanisole borylation in THF- $d_8$  against standard *n*-dodecane (top) and mass spectrum (EI) of anisole-4- $d_1$  (bottom).

First, using allyl *o*-chlorophenyl ether (**79a**) as substrate gave monoborylated product **79b**, but the cyclized (borylmethyl) indane (**79c**) was the main product, indicating an intramolecular trapping of the aryl radical by the olefin moiety, followed by coupling with the boryl species (Scheme 3-1). Second, when the reaction of **45a** with  $B_2pin_2$  was conducted in THF- $d_8$  instead of hexane, the borylation product **45b** was observed in a lower yield (61%), together with a significant amount of dehalogenation product anisole (**45d**, 10%) and anisole-4- $d_1$  (**45e**, 10%), due to hydrogen atom transfer from THF to *p*-MeO-C $_6$ H $_4$  $^{\bullet}$  (Table 3-2, entry 5, Scheme 3-2, and Figure 3-1). Thus, the hydrogen atom donor THF competes with the boryl species to react with the aryl radical. When the



reaction of **45a** was performed in the presence of 2 equiv of the hydrogen atom donor 9,10-dihydroanthracene as a radical trap, both borylation products were obtained in lower yields (**45b**: 73%; **45c**: 7%) with an increased yield of **45d** (17%). Increasing the amount of the dihydroanthracene radical trap to 10 equiv significantly reduced the yield of **45b** to 49% and **45c** to 1%, and increased the yield of **45d** to 42%, respectively. Only 0.4 equiv 2,2,6,6-tetramethylpiperidine 1-oxyl (TEMPO) as a radical trap shut down the reaction almost completely. The above intra- and intermolecular trapping reactions clearly indicate the generation of aryl radicals from the aryl chlorides.

### 3.4.2 EPR investigations

*In situ* EPR spectra at 70 K in frozen hexane after 1, 2, 3, and 5 minutes were recorded to confirm the formation of radical species. From Figure 3-2A, it can be seen that the signals continue to increase with time. Comparison of the *in situ* EPR spectrum at 70 K (Figure 3-2B) with the EPR spectrum of isolated  $[\text{Ni}^{\text{I}}(\text{IMes})_2\text{Cl}]$  (for synthesis and molecular structure please see SI) in frozen hexane (Figure 3-2C) revealed that they are essentially identical. The similarity of *in situ* EPR spectra of the reaction of  $[\text{Ni}(\text{IMes})_2]$  with chlorobenzene also confirmed that the formation of the complex  $[\text{Ni}^{\text{I}}(\text{IMes})_2\text{Cl}]$  during the reaction (Figure 3-3). While the main contribution to the observed EPR spectrum is from a  $[\text{Ni}^{\text{I}}(\text{IMes})_2\text{Cl}]$ , a second small signal which is attributed to  $[\text{Ni}^{\text{I}}(\text{IMes})_2\text{Ph}]$  was observed. The result is consistent with literature reports,<sup>279-281</sup> that steric impact of the IMes ligands prevents coordination of  $[\text{Ni}(\text{IMes})_2]$  to the chloroarene and leads to chlorine atom abstraction to form an aryl radical  $\text{Ar}^{\bullet}$  and the complex  $[\text{Ni}^{\text{I}}(\text{IMes})_2\text{Cl}]$ . No signal for  $\text{Ar}^{\bullet}$  was detected in the *in situ* EPR spectra, and neither benzene nor biphenyl compounds were detected by GC-MS. However, from our *in situ* NMR spectra and HRMS measurements of the reaction of chlorobenzene with  $[\text{Ni}(\text{IMes})_2]$ , the aryl complex  $[\text{Ni}^{\text{I}}(\text{IMes})_2\text{Ph}]$  was detected in addition to  $[\text{Ni}^{\text{I}}(\text{IMes})_2\text{Cl}]$ . Therefore, we speculated that the  $\text{Ar}^{\bullet}$  species likely reacts very quickly with  $[\text{Ni}(\text{IMes})_2]$  to form  $[\text{Ni}^{\text{I}}(\text{IMes})_2\text{Ar}]$ , whereas, in the catalytic reaction system,  $\text{Ar}^{\bullet}$  is more likely to react with  $\text{B}_2\text{pin}_2$  or more nucleophilic  $[\text{B}_2\text{pin}_2(\text{OMe})]^-$  to form the borylation product.

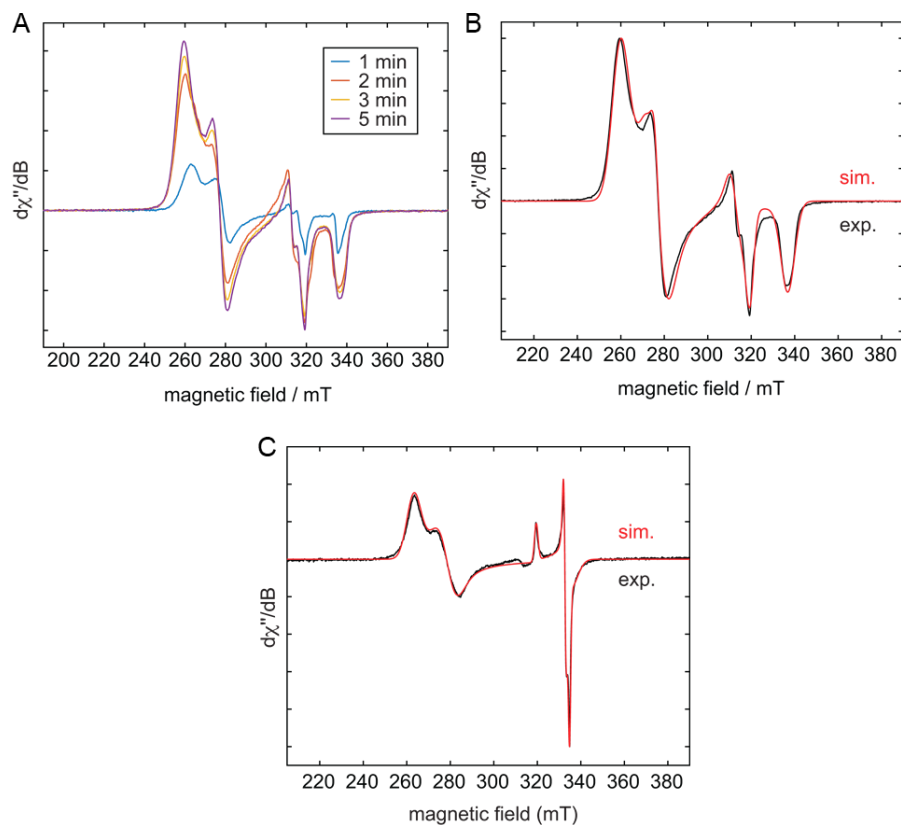


**Figure 3-2.** (A) Changes in the low-temperature CW EPR spectra of the reaction of  $[Ni(IMes)_2]$  and **45a** in hexane with the reaction time at 70 K and (B) the simulated spectrum is shown in red; (C) simulated (red) and experimental (black) CW EPR spectra of isolated  $[Ni^I(IMes)_2Cl]$  in frozen hexane.

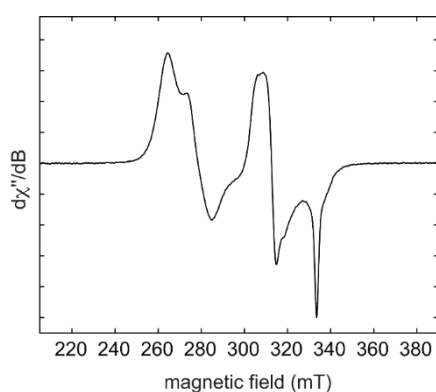


**Figure 3-3.** *In situ* CW EPR spectrum of the reaction of  $[Ni(IMes)_2]$  and chlorobenzene mixture in hexane at 70 K.

### 3.4.3 Photophysical properties of different Ni catalysts

To clarify the role of light, we investigated the photophysical properties of the different compounds in the reaction mixture. From the UV-vis spectra (Figure 3-4A), both IMes and  $K^+[B_2pin_2(OMe)]^-$  (product of KOMe reacting with  $B_2pin_2$ )<sup>92,93</sup> have almost no absorption at wavelengths  $> 300$  nm in hexane. The complex  $[Ni(IMes)_2]$  has very broad absorptions with two absorption maxima at 508 nm and 616 nm, while  $[Ni^I(IMes)_2Cl]$  has an absorption band between 300 - 450 nm with a maximum at 340 nm. However, both  $[Ni^I(IMes)_2Cl]$  and  $[Ni(IMes)_2]$  do not show any detectable emission, preventing us from obtaining the energies of the lowest singlet or triplet states via emission spectroscopy. We know that the chlorine atom abstraction of chloroarenes by  $[Ni(IMes)_2]$  to give  $[Ni^I(IMes)_2Cl]$  is very fast at room temperature, and therefore focused on the role of  $[Ni^I(IMes)_2Cl]$  in subsequent photochemical processes.

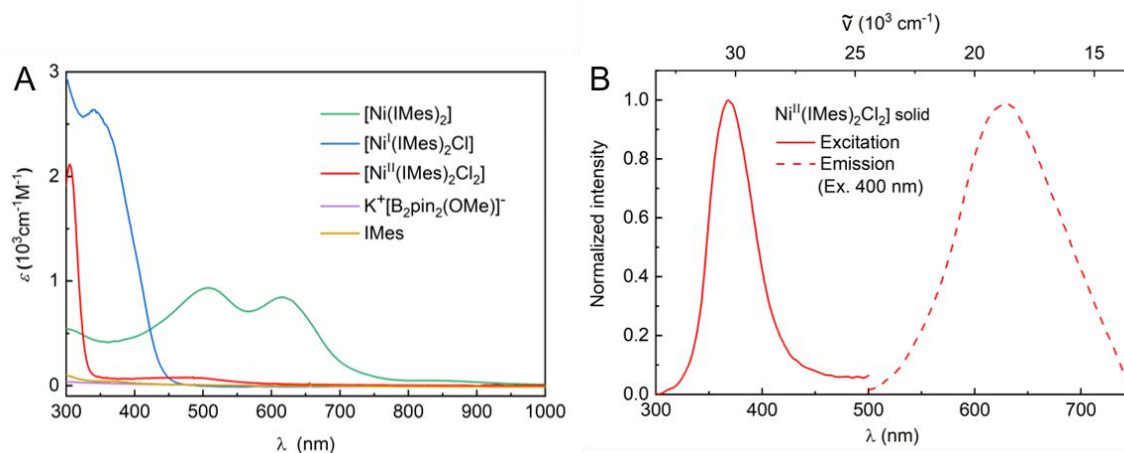


**Figure 3-4.** (A) UV-visible absorption spectra of  $[Ni(IMes)_2]$ ,  $[Ni^I(IMes)_2Cl]$ ,  $[Ni^{II}(IMes)_2Cl_2]$ ,  $K[B_2pin_2(OMe)]^-$  and IMes in degassed hexane solution at room temperature; (B) emission (excited at 400 nm) and excitation spectra of solid  $[Ni^{II}(IMes)_2Cl_2]$  under air at room temperature.

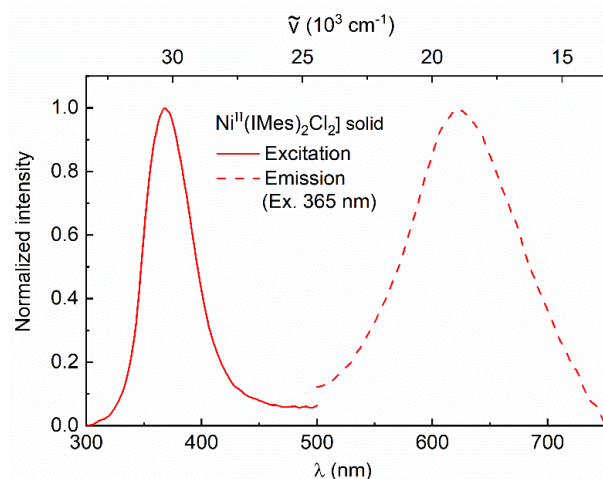
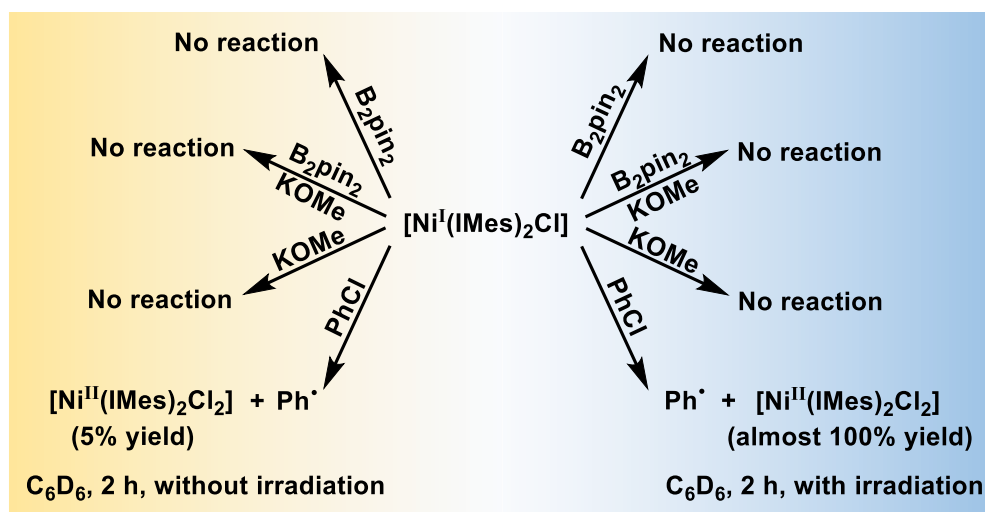


**Figure 3-5.** Emission (excited at 365 nm) and excitation spectra of solid  $[\text{Ni}^{\text{II}}(\text{IMes})_2\text{Cl}_2]$  under air at room temperature.

**Scheme 3-3.** Control reactions of  $[\text{Ni}^{\text{I}}(\text{IMes})_2\text{Cl}]$  with  $\text{B}_2\text{pin}_2$ , KOMe, and chlorobenzene, respectively, without (left) and with (right) irradiation



### 3.4.4 Photo-induced borylation of chlorobenzene with different Ni catalysts

The extinction coefficient of  $[\text{Ni}^{\text{I}}(\text{IMes})_2\text{Cl}]$  at 400 nm is ca.  $1320 \text{ cm}^{-1}\text{M}^{-1}$  (Figure 3-4A). Independently prepared  $[\text{Ni}^{\text{I}}(\text{IMes})_2\text{Cl}]$  was employed as catalyst instead of  $[\text{Ni}(\text{IMes})_2]$  for the photo-induced reaction of chlorobenzene (**63a**) with  $\text{B}_2\text{pin}_2$  under otherwise identical conditions, giving 68% and 17% yields of **63b** and **63c**, respectively (Table 3-5, entry 1). When the reaction was carried out in the dark the yield of **63b** was only 15% (Table 3-5, entry 2), indicating that light is necessary for an efficient reaction. Further control

experiments showed that  $[\text{Ni}^{\text{I}}(\text{IMes})_2\text{Cl}]$  had a good stability under continuous irradiation (Figure 3-6 and 3-7) for 2 h with 400 nm LEDs, and it did not react with  $\text{B}_2\text{pin}_2$  either in presence or absence of KOMe or light (Scheme 3-3 and Figure 3-8-3-15). The reaction of  $[\text{Ni}^{\text{I}}(\text{IMes})_2\text{Cl}]$  with **63a** yielded 5% of  $[\text{Ni}^{\text{II}}(\text{IMes})_2\text{Cl}_2]$  in the dark after 2 h (Scheme 3-3 and Figure 3-16 and 3-17). However, almost complete conversion of  $[\text{Ni}^{\text{I}}(\text{IMes})_2\text{Cl}]$  to  $[\text{Ni}^{\text{II}}(\text{IMes})_2\text{Cl}_2]$  in the presence of **63a** was observed under 400 nm LED irradiation for the same time (Scheme 3-3 and Figure 3-18 and 3-19), and biphenyl was detected by GC-MS from the photo-induced reaction, indicating a rapid photochemical reaction of  $[\text{Ni}^{\text{I}}(\text{IMes})_2\text{Cl}]$  with **63a** generates  $[\text{Ni}^{\text{II}}(\text{IMes})_2\text{Cl}_2]$  and a phenyl radical. Furthermore, the redox potentials of the participating and isolated metal complexes were investigated. The onset oxidation of  $[\text{Ni}^{\text{I}}(\text{IMes})_2\text{Cl}]$  was found to occur at  $E_{\text{pa}} = -0.94$  V (Figure 3-6), which is not sufficient to reduce chlorobenzene to its corresponding radical anion [ $E_{\text{red}}(\text{PhCl}/\text{PhCl}^{\cdot-}) = -2.78$  V vs  $\text{Fc}^{+/0}$ ].<sup>283</sup> Therefore,  $[\text{Ni}^{\text{I}}(\text{IMes})_2\text{Cl}]$  is expected to react with chlorobenzene via chlorine atom abstraction to generate a phenyl radical and  $[\text{Ni}^{\text{II}}(\text{IMes})_2\text{Cl}_2]$  complex. Light irradiation greatly enhances the efficiency of the reaction achieving almost 100% yield of  $[\text{Ni}^{\text{II}}(\text{IMes})_2\text{Cl}_2]$ .

The  $[\text{Ni}^{\text{II}}(\text{IMes})_2\text{Cl}_2]$  dissolved in degassed hexane has an absorption band at 305 nm and a very weak and broad absorption band between 350 to 600 nm, and its extinction coefficient at 400 nm is only  $66 \text{ cm}^{-1}\text{M}^{-1}$  (Figure 3-4A). Although there was no emission detected spectroscopically from  $[\text{Ni}^{\text{II}}(\text{IMes})_2\text{Cl}_2]$  in hexane, we observed that the “solution” appeared to be cloudy under UV irradiation and orange-red luminescence was observed by eye. This indicates the presence of very fine  $[\text{Ni}^{\text{II}}(\text{IMes})_2\text{Cl}_2]$  particles which did not dissolve in hexane. We therefore recorded the spectroscopic properties of  $[\text{Ni}^{\text{II}}(\text{IMes})_2\text{Cl}_2]$  in the solid state under air<sup>284</sup> at room temperature (Figures 3-4B and 3-5). Interestingly, in contrast to the absorption spectra in dilute solution, a broad excitation between 320-500 nm is visible with a maximum at 365 nm. A broad solid-state emission with  $\lambda_{\text{max}} = 625$  nm was observed for  $[\text{Ni}^{\text{II}}(\text{IMes})_2\text{Cl}_2]$ , which is absent in solution, probably due to rapid non-radiative decay processes.

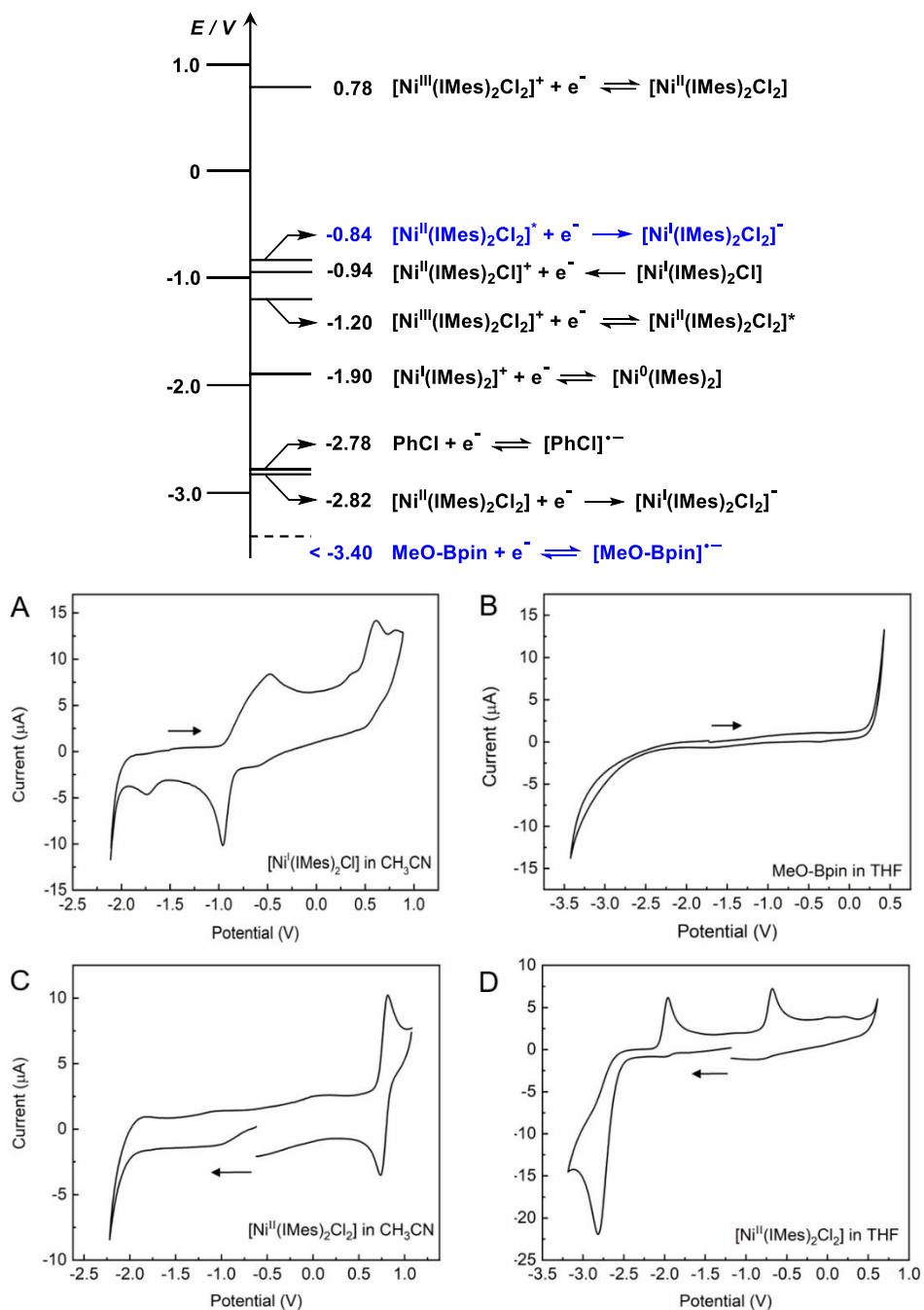
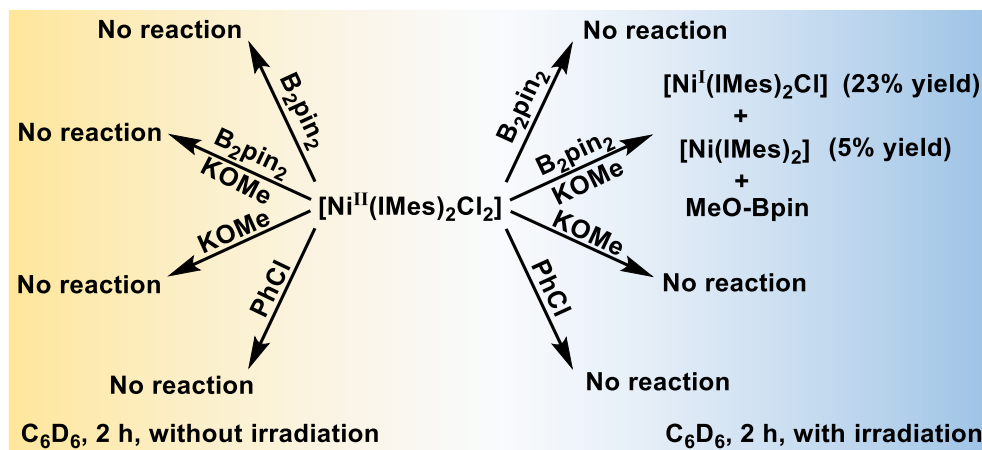


**Figure 3-6.** Comparison of redox potentials of the Ni species,  $\text{K}[\text{B}_{2}\text{pin}_2(\text{OMe})]$ , MeO-Bpin and chlorobenzene potentially involved in the photocatalytic C-Cl borylation reaction. Potentials are referenced to the ferrocene/ferrocenium couple. Solvent effects on the redox potentials have not been considered. Cyclic voltammograms of  $[\text{Ni}^{\text{I}}(\text{IMes})_2\text{Cl}]$  (A) and  $[\text{Ni}^{\text{II}}(\text{IMes})_2\text{Cl}_2]$  (C) in  $\text{CH}_3\text{CN}$ , and MeO-Bpin (B) and  $[\text{Ni}^{\text{II}}(\text{IMes})_2\text{Cl}_2]$  (D) in THF, respectively, using 0.1 M  $\text{TBAPF}_6$  as supporting electrolyte. Potentials are referenced to the ferrocene/ferrocenium couple.

**Scheme 3-4. Control reactions of  $[\text{Ni}^{\text{II}}(\text{IMes})_2\text{Cl}_2]$  with  $\text{B}_2\text{pin}_2$ , KOMe, chlorobenzene, and  $\text{B}_2\text{pin}_2/\text{KOMe}$ , respectively, without (left) and with (right) irradiation**

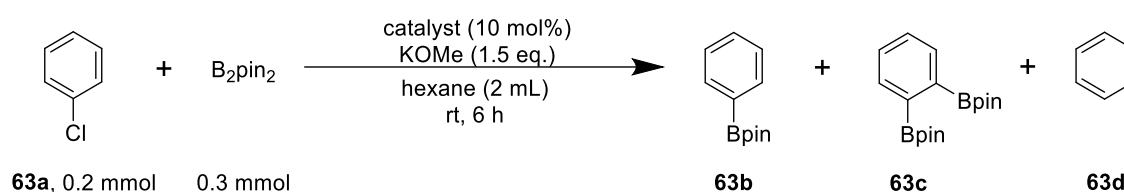


We then employed  $[\text{Ni}^{\text{II}}(\text{IMes})_2\text{Cl}_2]$  as a catalyst for the light reaction of **63a** with  $\text{B}_2\text{pin}_2$ , which resulted in a 75% yield of **63b** and an 11% yield of **63c**, respectively, after 6 h. No reaction was detected without irradiation. *In situ* NMR experiments showed that  $[\text{Ni}^{\text{II}}(\text{IMes})_2\text{Cl}_2]$  is stable under irradiation with 400 nm LEDs for 2 h (Scheme 3-4 and Figures 3-20 and 3-21) and did not react with **63a**,  $\text{B}_2\text{pin}_2$  or KOMe alone under either in the dark or under irradiation at 400 nm (Scheme 3-4 and Figures 3-22-3-33). Very recently, Doyle et al. reported that a metal-to-ligand charge transfer (MLCT) state of  $[\text{Ni}^{\text{II}}(\text{R}^{\text{bpy}})(\text{Ar})\text{X}]$  ( $\text{R}^{\text{bpy}}$  = substituted 2,2'-bipyridine) complexes, generated initially upon excitation, rapidly decays into a long-lived  $^3\text{d-d}$  state, which features a weak Ni-aryl bond.<sup>285</sup> This results in the excited  $\text{Ni}^{\text{II}}$  complexes undergoing Ni-C bond homolysis to generate aryl radicals and  $\text{Ni}^{\text{I}}$ . In our case, when  $[\text{Ni}^{\text{II}}(\text{IMes})_2\text{Cl}_2]$  was employed together with  $\text{B}_2\text{pin}_2$  and KOMe under irradiation for 2 h, the formation of  $[\text{Ni}^{\text{I}}(\text{IMes})_2\text{Cl}]$  and  $[\text{Ni}(\text{IMes})_2]$  in 23% and 7% yield, respectively, was observed accompanied by the formation of MeOBpin (Scheme 3-4 and Figures 3-36 and 3-37); both products were not detected when the reaction was performed in the dark (Scheme 3-4 and Figures 3-34 and 3-35).

Aryl radicals, as key intermediates, in our process should react with nucleophilic  $\text{sp}^2\text{-sp}^3$  diborane anion  $[\text{B}_2\text{pin}_2(\text{OMe})]^-$  from  $\text{B}_2\text{pin}_2$  and KOMe<sup>92,93</sup> to generate the corresponding borylated product and  $[\text{Bpin}(\text{OMe})]^-$  radical anion.<sup>74,264</sup> We collected the  $^{11}\text{B}$  NMR spectra

of MeO-Bpin using C<sub>6</sub>D<sub>6</sub>, CD<sub>3</sub>CN and THF-d<sub>8</sub> as the solvent, respectively. No obvious shift was found from the spectra, indicating that the MeO-Bpin is stable in these solvents and no adducts are formed. The redox behavior of MeO-Bpin was also investigated. No reduction or oxidation peaks were observed within the electrochemical window of the THF solvent (Figure 3-6), indicating that MeO-Bpin has a very negative reduction potential [ $E_{pc}(\text{MeO-Bpin}) < -3.4 \text{ V}$ ], making [Bpin(OMe)]<sup>-</sup> a particularly strong reducing agent. [Ni<sup>II</sup>(IMes)<sub>2</sub>Cl<sub>2</sub>] undergoes a reversible one-electron oxidation and an irreversible one-electron reduction at  $E_{pa} = 0.78 \text{ V}$  and  $E_{pc} = -2.82 \text{ V}$  in CH<sub>3</sub>CN and THF solution, respectively (Figure 3-6). The complex [Ni<sup>II</sup>(IMes)<sub>2</sub>Cl<sub>2</sub>] in the solid state exhibits a broad emission with  $\lambda_{max} = 625 \text{ nm}$ , therefore, the oxidation and reduction potentials of excited [Ni<sup>II</sup>(IMes)<sub>2</sub>Cl<sub>2</sub>]<sup>\*</sup> were calculated to be -1.20 V and -0.84 V [ $E(\text{Ni}^{\text{III}}/\text{Ni}^{\text{II}}) = E(\text{Ni}^{\text{III}}/\text{Ni}^{\text{II}}) - E_0 = 0.78 \text{ V} - 1.98 \text{ V} = -1.20 \text{ V}$ ,  $E(\text{Ni}^{\text{II}}/\text{Ni}^{\text{I}}) = E(\text{Ni}^{\text{II}}/\text{Ni}^{\text{I}}) + E_0 = -2.82 \text{ V} + 1.98 \text{ V} = -0.84 \text{ V}$ ,  $E_0$  is the emission energy]. Thus, electron transfer would be expected to occur from reactive [Bpin(OMe)]<sup>-</sup>, formed by the *in situ* reaction of aryl radical with [B<sub>2</sub>pin<sub>2</sub>(OMe)]<sup>-</sup>, to the excited [Ni<sup>II</sup>(IMes)<sub>2</sub>Cl<sub>2</sub>]<sup>\*</sup> [ $E(\text{Ni}^{\text{II}}/\text{Ni}^{\text{I}}) = -0.84 \text{ V}$ ] under irradiation, reducing it to [Ni<sup>I</sup>(IMes)<sub>2</sub>Cl] and then [Ni(IMes)<sub>2</sub>].

**Table 3-5. Photo-induced borylation of 63a with different catalyst**



Entry	Catalyst	400 nm LED	Yield (%) <sup>a</sup>		
			63b	63c	63d
1	[Ni <sup>I</sup> (IMes) <sub>2</sub> Cl]	✓	68	17	13
2	[Ni <sup>I</sup> (IMes) <sub>2</sub> Cl]	✗	15	-	trace
3	[Ni <sup>II</sup> (IMes) <sub>2</sub> Cl <sub>2</sub> ]	✓	75	11	11
4	[Ni <sup>II</sup> (IMes) <sub>2</sub> Cl <sub>2</sub> ]	✗	-	-	-

<sup>a</sup>The yields were determined by GC-MS analysis vs a calibrated internal standard and are averages of two runs.



To test the stability of the complex  $[\text{Ni}^{\text{I}}(\text{IMes})\text{Cl}]$  upon irradiation, a Young's tap NMR tube containing 14 mg of  $[\text{Ni}^{\text{I}}(\text{IMes})\text{Cl}]$  in 0.7 mL  $\text{C}_6\text{D}_6$  was placed between two 400 nm LEDs (1 W, 1 cm distance from either side of the tube) for 2 h. The  $^1\text{H}$  NMR spectra showed no sign of decomposition.

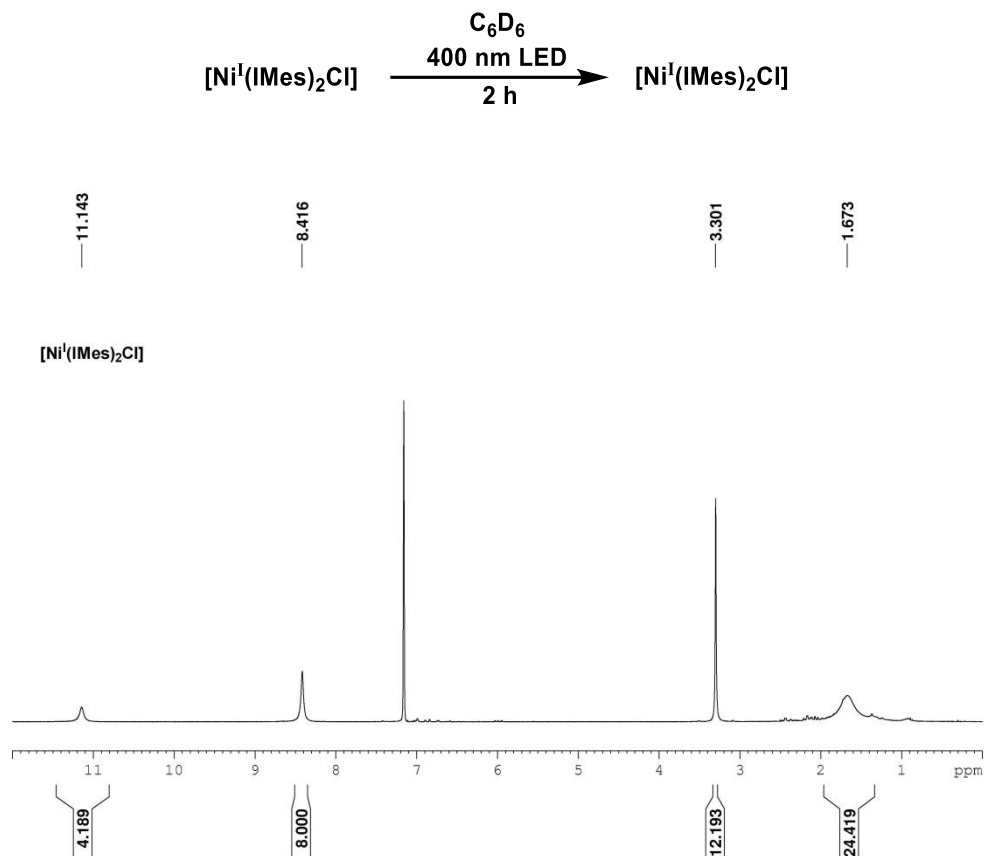


**Figure 3-7.**  $^1\text{H}$  NMR spectrum at 0 min (300 MHz,  $\text{C}_6\text{D}_6$ ).

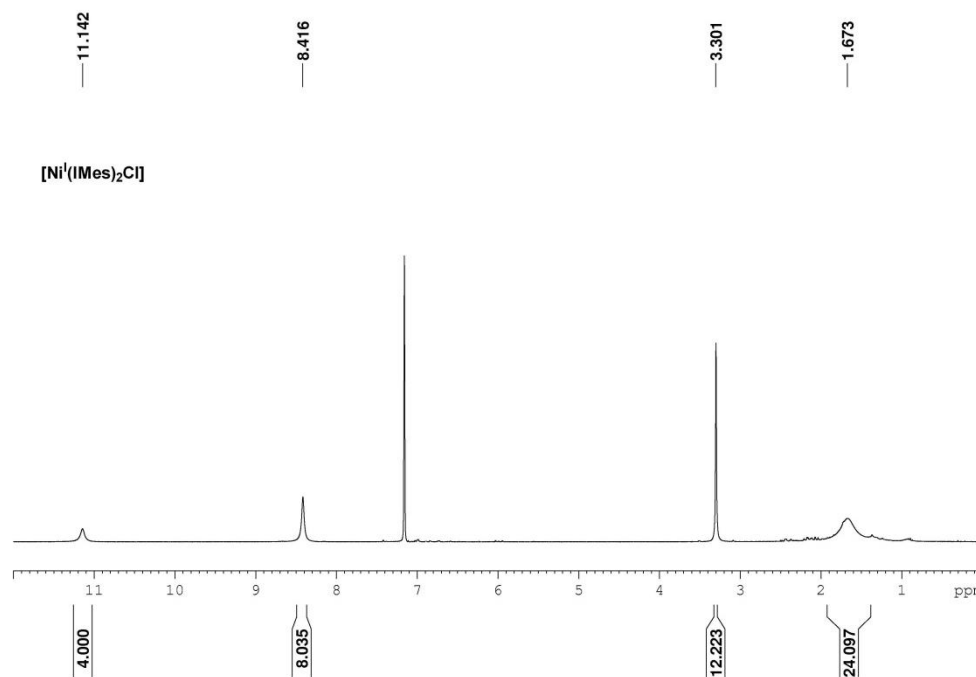


**Figure 3-8.**  $^1\text{H}$  NMR spectrum after 2 h irradiation (300 MHz,  $\text{C}_6\text{D}_6$ ).

We then studied the reactivity of  $[\text{Ni}^{\text{I}}(\text{IMes})\text{Cl}]$  with stoichiometric amounts of  $\text{B}_2\text{pin}_2$  under dark and light conditions in order to find out whether  $[\text{Ni}^{\text{I}}(\text{IMes})\text{Cl}]$  can be further transformed by  $\text{B}_2\text{pin}_2$ . A mixture of  $[\text{Ni}^{\text{I}}(\text{IMes})\text{Cl}]$  (0.02 mmol, 14 mg) and  $\text{B}_2\text{pin}_2$  (0.02 mmol, 5.1 mg, 1 equiv) was dissolved in 0.7 mL  $\text{C}_6\text{D}_6$  in a Young's tap NMR tube. For those components of which less than 6 mg were required we prepared a stock solution of known concentration and then added the respective volume as needed. Two identical samples were prepared according to the above method, and the  $^1\text{H}$  NMR spectra of the mixtures were recorded immediately. Then, one was kept in the dark and another one irradiated with a 400 nm LED. They subsequently were studied by  $^1\text{H}$  NMR spectroscopy after 2 h, which revealed no sign of a reaction.

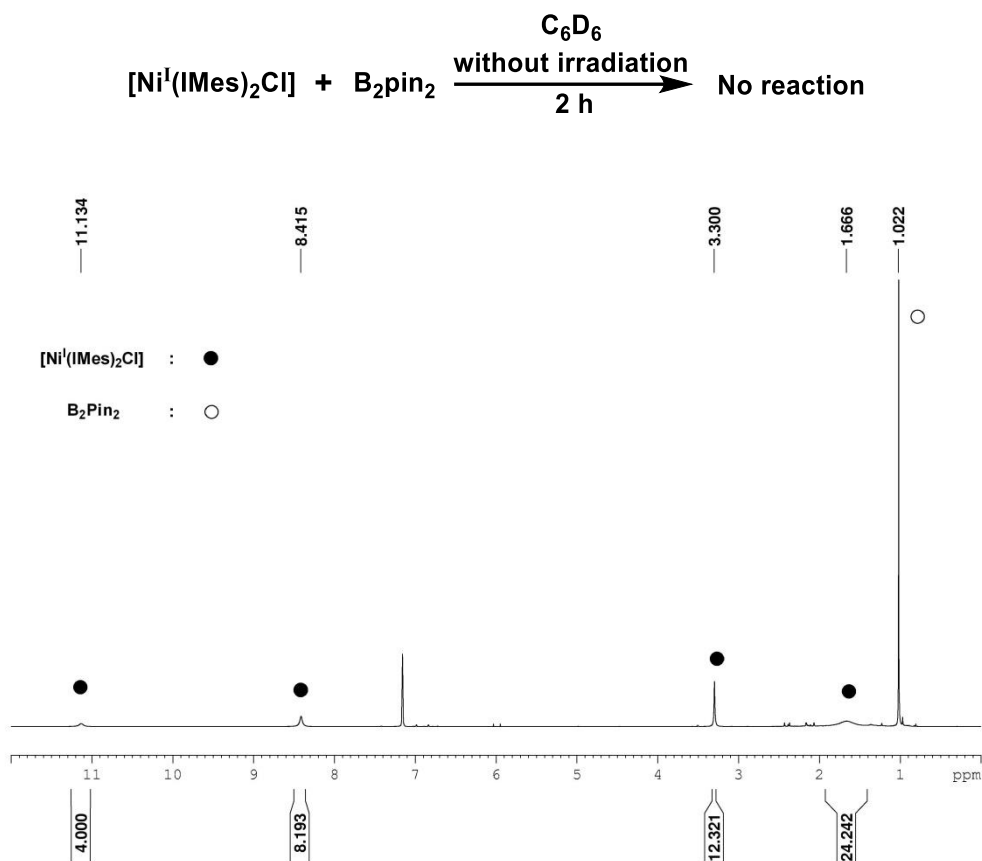


Figure 3-9.  $^1\text{H}$  NMR spectrum at 0 min (300 MHz,  $\text{C}_6\text{D}_6$ ).

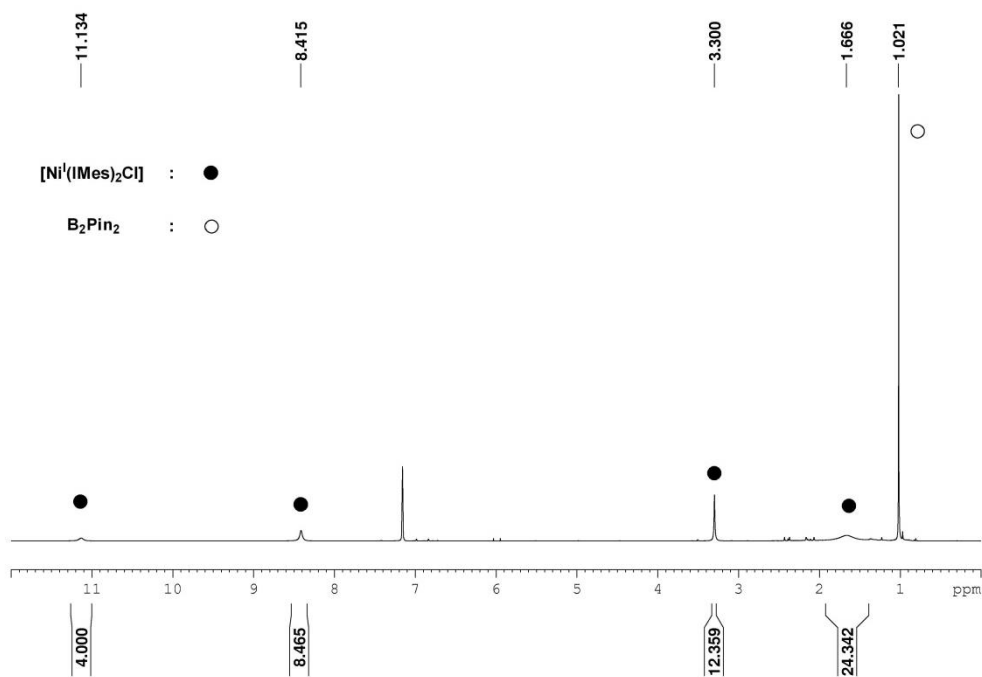


Figure 3-10.  $^1\text{H}$  NMR spectrum after 2 h in the dark (300 MHz,  $\text{C}_6\text{D}_6$ ).

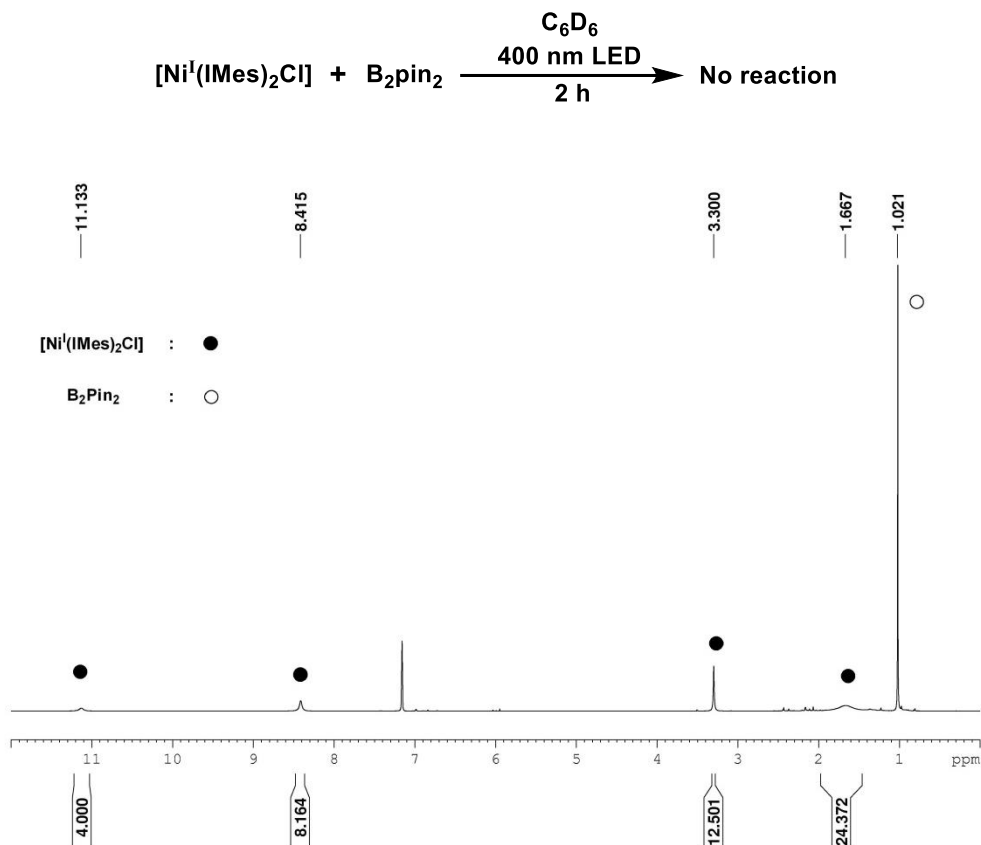


Figure 3-11. <sup>1</sup>H NMR spectrum at 0 min (300 MHz, C<sub>6</sub>D<sub>6</sub>).

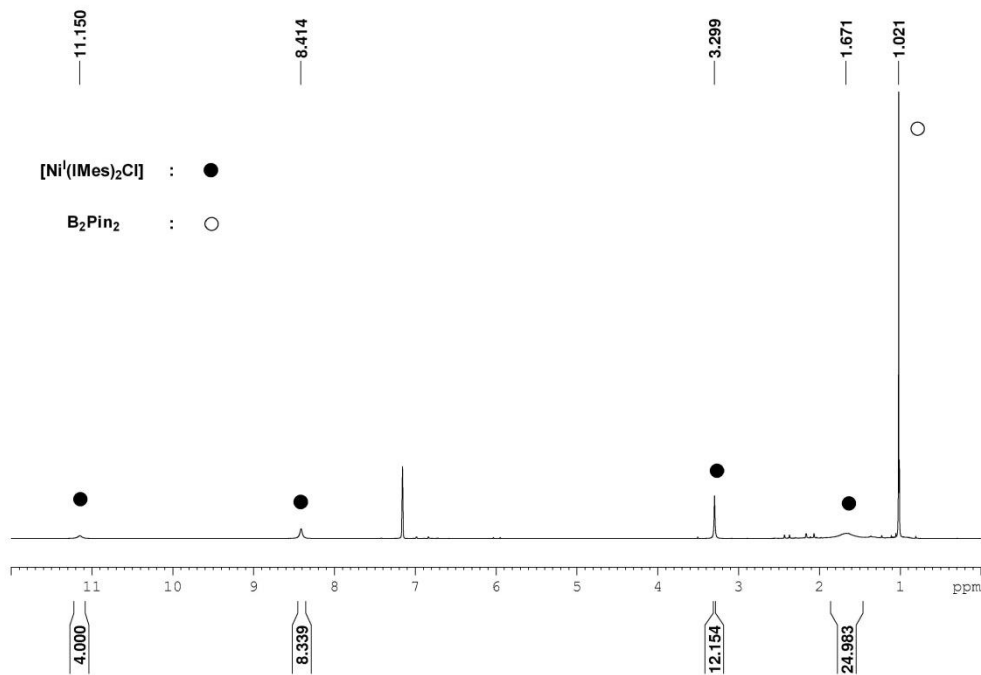
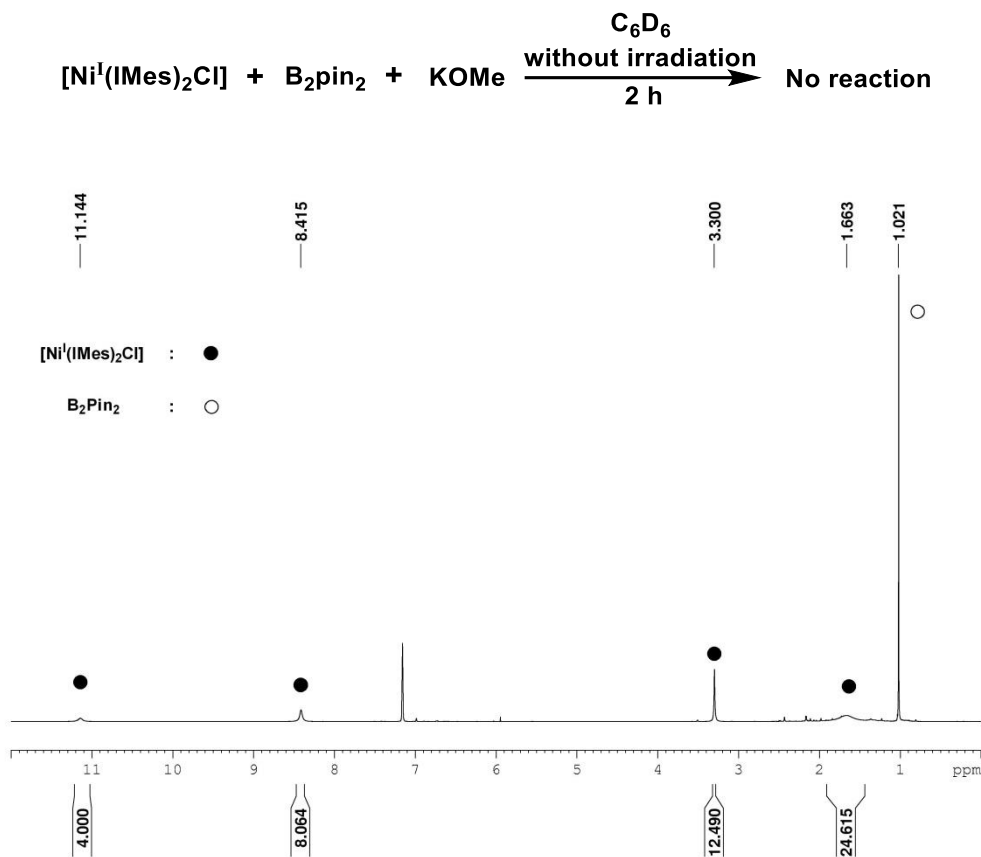


Figure 3-12. <sup>1</sup>H NMR spectrum after 2 h irradiation (300 MHz, C<sub>6</sub>D<sub>6</sub>).

The reactivity of  $[\text{Ni}^{\text{I}}(\text{IMes})\text{Cl}]$  with stoichiometric amounts of  $\text{B}_2\text{pin}_2$  in the presence of KOMe was also studied. A mixture of  $[\text{Ni}^{\text{I}}(\text{IMes})\text{Cl}]$  (0.02 mmol, 14 mg) and  $\text{B}_2\text{pin}_2$  (0.02 mmol, 5.1 mg, 1 equiv) was dissolved in 0.7 mL  $\text{C}_6\text{D}_6$  in a Young's tap NMR tube. Then KOMe (0.02 mmol, 1.4 mg, 1equiv) was added to the mixture. The  $^1\text{H}$  NMR spectra of both reactions in the dark and under irradiation reaction 2 h showed no signs of a reaction.



**Figure 3-13.**  $^1\text{H}$  NMR spectrum at 0 min (300 MHz,  $\text{C}_6\text{D}_6$ ).

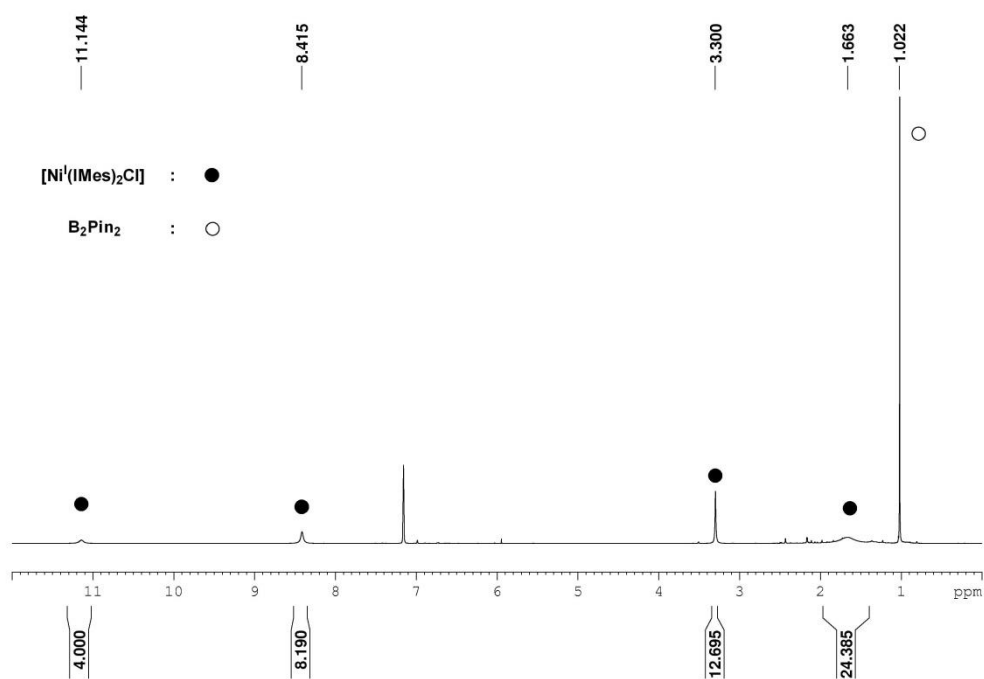


Figure 3-14.  $^1\text{H}$  NMR spectrum after 2 h in the dark (300 MHz,  $\text{C}_6\text{D}_6$ ).

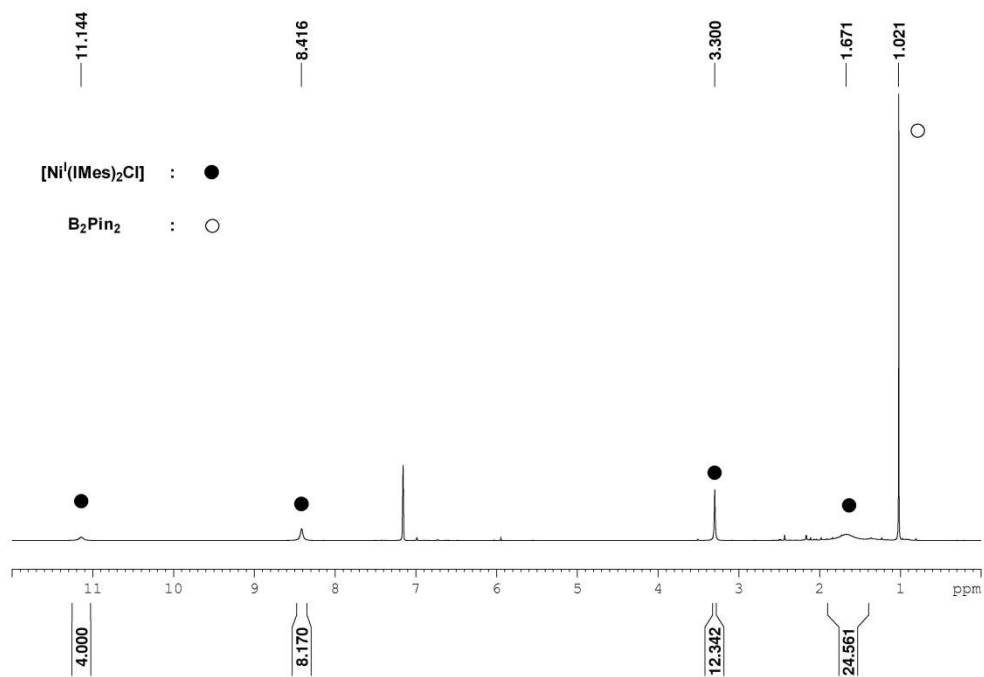
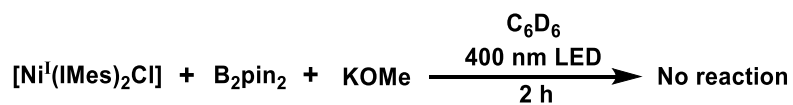
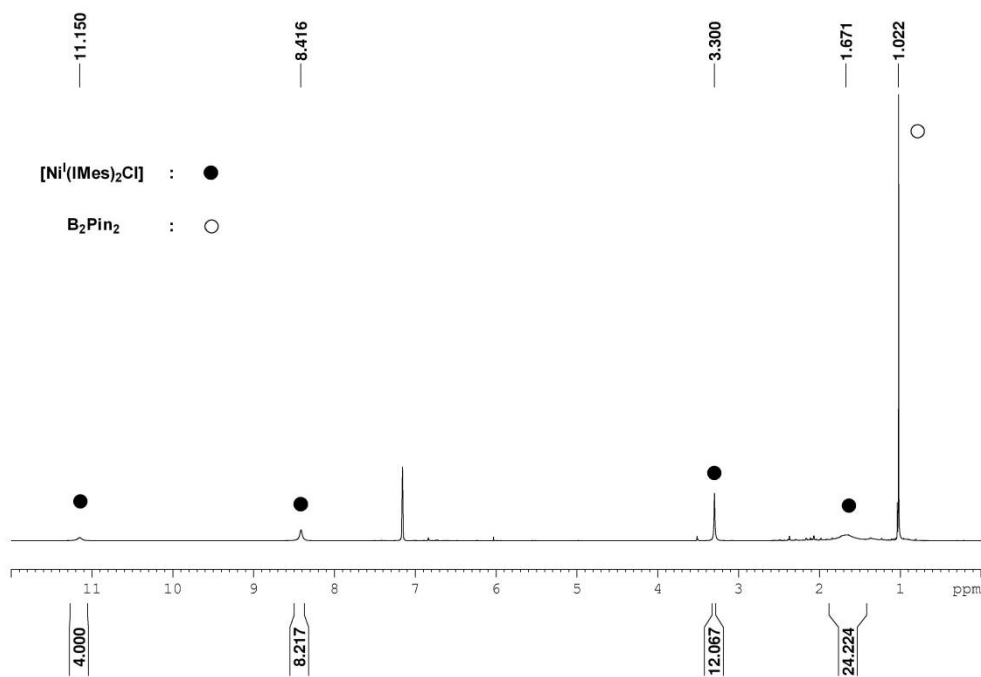
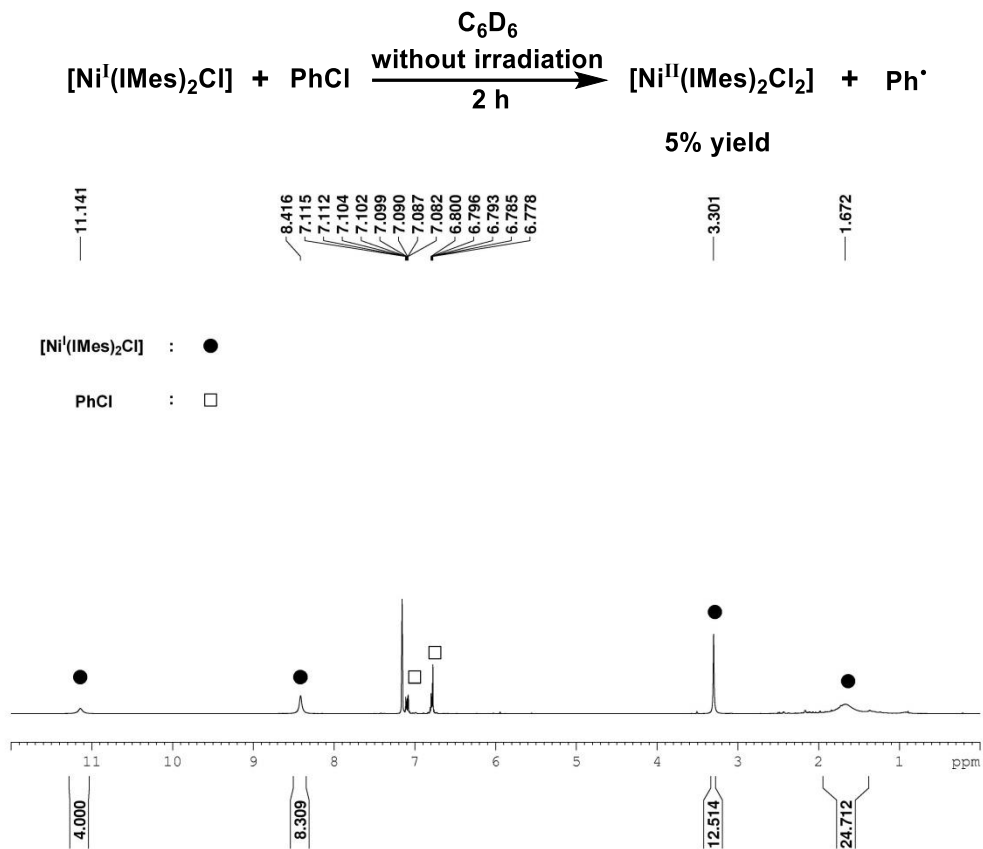
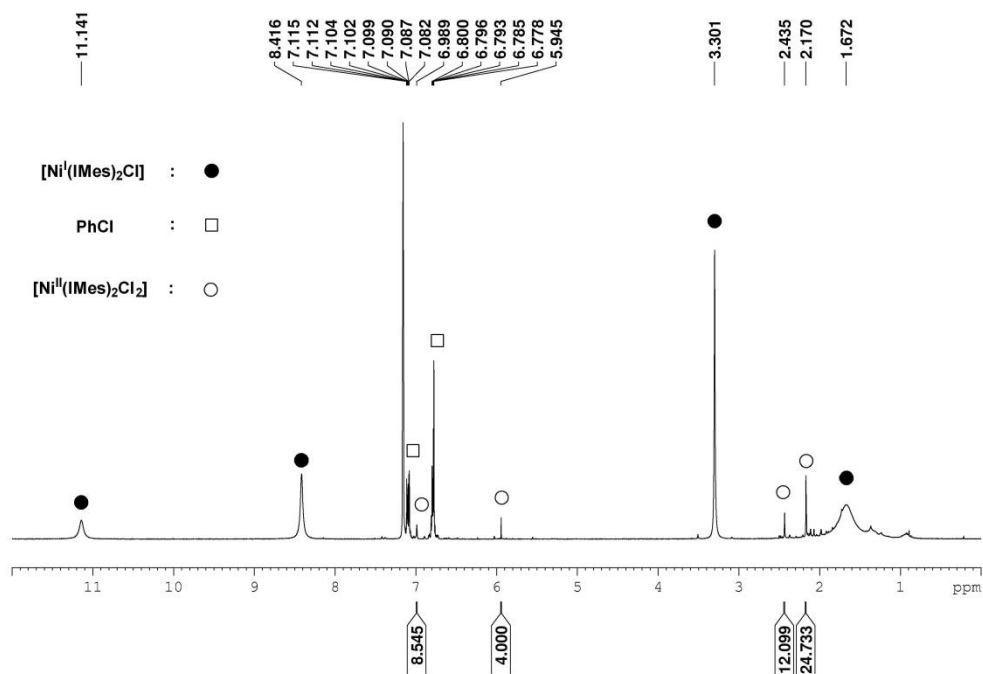


Figure 3-15.  $^1\text{H}$  NMR spectrum at 0 min (300 MHz,  $\text{C}_6\text{D}_6$ ).



**Figure 3-16.** <sup>1</sup>H NMR spectrum after 2 h irradiation (300 MHz, C<sub>6</sub>D<sub>6</sub>).

The reactivity of [Ni<sup>I</sup>(IMes)<sub>2</sub>Cl] with stoichiometric amounts of chlorobenzene was studied. A mixture of [Ni<sup>I</sup>(IMes)<sub>2</sub>Cl] (0.02 mmol, 14 mg) and chlorobenzene (0.02 mmol, 2 μL, 1equiv) was dissolved in 0.7 mL C<sub>6</sub>D<sub>6</sub> in a Young's tap NMR tube. From the <sup>1</sup>H NMR spectra recorded after 2 h, it was observed that [Ni<sup>I</sup>(IMes)<sub>2</sub>Cl] reacted with chlorobenzene to give 5% [Ni<sup>II</sup>(IMes)<sub>2</sub>Cl<sub>2</sub>] in the dark, while almost complete conversion of [Ni<sup>I</sup>(IMes)<sub>2</sub>Cl] to [Ni<sup>II</sup>(IMes)<sub>2</sub>Cl<sub>2</sub>] was observed under 400 nm LED irradiation.

Figure 3-17.  $^1\text{H}$  NMR spectrum at 0 min (300 MHz,  $\text{C}_6\text{D}_6$ ).Figure 3-18.  $^1\text{H}$  NMR spectrum after 2 h in the dark (300 MHz,  $\text{C}_6\text{D}_6$ ).



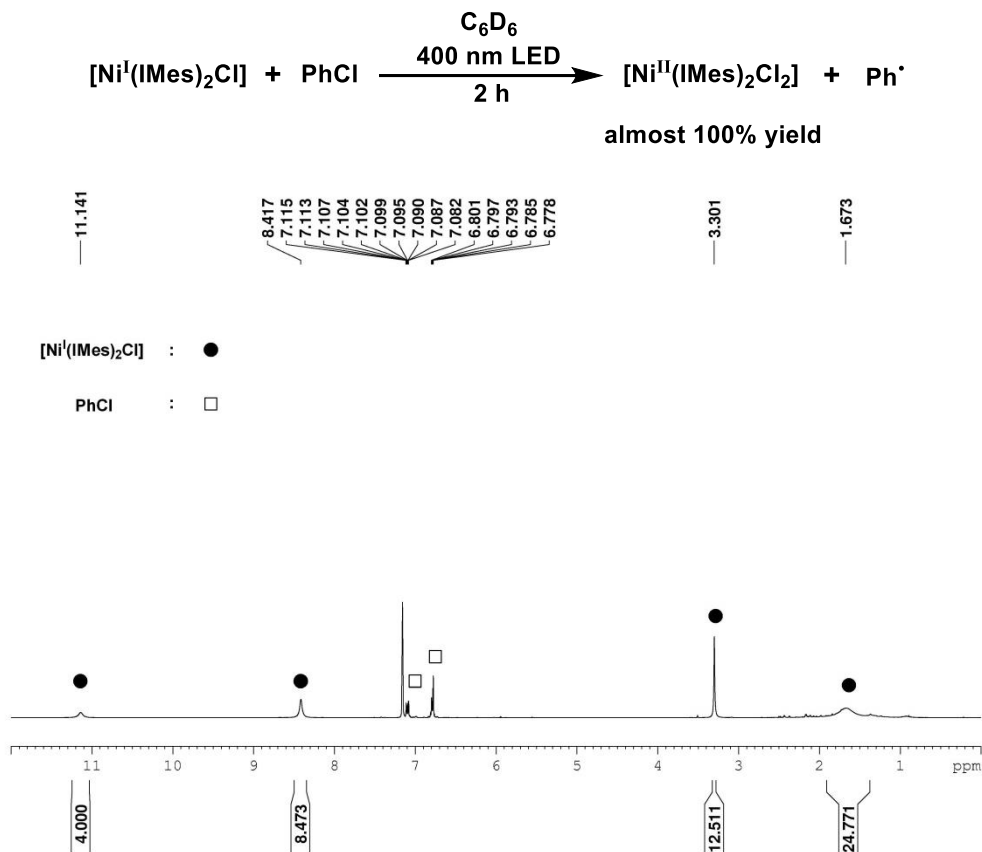


Figure 3-19.  $^1\text{H}$  NMR spectrum at 0 min (300 MHz,  $\text{C}_6\text{D}_6$ ).

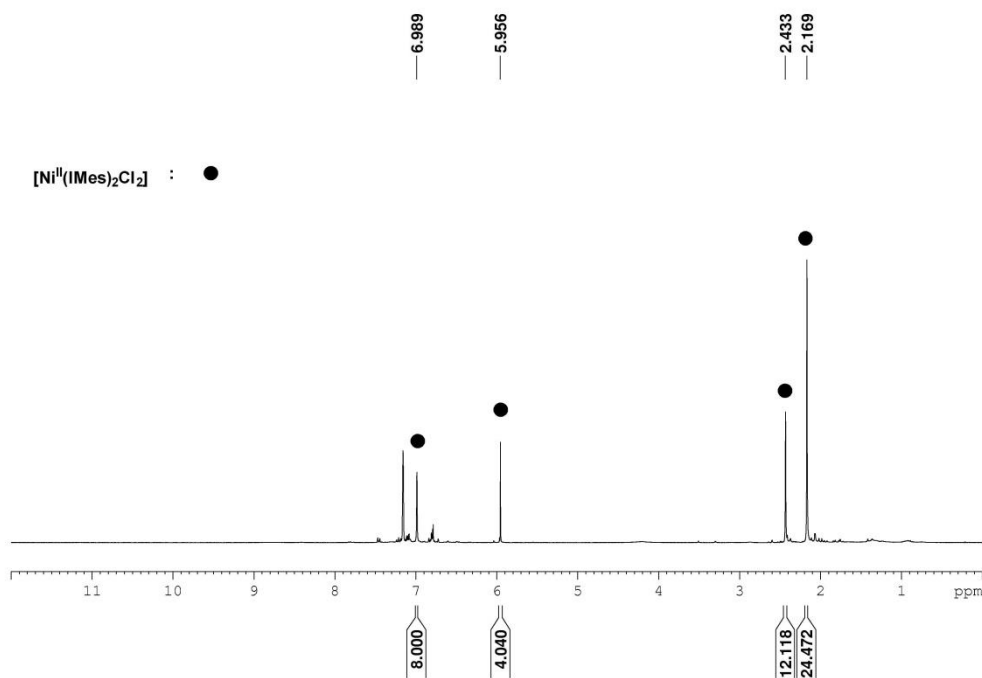
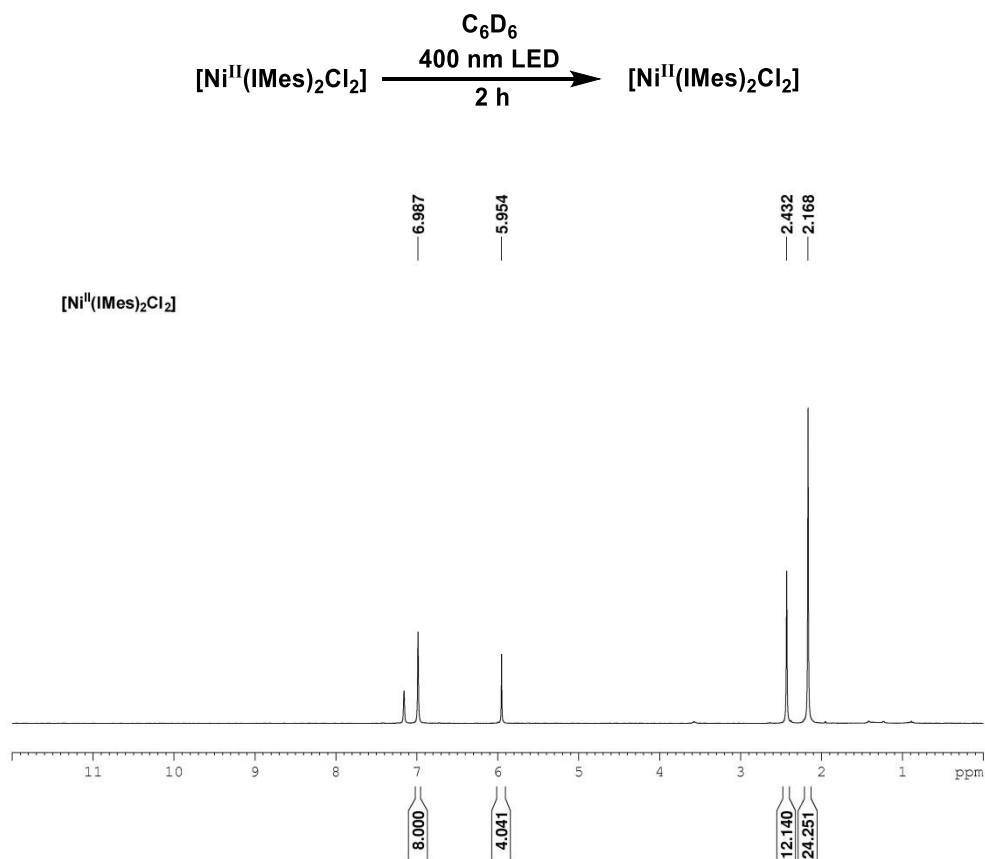
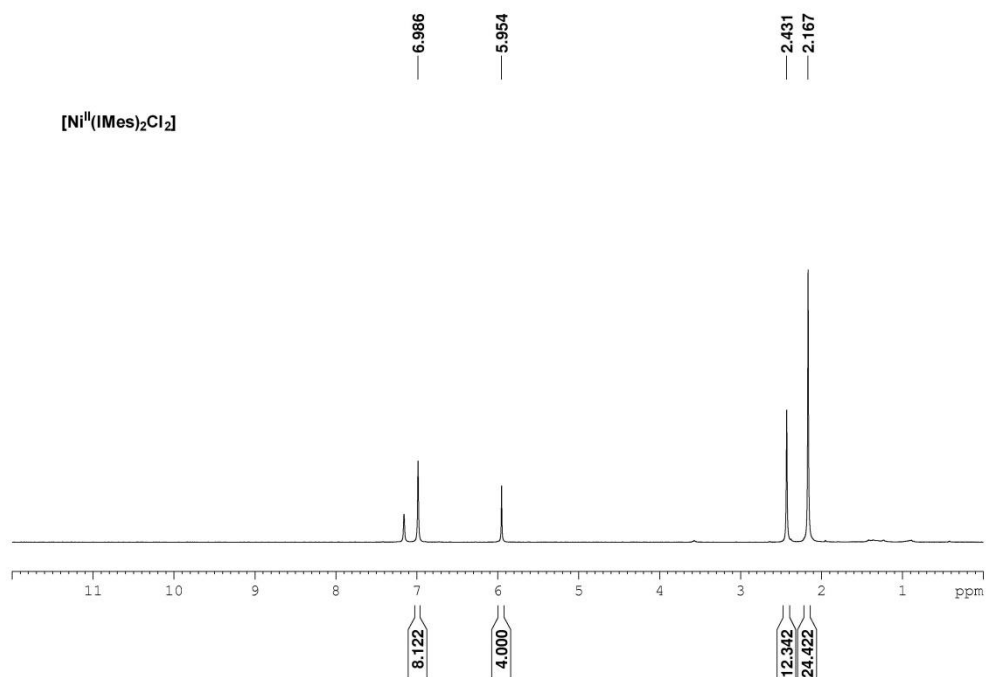


Figure 3-20.  $^1\text{H}$  NMR spectrum after 2 h irradiation (300 MHz,  $\text{C}_6\text{D}_6$ ).

To test the stability of the  $[\text{Ni}^{\text{II}}(\text{IMes})_2\text{Cl}_2]$  complex upon irradiation, a Young's tap NMR tube containing 15 mg of  $[\text{Ni}^{\text{II}}(\text{IMes})_2\text{Cl}_2]$  in 0.7 mL  $\text{C}_6\text{D}_6$  was placed between two 400 nm LEDs (1 W, one centimeter distance from either side of the tube) for 2 h. The  $^1\text{H}$  NMR spectra show no signs of decomposition.



**Figure 3-21.**  $^1\text{H}$  NMR spectrum at 0 min (300 MHz,  $\text{C}_6\text{D}_6$ ).



**Figure 3-22.**  $^1\text{H}$  NMR spectrum after 2 h irradiation (300 MHz,  $\text{C}_6\text{D}_6$ ).

The reactivity of  $[\text{Ni}^{\text{II}}(\text{IMes})_2\text{Cl}_2]$  with stoichiometric amounts of chlorobenzene was studied. A mixture of  $[\text{Ni}^{\text{II}}(\text{IMes})_2\text{Cl}_2]$  (0.02 mmol, 15 mg) and chlorobenzene (0.02 mmol, 2  $\mu\text{L}$ , 1 eq.) was dissolved in 0.7 mL  $\text{C}_6\text{D}_6$  in a Young's tap NMR tube. Two identical samples were prepared according to this method and the  $^1\text{H}$  NMR spectra of the mixtures were recorded immediately after preparation. Then, one was kept in the dark and the other one was irradiated with 400 nm LEDs. They were subsequently studied by  $^1\text{H}$  NMR spectroscopy after 2 h, which revealed no reaction.

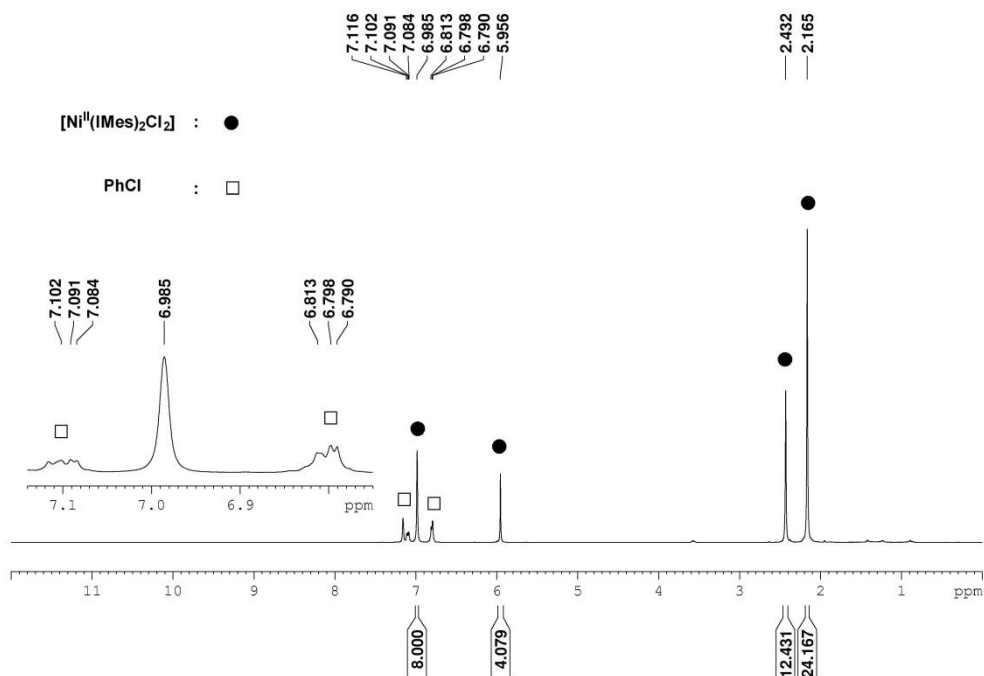
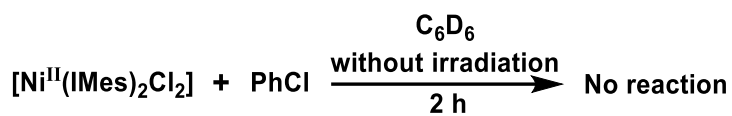


Figure 3-23.  $^1\text{H}$  NMR spectrum at 0 min (300 MHz,  $\text{C}_6\text{D}_6$ ).

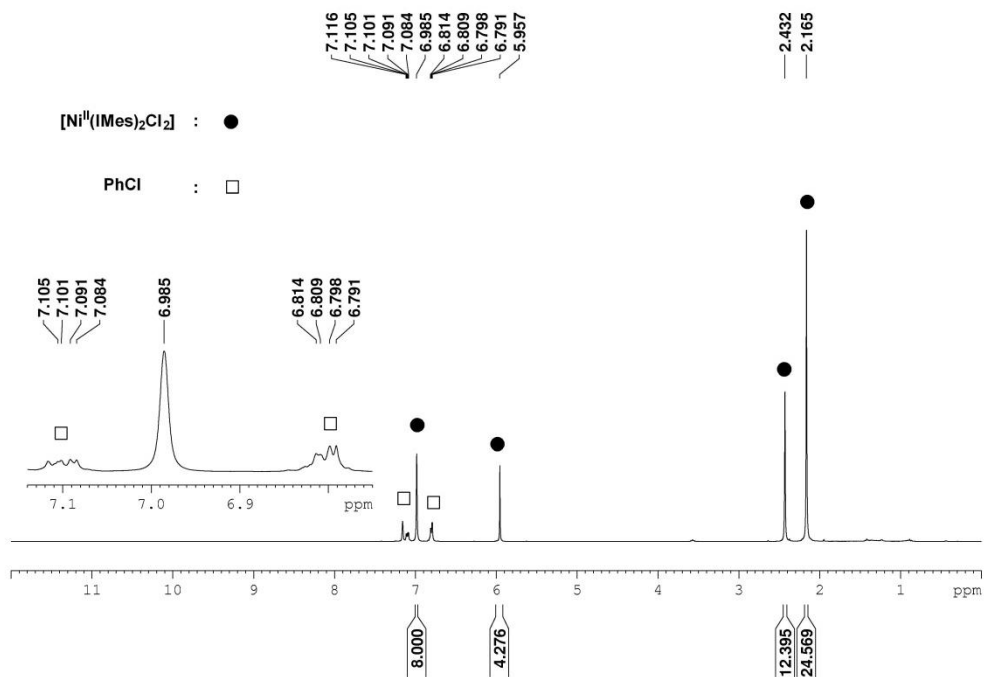


Figure 3-24.  $^1\text{H}$  NMR spectrum after 2 h in the dark (300 MHz,  $\text{C}_6\text{D}_6$ ).

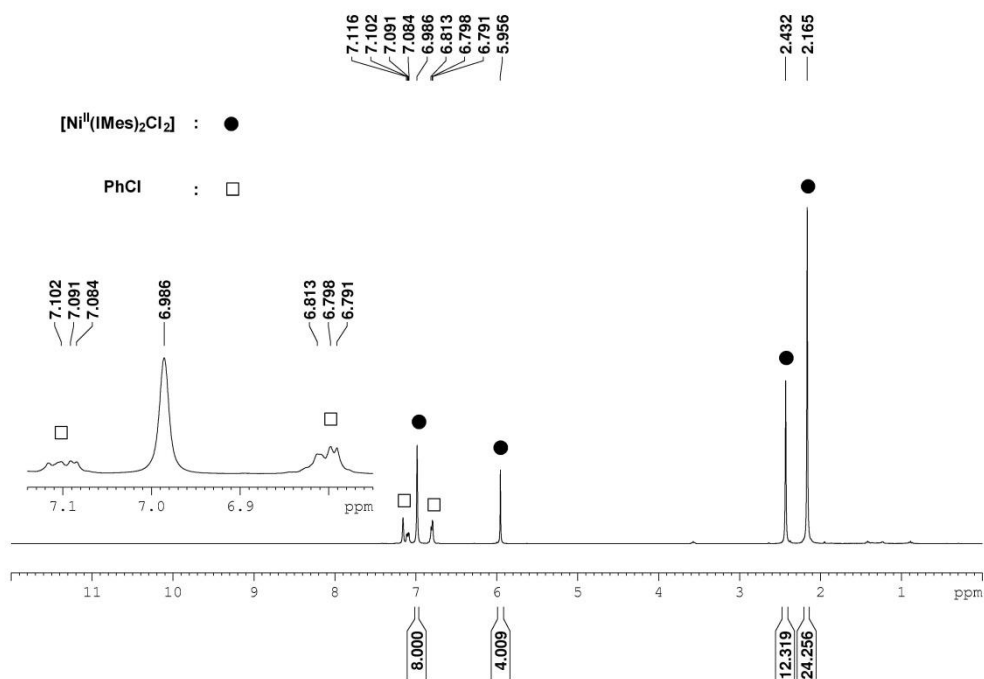
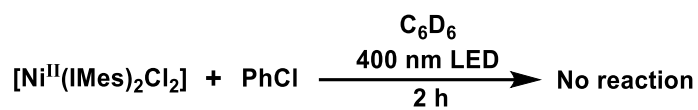


Figure 3-25.  $^1\text{H}$  NMR spectrum at 0 min (300 MHz,  $\text{C}_6\text{D}_6$ ).

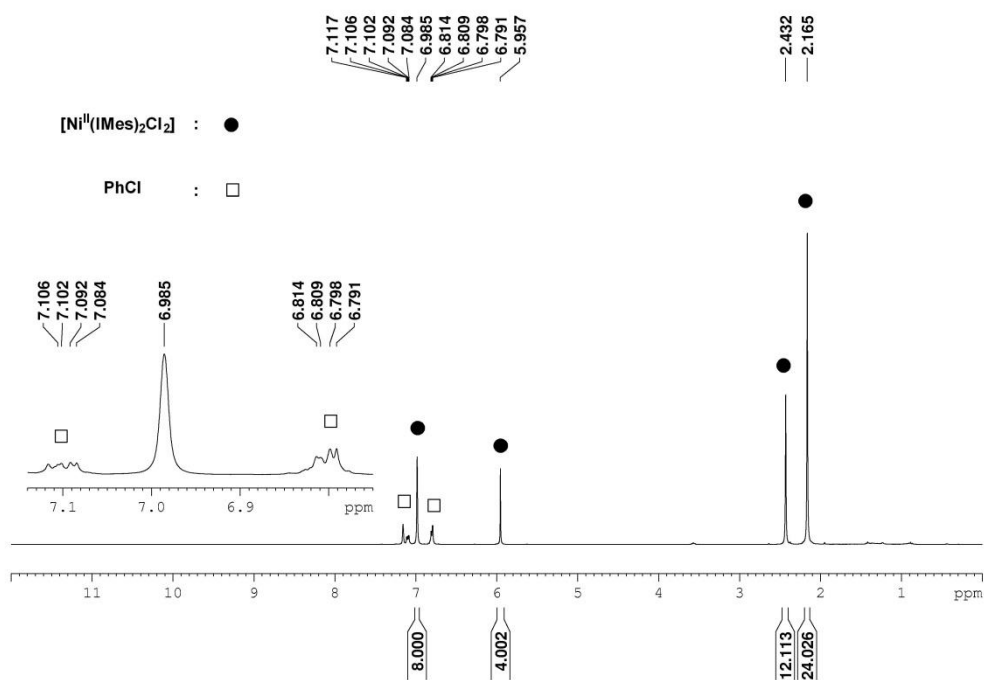
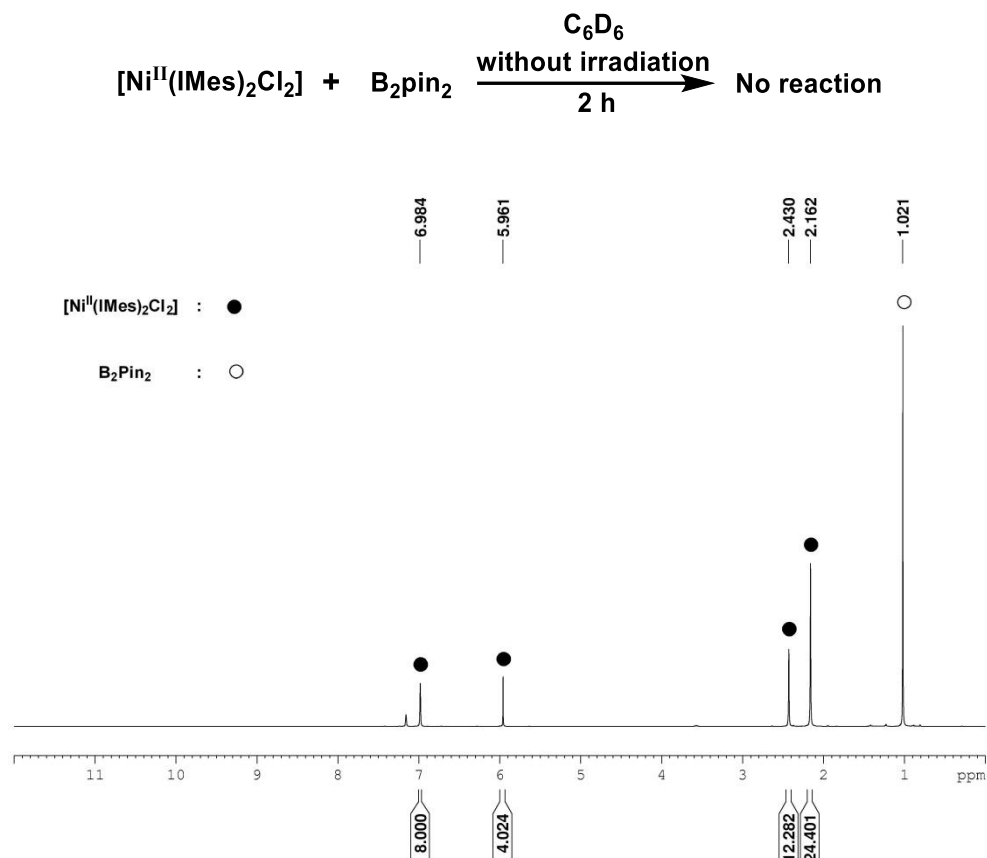


Figure 3-26.  $^1\text{H}$  NMR spectrum after 2 h irradiation (300 MHz,  $\text{C}_6\text{D}_6$ ).

The reactivity of  $[\text{Ni}^{\text{II}}(\text{IMes})_2\text{Cl}_2]$  with stoichiometric amounts of  $\text{B}_2\text{pin}_2$  was studied. The method was the same as above described for the reaction of  $[\text{Ni}^{\text{II}}(\text{IMes})_2\text{Cl}_2]$  with stoichiometric amounts of chlorobenzene, except that  $\text{B}_2\text{pin}_2$  (0.02 mmol, 5.1 mg, 1 equiv) was used instead of chlorobenzene. The  $^1\text{H}$  NMR spectra of reactions in the dark after 2 h, and under irradiation for 2 h, showed that no reaction had occurred.



**Figure 3-27.**  $^1\text{H}$  NMR spectrum at 0 min (300 MHz,  $\text{C}_6\text{D}_6$ ).

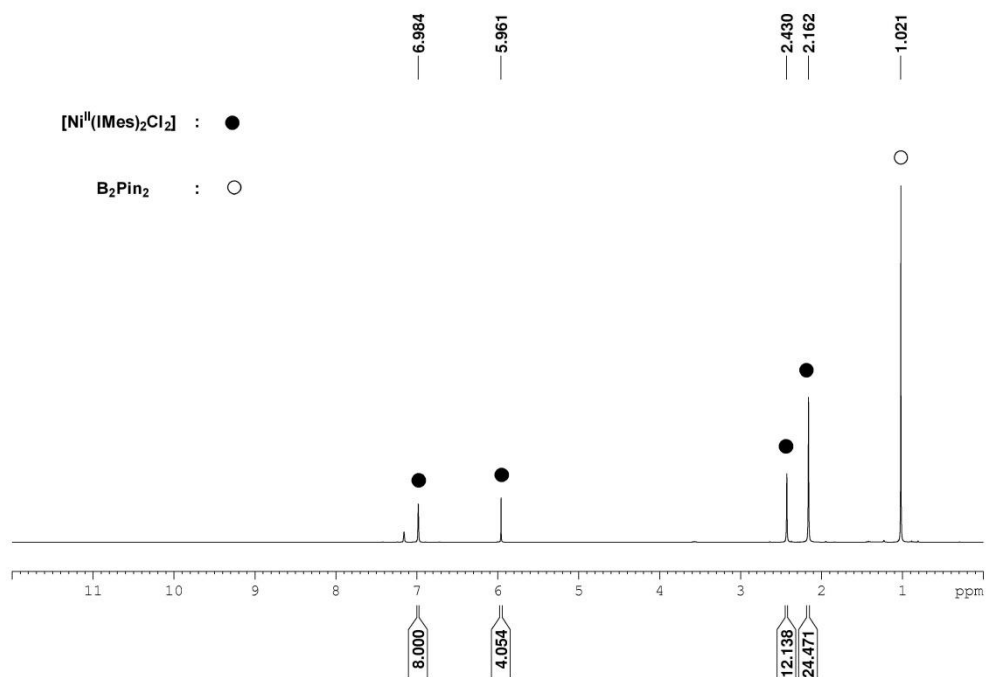


Figure 3-28.  $^1\text{H}$  NMR spectrum after 2 h in the dark (300 MHz,  $\text{C}_6\text{D}_6$ ).

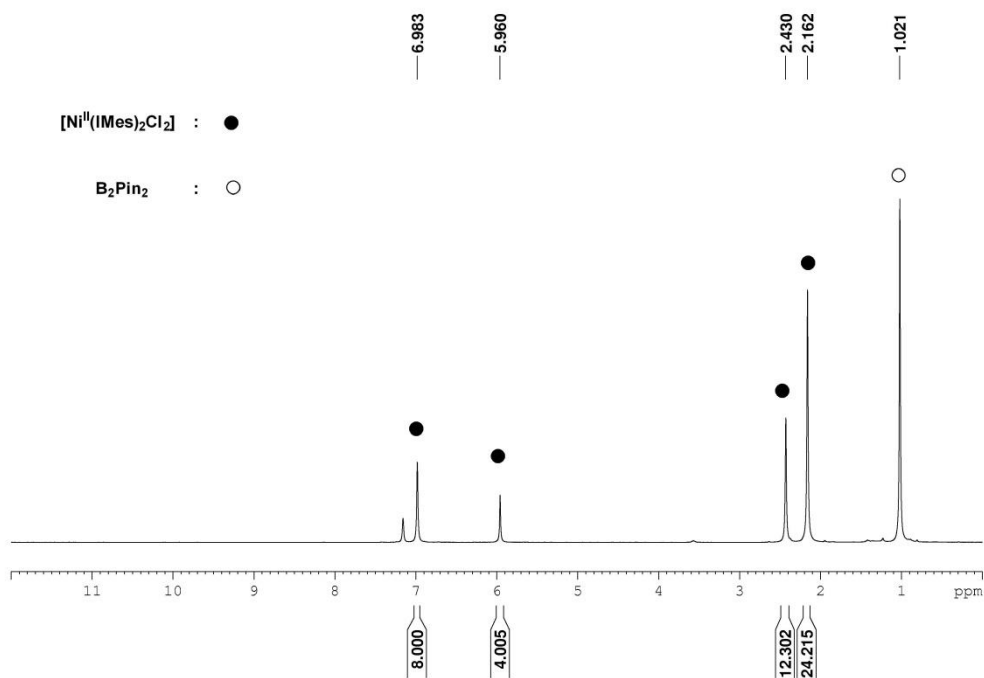
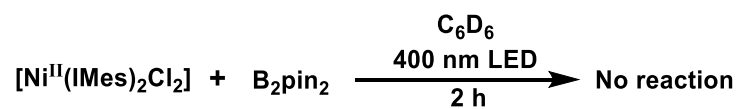
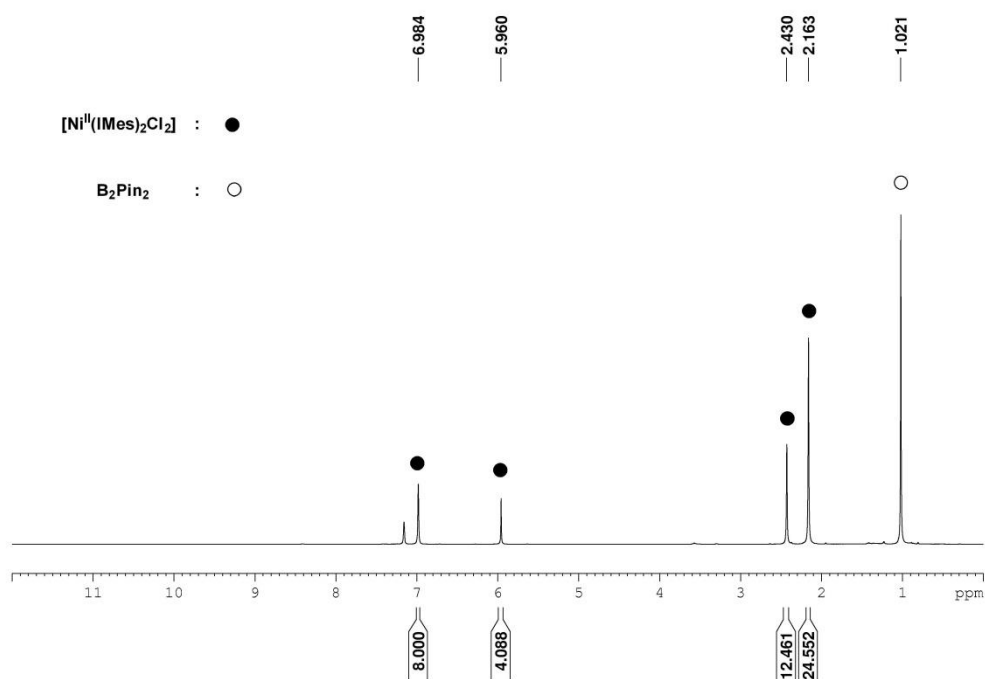


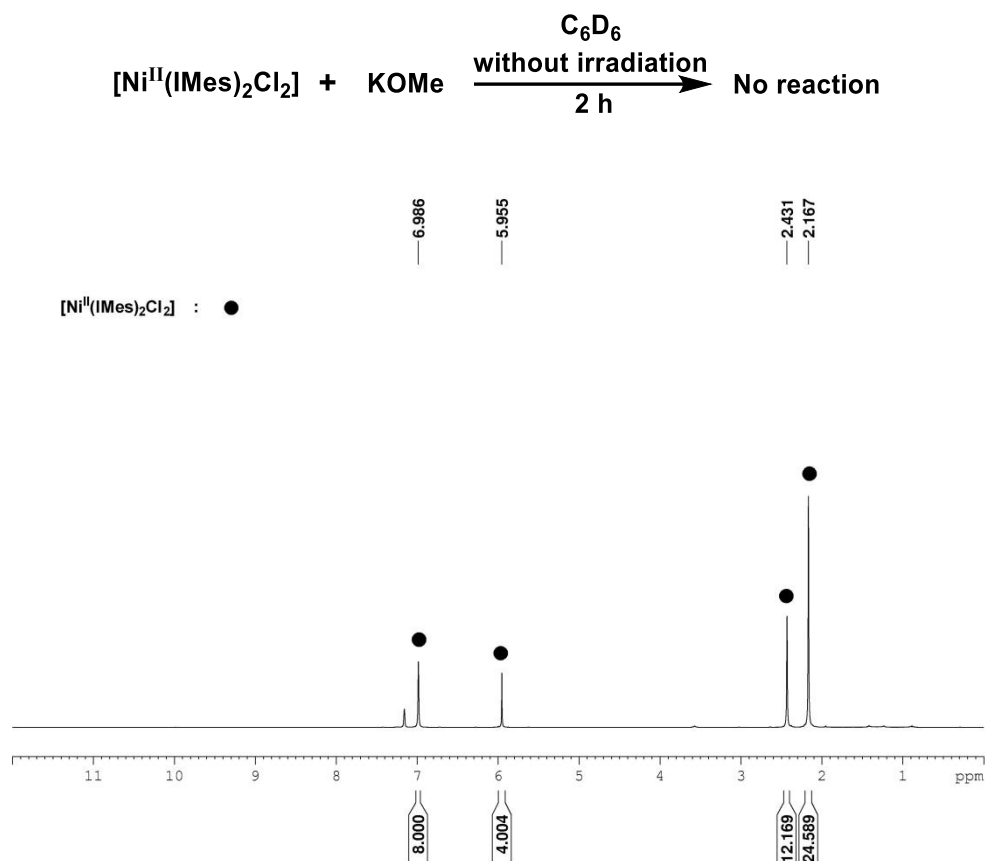
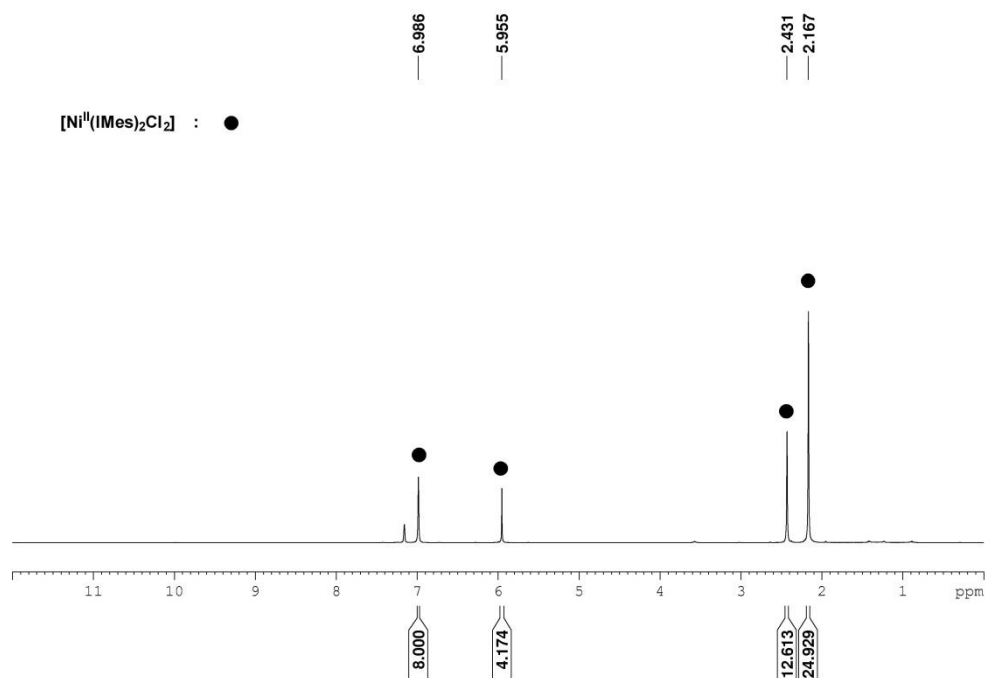
Figure 3-29.  $^1\text{H}$  NMR spectrum at 0 min (300 MHz,  $\text{C}_6\text{D}_6$ ).



**Figure 3-30.** <sup>1</sup>H NMR spectrum after 2 h irradiation (300 MHz, C<sub>6</sub>D<sub>6</sub>).

The reactivity of [Ni<sup>II</sup>(IMes)<sub>2</sub>Cl<sub>2</sub>] with stoichiometric amounts of KOMe was studied. The method was the same as described for the reaction of [Ni<sup>II</sup>(IMes)<sub>2</sub>Cl<sub>2</sub>] with stoichiometric amounts of chlorobenzene, except that KOMe (0.02 mmol, 1.4 mg, 1equiv) was used instead of chlorobenzene. The <sup>1</sup>H NMR spectra of reactions in the dark after 2 h, and under irradiation for 2 h, showed that no reaction had occurred.



Figure 3-31. <sup>1</sup>H NMR spectrum at 0 min (300 MHz, C<sub>6</sub>D<sub>6</sub>).Figure 3-32. <sup>1</sup>H NMR spectrum after 2 h in the dark (300 MHz, C<sub>6</sub>D<sub>6</sub>).

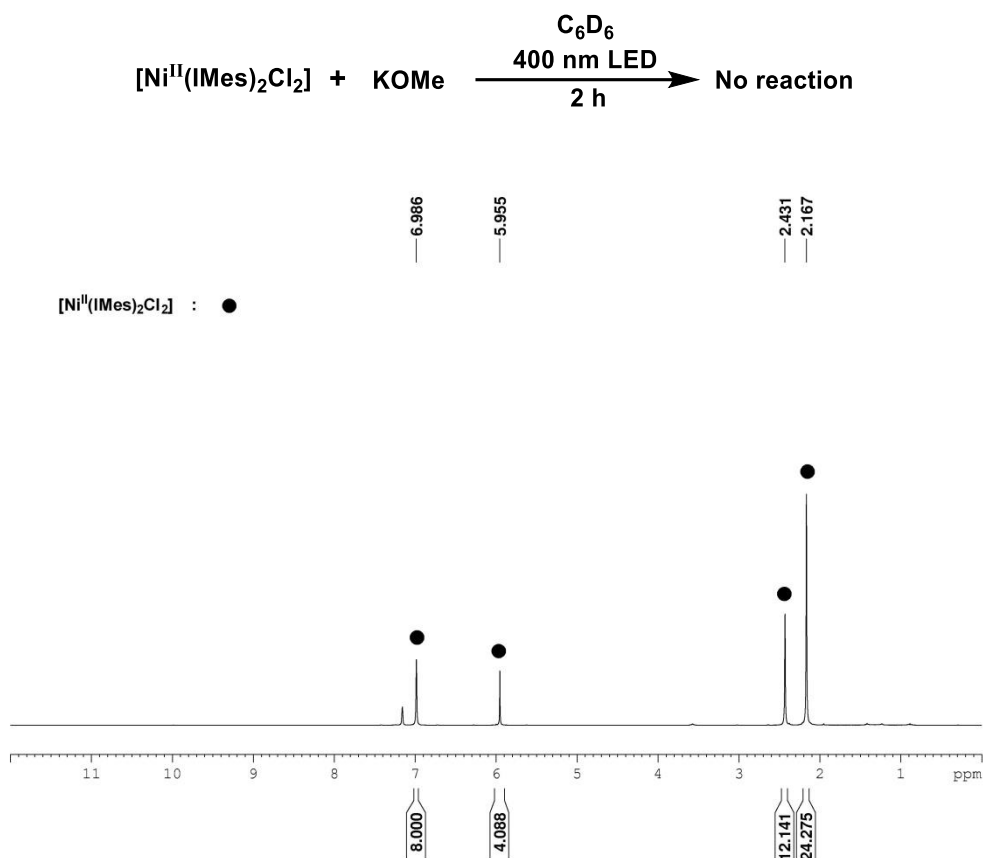


Figure 3-33.  $^1\text{H}$  NMR spectrum at 0 min (300 MHz,  $\text{C}_6\text{D}_6$ ).

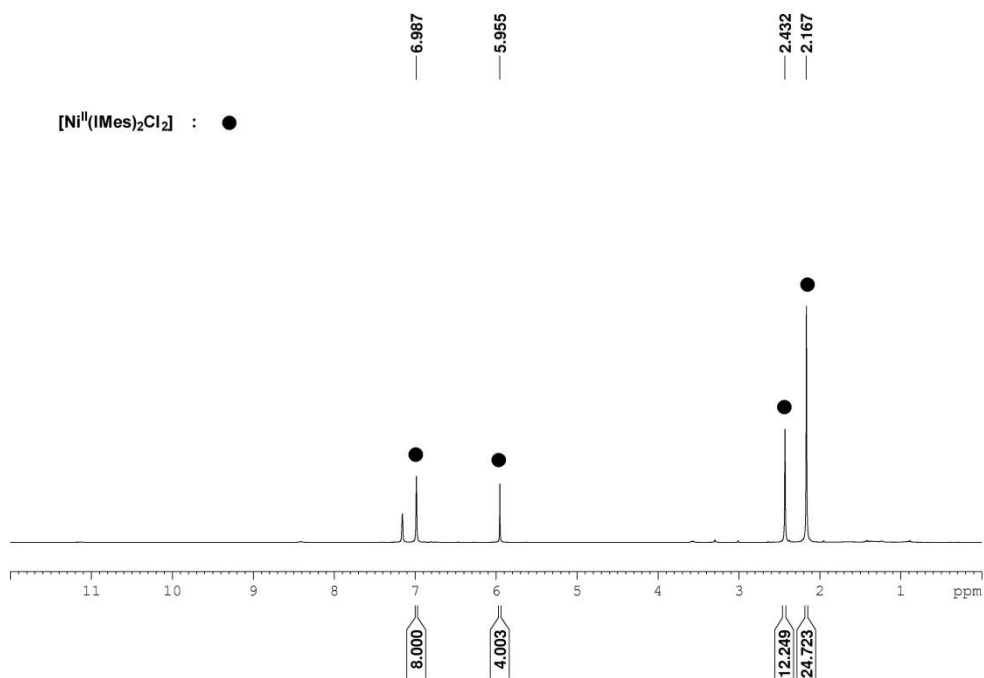
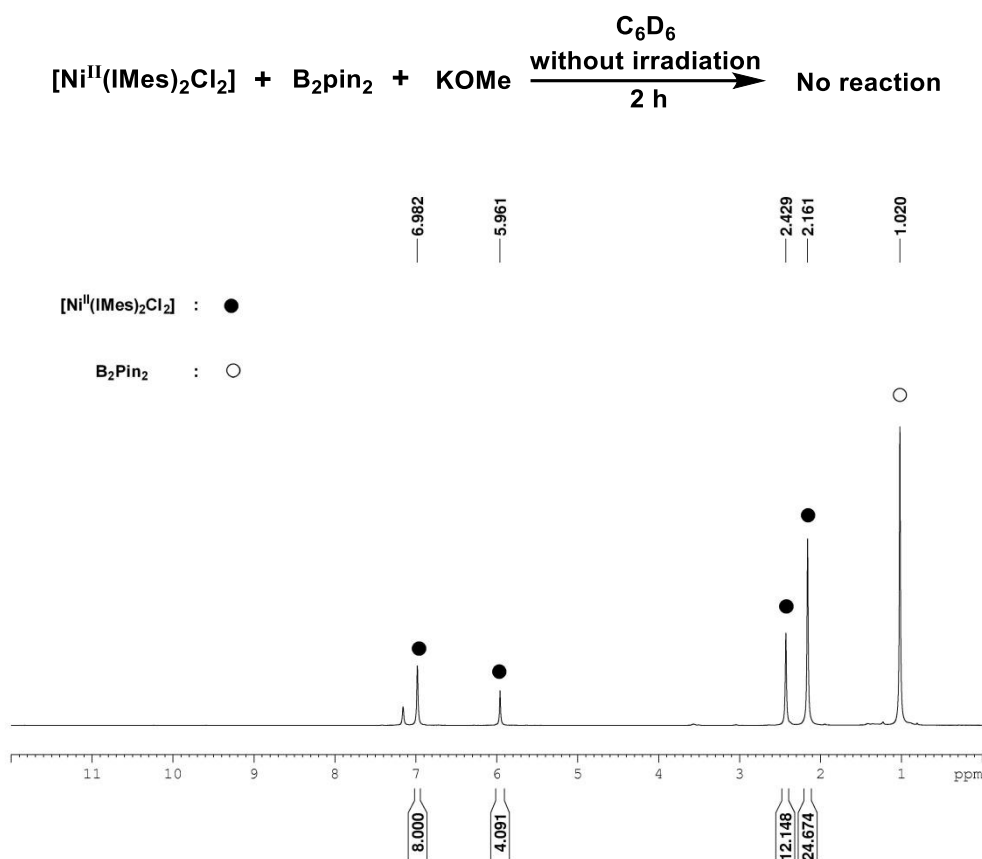
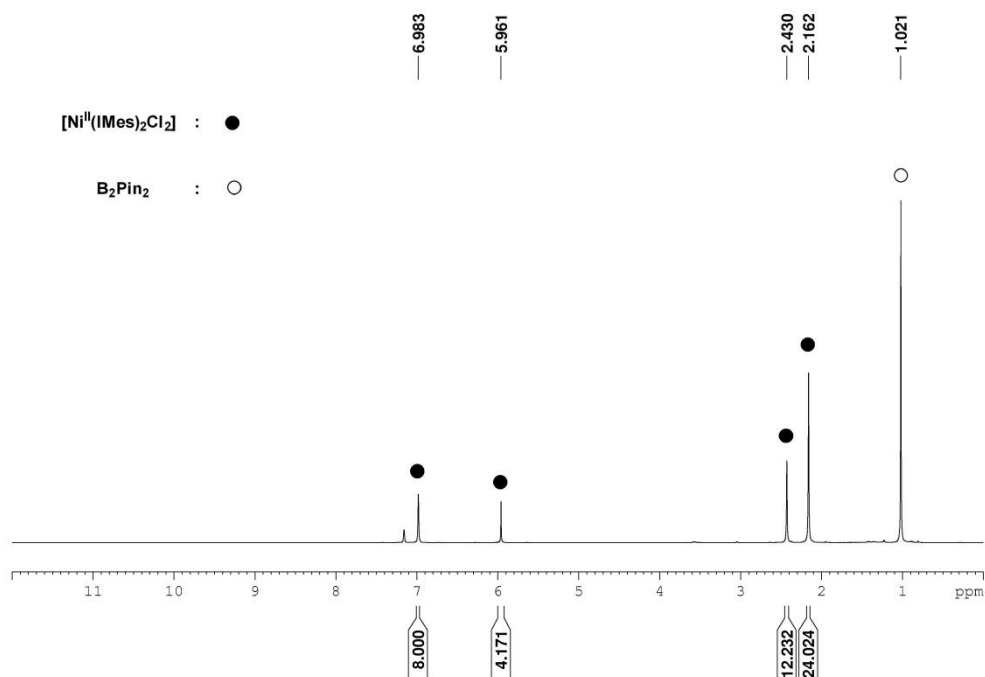


Figure 3-34.  $^1\text{H}$  NMR spectrum after 2 h irradiation (300 MHz,  $\text{C}_6\text{D}_6$ ).

The reactivity of  $[\text{Ni}^{\text{II}}(\text{IMes})_2\text{Cl}_2]$  with stoichiometric amounts of  $\text{B}_2\text{pin}_2$  in the presence of KOMe was studied. The method was the same as above described for the reaction of  $[\text{Ni}^{\text{II}}(\text{IMes})_2\text{Cl}_2]$  with stoichiometric amounts of  $\text{B}_2\text{pin}_2$ , except that KOMe (0.02 mmol, 1.4 mg, 1equiv) was added to the mixture. From the  $^1\text{H}$  NMR spectra recorded after 2 h, no reactivity was detected in the dark, while the formation of  $[\text{Ni}^{\text{I}}(\text{IMes})_2\text{Cl}]$  and  $[\text{Ni}(\text{IMes})_2]$  in 23% and 5% yield, respectively, was observed when the reaction was irradiated.



**Figure 3-35.**  $^1\text{H}$  NMR spectrum at 0 min (300 MHz,  $\text{C}_6\text{D}_6$ ).



**Figure 3-36.**  $^1\text{H}$  NMR spectrum after 2 h in the dark (300 MHz,  $\text{C}_6\text{D}_6$ ).

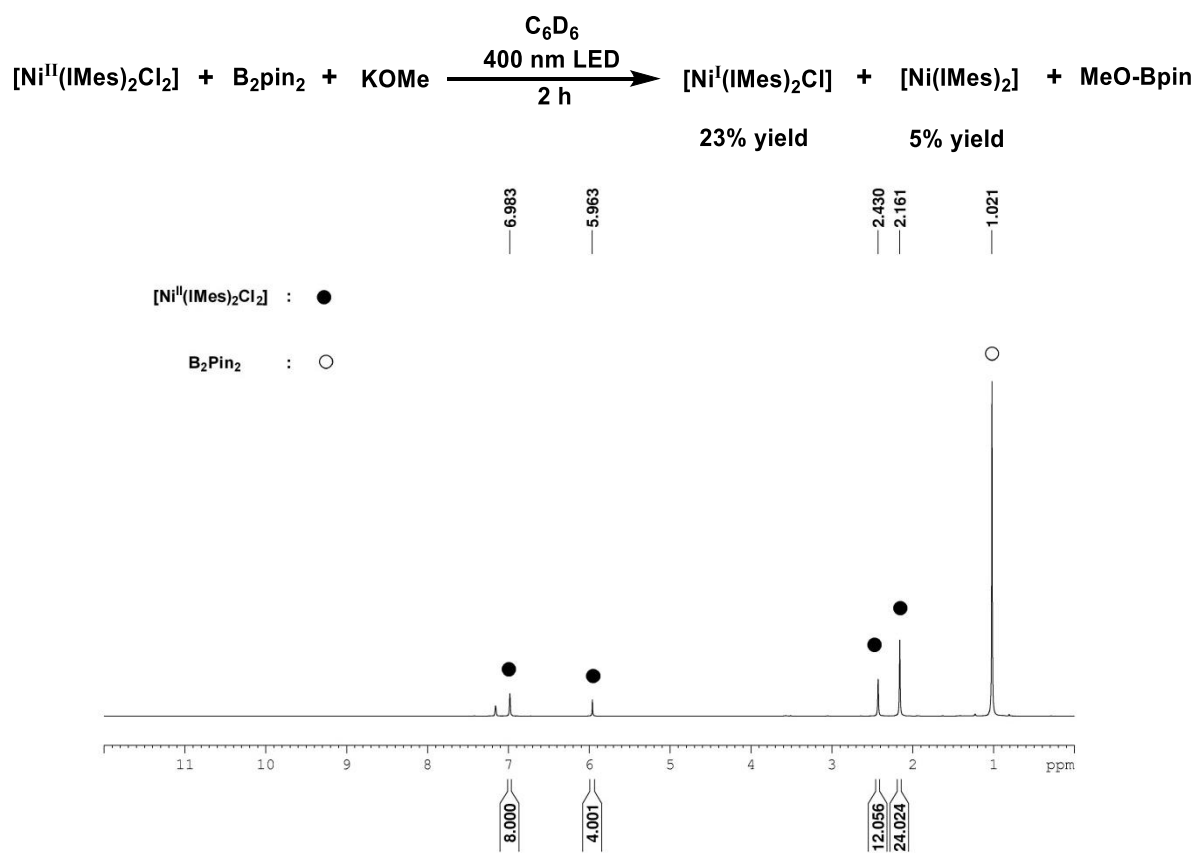


**Figure 3-37.**  $^1\text{H}$  NMR spectrum at 0 min (300 MHz,  $\text{C}_6\text{D}_6$ ).

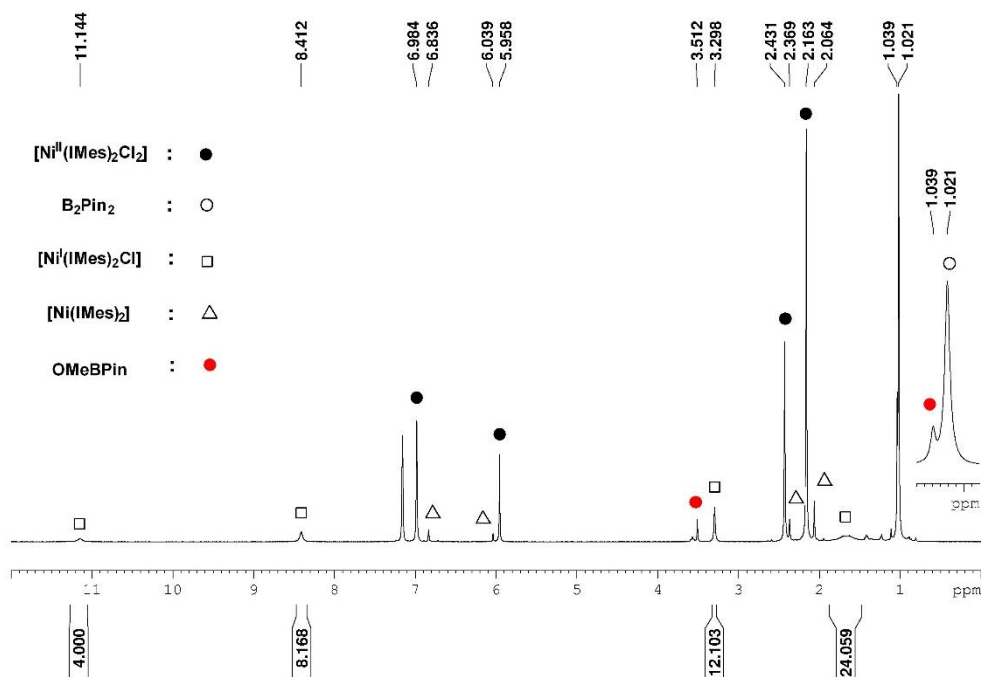


**Figure 3-38.**  $^1\text{H}$  NMR spectrum after 2 h irradiation (300 MHz,  $\text{C}_6\text{D}_6$ ).

The reactivity of  $[\text{Ni}^{\text{II}}(\text{IMes})_2\text{Cl}_2]$  with stoichiometric amounts of MeO-Bpin was studied. The method was the same as described for the reaction of  $[\text{Ni}^{\text{II}}(\text{IMes})_2\text{Cl}_2]$  with stoichiometric amounts of chlorobenzene, except that MeO-Bpin (0.02 mmol, 3.3  $\mu\text{L}$ , 1eq.) was used instead of chlorobenzene. The  $^1\text{H}$  and  $^{11}\text{B}$  NMR spectra of light reaction after 2 h showed no reactivity.

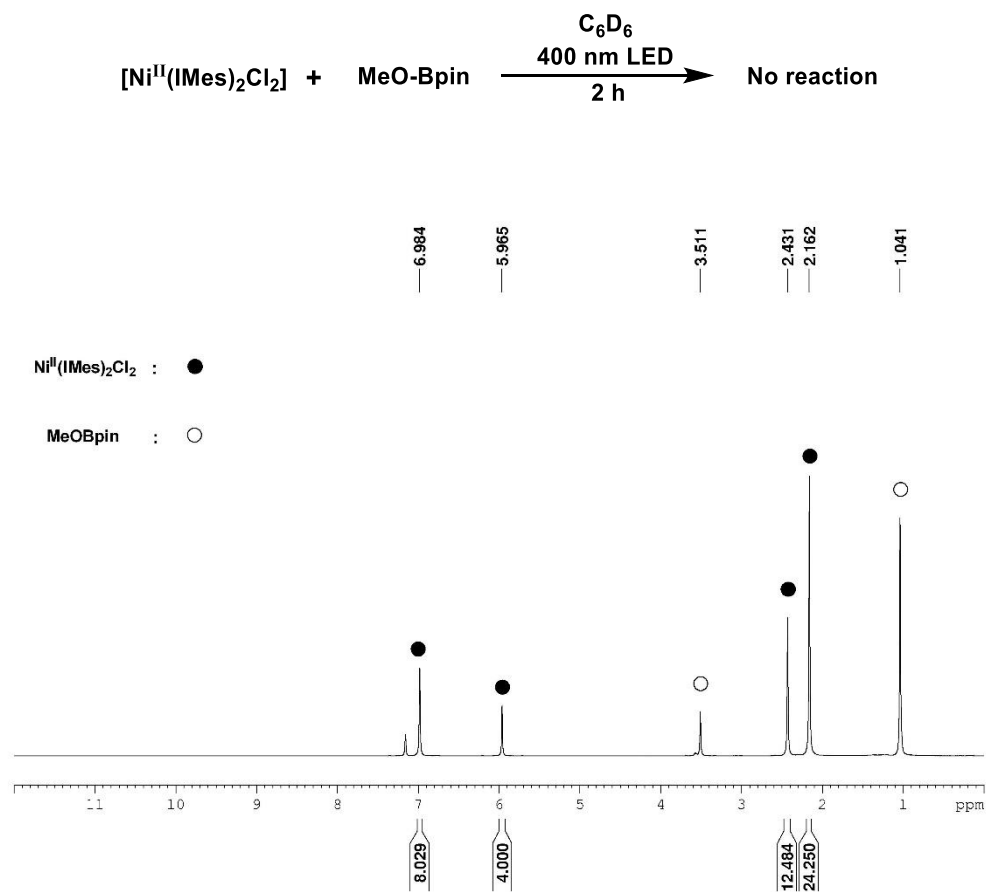


Figure 3-39.  $^1\text{H}$  NMR spectrum at 0 min (400 MHz,  $\text{C}_6\text{D}_6$ ).

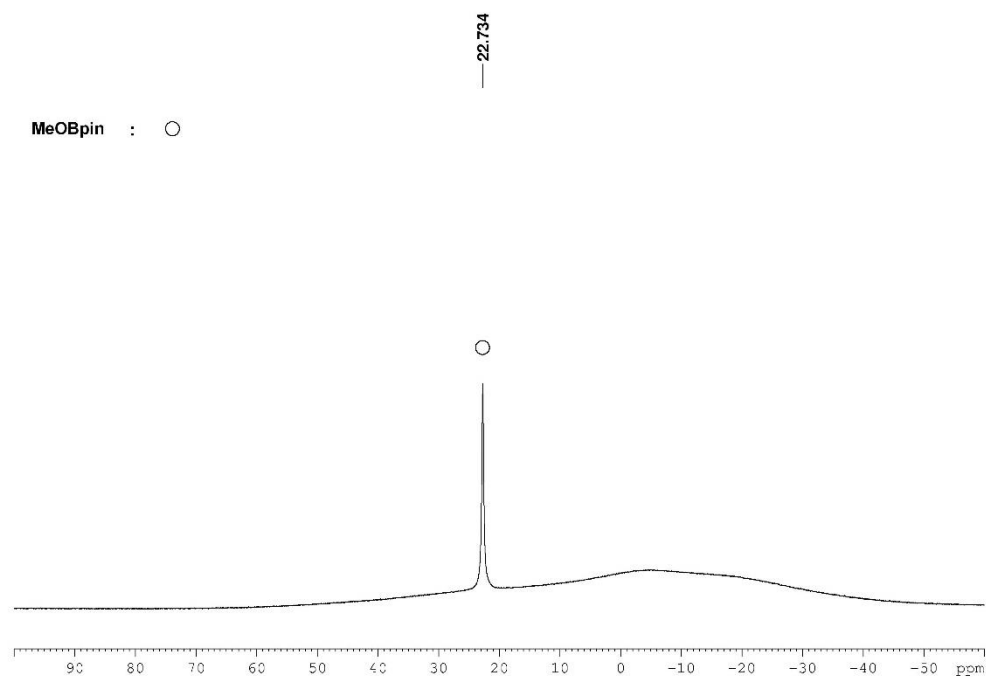


Figure 3-40.  $^{11}\text{B}$  NMR spectrum at 0 min (128 MHz,  $\text{C}_6\text{D}_6$ ).

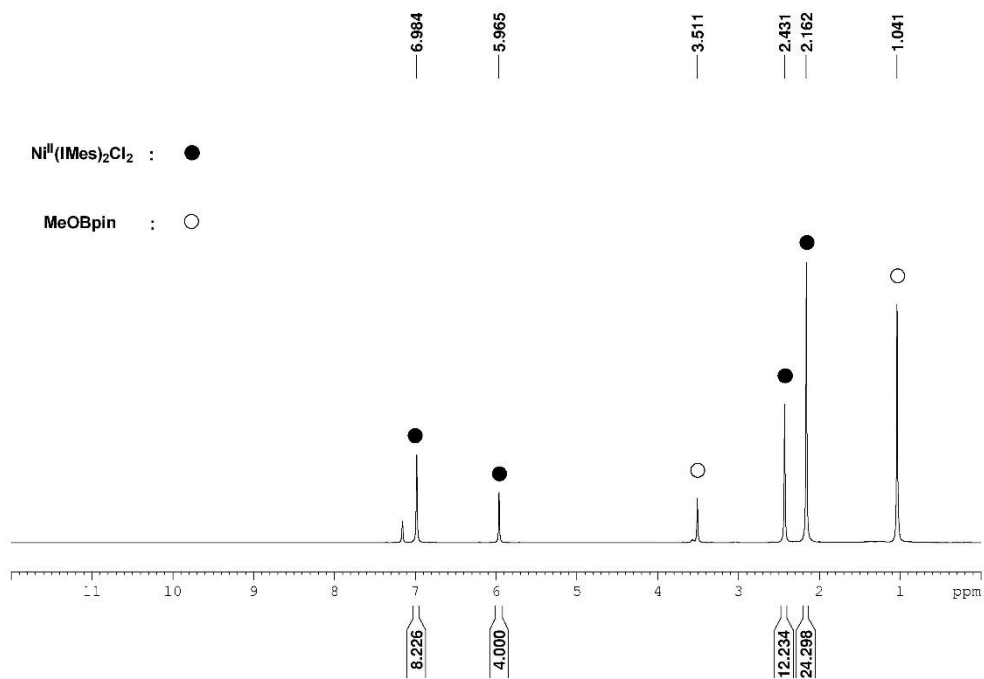


Figure 3-41.  $^1\text{H}$  NMR spectrum after 2 h irradiation (400 MHz,  $\text{C}_6\text{D}_6$ ).

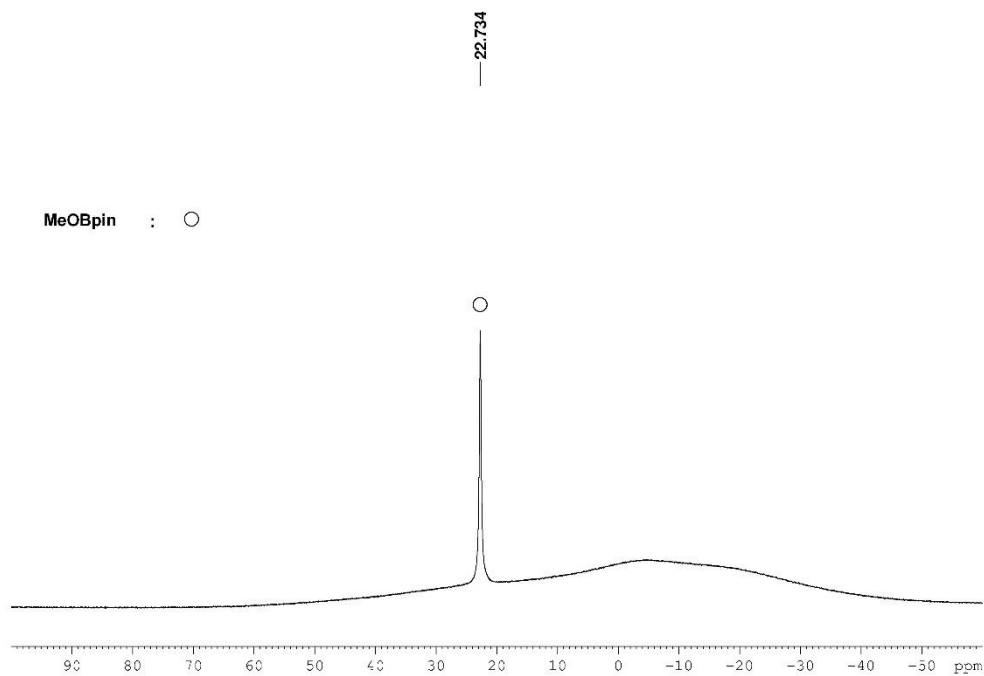
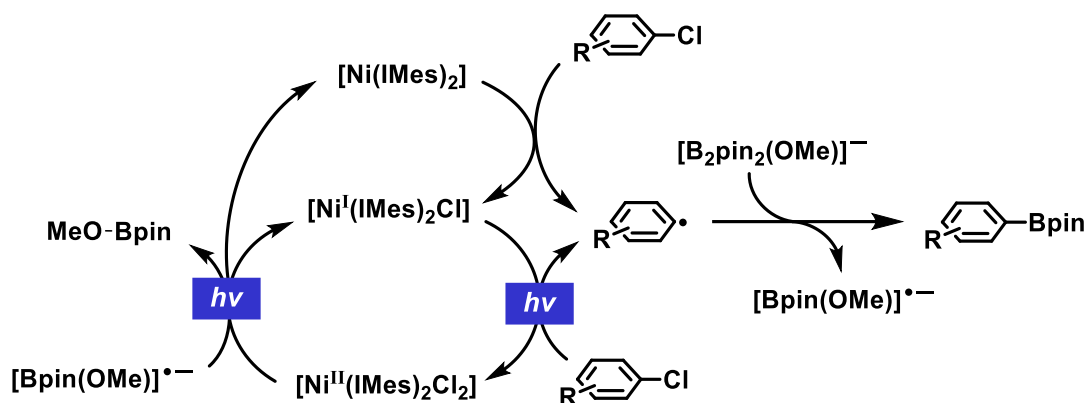


Figure 3-42.  $^{11}\text{B}$  NMR spectrum after 2 h irradiation (128 MHz,  $\text{C}_6\text{D}_6$ ).

### 3.4.5 Proposed mechanism

**Scheme 3-5. Plausible mechanism for the photo-induced borylation of aryl chlorides by transformations between Ni species in the 0, I and II oxidation states**



In light of these findings, a plausible mechanism for the borylation of chloroarenes under irradiation is shown in Scheme 3-5.  $[\text{Ni}(\text{IMes})_2]$  undergoes very fast chlorine atom abstraction from aryl chlorides to give  $[\text{Ni}^{\text{I}}(\text{IMes})_2\text{Cl}]$  and an active aryl radical. Under further irradiation,  $[\text{Ni}^{\text{I}}(\text{IMes})_2\text{Cl}]$  reacts with aryl chlorides to form  $[\text{Ni}^{\text{II}}(\text{IMes})_2\text{Cl}_2]$  and another aryl radical. The reaction of the generated aryl radicals with nucleophilic  $[\text{B}_2\text{pin}_2(\text{OMe})]^-$  yields the final borylated product and  $[\text{Bpin}(\text{OMe})]^{\bullet-}$  radical anion. The  $[\text{Bpin}(\text{OMe})]^{\bullet-}$  is a strong reducing agent, capable of converting  $[\text{Ni}^{\text{II}}(\text{IMes})_2\text{Cl}_2]$  to  $[\text{Ni}^{\text{I}}(\text{IMes})_2\text{Cl}]$  and  $[\text{Ni}(\text{IMes})_2]$ .

## 3.5 Conclusions

In conclusion, we have developed an efficient photocatalytic procedure for the C-Cl borylation of chloroarenes using  $[\text{Ni}(\text{IMes})_2]$  as catalyst operating with visible light. The reaction proceeds under mild conditions, displays broad scope and functional group tolerance, and furnishes arylboronates in good to excellent yields. Our investigations into mechanism suggest that abstraction of a chlorine atom from an aryl chloride by  $[\text{Ni}(\text{IMes})_2]$  is facile at room temperature, forming an aryl radical and  $[\text{Ni}^{\text{I}}(\text{IMes})_2\text{Cl}]$ . Aided by light, a similar process is expected to occur for  $[\text{Ni}^{\text{I}}(\text{IMes})_2\text{Cl}]$  producing additional aryl radicals and  $[\text{Ni}^{\text{II}}(\text{IMes})_2\text{Cl}_2]$ . The aryl radicals are believed to react with nucleophilic  $[\text{B}_2\text{pin}_2(\text{OMe})]^-$



to form the final borylation product and the [Bpin(OMe)]<sup>-</sup> radical anion, which in turn reduce [Ni<sup>II</sup>(IMes)<sub>2</sub>Cl<sub>2</sub>] to regenerate [Ni<sup>I</sup>(IMes)<sub>2</sub>Cl] and [Ni(IMes)<sub>2</sub>] for the next catalytic cycle.

## 3.6 Experimental procedures and characterization data

### 3.6.1 General information

Unless otherwise noted, all manipulations were performed using standard Schlenk or glovebox (Innovative Technology Inc.) techniques under argon. All reagents were purchased from Alfa-Aesar, Aldrich, ABCR or VWR, and were checked for purity by GC-MS and/or <sup>1</sup>H NMR spectroscopy and used as received. Bis(pinacolato)diboron (B<sub>2</sub>pin<sub>2</sub>) was kindly provided by Ally Chem Co. Ltd. (Dalian, China). HPLC grade solvents were argon saturated, dried using an Innovative Technology Inc. Pure-Solv Solvent Purification System, and further deoxygenated using the freeze-pump-thaw method. C<sub>6</sub>D<sub>6</sub> and CDCl<sub>3</sub> were purchased from Cambridge Isotope Laboratories, and dried over 4Å molecular sieves, deoxygenated using the freeze-pump-thaw method and vacuum transferred into a sealed vessel. 1,3-bis-(2,4,6-trimethylphenyl)imidazolin-2-ylidene (IMes)<sup>205</sup> and [Ni(IMes)<sub>2</sub>]<sup>206</sup> used were prepared according to the literature procedures.

Automated flash chromatography was performed using a Biotage<sup>®</sup> Isolera Four system, on silica gel (Biotage SNAP cartridge KP-Sil 10 g and KP-Sil 25 g). Commercially available, precoated TLC plates (Polygram<sup>®</sup> Sil G/UV254) were purchased from Machery-Nagel. The removal of solvent was performed on a rotary evaporator *in vacuo* at a maximum temperature of 30 °C. GC-MS analyses were performed using an Agilent 7890A gas chromatograph (column: HP-5MS 5% phenyl methyl siloxane, 10 m, Ø 0.25 mm, film 0.25 µm; injector: 250 °C; oven: 40 °C (2 min), 40 °C to 280 °C (20 °C·min<sup>-1</sup>); carrier gas: He (1.2 mL·min<sup>-1</sup>)) equipped with an Agilent 5975C inert MSD with triple-axis detector operating in EI mode and an Agilent 7693A series auto sampler/injector. HRMS were measured on a Thermo Scientific Exactive Plus equipped with an Orbitrap. ESI measurements were conducted using a HESI Source with an Aux-gas temperature of 50 °C. Measurements were conducted using an APCI Source with a Corona Needle;

aux-gas temperature was 400 °C.

All NMR spectra were recorded at ambient temperature using Bruker Avance III HD 300 NMR ( $^1\text{H}$ , 300 MHz;  $^{13}\text{C}\{^1\text{H}\}$ , 75 MHz;  $^{11}\text{B}$ , 96 MHz), or Bruker Avance 400 NMR ( $^1\text{H}$ , 400 MHz;  $^{13}\text{C}\{^1\text{H}\}$ , 100 MHz;  $^{11}\text{B}$ , 128 MHz), or Bruker Avance 500 NMR ( $^1\text{H}$ , 500 MHz;  $^{13}\text{C}\{^1\text{H}\}$ , 126 MHz;  $^{11}\text{B}$ , 160 MHz;  $^{19}\text{F}$ , 471 MHz) spectrometers.  $^1\text{H}$  NMR chemical shifts are reported relative to TMS and were referenced via residual proton resonances of the corresponding deuterated solvent ( $\text{CDCl}_3$ : 7.26 ppm,  $\text{C}_6\text{D}_6$ : 7.16 ppm) whereas  $^{13}\text{C}\{^1\text{H}\}$  NMR spectra are reported relative to TMS via the carbon signals of the deuterated solvent ( $\text{CDCl}_3$ : 77.16 ppm,  $\text{C}_6\text{D}_6$ : 128.06 ppm). However, signals for the carbon attach to boron, C(aryl)-B, are usually too broad to observe in the  $^{13}\text{C}\{^1\text{H}\}$  NMR spectra.  $^{11}\text{B}$  NMR chemical shifts are quoted relative to  $\text{BF}_3\cdot\text{Et}_2\text{O}$  as external standard.  $^{19}\text{F}$  NMR chemical shifts are quoted relative to  $\text{CFCl}_3$  as external standard. All  $^{13}\text{C}$  NMR spectra were broad-band  $^1\text{H}$  decoupled.

EPR measurements at X-band (9.38 GHz) were carried out using a Bruker ELEXSYS E580 CW EPR spectrometer equipped with an Oxford Instruments helium cryostat (ESR900) and a MercuryITC temperature controller.

A crystal suitable for single-crystal X-ray diffraction was selected, coated in perfluoropolyether oil, and mounted on a MiTeGen sample holder. Diffraction data were collected on a Bruker X8 Apex II 4-circle diffractometer with a CCD area detector using Mo-K $\alpha$  radiation generated by a Nonius FR591 rotating anode and monochromated by graphite. The crystal was cooled using an Oxford Cryostream low-temperature device. Data were collected at 100 K. The images were processed and corrected for Lorentz-polarization effects and absorption as implemented in the Bruker software packages. The structure was solved using the intrinsic phasing method (SHELXT)<sup>286</sup> and Fourier expansion technique. All non-hydrogen atoms were refined in anisotropic approximation, with hydrogen atoms 'riding' in idealized positions, by full-matrix least squares against  $F^2$  of all data, using SHELXL<sup>287</sup> software. Crystal data and experimental details are listed in Table 3-6; full structural information has been deposited with

Cambridge Structural Database. CCDC-1983919.

### 3.6.2 Experimental procedures

#### Method A

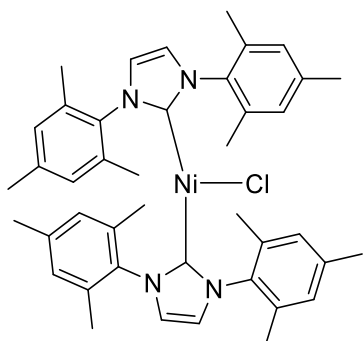
Unless specified otherwise, a mixture of  $[\text{Ni}(\text{IMes})_2]$  (0.02 mmol, 13 mg),  $\text{B}_2\text{pin}_2$  (0.3 mmol, 76 mg) and KOMe (0.3 mmol, 21 mg) was dissolved in the solvent (2 mL) in an oven-dried 10 mL vial equipped with a magnetic stirring bar. The aryl chloride (0.2 mmol) was then added to the solution, and then the vial was sealed. After removing from glove box, the vial was placed between two 400 nm LEDs (1W, one centimeter from either side of the vial). A fan of 40 W was used to avoid the temperature rising of the reaction system due to proximity to the lamp. The reaction mixture was stirred at room temperature for 6 h, then diluted with dichloromethane (DCM, 2 mL) and filtered through a plug of celite ( $\varnothing$  3 mm  $\times$  8 mm), and *n*-dodecane (34 mg, 0.2 mmol) was added as an internal standard. The product yield was determined by GC-MS using the calibrated *n*-dodecane internal standard. The yields are based on aryl chlorides.

#### Method B

A mixture of  $[\text{Ni}(\text{IMes})_2]$  (0.1 mmol, 65 mg),  $\text{B}_2\text{pin}_2$  (1.5 mmol, 381 mg) and KOMe (1.5 mmol, 105 mg) was dissolved in hexane (5 mL) in a Schlenk tube equipped with a magnetic stirring bar. The aryl chloride (1 mmol) was added to the solution. After removing from glove box, the Schlenk tube was placed between two 400 nm LEDs (1W, one centimeter from either side of the vial). A fan of 40 W was used to avoid the temperature rising of the reaction system due to proximity to the lamp. The reaction mixture was stirred at room temperature for 6 h, and was then filtered and the remaining solid was washed with diethyl ether (5 mL  $\text{Et}_2\text{O}$ ). The filtrate was concentrated *in vacuo* and purified by silica-gel column chromatography with hexane and afterwards a hexane and ethyl acetate mixture as eluent. The solvent of the product containing fraction of the eluent was evaporated *in vacuo*. The yields are based on aryl chlorides.

### 3.6.3 Synthesis of $[\text{Ni}^{\text{I}}(\text{IMes})_2\text{Cl}]$

For preparation of bis(1,3-dimesityl-imidazolin-2-ylidene)nickel(I) chloride ( $[\text{Ni}^{\text{I}}(\text{IMes})_2\text{Cl}]$ ), 4-chloroanisole (123  $\mu\text{L}$ , 1.00 mmol) was added to a solution of  $[\text{Ni}(\text{IMes})_2]$  (669 mg, 1.00 mmol) in hexane (10 mL). The solvent was removed under vacuum to yield the crude product. Recrystallization by slow diffusion of hexane into a saturated THF solution of  $[\text{Ni}^{\text{I}}(\text{IMes})_2\text{Cl}]$  at room temperature gave  $[\text{Ni}^{\text{I}}(\text{IMes})_2\text{Cl}]$  as an orange crystalline solid (75%, 526 mg).



$^1\text{H NMR}$  (500 MHz,  $\text{C}_6\text{D}_6$ ):  $\delta$  11.09 (br s, 4H), 8.42 (s, 8H), 3.30 (s, 12H), 1.68 (br s, 24H).

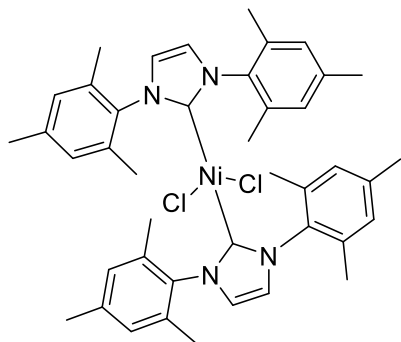
$^{13}\text{C}\{^1\text{H}\}$  NMR (126 MHz,  $\text{C}_6\text{D}_6$ ):  $\delta$  162.5, 143.4, 138.0, 136.6, 49.9, 22.8.

HRMS:  $m/z$  for  $[\text{C}_{42}\text{H}_{48}\text{ClNi}]^+ [\text{M}^+]$  calcd: 701.2915, found: 701.2912.

This is consistent with the results reported in the literature.<sup>280,288</sup>

### 3.6.4 Synthesis of $[\text{Ni}^{\text{II}}(\text{IMes})_2\text{Cl}_2]$

For the preparation of bis(1,3-dimesityl-imidazolin-2-ylidene)nickel(II) dichloride ( $[\text{Ni}^{\text{II}}(\text{IMes})_2\text{Cl}_2]$ ), 4-chloroanisole (123  $\mu\text{L}$ , 142 mg, 1.00 mmol) was added to a solution of  $[\text{Ni}^{\text{I}}(\text{IMes})_2\text{Cl}]$  (703 mg, 1.00 mmol) in toluene (10 mL), and then stirred under irradiation at 400 nm with LEDs for 2 h. The solvent was removed under vacuum to yield the crude product. Recrystallization by slow diffusion of hexane into a saturated toluene solution of  $[\text{Ni}^{\text{II}}(\text{IMes})_2\text{Cl}_2]$  at room temperature gave  $[\text{Ni}^{\text{II}}(\text{IMes})_2\text{Cl}_2]$  as orange-red hexagonal pillar crystals (88%, 650 mg).



**$^1\text{H}$  NMR (300 MHz,  $\text{C}_6\text{D}_6$ ):**  $\delta$  6.99 (s, 8H), 5.95 (s, 4H), 2.43 (s, 12H), 2.17 (s, 24H).

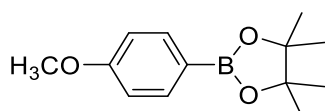
**$^{13}\text{C}\{^1\text{H}\}$  NMR (75 MHz,  $\text{C}_6\text{D}_6$ ):**  $\delta$  169.7, 136.8, 136.7, 136.6, 129.1, 121.9, 21.0, 19.2.

**HRMS:**  $m/z$  for  $[\text{C}_{42}\text{H}_{48}\text{Cl}_2\text{N}_4\text{Ni}]^+$   $[\text{M}^+]$  calcd: 736.2610, found: 736.2588.

This is consistent with the results reported in the literature.<sup>284</sup>

### 3.6.5 Compound characterization

#### 2-(4-Methoxyphenyl)-4,4,5,5-tetramethyl-1,3,2-dioxaborolane (45b)



**Isolated yield:** 79% (185.0 mg, colorless liquid).

**$^1\text{H}$  NMR (300 MHz,  $\text{CDCl}_3$ ):**  $\delta$  7.78-7.73 (m, 2H), 6.92-6.87 (m, 2H), 3.83 (s, 3H), 1.33 (s, 12H).

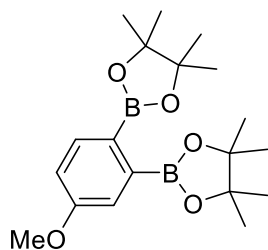
**$^{13}\text{C}\{^1\text{H}\}$  NMR (75 MHz,  $\text{CDCl}_3$ ):**  $\delta$  161.1, 135.5, 112.3, 82.5, 54.1, 23.8.

**$^{11}\text{B}$  NMR (96 MHz,  $\text{CDCl}_3$ ):**  $\delta$  30.8.

**HRMS:**  $m/z$  for  $[\text{C}_{13}\text{H}_{20}\text{BO}_3]^+$   $[\text{M}+\text{H}^+]$  calcd: 235.1500, found: 235.1500.

This is consistent with the results reported in the literature.<sup>97,289</sup>

#### 2,2'-(4-Methoxy-1,2-phenylene)-bis[4,4,5,5-tetramethyl-1,3,2-dioxaborolane] (45c)



**Isolated yield:** 5% (17.2 mg, colorless liquid).

**$^1\text{H}$  NMR (300 MHz,  $\text{CDCl}_3$ ):**  $\delta$  7.66 (d,  $J$  = 8 Hz, 1H), 7.11 (d,  $J$  = 3 Hz, 1H), 6.89 (dd,  $J$  = 8,

3 Hz, 1H), 3.81 (s, 3H), 1.37 (s, 12H), 1.34 (s, 12H).

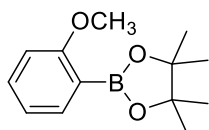
$^{13}\text{C}\{^1\text{H}\}$  NMR (75 MHz,  $\text{CDCl}_3$ ):  $\delta$  160.6, 136.1, 118.3, 114.6, 83.9, 83.6, 55.1, 24.91, 24.88.

$^{11}\text{B}$  NMR (96 MHz,  $\text{CDCl}_3$ ):  $\delta$  31.3.

**HRMS:**  $m/z$  for  $[\text{C}_{19}\text{H}_{31}\text{B}_2\text{O}_5]^+ [\text{M}+\text{H}^+]$  calcd: 361.2352, found: 361.2351.

This is consistent with the results reported in the literature.<sup>97,290</sup>

### 2-(2-Methoxyphenyl)-4,4,5,5-tetramethyl-1,3,2-dioxaborolane (46b)



**Isolated yield:** 60% (140.4 mg, colorless liquid).

$^1\text{H}$  NMR (400 MHz,  $\text{CDCl}_3$ ):  $\delta$  7.69 (dd,  $^1J = 2$  Hz,  $^2J = 7$  Hz, 1H), 7.42-7.38 (m, 1H), 6.97-6.93 (m, 1H), 6.86 (d,  $J = 8$  Hz, 1H), 3.83 (s, 3H), 1.36 (s, 12H).

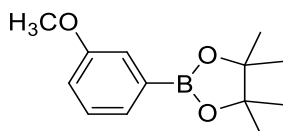
$^{13}\text{C}\{^1\text{H}\}$  NMR (101 MHz,  $\text{CDCl}_3$ ):  $\delta$  164.2, 136.7, 132.5, 120.2, 110.5, 83.4, 55.8, 24.8.

$^{11}\text{B}$  NMR (128 MHz,  $\text{CDCl}_3$ ):  $\delta$  31.0.

**HRMS:**  $m/z$  for  $[\text{C}_{13}\text{H}_{20}\text{BO}_3]^+ [\text{M}+\text{H}^+]$  calcd: 235.1500, found: 235.1499.

This is consistent with the results reported in the literature.<sup>291,292</sup>

### 2-(3-Methoxyphenyl)-4,4,5,5-tetramethyl-1,3,2-dioxaborolane (47b)



**Isolated yield:** 63% (147.4 mg, colorless liquid).

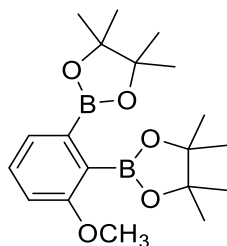
$^1\text{H}$  NMR (400 MHz,  $\text{CDCl}_3$ ):  $\delta$  7.46 (d,  $J = 7$  Hz, 1H), 7.39 (d,  $J = 2$  Hz, 1H), 7.33 (t,  $J = 8$  Hz, 1H), 7.06-7.03 (dm, 1H), 3.85 (s, 3H), 1.38 (s, 12H).

$^{13}\text{C}\{^1\text{H}\}$  NMR (101 MHz,  $\text{CDCl}_3$ ):  $\delta$  159.1, 129.0, 127.2, 118.8, 117.9, 83.8, 55.2, 24.9.

$^{11}\text{B}$  NMR (128 MHz,  $\text{CDCl}_3$ ):  $\delta$  30.9.

**HRMS:**  $m/z$  for  $[\text{C}_{13}\text{H}_{20}\text{BO}_3]^+ [\text{M}+\text{H}^+]$  calcd: 235.1500, found: 235.1499.

This is consistent with the results reported in the literature.<sup>97,292</sup>

**2,2'-(3-Methoxy-1,2-phenylene)-bis[4,4,5,5-tetramethyl-1,3,2-dioxaborolane] (47c)**

**Isolated yield:** 2% (7.2 mg, white solid).

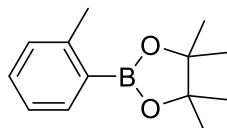
**<sup>1</sup>H NMR** (500 MHz, CDCl<sub>3</sub>): δ 7.41 (dd, *J* = 8, 1 Hz, 1H), 7.30-7.27 (m, 1H), 6.91 (dd, *J* = 8, 1 Hz, 1H), 3.77 (s, 3H), 1.42 (s, 12H), 1.32 (s, 12H).

**<sup>13</sup>C{<sup>1</sup>H} NMR** (126 MHz, CDCl<sub>3</sub>): δ 162.3, 129.4, 127.7, 112.9, 83.9, 83.8, 55.8, 25.1, 24.8.

**<sup>11</sup>B NMR** (160 MHz, CDCl<sub>3</sub>): δ 31.4.

**HRMS:** *m/z* for [C<sub>19</sub>H<sub>31</sub>B<sub>2</sub>O<sub>5</sub>]<sup>+</sup> [M+H<sup>+</sup>] calcd: 361.2352, found: 361.2351.

This is consistent with the results reported in the literature.<sup>97</sup>

**2-(2-Methyl-phenyl)-4,4,5,5-tetramethyl-[1,3,2]dioxaborolane (48b)**

**Isolated yield:** 62% (135.2 mg, colorless liquid).

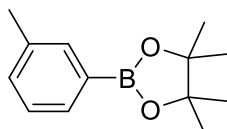
**<sup>1</sup>H NMR** (400 MHz, CDCl<sub>3</sub>): δ 7.92 (d, *J* = 8 Hz, 1H), 7.44 (t, *J* = 8 Hz, 1H), 7.29 (m, 2H), 2.69 (s, 3H), 1.45 (s, 12H).

**<sup>13</sup>C{<sup>1</sup>H} NMR** (101 MHz, CDCl<sub>3</sub>): δ 144.9, 136.1, 130.9, 129.9, 124.8, 83.5, 25.0, 22.4.

**<sup>11</sup>B NMR** (128 MHz, CDCl<sub>3</sub>): δ 31.5.

**HRMS:** *m/z* for [C<sub>13</sub>H<sub>20</sub>BO<sub>2</sub>]<sup>+</sup> [M+H<sup>+</sup>] calcd: 219.1551, found: 219.1550.

This is consistent with the results reported in the literature.<sup>97,292,293</sup>

**4,4,5,5-Tetramethyl-2-m-tolyl-1,3,2-dioxaborolane (49b)**

**Isolated yield:** 64% (139.5 mg, colorless liquid).

**<sup>1</sup>H NMR** (400 MHz, CDCl<sub>3</sub>): δ 7.68 (s, 1H), 7.67-7.63 (m, 1H), 7.31-7.30 (m, 2H), 2.39 (s,

3H), 1.38 (s, 12H).

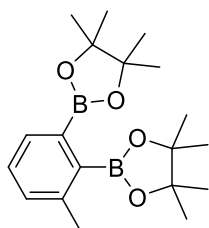
$^{13}\text{C}\{^1\text{H}\}$  NMR (101 MHz,  $\text{CDCl}_3$ ):  $\delta$  137.1, 135.4, 132.1, 131.8, 127.7, 83.7, 24.9, 21.3.

$^{11}\text{B}$  NMR (128 MHz,  $\text{CDCl}_3$ ):  $\delta$  31.0.

**HRMS:**  $m/z$  for  $[\text{C}_{13}\text{H}_{20}\text{BO}_2]^+ [\text{M}+\text{H}^+]$  calcd: 219.1551, found: 219.1551.

This is consistent with the results reported in the literature.<sup>97,292,293</sup>

### 2,2'-(3-Methyl-1,2-phenylene)-bis[4,4,5,5-tetramethyl-1,3,2-dioxaborolane] (49c)



**Isolated yield:** 3% (10.3 mg, white solid).

$^1\text{H}$  NMR (500 MHz,  $\text{CDCl}_3$ ):  $\delta$  7.63-7.61 (m, 1H), 7.24-7.20 (m, 2H), 2.41 (s, 3H), 1.43 (s, 12H), 1.33 (s, 12H).

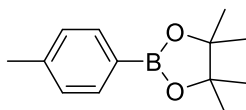
$^{13}\text{C}\{^1\text{H}\}$  NMR (126 MHz,  $\text{CDCl}_3$ ):  $\delta$  140.4, 132.2, 131.7, 128.1, 83.83, 83.82, 25.5, 24.8, 21.9.

$^{11}\text{B}$  NMR (160 MHz,  $\text{CDCl}_3$ ):  $\delta$  31.7.

**HRMS:**  $m/z$  for  $[\text{C}_{19}\text{H}_{31}\text{B}_2\text{O}_4]^+ [\text{M}+\text{H}^+]$  calcd: 345.2403, found: 345.2402.

This is consistent with the results reported in the literature.<sup>97</sup>

### 4,4,5,5-Tetramethyl-2-p-tolyl-1,3,2-dioxaborolane (50b)



**Isolated yield:** 67% (146.1 mg, white solid).

$^1\text{H}$  NMR (400 MHz,  $\text{CDCl}_3$ ):  $\delta$  7.73 (d,  $J = 8$  Hz, 2H), 7.20 (d,  $J = 8$  Hz, 2H), 2.38 (s, 3H), 1.35 (s, 12H).

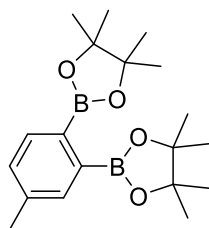
$^{13}\text{C}\{^1\text{H}\}$  NMR (101 MHz,  $\text{CDCl}_3$ ):  $\delta$  141.4, 134.8, 128.5, 83.6, 24.9, 21.8.

$^{11}\text{B}$  NMR (128 MHz,  $\text{CDCl}_3$ ):  $\delta$  31.0.

**HRMS:**  $m/z$  for  $[\text{C}_{13}\text{H}_{20}\text{BO}_2]^+ [\text{M}+\text{H}^+]$  calcd: 219.1551, found: 219.1550.

This is consistent with the results reported in the literature.<sup>97,292,293</sup>



**2,2'-(4-Methyl-1,2-phenylene)-bis[4,4,5,5-tetramethyl-1,3,2-dioxaborolane] (50c)**

**Isolated yield:** 5% (17.2 mg, pale yellow solid).

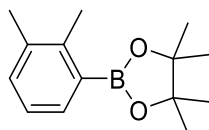
**<sup>1</sup>H NMR** (500 MHz, CDCl<sub>3</sub>): δ 7.57 (d, *J* = 8 Hz, 1H), 7.45-7.44 (m, 1H), 7.20-7.18 (m, 1H), 2.33 (s, 3H), 1.37 (s, 12H), 1.35 (s, 12H).

**<sup>13</sup>C{<sup>1</sup>H} NMR** (126 MHz, CDCl<sub>3</sub>): δ 139.0, 134.1, 133.9, 129.9, 83.8, 83.7, 24.9, 24.9, 21.5.

**<sup>11</sup>B NMR** (160 MHz, CDCl<sub>3</sub>): δ 31.6.

**HRMS:** *m/z* for [C<sub>19</sub>H<sub>31</sub>B<sub>2</sub>O<sub>4</sub>]<sup>+</sup> [M+H<sup>+</sup>] calcd: 345.2403, found: 345.2403.

This is consistent with the results reported in the literature.<sup>97,290</sup>

**4,4,5,5-Tetramethyl-2-(2,3-dimethylphenyl)-1,3,2-dioxaborolane (51b)**

**Isolated yield:** 55% (127.6 mg, white solid).

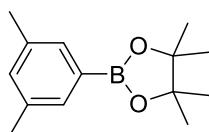
**<sup>1</sup>H NMR** (400 MHz, CDCl<sub>3</sub>): δ 7.61 (d, *J* = 7 Hz, 1H), 7.22 (d, *J* = 7 Hz, 1H), 7.10 (t, *J* = 7 Hz, 1H), 2.48 (s, 3H), 2.29 (s, 3H), 1.36 (s, 12H).

**<sup>13</sup>C{<sup>1</sup>H} NMR** (101 MHz, CDCl<sub>3</sub>): δ 143.1, 136.5, 133.5, 132.3, 124.9, 83.4, 24.9, 20.4, 18.5.

**<sup>11</sup>B NMR** (128 MHz, CDCl<sub>3</sub>): δ 31.6.

**HRMS:** *m/z* for [C<sub>14</sub>H<sub>22</sub>BO<sub>2</sub>]<sup>+</sup> [M+H<sup>+</sup>] calcd: 233.1707, found: 233.1705.

This is consistent with the results reported in the literature.<sup>292</sup>

**4,4,5,5-Tetramethyl-2-(3,5-dimethylphenyl)-1,3,2-dioxaborolane (52b)**

**Isolated yield:** 61% (141.5 mg, white solid).

$^1\text{H NMR}$  (400 MHz,  $\text{CDCl}_3$ ):  $\delta$  7.46 (s, 2H), 7.12 (s, 1H), 2.34 (s, 6H), 1.36 (s, 12H).

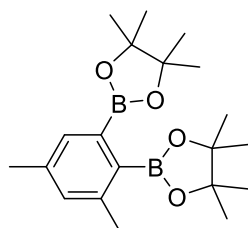
$^{13}\text{C}\{^1\text{H}\}$  NMR (101 MHz,  $\text{CDCl}_3$ ):  $\delta$  137.1, 133.0, 132.4, 83.7, 24.8, 21.1.

$^{11}\text{B NMR}$  (128 MHz,  $\text{CDCl}_3$ ):  $\delta$  31.1.

**HRMS:**  $m/z$  for  $[\text{C}_{14}\text{H}_{22}\text{BO}_2]^+ [\text{M}+\text{H}^+]$  calcd: 233.1707, found: 233.1706.

This is consistent with the results reported in the literature.<sup>97,292,294</sup>

### 2,2'-(3,5-Dimethyl-1,2-phenylene)-bis[4,4,5,5-tetramethyl-1,3,2-dioxaborolane] (52c)



**Isolated yield:** 3% (10.7 mg, white solid).

$^1\text{H NMR}$  (500 MHz,  $\text{CDCl}_3$ ):  $\delta$  7.44-7.43 (m, 1H), 7.02-7.01 (m, 1H), 2.38 (s, 3H), 2.27 (s, 3H), 1.42 (s, 12H), 1.33 (s, 12H).

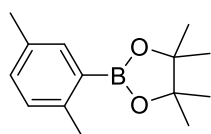
$^{13}\text{C}\{^1\text{H}\}$  NMR (126 MHz,  $\text{CDCl}_3$ ):  $\delta$  140.6, 137.5, 132.8, 132.6, 83.8, 83.7, 25.4, 24.8, 21.8, 21.1.

$^{11}\text{B NMR}$  (160 MHz,  $\text{CDCl}_3$ ):  $\delta$  31.7.

**HRMS:**  $m/z$  for  $[\text{C}_{20}\text{H}_{33}\text{B}_2\text{O}_4]^+ [\text{M}+\text{H}^+]$  calcd: 359.2559, found: 359.2558.

This is consistent with the results reported in the literature.<sup>97</sup>

### 4,4,5,5-Tetramethyl-2-(2,5-dimethylphenyl)-1,3,2-dioxaborolane (53b)



**Isolated yield:** 66% (153.1 mg, white solid).

$^1\text{H NMR}$  (500 MHz,  $\text{CDCl}_3$ ):  $\delta$  7.59 (d,  $J = 2$  Hz, 1H), 7.15-7.13 (m, 1H), 7.07 (d,  $J = 8$  Hz, 1H), 2.51 (s, 3H), 2.32 (s, 3H), 1.36 (s, 3H).

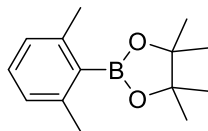
$^{13}\text{C}\{^1\text{H}\}$  NMR (126 MHz,  $\text{CDCl}_3$ ):  $\delta$  141.7, 136.4, 133.9, 131.6, 129.8, 83.4, 24.9, 21.7, 20.8.

$^{11}\text{B NMR}$  (160 MHz,  $\text{CDCl}_3$ ):  $\delta$  31.4.

**HRMS:**  $m/z$  for  $[\text{C}_{14}\text{H}_{22}\text{BO}_2]^+ [\text{M}+\text{H}^+]$  calcd: 233.1707, found: 233.1706.

This is consistent with the results reported in the literature.<sup>292,294</sup>

### 3-(2,6-Dimethylphenyl)-4,4,5,5-tetramethyl-1,3,2-dioxaborolane (54b)



**Isolated yield:** 38% (88.2 mg, white solid).

**<sup>1</sup>H NMR** (300 MHz, CDCl<sub>3</sub>): δ 7.12 (t, *J* = 7 Hz, 1H), 6.94 (d, *J* = 7 Hz, 2H), 2.39 (s, 6H), 1.39 (s, 12H).

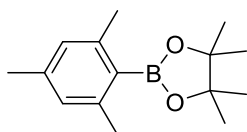
**<sup>13</sup>C{<sup>1</sup>H} NMR** (75 MHz, CDCl<sub>3</sub>): δ 141.8, 129.2, 126.4, 83.7, 25.0, 22.2.

**<sup>11</sup>B NMR** (96 MHz, CDCl<sub>3</sub>): δ 32.2.

**HRMS:** *m/z* for [C<sub>14</sub>H<sub>22</sub>BO<sub>2</sub>]<sup>+</sup> [M+H<sup>+</sup>] calcd: 233.1707, found: 233.1705.

This is consistent with the results reported in the literature.<sup>292,242</sup>

### 4,4,5,5-Tetramethyl-2-(2,4,6-trimethylphenyl)-1,3,2-dioxaborolane (55b)



**Isolated yield:** 35% (86.1 mg, white solid).

**<sup>1</sup>H NMR** (400 MHz, CDCl<sub>3</sub>): δ 6.82 (s, 2H), 2.42 (s, 6H), 2.28 (s, 3H), 1.41 (s, 12H).

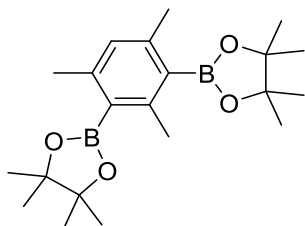
**<sup>13</sup>C{<sup>1</sup>H} NMR** (101 MHz, CDCl<sub>3</sub>): δ 142.2, 138.9, 127.5, 83.5, 25.0, 22.2, 21.3.

**<sup>11</sup>B NMR** (128 MHz, CDCl<sub>3</sub>): δ 32.3.

**HRMS:** *m/z* for [C<sub>15</sub>H<sub>24</sub>BO<sub>2</sub>]<sup>+</sup> [M+H<sup>+</sup>] calcd: 247.1864, found: 247.1863.

This is consistent with the results reported in the literature.<sup>94,97</sup>

### 2,2'-(2,4,6-Trimethyl-1,3-phenylene)-bis[4,4,5,5-tetramethyl-1,3,2-dioxaborolane] (55c)



**Isolated yield:** 9% (33.5 mg, white solid).

**<sup>1</sup>H NMR** (500 MHz, CDCl<sub>3</sub>): δ 6.73 (s, 1H), 2.44 (s, 3H), 2.32 (s, 6H), 1.36 (s, 24H).

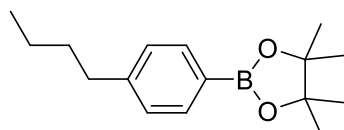
**<sup>13</sup>C{<sup>1</sup>H} NMR** (126 MHz, CDCl<sub>3</sub>): δ 145.5, 142.6, 127.5, 83.4, 25.0, 22.5, 22.2.

**<sup>11</sup>B NMR** (160 MHz, CDCl<sub>3</sub>): δ 32.1.

**HRMS:** *m/z* for [C<sub>21</sub>H<sub>35</sub>B<sub>2</sub>O<sub>4</sub>]<sup>+</sup> [M+H<sup>+</sup>] calcd: 373.2716, found: 373.2715.

This is consistent with the results reported in the literature.<sup>97</sup>

### 2-(4-Butylphenyl)-4,4,5,5-tetramethyl-1,3,2-dioxaborolane (56b)



**Isolated yield:** 63% (163.8 mg, colorless liquid).

**<sup>1</sup>H NMR** (400 MHz, CDCl<sub>3</sub>): δ 7.74 (d, *J* = 7 Hz, 2H), 7.20 (d, *J* = 7 Hz, 2H), 2.63 (t, *J* = 7 Hz, 2H), 1.60 (p, *J* = 7 Hz, 2H), 1.35 (m, 2H), 1.34 (s, 12H), 0.92 (t, *J* = 7 Hz, 3H).

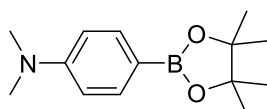
**<sup>13</sup>C{<sup>1</sup>H} NMR** (101 MHz, CDCl<sub>3</sub>): δ 146.4, 134.8, 127.9, 83.6, 35.9, 33.5, 24.9, 22.4, 14.0.

**<sup>11</sup>B NMR** (128 MHz, CDCl<sub>3</sub>): δ 30.9.

**HRMS:** *m/z* for [C<sub>16</sub>H<sub>26</sub>BO<sub>2</sub>]<sup>+</sup> [M+H<sup>+</sup>] calcd: 261.2020, found: 261.2018.

This is consistent with the results reported in the literature.<sup>220</sup>

### 2-(4-(Dimethylamino)phenyl)-4,4,5,5-tetramethyl-1,3,2-dioxaborolane (57b)



**Isolated yield:** 80% (197.6 mg, white solid).

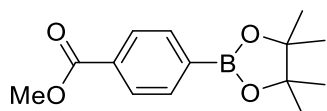
**<sup>1</sup>H NMR** (400 MHz, CDCl<sub>3</sub>): δ 7.71 (d, *J* = 8 Hz, 2H), 6.70 (d, *J* = 8 Hz, 2H), 3.00 (s, 6H), 1.34 (s, 12H).

**<sup>13</sup>C{<sup>1</sup>H} NMR** (101 MHz, CDCl<sub>3</sub>): δ 152.6, 136.2, 111.3, 83.2, 40.1, 24.9.

**<sup>11</sup>B NMR** (128 MHz, CDCl<sub>3</sub>): δ 30.9.

**HRMS:** *m/z* for [C<sub>14</sub>H<sub>23</sub>BNO<sub>2</sub>]<sup>+</sup> [M+H<sup>+</sup>] calcd: 248.1816, found: 248.1814.

This is consistent with the results reported in the literature.<sup>97,295</sup>

**4-(4,4,5,5-Tetramethyl-[1,3,2]dioxaborolan-2-yl)-benzoic acid methyl ester (58b)**

**Isolated yield:** 82% (214.8 mg, white solid).

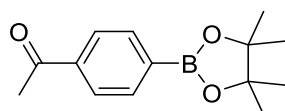
**<sup>1</sup>H NMR** (400 MHz, CDCl<sub>3</sub>): δ 8.02 (d, *J* = 8 Hz, 2H), 7.87 (d, *J* = 8 Hz, 2H), 3.91 (s, 3H), 1.35 (s, 12H).

**<sup>13</sup>C{<sup>1</sup>H} NMR** (101 MHz, CDCl<sub>3</sub>): δ 167.1, 134.7, 132.3, 128.6, 84.2, 52.1, 24.9.

**<sup>11</sup>B NMR** (128 MHz, CDCl<sub>3</sub>): δ 30.7.

**HRMS:** *m/z* for [C<sub>14</sub>H<sub>20</sub>BO<sub>4</sub>]<sup>+</sup> [M+H<sup>+</sup>] calcd: 263.1449, found: 263.1447.

This is consistent with the results reported in the literature.<sup>94,242,291</sup>

**3-(4-Acetylphenyl)-4,4,5,5-tetramethyl-1,3,2-dioxaborolane (59b)**

**Isolated yield:** 75% (184.5 mg, white solid).

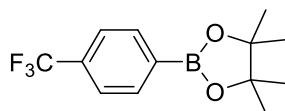
**<sup>1</sup>H NMR** (400 MHz, CDCl<sub>3</sub>): δ 7.90 (m, 4H), 2.61 (s, 3H), 1.35 (s, 12H).

**<sup>13</sup>C{<sup>1</sup>H} NMR** (101 MHz, CDCl<sub>3</sub>): δ 198.5, 139.0, 134.9, 127.3, 84.2, 26.8, 24.9.

**<sup>11</sup>B NMR** (128 MHz, CDCl<sub>3</sub>): δ 30.7.

**HRMS:** *m/z* for [C<sub>14</sub>H<sub>20</sub>BO<sub>3</sub>]<sup>+</sup> [M+H<sup>+</sup>] calcd: 247.1500, found: 247.1498.

This is consistent with the results reported in the literature.<sup>291,296</sup>

**4,4,5,5-Tetramethyl-2-(4-(trifluoromethyl)phenyl)-1,3,2-dioxaborolane (60b)**

**Isolated yield:** 90% (244.8 mg, yellow solid).

**<sup>1</sup>H NMR** (500 MHz, CDCl<sub>3</sub>): δ 7.91 (d, *J* = 8 Hz, 2H), 7.61 (d, *J* = 8 Hz, 2H), 1.36 (s, 12H).

**<sup>13</sup>C{<sup>1</sup>H} NMR** (126 MHz, CDCl<sub>3</sub>): δ 135.0, 132.8 (q, *J*<sub>C-F</sub> = 32.2 Hz), 124.3 (q, *J*<sub>C-F</sub> = 3.8 Hz), 124.1 (q, *J*<sub>C-F</sub> = 272.9 Hz), 84.3, 24.9.

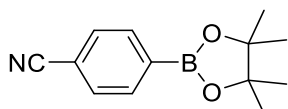
**<sup>19</sup>F{<sup>1</sup>H} NMR** (471 MHz, CDCl<sub>3</sub>): δ -63.0 (s, 3F).

**<sup>11</sup>B NMR** (160 MHz, CDCl<sub>3</sub>): δ 30.6.

**HRMS:**  $m/z$  for  $[C_{13}H_{17}BF_3O_2]^+ [M+H^+]$  calcd: 273.1268, found: 273.1267.

This is consistent with the results reported in the literature.<sup>94,97,291</sup>

#### 4-(4,4,5,5-Tetramethyl-[1,3,2]dioxaborolan-2-yl)-benzonitrile (61b)



**Isolated yield:** 15% (34.4 mg, yellow solid).

**<sup>1</sup>H NMR** (500 MHz, CDCl<sub>3</sub>): δ 7.88 (d,  $J$  = 9 Hz, 2H), 7.63 (d,  $J$  = 9 Hz, 2H), 1.35 (s, 12H).

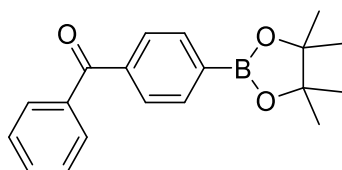
**<sup>13</sup>C{<sup>1</sup>H} NMR** (126 MHz, CDCl<sub>3</sub>): δ 135.1, 131.1, 118.9, 114.5, 84.5, 24.9.

**<sup>11</sup>B NMR** (160 MHz, CDCl<sub>3</sub>): δ 30.5.

**HRMS:**  $m/z$  for  $[C_{13}H_{17}BNO_2]^+ [M+H^+]$  calcd: 230.1347, found: 230.1346.

This is consistent with the results reported in the literature.<sup>291,297</sup>

#### 4-Benzoylphenylboronic acid pinacol ester (62b)



**Isolated yield:** 42% (129.4 mg, white solid).

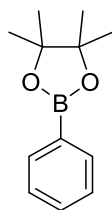
**<sup>1</sup>H NMR** (400 MHz, CDCl<sub>3</sub>): δ 8.22 (s, 1H), 8.02 (d,  $J$  = 7 Hz, 1H), 7.86 (d,  $J$  = 8 Hz, 1H), 7.80 (d,  $J$  = 8 Hz, 2H), 7.59 (t,  $J$  = 7 Hz, 1H), 7.49 (t,  $J$  = 8 Hz, 3H), 1.35 (s, 12H).

**<sup>13</sup>C{<sup>1</sup>H} NMR** (101 MHz, CDCl<sub>3</sub>): δ 196.9, 138.6, 137.7, 137.2, 136.0, 132.7, 132.4, 130.1, 128.3, 127.7, 84.1, 24.9.

**<sup>11</sup>B NMR** (128 MHz, CDCl<sub>3</sub>): δ 30.8.

**HRMS:**  $m/z$  for  $[C_{19}H_{22}BO_3]^+ [M+H^+]$  calcd: 309.1657, found: 309.1656.

This is consistent with the results reported in the literature.<sup>242,219</sup>

**(4,4,5,5-Tetramethyl-1,3,2-dioxaborolan-2-yl)benzene (63b)**

**Isolated yield:** 60% (122.5 mg, colorless liquid).

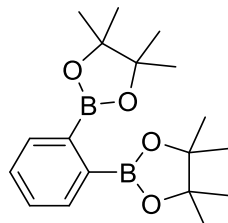
**<sup>1</sup>H NMR** (300 MHz, CDCl<sub>3</sub>): δ 7.85-7.82 (m, 2H), 7.51-7.45 (m, 1H), 7.42-7.36 (m, 2H), 1.37 (s, 12H).

**<sup>13</sup>C{<sup>1</sup>H} NMR** (75 MHz, CDCl<sub>3</sub>): δ 133.7, 130.2, 126.7, 82.7, 23.8.

**<sup>11</sup>B NMR** (96 MHz, CDCl<sub>3</sub>): δ 30.9.

**HRMS:** *m/z* for [C<sub>12</sub>H<sub>18</sub>BO<sub>2</sub>]<sup>+</sup> [M+H<sup>+</sup>] calcd: 205.1394, found: 205.1393.

This is consistent with the results reported in the literature.<sup>97,292</sup>

**1,2-Bis(4,4,5,5-tetramethyl-1,3,2-dioxaborolan-2-yl)benzene (63c)**

**Isolated yield:** 4% (13.2 mg, white solid).

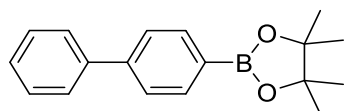
**<sup>1</sup>H NMR** (300 MHz, CDCl<sub>3</sub>): δ 7.66-7.64 (m, 2H), 7.39-7.36 (m, 2H), 1.37 (s, 24H).

**<sup>13</sup>C{<sup>1</sup>H} NMR** (75 MHz, CDCl<sub>3</sub>): δ 133.5, 129.2, 83.9, 24.9.

**<sup>11</sup>B NMR** (96 MHz, CDCl<sub>3</sub>): δ 31.5.

**HRMS:** *m/z* for [C<sub>18</sub>H<sub>29</sub>B<sub>2</sub>O<sub>4</sub>]<sup>+</sup> [M+H<sup>+</sup>] calcd: 331.2246, found: 331.2244.

This is consistent with the results reported in the literature.<sup>97,290</sup>

**2-(4-Biphenyl)-4,4,5,5-tetramethyl-1,3,2-dioxaborolane (64b)**

**Isolated yield:** 76% (212.8 mg, white solid).

**<sup>1</sup>H NMR** (400 MHz, CDCl<sub>3</sub>): δ 7.93 (d, *J* = 8 Hz, 2H), 7.64 (m, 4H), 7.47 (m, 2H), 7.38 (m,

1H), 1.39 (s, 12H).

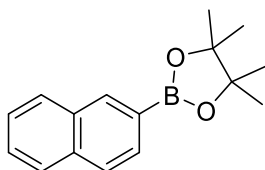
$^{13}\text{C}\{^1\text{H}\}$  NMR (101 MHz,  $\text{CDCl}_3$ ):  $\delta$  143.9, 141.1, 135.3, 128.8, 127.6, 127.3, 126.5, 83.8, 24.9.

$^{11}\text{B}$  NMR (128 MHz,  $\text{CDCl}_3$ ):  $\delta$  30.9.

**HRMS:**  $m/z$  for  $[\text{C}_{18}\text{H}_{22}\text{BO}_2]^+ [\text{M}+\text{H}^+]$  calcd: 281.1707, found: 281.1705.

This is consistent with the results reported in the literature.<sup>97,298</sup>

#### 4,4,5,5-Tetramethyl-2-(2-naphthalenyl)-1,3,2-dioxaborolane (65b)



**Isolated yield:** 62% (157.5 mg, colorless solid).

$^1\text{H}$  NMR (400 MHz,  $\text{CDCl}_3$ ):  $\delta$  8.42 (s, 1H), 7.93-7.85 (m, 4H), 7.55-7.48 (m, 2H), 1.42 (s, 12H).

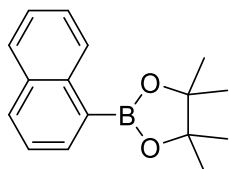
$^{13}\text{C}\{^1\text{H}\}$  NMR (101 MHz,  $\text{CDCl}_3$ ):  $\delta$  136.3, 135.1, 132.9, 130.5, 128.7, 127.8, 127.0, 126.9, 125.8, 84.0, 25.0.

$^{11}\text{B}$  NMR (128 MHz,  $\text{CDCl}_3$ ):  $\delta$  31.0.

**HRMS:**  $m/z$  for  $[\text{C}_{16}\text{H}_{20}\text{BO}_2]^+ [\text{M}+\text{H}^+]$  calcd: 255.1551, found: 255.1550.

This is consistent with the results reported in the literature.<sup>299</sup>

#### 4,4,5,5-Tetramethyl-2-(1-naphthalenyl)-1,3,2-dioxaborolane (66b)



**Isolated yield:** 71% (180.3 mg, pale brown solid).

$^1\text{H}$  NMR (400 MHz,  $\text{CDCl}_3$ ):  $\delta$  8.82 (m, 1H), 8.13 (m, 1H), 7.97 (m, 1H), 7.87 (m, 1H), 7.60-7.49 (m, 3H), 1.46 (s, 12H).

$^{13}\text{C}\{^1\text{H}\}$  NMR (101 MHz,  $\text{CDCl}_3$ ):  $\delta$  137.0, 135.7, 133.3, 131.7, 128.5, 128.4, 126.4, 125.5, 125.0, 83.8, 25.0.

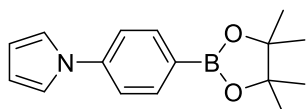
$^{11}\text{B}$  NMR (128 MHz,  $\text{CDCl}_3$ ):  $\delta$  31.6.



**HRMS:**  $m/z$  for  $[C_{16}H_{20}BO_2]^+$   $[M+H^+]$  calcd: 255.1551, found: 255.1550.

This is consistent with the results reported in the literature.<sup>94,300</sup>

**1-(4-(4,4,5,5-tetramethyl-1,3,2-dioxaborolan-2-yl)phenyl)-1H-pyrrole (67b)**



**Isolated yield:** 67% (180.2 mg, white solid).

**$^1H$  NMR** (300 MHz,  $CDCl_3$ ):  $\delta$  7.89 (m, 2H), 7.42 (m, 2H), 7.16 (m, 2H), 6.38 (m, 2H), 1.38 (s, 12H).

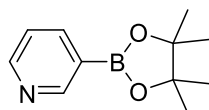
**$^{13}C\{^1H\}$  NMR** (75 MHz,  $CDCl_3$ ):  $\delta$  142.9, 136.3, 119.3, 119.1, 110.8, 83.9, 24.9.

**$^{11}B$  NMR** (96 MHz,  $CDCl_3$ ):  $\delta$  30.4.

**HRMS:**  $m/z$  for  $[C_{16}H_{21}BNO_2]^+$   $[M+H^+]$  calcd: 270.1660, found: 270.1659.

This is consistent with the results reported in the literature.<sup>219</sup>

**3-(4,4,5,5-tetramethyl-1,3,2-dioxaborolan-2-yl)pyridine (68b)**



**Isolated yield:** 50% (103 mg, white solid).

**$^1H$  NMR** (400 MHz,  $CDCl_3$ ):  $\delta$  8.94 (s, 1H), 8.65 (dd,  $J = 5$  Hz,  $J = 2$  Hz, 1H), 8.04 (dt,  $J = 8$  Hz,  $J = 2$  Hz, 1H), 7.26 (m, 1H), 1.34 (s, 12H).

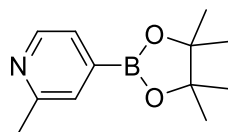
**$^{13}C\{^1H\}$  NMR** (101 MHz,  $CDCl_3$ ):  $\delta$  155.5, 152.0, 142.2, 123.1, 84.2, 24.9.

**$^{11}B$  NMR** (128 MHz,  $CDCl_3$ ):  $\delta$  30.6.

**HRMS:**  $m/z$  for  $[C_{11}H_{17}BNO_2]^+$   $[M+H^+]$  calcd: 206.1347, found: 206.1346.

This is consistent with the results reported in the literature.<sup>219</sup>

**2-(2-Methylpyridin-4-yl)-4,4,5,5-tetramethyl-1,3,2-dioxaborolane (69b)**



**Isolated yield:** 55% (120.5 mg, white solid).

**$^1H$  NMR** (400 MHz,  $CDCl_3$ ):  $\delta$  8.51 (d,  $J = 5$  Hz, 1H), 7.50 (s, 1H), 7.41 (d,  $J = 5$  Hz, 1H),

2.55 (s, 3H), 1.34 (s, 12H).

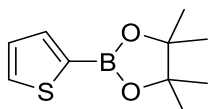
$^{13}\text{C}\{^1\text{H}\}$  NMR (101 MHz,  $\text{CDCl}_3$ ):  $\delta$  157.7, 148.6, 128.4, 125.6, 84.4, 24.9, 24.3.

$^{11}\text{B}$  NMR (128 MHz,  $\text{CDCl}_3$ ):  $\delta$  30.5.

**HRMS:**  $m/z$  for  $[\text{C}_{12}\text{H}_{19}\text{BNO}_2]^+$   $[\text{M}+\text{H}^+]$  calcd: 220.1503, found: 220.1500.

This is consistent with the results reported in the literature.<sup>301</sup>

#### 4,4,5,5-Tetramethyl-2-(2-thienyl)-1,3,2-dioxaborolane (70b)



**Isolated yield:** 53% (111.3 mg, white solid).

$^1\text{H}$  NMR (400 MHz,  $\text{CDCl}_3$ ):  $\delta$  7.67-7.63 (m, 2H), 7.21-7.19 (m, 1H), 1.35 (s, 12H).

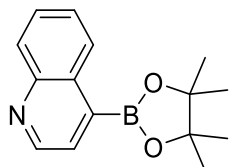
$^{13}\text{C}\{^1\text{H}\}$  NMR (101 MHz,  $\text{CDCl}_3$ ):  $\delta$  137.2, 132.4, 128.2, 84.1, 24.8.

$^{11}\text{B}$  NMR (128 MHz,  $\text{CDCl}_3$ ):  $\delta$  29.1.

**HRMS:**  $m/z$  for  $[\text{C}_{10}\text{H}_{16}\text{BO}_2\text{S}]^+$   $[\text{M}+\text{H}^+]$  calcd: 211.0959, found: 211.0958.

This is consistent with the results reported in the literature.<sup>94,293</sup>

#### 4-(4,4,5,5-Tetramethyl-1,3,2-dioxaborolan-2-yl)quinoline (71b)



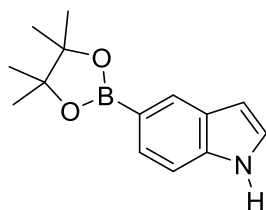
**Isolated yield:** 32% (81.6 mg, yellow solid).

$^1\text{H}$  NMR (400 MHz,  $\text{CDCl}_3$ ):  $\delta$  8.92 (d,  $J = 4$  Hz, 1H), 8.64 (dd,  $J = 8$  Hz,  $J = 1$  Hz, 1H), 8.11 (d,  $J = 8$  Hz, 1H), 7.84 (d,  $J = 4$  Hz, 1H), 7.72-7.67 (m, 1H), 7.59-7.55 (m, 1H), 1.42 (s, 12H).

$^{13}\text{C}\{^1\text{H}\}$  NMR (101 MHz,  $\text{CDCl}_3$ ):  $\delta$  149.6, 147.9, 131.1, 129.8, 129.0, 128.7, 128.4, 126.8, 84.5, 25.0.

$^{11}\text{B}$  NMR (128 MHz,  $\text{CDCl}_3$ ):  $\delta$  31.1.

**HRMS:**  $m/z$  for  $[\text{C}_{15}\text{H}_{19}\text{BNO}_2]^+$   $[\text{M}+\text{H}^+]$  calcd: 256.1503, found: 256.1502.

**5-(4,4,5,5-Tetramethyl-1,3,2-dioxaborolan-2-yl)-1H-indole (72b)**

**Isolated yield:** 40% (97.2 mg, white solid).

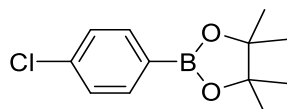
**<sup>1</sup>H NMR** (400 MHz, CDCl<sub>3</sub>): δ 8.33 (br s, 1H), 8.24 (s, 1H), 7.68 (dd, *J* = 1, 8 Hz, 1H), 7.36 (d, *J* = 8 Hz, 1H), 7.15 (t, *J* = 3 Hz, 1H), 6.58-6.57 (m, 1H), 1.40 (s, 12H).

**<sup>13</sup>C{<sup>1</sup>H} NMR** (101 MHz, CDCl<sub>3</sub>): δ 137.9, 128.7, 128.0, 127.7, 124.4, 110.6, 103.1, 83.6, 25.0.

**<sup>11</sup>B NMR** (128 MHz, CDCl<sub>3</sub>): δ 31.1.

**HRMS:** *m/z* for [C<sub>14</sub>H<sub>19</sub>BNO<sub>2</sub>]<sup>+</sup> [M+H<sup>+</sup>] calcd: 244.1503, found: 244.1501.

This is consistent with the results reported in the literature.<sup>219,302</sup>

**2-(4-Chlorophenyl)-4,4,5,5-tetramethyl-1,3,2-dioxaborolane (73b)**

**Isolated yield:** 25% (59.5 mg, colorless liquid).

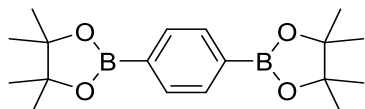
**<sup>1</sup>H NMR** (400 MHz, CDCl<sub>3</sub>): δ 7.73 (d, *J* = 8 Hz, 2H), 7.34 (d, *J* = 8 Hz, 2H), 1.34 (s, 12H).

**<sup>13</sup>C{<sup>1</sup>H} NMR** (101 MHz, CDCl<sub>3</sub>): δ 137.5, 136.1, 128.0, 84.0, 24.9.

**<sup>11</sup>B NMR** (128 MHz, CDCl<sub>3</sub>): δ 30.7.

**HRMS:** *m/z* for [C<sub>12</sub>H<sub>17</sub>BClO<sub>2</sub>]<sup>+</sup> [M+H<sup>+</sup>] calcd: 239.1005, found: 239.1004.

This is consistent with the results reported in the literature.<sup>291,303</sup>

**2,2'-(1,4-Phenylene)-bis[4,4,5,5-tetramethyl-1,3,2-dioxaborolane] (73c)**

**Isolated yield:** 40% (132.0 mg, colorless liquid).

**<sup>1</sup>H NMR** (400 MHz, CDCl<sub>3</sub>): δ 7.82 (s, 4H), 1.35 (s, 24H).

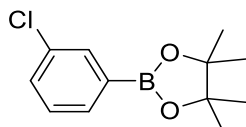
**<sup>13</sup>C{<sup>1</sup>H} NMR** (101 MHz, CDCl<sub>3</sub>): δ 133.9, 83.8, 24.9.

$^{11}\text{B}$  NMR (128 MHz,  $\text{CDCl}_3$ ):  $\delta$  31.0.

HRMS:  $m/z$  for  $[\text{C}_{18}\text{H}_{29}\text{B}_2\text{O}_4]^+$   $[\text{M}+\text{H}^+]$  calcd: 331.2246, found: 331.2244.

This is consistent with the results reported in the literature.<sup>94,293</sup>

### 2-(3-Chlorophenyl)-4,4,5,5-tetramethyl-1,3,2-dioxaborolane (74b)



Isolated yield: 41% (97.6 mg, colorless liquid).

$^1\text{H}$  NMR (400 MHz,  $\text{CDCl}_3$ ):  $\delta$  7.81 (d,  $J = 2$  Hz, 1H), 7.69 (dd,  $J = 8$  Hz,  $J = 1$  Hz, 1H), 7.43-7.40 (m, 1H), 7.29 (t,  $J = 8$  Hz, 1H), 1.34 (s, 12H).

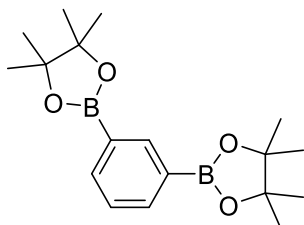
$^{13}\text{C}\{^1\text{H}\}$  NMR (101 MHz,  $\text{CDCl}_3$ ):  $\delta$  134.6, 134.0, 132.7, 131.3, 129.2, 84.1, 24.9.

$^{11}\text{B}$  NMR (128 MHz,  $\text{CDCl}_3$ ):  $\delta$  30.5.

HRMS:  $m/z$  for  $[\text{C}_{12}\text{H}_{17}\text{BClO}_2]^+$   $[\text{M}+\text{H}^+]$  calcd: 239.1005, found: 239.1003.

This is consistent with the results reported in the literature.<sup>303,304</sup>

### 2,2'-(1,3-Phenylene)-bis[4,4,5,5-tetramethyl-1,3,2-dioxaborolane] (74c)



Isolated yield: 15% (49.5 mg, white solid).

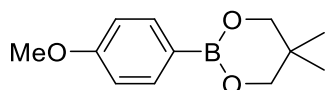
$^1\text{H}$  NMR (400 MHz,  $\text{CDCl}_3$ ):  $\delta$  8.28 (s, 1H), 7.90 (dd,  $J = 7$  Hz,  $J = 1$  Hz, 2H), 7.38 (t,  $J = 7$  Hz, 1H), 1.34 (s, 24H).

$^{13}\text{C}\{^1\text{H}\}$  NMR (101 MHz,  $\text{CDCl}_3$ ):  $\delta$  141.2, 137.6, 127.1, 83.7, 24.9.

$^{11}\text{B}$  NMR (128 MHz,  $\text{CDCl}_3$ ):  $\delta$  31.1.

HRMS:  $m/z$  for  $[\text{C}_{18}\text{H}_{29}\text{B}_2\text{O}_4]^+$   $[\text{M}+\text{H}^+]$  calcd: 331.2246, found: 331.2245.

This is consistent with the results reported in the literature.<sup>305,306</sup>

**2-(4-methoxyphenyl)-5,5-dimethyl-1,3,2-dioxaborinane (75b)**

**Isolated yield:** 75% (165.0 mg, colorless liquid).

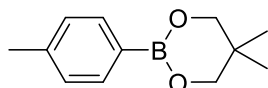
**<sup>1</sup>H NMR** (300 MHz, CDCl<sub>3</sub>): δ 7.75 (m, 2H), 6.89 (m, 2H), 3.83 (s, 3H), 3.76 (s, 4H), 1.02 (s, 6H).

**<sup>13</sup>C{<sup>1</sup>H} NMR** (75 MHz, CDCl<sub>3</sub>): δ 161.8, 135.5, 113.2, 72.3, 55.1, 31.9, 21.9.

**<sup>11</sup>B NMR** (96 MHz, CDCl<sub>3</sub>): δ 26.7.

**HRMS:** *m/z* for [C<sub>12</sub>H<sub>18</sub>BO<sub>3</sub>]<sup>+</sup> [M+H<sup>+</sup>] calcd: 221.1344, found: 221.1343.

This is consistent with the results reported in the literature.<sup>94</sup>

**5,5-dimethyl-2-*p*-tolyl-1,3,2-dioxaborinane (76b)**

**Isolated yield:** 76% (155.0 mg, white solid).

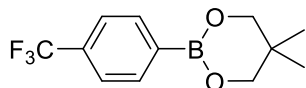
**<sup>1</sup>H NMR** (500 MHz, CDCl<sub>3</sub>): δ 7.71 (d, *J* = 8 Hz, 2H), 7.18 (d, *J* = 8 Hz, 2H), 3.77 (s, 4H), 2.37 (s, 3H), 1.03 (s, 6H).

**<sup>13</sup>C{<sup>1</sup>H} NMR** (126 MHz, CDCl<sub>3</sub>): δ 140.7, 133.9, 128.4, 72.3, 31.9, 21.9, 21.7.

**<sup>11</sup>B NMR** (160 MHz, CDCl<sub>3</sub>): δ 26.9.

**HRMS:** *m/z* for [C<sub>12</sub>H<sub>18</sub>BO<sub>2</sub>]<sup>+</sup> [M+H<sup>+</sup>] calcd: 205.1394, found: 205.1392.

This is consistent with the results reported in the literature.<sup>307,308</sup>

**5,5-dimethyl-2-(4-(trifluoromethylphenyl)-1,3,2-dioxaborinane (77b)**

**Isolated yield:** 89% (229.6 mg, yellow solid).

**<sup>1</sup>H NMR** (500 MHz, CDCl<sub>3</sub>): δ 7.90 (d, *J* = 8 Hz, 2H), 7.59 (d, *J* = 8 Hz, 2H), 3.79 (s, 4H), 1.03 (s, 6H).

**<sup>13</sup>C{<sup>1</sup>H} NMR** (126 MHz, CDCl<sub>3</sub>): δ 134.1, 132.3 (q, *J*<sub>C-F</sub> = 32 Hz), 124.3 (q, *J*<sub>C-F</sub> = 273 Hz), 124.2 (q, *J*<sub>C-F</sub> = 4 Hz), 72.4, 31.9, 21.9.

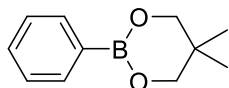
$^{19}\text{F}$  NMR (471 MHz,  $\text{CDCl}_3$ ):  $\delta$  -62.9 (s, 3F).

$^{11}\text{B}$  NMR (160 MHz,  $\text{CDCl}_3$ ):  $\delta$  26.5.

HRMS:  $m/z$  for  $[\text{C}_{12}\text{H}_{15}\text{BF}_3\text{O}_2]^+$   $[\text{M}+\text{H}^+]$  calcd: 259.1112, found: 259.1109.

This is consistent with the results reported in the literature.<sup>307,309</sup>

### 5,5-dimethyl-2-phenyl-1,3,2-dioxaborinane (78b)



Isolated yield: 79% (150.2 mg, white solid).

$^1\text{H}$  NMR (500 MHz,  $\text{CDCl}_3$ ):  $\delta$  7.81 (dd,  $J = 8$  Hz,  $J = 2$  Hz, 2H), 7.45-7.42 (m, 1H), 7.38-7.35 (m, 2H), 3.78 (s, 4H), 1.03 (s, 6H).

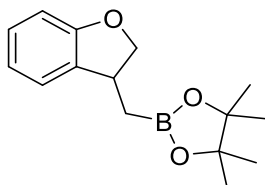
$^{13}\text{C}\{^1\text{H}\}$  NMR (126 MHz,  $\text{CDCl}_3$ ):  $\delta$  133.8, 130.7, 127.6, 72.3, 31.9, 21.9.

$^{11}\text{B}$  NMR (160 MHz,  $\text{CDCl}_3$ ):  $\delta$  26.9.

HRMS:  $m/z$  for  $[\text{C}_{11}\text{H}_{16}\text{BO}_2]^+$   $[\text{M}+\text{H}^+]$  calcd: 191.1238, found: 191.1238.

This is consistent with the results reported in the literature.<sup>237,310</sup>

### 2,3-Dihydro-3-[(4,4,5,5-tetramethyl-1,3,2-dioxaborolan-2-yl)methyl]benzofuran (79c)



Isolated yield: 52% (135.3 mg, colorless liquid).

$^1\text{H}$  NMR (400 MHz,  $\text{CDCl}_3$ ):  $\delta$  7.20 (d,  $J = 7$  Hz, 1H), 7.09 (t,  $J = 8$  Hz, 1H), 6.84 (t,  $J = 7$  Hz, 1H), 6.76 (d,  $J = 8$  Hz, 1H), 4.70 (t,  $J = 9$  Hz, 1H), 4.11 (dd,  $J = 9$  Hz and 8 Hz, 1H), 3.68-3.60 (m, 1H), 1.36-1.30 (m, 1H), 1.26 (s, 12H), 1.13-1.07 (m, 1H).

$^{13}\text{C}\{^1\text{H}\}$  NMR (101 MHz,  $\text{CDCl}_3$ ):  $\delta$  158.7, 131.7, 126.8, 123.0, 119.3, 108.3, 82.4, 77.6, 36.7, 23.9, 23.7.

$^{11}\text{B}$  NMR (128 MHz,  $\text{CDCl}_3$ ):  $\delta$  33.5.

HRMS:  $m/z$  for  $[\text{C}_{15}\text{H}_{22}\text{BO}_3]^+$   $[\text{M}+\text{H}^+]$  calcd: 261.1657, found: 261.1654.

This is consistent with the results reported in the literature.<sup>72,77</sup>

### 3.6.6 Single-crystal X-ray diffraction analyses

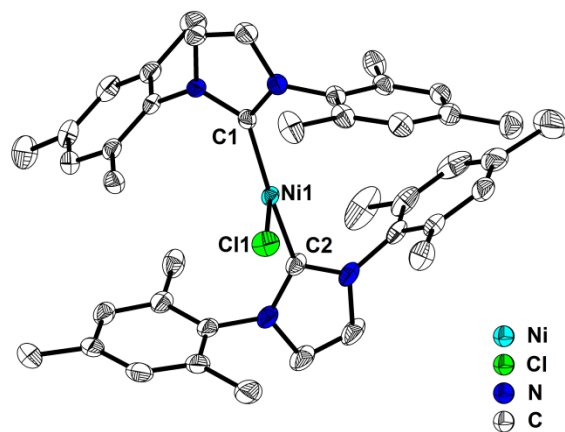


**Figure 3-43.** Molecular structures of  $[\text{Ni}'(\text{IMes})_2\text{Cl}]$  from single-crystal X-ray diffraction data at 100 K. Atomic displacement ellipsoids are drawn at the 50% probability level, and hydrogen atoms are omitted for clarity. Selected bond lengths ( $\text{\AA}$ ) and angles (deg):  $\text{Ni}(1)\text{-C}(1) = 1.921(3)$ ,  $\text{Ni}(1)\text{-C}(2) = 1.917(3)$ ,  $\text{Ni}(1)\text{-Cl}(1) = 2.3043(13)$ ;  $\text{C}(1)\text{-Ni}(1)\text{-Cl}(1) = 96.93(8)$ ,  $\text{C}(2)\text{-Ni}(1)\text{-Cl}(1) = 94.98(9)$ ,  $\text{C}(1)\text{-Ni}(1)\text{-C}(2) = 168.03(11)$ .





## **Chapter Four**

### **Ni-catalyzed traceless, directed C3-selective C-H borylation of indoles**



## 4 Ni-catalyzed traceless, directed C3-selective C-H borylation of indoles

### 4.1 Abstract

A highly efficient and general protocol for traceless, directed C3-selective C-H borylation of indoles with  $[\text{Ni}(\text{IMes})_2]$  as the catalyst was achieved. Activation and borylation of N-H bonds by  $[\text{Ni}(\text{IMes})_2]$  is essential to install a Bpin moiety at the N-position as a traceless directing group, which enables the C3-selective borylation of C-H bonds. The N-Bpin group which is formed is easily converted *in situ* back to an N-H group by the oxidative addition product of  $[\text{Ni}(\text{IMes})_2]$  and *in situ*-generated HBpin. The catalytic reactions are operationally simple, allowing borylation of a variety of substituted indoles with  $\text{B}_2\text{pin}_2$  in excellent yields and with high selectivity. The C-H borylation can be followed by Suzuki-Miyaura cross-coupling of the C-borylated indoles in an overall two-step, one-pot process providing an efficient method for synthesizing C3-functionalized heteroarenes.

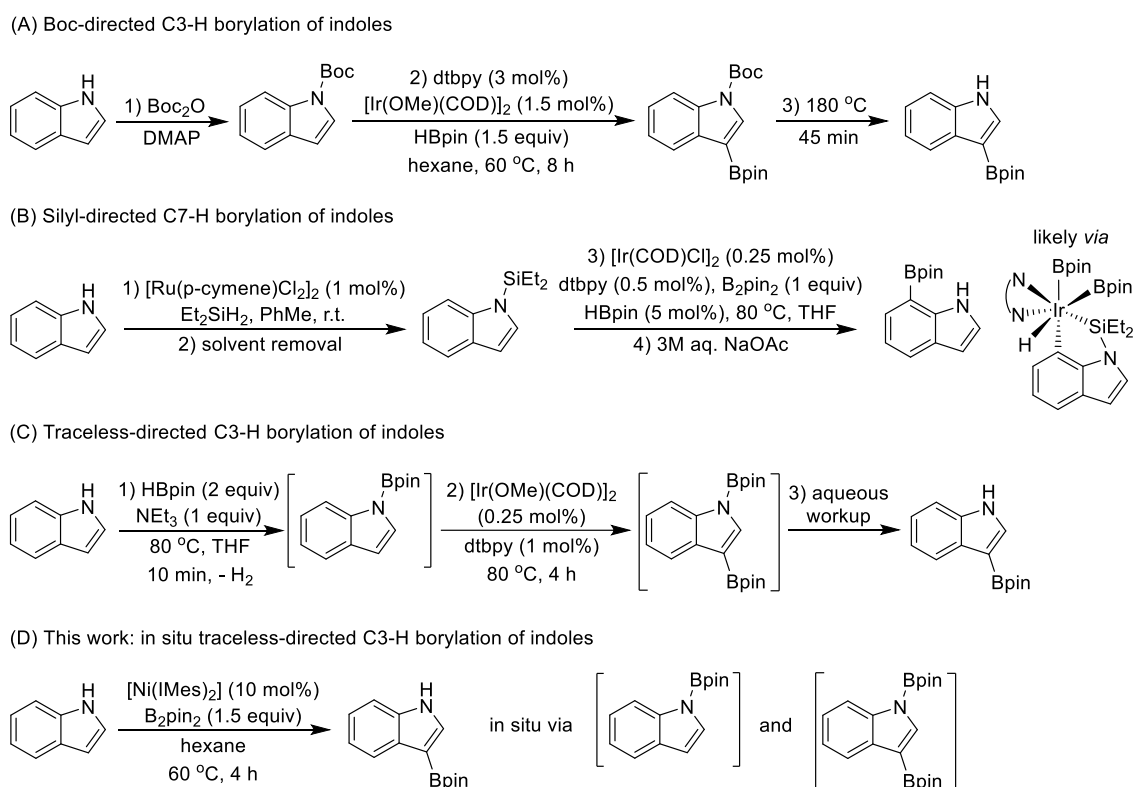
## 4.2 Introduction

Indoles have important biological functions, and construction of the ring from other substrates or direct functionalization of an existing indole are the usual approaches employed in synthesizing substituted derivatives.<sup>311-320</sup> Borylated indoles are of particular interest because they can serve as versatile building blocks for the construction of functional molecules.<sup>1-3,42,321</sup> Recently, transition metal-catalyzed direct C-H borylation has emerged as a powerful tool for the construction of C-B bonds due to its broad functional group tolerance and substrate scope allowing late-stage functionalization without the use of protecting groups.<sup>1-4,38-40,42,53,119,321-331</sup> The regioselectivity of the C-H functionalization of unprotected indoles, which have seven different sites, is typically driven by electronic effects. Therefore, C-H borylation reactions occur predominantly at the C2 position which contains the most acidic and reactive C-H bond.<sup>332,333</sup> However, the selectivity can be overridden by steric factors. Many groups including Ishiyama and Miyaura,<sup>332,333</sup> Hartwig,<sup>334,335</sup> Ito,<sup>336,337</sup> Marder,<sup>294,338,339</sup> Tobisu and Chatani,<sup>179,211</sup> Chattopadhyay,<sup>340,341</sup> Maleczka and Smith<sup>342-346</sup> *et al.* have reported the selective borylation of indoles using mainly Ir, but also Rh, Pt, Co, Ni and other catalysts.<sup>347-353</sup> Metal-free catalytic C-H borylation is also an attractive alternative as it offers a simple and cheap route to borylated indoles under mild conditions.<sup>354-365</sup>

Directing groups are usually employed to control regioselectivity in C-H functionalizations.<sup>366-375</sup> For example, Maleczka and Smith *et al.* used *tert*-butoxycarbonyl (Boc) as a directing group in the Ir-catalyzed C-H borylations of pyrroles, indoles, azaindoles, and pyrazoles, and observed selective functionalization of the N-Boc-protected heterocycles at positions  $\beta$  to the N atoms (Scheme 4-1A).<sup>343</sup> Hartwig and co-workers developed a one-pot protocol consisting of the Ru-catalyzed installation of a silyl group at the indole N-atom, Ir-catalyzed borylation of the silylindole, and subsequent hydrolysis of the N-silyl group to obtain C7-borylated indoles selectively (Scheme 4-1B).<sup>335</sup> The groups of Ingleson, Houk and Shi employed a pivaloyl moiety as an effective directing group at the N-position to enable the C7 borylation of indoles and *ortho*-borylation of anilines simply by using BBr<sub>3</sub>.<sup>363,365</sup> The latter group also found that installation of pivaloyl

groups at the C3 position of indoles enables borylation at the unfavorable C4 position.<sup>365</sup> Although site-selective C-H functionalization can be efficiently achieved with the assistance of directing groups, some difficult to remove or modify, thus limiting the practical application of this methodology. Therefore, employing traceless directing groups would be an attractive alternative to the traditional methods. Krska, Maleczka, Smith *et al.* demonstrated that the (pinacolato)boryl (Bpin) moiety can serve as a traceless directing group for selective Ir-catalyzed C-H borylation of indoles at the C3 position (Scheme 4-1C).<sup>345</sup> The addition of a tertiary amine base ensures the borylation of the nitrogen atom. The N-Bpin moiety formed enables further Ir-catalyzed regioselective borylation of C3-H bonds, and an aqueous workup was subsequently required to remove the N-bound Bpin group to give the final 3-Bpin-indole product.

### Scheme 4-1. Examples of directed C-H borylation of indoles



N-Heterocyclic carbene (NHC) transition metal complexes have proven to be efficient for homogeneous catalytic C-H activation.<sup>179,211,376-383</sup> Nakao, Hartwig *et al.* demonstrated an *anti*-Markovnikov addition of arenes and heteroarenes to alkenes catalyzed by a hindered Ni-NHC system.<sup>377,383</sup> Tobisu, Chatani *et al.* developed [Ni(ICy)<sub>2</sub>] (ICy =

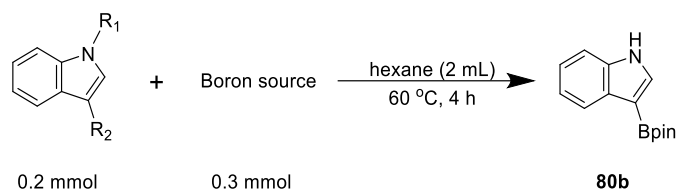
1,3-dicyclohexylimidazolin-2-ylidene) which showed excellent activity for the borylation of arenes and N-substituted heteroarenes with B<sub>2</sub>pin<sub>2</sub>.<sup>179</sup> Selective borylation of indoles was achieved at the reactive C2 position. Recently, Hahn *et al.* reported that unsubstituted 2-halogenoazoles undergo N-H oxidative addition with [Ni(PEt<sub>3</sub>)<sub>2</sub>] forming a Ni<sup>II</sup> hydride complex, rather than C-metalation of the C-Cl bond, at low temperature in THF.<sup>384</sup> In light of these findings and our long-standing interest in catalytic borylation reactions based on different NHC-metal complexes,<sup>126,130,177,244,256,277,385,386</sup> we report herein a highly selective traceless, directed C3-H borylation of indoles that employs [Ni(IMes)<sub>2</sub>] as a catalyst without an additional base or hydrolysis to achieve: 1) *in situ* installation of Bpin as a traceless directing group at the indole N-position; 2) catalytic C3-H borylation; and 3) deprotection of the N-Bpin moiety back to an N-H group to provide C3-borylated indoles with excellent activity and selectivity (Scheme 4-1D).

## 4.3 Results and discussions

### 4.3.1 Borylation of indole

We first investigated the efficiency of the directed borylation reaction of indole (**80a**) with B<sub>2</sub>pin<sub>2</sub> using 10 mol % [Ni(IMes)<sub>2</sub>] as the catalyst and hexane as solvent at 60 °C. This initial result gave 3-Bpin-indole (**80b**) in an excellent yield of 89% with high selectivity for the C3 position after 4 h (Table 4-1, entry 1). A range of solvents was screened, with hexane proving to be optimal (Table 4-2). The non-polar solvent methylcyclohexane gave almost the same yield of **80b** as obtained in hexane, but the reactivity was low in polar solvents. Dichloromethane and acetonitrile, respectively, completely quench the reaction. Meanwhile, the yield of **80b** is higher at a reaction temperature of 60 °C than that at 30-50 °C, but decreased significantly with decreasing number of equiv of B<sub>2</sub>pin<sub>2</sub> (Figure 4-1). For molar ratios of 1 : 0.5 and 1 : 0.75, prolonging the reaction time from 4 h to 22 h only slightly increased the yield of **80b**, which remained below 50%. Using 1 equiv of B<sub>2</sub>pin<sub>2</sub> yielded 83% of **80b** after 22 h, which is similar to the result obtained when 1.5 equiv of B<sub>2</sub>pin<sub>2</sub> was used to borylate **80a** for 4 h. When HBpin was employed as the boron source instead of B<sub>2</sub>pin<sub>2</sub>, only a 7% yield of **80b** was achieved (Table 4-1, entry 3). It is important to note that no reaction occurred in the absence of the [Ni(IMes)<sub>2</sub>] catalyst (Table

4-1, entries 2 and 4).

**Table 4-1. Control experiments of directed C3-H borylation of different indoles**

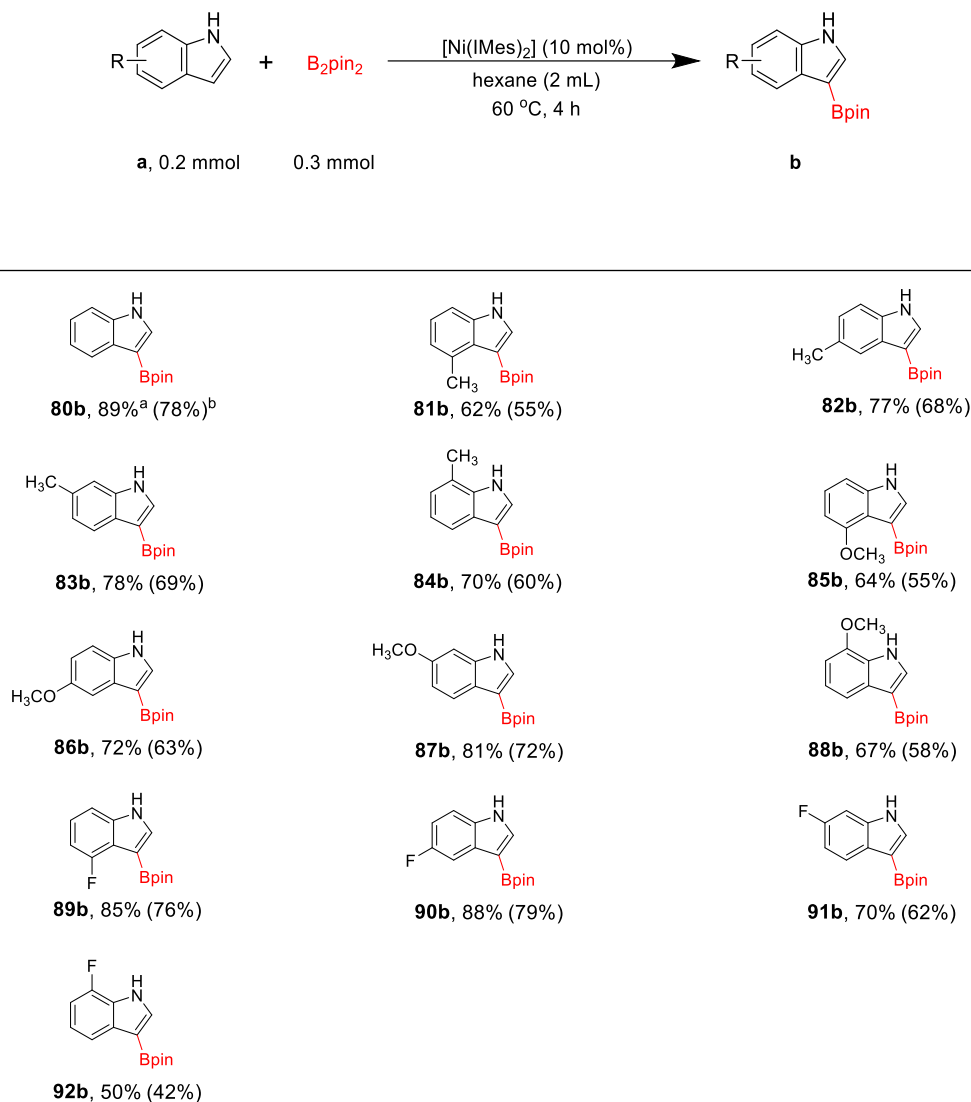
Entry	Substrate	Boron source	[Ni(IMes) <sub>2</sub> ] (10 mol%)	Yield of 80b (%) <sup>a</sup>
1	R <sub>1</sub> = H, R <sub>2</sub> = H	B <sub>2</sub> pin <sub>2</sub>	✓	89
2	R <sub>1</sub> = H, R <sub>2</sub> = H	B <sub>2</sub> pin <sub>2</sub>	✗	-
3	R <sub>1</sub> = H, R <sub>2</sub> = H	HBpin	✓	7
4	R <sub>1</sub> = H, R <sub>2</sub> = H	HBpin	✗	-
5	R <sub>1</sub> = Bpin, R <sub>2</sub> = H	B <sub>2</sub> pin <sub>2</sub>	✓	91
6	R <sub>1</sub> = Bpin, R <sub>2</sub> = H	B <sub>2</sub> pin <sub>2</sub>	✗	-
7	R <sub>1</sub> = Bpin, R <sub>2</sub> = H	HBpin	✓	trace <sup>b</sup>
8	R <sub>1</sub> = Bpin, R <sub>2</sub> = H	HBpin	✗	-
9	R <sub>1</sub> = Bpin, R <sub>2</sub> = Bpin	B <sub>2</sub> pin <sub>2</sub>	✓	trace
10	R <sub>1</sub> = Bpin, R <sub>2</sub> = Bpin	B <sub>2</sub> pin <sub>2</sub>	✗	-
11	R <sub>1</sub> = Bpin, R <sub>2</sub> = Bpin	HBpin	✓	94
12	R <sub>1</sub> = Bpin, R <sub>2</sub> = Bpin	HBpin	✗	-

<sup>a</sup>Yields are based on indoles and were determined by GC-MS analysis vs. a calibrated internal standard and are averages of two runs. <sup>b</sup>The yield of indole was ca. 50% apart from **80b**.





## 4.3.2 Substrate scope

Table 4-3. Substrate scope for the C3-H borylation of indoles with [Ni(IMes)<sub>2</sub>]

<sup>a</sup>Yields are based on indoles and were determined by GC-MS analysis vs. a calibrated internal standard and are averages of two runs. <sup>b</sup>Isolated yields based on 1 mmol indoles are given in parentheses.

We further examined the scope of indoles for the directed borylation with [Ni(IMes)<sub>2</sub>] under the optimized conditions, and the results are summarized in Table 4-3. Indoles with either electron-donating (**81a-88a**) or electron-withdrawing (**89a-92a**) groups reacted smoothly to afford corresponding C3-borylated indoles in good to excellent yields, suggesting the excellent functional group tolerance of this method. The positions of Me and MeO substituents on the benzenoid unit of indole did not significantly affect the catalytic activity;

placing them at the C5 or C6 positions resulted in slightly higher yields of products than when they were placed at the C4 or C7 positions (**81a-88a**). Because fluorinated organic compounds have exceptional properties that are being exploited in many applications,<sup>100-104</sup> it is important to note that fluoroindoles underwent C3-H borylation with fluoride moiety remaining intact under our conditions (**89a-92a**). Interestingly, 4-F-indole (**89a**) and 5-F-indole (**90a**) exhibited higher yields of products than 6-F-indole (**91a**) and 7-F-indole (**92a**) revealed the lowest activity with only a 50% yield of 3-Bpin-7-F-indole (**92b**). The C3 selectivity of the C-H borylation reported here was confirmed by the molecular structures of **80b**, **82b-84b**, **86b**, and **88b-91b** obtained by single-crystal X-ray diffraction.

## 4.4 Mechanistic studies

### 4.4.1 Monitoring the borylation of indole at different times

First, we monitored the borylation of **80a** by GC–MS analysis. As shown in Table 4-4 and Figure 4-2, the yield of **80b** increased with longer reaction times. Importantly, the N-H monoborylation product 1-Bpin-indole (**80c**) and diborylation product 1,3-(Bpin)<sub>2</sub>-indole (**80d**) were detected during the reaction. Compounds **80c** and **80d** reached their maximum yields of 36% and 28% after 10 min and 30 min, respectively, and then the yields decreased to trace amounts at 1.5 and 4 h, respectively. The above results suggest that the N-borylated compound **80c** and the bis N/C3-borylated compound **80d** are important intermediates in the formation of **80b**.





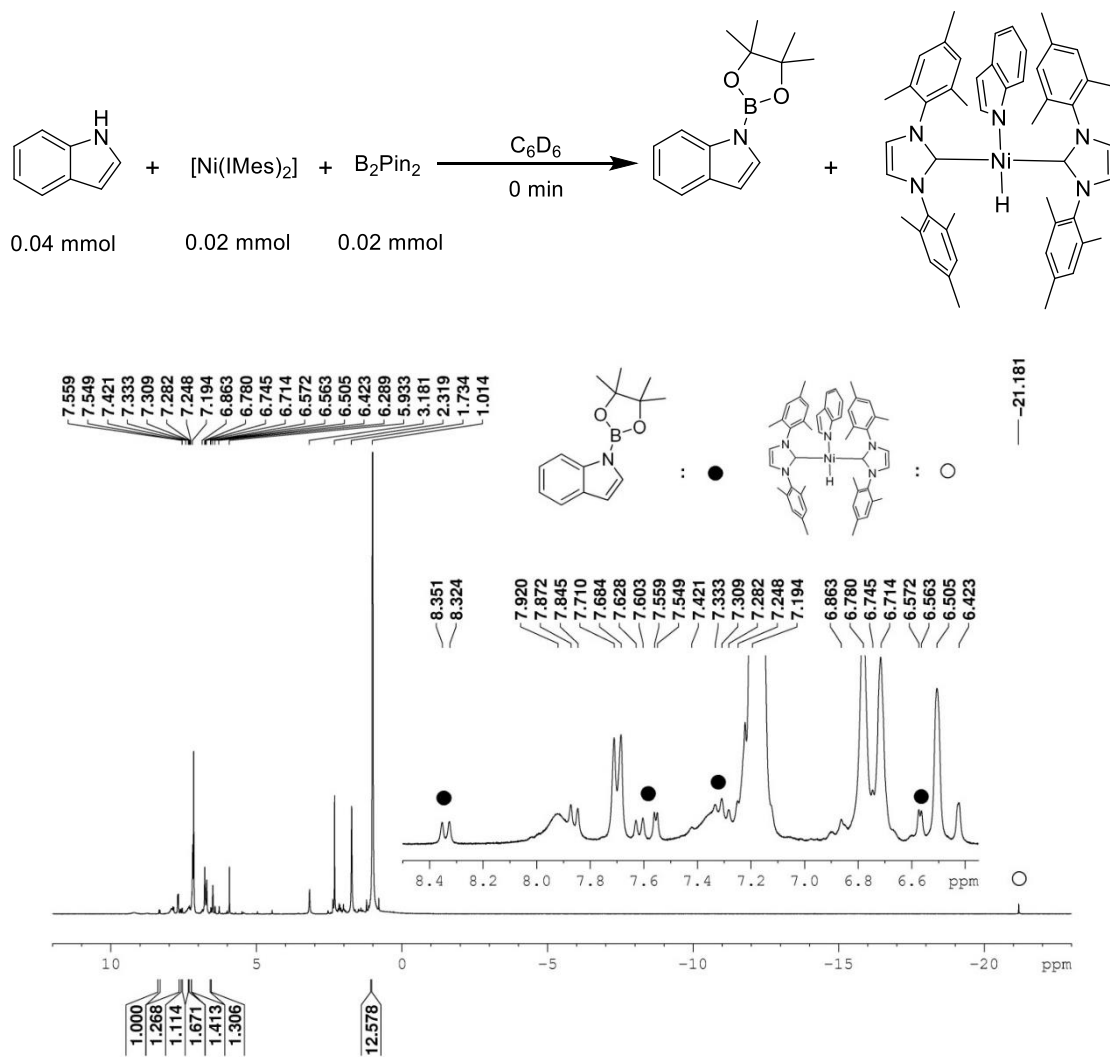
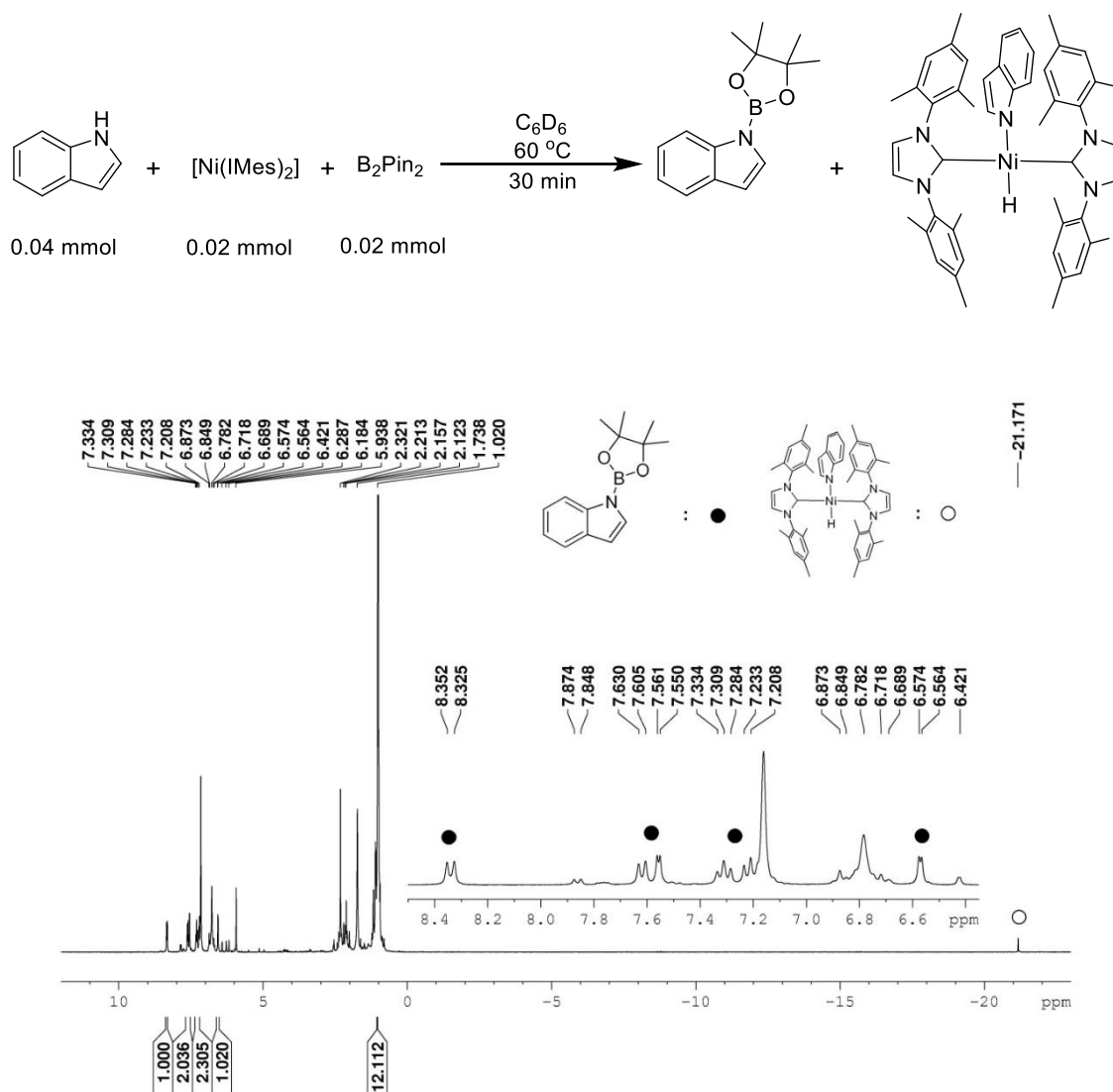
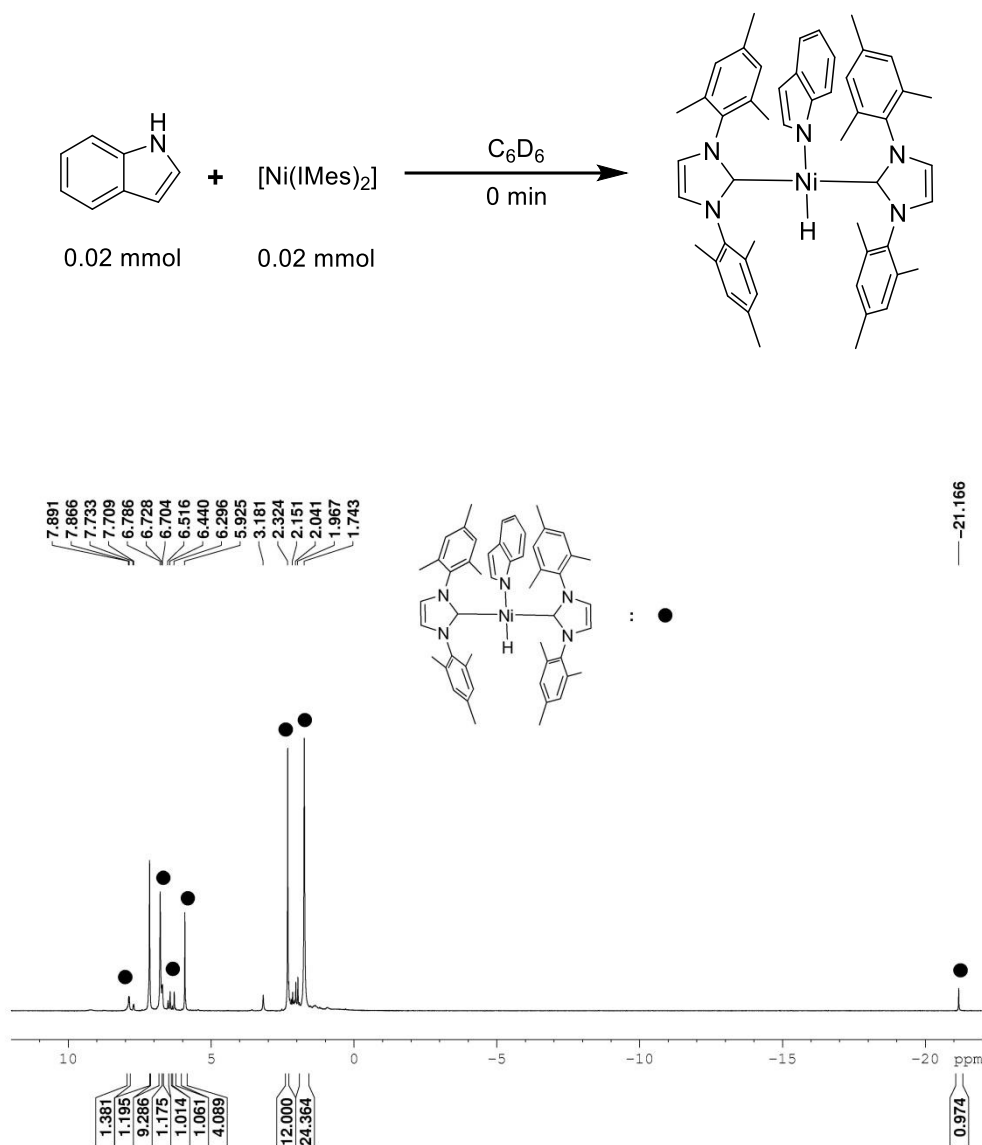


Figure 4-3.  $^1\text{H}$  NMR spectrum at 0 min (300 MHz,  $C_6D_6$ ).



**Figure 4-4.**  $^1\text{H}$  NMR spectrum after 30 min of heating (300 MHz,  $\text{C}_6\text{D}_6$ ).

The reactivity of indole with  $[\text{Ni}(\text{IMes})_2]$  was further studied. A mixture of indole (0.02 mmol, 2.3 mg) and  $[\text{Ni}(\text{IMes})_2]$  (0.02 mmol, 14 mg) was dissolved in 0.7 mL of  $\text{C}_6\text{D}_6$  in a Youngs' tap NMR tube. The  $^1\text{H}$  NMR spectrum of the mixture was recorded immediately, and nearly complete conversion to  $[\text{Ni}(\text{IMes})_2(\text{H})(\text{indole})]$  was observed.



**Figure 4-5.**  $^1\text{H}$  NMR spectrum at 0 min (300 MHz,  $\text{C}_6\text{D}_6$ ).

Then, the reaction of 1.00 mmol of **80a** and 1.00 mmol of **91a**, respectively, with 1 equiv of  $[\text{Ni}(\text{IMes})_2]$  in hexane (i.e., without  $\text{B}_2\text{pin}_2$ ) was conducted at  $60^\circ\text{C}$  for 4 h, yielding 76% and 75% of the corresponding  $\text{Ni}^{\text{II}}$  complexes  $[\text{Ni}(\text{IMes})_2(\text{H})(N\text{-indolyl})]$  (**I1**) and  $[\text{Ni}(\text{IMes})_2(\text{H})(6\text{F-}N\text{-indolyl})]$  (**I1-6F**). After isolation, the NMR spectra and X-ray diffraction analysis (Figure 4-6) confirmed the formation of  $\text{Ni}^{\text{II}}$  complexes **I1** and **I1-6F**, which result from an oxidative addition of the indole N-H bond to the  $\text{Ni}^0$  complex  $[\text{Ni}(\text{IMes})_2]$ . These results indicate that the facile activation of the N-H bond by  $[\text{Ni}(\text{IMes})_2]$  generates intermediate **I1**, which then reacts with  $\text{B}_2\text{pin}_2$  to give **80c**.

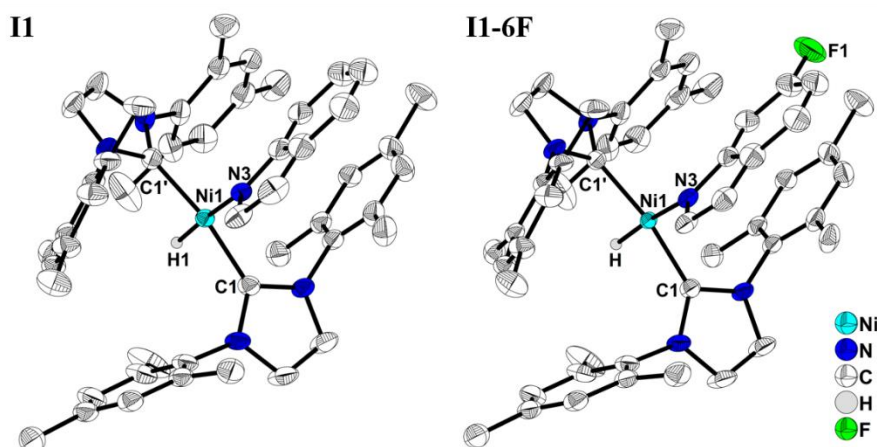
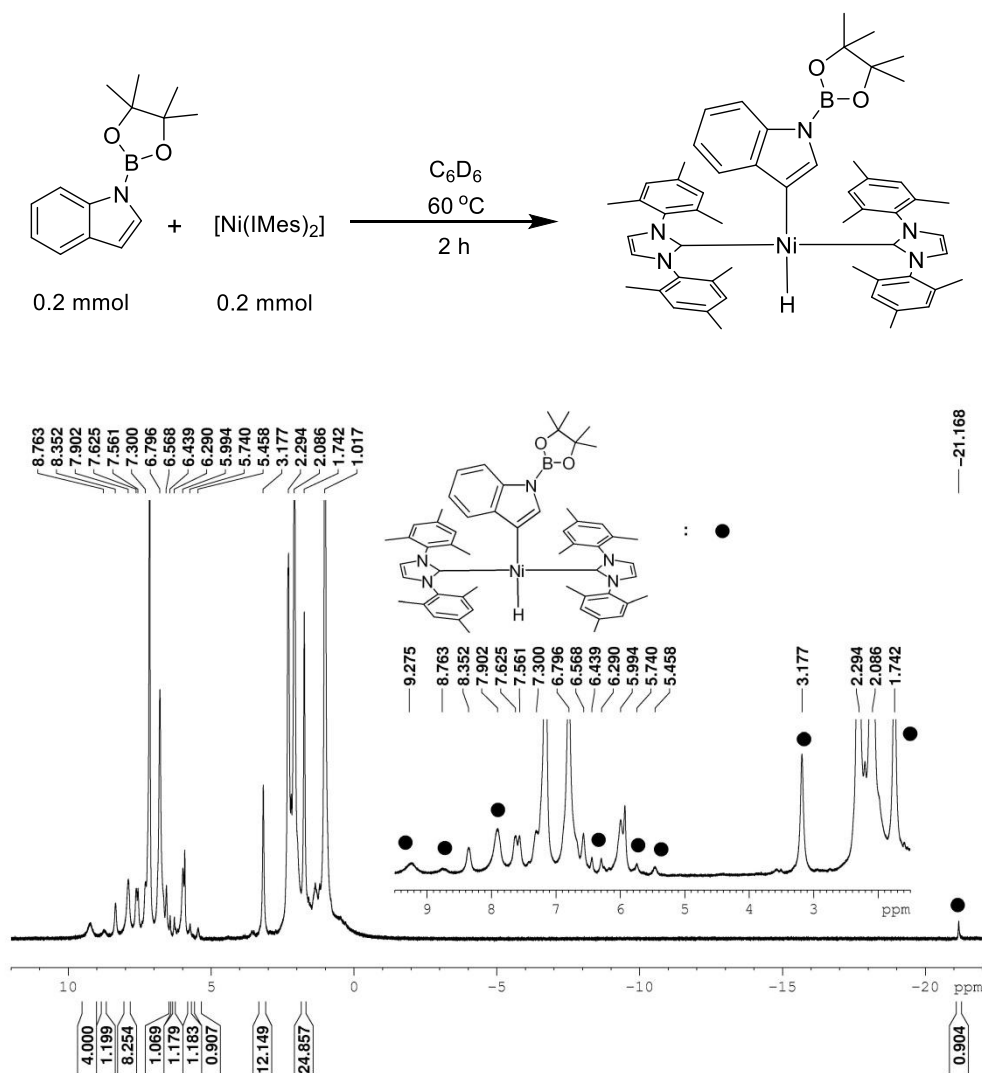


**Figure 4-6.** Molecular structures of  $[\text{Ni}(\text{IMes})_2(\text{H})(N\text{-indolyl})]$  (**I1**) and  $[\text{Ni}(\text{IMes})_2(\text{H})(6\text{F-}N\text{-indolyl})]$  (**I1-6F**) from single-crystal X-ray diffraction data at 100 K. Atomic displacement ellipsoids are drawn at the 50% probability level, and some hydrogen atoms are omitted for clarity. The molecules have 2-fold rotational symmetry and only one of the two disordered parts of each indole moiety is shown here for clarity. Selected bond lengths (Å) and angles (deg) for **I1**: Ni1–C1 1.9047(18), Ni1–C1' 1.9047(18), Ni1–N3 1.954(3), Ni1–H1 1.38(3); C1–Ni1–N3 93.3(2), C1–Ni1–H1 83.16(6), C1–Ni1–C1' 166.3(1), C1'–Ni1–N3 100.3(2), C1'–Ni1–H1 83.16(6), N3–Ni1–H1 172.3(1). Selected bond lengths (Å) and angles (deg) for **I1-6F**: Ni1–C1 1.906(3), Ni1–C1' 1.906(3), Ni1–N3 1.950(5), Ni1–H 1.43(7); C1–Ni1–N3 92.8(2), C1–Ni1–H 83.2(1), C1–Ni1–C1' 166.3(2), C1'–Ni1–N3 100.7(2), C1'–Ni1–H 83.2(1), N3–Ni1–H 170.7(1).

#### 4.4.3 Investigation of the catalytic selective C3-H borylation step

Reaction of **80c** with  $\text{B}_2\text{pin}_2$  in the absence of  $[\text{Ni}(\text{IMes})_2]$  was not detected (Table 4-1, entry 6). However, the reaction with 10 mol %  $[\text{Ni}(\text{IMes})_2]$  gave **80b** in an excellent yield of 91% and a trace of **80d** at 60 °C for 4 h (Table 4-1, entry 5), indicating that **80c** requires the Ni-catalyst to form **80d**. We also studied the reactivity of **80c** with  $[\text{Ni}(\text{IMes})_2]$ . A mixture of 1-Bpin-indole (**80c**, 0.02 mmol, 4.9 mg) and  $[\text{Ni}(\text{IMes})_2]$  (0.02 mmol, 14 mg) was dissolved in 0.7 mL of  $\text{C}_6\text{D}_6$  in a Youngs' tap NMR tube. *In situ*  $^1\text{H}$  NMR spectra of the reaction clearly showed that the oxidative addition of the C3-H bond by the  $\text{Ni}^0$  complex formed  $[\text{Ni}^{\text{II}}(\text{IMes})_2(\text{H}_{\text{C}3})(1\text{-Bpin-indole})]$  (**I2**, Figure 4-7) after heating at 60 °C for 2 h. Therefore, with  $[\text{Ni}(\text{IMes})_2]$  and  $\text{B}_2\text{pin}_2$ , the conversion of **80c** to **80d** appears to occur *via* formation of intermediate **I2**.



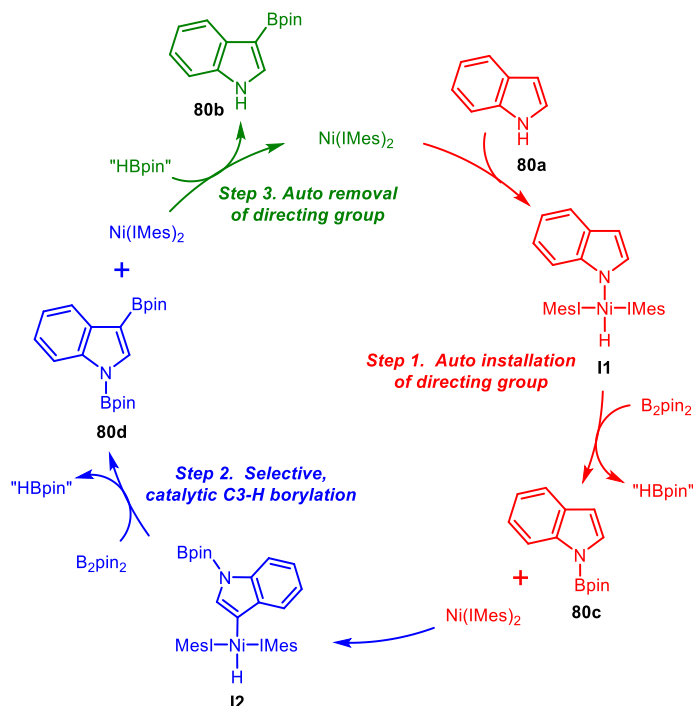


**Figure 4-7.** <sup>1</sup>H NMR spectrum after 2 h of heating (300 MHz, C<sub>6</sub>D<sub>6</sub>).

#### 4.4.4 Investigation of the removal of the directing group

When HBpin was employed as the boron source instead of B<sub>2</sub>pin<sub>2</sub> for the borylation of **80c**, there was no reaction without [Ni(IMes)<sub>2</sub>] (Table 4-1, entry 8). When [Ni(IMes)<sub>2</sub>] was present, HBpin as the boron source led to only trace amounts of **80d**; however, *ca.* half of **80c** was converted to **80a** (Table 4-1, entry 7). This suggests that the conversion of N-Bpin to N-H is achieved by reaction with HBpin in the presence of [Ni(IMes)<sub>2</sub>]. When **80d** was used as the substrate, it did not react with either B<sub>2</sub>pin<sub>2</sub> or HBpin in the absence of [Ni(IMes)<sub>2</sub>] (Table 4-1, entries 10 and 12). With [Ni(IMes)<sub>2</sub>], B<sub>2</sub>pin<sub>2</sub> as the boron source gave only a trace of **80b** (Table 4-1, entry 9), whereas reaction of HBpin with **80d** efficiently yielded 94% of **80b** (Table 4-1, entry 11).

## 4.4.5 Proposed mechanism

Scheme 4-2. Plausible mechanism for the traceless-directed C3-selective C-H borylation of indoles with  $[\text{Ni}(\text{IMes})_2]$ 

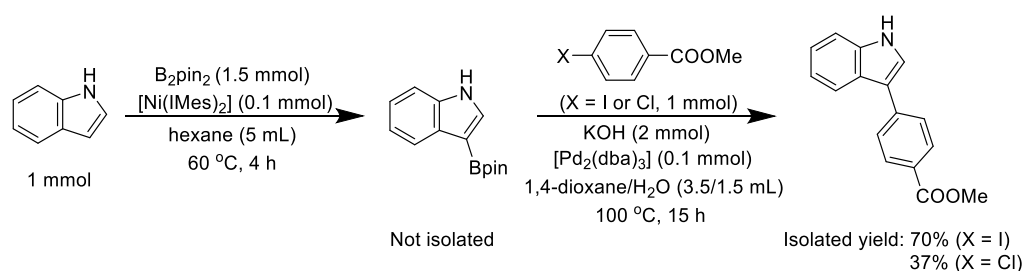
In light of these findings, a plausible mechanism for the C3-selective borylation of indoles with  $[\text{Ni}(\text{IMes})_2]$  is shown in Scheme 4-2. First, the indoles undergo rapid N-H oxidative addition to  $[\text{Ni}(\text{IMes})_2]$  to give the  $\text{Ni}^{\text{II}}$  hydride complex **11**, which further reacts with  $\text{B}_2\text{pin}_2$  *in situ* to install Bpin as a traceless directing group at the indole N-position to produce **80c** and release  $[\text{Ni}(\text{IMes})_2]$ . Then, the regenerated  $[\text{Ni}(\text{IMes})_2]$  catalyzes the C3-borylation of **80c**;  $[\text{Ni}(\text{IMes})_2]$  thus inserts into the C3-H bond of **80c** to form the  $\text{Ni}^{\text{II}}$  hydride complex **12**, which is converted with  $\text{B}_2\text{pin}_2$  to the bis-N/C3-borylated indole **80d**, a step which also regenerates the  $\text{Ni}^0$  complex  $[\text{Ni}(\text{IMes})_2]$ . Finally, it appears that this, or another Ni-complex present in the reaction mixture, also catalyzes the removal of the directing group, i.e., that the conversion of N-Bpin to N-H to form the final C3-borylated indole **80b** is achieved by the  $[\text{Ni}(\text{IMes})_2]$ -catalyzed reaction of **80d** with a source of hydrogen atoms, which we depict in Scheme 4-2 as *in situ* generated HBpin. While we do not observe HBpin by *in situ* GC-MS during the course of the reactions, and do not yet know the

intimate details of this final step in the cycle, as the reaction proceed smoothly under an inert atmosphere and in carefully dried solvents, it would appear that the hydrogen atom source must be generated in the N-H or C-H activation steps.

#### 4.4.6 Synthetic applications of C3-borylated indoles

Arylindoles are key building blocks in many natural products and pharmaceuticals.<sup>311,313</sup> C3-Arylated indoles are particularly important because of their diverse biological activities such as antimicrobial, anti-inflammatory, and anticancer activities.<sup>387-394</sup> Thus, as a proof of principle, to demonstrate the synthetic utility of our protocol, a one-pot C3-H borylation / Suzuki-Miyaura cross-coupling sequence for the direct synthesis of C3-arylated indole was also investigated using the parent indole **80a**. The *in situ* formed 3-borylated indole **80b** was directly employed in one-pot cross-coupling reactions with methyl 4-iodobenzoate and methyl 4-chlorobenzoate, using  $[\text{Pd}_2(\text{dba})_3]$  (dba = dibenzylideneacetone) as the catalyst precursor (Scheme 4-3). The product 3-(methyl-4-benzoate)-indole was obtained in 70% and 37% isolated yield, respectively, demonstrating the potential for employing this C3-borylation methodology for the tandem synthesis of C3-arylated indoles.

#### Scheme 4-3. A one-pot C3-H borylation/Suzuki-Miyaura cross-coupling sequence for synthesis of C3-arylated indole



## 4.5 Conclusions

We have developed an efficient, traceless, directed C3-selective C-H borylation of indoles with  $\text{B}_2\text{pin}_2$  using  $[\text{Ni}(\text{IMes})_2]$  as the catalyst. The reaction proceeds without any base and under mild conditions, displays broad scope and functional group tolerance, and furnishes borylated indoles in good to excellent yields with high selectivity. Bpin, as a traceless

directing, group is installed at the N-position via activation of the N-H bond by  $[\text{Ni}(\text{IMes})_2]$ . The N-borylated indole formed undergoes catalytic C3-selective C-H borylation with regenerated  $[\text{Ni}(\text{IMes})_2]$  to form the bis-N/C3-borylated indole, which then generates the desired C3-borylated indole product by conversion of N-Bpin to N-H with  $[\text{Ni}(\text{IMes})_2]$  and *in situ*-generated HBpin. This protocol enables the *in situ* installation and removal of the directing group without additional operations, using a first-row transition metal catalyst, and can be followed, in the same pot, by a Suzuki-Miyaura cross-coupling with an aryl halide.

## 4.6 Experimental procedures and characterization data

### 4.6.1 General information

Unless otherwise noted, all manipulations were performed using standard Schlenk or glovebox (Innovative Technology Inc.) techniques under argon. All reagents were purchased from Alfa-Aesar, Aldrich, ABCR or VWR, and were checked for purity by GC-MS and/or  $^1\text{H}$  NMR spectroscopy and used as received. Bis(pinacolato)diboron ( $\text{B}_2\text{pin}_2$ ) was kindly provided by AllyChem Co. Ltd. (Dalian, China). HPLC grade solvents were argon saturated, dried using an Innovative Technology Inc. Pure-Solv Solvent Purification System, and further deoxygenated using the freeze-pump-thaw method.  $\text{C}_6\text{D}_6$  and  $\text{CDCl}_3$  were purchased from Cambridge Isotope Laboratories, and dried over 4Å molecular sieves, deoxygenated using the freeze-pump-thaw method and vacuum transferred into a sealed vessel. 1,3-bis-(2,4,6-trimethylphenyl)imidazolin-2-ylidene (IMes),<sup>205</sup>  $[\text{Ni}(\text{IMes})_2]$ ,<sup>206</sup> and 1-Bpin-indole<sup>345</sup> used were prepared according to the literature procedures.

Automated flash chromatography was performed using a Biotage<sup>®</sup> Isolera Four system, on silica gel (Biotage SNAP cartridge KP-Sil 10 g and KP-Sil 25 g). Commercially available, precoated TLC plates (Polygram<sup>®</sup> Sil G/UV254) were purchased from Machery-Nagel. The removal of solvent was performed on a rotary evaporator *in vacuo* at a maximum temperature of 30 °C. GC-MS analyses were performed using an Agilent 7890A gas chromatograph (column: HP-5MS 5% phenyl methyl siloxane, 10 m, Ø 0.25 mm, film 0.25

$\mu\text{m}$ ; injector: 250 °C; oven: 40 °C (2 min), 40 °C to 280 °C (20 °C·min<sup>-1</sup>); carrier gas: He (1.2 mL·min<sup>-1</sup>) equipped with an Agilent 5975C inert MSD with triple-axis detector operating in EI mode and an Agilent 7693A series auto sampler/injector. HRMS were measured on a Thermo Scientific Exactive Plus equipped with an Orbitrap. ESI measurements were conducted using a HESI Source with an aux-gas temperature of 50 °C. Measurements were conducted using an APCI Source with a Corona Needle; aux-gas temperature was 400 °C.

All NMR spectra were recorded at ambient temperature using Bruker Avance III HD 300 NMR (<sup>1</sup>H, 300 MHz; <sup>13</sup>C{<sup>1</sup>H}, 75 MHz; <sup>11</sup>B, 96 MHz), Bruker Avance 400 NMR (<sup>1</sup>H, 400 MHz; <sup>13</sup>C{<sup>1</sup>H}, 100 MHz; <sup>11</sup>B, 128 MHz), or Bruker Avance 500 NMR (<sup>1</sup>H, 500 MHz; <sup>13</sup>C{<sup>1</sup>H}, 126 MHz; <sup>11</sup>B, 160 MHz; <sup>19</sup>F, 471 MHz) spectrometers. <sup>1</sup>H NMR chemical shifts are reported relative to TMS and were referenced via residual proton resonances of the corresponding deuterated solvent (CDCl<sub>3</sub>: 7.26 ppm, C<sub>6</sub>D<sub>6</sub>: 7.16 ppm) whereas <sup>13</sup>C{<sup>1</sup>H} NMR spectra are reported relative to TMS *via* the carbon signals of the deuterated solvent (CDCl<sub>3</sub>: 77.16 ppm, C<sub>6</sub>D<sub>6</sub>: 128.06 ppm). However, signals for the carbon attach to boron, C(aryl)-B, are usually too broad to observe in the <sup>13</sup>C{<sup>1</sup>H} NMR spectra. <sup>11</sup>B NMR chemical shifts are quoted relative to BF<sub>3</sub>·Et<sub>2</sub>O as external standard. <sup>19</sup>F NMR chemical shifts are quoted relative to CFC<sub>3</sub> as the external standard. All <sup>13</sup>C NMR spectra were broad-band <sup>1</sup>H decoupled. Elemental analyses were performed on a Elementar Vario MICRO cube elemental analyzer.

Crystals suitable for single-crystal X-ray diffraction were selected, coated in perfluoropolyether oil, and mounted on MiTeGen sample holders. Diffraction data were collected on Bruker X8 Apex II 4-circle diffractometers with CCD area detectors using Mo-K<sub>α</sub> radiation generated by a Nonius FR591 rotating anode and monochromated by graphite (5-Me-3-Bpin-indole, 5-MeO-3-Bpin-indole, 7-MeO-3-Bpin-indole, 5F-3-Bpin-indole, 6F-3-Bpin-indole) or multi-layer focusing mirrors (6-Me-3-Bpin-indole, 4F-3-Bpin-indole). However, diffraction data of 3-Bpin-indole, 7-Me-3-Bpin-indole, [Ni(IMes)<sub>2</sub>(H)(indole)], and [Ni(IMes)<sub>2</sub>(H)(6F-indole)] were collected on a RIGAKU

OXFORD DIFFRACTION XtaLAB Synergy diffractometer with a semiconductor HPA-detector (HyPix-6000) and multi-layer mirror monochromated Cu-K $\alpha$  radiation. The crystals were cooled using Oxford Cryostream low-temperature devices. Data were collected at 100 K. The images of were processed and corrected for Lorentz-polarization effects and absorption as implemented in the Bruker software packages or in the CrysAlis<sup>Pro</sup> software (Rigaku OD), respectively. The structures were solved using the intrinsic phasing method (SHELXT)<sup>286</sup> and Fourier expansion technique. All non-hydrogen atoms were refined in anisotropic approximation, with hydrogen atoms 'riding' in idealized positions, by full-matrix least squares against F<sup>2</sup> of all data, using SHELXL<sup>287</sup> software and the SHELXLE graphical user interface<sup>395</sup>. Only the H1 and H hydrogen atoms bonded to the nickel atoms of [Ni(IMes)<sub>2</sub>(H)(indole)] and [Ni(IMes)<sub>2</sub>(H)(6F-indole)], respectively, were refined freely. Diamond<sup>396</sup> software was used for graphical representation. Crystal data and experimental details are listed in Tables 4-5-4-7; full structural information has been deposited with the Cambridge Crystallographic Data Centre. CCDC-2002670 (3-Bpin-indole), CCDC-2002671 (5-Me-3-Bpin-indole), CCDC-2002672 (6-Me-3-Bpin-indole), CCDC-2002673 (7-Me-3-Bpin-indole), CCDC-2002674 (5-MeO-3-Bpin-indole), CCDC-2002675 (7-MeO-3-Bpin-indole), CCDC-2002676 (4F-3-Bpin-indole), CCDC-2002677 (5F-3-Bpin-indole), CCDC-2002678 (6F-3-Bpin-indole), CCDC-2002679 ([Ni(IMes)<sub>2</sub>(H)(indole)]), and CCDC-2002680 ([Ni(IMes)<sub>2</sub>(H)(6F-indole)]).

## 4.6.2 Experimental procedures

### Method A

Unless specified otherwise, a mixture of [Ni(IMes)<sub>2</sub>] (0.02 mmol, 13 mg) and B<sub>2</sub>pin<sub>2</sub> (0.3 mmol, 76 mg) was dissolved in the solvent (2 mL) in an oven-dried 10 mL vial equipped with a magnetic stirring bar. The indole (0.2 mmol) was then added to the solution, and then the vial was sealed. After removal from glove box, the reaction mixture was heated at 60 °C for 4 h, then diluted with dichloromethane (DCM, 2 mL) and filtered through a plug of celite (Ø 3 mm × 8 mm), and *n*-dodecane (34 mg, 0.2 mmol) was added as an internal standard. The product yield was determined by GC-MS using the calibrated *n*-dodecane

internal standard. The yields are based on indoles.

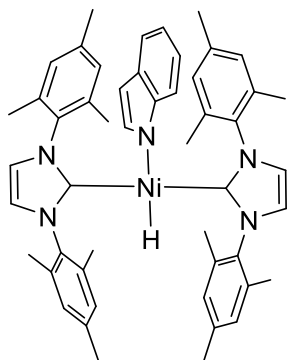
### Method B

A mixture of  $[\text{Ni}(\text{IMes})_2]$  (0.1 mmol, 65 mg) and  $\text{B}_2\text{pin}_2$  (1.5 mmol, 381 mg) was dissolved in hexane (5 mL) in a Schlenk tube equipped with a magnetic stirring bar. The indole (1 mmol) was added to the solution. After removal from glove box, the reaction mixture was heated at 60 °C for 4 h, and was then concentrated *in vacuo* and purified by silica-gel column chromatography with hexane and then a hexane and ethyl acetate mixture as eluent. The solvent of the product containing fraction of the eluent was evaporated *in vacuo*. The isolated yields are based on indoles.

### 4.6.3 Synthesis of $[\text{Ni}(\text{IMes})_2(\text{H})(\text{indole})]$ and $[\text{Ni}(\text{IMes})_2(\text{H})(6\text{F-indole})]$

Indole (117 mg, 1.00 mmol) or 6F-indole (135 mg, 1.00 mmol), respectively, were added to solutions of  $[\text{Ni}(\text{IMes})_2]$  (669 mg, 1.00 mmol) in hexane (10 mL) under argon, and then the reactions were heated at 60 °C for 4 h. In each case, the solvent was removed under vacuum to yield the crude product. Recrystallization by slow diffusion of hexane into saturated THF solutions of the resulting Ni complexes at room temperature gave **I1** (595 mg, 76%) and **I1-6F** (601 mg, 75%,) in form of yellow-orange crystalline solids.

#### $[\text{Ni}(\text{IMes})_2(\text{H})(\text{indole})]$ (**I1**)



$^1\text{H NMR}$  (500 MHz,  $\text{C}_6\text{D}_6$ ):  $\delta$  8.56 (d,  $J = 7$  Hz, 1H), 7.15-7.13 (m, 1H), 6.79 (s, 8H), 6.77-6.76 (m, 1H), 6.72-6.70 (m, 1H), 6.43 (dd,  $J = 1$  Hz, 2Hz, 1H), 6.29 (d,  $J = 2$  Hz, 1H), 5.93 (s, 4H), 2.32 (s, 12H), 1.74 (s, 24H), -21.2 (s, 1H).

$^{13}\text{C}\{^1\text{H}\}$  NMR (126 MHz,  $\text{C}_6\text{D}_6$ ):  $\delta$  187.7, 146.4, 137.1, 137.0, 135.6, 131.0, 128.8, 121.0,

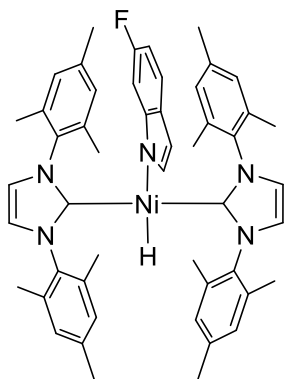
117.6, 116.6, 114.9, 114.4, 97.7, 20.9, 17.9.

**HRMS:**  $m/z$  for  $[\text{C}_{50}\text{H}_{55}\text{N}_5\text{Ni}]^+$   $[\text{M}^+]$  calcd: 783.3805, found: 783.3794.

**Anal.** for  $\text{C}_{50}\text{H}_{55}\text{N}_5\text{Ni}$  calcd: C, 76.53; H, 7.06; N, 8.92. found: C, 76.16; H, 7.14; N, 8.76.

**IR (ATR):**  $\nu_{\text{Ni-H}} = 1950 \text{ cm}^{-1}$ .

**[Ni(IMes)<sub>2</sub>(H)(6F-indole)] (I1-6F)**



**<sup>1</sup>H NMR** (500 MHz,  $\text{C}_6\text{D}_6$ ):  $\delta$  7.61-7.58 (m, 1H), 6.92-6.88 (m, 1H), 6.82 (s, 8H), 6.41-6.40 (m, 1H), 6.34-6.32 (m, 1H), 6.27 (d,  $J = 2$  Hz, 1H), 5.91 (s, 4H), 2.36 (s, 12H), 1.73 (s, 24H), -21.3 (s, 1H).

**<sup>13</sup>C{<sup>1</sup>H} NMR** (126 MHz,  $\text{C}_6\text{D}_6$ ):  $\delta$  187.2, 157.3 (d,  $J = 226$  Hz), 146.0 (d,  $J = 12$  Hz), 137.7 (d,  $J = 3$  Hz), 137.4, 136.9, 135.7, 128.8, 121.1, 117.1 (d,  $J = 11$  Hz), 102.6 (d,  $J = 25$  Hz), 101.2 (d,  $J = 22$  Hz), 97.8, 20.9, 17.8.

**<sup>19</sup>F NMR** (471 MHz,  $\text{C}_6\text{D}_6$ ):  $\delta$  -130.4 - -130.5 (m, 1F).

**HRMS:**  $m/z$  for  $[\text{C}_{50}\text{H}_{54}\text{FN}_5\text{Ni}]^+$   $[\text{M}^+]$  calcd: 801.3711, found: 801.3700.

**Anal.** for  $\text{C}_{50}\text{H}_{54}\text{FN}_5\text{Ni}$  calcd: C, 74.82; H, 6.78; N, 8.72. found: C, 74.81; H, 6.94; N, 8.71.

**IR (ATR):**  $\nu_{\text{Ni-H}} = 1950 \text{ cm}^{-1}$ .



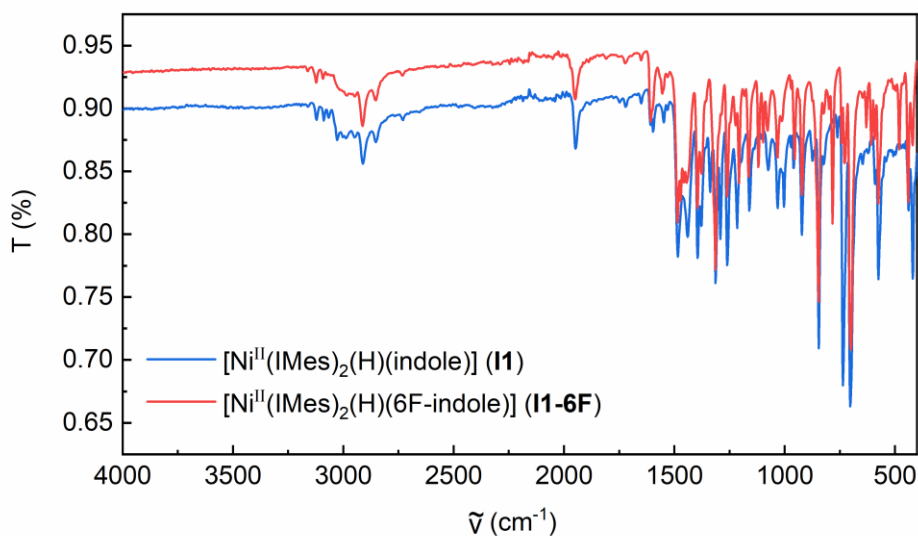
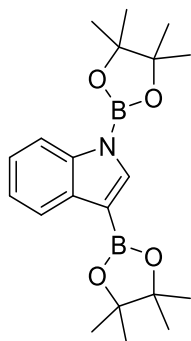


**Figure 4-8.** IR spectra of the  $[\text{Ni}^{\text{II}}(\text{IMes})_2(\text{H})(\text{indole})]$  (**11**) and  $[\text{Ni}^{\text{II}}(\text{IMes})_2(\text{H})(6\text{F-indole})]$  (**11-6F**) in the solid state.

#### 4.6.4 Synthesis of 1,3-(Bpin)<sub>2</sub>-indole

For the preparation of 1,3-(Bpin)<sub>2</sub>-indole (**80d**), 3-Bpin-indole (117 mg, 1 mmol) was dissolved in 1 mL of THF in an oven-dried 10 mL vial equipped with a magnetic stirring bar. HBpin (290  $\mu\text{L}$ , 2 mmol) and  $\text{NEt}_3$  (140  $\mu\text{L}$ , 1 mmol) were added to the solution, and then the vial was sealed. After removal from glove box, the reaction mixture was heated at 80  $^\circ\text{C}$  for 1 h, then the solvent was removed under vacuum to yield the **80d** (95%, 351 mg) as a white solid.

#### 1,3-bis(4,4,5,5-tetramethyl-1,3,2-dioxaborolan-2-yl)-1H-indole (**80d**)



$^1\text{H NMR}$  (500 MHz,  $\text{C}_6\text{D}_6$ ):  $\delta$  8.53-8.51 (m, 1H), 8.31-8.28 (m, 2H), 7.32-7.30 (m, 2H), 1.17 (s, 12H), 0.99 (s, 12H).

$^{13}\text{C}\{^1\text{H}\}$  NMR (126 MHz,  $\text{C}_6\text{D}_6$ ):  $\delta$  140.6, 140.0, 135.0, 123.0, 122.8, 122.0, 114.6, 84.0,

82.6, 24.7, 24.2.

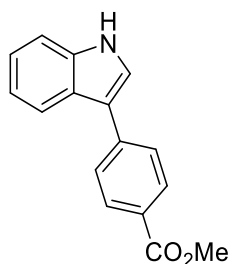
$^{11}\text{B}$  NMR (160 MHz,  $\text{C}_6\text{D}_6$ ):  $\delta$  30.7, 24.7.

**HRMS:**  $m/z$  for  $[\text{C}_{20}\text{H}_{30}\text{B}_2\text{NO}_4]^+ [\text{M}+\text{H}^+]$  calcd: 370.2355, found: 370.2349.

Our data are consistent with those in the literature.<sup>345</sup>

#### 4.6.5 Synthesis of methyl-4-(1*H*-indol-3-yl)-benzoate

A mixture of  $[\text{Ni}(\text{IMes})_2]$  (0.1 mmol, 67 mg) and  $\text{B}_2\text{pin}_2$  (1.5 mmol, 381 mg) dissolved in hexane (5 mL) in a Schlenk tube equipped with a magnetic stirring bar. The indole (1 mmol, 117 mg) was added to the solution. After removal from glove box, the reaction mixture was heated at 60 °C for 4 h, and was then concentrated *in vacuo*. A mixture of methyl 4-iodobenzoate (1 mmol, 262 mg), KOH (2 mmol, 112 mg) and tris(dibenzylideneacetone)dipalladium(0) (0.1 mmol, 92 mg) was then added into the Schlenk tube and dissolved in the mixture of 1,4-dioxane (3.5 mL) and water (1.5 mL) under Argon. The reaction mixture was heated 100 °C for 15h and was then concentrated *in vacuo* to yield the crude product which was purified by column chromatography on silica-gel with hexane and then a hexane and ethyl acetate mixture as eluent to yield the desired C3-arylated product 3-(methyl-4-benzoate)-indole (70%, 176 mg) as a white solid. Methyl 4-chlorobenzoate (1 mmol, 171 mg) was also successfully employed to synthesize the methyl-4-(1*H*-indole-3-yl)-benzoate under the same conditions, and the isolated yield was 37% (93 mg).



**Isolated yield:** 70% (175.7 mg, white solid) from methyl 4-iodobenzoate and 37% (93 mg, white solid) from methyl 4-chlorobenzoate.

$^1\text{H}$  NMR (500 MHz,  $\text{CDCl}_3$ ):  $\delta$  8.38 (s, 1H), 8.13-8.11 (m, 2H), 7.99-7.96 (m, 1H), 7.77-7.75 (m, 2H), 7.48-7.45 (m, 2H), 7.30-7.22 (m, 2H), 3.95 (s, 3H).

$^{13}\text{C}\{^1\text{H}\}$  NMR (126 MHz,  $\text{CDCl}_3$ ):  $\delta$  167.2, 140.5, 136.8, 130.2, 127.3, 126.9, 125.4, 122.8,

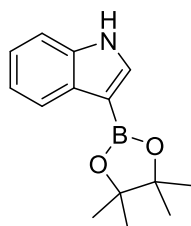
122.7, 120.8, 119.8, 117.4, 111.6, 52.0.

**HRMS:**  $m/z$  for  $[C_{16}H_{14}NO_2]^+$   $[M+H]^+$  calcd: 252.1019, found: 252.1013.

**Anal.** for  $C_{16}H_{14}NO_2$  calcd: C, 76.48; H, 5.21; N, 5.57. found: C, 76.51; H, 5.20; N, 5.48.

#### 4.6.6 Compound characterization

##### 3-Bpin-indole (80b)



**Isolated yield:** 78% (189.5 mg, white solid).

**$^1H$  NMR** (500 MHz,  $CDCl_3$ ):  $\delta$  8.43 (s, 1H), 8.07-8.05 (m, 1H), 7.65 (d,  $J = 3$  Hz, 1H), 7.40-7.38 (m, 1H), 7.22-7.16 (m, 2H), 1.37 (s, 12H).

**$^{13}C\{^1H\}$  NMR** (126 MHz,  $CDCl_3$ ):  $\delta$  136.7, 133.8, 131.6, 122.5, 122.2, 120.5, 110.8, 82.9, 24.9.

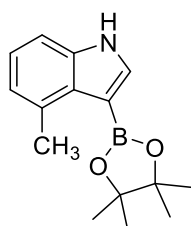
**$^{11}B$  NMR** (160 MHz,  $CDCl_3$ ):  $\delta$  30.3.

**HRMS:**  $m/z$  for  $[C_{14}H_{19}BNO_2]^+$   $[M+H]^+$  calcd: 244.1503, found: 244.1495.

**Anal.** for  $C_{14}H_{18}BNO_2$  calcd: C, 69.17; H, 7.46; N, 5.76. found: C, 69.06; H, 7.42; N, 5.56.

Our data are consistent with those in the literature.<sup>345,343</sup>

##### 4-Me-3-Bpin-indole (81b)



**Isolated yield:** 55% (141.4 mg, white solid).

**$^1H$  NMR** (500 MHz,  $CDCl_3$ ):  $\delta$  8.43 (s, 1H), 7.68 (d,  $J = 3$  Hz, 1H), 7.23-7.21 (m, 1H), 7.10 (t,  $J = 7$  Hz, 1H), 6.96-6.94 (m, 1H), 2.78 (s, 3H), 1.37 (s, 12H).

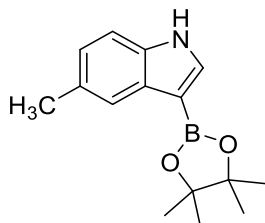
**$^{13}C\{^1H\}$  NMR** (126 MHz,  $CDCl_3$ ):  $\delta$  137.3, 135.0, 132.9, 129.8, 122.3, 121.9, 108.6, 83.0, 24.8, 21.3.

$^{11}\text{B}$  NMR (160 MHz,  $\text{CDCl}_3$ ):  $\delta$  30.6.

**HRMS:**  $m/z$  for  $[\text{C}_{15}\text{H}_{21}\text{BNO}_2]^+$   $[\text{M}+\text{H}^+]$  calcd: 258.1660, found: 258.1653.

**Anal.** for  $\text{C}_{15}\text{H}_{20}\text{BNO}_2$  calcd: C, 70.06; H, 7.84; N, 5.45. found: C, 69.91; H, 7.83; N, 5.29.

### 5-Me-3-Bpin-indole (82b)



**Isolated yield:** 68% (174.8 mg, white solid).

$^1\text{H}$  NMR (500 MHz,  $\text{CDCl}_3$ ):  $\delta$  8.35 (s, 1H), 7.83-7.82 (m, 1H), 7.61 (d,  $J = 3$  Hz, 1H), 7.27 (d,  $J = 8$  Hz, 1H), 7.04-7.02 (m, 1H), 2.48 (s, 3H), 1.37 (s, 12H).

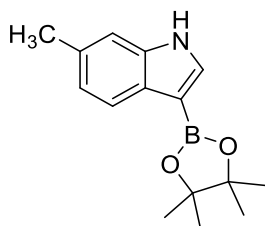
$^{13}\text{C}\{^1\text{H}\}$  NMR (126 MHz,  $\text{CDCl}_3$ ):  $\delta$  135.0, 134.0, 131.9, 129.9, 123.8, 122.1, 110.5, 82.8, 24.9, 21.5.

$^{11}\text{B}$  NMR (160 MHz,  $\text{CDCl}_3$ ):  $\delta$  30.3.

**HRMS:**  $m/z$  for  $[\text{C}_{15}\text{H}_{21}\text{BNO}_2]^+$   $[\text{M}+\text{H}^+]$  calcd: 258.1660, found: 258.1653.

**Anal.** for  $\text{C}_{15}\text{H}_{20}\text{BNO}_2$  calcd: C, 70.06; H, 7.84; N, 5.45. found: C, 70.03; H, 7.83; N, 5.28.

### 6-Me-3-Bpin-indole (83b)



**Isolated yield:** 69% (177.3 mg, white solid).

$^1\text{H}$  NMR (500 MHz,  $\text{CDCl}_3$ ):  $\delta$  8.30 (s, 1H), 7.91 (d,  $J = 8$  Hz, 1H), 7.58 (d,  $J = 3$  Hz, 1H), 7.18-7.17 (m, 1H), 7.02-7.00 (m, 1H), 2.46 (s, 3H), 1.37 (s, 12H).

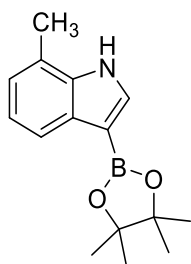
$^{13}\text{C}\{^1\text{H}\}$  NMR (126 MHz,  $\text{CDCl}_3$ ):  $\delta$  137.1, 133.3, 132.0, 129.4, 122.3, 122.1, 110.8, 82.8, 24.9, 21.7.

$^{11}\text{B}$  NMR (160 MHz,  $\text{CDCl}_3$ ):  $\delta$  30.4.

**HRMS:**  $m/z$  for  $[\text{C}_{15}\text{H}_{21}\text{BNO}_2]^+$   $[\text{M}+\text{H}^+]$  calcd: 258.1660, found: 258.1655.

**Anal.** for C<sub>15</sub>H<sub>20</sub>BNO<sub>2</sub> calcd: C, 70.06; H, 7.84; N, 5.45. found: C, 70.07; H, 7.94; N, 5.36.

#### 7-Me-3-Bpin-indole (84b)



**Isolated yield:** 60% (154.2 mg, white solid).

**<sup>1</sup>H NMR** (500 MHz, CDCl<sub>3</sub>): δ 8.39 (s, 1H), 7.92-7.90 (m, 1H), 7.65 (d, *J* = 3 Hz, 1H), 7.11 (t, *J* = 7 Hz, 1H), 7.02-7.00 (m, 1H), 2.49 (s, 3H), 1.38 (s, 12H).

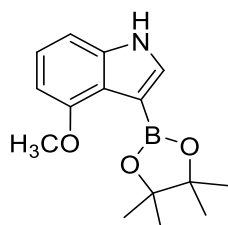
**<sup>13</sup>C{<sup>1</sup>H} NMR** (126 MHz, CDCl<sub>3</sub>): δ 136.3, 133.5, 131.2, 122.7, 120.7, 120.2, 120.0, 82.8, 24.9, 16.8.

**<sup>11</sup>B NMR** (160 MHz, CDCl<sub>3</sub>): δ 30.4.

**HRMS:** *m/z* for [C<sub>15</sub>H<sub>21</sub>BNO<sub>2</sub>]<sup>+</sup> [M+H<sup>+</sup>] calcd: 258.1660, found: 258.1653.

**Anal.** for C<sub>15</sub>H<sub>20</sub>BNO<sub>2</sub> calcd: C, 70.06; H, 7.84; N, 5.45. found: C, 70.11; H, 7.71; N, 5.33.

#### 4-MeO-3-Bpin-indole (85b)



**Isolated yield:** 55% (150.2 mg, pale yellow liquid).

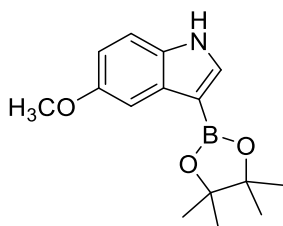
**<sup>1</sup>H NMR** (500 MHz, CDCl<sub>3</sub>): δ 8.37 (s, 1H), 7.52 (d, *J* = 3 Hz, 1H), 7.11 (t, *J* = 8 Hz, 1H), 7.01-6.99 (m, 1H), 6.57-6.55 (m, 1H), 3.95 (s, 3H), 1.38 (s, 12H).

**<sup>13</sup>C{<sup>1</sup>H} NMR** (126 MHz, CDCl<sub>3</sub>): δ 154.7, 138.5, 132.5, 123.1, 121.0, 104.2, 101.1, 82.9, 55.4, 24.9.

**<sup>11</sup>B NMR** (160 MHz, CDCl<sub>3</sub>): δ 30.8.

**HRMS:** *m/z* for [C<sub>15</sub>H<sub>21</sub>BNO<sub>3</sub>]<sup>+</sup> [M+H<sup>+</sup>] calcd: 274.1609, found: 274.1604.

**Anal.** for C<sub>15</sub>H<sub>20</sub>BNO<sub>3</sub> calcd: C, 65.96; H, 7.38; N, 5.13. found: C, 65.81; H, 7.24; N, 4.92.

**5-MeO-3-Bpin-indole (86b)**

**Isolated yield:** 63% (172.0 mg, white solid).

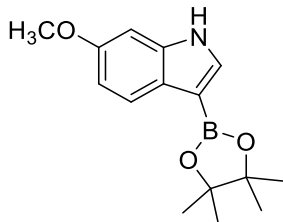
**<sup>1</sup>H NMR** (500 MHz, CDCl<sub>3</sub>): δ 8.34 (s, 1H), 7.62-7.61 (m, 1H), 7.54 (d, *J* = 3 Hz, 1H), 7.29-7.27 (m, 1H), 6.88-6.85 (m, 1H), 3.89 (s, 3H), 1.37 (s, 12H).

**<sup>13</sup>C{<sup>1</sup>H} NMR** (126 MHz, CDCl<sub>3</sub>): δ 154.8, 134.4, 132.4, 131.8, 112.2, 111.4, 104.6, 82.8, 56.0, 25.0.

**<sup>11</sup>B NMR** (160 MHz, CDCl<sub>3</sub>): δ 30.4.

**HRMS:** *m/z* for [C<sub>15</sub>H<sub>21</sub>BNO<sub>3</sub>]<sup>+</sup> [M+H<sup>+</sup>] calcd: 274.1609, found: 274.1604.

**Anal.** for C<sub>15</sub>H<sub>20</sub>BNO<sub>3</sub> calcd: C, 65.96; H, 7.38; N, 5.13. found: C, 65.74; H, 7.23; N, 4.94.

**6-MeO-3-Bpin-indole (87b)**

**Isolated yield:** 72% (196.6 mg, white solid).

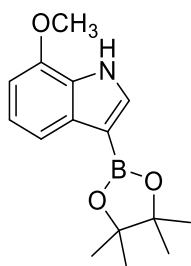
**<sup>1</sup>H NMR** (500 MHz, CDCl<sub>3</sub>): δ 8.31 (s, 1H), 7.92-7.90 (m, 1H), 7.55 (d, *J* = 2 Hz, 1H), 6.88-6.84 (m, 2H), 3.84 (s, 3H), 1.36 (s, 12H).

**<sup>13</sup>C{<sup>1</sup>H} NMR** (126 MHz, CDCl<sub>3</sub>): δ 156.6, 137.4, 132.8, 125.8, 123.1, 110.4, 94.4, 82.8, 55.7, 24.9.

**<sup>11</sup>B NMR** (160 MHz, CDCl<sub>3</sub>): δ 30.3.

**HRMS:** *m/z* for [C<sub>15</sub>H<sub>21</sub>BNO<sub>3</sub>]<sup>+</sup> [M+H<sup>+</sup>] calcd: 274.1609, found: 274.1603.

**Anal.** for C<sub>15</sub>H<sub>20</sub>BNO<sub>3</sub> calcd: C, 65.96; H, 7.38; N, 5.13. found: C, 65.79; H, 7.31; N, 4.90.

**7-MeO-3-Bpin-indole (88b)**

**Isolated yield:** 58% (158.3 mg, white solid).

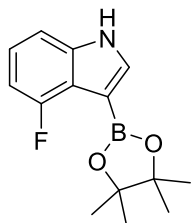
**<sup>1</sup>H NMR** (500 MHz, CDCl<sub>3</sub>): δ 8.65 (s, 1H), 7.64 (d, *J* = 8 Hz, 1H), 7.62 (d, *J* = 3 Hz, 1H), 7.09 (t, *J* = 8 Hz, 1H), 6.65 (d, *J* = 8 Hz, 1H), 3.95 (s, 3H), 1.36 (s, 12H).

**<sup>13</sup>C{<sup>1</sup>H} NMR** (126 MHz, CDCl<sub>3</sub>): δ 146.1, 133.2, 133.1, 127.2, 120.9, 115.1, 102.1, 82.8, 55.3, 24.9.

**<sup>11</sup>B NMR** (160 MHz, CDCl<sub>3</sub>): δ 30.3.

**HRMS:** *m/z* for [C<sub>15</sub>H<sub>21</sub>BNO<sub>3</sub>]<sup>+</sup> [M+H<sup>+</sup>] calcd: 274.1609, found: 274.1604.

**Anal.** for C<sub>15</sub>H<sub>20</sub>BNO<sub>3</sub> calcd: C, 65.96; H, 7.38; N, 5.13. found: C, 65.92; H, 7.34; N, 4.93.

**4-F-3-Bpin-indole (89b)**

**Isolated yield:** 76% (198.4 mg, white solid).

**<sup>1</sup>H NMR** (500 MHz, CDCl<sub>3</sub>): δ 8.61 (s, 1H), 7.63 (d, *J* = 3 Hz, 1H), 7.17-7.15 (m, 1H), 7.12-7.08 (m, 1H), 6.84-6.80 (m, 1H), 1.38 (s, 12H).

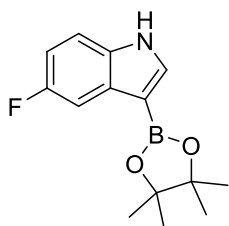
**<sup>13</sup>C{<sup>1</sup>H} NMR** (126 MHz, CDCl<sub>3</sub>): δ 157.4 (d, *J* = 250 Hz), 139.7 (d, *J* = 12 Hz), 134.6, 122.9 (d, *J* = 8 Hz), 119.4 (d, *J* = 23 Hz), 107.0 (d, *J* = 4 Hz), 106.0 (d, *J* = 20 Hz), 83.2, 24.8.

**<sup>19</sup>F NMR** (471 MHz, CDCl<sub>3</sub>): δ -115.7- -115.8 (m, 1F).

**<sup>11</sup>B NMR** (160 MHz, CDCl<sub>3</sub>): δ 30.3.

**HRMS:** *m/z* for [C<sub>14</sub>H<sub>18</sub>BFNO<sub>2</sub>]<sup>+</sup> [M+H<sup>+</sup>] calcd: 262.1409, found: 262.1404.

**Anal.** for C<sub>14</sub>H<sub>17</sub>BFNO<sub>2</sub> calcd: C, 64.40; H, 6.56; N, 5.36. found: C, 64.35; H, 6.66; N, 5.32.

**5-F-3-Bpin-indole (90b)**

**Isolated yield:** 79% (206.2 mg, white solid).

**<sup>1</sup>H NMR** (500 MHz, CDCl<sub>3</sub>): δ 8.43 (s, 1H), 7.72-7.70 (m, 1H), 7.67 (d, *J* = 3 Hz, 1H), 7.31-7.28 (m, 1H), 6.97-6.93 (m, 1H), 1.37 (s, 12H).

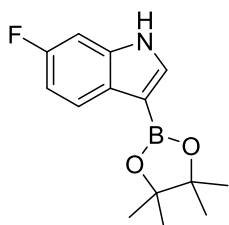
**<sup>13</sup>C{<sup>1</sup>H} NMR** (126 MHz, CDCl<sub>3</sub>): δ 158.5 (d, *J* = 235 Hz), 135.2, 133.1, 132.4 (d, *J* = 11 Hz), 111.3 (d, *J* = 10 Hz), 110.6 (d, *J* = 27 Hz), 107.5 (d, *J* = 23 Hz), 83.0, 24.9.

**<sup>19</sup>F NMR** (471 MHz, CDCl<sub>3</sub>): δ -123.9- -124.0 (m, 1F).

**<sup>11</sup>B NMR** (160 MHz, CDCl<sub>3</sub>): δ 30.1.

**HRMS:** *m/z* for [C<sub>14</sub>H<sub>18</sub>BFNO<sub>2</sub>]<sup>+</sup> [M+H<sup>+</sup>] calcd: 262.1409, found: 262.1401.

**Anal.** for C<sub>14</sub>H<sub>17</sub>BFNO<sub>2</sub> calcd: C, 64.40; H, 6.56; N, 5.36. found: C, 64.68; H, 6.65; N, 5.23.

**6-F-3-Bpin-indole (91b)**

**Isolated yield:** 62% (161.8 mg, white solid).

**<sup>1</sup>H NMR** (500 MHz, CDCl<sub>3</sub>): δ 8.47 (s, 1H), 7.98-7.95 (m, 1H), 7.61 (d, *J* = 2 Hz, 1H), 7.07-7.05 (m, 1H), 6.96-6.92 (m, 1H), 1.37 (s, 12H).

**<sup>13</sup>C{<sup>1</sup>H} NMR** (126 MHz, CDCl<sub>3</sub>): δ 160.0 (d, *J* = 238 Hz), 136.6 (d, *J* = 13 Hz), 134.2 (d, *J* = 3 Hz), 128.0, 123.3 (d, *J* = 10 Hz), 109.2 (d, *J* = 24 Hz), 97.2 (d, *J* = 26 Hz), 83.0, 24.9.

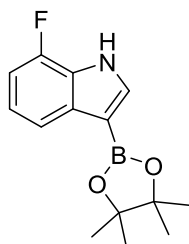
**<sup>19</sup>F NMR** (471 MHz, CDCl<sub>3</sub>): δ -121.0- -121.1 (m, 1F).

**<sup>11</sup>B NMR** (160 MHz, CDCl<sub>3</sub>): δ 30.3.

**HRMS:** *m/z* for [C<sub>14</sub>H<sub>18</sub>BFNO<sub>2</sub>]<sup>+</sup> [M+H<sup>+</sup>] calcd: 262.1409, found: 262.1402.

**Anal.** for C<sub>14</sub>H<sub>17</sub>BFNO<sub>2</sub> calcd: C, 64.40; H, 6.56; N, 5.36. found: C, 64.36; H, 6.69; N, 5.39.



**7-F-3-Bpin-indole (92b)**

**Isolated yield:** 42% (109.6 mg, light purple solid).

**<sup>1</sup>H NMR** (500 MHz, CDCl<sub>3</sub>): δ 8.61 (s, 1H), 7.81-7.80 (m, 1H), 7.66 (d, *J* = 2 Hz, 1H), 7.10-7.06 (m, 1H), 6.93-6.89 (m, 1H), 1.37 (s, 12H).

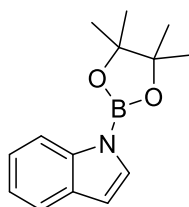
**<sup>13</sup>C{<sup>1</sup>H} NMR** (126 MHz, CDCl<sub>3</sub>): δ 149.5 (d, *J* = 244 Hz), 135.3 (d, *J* = 4 Hz), 134.2, 125.0 (d, *J* = 12 Hz), 120.8 (d, *J* = 6 Hz), 118.2 (d, *J* = 4 Hz), 107.1 (d, *J* = 16 Hz), 83.0, 24.9.

**<sup>19</sup>F NMR** (471 MHz, CDCl<sub>3</sub>): δ -135.0- -135.1 (m, 1F).

**<sup>11</sup>B NMR** (160 MHz, CDCl<sub>3</sub>): δ 30.2.

**HRMS:** *m/z* for [C<sub>14</sub>H<sub>18</sub>BFNO<sub>2</sub>]<sup>+</sup> [M+H<sup>+</sup>] calcd: 262.1409, found: 262.1402.

**Anal.** for C<sub>14</sub>H<sub>17</sub>BFNO<sub>2</sub> calcd: C, 64.40; H, 6.56; N, 5.36. found: C, 64.61; H, 6.55; N, 5.38.

**1-Bpin-indole (80c)**

**<sup>1</sup>H NMR** (500 MHz, C<sub>6</sub>D<sub>6</sub>): δ 8.36-8.33 (m, 1H), 7.63-7.61 (m, 1H), 7.56 (d, *J* = 3 Hz, 1H), 7.33-7.30 (m, 1H), 7.23-7.20 (m, 1H), 6.57 (dd, *J* = 1 Hz, *J* = 3 Hz, 1H), 1.02 (s, 12H).

**<sup>13</sup>C{<sup>1</sup>H} NMR** (126 MHz, C<sub>6</sub>D<sub>6</sub>): δ 139.7, 131.6, 128.8, 122.9, 121.6, 120.7, 114.8, 107.5, 83.9, 24.2.

**<sup>11</sup>B NMR** (160 MHz, C<sub>6</sub>D<sub>6</sub>): δ 24.7.

**HRMS:** *m/z* for [C<sub>14</sub>H<sub>19</sub>BNO<sub>2</sub>]<sup>+</sup> [M+H<sup>+</sup>] calcd: 244.1503, found: 244.1495.

Our data are consistent with those in the literature.<sup>345</sup>

## 4.6.7 Single-crystal X-ray diffraction analyses of C3-borylated indoles

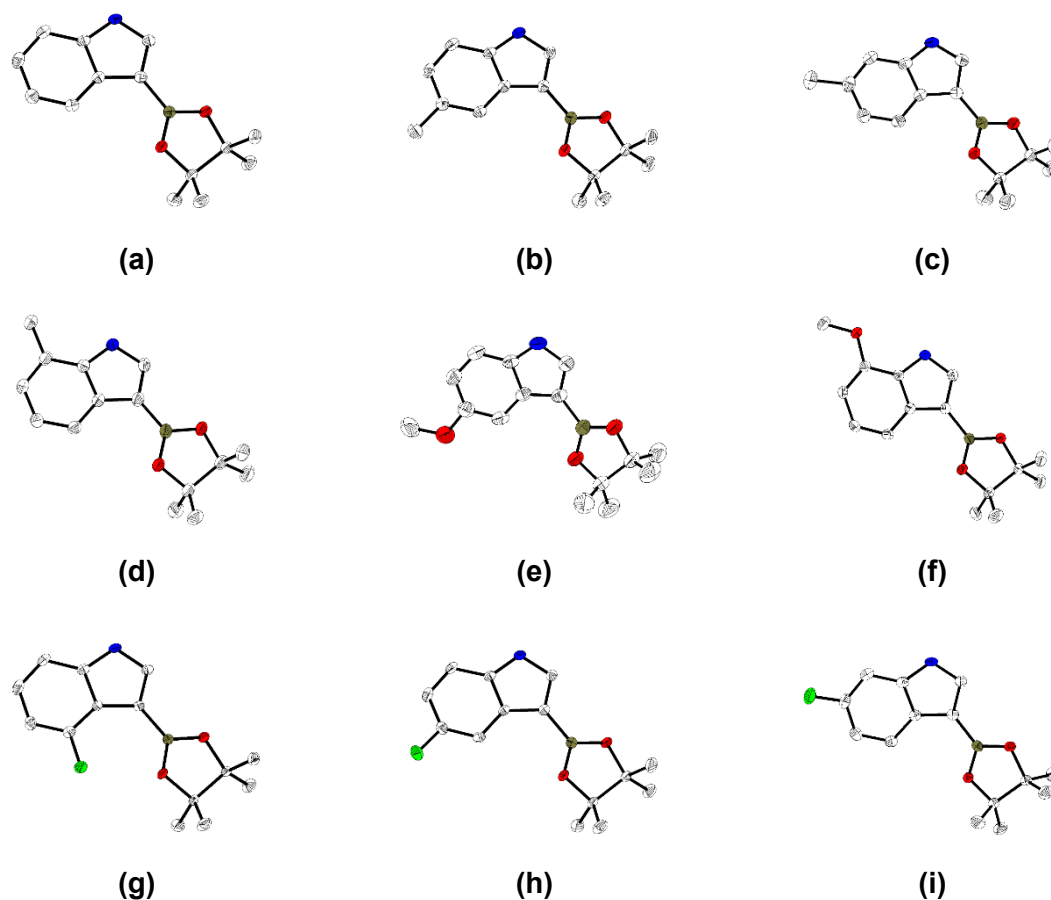
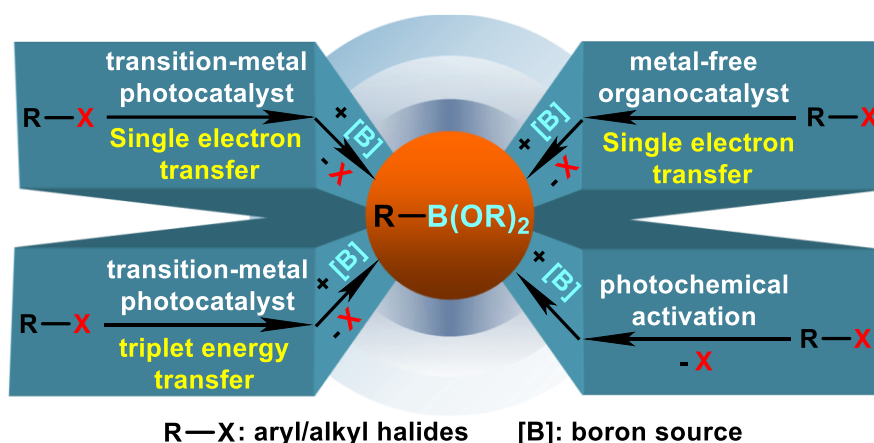


**Figure 4-9.** Molecular structure of 3-Bpin-indole **(a)**, 5-Me-3-Bpin-indole **(b)**, 6-Me-3-Bpin-indole **(c)**, 7-Me-3-Bpin-indole **(d)**, 5-MeO-3-Bpin-indole **(e)**, 7-MeO-3-Bpin-indole **(f)**, 4F-3-Bpin-indole **(g)**, 5F-3-Bpin-indole **(h)**, 6F-3-Bpin-indole **(i)** in the solid state at 100 K. Atomic displacement ellipsoids are drawn at the 50% probability level, and H atoms are omitted for clarity. Colors: white (carbon), blue (nitrogen), brown (boron), red (oxygen).

## Summary

Efficient and general methodologies have been developed for the selective construction of C-B bonds via  $[\text{Ni}(\text{IMes})_2]$ -catalyzed borylations of aryl fluorides, aryl chlorides and substituted indoles, which are readily available substrates.

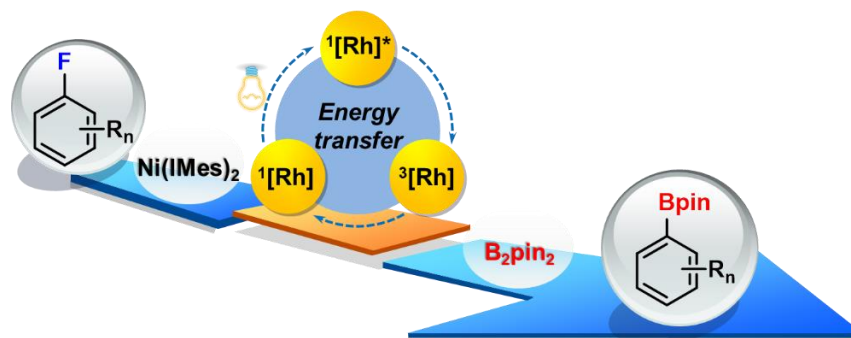
### Chapter 1



Chapter 1 summarizes the development of photoinduced C-X borylations for the synthesis of organoboron compounds. Clarifying the nature of the key steps in the interaction of an incident photon with a photocatalyst or the starting materials, and how these interactions facilitate borylation are very important to understand the mechanisms of photoinduced borylations. First, the photon energy must match the energy of the C-X bond that needs to be cleaved in the substrate. These photochemically activated molecules normally have good leaving groups, such as -Br, -I, and  $-\text{NR}_3^+$  etc. The borylation reactions are usually carried out using short wavelength irradiation, such as “hard” UV, and undergo radical processes. Second, if bonds between leaving groups and substrates are so strong that the light alone can not cleave them, or lower energy visible light is employed, a photoredox catalyst, e.g.,  $[\text{Ru}(\text{bpy})_3]^{2+}$ , *fac*- $\text{Ir}(\text{ppy})_3$ , or Eosin Y etc., are employed. Their redox potentials are modified upon irradiation such that many organic substrates can be reduced or oxidized to form reactive species, such as radicals. The direct energy transfer from the excited photoredox catalyst to a substrate molecule can also initiate the subsequent reactions. Third, activation of the diboron reagent via adduct formation or B-B bond fission

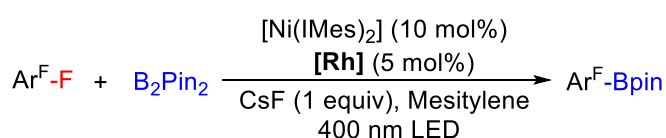
to produce photoreactive intermediates can promote the reaction.

## Chapter 2



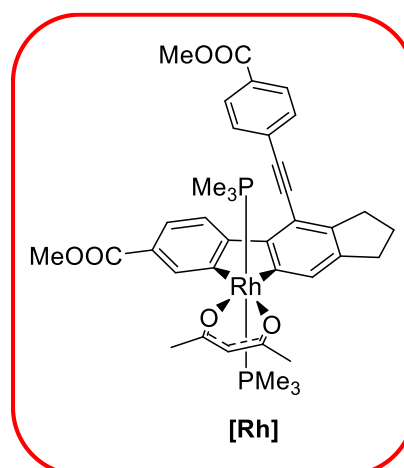
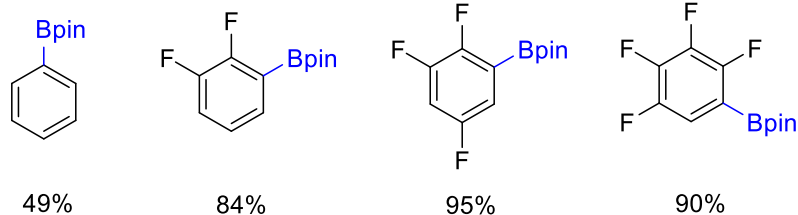
Chapter 2 reports a dual photocatalysis system that employs a rhodium-biphenyl complex as a triplet sensitizer and a nickel catalyst  $[\text{Ni}(\text{IMes})_2]$  for the selective activation and borylation of C-F bond of fluoroarenes with  $\text{B}_2\text{pin}_2$  (Scheme S-1). The strategy operates with visible (400 nm) light and achieves borylation at room temperature in excellent yields and with high selectivity. The efficient triplet energy transfer from the exceptionally long-lived triplet excited state of the Rh-biphenyl complex to the intermediary C-F bond oxidative addition product  $\text{trans}-[\text{NiF}(\text{Ar}^{\text{F}})(\text{IMes})_2]$  leads to NHC ligand dissociation and subsequently to a greatly enhanced rate constant for the transmetalation step at room temperature. Meanwhile, the indirect excitation of the triplet states  $\text{trans}-[\text{NiF}(\text{Ar}^{\text{F}})(\text{IMes})_2]$  by the photoexcited Rh biphenyl complex can also bypass its fast decomposition upon direct irradiation.

### Scheme S-1. Selective photocatalytic C-F borylation of polyfluoroarenes

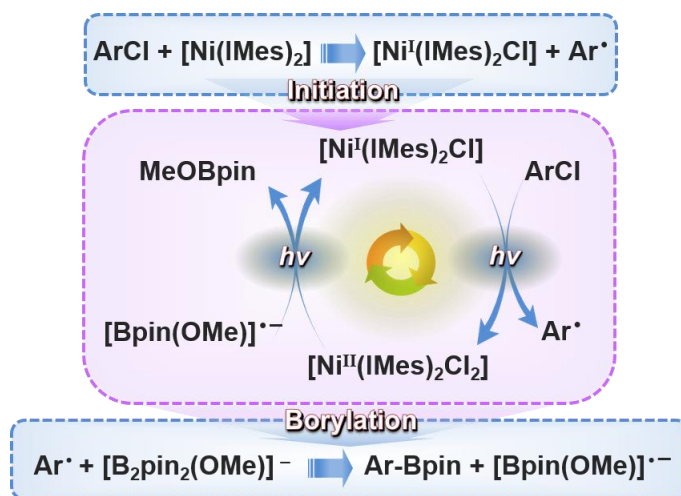


11 examples from monofluorobenzene to hexafluorobenzene

For example:

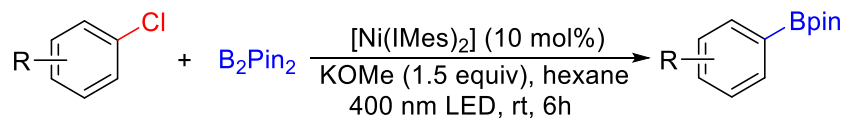


## Chapter 3



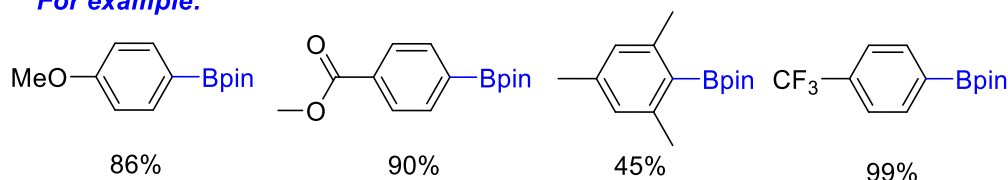
Chapter 3 reports a highly selective and general photo-induced protocol for the C-Cl borylation of chloroarenes using  $[\text{Ni}(\text{IMes})_2]$  as the catalyst with irradiation by 400 nm LEDs (Scheme S-2). The protocol displays broad scope and functional group tolerance, and furnishes arylboronates in good to excellent yields. The photo-induced  $[\text{Ni}^{\text{I}}(\text{IMes})_2\text{Cl}]/[\text{Ni}^{\text{II}}(\text{IMes})_2\text{Cl}_2]$  transformation acts as a novel redox shuttle which efficiently promotes the borylation. Halide abstraction from aryl chlorides by  $[\text{Ni}(\text{IMes})_2]$  is facile at room temperature to give  $[\text{Ni}^{\text{I}}(\text{IMes})_2\text{Cl}]$  and aryl radicals. Light also promotes the reaction of  $[\text{Ni}^{\text{I}}(\text{IMes})_2\text{Cl}]$  with aryl chlorides to form more aryl radicals and  $[\text{Ni}^{\text{II}}(\text{IMes})_2\text{Cl}_2]$ . Aryl radicals, as key intermediates, react with  $[\text{B}_2\text{pin}_2(\text{OMe})]^\bullet-$  to generate the corresponding borylation product and the  $[\text{Bpin}(\text{OMe})]^\bullet-$  radical anion.  $[\text{Bpin}(\text{OMe})]^\bullet-$  is a strong reducing agent, capable of converting  $[\text{Ni}^{\text{II}}(\text{IMes})_2\text{Cl}_2]$  to  $[\text{Ni}^{\text{I}}(\text{IMes})_2\text{Cl}]$  and  $[\text{Ni}(\text{IMes})_2]$  for the next catalytic cycle.

## Scheme S-2. Photo-induced Ni-catalyzed radical borylation of chloroarenes

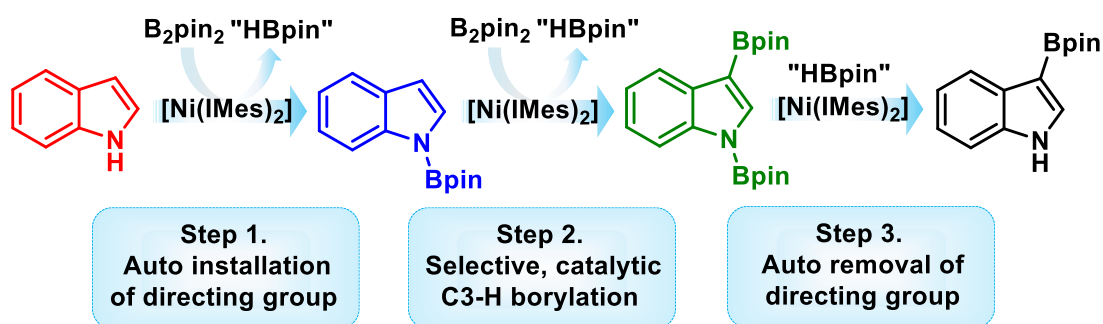


34 examples were successfully borylated

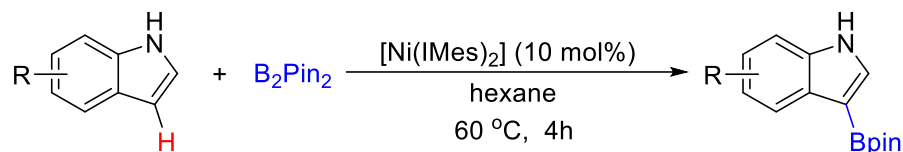
For example:



## Chapter 4

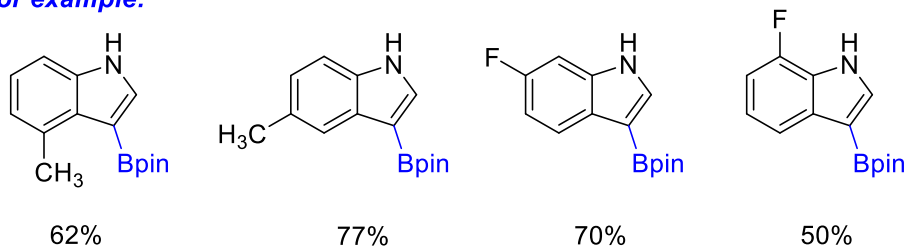


Chapter 4 reports an efficient and general protocol for the traceless, directed C3-selective C-H borylation of indoles with  $B_2pin_2$  using  $[Ni(IMes)_2]$  as the catalyst (Scheme S-3). The borylation of most indoles, bearing different functional groups, proceeds without base and under mild conditions, resulting in borylated products in good to excellent yields. A one-pot C3-H borylation/ Suzuki-Miyaura cross-coupling sequence for the direct synthesis of C3-arylated indoles was also achieved. Mechanistic studies suggest that indoles undergo fast oxidative addition to  $[Ni(IMes)_2]$  and further react with  $B_2pin_2$  to install Bpin *in situ* as a traceless directing group at the indole N-position. The regenerated  $[Ni(IMes)_2]$  inserts into the C3-H bond of the N-borylated indole to form the bis-N/C3-borylated indole. In the last step, the Bpin directing group from N-Bpin is removed to form the corresponding C3-borylated indoles.

**Scheme S-3. Ni-catalyzed C3-selective C-H borylation of indoles**

**13 examples were selectively borylated at C3-position**

**For example:**



In summary, highly selective and general C-X (X = F, Cl) and C-H borylation protocols that employ  $[\text{Ni}(\text{IMes})_2]$  as a catalyst to construct the C-B bond have been developed. Easily accessible aryl fluorides/chlorides and substituted indoles were successfully borylated in good to excellent yields. A Rh biphenyl complex, developed by our group, proved to be an effective photocatalyst, providing a powerful tool for the selective borylation of polyfluoroarenes via a triplet energy transfer pathway. Generation of aryl radicals from aryl chlorides by photoinduced transformations of  $[\text{Ni}^{\text{I}}(\text{IMes})_2\text{Cl}]/[\text{Ni}^{\text{II}}(\text{IMes})_2\text{Cl}_2]$  provide a mechanism by which aryl chlorides can be catalytically borylated.  $[\text{Ni}(\text{IMes})_2]$ -catalyzed C3-selective C-H borylation of indoles, using *in situ* installation of Bpin as a traceless directing group at the indole N-position, provides a simple and effective method by which to synthesize C3-borylated indoles. All of the protocols developed may be applied in the future for the late-stage functionalization of organic molecules, natural products and drug precursors containing aryl C-F-, aryl C-Cl or indole-C-H moieties.

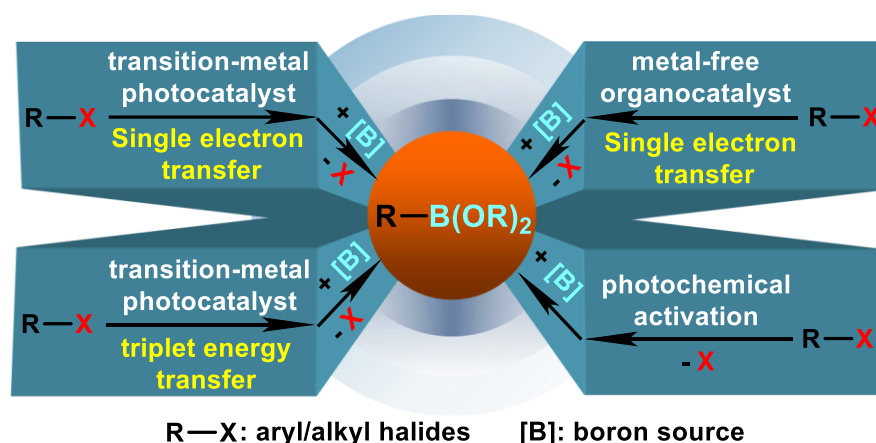




## Zusammenfassung

Es wurden effiziente und allgemeine Methoden für die selektive C-B-Verknüpfung mittels  $[\text{Ni}(\text{IMes})_2]$ -katalysierter Borylierungen von Arylfluoriden, Arylchloriden und substituierten Indolen entwickelt, welches alles leicht verfügbare Substrate sind.

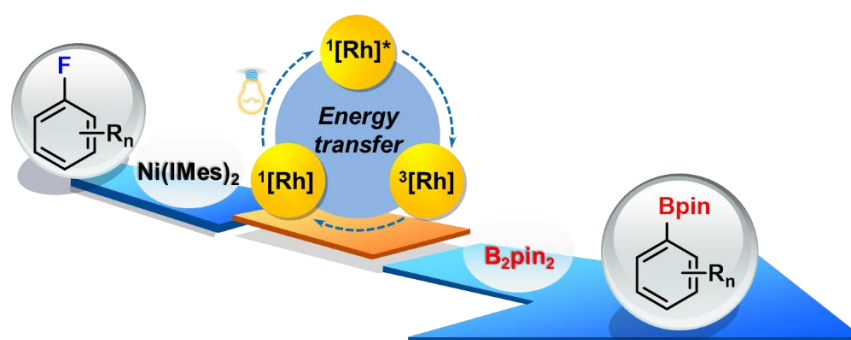
### Kapitel 1



Kapitel 1 fasst die Entwicklung von photoinduzierten C-X-Borylierungen für die Synthese von Organoborverbindungen zusammen. Die Natur der einzelnen Schlüsselschritte, von der Wechselwirkung eines einfallenden Photons mit einem Photokatalysator oder den Edukten, bis zu der Art und Weise, wie diese Wechselwirkungen die Borylierung erleichtern, zu erklären, ist sehr wichtig um den Mechanismus der photoinduzierter Borylierungen zu verstehen. Erstens muss die Energie des Photons mit der Energie der C-X-Bindung übereinstimmen, die im Substrat gespalten wird. Diese photochemisch aktivierten Moleküle haben normalerweise gute Abgangsgruppen, wie  $-\text{Br}$ ,  $-\text{I}$ , und  $-\text{NR}_3^+$  etc. Die Borylierungsreaktionen werden in der Regel mit kurzweiliger Bestrahlung, wie z.B. "hartem" UV, durchgeführt und durchlaufen radikalische Prozesse. Zweitens, wenn die Bindungen zwischen den Abgangsgruppen und den Substraten so stark sind, dass das Licht allein sie nicht spalten kann, oder wenn sichtbares Licht geringerer Energie verwendet wird, wird ein Photoredox-Katalysator, wie zum Beispiel  $[\text{Ru}(\text{bpy})_3]^{2+}$ , *fac*- $\text{Ir}(\text{ppy})_3$  oder Eosin Y etc. verwendet. Ihre Redoxpotentiale werden bei Bestrahlung so modifiziert, dass viele organische Substrate reduziert oder oxidiert werden können, um

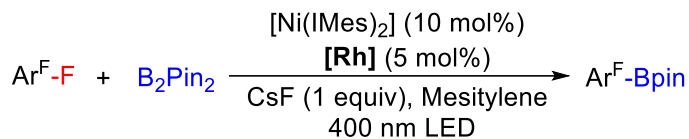
reaktive Spezies, wie z.B. Radikale, zu bilden. Die direkte Energieübertragung vom angeregten Photoredox-Katalysator auf ein Substratmolekül kann auch die nachfolgenden Reaktionen auslösen. Drittens kann die Aktivierung des Diborreagenzes durch Adduktbildung oder B-B-Bindungsspaltung, unter Bildung photoreaktiver Intermediate, auch die Reaktion fördern.

## Kapitel 2



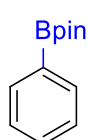
Kapitel 2 handelt von einem dualen Photokatalyse-System, das einen Rh-Biphenyl-Komplex als Triplett-Sensibilisator und einen Nickel-Katalysator  $[\text{Ni}(\text{IMes})_2]$  zur selektiven Aktivierung und Borylierung der C-F-Bindung von Fluorarenen mit  $\text{B}_2\text{pin}_2$  verwendet (Schema S-1). Nach dieser Strategie verläuft die Reaktion mit sichtbarem (400 nm) Licht, wobei Borylierungen schon bei Raumtemperatur in hervorragenden Ausbeuten und mit hoher Selektivität erreicht werden. Der effiziente Triplett-Energietransfer des außergewöhnlich langlebigen angeregten Triplett-Zustands des Rh-Biphenyl-Komplexes zum intermediären oxidativen Additionsprodukt  $\text{trans-}[\text{NiF}(\text{Ar}^{\text{F}})(\text{IMes})_2]$  der C-F-Bindung führt zu einer Dissoziation des NHC-Liganden und anschließend zu einer stark verbesserten Geschwindigkeitskonstante für den Transmetallierungsschritt bei Raumtemperatur. Währenddessen kann die indirekte Anregung der Triplettzustände von  $\text{trans-}[\text{NiF}(\text{Ar}^{\text{F}})(\text{IMes})_2]$  durch den photoangeregten Rh-Biphenyl-Komplex auch seine schnelle Zersetzung durch Bestrahlung umgehen.

### Schema S-1. Selektive photokatalytische C-F-Borylierung von Polyfluorarenen

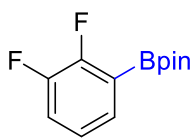


#### 11 Beispiele von Monofluorobenzol bis Hexafluorobenzol

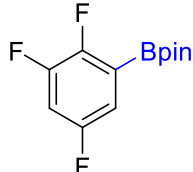
Zum Beispiel:



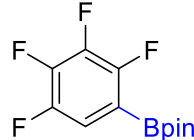
49%



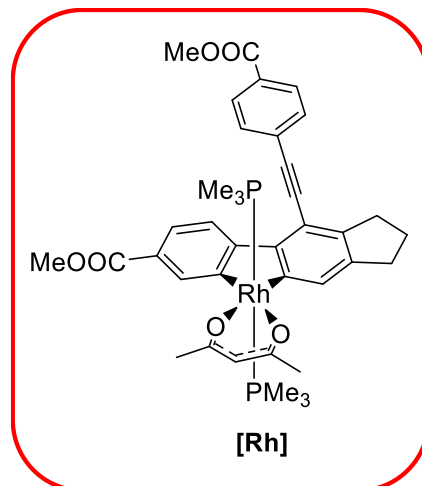
84%



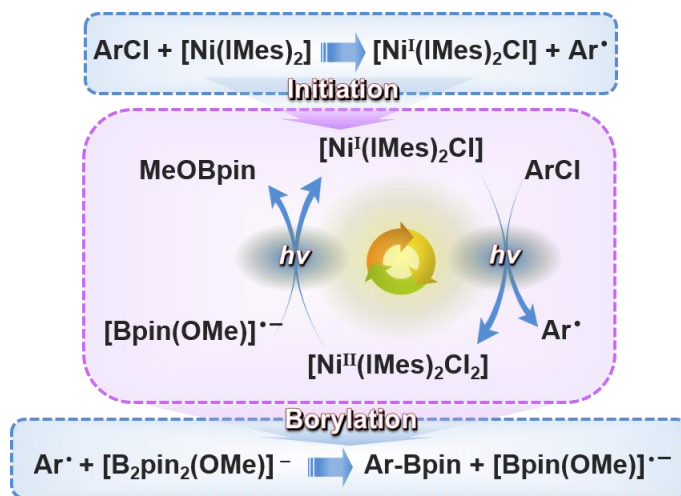
95%



90%



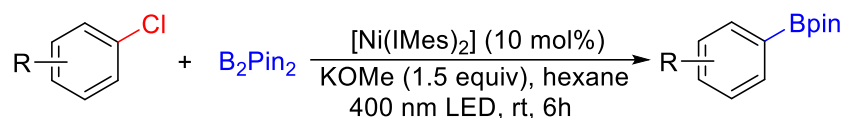
### Kapitel 3



Kapitel 3 handelt von einem hochselektiven und allgemeinen photoinduzierten Protokoll für die C-Cl-Borylierung von Arylchloriden unter Verwendung des Katalysators  $[\text{Ni}(\text{IMes})_2]$  und bei Bestrahlung mit einer 400-nm-LED (Schema S-2). Dieses Protokoll zeigt einen breiten Anwendungsbereich und eine hohe Toleranz gegenüber verschiedenen funktionellen Gruppen und liefert Arylboronate in guten bis ausgezeichneten Ausbeuten. Die photoinduzierte  $[\text{Ni}^{\text{I}}(\text{IMes})_2\text{Cl}]/[\text{Ni}^{\text{II}}(\text{IMes})_2\text{Cl}_2]$ -Transformation agiert als neuartiges Redox-System, das die Borylierung effizient fördert. Die Halogenidabstraktion von

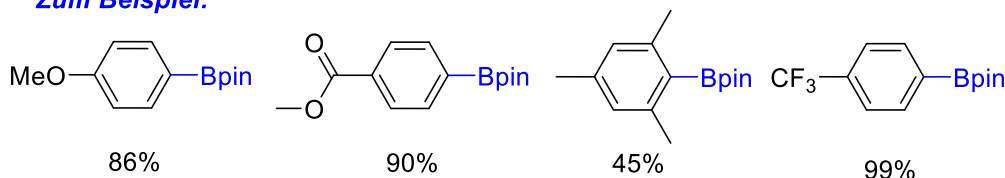
Arylchloriden durch  $[\text{Ni}(\text{IMes})_2]$  ist bei Raumtemperatur leicht, um  $[\text{Ni}^{\text{I}}(\text{IMes})_2\text{Cl}]$  und aktive Arylradikale zu bilden. Licht fördert auch die Reaktion von  $[\text{Ni}^{\text{I}}(\text{IMes})_2\text{Cl}]$  mit Arylchloriden zur Bildung von weiteren Arylradikalen und  $[\text{Ni}^{\text{II}}(\text{IMes})_2\text{Cl}_2]$ . Arylradikale als Schlüsselzwischenprodukte reagieren mit  $[\text{B}_2\text{pin}_2(\text{OMe})]^-$  unter Bildung des entsprechenden Borylierungsprodukts und des radikalischen Anions  $[\text{Bpin}(\text{OMe})]^-$ .  $[\text{Bpin}(\text{OMe})]^-$  ist ein starkes Reduktionsmittel, das in der Lage ist,  $[\text{Ni}^{\text{II}}(\text{IMes})_2\text{Cl}_2]$  in  $[\text{Ni}^{\text{I}}(\text{IMes})_2\text{Cl}]$  und  $[\text{Ni}(\text{IMes})_2]$  für den nächsten katalytischen Zyklus umzuwandeln.

### Schema S-2. Photoinduzierte Ni-katalysierte radikalische Borylierung von Chlorarenen

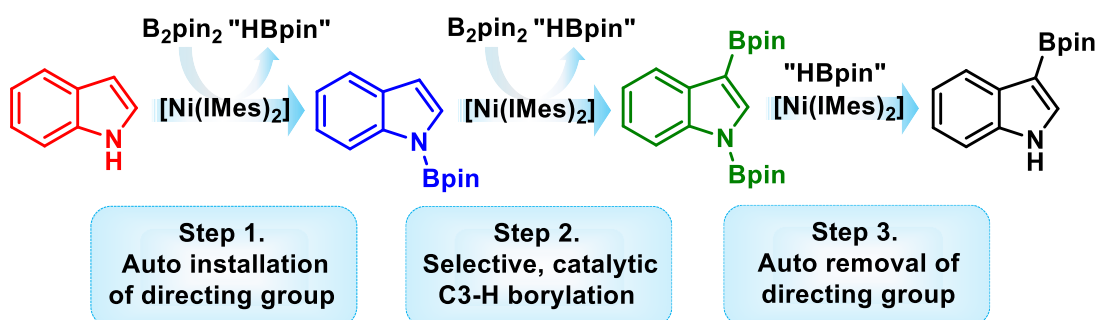


*34 Beispiele wurden erfolgreich boryliert*

*Zum Beispiel:*



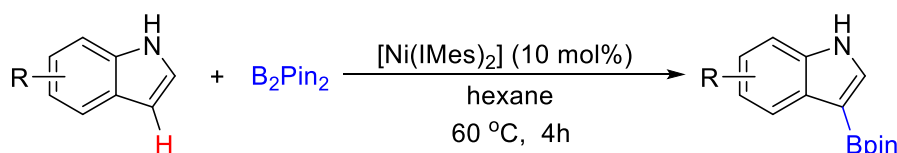
### Kapitel 4



In Kapitel 4 wird über ein effizientes und allgemeines Protokoll für eine dirigierte, selektive C-H-Borylierung von Indolen an C3 mit  $\text{B}_2\text{pin}_2$  und dem Katalysator  $[\text{Ni}(\text{IMes})_2]$  berichtet (Schema S-3). Die Borylierung der meisten Indole, mit den unterschiedlichsten funktionellen Gruppen, verläuft ohne Base und unter milden Bedingungen, was zu

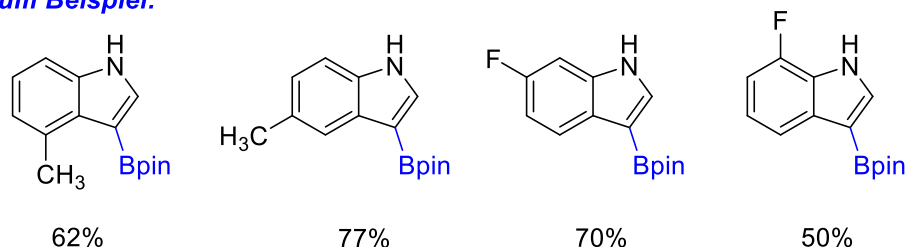
borylierten Produkten in guten bis ausgezeichneten Ausbeuten führt. Eine Eintopfsynthese bestehend aus einer C3-H-Borylierung und einer Suzuki-Miyaura-Kreuzkupplungsreaktion für die direkte Synthese von C3-arylierten Indolen wurde ebenfalls erreicht. Mechanistische Studien legen nahe, dass Indole eine schnelle oxidative Addition mit  $[\text{Ni}(\text{IMes})_2]$  eingehen und dann weiter mit  $\text{B}_2\text{pin}_2$  reagieren, um Bpin *in situ* als dirigierende Gruppe an der Indol-N-Position zu installieren. Das regenerierte  $[\text{Ni}(\text{IMes})_2]$ -System fügt sich nun in die C3-H-Bindung des N-borylierten Indols um das Bis-N/C3-borylierte Indol zu bilden. Im letzten Schritt wird die dirigierende Gruppe Bpin von N-Bpin entfernt, um das entsprechende C3-borylierte Indol zu bilden.

### Schema S-3. Ni-katalysierte C3-selektive C-H Borylierung von Indolen



**13 Beispiele wurden selektiv an der C3-Position boryliert**

**Zum Beispiel:**



Zusammenfassend werden in dieser Arbeit hochselektive und allgemeine C-X- ( $X = \text{F}, \text{Cl}$ ) und C-H-Borylierungsprotokolle entwickelt, bei denen der Komplex  $[\text{Ni}(\text{IMes})_2]$  als Katalysator zur Knüpfung der C-B-Bindung verwendet wurde. Demnach wurden leicht zugängliche Arylfluoride/-chloride und substituierte Indole erfolgreich in guten bis ausgezeichneten Ausbeuten boryliert. Ein neuer Rh-Biphenyl-Komplex, der von unserer Gruppe entwickelt wurde, hat sich als wirksamer Photokatalysator erwiesen und bietet damit ein leistungsstarkes Mittel für die selektive Borylierung von Polyfluorarenen über einen Triplett-Energieübertragungsweg. Die Bildung von Arylradikalen aus Arylchloriden durch die photoinduzierte Umwandlung von  $[\text{Ni}^{\text{I}}(\text{IMes})_2\text{Cl}]/[\text{Ni}^{\text{II}}(\text{IMes})_2\text{Cl}_2]$  liefert eine zuverlässige und nützliche Referenz für zukünftige Reaktionen, die auch Radikalwege

durchlaufen. Die  $[\text{Ni}(\text{IMes})_2]$ -katalysierte C3-selektive C-H-Borylierung von Indolen mit der *in-situ* eingeführten dirigierenden Bpin-Gruppe an der Indol-N-Position bietet eine einfache und effektive Methode zur Synthese von C3-borylierten Indolen. Alle hier entwickelten Protokolle können in Zukunft für die Spätfunktionalisierung von organischen Molekülen, Naturstoffen und Arzneimitteln angewendet werden, die Aryl-C-F-, Aryl-C-Cl- oder Indol-C-H-Gruppen enthalten.

## Notes and References

1. Hall, D. G. 2nd ed., Willey-VCH, Weinheim **2011**.
2. Neeve, E. C.; Geier, S. J.; Mkhaliid, I. A. I.; Westcott, S. A.; Marder, T. B. *Chem. Rev.* **2016**, *116*, 9091.
3. Cuenca, A. B.; Shishido, R.; Ito, H.; Fernández, E. *Chem. Soc. Rev.* **2017**, *46*, 415.
4. Mkhaliid, I. A. I.; Barnard, J. H.; Marder, T. B.; Murphy, J. M.; Hartwig, J. F. *Chem. Rev.* **2010**, *110*, 890.
5. Corey, E. J. *Angew. Chem. Int. Ed.* **2002**, *41*, 1650.
6. Dimitrijević, E.; Taylor, M. S. *ACS Catal.* **2013**, *3*, 945.
7. Taylor, M. S. *Acc. Chem. Res.* **2015**, *48*, 295.
8. Ji, L.; Griesbeck, S.; Marder, T. B. *Chem. Sci.* **2017**, *8*, 846.
9. Shoji, Y.; Iwabata, Y.; Wang, Q.; Nemoto, D.; Sakamoto, A.; Tanaka, N.; Seino, J.; Nakai, H.; Fukushima, T. *J. Am. Chem. Soc.* **2017**, *139*, 2728.
10. He, J.; Rauch, F.; Friedrich, A.; Sieh, D.; Ribbeck, T.; Krummenacher, I.; Braunschweig, H.; Finze, M.; Marder, T. B. *Chem. Eur. J.* **2019**, *25*, 13777.
11. Merz, J.; Steffen, A.; Nitsch, J.; Fink, J.; Schürger, C. B.; Friedrich, A.; Krummenacher, I.; Braunschweig, H.; Moos, M.; Mims, D.; Lambert, C.; Marder, T. B. *Chem. Sci.* **2019**, *10*, 7516.
12. Lorbach, A.; Hübner, A.; Wagner, M. *Dalton Trans.* **2012**, *41*, 6048.
13. Zhao, F.; Liu, H.; Mathe, S. D. R.; Dong, A.; Zhang, J. *Nanomaterials* **2018**, *8*, 15.
14. Qiu, F.; Zhao, W.; Han, S.; Zhuang, X.; Lin, H.; Zhang, F. *Polymers* **2016**, *8*, 191.
15. Wang, H.; Wang, H.; Wang, Z.; Tang, L.; Zeng, G.; Xu, P.; Chen, M.; Xiong, T.; Zhou, C.; Li, X.; Huang, D.; Zhu, Y.; Wang, Z.; Tang, J. *Chem. Soc. Rev.* **2020**, *49*, 4135.
16. Demirci, S.; Doğan, A.; Karakuş, E.; Halıcı, Z.; Topçu, A.; Demirci, E.; Sahin, F. *Biol Trace Elem Res.* **2015**, *168*, 169.
17. Tong, X.; Du, L.; Xu, Q. *J. Mater. Chem. A* **2018**, *6*, 3091.
18. Ahtzaz, S.; Waris, T. S.; Shahzadi, L.; Chaudhry, A. A.; Rehman, I. U.; Yar, M. *Int. J. Polym. Mater. Polym. Biomater.* **2019**, *69*, 525.

19. Das, B. C.; Thapa, P.; Karki, R.; Schinke, C.; Das, S.; Kambhampati, S.; Banerjee, S. K.; Van Veldhuizen, P.; Verma, A.; Weiss, L. M. *Future Med. Chem.* **2013**, *5*, 653.
20. Scorei, R. I.; Popa, R. *Anti Cancer Agents Med. Chem.* **2010**, *10*, 346.
21. Kouroukis, T. C.; Baldassarre, F. G.; Haynes, A. E.; Imrie, K.; Reece, D. E.; Cheung, M. C. *Curr. Oncol.* **2014**, *21*, e573.
22. Khotinsky, E.; Melamed, M. *Ber. Dtsch. Chem. Ges.* **1909**, *42*, 3090.
23. Letsinger, R. L.; Skoog, I. H. *J. Org. Chem.* **1953**, *18*, 895.
24. Dang, L.; Lin, Z.; Marder, T. B. *Chem. Commun.* **2009**, 3987.
25. Suginome, M.; Ito, Y. *J. Organomet. Chem.* **2003**, *680*, 43.
26. Cipot, J.; Vogels, C. M.; McDonald, R.; Westcott, S. A.; Stradiotto, M. *Organometallics* **2006**, *25*, 5965.
27. Takaya, J.; Iwasawa, N. *ACS Catal.* **2012**, *2*, 1993.
28. Yun, J. *Asian J. Org. Chem.* **2013**, *2*, 1016.
29. Issaian, A.; Tu, K. N.; Blum, S. A. *Acc. Chem. Res.* **2017**, *50*, 2598.
30. Zhao, F.; Jia, X.; Li, P.; Zhao, J.; Zhou, Y.; Wang, J.; Liu, H. *Org. Chem. Front.* **2017**, *4*, 2235.
31. Hemming, D.; Fritzeimer, R.; Westcott, S. A.; Santos, W. L.; Steel, P. G. *Chem. Soc. Rev.* **2018**, *47*, 7477.
32. Nallagonda, R.; Padala, K.; Masarwa, A. *Org. Biomol. Chem.* **2018**, *16*, 1050.
33. Verma, P. K.; Shegavi, M. L.; Bose, S. K.; Geetharani, K. *Org. Biomol. Chem.* **2018**, *16*, 857.
34. Carreras, J.; Caballero, A.; Pérez, P. J. *Chem. Asian J.* **2019**, *14*, 329.
35. Ding, S.; Xu, L.; Miao, Z. *Molecules* **2019**, *24*, 1325.
36. Takale, B. S.; Thakore, R. R.; Etemadi-Davan, E.; Lipshutz, B. H. *Beilstein J. Org. Chem.* **2020**, *16*, 691.
37. Ishiyama, T.; Miyaura, N. *J. Organomet. Chem.* **2003**, *680*, 3.
38. Hartwig, J. F. *Chem. Soc. Rev.* **2011**, *40*, 1992.
39. Hartwig, J. F. *Acc. Chem. Res.* **2012**, *45*, 864.
40. Ros, A.; Fernández, R. Lassaletta, J. M. *Chem. Soc. Rev.* **2014**, *43*, 3229.
41. Kuroda, Y.; Nakao, Y. *Chem. Lett.* **2019**, *48*, 1092.



42. Čubiňák, M.; Edlová, T.; Polák, P.; Tobrman, T. *Molecules* **2019**, *24*, 3523.
43. Iqbal, S. A.; Pahl, J.; Yuan, K.; Ingleson, M. J. *Chem. Soc. Rev.* **2020**, *49*, 4564.
44. Tian, Y.-M.; Guo, X.-N.; Wu, Z.; Friedrich, A.; Westcott, S. A.; Braunschweig, H.; Radius, U.; Marder, T. B. *J. Am. Chem. Soc.* **2020**, *142*, 13136.
45. Chen, K.; Wang, L. H.; Meng, G.; Li, P. F. *Synthesis* **2017**, *49*, 4719.
46. Chow, W. K.; Yuen, O. Y.; Choy, P. Y.; So, C. M.; Lau, C. P.; Wong, W. T.; Kwong, F. Y. *RSC Adv.* **2013**, *3*, 12518.
47. Kubota, K.; Iwamoto, H.; Ito, H. *Org. Biomol. Chem.* **2017**, *15*, 285.
48. Wang, M.; Shi, Z. *Chem. Rev.* **2020**, *120*, 7348.
49. Vogels, C. M.; Westcott, S. A. *ChemCatChem* **2012**, *4*, 47.
50. Wen, Y.; Deng, C.; Xie, J.; Kang, X. *Molecules* **2019**, *24*, 101.
51. Yan, G. B.; Huang, D. Y.; Wu, X. M. *Adv. Synth. Catal.* **2018**, *360*, 1040.
52. Nguyen, V. D.; Nguyen, V. T.; Jin, S. F.; Dang, H. T.; Larionov, O. V. *Tetrahedron* **2019**, *75*, 584.
53. Xu, L.; Wang, G. H.; Zhang, S.; Wang, H.; Wang, L. H.; Liu, L.; Jiao, J.; Li, P. F. *Tetrahedron* **2017**, *73*, 7123.
54. Prier, C. K.; Rankic, D. A.; MacMillan, D. W. C. *Chem. Rev.* **2013**, *113*, 5322.
55. Twilton, J.; Le, C.; Zhang, P.; Shaw, M. H.; Evans, R. W.; MacMillan, D. W. C. *Nat. Rev. Chem.* **2017**, *1*, 0052.
56. Narayanam, J. M. R.; Stephenson, C. R. J. *Chem. Soc. Rev.* **2011**, *40*, 102.
57. Tellis, J. C.; Primer, D. N.; Molander, G. A. *Science* **2014**, *345*, 433.
58. Zuo, Z. W.; Ahneman, D. T.; Chu, L. L.; Terrett, J. A.; Doyle, A. G.; MacMillan, D. W. C. *Science* **2014**, *345*, 437.
59. Romero, N. A.; Nicewicz, D. A. *Chem. Rev.* **2016**, *116*, 10075.
60. Arias-Rotondo, D. M.; McCusker, J. K. *Chem. Soc. Rev.* **2016**, *45*, 5803.
61. Wang, C. S.; Dixneuf, P. H.; Soulé, J.-F. *Chem. Rev.* **2018**, *118*, 7532.
62. Marzo, L.; Pagire, S. K.; Reiser, O.; König, B. *Angew. Chem. Int. Ed.* **2018**, *57*, 10034.
63. Buzzetti, L.; Crisenza, G. E. M.; Melchiorre, P. *Angew. Chem. Int. Ed.* **2019**, *58*, 3730.
64. Ishiyama, T.; Murata, M.; Miyaura, N. *J. Org. Chem.* **1995**, *60*, 7508.

65. Jiang, M.; Yang, H. J.; Fu, H. *Org. Lett.* **2016**, *18*, 5248.
66. Wayner, D. D. M.; Dannenberg, J. J.; Griller, D. *Chem. Phys. Lett.* **1986**, *131*, 189.
67. Yin, H.; Carroll, P. J.; Anna, J. M.; Schelter, E. J. *J. Am. Chem. Soc.* **2015**, *137*, 9234.
68. Yin, H.; Carroll, P. J.; Manor, B. C.; Anna, J. M.; Schelter, E. J. *J. Am. Chem. Soc.* **2016**, *138*, 5984.
69. Yin, H.; Jin, Y.; Hertzog, J. E.; Mullane, K. C.; Carroll, P. J.; Manor, B. C.; Anna, J. M.; Schelter, E. J. *J. Am. Chem. Soc.* **2016**, *138*, 16266.
70. Qiao, Y.; Schelter, E. J. *Acc. Chem. Res.* **2018**, *51*, 2926.
71. Qiao, Y.; Yang, Q.; Schelter, E. J. *Angew. Chem. Int. Ed.* **2018**, *57*, 10999.
72. Zhang, L.; Jiao, L. *J. Am. Chem. Soc.* **2017**, *139*, 607.
73. Mfuh, A. M.; Doyle, J. D.; Chhetri, B.; Arman, H. D.; Larionov, O. V. *J. Am. Chem. Soc.* **2016**, *138*, 2985.
74. Chen, K.; Zhang, S.; He, P.; Li, P. F. *Chem. Sci.* **2016**, *7*, 3676.
75. Mfuh, A. M.; Nguyen, V. T.; Chhetri, B.; Burch, J. E.; Doyle, J. D.; Nesterov, V. N.; Arman, H. D.; Larionov, O. V. *J. Am. Chem. Soc.* **2016**, *138*, 8408.
76. Liu, W.; Yang, X.; Gao, Y.; Li, C. J. *J. Am. Chem. Soc.* **2017**, *139*, 8621.
77. Nitelet, A.; Thevenet, D.; Schiavi, B.; Hardouin, C.; Fournier, J.; Tamion, R.; Pannecoucke, X.; Jubault, P.; Poisson, T. *Chem. Eur. J.* **2019**, *25*, 3262.
78. Xu, W. G.; Jiang, H. M.; Leng, J.; Ong, H. W.; Wu, J. *Angew. Chem. Int. Ed.* **2020**, *59*, 4009.
79. Yu, D.; To, W. P.; Tong, G. S. M.; Wu, L.-L.; Chan, K.-T.; Du, L.; Phillips, D. L.; Liu, Y.; Che, C.-M. *Chem. Sci.* **2020**, *11*, 6370.
80. Zhao, J.-H.; Zhou, Z.-Z.; Zhang, Y.; Su, X.; Chen, X.-M.; Liang, Y.-M. *Org. Biomol. Chem.* **2020**, *18*, 4390.
81. Jiao, Z. F.; Zhao, J. X.; Guo, X. N.; Guo, X. Y. *Chinese J. Catal.* **2020**, *41*, 357.
82. Mazzarella, D.; Magagnano, G.; Schweitzer-Chaput, B.; Melchiorre, P. *ACS Catal.* **2019**, *9*, 5876.
83. Schweitzer-Chaput, B.; Horwitz, M. A.; de Pedro Beato, E.; Melchiorre, P. *Nat. Chem.* **2019**, *11*, 129.
84. Zhang, L.; Jiao, L. *Chem. Sci.* **2018**, *9*, 2711.

85. Zhang, L.; Jiao, L. *J. Am. Chem. Soc.* **2019**, *141*, 9124.
86. Zhang, L.; Wu, Z. Q.; Jiao, L. *Angew. Chem. Int. Ed.* **2020**, *59*, 2095.
87. Lee, D. S.; Iqbal, C. S.; Kim, N.; Park, G. S.; Son, K.-S.; Cho, E. J. *Org. Lett.* **2019**, *21*, 9950.
88. Kim, H.; Kim, H.; Lambert, T. H.; Lin, S. *J. Am. Chem. Soc.* **2020**, *142*, 2087.
89. Schutt, L.; Bunce, N. J. 2nd ed.; Horspool, W. M.; Lenci, F.; Eds.; CRC Press: Boca Raton, **2004**.
90. Albin, A., Fagnoni, M., Eds.; Wiley-VCH: Weinheim, **2010**.
91. Albin, A.; Fagnoni, M. John Wiley & Sons, Inc.: Hoboken, **2013**.
92. Pietch, S.; Neeve, E. C.; Apperley, D. C.; Bertermann, R.; Mo, F.; Qiu, D.; Cheung, M. S.; Dang, L.; Wang, J.; Radius, U.; Lin, Z.; Kleeberg, C.; Marder, T. B. *Chem. Eur. J.* **2015**, *21*, 7082.
93. Dewhurst, R. D.; Neeve, E. C.; Braunschweig, H.; Marder, T. B. *Chem. Commun.* **2015**, *51*, 9594.
94. Kleeberg, C.; Dang, L.; Lin, Z. Y.; Marder, T. B. *Angew. Chem. Int. Ed.* **2009**, *48*, 5350.
95. Chen, K.; Cheung, M. S.; Lin, Z. Y.; Li, P. F. *Org. Chem. Front.* **2016**, *3*, 875.
96. Mfuh, A. M.; Schneider, B. D.; Cruces, W.; Larionov, O. V. *Nat. Protoc.* **2017**, *12*, 604.
97. Bose, S. K.; Deißnerberger, A.; Eichhorn, A.; Steel, P. G.; Lin, Z. Y.; Marder, T. B. *Angew. Chem. Int. Ed.* **2015**, *54*, 11843.
98. Mukai, K.; de Sant'Ana, D. P.; Hirooka, Y.; Mercado-Marin, E. V.; Stephens, D. E.; Kou, K. G. M.; Richter, S. C.; Kelley, N.; Sarpong, R. *Nat. Chem.* **2018**, *10*, 38.
99. Cheng, Y.; Mgck-Lichtenfeld, C.; Studer, A. *Angew. Chem. Int. Ed.* **2018**, *57*, 16832.
100. Wang, J.; Sánchez-Roselló, M.; Aceña, J. L.; del Pozo, C.; Sorochinsky, A. E.; Fustero, S.; Soloshonok, V. A.; Liu H. *Chem. Rev.* **2014**, *114*, 2432.
101. Purser, S.; Moore, P. R.; Swallow, S.; Gouverneur, V. *Chem. Soc. Rev.* **2008**, *37*, 320.
102. Dolbier, W. R. J. *Fluorine Chem.* **2005**, *126*, 157.
103. Uneyama, K. Wiley-Blackwell: Oxford, U.K., **2006**.
104. Doherty, N. M.; Hoffmann, N. W. *Chem. Rev.* **1991**, *91*, 553.
105. Sun, A. D.; Love, J. A. *Dalton Trans.* **2010**, *39*, 10362.
106. Clot, E.; Eisenstein, O.; Jasim, N.; Macgregor, S. A.; McGrady, J. E.; Perutz, R. N. *Acc.*

- Chem. Res.* **2011**, *44*, 333.
107. Johnson, S. A.; Hatnean, J. A.; Doster, M. E. John Wiley & Sons, Inc.: Hoboken, N. J.; **2012**; Vol 57, p 255.
108. Kuehnel, M. F.; Lentz, D.; Braun, T. *Angew. Chem. Int. Ed.* **2013**, *52*, 3328.
109. Keyes, L.; Love, J. A. Ribas, X., Ed.; RSC: Cambridge, U.K., **2013**.
110. Weaver, J.; Senaweera, S. *Tetrahedron* **2014**, *70*, 7413.
111. LaBerge, N. A.; Love, J. A. *Top. Organomet. Chem.* **2015**, *52*, 55.
112. Eisenstein, O.; Milani, J.; Perutz, R. N. *Chem. Rev.* **2017**, *117*, 8710.
113. Hall, D. G., Ed.; Wiley-VCH: Weinheim, Germany, **2006**.
114. Suzuki, A. *Angew. Chem., Int. Ed.* **2011**, *50*, 6722.
115. Ros, A.; Fernandez, R.; Lassaletta, J. M. *Chem. Soc. Rev.* **2014**, *43*, 3229.
116. Bose, S. K.; Marder, T. B. *Org. Lett.* **2014**, *16*, 4562.
117. Ahrens, T.; Kohlmann, J.; Ahrens, M.; Braun, T. *Chem. Rev.* **2015**, *115*, 931.
118. Amii, H.; Uneyama, K. *Chem. Rev.* **2009**, *109*, 2119.
119. Cho, J. Y.; Iverson, C. N.; Smith, M. R., III. *J. Am. Chem. Soc.* **2000**, *122*, 12868.
120. Braun, T.; Ahijado Salomon, M.; Altenhöner, K.; Teltewskoi, M.; Hinze, S. *Angew. Chem. Int. Ed.* **2009**, *48*, 1818.
121. Teltewskoi, M.; Panetier, J. A.; Macgregor, S. A.; Braun, T. *Angew. Chem. Int. Ed.* **2010**, *49*, 3947.
122. Guo, W. H.; Min, Q. Q.; Gu, J. W.; Zhang, X. *Angew. Chem. Int. Ed.* **2015**, *54*, 9075.
123. Lindup, R. J.; Marder, T. B.; Perutz, R. N.; Whitwood, A. C. *Chem. Commun.* **2007**, 3664.
124. Liu, X. W.; Echavarren, J.; Zarate, C.; Martin, R. *J. Am. Chem. Soc.* **2015**, *137*, 12470.
125. Niwa, T.; Ochiai, H.; Watanabe, Y.; Hosoya, T. *J. Am. Chem. Soc.* **2015**, *137*, 14313.
126. Zhou, J.; Kuntze-Fechner, M. W.; Bertermann, R.; Paul, U. S. D.; Berthel, J. H. J.; Friedrich, A.; Du, Z.; Marder, T. B.; Radius, U. *J. Am. Chem. Soc.* **2016**, *138*, 5250.
127. Schaub, T.; Radius, U. *Chem. Eur. J.* **2005**, *11*, 5024.
128. Schaub, T.; Backes, M.; Radius, U. *J. Am. Chem. Soc.* **2006**, *128*, 15964.
129. Schaub, T.; Backes, M.; Radius, U. *Eur. J. Inorg. Chem.* **2008**, 2680.
130. Schaub, T.; Fischer, P.; Steffen, A.; Braun, T.; Radius, U.; Mix, A. *J. Am. Chem. Soc.*

- 2008**, 130, 9304.
- 131.Schaub, T.; Fischer, P.; Meins, T.; Radius, U. *Eur. J. Inorg. Chem.* **2011**, 3122.
- 132.Zell, T.; Feierabend, M.; Halfter, B.; Radius, U. *J. Organomet. Chem.* **2011**, 696, 1380.
- 133.Fischer, P.; Götz, K.; Eichhorn, A.; Radius, U. *Organometallics* **2012**, 31, 1374.
- 134.Steffen, A.; Sladek, M. I.; Braun, T.; Neumann, B.; Stammler, H. G. *Organometallics* **2005**, 24, 4057.
- 135.Saito, S.; Oh-tani, S.; Miyaura, N. *J. Org. Chem.* **1997**, 62, 8024.
- 136.Chen, J. R.; Hu, X. Q.; Lu, L. Q.; Xiao, W. J. *Acc. Chem. Res.* **2016**, 49, 1911.
- 137.Yi, H.; Zhang, G. T.; Wang, H. M.; Huang, Z. Y.; Wang, J.; Singh, A. K.; Lei, A. W. *Chem. Rev.* **2017**, 117, 9016.
- 138.Yu, J.; Zhang, L.; Yan, G. B. *Adv. Synth. Catal.* **2012**, 354, 2625.
- 139.Ahammed, S.; Nandi, S.; Kundu, D.; Ranu, B. C. *Tetrahedron Lett.* **2016**, 57, 1551.
- 140.Teders, M.; Pitzer, L.; Hopkinson, M. N.; Glorius, F. *Angew. Chem. Int. Ed.* **2017**, 56, 902.
- 141.Hu, D. W.; Wang, L. H.; Li, P. F. *Org. Lett.* **2017**, 19, 2770.
- 142.Candish, L.; Teders, M.; Glorius, F. *J. Am. Chem. Soc.* **2017**, 139, 7440.
- 143.Fawcett, A.; Pradeilles, J.; Wang, Y.; Mutsuga, T.; Myers, E. L.; Aggarwal, V. K. *Science* **2017**, 357, 283.
- 144.Mazzacano, T. J.; Mankad, N. P. *J. Am. Chem. Soc.* **2013**, 135, 17258.
- 145.Hartwig, J. F.; Bergman, R. G.; Andersen, R. A. *J. Am. Chem. Soc.* **1991**, 113, 3404.
- 146.Hartwig, J. F.; Bhandari, S.; Rablen, P. R. *J. Am. Chem. Soc.* **1994**, 116, 1839.
- 147.Webster, C. E.; Fan, Y.; Hall, M. B.; Kunz, D.; Hartwig, J. F. *J. Am. Chem. Soc.* **2003**, 125, 858.
- 148.Hartwig, J. F.; Cook, K. S.; Hapke, M.; Incarvito, C. D.; Fan, Y.; Webster, C. E.; Hall, M. B. *J. Am. Chem. Soc.* **2005**, 127, 2538.
- 149.Boebel, T. A.; Hartwig, J. F. *J. Am. Chem. Soc.* **2008**, 130, 7534.
- 150.Sawyer, K. R.; Cahoon, J. F.; Shanoski, J. E.; Glascoe, E. A.; Kling, M. F.; Schlegel, J. P.; Zoerb, M. C.; Hapke, M.; Hartwig, J. F.; Webster, C. E.; Harris, C. B. *J. Am. Chem. Soc.* **2010**, 132, 1848.
- 151.Bheeter, C. B.; Chowdhury, A. D.; Adam, R.; Jackstell, R.; Beller, M. *Org. Biomol.*

- Chem.* **2015**, *13*, 10336.
152. Dombray, T.; Werncke, C. G.; Jiang, S.; Grellier, M.; Vendier, L.; Bontemps, S.; Sortais, J. B.; Sabo-Etienne, S.; Darcel, C. *J. Am. Chem. Soc.* **2015**, *137*, 4062.
153. Kalyani, D.; McMurtrey, K. B.; Neufeldt, S. R.; Sanford, M. S. *J. Am. Chem. Soc.* **2011**, *133*, 18566.
154. Ye, Y.; Sanford, M. S. *J. Am. Chem. Soc.* **2012**, *134*, 9034.
155. Sahoo, B.; Hopkinson, M. N.; Glorius, F. *J. Am. Chem. Soc.* **2013**, *135*, 5505.
156. Hopkinson, M. N.; Tlahuext-Aca, A.; Glorius, F. *Acc. Chem. Res.* **2016**, *49*, 2261.
157. Mori, K.; Kawashima, M.; Yamashita, H. *Chem. Commun.* **2014**, *50*, 14501.
158. Senaweera, S. M.; Singh, A.; Weaver, J. D. *J. Am. Chem. Soc.* **2014**, *136*, 3002.
159. Singh, A.; Kubik, J. J.; Weaver, J. D. *Chem. Sci.* **2015**, *6*, 7206.
160. Senaweera, S. M.; Weaver, J. D. *J. Am. Chem. Soc.* **2016**, *138*, 2520.
161. Singh, A.; Fennell, C. J.; Weaver, J. D. *Chem. Sci.* **2016**, *7*, 6796.
162. Chow, P. K.; Cheng, G.; Tong, G. S. M.; Ma, C.; Kwok, W. M.; Ang, W. H.; Chung, C. Y. S.; Yang, C.; Wang, F.; Che, C. M. *Chem. Sci.* **2016**, *7*, 6083.
163. Yang, C.; Mehmood, F.; Lam, T. L.; Chan, S. L. F.; Wu, Y.; Yeung, C. S.; Guan, X.; Li, K.; Chung, C. Y. S.; Zhou, C. Y.; Zou, T.; Che, C. M. *Chem. Sci.* **2016**, *7*, 3123.
164. Sun, C. Y.; To, W. P.; Wang, X. L.; Chan, K. T.; Su, Z. M.; Che, C. M. *Chem. Sci.* **2015**, *6*, 7105.
165. Sieck, C.; Sieh, D.; Sapotta, M.; Haehnel, M.; Edkins, K.; Lorbach, A.; Steffen, A.; Marder, T. B. *J. Organomet. Chem.* **2017**, *847*, 184.
166. Steffen, A.; Ward, R. M.; Tay, M. G.; Edkins, R. M.; Seeler, F.; van Leeuwen, M.; Pålsson, L.-O.; Beeby, A.; Batsanov, A. S.; Howard, J. A. K.; Marder, T. B. *Chem. Eur. J.* **2014**, *20*, 3652.
167. Steffen, A.; Costuas, K.; Boucekkine, A.; Thibault, M.-H.; Beeby, A.; Batsanov, A. S.; Charaf-Eddin, A.; Jacquemin, D.; Halet, J.-F.; Marder, T. B. *Inorg. Chem.* **2014**, *53*, 7055.
168. Steffen, A.; Tay, M. G.; Batsanov, A. S.; Howard, J. A. K.; Beeby, A.; Vuong, K. Q.; Sun, X. Z.; George, M. W.; Marder, T. B. *Angew. Chem. Int. Ed.* **2010**, *49*, 2349.
169. Rourke, J. P.; Batsanov, A. S.; Howard, J. A. K.; Marder, T. B. *Chem. Commun.* **2001**,

- 2626.
170. Sieck, C.; Tay, M. G.; Thibault, M. H.; Edkins, R. M.; Costuas, K.; Halet, J. F.; Batsanov, A. S.; Haehnel, M.; Edkins, K.; Lorbach, A.; Steffen, A.; Marder, T. B. *Chem. Eur. J.* **2016**, *22*, 10523.
171. Srivastava, V.; Singh, P. P. *RSC Adv.* **2017**, *7*, 31377.
172. Mao, L.; Bertermann, R.; Emmert, K.; Szabó, K. J.; Marder, T. B. *Org. Lett.* **2017**, *19*, 6586.
173. Mao, L.; Szabó, K. J.; Marder, T. B. *Org. Lett.* **2017**, *19*, 1204.
174. Neeve, E. C.; Geier, S. J.; Mkhaliid, I. A. I.; Westcott, S. A.; Marder, T. B. *Chem. Rev.* **2016**, *116*, 9091.
175. Batsanov, A. S.; Cabeza, J. A.; Crestani, M. G.; Fructos, M. R.; García-Álvarez, P.; Gille, M.; Lin, Z. Y.; Marder, T. B. *Angew. Chem. Int. Ed.* **2016**, *55*, 4707.
176. Pietsch, S.; Paul, U.; Cade, L. A.; Ingleson, M. J.; Radius, U.; Marder, T. B. *Chem. Eur. J.* **2015**, *21*, 9018.
177. Bose, S. K.; Fucke, K.; Liu, L.; Steel, P. G.; Marder, T. B. *Angew. Chem. Int. Ed.* **2014**, *53*, 1799.
178. Singh, A.; Fennell, C. J.; Weaver, J. D. *Chem. Sci.* **2016**, *7*, 6796.
179. Furukawa, T.; Tobisu, M.; Chatani, N. *Chem. Commun.* **2015**, *51*, 6508.
180. Reinhold, M.; McGrady, J. E.; Perutz, R. N. *J. Am. Chem. Soc.* **2004**, *126*, 5268.
181. Balzani, V.; Bolletta, F.; Scandola, F.; Ballardini, R. *Pure Appl. Chem.* **1979**, *51*, 299.
182. Rehm, D.; Weller, A. *Isr. J. Chem.* **1970**, *8*, 259.
183. Creutz, C.; Sutin, N. *Inorg. Chem.* **1976**, *15*, 496.
184. Neese, F. *WIREs Comput. Mol. Sci.* **2012**, *2*, 73.
185. Neese, F. *WIREs Comput. Mol. Sci.* **2018**, *8*:e1327.
186. Perdew, J. P.; Burke, K.; Ernzerhof, M. *Phys. Rev. Lett.* **1996**, *77*, 3865.
187. Perdew, J. P.; Ernzerhof, M.; Burke, K. *J. Chem. Phys.* **1996**, *105*, 9982.
188. Perdew, J. P.; Burke, K.; Ernzerhof, M. *Phys. Rev. Lett.* **1997**, *78*, 1396.
189. Adamo, C.; Barone, V. *J. Chem. Phys.* **1999**, *110*, 6158.
190. Ernzerhof, M.; Scuseria, G. E. *J. Chem. Phys.* **1999**, *110*, 5029.
191. Tao, J. M.; Perdew, J. P.; Staroverov, V. N.; Scuseria, G. E. *Phys. Rev. Lett.* **2003**, *91*,

- 146401.
192. Perdew, J. P.; Tao, J. M.; Staroverov, V. N.; Scuseria, G. E. *J. Chem. Phys.* **2004**, *120*, 6898.
193. Grimme, S.; Antony, J.; Ehrlich, S.; Krieg, H. *J. Chem. Phys.* **2010**, *132*, 154104.
194. Grimme, S.; Ehrlich, S.; Goerigk, L. *J. Comput. Chem.* **2011**, *32*, 1456.
195. Schafer, A.; Horn, H.; Ahlrichs, R. *J. Chem. Phys.* **1992**, *97*, 2571.
196. Weigend, F.; Ahlrichs, R. *Phys. Chem. Chem. Phys.* **2005**, *7*, 3297.
197. Weigend, F. *Phys. Chem. Chem. Phys.* **2006**, *8*, 1057.
198. Laaksonen, L. *J. Mol. Graphics* **1992**, *10*, 33.
199. Bergman, D. L.; Laaksonen, L.; Laaksonen, A. *J. Mol. Graph. Model.* **1997**, *15*, 301.
200. Gaussian 16, Revision B.01, Frisch, M. J.; Trucks, G. W.; Schlegel, H. B.; Scuseria, G. E.; Robb, M. A.; Cheeseman, J. R.; Scalmani, G.; Barone, V.; Petersson, G. A.; Nakatsuji, H.; Li, X.; Caricato, M.; Marenich, A. V.; Bloino, J.; Janesko, B. G.; Gomperts, R.; Mennucci, B.; Hratchian, H. P.; Ortiz, J. V.; Izmaylov, A. F.; Sonnenberg, J. L.; Williams-Young, D.; Ding, F.; Lipparini, F.; Egidi, F.; Goings, J.; Peng, B.; Petrone, A.; Henderson, T.; Ranasinghe, D.; Zakrzewski, V. G.; Gao, J.; Rega, N.; Zheng, G.; Liang, W.; Hada, M.; Ehara, M.; Toyota, K.; Fukuda, R.; Hasegawa, J.; Ishida, M.; Nakajima, T.; Honda, Y.; Kitao, O.; Nakai, H.; Vreven, T.; Throssell, K.; Montgomery, J. A., Jr.; Peralta, J. E.; Ogliaro, F.; Bearpark, M. J.; Heyd, J. J.; Brothers, E. N.; Kudin, K. N.; Staroverov, V. N.; Keith, T. A.; Kobayashi, R.; Normand, J.; Raghavachari, K.; Rendell, A. P.; Burant, J. C.; Iyengar, S. S.; Tomasi, J.; Cossi, M.; Millam, J. M.; Klene, M.; Adamo, C.; Cammi, R.; Ochterski, J. W.; Martin, R. L.; Morokuma, K.; Farkas, O.; Foresman, J. B.; Fox, D. J. Gaussian, Inc., Wallingford CT, **2016**.
201. Lockwood, G.; McGarvey, J. J.; Devonshire, R. *Chem. Phys. Lett.* **1982**, *86*, 127.
202. Harriman, A. *J. Chem. Soc., Faraday Trans. 1*, **1980**, *76*, 1978.
203. Valeur B. Wiley-VCH Verlag GmbH, Weinheim, **2001**, p 77-78.
204. Cheung, M. S.; Sheong, F. K.; Marder, T. B.; Lin, Z. Y. *Chem. Eur. J.* **2015**, *21*, 7480.
205. Bantreil, X.; Nolan, S. P. *Nat. Protoc.* **2011**, *6*, 69.
206. Arduengo, A. J.; Gamper, S. F.; Calabrese, J. C.; Davidson, F. *J. Am. Chem. Soc.* **1994**, *116*, 4391.



207. Dümmling, S.; Eichhorn, E.; Schneider, S.; Speiser, B.; Würde, M. *Curr. Sep.* **1996**, *15*, 53.
208. Qiu, D.; Jin, L.; Zheng, Z.; Meng, H.; Mo, F.; Wang, X.; Zhang, Y.; Wang, J. *J. Org. Chem.* **2012**, *78*, 1923.
209. Ebner, D. C.; Bagdanoff, J. T.; Ferreira, E. M.; McFadden, R. M.; Caspi, D. D.; Trend, R. M.; Stoltz, B. M. *Chem. Eur. J.* **2009**, *15*, 12978.
210. Furukawa, T.; Tobisu, M.; Chatani, N. *J. Am. Chem. Soc.* **2015**, *137*, 12211.
211. Park, J. H.; Jung, E. H.; Jung, J. W.; Jo, W. H. *Adv. Mat.* **2013**, *25*, 2583.
212. Tsoi, Y. T.; Zhou, Z.; Yu, W. Y. *Org. Lett.* **2011**, *13*, 5370.
213. Murata, M.; Oyama, T.; Watanabe, S.; Masuda, Y. *J. Org. Chem.* **2000**, *65*, 164.
214. Baudoin, O.; Guénard, D.; Guéritte, F. *J. Org. Chem.* **2000**, *65*, 9268.
215. Ishiyama, T.; Ishida, K.; Miyaura, N. *Tetrahedron* **2001**, *57*, 9813.
216. Fürstner, A.; Seidel, G. *Org. Lett.* **2002**, *4*, 541.
217. Ishiyama, T.; Miyaura, N. *Chem. Rec.* **2004**, *3*, 271.
218. Broutin, P. E.; Čerňa, I.; Campaniello, M.; Leroux, F.; Colobert, F. *Org. Lett.* **2004**, *6*, 4419.
219. Billingsley, K. L.; Barder, T. E.; Buchwald, S. L. *Angew. Chem. Int. Ed.* **2007**, *46*, 5359.
220. Billingsley, K. L.; Buchwald, S. L. *J. Org. Chem.* **2008**, *73*, 5589.
221. Ma, N.; Zhu, Z.; Wu, Y. *Tetrahedron* **2007**, *63*, 4625.
222. Wang, L.; Li, J.; Cui, X.; Wu, Y.; Zhu, Z.; Wu, Y. *Adv. Synth. Catal.* **2010**, *352*, 2002.
223. Leng, Y.; Yang, F.; Zhu, W.; Zou, D.; Wu, Y.; Cai, R. *Tetrahedron* **2011**, *67*, 6191.
224. Kawamorita, S.; Ohmiya, H.; Iwai, T.; Sawamura, M. *Angew. Chem. Int. Ed.* **2011**, *50*, 8363.
225. Murata, M. *Heterocycles* **2012**, *85*, 1795.
226. Wang, L.; Cui, X.; Li, J.; Wu, Y.; Zhu, Z.; Wu, Y. *Eur. J. Org. Chem.* **2012**, 595.
227. Molander, G. A.; Trice, S. L. J.; Kennedy, S. M. P. *Org. Lett.* **2012**, *14*, 4814.
228. Chow, W. K.; Yuen, O. Y.; So, C. M.; Wong, W. T.; Kwong, F. Y. *J. Org. Chem.* **2012**, *77*, 3543.
229. Molander, G. A.; Trice, S. L. J.; Kennedy, S. M.; Dreher, S. D.; Tudge, M. T. *J. Am. Chem. Soc.* **2012**, *134*, 11667.

230. Guerrand, H. D. S.; Marciasini, L. D.; Jousseau, M.; Vaultier, M.; Pucheault, M. *Chem. Eur. J.* **2014**, *20*, 5573.
231. Li, P.; Fu, C.; Ma, S. *Org. Biomol. Chem.* **2014**, *12*, 3604.
232. Xu, L.; Li, P. *Chem. Commun.* **2015**, *51*, 5656.
233. Dzhevakov, P. B.; Topchiy, M. A.; Zharkova, D. A.; Morozov, O. S.; Asachenko, A. F.; Nechaev, M. S. *Adv. Synth. Catal.* **2016**, *358*, 977.
234. Yamamoto, Y.; Matsubara, H.; Yorimitsu, H.; Osuka, A. *ChemCatChem* **2016**, *8*, 2317.
235. Rosen, B. M.; Huang, C.; Percec, V. *Org. Lett.* **2008**, *10*, 2597.
236. Moldoveanu, C.; Wilson, D. A.; Wilson, C. J.; Corcoran, P.; Rosen, B. M.; Percec, V. *Org. Lett.* **2009**, *11*, 4974.
237. Wilson, V.; Wilson, C. J.; Moldoveanu, C.; Resmerita, A. M.; Corcoran, P.; Hoang, L. M.; Rosen, B. M.; Percec, V. *J. Am. Chem. Soc.* **2010**, *132*, 1800.
238. Moldoveanu, C.; Wilson, D. A.; Wilson, C. J.; Leowanawat, P.; Resmerita, A. M.; Liu, C.; Rosen, B. M.; Percec, V. *J. Org. Chem.* **2010**, *75*, 5438.
239. Leowanawat, P.; Resmerita, A. M.; Moldoveanu, C.; Liu, C.; Zhang, N.; Wilson, D. A.; Hoang, L. M.; Rosen, B. M.; Percec, V. *Z. J. Org. Chem.* **2010**, *75*, 7822.
240. Murata, M.; Sambommatsu, T.; Oda, T.; Watanabe, S.; Masuda, Y. *Heterocycles* **2010**, *80*, 213.
241. Huang, K.; Yu, D.-G.; Zheng, S. F.; Wu, Z. H.; Shi, Z. J. *Chem. Eur. J.* **2011**, *17*, 786.
242. Yamamoto, T.; Morita, T.; Takagi, J.; Yamakawa, T. *Org. Lett.* **2011**, *13*, 5766.
243. Molander, G. A.; Cavalcanti, L. N.; García-García, C. *J. Org. Chem.* **2013**, *78*, 6427.
244. Kuehn, L.; Jammal, D. G.; Lubitz, K.; Marder, T. B.; Radius, U. *Chem. Eur. J.* **2019**, *25*, 9514.
245. Marciasini, L. D.; Richy, N.; Vaultier, M.; Pucheault, M. *Adv. Synth. Catal.* **2013**, *355*, 1083.
246. Bedford, R. B.; Brenner, P. B.; Carter, E.; Clifton, J.; Cogswell, P. M.; Gower, N. J.; Haddow, M. F.; Harvey, J. N.; Kehl, J. A.; Murphy, D. M.; Neeve, E. C.; Neidig, M.; Nunn, J.; Snyder, B. E. R.; Taylor, J. *Organometallics* **2014**, *33*, 5767.
247. Bedford, R. B.; Brenner, P. B.; Carter, E.; Gallagher, T.; Murphy, D. M.; Pye, D. R. *Organometallics* **2014**, *33*, 5940.

248. Atack, T.; Lecker, R. M.; Cook, S. P. *J. Am. Chem. Soc.* **2014**, *136*, 9521.
249. Bedford, R. B. *Acc. Chem. Res.* **2015**, *48*, 1485.
250. Yoshida, T.; Ilies, L.; Nakamura, E. *ACS Catal.* **2017**, *7*, 3199.
251. Zhu, W.; Ma, D. *Org. Lett.* **2006**, *8*, 261.
252. Grigg, R. D.; Van Hoveln, R.; Schomaker, J. M. *J. Am. Chem. Soc.* **2012**, *134*, 16131.
253. Labre, F.; Gimbert, Y.; Bannwarth, P.; Olivero, S.; Duñach, E.; Chavant, P. Y. *Org. Lett.* **2014**, *16*, 2366.
254. Ando, S.; Matsunaga, H.; Ishizuka, T. *J. Org. Chem.* **2015**, *80*, 9671.
255. Schmid, S. C.; Van Hoveln, R.; Rigoli, J. W.; Schomaker, J. M. *Organometallics* **2015**, *34*, 4164.
256. Kuehn, L.; Huang, M. M.; Marder, T. B.; Radius, U. *Org. Biomol. Chem.* **2019**, *17*, 6601.
257. Adams, C. J.; Baber, R. A.; Batsanov, A. S.; Bramham, G.; Charmant, J. P. H.; Haddow, M. F.; Howard, J. A. K.; Lam, W. H.; Lin, Z.; Marder, T. B.; Norman, N. C.; Orpen, A. G. *Dalton. Trans.* **2006**, *11*, 1370.
258. Dai, C.; Stringer, G.; Corrigan, J. F.; Taylor, N. J.; Marder, T. B.; Norman, N. C. *J. Organomet. Chem.* **1996**, *513*, 273.
259. Frank, R.; Howell, J.; Campos, J.; Tirfoin, R.; Phillips, N.; Zahn, S.; Mingos, D. M. P.; Aldridge, S. *Angew. Chem. Int. Ed.* **2015**, *54*, 9586.
260. Komeyama, K.; Kiguchi, S.; Takaki, K. *Chem. Commun.* **2016**, *52*, 7009.
261. Yao, W. B.; Fang, H. Q.; Peng, S. H.; Wen, H. A.; Zheng, L.; Hu, A. G.; Huang, Z. *Organometallics* **2016**, *35*, 1559.
262. Verma, P. K.; Mandal, S.; Geetharani, K. *ACS Catal.* **2018**, *8*, 4049.
263. Nagashima, Y.; Takita, R.; Yoshida, K.; Hirano, K.; Uchiyama, M. *J. Am. Chem. Soc.* **2013**, *135*, 18730.
264. Zhang, L.; Jiao, L. *J. Am. Chem. Soc.* **2017**, *139*, 607.
265. Yamamoto, E.; Izumi, K.; Horita, Y.; Ito, H. *J. Am. Chem. Soc.* **2012**, *134*, 19997.
266. Yamamoto, E.; Ukigai, S.; Ito, H. *Chem. Sci.* **2015**, *6*, 2943.
267. Uematsu, R.; Yamamoto, E.; Maeda, S.; Ito, H.; Taketsugu, T. *J. Am. Chem. Soc.* **2015**, *137*, 4090.

268. Cheung, M. S.; Marder, T. B.; Lin, Z. *Organometallics* **2011**, *30*, 3018.
269. Zhang, J. M.; Wu, H. H.; Zhang, J. L. *Eur. J. Org. Chem.* **2013**, 6263.
270. Miralles, N.; Romero, R. M.; Fernández, E.; Muñoz, K. A *Mild Chem. Commun.* **2015**, *51*, 14068.
271. Lu, D. M.; Wu, C.; Li, P. F. *Chem. Eur. J.* **2014**, *20*, 1630.
272. Lu, D. M.; Wu, C.; Li, P. F. *Org. Lett.* **2014**, *16*, 1486.
273. Cambié, D.; Bottecchia, C.; Straathof, N. J. W.; Hessel, V.; Noël, T. *Chem. Rev.* **2016**, *116*, 10276.
274. Su, Y.; Straathof, N. J. W.; Hessel, V.; Noël, T. *Chem. Eur. J.* **2014**, *20*, 10562.
275. Lee, Y.; Baek, S.; Park, J.; Kim, S. T.; Tussupbayev, S.; Kim, J.; Baik, M. H.; Cho, S. H. *J. Am. Chem. Soc.* **2017**, *139*, 976.
276. Jin, S.; Dang, H. T.; Haug, G. C.; He, R.; Nguyen, V. D.; Nguyen, V. T.; Arman, H. D.; Schanze, K. S.; Larionov, O. V. *J. Am. Chem. Soc.* **2020**, *142*, 1603.
277. Tian, Y. M.; Guo, X. N.; Kuntze-Fechner, M. W.; Krummenacher, I.; Braunschweig, H.; Radius, U.; Steffen, A.; Marder, T. B. *J. Am. Chem. Soc.* **2018**, *140*, 17612.
278. McGuinness, D. S.; Cavell, K. J.; Skelton, B. W.; White, A. H. *Organometallics* **1999**, *18*, 1596.
279. Miyazaki, S.; Koga, Y.; Matsumoto, T.; Matsubara, K. *Chem. Commun.* **2010**, *46*, 1932.
280. Zhang, K.; Conda-Sheridan, M.; Cooke, S. R.; Louie, J. *Organometallics* **2011**, *30*, 2546.
281. Nelson, D. J.; Maseras, F. *Chem. Commun.* **2018**, *54*, 10646.
282. Nguyen, P.; Lesley, G.; Taylor, N. J.; Marder, T. B.; Pickett, N. L.; Clegg, W.; Elsegood, M. R. J.; Norman, N. C. *Inorg. Chem.* **1994**, *33*, 4623.
283. Pause, L.; Robert, M.; Savéant, J.-M. *J. Am. Chem. Soc.* **1999**, *121*, 7158.
284. Matsubara, K.; Ueno, K.; Shibata, Y. *Organometallics* **2006**, *25*, 3422.
285. Ting, S. I.; Garakyaraghi, S.; Taliaferro, C. M.; Shields, B. J.; Scholes, G. D.; Castellano, F. N.; Doyle, A. G. *J. Am. Chem. Soc.* **2020**, *142*, 5800.
286. Sheldrick, G. M. *Acta Crystallogr., Sect. A: Found. Adv.* **2015**, *71*, 3.
287. Sheldrick, G. M. *Acta Crystallogr., Sect. A: Found. Crystallogr.* **2008**, *64*, 112.

288. Lee, C. H.; Cook, T. R.; Nocera, D. G. *Inorg. Chem.* **2011**, *50*, 714.
289. Molander, G. A.; Cavalcanti, L. N.; Canturk, B.; Pan, P. S.; Kennedy, L. E. *J. Org. Chem.* **2009**, *74*, 7364.
290. Yoshida, H.; Okada, K.; Kawashima, S.; Tanino, K.; Ohshita, J. *Chem. Commun.* **2010**, *46*, 1763.
291. Claudel, S.; Gosmini, C.; Paris, J. M.; Périchon, J. *Chem. Commun.* **2007**, 3667.
292. Jiang, Y.; Kuang, C.; Wang, S.; Liu, H.; Zhang, Y.; Wang, J. *Chem. Commun.* **2010**, *46*, 3170.
293. Clary, J. W.; Rettenmaier, T. J.; Snelling, R.; Bryks, W.; Banwell, J.; Wipke, W. T.; Singaram, B. *J. Org. Chem.* **2011**, *76*, 9602.
294. Harisson, P.; Morris, J.; Marder, T. B.; Steel, P. G. *Org. Lett.* **2009**, *11*, 3586.
295. Grosso, A. D.; Singleton, P. J.; Murn, C. A.; Ingleson, M. J. *Angew. Chem. Int. Ed.* **2011**, *50*, 2102.
296. Andrade, L. H.; Barcellos, T. *Org. Lett.* **2009**, *11*, 3052.
297. Chotana, G. A.; Rak, M. A.; Smith, III, M. R. *J. Am. Chem. Soc.* **2005**, *127*, 10539.
298. Chen, H. B.; Zhou, Y.; Yin, J.; Yan, J.; Ma, Y.; Wang, L.; Cao, Y.; Wang, J.; Pei, J. *Langmuir.* **2009**, *25*, 5459.
299. Brimble, M. A.; Lai, M. Y. H. *Org. Biomol. Chem.*, **2003**, *1*, 2084.
300. Yan, J. M.; Qiu, D.; Li, F.; Zhang, Y.; Wang, J. *Angew. Chem. Int. Ed.* **2010**, *49*, 2028.
301. Yang, L.; Semba, K.; Nakao, Y. *Angew. Chem. Int. Ed.* **2017**, *56*, 4853.
302. Chow, W. K.; So, C. M.; Lau, C. P.; Kwong, F. Y. *Chem. Eur. J.* **2011**, *17*, 6913.
303. Boebel, T. A.; Hartwig, J. F. *Organometallics* **2008**, *27*, 6013.
304. Mo, F.; Jiang, Y.; Qiu, D.; Zhang, Y.; Wang, J. *Angew. Chem. Int. Ed.* **2010**, *49*, 1846.
305. Han, F. S.; Higuchi, M.; Kurth, D. G. *Org. Lett.* **2007**, *9*, 559.
306. Büldt, L. A.; Guo, X.; Prescimone, A.; Wenger, O. S. *Angew. Chem. Int. Ed.* **2016**, *55*, 11247.
307. Liu, Q.; Li, G.; He, J.; Liu, J.; Li, P.; Lei, A. *Angew. Chem. Int. Ed.* **2010**, *49*, 3371.
308. Haddenham, D.; Bailey, C. L.; Vu, C.; Nepomuceno, G.; Eagon, S.; Pasumansky, L.; Singaram, B. *Tetrahedron.* **2011**, *67*, 576.
309. Ukai, K.; Aoki, M.; Takaya, J.; Iwasawa, N. *J. Am. Chem. Soc.* **2006**, *128*, 8706.

310. Blakemore, P. R.; Marsden, S. P.; Vater, H. D. *Org. Lett.* **2006**, *8*, 773.
311. Humphrey, G. R.; Kuethe, J. T. *Chem. Rev.* **2006**, *106*, 2875.
312. Sundberg, R. J. Academic Press, San Diego, **1996**.
313. Bandini, M.; Eichholzer, A. *Angew. Chem. Int. Ed.* **2009**, *48*, 9608.
314. Joucla, L.; Djakovitch, L. Transition Metal-Catalysed, Direct and Site-Selective N1-, C2- or C3-Arylation of the Indole Nucleus: 20 Years of Improvements. *Adv. Synth. Catal.* **2009**, *351*, 673.
315. Gribble, G. W.; Badenock, J. C. Springer, Berlin, **2010**.
316. Cacchi, S.; Fabrizi, G. *Chem. Rev.* **2011**, *111*, PR215.
317. Lebrasseur, N.; Larrosa, I. *Adv. Heterocycl. Chem.* **2012**, *105*, 309.
318. Sandtorv, A. H. *Adv. Synth. Catal.* **2015**, *357*, 2403.
319. Cheng, H. G.; Chen, S. Q.; Chen, R. M.; Zhou, Q. H. *Angew. Chem. Int. Ed.* **2019**, *58*, 5832.
320. Qiu, X. D.; Wang, P. P.; Wang, D. Y.; Wang, M. Y.; Yuan, Y.; Shi, Z. Z. *Angew. Chem. Int. Ed.* **2019**, *58*, 1504.
321. Miyaura, N.; Suzuki, A. *Chem. Rev.* **1995**, *95*, 2457.
322. Iverson, C. N.; Smith, M. R., III. *J. Am. Chem. Soc.* **1999**, *121*, 7696.
323. Cho, J. Y.; Tse, M. K.; Holmes, D.; Maleczka, R. E., Jr.; Smith, M. R., III. *Science* **2002**, *295*, 305.
324. Ishiyama, T.; Takagi, J.; Ishida, K.; Miyaura, N.; Anastasi, N. R.; Hartwig, J. F. *J. Am. Chem. Soc.* **2002**, *124*, 390.
325. Tajuddin, H.; Harrisson, P.; Bitterlich, B.; Collings, J. C.; Sim, N.; Batsanov, A. S.; Cheung, M. S.; Kawamorita, S.; Maxwell, A. C.; Shukla, L.; Morris, J.; Lin, Z. Y.; Marder, T. B.; Steel, P. G. *Chem. Sci.* **2012**, *3*, 3505.
326. Roosen, P. C.; Kallepalli, V. A.; Chattopadhyay, B.; Singleton, D. A.; Maleczka, R. E., Jr.; Smith, M. R., III. *J. Am. Chem. Soc.* **2012**, *134*, 11350.
327. Larsen, M. A.; Hartwig, J. F. *J. Am. Chem. Soc.* **2014**, *136*, 4287.
328. Sadler, S. A.; Hones, A. C.; Roberts, B.; Blakemore, D.; Marder, T. B.; Steel, P. G. *J. Org. Chem.* **2015**, *80*, 5308.
329. Wang, G. H.; Xu, L.; Li, P. F. *J. Am. Chem. Soc.* **2015**, *137*, 8058.

330. Chattopadhyay, B.; Dannatt, J. E.; Andujar-De Sanctis, I. L.; Gore, K. A.; Maleczka, R. E., Jr.; Singleton, D. A.; Smith, M. R., III. *J. Am. Chem. Soc.* **2017**, *139*, 7864.
331. Kanwal, S.; Ann, N.; Fatima, S.; Emwas, A.-H.; Alazmi, M.; Gao, X.; Ibrar, M.; Saleem, R. S. Z.; Chotana, G. A. *Molecules* **2020**, *25*, 2106.
332. Takagi, J.; Sato, K.; Hartwig, J. F.; Ishiyama, T.; Miyaura, N. *Tetrahedron Lett.* **2002**, *43*, 5649.
333. Ishiyama, T.; Takagi, J.; Hartwig, J. F.; Miyaura, N. *Angew. Chem. Int. Ed.* **2002**, *41*, 3056.
334. Boller, T. M.; Murphy, J. M.; Hapke, M.; Ishiyama, T.; Miyaura, N.; Hartwig, J. F. *J. Am. Chem. Soc.* **2005**, *127*, 14263.
335. Robbins, D. W.; Boebel, T. A.; Hartwig, J. F. *J. Am. Chem. Soc.* **2010**, *132*, 4068.
336. Kubota, K.; Hayama, K.; Iwamoto, H.; Ito, H. *Angew. Chem. Int. Ed.* **2015**, *54*, 8809.
337. Pang, Y.; Ishiyama, T.; Kubota, K.; Ito, H. *Chem. Eur. J.* **2019**, *25*, 4654.
338. Mkhalid, I. A. I.; Coventry, D. N.; Albesa-Jove, D.; Batsanov, A. S.; Howard, J. A. K.; Perutz, R. N.; Marder, T. B. *Angew. Chem. Int. Ed.* **2006**, *45*, 489.
339. Sadler, S. A.; Tajuddin, H.; Mkhalid, I. A. I.; Batsanov, A. S.; Albesa-Jove, D.; Cheung, M. S.; Maxwell, A. C.; Shukla, L.; Roberts, B.; Blakemore, D. C.; Lin, Z.; Marder, T. B.; Steel, P. G. *Org. Biomol. Chem.* **2014**, *12*, 7318.
340. Hoque, M. E.; Bisht, R.; Haldar, C.; Chattopadhyay, B. *J. Am. Chem. Soc.* **2017**, *139*, 7745.
341. Smith, M. R., III; Bisht, R.; Haldar, C.; Pandey, G.; Dannatt, J. E.; Ghaffari, B.; Maleczka, R. E., Jr.; Chattopadhyay, B. *ACS Catal.* **2018**, *8*, 6216.
342. Paul, S.; Chotana, G. A.; Holmes, D.; Reichle, R. C.; Maleczka, R. E., Jr.; Smith, M. R., III. *J. Am. Chem. Soc.* **2006**, *128*, 15552.
343. Kallepalli, V. A.; Shi, F.; Paul, S.; Onyeozili, E. N.; Maleczka, R. E., Jr.; Smith, M. R., III. *J. Org. Chem.* **2009**, *74*, 9199.
344. Kallepalli, V. A.; Gore, K. A.; Shi, F.; Sanchez, L.; Chotana, G. A.; Miller, S. L.; Maleczka, R. E., Jr.; Smith, M. R., III. *J. Org. Chem.* **2015**, *80*, 8341.
345. Preshlock, S. M.; Plattner, D. L.; Maligres, P. E.; Krska, S. W.; Maleczka, R. E., Jr.; Smith, M. R., III. *Angew. Chem. Int. Ed.* **2013**, *52*, 12915.

346. Shen, F.; Tyagarajan, S.; Perera, D.; Krska, S. W. Maligres, P. E.; Smith, M. R., III; Maleczka, R. E., Jr. *Org. Lett.* **2016**, *18*, 1554.
347. Mertins, K.; Zapf, A.; Beller, M. *J. Mol. Catal. A: Chem.* **2004**, *207*, 21.
348. Lo, W. F.; Kaiser, H. M.; Spannenberg, A.; Beller, M.; Tse, M. K. *Tetrahedron Lett.* **2007**, *48*, 371.
349. Zhang, H.; Hagihara, S.; Itami, K. *Chem. Lett.* **2015**, *44*, 779.
350. Léonard, N. G.; Bezdek, M. J.; Chirik, P. J. *Organometallics* **2017**, *36*, 142.
351. Thongpaen, J.; Schmid, T. E.; Toupet, L.; Dorcet, V.; Mauduit, M.; Baslé, O. *Chem. Commun.* **2018**, *54*, 8202.
352. Das, A.; Hota, P. K.; Mandal, S. K. *Organometallics* **2019**, *38*, 3286.
353. Manguin, R.; Dorcet, V.; Vives, T.; Duhayon, C.; Mauduit, M.; Baslé, O. *Angew. Chem. Int. Ed.* **2019**, *58*, 15244.
354. Bagutski, V.; Grosso, A. D.; Carrillo, J. A.; Cade, I. A.; Helm, M. D.; Lawson, J. R.; Singleton, P. J.; Solomon, S. A.; Marcelli, T.; Ingleson, M. J. *J. Am. Chem. Soc.* **2013**, *135*, 474.
355. Stahl, T.; Müther, K.; Ohki, Y.; Tatsumi, K.; Oestreich, M. *J. Am. Chem. Soc.* **2013**, *135*, 10978.
356. Légaré, M.-A.; Courtemanche, M.-A.; Rochette, É.; Fontaine, F.-G. *Science* **2015**, *349*, 513.
357. Bose, S. K.; Marder, T. B. *Science*, **2015**, *349*, 473.
358. Lavergne, J. L.; Jayaraman, A.; Misal Castro, L. C.; Rochette, É.; Fontaine, F.-G. *J. Am. Chem. Soc.* **2017**, *139*, 14714.
359. Lavergne, J. L.; Misal Castro, L. C.; Desrosiers, V.; Fontaine, F.-G. *Chem. Sci.* **2018**, *9*, 5057.
360. Han, Y.; Zhang, S.; He, J.; Zhang, Y. *ACS Catal.* **2018**, *8*, 8765.
361. Zhang, S.; Han Y.; He, J.; Zhang, Y. *J. Org. Chem.* **2018**, *83*, 1377.
362. Zhong, Q.; Qin, S.; Yin, Y.; Hu, J.; Zhang, H. *Angew. Chem. Int. Ed.* **2018**, *57*, 14891.
363. Iqbal, S. A.; Cid, J.; Procter, R. J.; Uzelac, M.; Yuan, K.; Ingleson, M. J. *Angew. Chem. Int. Ed.* **2019**, *58*, 15381.
364. Rochette, É.; Desrosiers, V.; Soltani, Y.; Fontaine, F.-G. *J. Am. Chem. Soc.* **2019**, *141*,



- 12305.
- 365.Lv, J.; Chen, X.; Xue, X.-S.; Zhao, B.; Liang, Y.; Wang, M.; Jin, L.; Yuan, Y.; Han, Y.; Zhao, Y.; Lu, Y.; Zhao, J.; Sun, W.-Y.; Houk, K. N.; Shi, Z. *Nature* **2019**, *575*, 336.
- 366.Murai, S.; Kakiuchi, F.; Sekine, S.; Tanaka, Y.; Kamatani, A.; Sonoda, M.; Chatani, N. *Nature* **1993**, *366*, 529.
- 367.Ishiyama, T.; Isou, H.; Kikuchi, T.; Miyaura, N. *Chem. Commun.* **2010**, *46*, 159.
- 368.Kawamorita, S.; Ohmiya, H.; Hara, K.; Fukuoka, A.; Sawamura, M. *J. Am. Chem. Soc.* **2009**, *131*, 5058.
- 369.Colby, D. A.; Bergman, R. G.; Ellman, J. A. *Chem. Rev.* **2010**, *110*, 624.
- 370.Kawamorita, S.; Ohmiya, H.; Sawamura, M. *J. Org. Chem.* **2010**, *75*, 3855.
- 371.Lyons, T. W.; Sanford, M. S. *Chem. Rev.* **2010**, *110*, 1147.
- 372.Ros, A.; López-Rodríguez, R.; Estepa, B.; Álvarez, E.; Fernández, R.; Lassaletta, J. M. *J. Am. Chem. Soc.* **2012**, *134*, 4573.
- 373.Gulevich, A. V.; Melkonyan, F. S.; Sarkar, D.; Gevorgyan, V. *J. Am. Chem. Soc.* **2012**, *134*, 5528.
- 374.Zhang, F.; Spring, D. R. *Chem. Soc. Rev.* **2014**, *43*, 6906.
- 375.Ping, L.; Chung, D. S.; Bouffard, J.; Lee, S. *Chem. Soc. Rev.* **2017**, *46*, 4299.
- 376.Zhao, H. T.; Dang, L.; Marder, T. B.; Lin, Z. Y. *J. Am. Chem. Soc.* **2008**, *130*, 5586.
- 377.Schramm, Y.; Takeuchi, M.; Semba, K.; Nakao, Y.; Hartwig, J. F. *J. Am. Chem. Soc.* **2015**, *137*, 12215.
- 378.Parmelee, S. R.; Mazzacano, T. J.; Zhu, Y.; Mankad, N. P.; Keith, J. A. *ACS Catal.* **2015**, *5*, 3689.
- 379.Tobisu, M.; Igarashi, T.; Chatani, N. *J. Org. Chem.* **2016**, *12*, 654.
- 380.Procter, R. J.; Uzelac, M.; Cid, J.; Rushworth, P. J.; Ingleson, M. J. *ACS Catal.* **2019**, *9*, 5760.
- 381.McGough, J. S.; Cid, J.; Ingleson, M. J. *Chem. Eur. J.* **2017**, *23*, 8180.
- 382.Jayasundara, C. R. K.; Sabasovs, D.; Staples, R. J.; Oppenheimer, J.; Smith, M. R., III; Maleczka, R. E. Jr. *Organometallics* **2018**, *37*, 1567.
- 383.Saper, N. I.; Ohgi, A.; Small, D. W.; Semba, K.; Nakao, Y.; Hartwig, J. F. *Nat. Chem.* **2020**, *12*, 276.

384. Das, R.; Blumenberg, J.; Daniliuc, C. G.; Schnieders, D.; Neugebauer, J.; Han, Y. F.; Hahn, F. E. *Organometallics* **2019**, *38*, 3278.
385. Zhou, J.; Berthel, J. H. J.; Kuntze-Fechner, M. W.; Friedrich, A.; Marder, T. B.; Radius, U. *NHC J. Org. Chem.* **2016**, *81*, 5789.
386. Bose, S. K.; Brand, S.; Omoregie, H. O.; Haehnel, M.; Maier, J.; Bringmann, G.; Marder, T. B. *ACS Catal.* **2016**, *6*, 8332.
387. Stuart, D. R.; Villemure, E.; Fagnou, K. *J. Am. Chem. Soc.* **2007**, *129*, 12072.
388. Phipps, R. J.; Grimster, N. P.; Gaunt, M. J. *J. Am. Chem. Soc.* **2008**, *130*, 8172.
389. Roy, D.; Mom, S.; Royer, S.; Lucas, D.; Hierso, J.-C.; Doucet, H. *ACS Catal.* **2012**, *2*, 1033.
390. Li, X.; Gu, X. Y.; Li, Y. J.; Li, P. X. *ACS Catal.* **2014**, *4*, 1897.
391. Jin, L.-K.; Wan, L.; Feng, J.; Cai, C. *Org. Lett.* **2015**, *17*, 4726.
392. Chen, J.; Wu, J. *Angew. Chem. Int. Ed.* **2017**, *56*, 3951.
393. Yamaguchi, M.; Suzuki, K.; Sato, Y.; Manabe, K. *Org. Lett.* **2017**, *19*, 5388.
394. Mohr, Y.; Renom-Carrasco, M.; Demarcy, C.; Quadrelli, E. A.; Camp, C.; Wisser, F. M.; Clot, E.; Thieuleux, C.; Canivet, J. *ACS Catal.* **2020**, *10*, 2713.
395. Hübschle, C. B.; Sheldrick, G. M.; Dittrich, B. *J. Appl. Cryst.* **2011**, *44*, 1281.
396. Putz, K. B. H. *crystal impact*, H. Putz & K., Brandenburg GbR, Bonn (Germany), **2017**.

# Appendix

## Coordinates (x,y,z) of the geometry optimized $S_0$ state of *trans*-[NiF(2,3,5-C<sub>6</sub>F<sub>3</sub>H<sub>2</sub>)(IMes)<sub>2</sub>]

C	0.474282	1.886627	-3.755363	H	-5.299709	-5.605724	-0.826241
C	-0.853269	1.621645	-3.719470	H	4.537009	3.755257	-1.049134
C	2.855289	-0.784842	-3.419660	H	6.839427	3.135214	-1.485208
C	-1.915939	-1.848444	-2.998248	H	-2.900967	-5.180298	-1.340457
C	3.325085	0.453854	-2.722381	H	6.944024	1.528524	-0.750833
C	4.679995	0.688862	-2.486655	H	0.832850	3.411840	-1.369566
C	2.413028	1.443108	-2.317398	H	2.096232	4.194910	-0.423140
C	-2.784186	-0.847930	-2.297570	H	-6.789461	-1.231108	-1.350614
C	5.138149	1.865745	-1.884826	H	-0.564368	-5.179095	-1.531779
C	-2.361967	0.476128	-2.121258	H	-6.785737	0.184334	-0.280572
C	2.829419	2.646234	-1.729834	H	0.227269	-3.639785	-1.072977
C	6.605674	2.076638	-1.641722	H	-1.663299	2.870633	-0.888615
C	-4.044311	-1.189363	-1.808036	H	-3.332355	3.405854	-0.644411
C	4.199500	2.826277	-1.510085	H	-6.127840	-4.669286	0.434669
C	1.869588	3.755183	-1.400700	H	-5.036956	1.786755	-0.522041
C	0.085805	0.631015	-1.907193	H	4.475984	-1.504277	-0.442913
C	-3.160498	1.447688	-1.504621	H	2.718189	-1.791585	-0.446327
C	-5.383107	-4.614296	-0.367181	H	-6.057453	-1.339792	0.255482
C	-2.671585	2.855030	-1.320499	H	0.284200	-5.032566	0.019870
C	-4.868556	-0.259435	-1.168532	H	1.489237	2.029745	0.640082
C	-4.414235	1.053130	-1.034393	H	5.147061	0.543940	0.489201
C	-6.197776	-0.678742	-0.609950	H	3.745355	-2.625876	0.724657
C	-2.865533	-4.500234	-0.488317	H	-4.896083	-3.015820	1.783095
C	-0.350269	-4.499001	-0.701192	H	5.803076	2.715487	1.248105
C	-4.056195	-4.131952	0.145472	H	-3.537503	-1.229591	2.970012
C	-1.620202	-4.043613	-0.051173	H	4.602586	3.689853	2.118063
C	3.603430	-1.674412	0.194488	H	5.774292	2.721889	3.020188
C	-3.981145	-3.293947	1.258227	H	-1.641233	3.874380	2.928176
C	-0.365259	0.911492	0.695430	H	-1.790251	-1.424875	3.093469
C	-1.596959	-3.171083	1.048175	H	-0.181855	-4.218587	3.115067
C	0.462729	2.001913	0.998510	H	-2.862231	-2.600050	3.873397
C	4.327292	0.527665	1.204787	H	0.090657	0.451812	3.386434
C	3.433193	-0.546046	1.166157	H	2.984988	2.359620	3.722896
C	0.377977	-1.641981	1.158227	H	2.101479	-2.735926	3.735704
C	-2.762133	-2.807019	1.737159	H	1.014828	1.404578	4.559197
C	-1.651803	0.929603	1.221712	H	1.038040	-0.368382	4.635374
C	0.009126	3.044362	1.793560	N	1.028580	1.281143	-2.638099
C	5.143492	2.735341	2.121404	N	-1.067133	0.864228	-2.583013
C	4.185428	1.578622	2.112722	N	-0.337023	-2.725365	1.561688
C	-2.111659	1.976983	2.015949	N	1.406287	-1.584142	2.042967
C	2.372617	-0.533019	2.078632	F	0.868885	-1.868960	-1.451910
C	-1.283069	3.054548	2.310788	F	-2.492376	-0.074105	0.969853
C	-2.731234	-1.969283	2.983707	F	0.827336	4.059366	2.070929
C	0.247752	-3.336063	2.659443	F	-3.353520	1.945535	2.482074
C	1.352703	-2.614145	2.963605	Ni	0.227556	-0.498312	-0.372342
C	3.126081	1.535354	3.023400				
C	2.203222	0.490105	3.023456				
C	1.028564	0.492626	3.955350				
H	1.078194	2.444121	-4.459500				
H	-1.659171	1.893801	-4.388447				
H	2.356701	-0.531791	-4.365393				
H	-1.725737	-1.540658	-4.035422				
H	3.698670	-1.443863	-3.647945				
H	-2.400335	-2.829107	-3.016556				
H	7.205501	1.716011	-2.485305				
H	1.939225	4.555328	-2.150066				
H	5.401331	-0.065202	-2.803735				
H	2.124619	-1.326387	-2.800193				
H	-0.939297	-1.949634	-2.504888				
H	-2.630257	3.401716	-2.271791				
H	-4.382400	-2.217903	-1.924263				
H	-5.780221	-3.932940	-1.133070				

Coordinates (x,y,z) of the geometry optimized T<sub>1</sub> state of *trans*-[NiF(2,3,5-C<sub>6</sub>F<sub>3</sub>H<sub>2</sub>)(IMes)<sub>2</sub>]

C	-0.008855	1.869346	-3.914742	H	-5.351054	-4.683920	-1.648638
C	-1.309225	1.495450	-3.831269	H	-5.224146	-5.939922	-0.417610
C	2.696455	-0.582789	-3.353419	H	3.753086	4.187533	-1.070384
C	-2.002595	-1.999587	-3.112743	H	5.995302	3.404020	-0.500983
C	2.992278	0.727430	-2.692862	H	-2.676787	-5.386069	-1.286004
C	4.285349	1.067540	-2.286695	H	6.510175	1.754959	-0.904562
C	1.977307	1.665640	-2.459943	H	0.308264	3.459609	-1.118076
C	-2.980766	-1.092248	-2.426876	H	1.488304	4.777434	-1.113813
C	4.581127	2.302382	-1.702531	H	-6.641564	-2.248449	-1.215627
C	-2.660695	0.248612	-2.178064	H	-0.317550	-5.272869	-1.306000
C	2.234365	2.930043	-1.911687	H	-7.293191	-0.610021	-1.390105
C	5.984350	2.638315	-1.284341	H	0.356059	-3.663581	-0.897417
C	-4.236976	-1.540379	-2.017597	H	-2.084252	2.719493	-1.292360
C	3.547758	3.227498	-1.543550	H	-3.481264	2.845976	-0.226611
C	1.127852	3.917449	-1.685396	H	-6.133469	-4.458763	-0.073636
C	-0.238584	0.646063	-2.019486	H	-5.445570	1.271663	-0.557102
C	-3.525235	1.119499	-1.500750	H	4.454615	-1.921304	-0.169758
C	-5.240068	-4.853238	-0.568967	H	2.672670	-1.943615	-0.237459
C	-3.163063	2.552030	-1.231872	H	-6.616630	-1.126313	0.157359
C	-5.140005	-0.704737	-1.356165	H	0.393144	-4.974543	0.292298
C	-4.759981	0.612770	-1.091893	H	2.679774	1.742386	0.633981
C	-6.491758	-1.202558	-0.930588	H	5.401314	-0.053046	0.882502
C	-2.735648	-4.618531	-0.512909	H	3.526381	-2.967975	0.922616
C	-0.206928	-4.527859	-0.511657	H	-5.010594	-2.875628	1.299785
C	-3.987460	-4.216087	-0.037348	H	6.503215	1.792797	1.968018
C	-1.547803	-4.086035	-0.008305	H	-2.565853	-0.614774	2.104275
C	3.543160	-1.984440	0.433072	H	5.247880	3.029453	2.185675
C	-4.041460	-3.215759	0.934711	H	5.983155	2.264242	3.600888
C	0.548051	1.365395	0.718790	H	0.387844	4.841153	2.524350
C	-1.651330	-3.113014	0.998164	H	-2.340891	-1.807439	3.384476
C	1.706688	2.110231	0.951329	H	-0.385012	-4.292507	3.094547
C	4.559418	0.030136	1.570131	H	-3.979844	-1.399606	2.835316
C	3.508157	-0.885382	1.450684	H	0.346647	0.840663	3.540279
C	0.294272	-1.599597	1.338243	H	3.438680	1.921845	4.148172
C	-2.883789	-2.642492	1.467304	H	1.951517	-2.949519	3.833810
C	-0.641602	1.906427	1.174818	H	1.359096	1.173671	4.959237
C	1.641822	3.335515	1.599261	H	0.816533	-0.483555	4.615176
C	5.639398	2.080547	2.575995	N	0.623217	1.349146	-2.799795
C	4.555334	1.043391	2.530435	N	-1.420632	0.756795	-2.666627
C	-0.730539	3.142162	1.807300	N	-0.456266	-2.681430	1.652463
C	2.418600	-0.734963	2.317949	N	1.321775	-1.651560	2.225091
C	0.431341	3.874956	2.027932	F	0.994519	-1.787119	-1.269563
C	-2.948916	-1.560854	2.505235	F	-1.784036	1.203345	0.985972
C	0.083716	-3.396730	2.707984	F	2.762019	4.031619	1.811383
C	1.214899	-2.743625	3.067525	F	-1.908349	3.620576	2.191321
C	3.470018	1.123128	3.406572	Ni	0.198657	-0.345826	-0.276683
C	2.382465	0.256519	3.308335				
C	1.165626	0.451147	4.160975				
H	0.522957	2.452610	-4.655591				
H	-2.155037	1.681262	-4.480349				
H	2.156749	-0.432084	-4.297584				
H	-1.767854	-1.638982	-4.123103				
H	3.622519	-1.124073	-3.571157				
H	-2.409509	-3.011665	-3.195269				
H	6.565368	3.023772	-2.133376				
H	0.712274	4.286749	-2.631979				
H	5.085214	0.342163	-2.439755				
H	2.060151	-1.199221	-2.699507				
H	-1.052224	-2.051997	-2.563167				
H	-3.648437	3.223122	-1.953023				
H	-4.512154	-2.573584	-2.219429				

Coordinates (x,y,z) of the geometry optimized T<sub>2</sub> state of *trans*-[NiF(2,3,5-C<sub>6</sub>F<sub>3</sub>H<sub>2</sub>)(IMes)<sub>2</sub>]

C	-0.48852300	-3.95863800	H	5.40728900	-1.14075700
-1.71863900			-1.01698400		
C	0.80988800	-4.04638900	H	7.27517700	0.34276700
-1.33798500			-1.24919700		
C	-1.59333800	-1.16247100	H	7.63515900	2.07361300
-3.78956900			-1.29009300		
C	3.11074300	-1.47710100	H	-5.20232500	-2.32606800
-2.44724700			0.05231200		
C	-2.59373700	-1.46061400	H	-6.72970400	-0.62912600
-2.71664200			-0.97102900		
C	-3.91477500	-1.01163000	H	5.33941500	1.83087800
-2.80075200			-2.69381500		
C	-2.24249100	-2.21405900	H	-6.34578000	0.08152200
-1.58849500			-2.55873600		
C	3.38917200	-1.86440700	H	-1.87446200	-2.96172200
-1.02599900			1.07914700		
C	-4.86541800	-1.31165600	H	-3.56968300	-3.42961900
-1.82207400			1.32951800		
C	2.40968200	-2.49186300	H	6.91632100	-1.23331000
-0.24643000			0.82113000		
C	-3.16933500	-2.56232700	H	3.29702300	2.37825000
-0.59530300			-3.73813700		
C	-6.28246700	-0.83468900	H	6.67203100	-2.61316500
-1.95392100			1.91696500		
C	4.62533300	-1.61834200	H	1.83196500	1.81588500
-0.42389100			-2.85750100		
C	-4.47754200	-2.09616900	H	0.54773500	-3.12456500
-0.73313000			1.64901400		
C	-2.76171600	-3.38862500	H	1.70375900	-3.35378500
0.58781600			2.97337600		
C	0.11248800	-1.93472300	H	7.61013300	1.21128900
-0.89668200			0.26594000		
C	2.61654200	-2.84232400	H	4.04116500	-2.81218000
1.09560600			2.70066900		
C	7.11666400	1.29283200	H	-2.71368200	2.17095200
-0.71236000			-3.16243900		
C	1.54351500	-3.51452000	H	-1.14377100	1.73473900
1.89946600			-2.42400400		
C	4.88117000	-1.95767900	H	6.11699500	-1.00083900
0.90599000			2.39303000		
C	3.86280900	-2.55703100	H	2.30880200	3.52794600
1.65205700			-2.80495500		
C	6.21619700	-1.68574000	H	-3.02475300	0.07361500
1.53581600			0.41008700		
C	4.87744100	1.86808500	H	-4.59962900	2.05763600
-1.70273100			-1.76931200		
C	2.70082600	2.49812800	H	-1.56431600	3.43657600
-2.82349400			-2.66807000		
C	5.65492900	1.60520500	H	5.62993400	1.41722000
-0.57066600			1.57536500		
C	3.52666700	2.20577400	H	-6.61309000	2.07539100
-1.60907600			-0.44002400		
C	-1.98114700	2.45303800	H	3.79075600	1.90354200
-2.39430400			2.97954300		
C	5.04009600	1.63613400	H	-6.20963400	1.08737300
0.68142900			0.98715400		
C	-1.05582500	-0.24639900	H	-6.57890100	2.81023500
1.28628200			1.18434800		
C	2.96106600	2.26278300	H	-3.10129200	-1.15613200
-0.32522500			4.52714000		
C	-2.45696000	-0.20748500	H	2.33260000	1.14847100
1.29867400			2.29461600		
C	-4.00333800	2.29786700	H	2.20634600	4.86676400
-0.88521700			-0.21692200		
C	-2.62935800	2.50960000	H	2.46692000	2.91256300
-1.04424800			2.34124700		

## Appendix

C	0.48530400	2.06729800	H	-0.95029600	2.22748100
-0.10118600			2.73357200		
C	3.68860100	1.95978700	H	-4.31374600	2.73588200
0.83197300			2.46450600		
C	-0.44087100	-0.60576900	H	-0.56842300	5.18126000
2.47273000			0.00419800		
C	-3.16470600	-0.52583800	H	-2.24755000	3.17916300
2.44771000			3.49723000		
C	-6.08665700	2.08023600	H	-0.99174500	3.98778700
0.52435800			2.52351800		
C	-4.62679100	2.38165100	N	-0.89392000	-2.66575700
0.36096500			-1.43527200		
C	-1.14699400	-0.94031300	N	1.14802400	-2.80092100
3.62658600			-0.83867900		
C	-1.88337300	2.78660000	N	1.63384800	2.77830100
0.10799200			-0.18998100		
C	-2.53613800	-0.90123700	N	-0.47680300	3.01917400
3.63064200			-0.01076100		
C	3.03936500	1.98568300	F	0.46567400	0.44516600
2.18284700			-2.27635500		
C	1.39839200	4.14325500	F	0.91349600	-0.65334500
-0.15872100			2.54802800		
C	0.05723100	4.29501400	F	-4.50957500	-0.48016500
-0.04907700			2.42844400		
C	-3.84536000	2.69097300	F	-0.48933700	-1.30062500
1.47757500			4.73173100		
C	-2.46852500	2.88146700	Ni	0.13686700	0.05891400
1.37864700			-0.38412700		
C	-1.62395400	3.08984800			
2.59818900					
H	-1.16013400	-4.68719600			
-2.16349800					
H	1.52055900	-4.86674600			
-1.37611000					
H	-1.15924400	-2.09360500			
-4.18860200					
H	2.85807100	-2.35948800			
-3.05746900					
H	-2.06628900	-0.62326500			
-4.62161700					
H	3.98757600	-0.98967000			
-2.89367500					
H	-6.90939500	-1.59630700			
-2.44700300					
H	-2.51253800	-4.42129600			
0.29487900					
H	-4.20718100	-0.41173900			
-3.66753200					
H	-0.75955800	-0.55517100			
-3.39224800					
H	2.25233100	-0.78556500			
-2.51298800					
H	1.52772700	-4.60126300			
1.71350500					

Coordinates (x,y,z) of the geometry optimized T<sub>3</sub> state of *trans*-[NiF(2,3,5-C<sub>6</sub>F<sub>3</sub>H<sub>2</sub>)(IMes)<sub>2</sub>]

C	-1.65458100	-3.98815600	H	4.52949800	-1.73815600
-0.99278000			-1.36889800		
C	-0.34900100	-4.23129600	H	6.52308300	-0.71967000
-0.71948000			-2.36600000		
C	-2.52622100	-1.64079300	H	7.10640900	0.83065500
-3.50153800			-2.98717300		
C	2.08349500	-2.16271900	H	-5.90877400	-1.30145800
-2.48096500			0.68954400		
C	-3.46861700	-1.53344700	H	-7.65276100	-0.49273100
-2.34468500			-0.73709500		
C	-4.74708900	-0.98884800	H	4.50587600	0.63032200
-2.48443900			-3.79373100		
C	-3.09559300	-1.98369500	H	-6.94109200	0.79361300
-1.06898900			-1.73423700		
C	2.50106200	-2.36028600	H	-2.51938400	-2.11831100
-1.05415100			1.63874500		
C	-5.63841200	-0.89953200	H	-4.22119700	-2.10620200
-1.41085600			2.16282700		
C	1.58996700	-2.79803200	H	6.26580900	-1.74961000
-0.08506500			0.28764600		
C	-3.95452700	-1.91110500	H	2.38586500	1.29657100
0.03511200			-4.56769500		
C	-7.00168000	-0.29992200	H	6.02837300	-2.67622700
-1.60121600			1.79430400		
C	3.81036000	-2.10829000	H	1.11200600	1.06386700
-0.63540000			-3.32119300		
C	-5.22412800	-1.36181100	H	0.12713200	-2.70312300
-0.16067800			2.34124200		
C	-3.53557000	-2.44266400	H	1.39598100	-3.54336500
1.37356600			3.26074900		
C	-0.66861000	-1.99095900	H	7.31728100	0.42959200
-0.57305100			-1.26603600		
C	1.95337800	-3.01618900	H	3.56963800	-2.89043600
1.25269500			2.65833400		
C	6.62914500	0.34955900	H	-3.40611200	1.92862500
-2.11906500			-2.80963100		
C	0.93729600	-3.44653700	H	-1.72167100	1.43896600
2.26804700			-2.46158600		
C	4.20934600	-2.28577100	H	5.54595700	-0.97092200
0.68880300			1.71597500		
C	3.27469100	-2.76145100	H	1.65252200	2.70101600
1.61326200			-3.75260700		
C	5.58915100	-1.90926100	H	-2.01611900	-0.04206500
1.13859600			2.34376800		
C	4.30155000	1.02982000	H	-4.82345900	1.67810700
-2.79587400			-0.95647100		
C	1.99609100	1.66376800	H	-2.11969700	3.15591500
-3.60856000			-2.66357700		
C	5.29749700	0.97293700	H	5.78765100	1.46636700
-1.81463800			0.22361500		
C	3.04904200	1.59176000	H	-6.39125100	1.53969600
-2.54732000			0.82770700		
C	-2.49558300	2.20201500	H	4.03020500	2.07234100
-2.26003900			1.88155900		
C	5.02127600	1.50376500	H	-5.62071600	0.87980800
-0.55567300			2.28720500		
C	0.04187500	-0.00177700	H	-6.09668300	2.58506200
1.61493700			2.23965000		
C	2.81038500	2.09723100	H	0.95398400	-0.09060300
-1.25853000			5.45022100		
C	-0.95396300	-0.05207300	H	2.46842200	2.71491200
2.60221300			1.34623300		
C	-4.04390900	2.01344400	H	2.11679000	4.75900600
-0.27028200			-1.26767300		
C	-2.78282900	2.31630100	H	3.93685600	3.69779300
-0.79317500			1.16270100		

Appendix

C	0.42376800	2.02296100	H	-0.05553400	2.68083800
-0.60116700			2.29556600		
C	3.78370900	2.07996300	H	-3.51496100	2.63685000
-0.25287600			3.02541200		
C	1.34838300	0.01673900	H	-0.54034200	5.16752100
2.07136800			-0.49056000		
C	-0.61879300	-0.07525100	H	-1.27772600	3.22734100
3.95178200			3.46428000		
C	-5.68018000	1.76534800	H	-0.65144100	4.35292200
1.63391200			2.23379700		
C	-4.32638700	2.12060800	N	-1.82494500	-2.61580000
1.09182200			-0.89665500		
C	1.69430500	-0.01941400	N	0.22582000	-3.00037700
3.41750000			-0.46122700		
C	-1.79687700	2.73433400	N	1.54049700	2.69217000
0.11014300			-0.97406500		
C	0.70239200	-0.06620000	N	-0.48175400	3.00324900
4.38996400			-0.37639000		
C	3.53768300	2.67148900	F	-0.24618600	0.01562400
1.10400000			-2.40864500		
C	1.33190000	4.06187100	F	2.35584600	0.06301600
-0.98909000			1.17356300		
C	0.04498400	4.26044400	F	-1.59335500	-0.10168000
-0.61009400			4.87263300		
C	-3.31428900	2.55706400	F	2.98298800	-0.01496500
1.95314700			3.77634400	Ni	-0.12123700
C	-2.03852400	2.86960600	0.01483600	-0.42276800	
1.48611800					
C	-0.95088400	3.30901300			
2.41955500					
H	-2.47444900	-4.65337800			
-1.24809100					
H	0.22217500	-5.15466700			
-0.68954400					
H	-2.20761800	-2.68407100			
-3.65767000					
H	1.68443900	-3.09707400			
-2.90829200					
H	-3.00071000	-1.28527800			
-4.42610700					
H	2.93947100	-1.84418600			
-3.09052800					
H	-7.49544100	-0.70260200			
-2.49848800					
H	-3.53121300	-3.54511900			
1.37988600					
H	-5.05788400	-0.63500500			
-3.47189100					
H	-1.61537100	-1.04540700			
-3.30070800					
H	1.28769200	-1.40247900			
-2.57475400					
H	0.47324800	-4.41100700			
2.00890400					



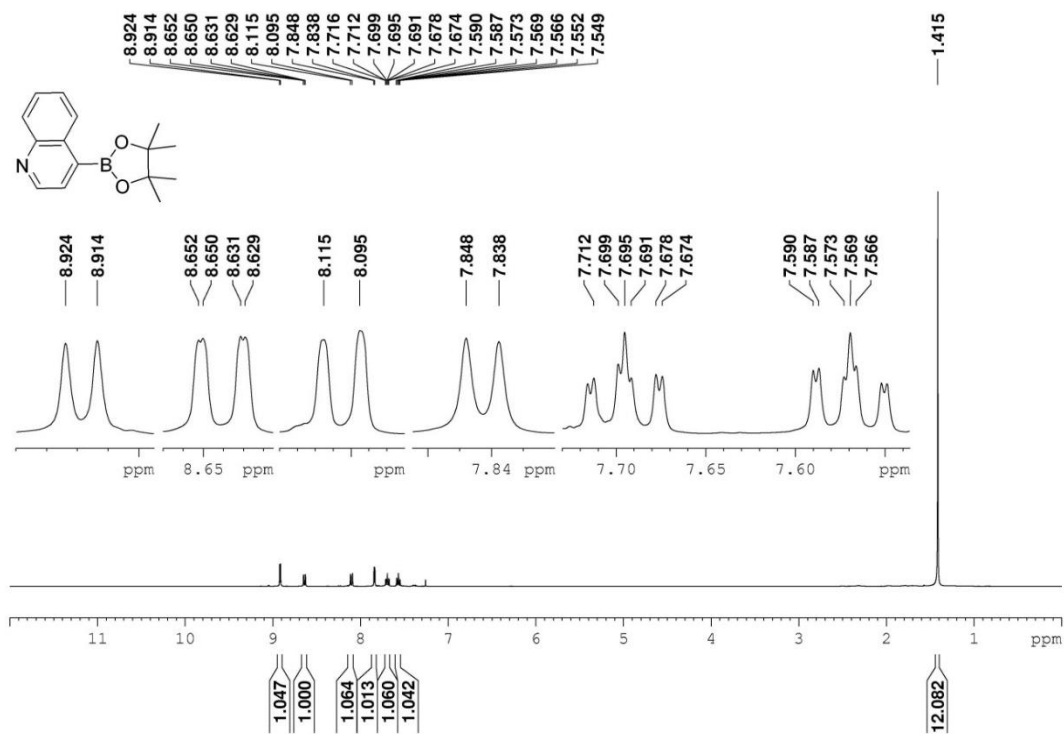
Coordinates (x,y,z) of the geometry optimized T<sub>4</sub> state of *trans*-[NiF(2,3,5-C<sub>6</sub>F<sub>3</sub>H<sub>2</sub>)(IMes)<sub>2</sub>]

C	-0.90166800	-4.04035800	H	1.27040700	-4.52891600
-1.38862800			2.05568800		
C	0.39173900	-4.18356200	H	5.13859000	-1.44231100
-1.00420300			-1.13045100		
C	-1.61120100	-1.36096200	H	7.02987200	-0.07453800
-3.76122900			-1.66845100		
C	2.79845200	-1.85085900	H	7.52266200	1.60097600
-2.44919900			-1.94831800		
C	-2.70554800	-1.48132000	H	-5.55243200	-1.85043500
-2.74729700			-0.10900600		
C	-3.97659100	-0.95252100	H	-6.98828900	-0.44796200
-2.97766600			-1.43283400		
C	-2.49095400	-2.14166800	H	5.11482700	1.49527700
-1.52683400			-3.11495900		
C	3.10829500	-2.11850200	H	-6.31295500	0.48652000
-1.00849100			-2.79095000		
C	-5.01199000	-1.07365700	H	-2.25142200	-2.93318600
-2.04561700			1.07414900		
C	2.13684000	-2.63552900	H	-3.96732100	-2.72568200
-0.14103600			1.48085200		
C	-3.50413900	-2.30481200	H	6.70433700	-1.39289900
-0.57330700			0.65676600		
C	-6.37430000	-0.51658500	H	3.07982600	2.22523400
-2.34157900			-4.04207600		
C	4.36921600	-1.84978100	H	6.48129800	-2.65982800
-0.47153000			1.88660700		
C	-4.75657100	-1.74962900	H	1.67925600	1.65213400
-0.85223000			-3.06953600		
C	-3.27481300	-3.06540400	H	0.33523300	-3.03320600
0.69934100			1.86555000		
C	-0.13492200	-1.98956700	H	1.53573000	-3.16252300
-0.80868600			3.16624800		
C	2.38938700	-2.88085900	H	7.57547200	0.92436600
1.21564700			-0.30303400		
C	7.00005700	0.94074900	H	3.87208400	-2.75521500
-1.23907700			2.76144700		
C	1.32754000	-3.42962600	H	-2.80114500	2.02838400
2.12170100			-3.07339100		
C	4.66523900	-2.07557600	H	-1.20533500	1.58378000
0.87382000			-2.40479100		
C	3.66385100	-2.58985200	H	5.95868800	-1.00141800
1.70055300			2.22325400		
C	6.02336600	-1.76654200	H	2.12877400	3.37471800
1.43321900			-3.06764000		
C	4.73995000	1.63800800	H	-2.72340500	-0.04221800
-2.09712300			0.75422000		
C	2.53424300	2.35078300	H	-4.57403300	1.78354800
-3.09714600			-1.55729700		
C	5.58726100	1.39553600	H	-1.60844400	3.28698700
-1.01180200			-2.66112100		
C	3.42756200	2.08124000	H	5.73811800	1.40514900
-1.92696900			1.13731800		
C	-2.02812000	2.31680100	H	-6.51727800	1.76258500
-2.34893300			-0.11005900		
C	5.08878700	1.58728600	H	4.08028700	2.18282400
0.27691700			2.62667600		
C	-0.66839900	-0.18356000	H	-5.94453700	0.77961400
1.46667400			1.26070500		
C	2.97015400	2.26111300	H	-6.42013600	2.46641600
-0.61218700			1.52582700		
C	-2.06448700	-0.19429700	H	-2.36088100	-0.77151300
1.61301600			4.97481200		
C	-3.94952000	2.10512700	H	2.53666100	1.43642800
-0.72107000			2.15784100		
C	-2.60632100	2.40351300	H	2.23567900	4.89012500
-0.96859000			-0.49370200		

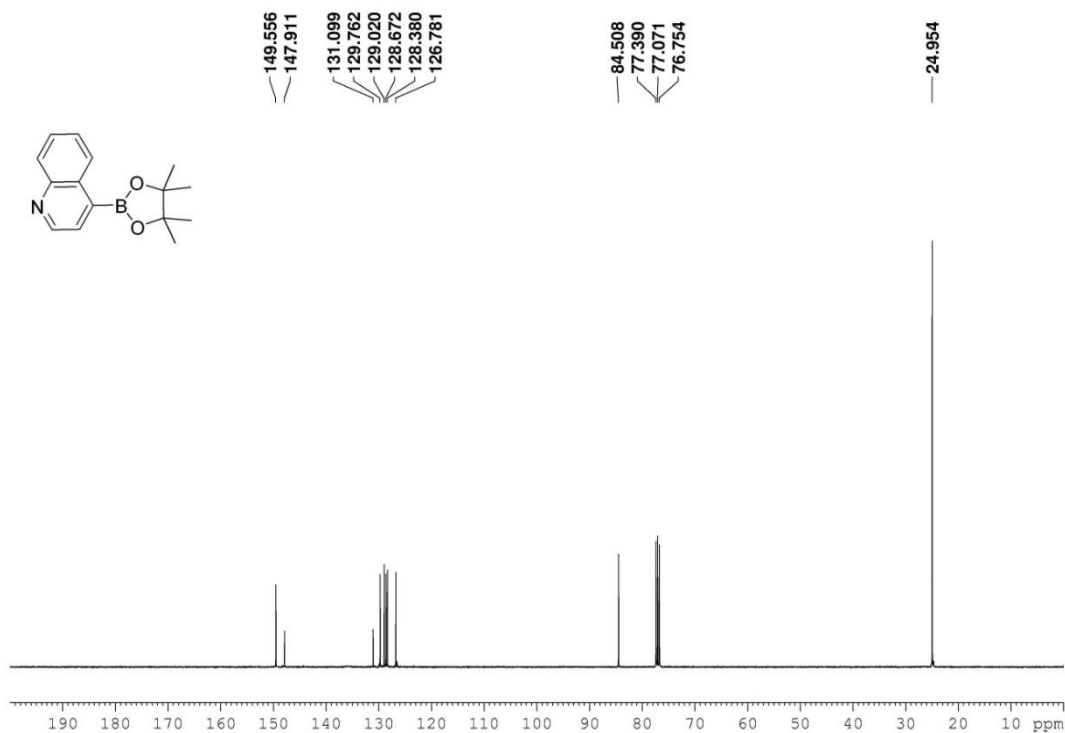
Appendix

C	0.51748400	2.10236500	H	2.74801800	3.18964700
-0.23272600			2.00490200		
C	3.77960300	2.02105100	H	-0.68003900	2.43562700
0.50440900			2.69305300		
C	0.07250400	-0.38106700	H	-4.10500000	2.67328900
2.61996900			2.62024600		
C	-2.64922100	-0.39584900	H	-0.51332500	5.22154400
2.85362300			-0.08038700		
C	-5.92512800	1.78807400	H	-2.01878800	3.27201700
0.81517800			3.51626000		
C	-4.50608000	2.19820800	H	-0.91266200	4.17655300
0.55612500			2.45147200		
C	-0.51278900	-0.59625000	N	-1.20036500	-2.69496300
3.86661700			-1.25808200		
C	-1.81982300	2.78648800	N	0.83302000	-2.92072300
0.12533900			-0.65426800		
C	-1.89529100	-0.60219800	N	1.66151000	2.80422000
4.00380500			-0.40637400		
C	3.26109100	2.22191700	N	-0.43185500	3.05713900
1.89614300			-0.08282600		
C	1.43234100	4.16945100	F	0.49221800	0.27902600
-0.37022600			-2.27992100		
C	0.10129700	4.33009300	F	1.42184200	-0.39580200
-0.16660800			2.57757400		
C	-3.69040000	2.61740600	F	-3.99056100	-0.40586300
1.61016900			2.95859400		
C	-2.33814800	2.90013400	F	0.25993000	-0.81472600
1.42267800			4.93350900		
C	-1.44484600	3.22192700	Ni	0.09545300	0.05507700
2.58184100			-0.40226700		
H	-1.63172500	-4.76180800			
-1.74397100					
H	1.03550000	-5.05671100			
-0.95066000					
H	-1.19091100	-2.34981700			
-4.00547900					
H	2.39897100	-2.74945900			
-2.94632600					
H	-1.98936600	-0.91063600			
-4.68897600					
H	3.70190900	-1.53171300			
-2.98595200					
H	-6.91295000	-1.15664600			
-3.05966600					
H	-3.43869100	-4.14543800			
0.54727800					
H	-4.16220600	-0.43393800			
-3.92292900					
H	-0.78188600	-0.74292600			
-3.37117700					
H	2.03329200	-1.05966800			
-2.54227400					

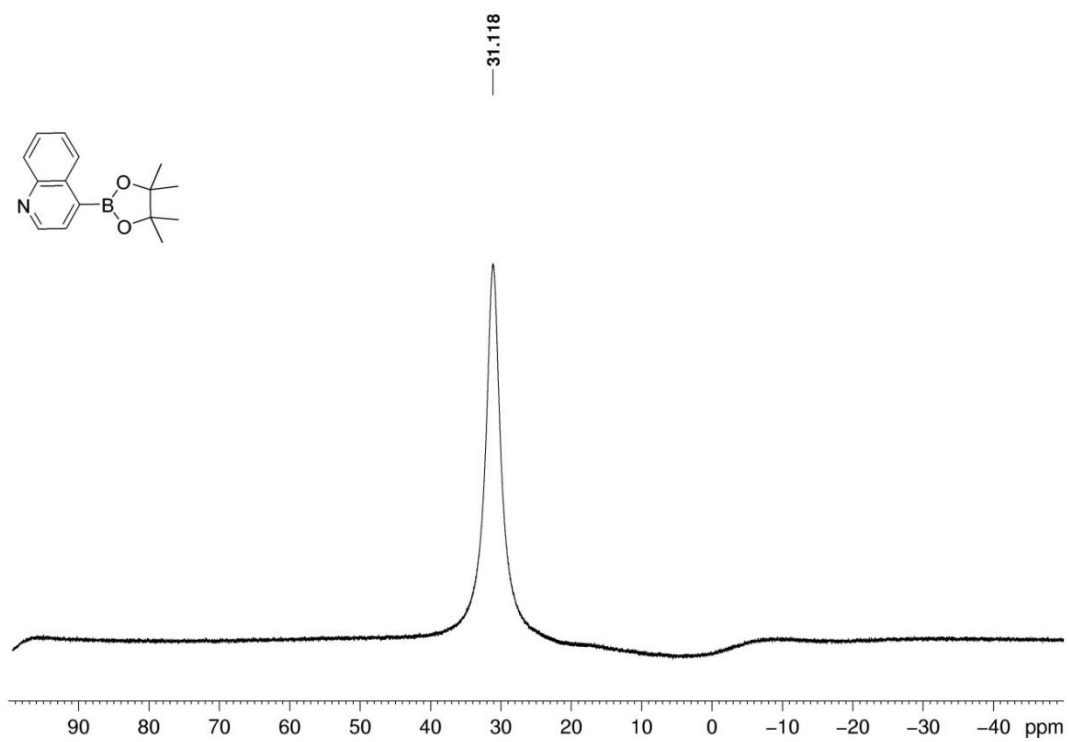
## 4-(4,4,5,5-Tetramethyl-1,3,2-dioxaborolan-2-yl)quinoline



<sup>1</sup>H NMR spectrum (400 MHz, CDCl<sub>3</sub>).




<sup>13</sup>C{<sup>1</sup>H} NMR (101 MHz, CDCl<sub>3</sub>).



$^{11}\text{B}$  NMR (128 MHz,  $\text{CDCl}_3$ ).

## Permission of American Chemical Society



# RightsLink


[Home](#)

[Help](#)

[Email Support](#)

[Sign in](#)

[Create Account](#)



**ACS Publications**  
Most Trusted. Most Cited. Most Read.

## Selective Photocatalytic C-F Borylation of Polyfluoroarenes by Rh/Ni Dual Catalysis Providing Valuable Fluorinated Arylboronate Esters

Author: Ya-Ming Tian, Xiao-Ning Guo, Maximilian W. Kuntze-Fechner, et al

Publication: Journal of the American Chemical Society

Publisher: American Chemical Society

Date: Dec 1, 2018

Copyright © 2018, American Chemical Society

### Quick Price Estimate

This service provides permission for reuse only. If you do not have a copy of the portion you are using, you may copy and paste the content and reuse according to the terms of your agreement. Please be advised that obtaining the content you license is a separate transaction not involving RightsLink.

☑ Permission for this particular request is granted for print and electronic formats, and translations, at no charge. Figures and tables may be modified. Appropriate credit should be given. Please print this page for your records and provide a copy to your publisher. Requests for up to 4 figures require only this record. Five or more figures will generate a printout of additional terms and conditions. Appropriate credit should read: "Reprinted with permission from {COMPLETE REFERENCE CITATION}. Copyright {YEAR} American Chemical Society." Insert appropriate information in place of the capitalized words.

I would like to...	<input type="text" value="reuse in a Thesis/Dissertatio"/>	Will you be translating?	<input type="text" value="No"/>
Requestor Type	<input type="text" value="Author (original work)"/>	Select your currency	<input type="text" value="EUR - €"/>
Portion	<input type="text" value="Full article"/>	Quick Price	Click Quick Price
Format	<input type="text" value="Print"/>	<input type="button" value="QUICK PRICE"/> <input type="button" value="CONTINUE"/>	

To request permission for a type of use not listed, please contact [the publisher](#) directly.

© 2020 Copyright - All Rights Reserved | [Copyright Clearance Center, Inc.](#) | [Privacy statement](#) | [Terms and Conditions](#)  
Comments? We would like to hear from you. E-mail us at [customer@copyright.com](mailto:customer@copyright.com)



RightsLink



Home



Help



Email Support



Sign in



Create Account

### Selective Photocatalytic C-F Borylation of Polyfluoroarenes by Rh/Ni Dual Catalysis Providing Valuable Fluorinated Arylboronate Esters



Author: Ya-Ming Tian, Xiao-Ning Guo, Maximilian W. Kuntze-Fechner, et al

Publication: Journal of the American Chemical Society

Publisher: American Chemical Society

Date: Dec 1, 2018

Copyright © 2018, American Chemical Society

#### PERMISSION/LICENSE IS GRANTED FOR YOUR ORDER AT NO CHARGE

This type of permission/license, instead of the standard Terms & Conditions, is sent to you because no fee is being charged for your order. Please note the following:

- Permission is granted for your request in both print and electronic formats, and translations.
- If figures and/or tables were requested, they may be adapted or used in part.
- Please print this page for your records and send a copy of it to your publisher/graduate school.
- Appropriate credit for the requested material should be given as follows: "Reprinted (adapted) with permission from (COMPLETE REFERENCE CITATION). Copyright (YEAR) American Chemical Society." Insert appropriate information in place of the capitalized words.
- One-time permission is granted only for the use specified in your request. No additional uses are granted (such as derivative works or other editions). For any other uses, please submit a new request.

[BACK](#)[CLOSE WINDOW](#)



RightsLink



Home



Help



Email Support



Sign in



Create Account

## Ni-Catalyzed Traceless, Directed C3-Selective C-H Borylation of Indoles



Author: Ya-Ming Tian, Xiao-Ning Guo, Zhu Wu, et al

Publication: Journal of the American Chemical Society

Publisher: American Chemical Society

Date: Jul 1, 2020

Copyright © 2020, American Chemical Society

### Quick Price Estimate

This service provides permission for reuse only. If you do not have a copy of the portion you are using, you may copy and paste the content and reuse according to the terms of your agreement. Please be advised that obtaining the content you license is a separate transaction not involving RightsLink.

Permission for this particular request is granted for print and electronic formats, and translations, at no charge. Figures and tables may be modified. Appropriate credit should be given. Please print this page for your records and provide a copy to your publisher. Requests for up to 4 figures require only this record. Five or more figures will generate a printout of additional terms and conditions. Appropriate credit should read: "Reprinted with permission from {COMPLETE REFERENCE CITATION}. Copyright {YEAR} American Chemical Society." Insert appropriate information in place of the capitalized words.

I would like to...	<input type="text" value="reuse in a Thesis/Dissertatio"/>	Will you be translating?	<input type="text" value="No"/>
Requestor Type	<input type="text" value="Author (original work)"/>	Select your currency	<input type="text" value="EUR - €"/>
Portion	<input type="text" value="Full article"/>	Quick Price	Click Quick Price
Format	<input type="text" value="Print"/>		



To request permission for a type of use not listed, please contact the publisher directly.



RightsLink



Home



Help



Email Support



Sign in



Create Account

### Ni-Catalyzed Traceless, Directed C3-Selective C–H Borylation of Indoles



Author: Ya-Ming Tian, Xiao-Ning Guo, Zhu Wu, et al

Publication: Journal of the American Chemical Society

Publisher: American Chemical Society

Date: Jul 1, 2020

Copyright © 2020, American Chemical Society

#### PERMISSION/LICENSE IS GRANTED FOR YOUR ORDER AT NO CHARGE

This type of permission/license, instead of the standard Terms & Conditions, is sent to you because no fee is being charged for your order. Please note the following:

- Permission is granted for your request in both print and electronic formats, and translations.
- If figures and/or tables were requested, they may be adapted or used in part.
- Please print this page for your records and send a copy of it to your publisher/graduate school.
- Appropriate credit for the requested material should be given as follows: "Reprinted (adapted) with permission from (COMPLETE REFERENCE CITATION). Copyright (YEAR) American Chemical Society." Insert appropriate information in place of the capitalized words.
- One-time permission is granted only for the use specified in your request. No additional uses are granted (such as derivative works or other editions). For any other uses, please submit a new request.

[BACK](#)[CLOSE WINDOW](#)



## Affidavit

I hereby confirm that my theses entitled “*Selective C-X and C-H Borylation by N-Heterocyclic Carbene Nickel(0) Complex*” is the result of my own work. I did not receive any help or support from commercial consultants. All sources and/or materials applied are listed and specified in the thesis. Furthermore, I confirm that this thesis has not yet been submitted as part of another examination process neither in identical nor similar form.

Würzburg, 25. 08. 2020

---

Signature

## Eidesstaatliche Erklärung

Hiermit erkläre ich an Eides statt, die Dissertation „*Selective C-X and C-H Borylation by N-Heterocyclic Carbene Nickel(0) Complex*” eigenständig, d.h. insbesondere selbstständig und ohne Hilfe eines kommerziellen Promotionsberaters angefertigt und keinen anderen als die von mir angegebenen Quellen und Hilfsmittel verwendet zu haben. Ich erkläre außerdem, dass die Dissertation weder in gleicher noch ähnlicher Form bereits in einem anderen Prüfungsverfahren vorgelegen hat.

Würzburg, 25. 08. 2020

---

Unterschrift